

ADVANCES IN SUPERCAPACITOR AND SUPERCAPATTERY



ADVANCES IN SUPERCAPACITOR AND SUPERCAPATTERY

Innovations in Energy Storage Devices

Edited by

NUMAN ARSHID

*State Key Laboratory of ASIC and System, SIST, Fudan
University, Shanghai, P.R. China*

MOHAMMAD KHALID

*Graphene & Advanced 2D Materials Research Group
(GAMRG), School of Science and Technology, Sunway
University, Selangor, Malaysia*

ANDREWS NIRMALA GRACE

*Centre for Nanotechnology Research, Vellore Institute of
Technology (VIT), Vellore, India*



ELSEVIER

Elsevier

Radarweg 29, PO Box 211, 1000 AE Amsterdam, Netherlands
The Boulevard, Langford Lane, Kidlington, Oxford OX5 1GB, United Kingdom
50 Hampshire Street, 5th Floor, Cambridge, MA 02139, United States

Copyright © 2021 Elsevier Inc. All rights reserved.

No part of this publication may be reproduced or transmitted in any form or by any means, electronic or mechanical, including photocopying, recording, or any information storage and retrieval system, without permission in writing from the publisher. Details on how to seek permission, further information about the Publisher's permissions policies and our arrangements with organizations such as the Copyright Clearance Center and the Copyright Licensing Agency, can be found at our website: www.elsevier.com/permissions.

This book and the individual contributions contained in it are protected under copyright by the Publisher (other than as may be noted herein).

Notices

Knowledge and best practice in this field are constantly changing. As new research and experience broaden our understanding, changes in research methods, professional practices, or medical treatment may become necessary.

Practitioners and researchers must always rely on their own experience and knowledge in evaluating and using any information, methods, compounds, or experiments described herein. In using such information or methods they should be mindful of their own safety and the safety of others, including parties for whom they have a professional responsibility.

To the fullest extent of the law, neither the Publisher nor the authors, contributors, or editors, assume any liability for any injury and/or damage to persons or property as a matter of products liability, negligence or otherwise, or from any use or operation of any methods, products, instructions, or ideas contained in the material herein.

British Library Cataloguing-in-Publication Data

A catalogue record for this book is available from the British Library

Library of Congress Cataloging-in-Publication Data

A catalog record for this book is available from the Library of Congress

ISBN: 978-0-12-819897-1

For Information on all Elsevier publications
visit our website at <https://www.elsevier.com/books-and-journals>

Publisher: Matthew Deans

Acquisitions Editor: Christina Gifford

Editorial Project Manager: Charlotte Rowley

Production Project Manager: Kamesh Ramajogi

Cover Designer: Christian J. Bilbow

Typeset by MPS Limited, Chennai, India



Contents

<i>List of contributors</i>	<i>xi</i>
<i>Preface</i>	<i>xv</i>
<i>Introduction</i>	<i>xvii</i>

1. Background of energy storage **1**

Suresh Sagadevan, Mohd Rafie Johan, A.R. Marlinda, Omid Akbarzadeh, Karuppasamy Pandian, M.M. Shahid, Faruq Mohammad and Jiban Podder

1.1	Introduction	1
1.2	Importance of energy storage	4
1.3	Batteries and capacitors	5
1.4	Fundamentals of energy storage	6
1.5	Electrochemical energy storage systems and materials	8
1.6	Status of energy storage technology development	10
1.6.1	Mechanical energy storage	11
1.6.2	Heat storage	15
1.6.3	Electrochemical energy storage	16
1.6.4	Electromagnetic energy storage	17
1.6.5	Chemical energy storage	18
1.6.6	Other storage	18
1.7	Challenges and prospects of energy storage technologies	18
1.7.1	Challenges of the energy storage application	18
1.7.2	Prospects of energy storage technology development	19
1.8	Energy storage systems costs and values	20
1.9	Technology frontiers	21
1.9.1	Improvements in traditional battery technology	21
1.9.2	Lithium-ion battery safety research	22
1.9.3	Solid-state battery R&D	23
1.9.4	Emerging battery systems	23
1.10	Conclusion	24
	References	24

2. Fundamental electrochemical energy storage systems **27**

Suresh Sagadevan, A.R. Marlinda, Zaira Zaman Chowdhury, Yasmin Binti Abdul Wahab, Nor Aliya Hamizi, M.M. Shahid, Faruq Mohammad, Jiban Podder and Mohd Rafie Johan

2.1	Introduction	27
2.2	Background of energy storage	28

2.3	Electrochemical capacitors	29
2.4	Principle of energy storage in electrochemical capacitors	31
2.5	Charge storage mechanism in electrical dual layer condensers	31
2.6	Electrical double-layer capacitor	32
2.7	Pseudocapacitor	37
2.8	Types of pseudocapacitance	39
2.8.1	Underpotential deposition	39
2.8.5	Redox pseudocapacitance	40
2.8.3	Intercalation pseudocapacitance	41
2.9	Conclusion	41
	References	42
3.	Introduction to supercapattery	45
	Arshid Numan, Yiqiang Zhan, Mohammad Khalid and Mohammad Hatamvand	
3.1	Introduction	45
3.2	Charge storage mechanism in electrochemical energy storage systems	48
3.2.1	Electrical double-layer capacitive electrode	50
3.2.2	Pseudocapacitive electrode	50
3.2.3	Battery electrode	51
3.3	Difference between pseudocapacitive and battery-grade materials	52
3.3.1	Why pseudocapacitive materials are considered capacitive?	52
3.3.2	Confusion between pseudocapacitive and battery-grade materials	54
3.4	Conclusions	58
	References	59
4.	Conducting polymeric nanocomposite for supercapattery	63
	Meenakshi Gusain, Irfan Ahmed and Yiqiang Zhan	
4.1	Introduction to conducting polymers	63
4.2	Types of C-polymers	64
4.2.1	Based on conductivity	65
4.2.2	Based on structural backbone	66
4.3	Problems related to conducting polymers based electrodes	67
4.4	Polymer nanocomposite	71
4.4.1	In situ synthesis	72
4.4.2	Ex situ synthesis	72
4.4.3	Carbonaceous—polymer nanocomposites	73
4.4.4	Chalcogenide—polymer nanocomposite	74
4.4.5	Polymer/layered silicates nanocomposite	75

4.5	Nanocomposites of conducting polymer with various nanomaterials	77
4.5.1	Carbon-based nanocomposite materials	77
4.5.2	Metal oxide-based composites materials	79
4.5.3	MXene and transition metal dichalcogenides composites	80
4.6	Conclusion	86
4.7	Abbreviations	87
	References	87
5.	Carbonaceous nanocomposites for supercapattery	93
	Andrews Nirmala Grace, Sandhya Venkateshalu and Subashini Gnanasekar	
5.1	Introduction	93
5.2	Carbonaceous electrode materials	95
5.2.1	Graphene and its composites	95
5.2.2	Carbon nanotube and its composites	98
5.2.3	Activated carbon and its composites	102
5.3	Summary and outlook	107
	References	107
6.	Binary metal oxides for supercapattery devices	111
	Muhammad Zahir Iqbal and Abbas Khan	
6.1	Introduction	111
6.2	Binary metal oxides	114
6.2.1	Synthesis of binary metal oxides	115
6.2.2	Binary metal oxides for supercapattery applications	120
6.3	Summary and future outlook	131
	References	133
7.	Ternary nanocomposites for supercapattery	141
	Javed Iqbal, Shahid Bashir, Mohammad Omaish Ansari, Rashida Jafer, Asim Jilani, Sharifah Mohammad, K. Ramesh and S. Ramesh	
7.1	Introduction	141
7.2	Noble metals	144
7.3	Metal oxides	145
7.3.1	Gold-containing ternary nanocomposites	147
7.3.2	Platinum-containing ternary nanocomposites	147
7.4	Carbonaceous materials	151
7.4.1	Carbon nanotubes	152
7.4.2	Graphene	155

7.5	Conducting polymers	158
7.5.1	Ternary composites of polyaniline	158
7.5.2	Ternary nanocomposites of polypyrrole containing noble metals	163
7.5.3	Ternary nanocomposites of polythiophene or other polymers containing noble metals	164
7.6	Conclusions and future work	165
	Acknowledgments	167
	References	167
8.	Metal/metal oxide thin film electrodes for supercapatteries	175
	Mohammad Islam, Sofia Javed, Muhammad Aftab Akram and Muhammad Usman	
8.1	Hybrid supercapacitors or supercapatteries	175
8.1.1	Prerequisites for a supercapattery	176
8.2	Metal oxides as electrode materials	178
8.2.1	Promising metal oxides	178
8.2.2	Technical issues with pure metal oxides	179
8.3	Performance of metal oxide electrodes	180
8.3.1	Nickel oxide	180
8.3.2	Copper oxide	181
8.3.3	Vanadium pentoxide (V_2O_5)	182
8.3.4	Ruthenium oxide (RuO_2)	183
8.3.5	Manganese dioxide (MnO_2)	183
8.3.6	Cobalt oxide (Co_3O_4)	185
8.4	Hybridization of metal oxides	189
8.5	Summary	192
	References	192
9.	Layered double hydroxide as electrode material for high-performance supercapattery	199
	Aruni Shajkumar, Sarbani Sahu, Navaneethan Duraisamy, Lukas Schmidt-Mende and Ananthakumar Ramadoss	
9.1	Introduction	199
9.2	Energy storage mechanism	201
9.3	Synthesis of layered double hydroxides nanostructures	203
9.3.1	Direct synthesis	205
9.3.2	Indirect synthesis	208
9.4	Transition metal layered double hydroxides for supercapattery	210
9.4.1	Nickel–Cobalt layered double hydroxides (Ni–Co LDH)	210

9.5	Core–shell layered double hydroxides	226
9.6	Carbon material/layered double hydroxide composites for supercapattery	237
9.7	Summary	245
	Acknowledgments	246
	References	246
10.	MXene	255
	Ghulam Ali, Muhammad Zahir Iqbal and Faiza Jan Iftikhar	
10.1	MXene	255
10.2	Structure and types of MXene	256
10.3	MXene in supercapacitors	256
10.4	MXene in rechargeable batteries	259
10.5	MXene in supercapattery	261
10.6	Conclusion	266
	References	267
11.	Aqueous solid and gel electrolytes for supercapattery	271
	Shahid Bashir, Mee Yoke Chong, Maryam Hina, Kashif Kamran, S. Ramesh and K. Ramesh	
11.1	Introduction	271
11.2	Polymer electrolytes	273
11.2.1	Ion conduction pattern in polymer electrolytes	274
11.2.2	Classification of polymer electrolytes	276
11.2.3	Classifications of solid polymer electrolytes	277
11.2.4	Methods to improve the performance of the solid polymer electrolyte	281
11.2.5	Gel polymer electrolytes	285
11.2.6	Hydrogel electrolytes	285
11.3	Conclusion and future challenges	302
	Acknowledgments	302
	References	303
12.	Applications of supercapattery	311
	Syam G. Krishnan, Arulraj Arunachalam and Priyanka Jagadish	
12.1	Introduction	311
12.2	Metal oxide/metal hydroxide–based supercabattery	312
12.2.1	CuO supercabattery	313
12.2.2	NiO supercabattery	318

12.2.3	Co ₃ O ₄ supercabattery	321
12.2.4	Cu(OH) ₂ supercabattery	325
12.2.5	Ni(OH) ₂ supercabattery	328
12.2.6	TMC supercabattery	330
12.3	Chalcogenides supercabatteries	334
12.4	Importance of supercabattery commercialization and applications	339
12.5	Conclusion	341
	References	342
13.	Supercapattery: technical challenges and future prospects	349
	M.N.M. Ansari and Noor Afeefah Nordin	
13.1	Introduction	349
13.2	Technical challenges	354
13.2.1	Pairing of electrode materials	355
13.2.2	Diffusion issues related to electronic property	356
13.2.3	Influence of redox electrolyte on performance of charge storage capacity	357
13.2.4	Inadequate properties that can contribute to the electrochemical performances	359
13.2.5	Insolubility and intractability of conducting polymers	361
13.3	Prospects	363
13.4	Market potential	367
13.5	Conclusion	372
	Acknowledgments	373
	References	373
	<i>Index</i>	379

List of contributors

Irfan Ahmed

State Key Laboratory of ASIC and System, Centre of Micro-Nano System, SIST, Fudan University, Shanghai, China; Department of Physics, Government Postgraduate College, Mansehra, (Higher Education Department-HED) Khyber Pakhtunkhwa, Pakistan

Omid Akbarzadeh

Nanotechnology & Catalysis Research Centre, University of Malaya, Kuala Lumpur, Malaysia

Muhammad Aftab Akram

Department of Materials Engineering, School of Chemical and Materials Engineering, National University of Sciences and Technology, Islamabad, Pakistan

Ghulam Ali

U.S.-Pakistan Center for Advanced Studies in Energy, National University of Sciences and Technology, H-12, Islamabad, Pakistan

M.N.M. Ansari

Institute of Power Engineering, Universiti Tenaga Nasional, Kajang, Malaysia

Mohammad Omaish Ansari

Center of Nanotechnology, King Abdulaziz University, Jeddah, Saudi Arabia

Arulraj Arunachalam

Graphene & Advanced 2D Materials Research Group (GAMRG), School of Science and Technology, Sunway University, Selangor, Malaysia

Shahid Bashir

Centre for Ionics University of Malaya, Department of Physics, Faculty of Science, University of Malaya, Kuala Lumpur, Malaysia

Mee Yoke Chong

Centre for American Education, INTI International University, Persiaran Bandar Baru Nilai, Malaysia

Zaira Zaman Chowdhury

Nanotechnology & Catalysis Research Centre, University of Malaya, Kuala Lumpur, Malaysia

Navaneethan Duraisamy

Department of Chemistry, J.K.K. Nataraja College of Arts and Science, TN, India

Subashini Gnanasekar

Centre for Nanotechnology Research, Vellore Institute of Technology (VIT), Vellore, India

Andrews Nirmala Grace

Centre for Nanotechnology Research, Vellore Institute of Technology (VIT), Vellore, India

Meenakshi Gusain

State Key Laboratory of ASIC and System, Centre of Micro-Nano System, SIST, Fudan University, Shanghai, China

Nor Aliya Hamizi

Nanotechnology & Catalysis Research Centre, University of Malaya, Kuala Lumpur, Malaysia

Mohammad Hatamvand

State Key Laboratory of ASIC and System, SIST, Fudan University, Shanghai, China

Maryam Hina

Centre for Ionics University of Malaya, Department of Physics, Faculty of Science, University of Malaya, Kuala Lumpur, Malaysia

Javed Iqbal

Department of Chemistry, Faculty of Science, University of Malaya, Kuala Lumpur, Malaysia; Center of Nanotechnology, King Abdulaziz University, Jeddah, Saudi Arabia

Muhammad Zahir Iqbal

Faculty of Engineering Sciences, GIK Institute of Engineering Sciences and Technology, Topi, Pakistan; Nanotechnology Research Laboratory, Faculty of Engineering Sciences, GIK Institute of Engineering Sciences and Technology, Topi, Pakistan

Mohammad Islam

Center of Excellence for Research in Engineering Materials, Deanship of Scientific Research, King Saud University, Riyadh, Saudi Arabia

Rashida Jafer

Department of Physics, Faculty of Science, King Abdulaziz University, Jeddah, Saudi Arabia

Priyanka Jagadish

Graphene & Advanced 2D Materials Research Group (GAMRG), School of Science and Technology, Sunway University, Selangor, Malaysia

Faiza Jan Iftikhar

NUTECH School of Applied Sciences and Humanities, National University of Technology, Islamabad, Pakistan

Sofia Javed

Department of Materials Engineering, School of Chemical and Materials Engineering, National University of Sciences and Technology, Islamabad, Pakistan

Asim Jilani

Center of Nanotechnology, King Abdulaziz University, Jeddah, Saudi Arabia

Mohd Rafie Johan

Nanotechnology & Catalysis Research Centre, University of Malaya, Kuala Lumpur, Malaysia

Kashif Kamran

Department of Physics, University of Agriculture, Faisalabad, Pakistan

Mohammad Khalid

Graphene & Advanced 2D Materials Research Group (GAMRG), School of Science and Technology, Sunway University, Selangor, Malaysia

Abbas Khan

Nanotechnology Research Laboratory, Faculty of Engineering Sciences, GIK Institute of Engineering Sciences and Technology, Topi, Pakistan

Syam G. Krishnan

Graphene & Advanced 2D Materials Research Group (GAMRG), School of Science and Technology, Sunway University, Selangor, Malaysia

A.R. Marlinda

Nanotechnology & Catalysis Research Centre, University of Malaya, Kuala Lumpur, Malaysia

Faruq Mohammad

Department of Chemistry, College of Science, King Saud University, Riyadh, Kingdom of Saudi Arabia

Sharifah Mohammad

Department of Chemistry, Faculty of Science, University of Malaya, Kuala Lumpur, Malaysia

Noor Afeefah Nordin

Institute of Power Engineering, Universiti Tenaga Nasional, Kajang, Malaysia

Arshid Numan

State Key Laboratory of ASIC and System, SIST, Fudan University, Shanghai, China; Graphene & Advanced 2D Materials Research Group (GAMRG), School of Science and Technology, Sunway University, Selangor, Malaysia

Karuppasamy Pandian

Quantum Nano-Optoelectronics Group, The Institute of Photonic Sciences, Castelldefels (Barcelona), Spain

Jiban Podder

Department of Physics, Bangladesh University of Engineering and Technology, Dhaka, Bangladesh

Ananthakumar Ramadoss

School for Advanced Research in Polymers: Laboratory for Advanced Research in Polymeric Materials, Central Institute of Plastics Engineering and Technology, Bhubaneswar, India

K. Ramesh

Centre for Ionics University of Malaya, Department of Physics, Faculty of Science, University of Malaya, Kuala Lumpur, Malaysia

S. Ramesh

Centre for Ionics University of Malaya, Department of Physics, Faculty of Science, University of Malaya, Kuala Lumpur, Malaysia

Suresh Sagadevan

Nanotechnology & Catalysis Research Centre, University of Malaya, Kuala Lumpur, Malaysia

Sarbani Sahu

School for Advanced Research in Polymers: Laboratory for Advanced Research in Polymeric Materials, Central Institute of Plastics Engineering and Technology, Bhubaneswar, India

Lukas Schmidt-Mende

Department of Physics, University of Konstanz, Konstanz, Germany

M.M. Shahid

Center of Micro-Nano System, School of Information Science and Technology, Fudan University, Shanghai, P.R. China

Aruni Shajkumar

School for Advanced Research in Polymers: Laboratory for Advanced Research in Polymeric Materials, Central Institute of Plastics Engineering and Technology, Bhubaneswar, India

Muhammad Usman

Department of Materials Engineering, School of Chemical and Materials Engineering, National University of Sciences and Technology, Islamabad, Pakistan

Sandhya Venkateshalu

Centre for Nanotechnology Research, Vellore Institute of Technology (VIT), Vellore, India

Yasmin Binti Abdul Wahab

Nanotechnology & Catalysis Research Centre, University of Malaya, Kuala Lumpur, Malaysia

Yiqiang Zhan

State Key Laboratory of ASIC and System, Centre of Micro-Nano System, SIST, Fudan University, Shanghai, China; State Key Laboratory of ASIC and System, SIST, Fudan University, Shanghai, China

Preface

Since the beginning of the 20th century, global energy demand has rapidly increased because of population and economic growth. Additionally, rapid industrialization and the quest for smart technologies require more energy resources than ever. As a result, fossil fuel consumption has increased tremendously, leading to its rapid depletion, creating new energy security challenges and causing environmental issues and global warming. The growing demand for energy and the scarcity of conventional energy resources has catalyzed research toward alternative energy resources and energy storage devices. The energy storage through electrochemical methods has been recognized as one of the most important inventions among all the energy storage and conversion technologies.

There are two major kinds of energy storage devices, namely supercapacitors and batteries. The former has the distinctive advantages of high-power density and rapid energy storage capability, but suffers from low energy density compared to batteries. Conversely, batteries have high energy but low power density, which limits their application where power surges are required. The advantages of both devices can be harvested in a single device by fabricating the hybrid device (supercapattery) using a single electrode from each device (battery and capacitor). A supercapattery can deliver high energy density and high-power density compared to a supercapacitor and battery, and thus it can cover a wide range of applications.

This book is focused on the fundamentals of supercapattery from a technical and practical point of view. There are misleading concepts that are associated with pseudocapacitive materials. Many research articles have critically highlighted this issue by signifying the difference between pseudocapacitive and battery-grade materials. This book will explain the energy storage mechanism of both materials (pseudocapacitive and battery grade) based on the fundamental concepts of physics and electrochemistry. The main driver of this book is to describe the innovative electrode materials to enable new devices and improve existing device designs for energy storage, especially supercapattery. The book will help to illuminate practical aspects of understanding and applying the technology in the industry and providing enough technical details about new materials developed by experts in the field that may surface in the future. Furthermore, the

technical challenges are also discussed in this book to give readers an understanding of the practical limitations and their associated parameters in electrochemical energy storage technology.

This book is equally beneficial for research scientists, engineers, graduate and undergraduate students wanting to specialize in energy storage systems. It provides the latest developments and fundamentals of energy storage mechanism and clarifies the misleading concepts in this field. Additionally, this book will also cover the potential of the supercapattery in industry and how it can bridge the gap between the traditional capacitor and a battery.

Introduction

Advances in Supercapacitor and Supercapattery: An Innovation In Energy Storage Devices provides an in-depth overview of the present status of the rapidly growing field of electrochemical energy storage systems. This book will cover the fundamentals, the latest developments, and innovative materials used for the hybrid electrochemical energy storage systems as well as their potential for the latest technological energy storage applications. Currently, the literature available to boost the performance of supercapacitors is scattered. Moreover, there are some misperceptions between the concepts for the pseudocapacitive and battery grade materials. This book comprehensively covers the synthesis strategies to enhance the overall performance of the supercapacitor device. The misleading concepts will be explained in detail based on electrochemical reactions and their corresponding electrochemical signatures.

The first two chapters cover the detailed background, the fundamentals of the charge storage mechanism, and different supercapacitor types. The third chapter presents the hybrid device (supercapattery), comprising a battery and capacitive electrode. The main advantages of supercapattery over batteries and supercapacitors are covered in this chapter. The following seven chapters cover innovative nanomaterials, such as carbonaceous materials, conducting polymers, metal oxides and hydroxides, and the latest 2D material (MXene), as electrodes for energy storage applications. The electrolyte is a crucial part of an energy storage device that significantly contributes to its performance. Therefore different kinds of electrolytes and their suitability are discussed in Chapter 11. The book concludes with a discussion on the potential applications, challenges, and perspectives of supercapattery in Chapters 12 and 13.



Background of energy storage

Suresh Sagadevan¹, Mohd Rafie Johan¹, A.R. Marlinda¹,
Omid Akbarzadeh¹, Karuppasamy Pandian², M.M. Shahid³,
Faruq Mohammad⁴ and Jiban Podder⁵

¹Nanotechnology & Catalysis Research Centre, University of Malaya, Kuala Lumpur, Malaysia

²Quantum Nano-Optoelectronics Group, The Institute of Photonic Sciences, Castelldefels (Barcelona), Spain

³Center of Micro-Nano System, School of Information Science and Technology, Fudan University, Shanghai, P.R. China

⁴Department of Chemistry, College of Science, King Saud University, Riyadh, Kingdom of Saudi Arabia

⁵Department of Physics, Bangladesh University of Engineering and Technology, Dhaka, Bangladesh



1.1 Introduction

Currently used, conventional power generation and distribution infrastructure require an extremely sensitive, low-error margin, and a near-instant equilibrium between electricity supply and demand on the electrical grid system. To achieve equilibrium, thousands of turbines around the globe need to be immediately brought online or taken off to meet the variability in demand for electricity. Most of these turbines usually remain idle most of the time resulting in a loss of ability for generation. Also, because of the absence of adequate storage capability, the energy produced by these sources during off-peak times is often lost. The fundamental assumption of energy storage includes transforming one type of energy into another type that can efficiently, cost-effectively, and reliably produce the stored energy when required. Electrical energy storage techniques and systems demonstrate an equally wide variety in a way comparable to the broad variety of power generation techniques. Each offers a separate set of benefits, but also disadvantages, difficulties, and weaknesses. Since there is no single winning power generation technology capable of meeting the broad variety of demands including environmental, price, efficiency, accessibility, client request, portability, scalability, etc., there is no single bullet to tackle our impending electrical energy storage needs as well. Therefore it is best to create a multipronged portfolio approach to create a variety of storage techniques and systems. Each

one provides its strengths and weaknesses and distinct technological bases governing its working theory.

Global excitement, momentum, and huge investments as one of the main sources of energy production are essential to pave the way for decarbonization of today's fossil-fuel energy economy, particularly electricity generation. Nevertheless, most renewable energy sources are a significant obstacle to the efficient generation of electricity and global mass use. As is currently the case, the distribution of renewable sources offers a substantial benefit in reducing the financial and environmental impacts of centralized transmission. In poor and underdeveloped parts of the globe, where large communities often lack electricity and other resources for their daily tasks, renewables are also important. In this respect, in many of these societies, renewables can boost economic growth and significantly enhance the quality of life.

To create a sustainable energy infrastructure to address the energy and environmental problems produced by carbon fuels, the new energy revolution is shaping electricity as the main energy source. It is determined by the large-scale development and use of renewable energy. With the expansion of the smart grid, innovation and government policies the opportunities of power storage are slowly emerging [1–4]. The potential use throughout the spectrum of power systems, including generation, transmission, delivery, and consumption, could be explored. The objectives include the increased adoption of large-scale renewable electricity, improved electricity grid capacity, postponement and reduction of the cost of output and power systems development, enhancement of electricity quality and efficiency, ensuring a high level of safe, viable supply of energy, promoting the best possible control of grids and the operating schedule [5–9]. The design of potential applications will have a major effect on the energy storage industry by designing and promoting energy storage technologies [10]. Both engineering and academic study have grown rapidly in the latest years, leading to many accomplishments. The research and demonstration of energy storage have been extended by the rapid growth of energy storage technologies from small to large scale.

However, energy storage demands vary extensively, driven mainly by the application type. No single technology meets all large-scale grid performance storage demands and metrics. For some applications, a particular technology may give characteristics and merits, but not for others. Electrochemical techniques such as Na-S and Li-ion batteries have become commercially feasible in some industries, even though they do

not meet all the necessary metrics. Considering an appropriate combination of distinct storage technologies, such deficiencies can be alleviated to meet the specific demands of a specific implementation. Considering an appropriate mix of distinct storage technologies, such deficiencies can be alleviated to meet the specific demands of a specific implementation. Instead, this chapter distinguishes itself by taking a broad brush and presenting an in-depth overview of a wide range of techniques, equipment, and systems for storing electrical energy with an eye for large-scale storage of electrical grids. Furthermore, the chapter describes an extensive debate of the status of four main classes of electricity storage techniques including electrochemical, chemical, mechanical, and thermal storage systems covering a broad variety of alternatives from pumped hydro and flywheels to hydrogen and ammonia, to supercapacitors, batteries, regenerative fuel cells, flow batteries, and storage of phase-changing products. Where necessary, the chapter also provides the interested reader with tutorial data to obtain a greater understanding and recognition of the basic factors and difficulties in storing electrical energy. This evaluation is intended to help noninitiated scientists and engineers who have invested in electrical energy storage systems. Fig. 1.1 displays a standard electrical demand profile. The primary power generator could work during the night when a low-cost

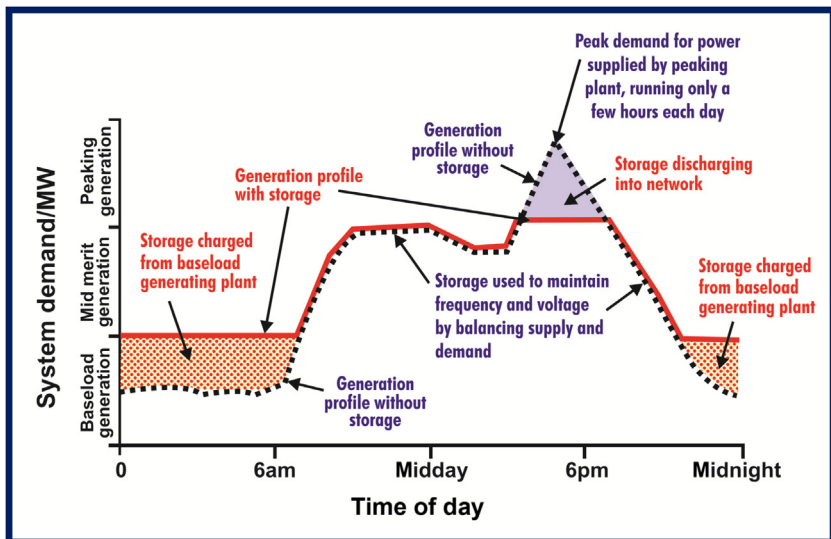


Figure 1.1 A typical electrical power profile, showing the large variations during a 24-h period.

power storage facility was available, and the storage systems could be supplied with energy during peak demand hours to remove the need for power stations alone.



1.2 Importance of energy storage

Energy storage makes a critical contribution to the energy security of current energy networks. Today, much energy is stored in the form of raw or refined hydrocarbons, whether as coal heaps or oil and gas reserves. Since energy storage is far more efficient, power precursors are stored instead of electricity, and demand for generation varies. The only exception is a pumped hydroelectric plant, which can provide a great energy output for a short period and tends to improve electric system reliability at very short notice. When energy systems increasingly evolve to use low-carbon technology, the purpose and form of energy storage are likely to change considerably. Perhaps two broad trends will push this move. Firstly, with intermittent nuclear power and fixed production playing an ever-growing role, the supply of electricity will become increasingly difficult to match with demand, whereas imbalances will expand and dominate over time. Moving away from fossil production means that most power suppliers, except flexible gas generation, can no longer be stored as hydrocarbons. Furthermore, the structure of the demand for electricity will change significantly if low-carbon power displaces the oil and gas for transport and heat supply, where there is the highest demand. In developing energy storage technologies, electricity is stored at times of surplus energy supply to meet demand. For example, other storage techniques could in other areas support the energy system by storing surplus electricity such as heat or hydrogen for use in other industries. The way energy storage is used will only cause a revolution in going toward a low-carbon society. The correlation of multisystem storage capability has been shown clearly in Fig. 1.2. Condenser energy is typical of poor quality, that is, the supplied voltage is a powerful function of the discharge state, while the output capacity of the batteries is relatively stable. Fuel cells with liquid fuels, for example, methanol, allow a high storage of energy, but their power output is limited. Li-oxygen batteries can also have high energy density but have low power. Therefore their performance is optimum

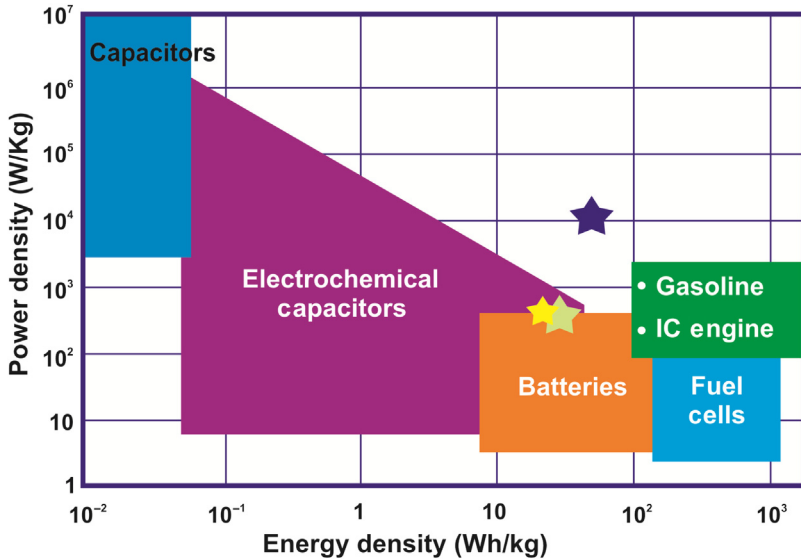


Figure 1.2 Comparison of the power versus energy density characteristics of different storage media.

only in continuous output and their lack of response time involves the combination of a storage medium like batteries. No storage medium, as shown in Fig. 1.2 exceeds the efficiency of oil production.



1.3 Batteries and capacitors

Electric power storage has two primary types: the battery and the condenser. Like chemical energy in a battery, electric energy is stored, while electricity is stored in condensers as a surface charge. Chemical reactions occur in the whole solid bulk of the battery, so that the reacting species may join the product and be expelled thereafter. It needs to be done tens of times to provide a commercially feasible rechargeable battery. Nevertheless, large quantities of the surface area are used for a condenser, and the storage capacity is directly connected to the surface area. As no question is raised as to the structural integrity of a condensing component, pure condensers can, without substantial product loss, be loaded and discharged several million times, whereas battery chemical reactions cannot always reverse due to structural material modifications. The

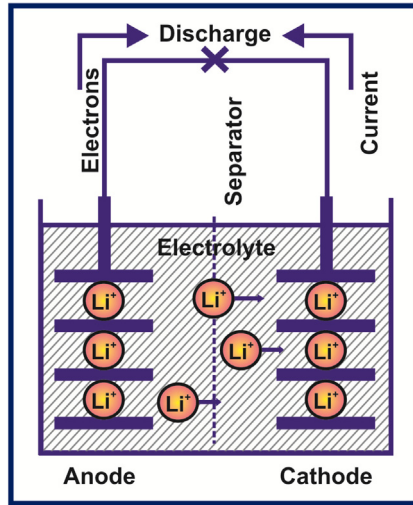


Figure 1.3 Schematic of a battery.

supercapacitors are a hybrid between the two, with both ground load and certain faradic reactions. Batteries and supercapacitors contain two electrodes, the anode, and the cathode, as shown schematically in Fig. 1.3. The cathode is the electrode to which electrons flow through the operating circuit. The anode is the electrode from which electrons flow through the functioning external circuit. Cations usually flow from anode to cathode through the electrolyte of the battery to balance the electron stream. The single-ion and not electrons escape from such a liquid or solid electrolyte. In the case of common dry cells of Zn/MnO₂, it is sulfuric acid, in the battery of Pb-acid and potassium hydroxide in water, this solution is usually aqueous. A porous separator is placed between the two electrodes to ensure that the two do not contact each other. Whether the device is packed or unloaded, the more electropositive electrode in the charged state as the anode is typically in the battery/capacitor region.



1.4 Fundamentals of energy storage

The first thermodynamic law states that the total energy is fixed in a closed system and that energy cannot be produced or destroyed. Only from one type to another can it be transformed. This basic idea serves as

the basis for the transformation and storage of almost all types of energy. The majority of storage techniques therefore come under four broad categories: mechanical energy storage, chemical energy stockpiling, electrochemical energy stockpiling, and electric energy storage. The maximum amount of electrical work that can be extracted from a storage system is given by,

$$G = H - TS \quad (1.1)$$

Here, G is Gibbs free energy, H is enthalpy, T is temperature, and S is entropy. In other words, G represents the maximum energy available to do either mechanical or electrical work. Mechanical energy storage, such as pumped hydro, manifests itself by potential, E_{pot} , and/or kinetic, E_{kin} , energies that can be represented by,

$$E_{pot} = fd \quad (1.2)$$

$$E_{kin} = (1/2)mv^2 \quad (1.3)$$

Here, f denotes force, d is distance, m is mass, and v denotes velocity. For a rotating body such as a flywheel or a wind turbine, the kinetic energy is described in a similar expression by,

$$E_{kin} = (1/2)I\omega^2 \quad (1.4)$$

where I denotes the moment of inertia and ω is the angular velocity of the rotating system. In other words, stored energy increases with the system's inertia and the square of its angular velocity. The moment of inertia for a body of mass (m), radius (r), length (l), and density (ρ) can be given by

$$I = (1/2)mr^2, \text{ or } = (1/2)\rho l\pi r^4 \quad (1.5)$$

Accordingly, high-density materials with a large radius help store more energy. For mechanical energy storage in flywheels, [Eq. \(1.5\)](#) can also be expressed as

$$E_{kin} = \frac{\sigma_m s}{\rho} \quad (1.6)$$

Here, σ_m denotes maximum stress, s is a shape factor, and ρ is material density. For modern flywheels made from reinforced high-strength carbon fibers, it is possible to achieve storage capacities greater than 200 kJ per kilogram of flywheel mass. Compressed air storage in salt caverns or

underground aquifers relies on the gas law ($PV = nRT$), and the available work, w , is given by PdV integrated over the incremental volume change (dV).

Thermal storage relies on the amount of heat, q , one can store in a medium or material of defined volume (V) materials density, ρ , and specific heat (C_p), resulting in a temperature rise of ΔT . This can be expressed by,

$$q = \rho C_p V \Delta T \quad (1.7)$$

In the case of a phase transition in the thermal energy processing medium or matter, the total energy retained must take account of the latent heat associated with that transformation. Chemical storage relies on the energy storage of the chemical bonds of fuels which are intrinsically solid and therefore provide very broad densities of energy. Nonetheless, electric or thermal power usually needs to be used to manufacture chemicals. Electrochemical processing systems are based on the containment of electrical condensers and supercapacitors or the chemical bonds of fuel cells in cases of electrical batteries or electrochemical interfaces. The intrinsic high efficiency of electrical energy processing is characterized by the ratios of ($\Delta G/\Delta H$). Electrochemical energy storage provides high efficiencies. Finally, the electric and magnetic power storage can also be carried out.



1.5 Electrochemical energy storage systems and materials

The basic working theory of electrochemical and photoelectrochemical processes (photovoltaic system) covers three important process steps: charging separation (or ionization), charged species transport, and charging recombination. This basic concept controls the function of a broad spectrum of devices including photochemical and photovoltaic structures, batteries, fuel cells, supercapacitors, and electrolytes. Their working theories, however, require different systems in which interfaces play a crucial role. As batteries hold charges in the electrodes, for example, fuel cells and battery charge flows are contained in the gas, which is pumped to the surface of the electrode externally. Supercapacitors charge either on the electrode/electrolyte interface in the double-layer electric or

as opt-outs of redox-surface responses. Some of them work at ambient or room temperatures, such as PEMFC, supercapacitors, and batteries while others require high temperatures like sodium or molten carbonate and solid oxide fuel cells. In other words, product requirements for each electrochemical storage system are different and many are analyzed in depth elsewhere [11–18]. A new review article has presented a description of the basic and operating concepts of batteries, fuel cells, and supercapacitors [19]. The fundamental principle behind electrochemical energy storage is the reciprocity between converting the chemical energy stored in fuel bonds into electricity and using electric power, by synthesizing chemicals or fuels in the opposite direction. The driving force for this conversion is the Gibbs free energy change (ΔG) of the electrically neutral species at the electrodes participating in the chemical reaction,

$$A + B = C \quad \Delta G(\text{kJ/mole}) \quad (1.8)$$

This free change in energy is the same if reactants A and B are to be subjected to a purely chemical reaction, as in Eq. (1.8), or an electrochemical reaction involving the transmission of ions and electrons through the cell. As these species are electrically charged, the electrostatic energy transported across by a mole of such species is given by zEF , where F is Faraday's constant, z is the charge number of the transporting species, and E is the cell voltage. Under open-circuit conditions, the cell voltage is related to the Gibbs free energy change by,

$$\Delta G = -zEF \quad (1.9)$$

In other words, the chemical potential distinction between neutral species at the electrodes describes the fundamental force driving an electrochemical cell to form an electrically neutral product, C , through a chemical reaction between electrically neutral reactants, A and B . The systems contain fundamental elements for electrical processing that have a vital role, including two dedicated electrode bodies separated by an ionically conducting yet electronically segregated “electrolyte.” Electrodes with excellent electronic conductivity, excellent stability, and high catalytic activity are preferably selected from abundant and economic materials. A conversion and storage system, whether a battery, a fuel cell, or an electrochemical capacitor, is schematically illustrated in Fig. 1.4, which shows the storage of electrical energy in the form of chemical energy, and the conversion of chemical reacting energy. Fig. 1.4A shows an electrolytic cell which is used for the production of fuel B using internal energy

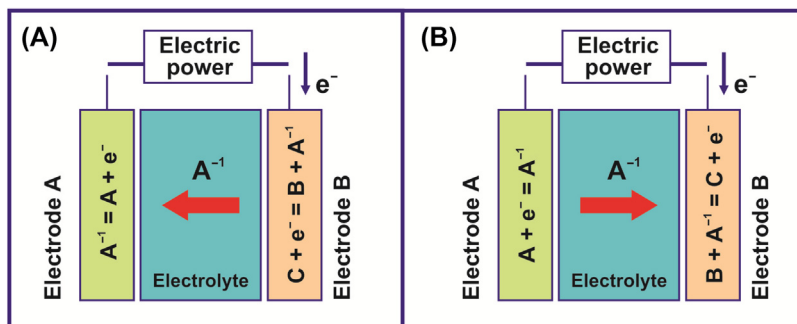


Figure 1.4 Basic operating principle of electrochemical energy storage, illustrating (A) electrical energy to chemical energy conversion, and (B) chemical energy back to electrical conversion for reaction $A + B = C$.

(i.e., storage). Fig. 1.4B demonstrates an electricity fuel cell using fuel B and oxidant A (i.e., electricity generation mode). Chemical energy storage is addressed, although regenerative solid oxide combustible fuel cells offer the opportunity to work bidirectionally. It is worth noting that batteries, electric condensers, and supercapacitors combine specific energy and specific power with chemistry and choice of battery materials. Nevertheless, energy efficiency is determined by fuel choice, and is related to the kinetic and transport features of cellular materials. Such decoupling provides tremendous benefits for many uses. The electrical storage device volumetric densities are also significant. Volume is particularly important for travel, storage, and mobile apps. The focus is on whether Li-ion batteries or fuel cells can ultimately overtake mobile applications, and specifically which transport market will be operated [20].

1.6 Status of energy storage technology development

Energy storage technologies can be classified into five main energy storage categories: mechanical storage of power, heat energy storage, electrical processing, magnetic energy storage, and chemical energy storage [21]. These vary between physical and chemical as well as electromagnetic technology such as hydrogen energy storage. Each technology has its own specific features and suitability for various applications. The world's energy

stock technology until 2016 consisted overwhelmingly of pumped hydro storage (Fig. 1.5).

Growth in pumped hydro has slowed since 2015, with an annual rise of only 1.8%. In terms of cumulative worldwide capability, molten salt heat energy storage takes second place. Electrochemical energy storage capability comes in third, having experienced the highest development with a complete capability of 1769.9 MW, up 56% from the prior year. Lithium-ion power storage has the biggest installed capability worldwide among electrochemical power storage systems, accounting for 65% of capacity. Since 2015 this figure has risen by 89%. A schematic representation of energy storage technologies is shown in Fig. 1.6.

1.6.1 Mechanical energy storage

Mechanical technology for energy storage primarily involves the storage of pumped gas, storage of compressed air, and flywheel control. The most mature technology is pumped storage, which is characterized by high ability, lengthy service life, and low unit cost. However, geographical circumstances restrict the development of the pumped storage power station, the building period is longer, and the general investment is big. The benefits of compressed air energy storage are big capacity, lengthy operating time, lengthy service life, etc. And it can also supply combined heat, cold, and electricity by turning the compressed air into alternative energy. Even though its effectiveness is small, the system is complicated, and the air storage mine tunnel location requirement is high [22,23]. The flywheel energy storage has the benefits of high effectiveness, quick reaction, lengthy service life, lower operating and maintenance requirements,

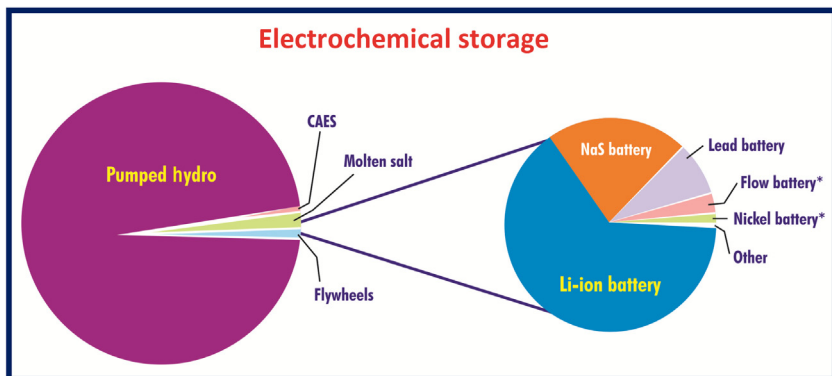


Figure 1.5 Global energy storage capacity by technology.

	Technologies	Characteristics
Physical storage	Pumped hydro compressed air (supercritical CAES) flywheel	Uses water/air as storage medium No chemical change Mechanical-electric energy
Chemical storage	Lead-acid battery Li-ion battery Flow battery (Vanadium, Zn-Br) Na-S battery	Uses chemicals as storage medium Battery charges/discharges with chemical change/valence change
E&M storage	Supercapacitor	Fast response, can release large amounts electric power in short times, high number of cycles
Other storage	Fuel cell* Metal-air battery*	Does not possess "charging" characteristics

Figure 1.6 Energy storage technologies.

excellent stability, brief building time, low footprint, and no pollution, but the energy density is low and it is easy for it to self-discharge which is only appropriate for short-term applications [24,25].

1.6.1.1 Pumped hydro storage

Pumped hydro storage is currently the most advanced type of storage technology, accounting for about 95% of worldwide energy storage capacity. Most frequently, water kept at distinct heights in two reservoirs is pumped against gravity, stored, and then released to run through an electricity-generating turbine. More traditional open-loop systems are linked to a natural water structure that either refill the upper or lower reservoir. The primary disadvantages include geographical constraints as well as effects on aquatic life and flows. Many latest design ideas and demonstration projects favour closed-loop schemes separate from naturally flowing water to solve these difficulties, including subterranean structures with a lower footprint and environmental concerns. Current pumped hydro projects can serve many tasks to deliver energy balance, reserve power, and stabilization features to the electricity grid. Modified pumped hydro installations with variable-speed turbines are best suited for renewable generation and frequency regulatory services.

1.6.1.2 Compressed air energy storage

Compressed air energy storage (CAES) utilizes compressed air expansion to drive a turbine and generate electricity. The world presently operates relatively few projects but reported capital and operating costs can be competitive to pumped hydro. The heat produced during air compression is lost in adiabatic setups, requiring fresh heat to be produced during an expansion (often through natural gas burning). Instead, adiabatic systems store the heat in a heat sink to reinject the round-trip effectiveness during development. During compression, heat is continually stored in an isothermal setup and reintroduced continually in expansion to mimic isothermal circumstances and boost effectiveness. Because of the low storage density, how to store the compressed air is a significant factor in CAES schemes. To date, subterranean CAES has been mostly implemented in subterranean salt caverns of steady quantity, introducing geographical constraints, of course. Another alternative is the emptied natural gas wells and abandoned mines. Some projects also used the piping system above ground to store compressed air, presenting a rise in price but providing more flexibility on site. With a variable volume vessel, Hydrostor, air can also be stored under constant pressure by building an underwater cavern with a changing volume of water to keep the air at constant pressure. As the pumping machinery operates optimally under continuous stress, isobaric systems can attain even higher efficiencies.

1.6.1.3 Flywheel storage

Flywheels use the fine energy of a rotating mass, which is often stored in a vacuum in a magnetic coil, to discharge the rotational frequency by slowing down, to generate energy through a motor. The material used for the rotating mass has a huge impact on the price, weight, and quality of steel or carbon composite steel. Rapid response velocity and durability are key benefits of flywheels compared to battery devices. On a scale of seconds, flywheels can charge/discharge and most devices can complete 170,000 discharge cycles. For an extended discharge period, several flywheel units can be incorporated together. Besides, they are ideal for high-power low-energy applications, such as an average asset, and a slower generation to ensure the accuracy of power and frequency responses. [Fig. 1.7](#) plots select techniques for energy storage with a rated power and discharge moment. Flywheels are one of the resources that are fastest to respond.

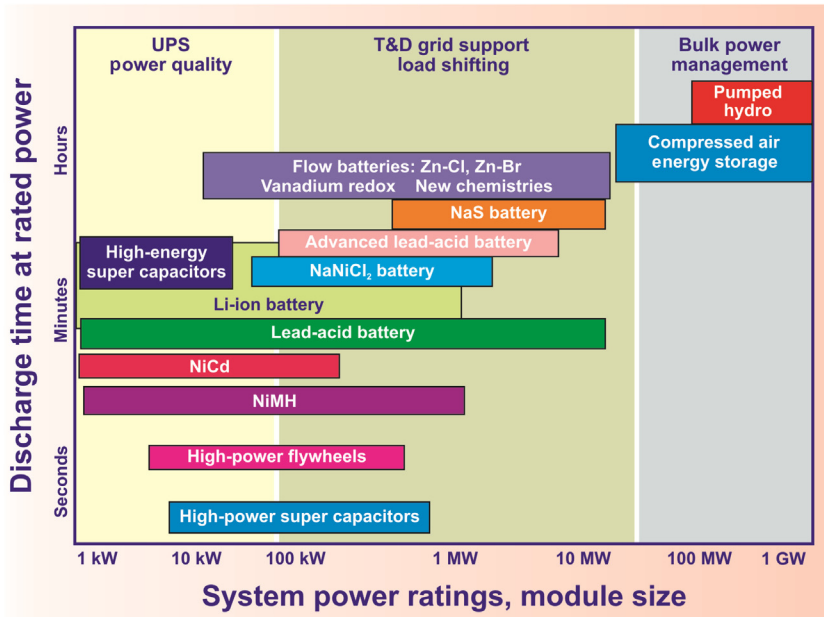


Figure 1.7 Energy storage rated power and discharge time across technology types.

1.6.1.4 Flow battery

In a flow battery, the energy is stored in the electrolyte solution. The chemical energy is converted to the electric energy when the electrolytes flow through the external tanks. The volume of the electrolyte and the surface area of the electrode influence the performance of the flow battery. Flow batteries can be employed both as a rechargeable secondary battery and a fuel cell. The earlier loaded electrolyte will be the alternative for the discharged electrolyte and thus it has the synergic significance. There are different types of flow batteries and they are the following: redox flow batteries, hybrid flow batteries, and fewer batteries for membrane. The costlier one is the membrane flow battery and their battery parts are very brittle and can be easily corroded by the reactants of the operation. The membrane flow battery uses laminar flow which paves the way for the electrodes to move sides without mixing, and also without the help of a membrane. Thus the membrane flow battery has a high energy density. The large-scale industries of energy storage use flow batteries as they are very long-lasting and have a higher power density than the Li-ion battery. One of the disadvantages of this type of battery is that it has a lower energy density compared to the Li-ion battery and it is not

suitable for portable energy storage device applications. The traditional flow battery configuration with a membrane is depicted in Fig. 1.8.

1.6.1.5 Na-S battery

Molten sulfur and molten sodium are used as the electrode materials for the sodium-sulfur batteries. This kind of battery operates at higher temperatures ranging from 300°C to 350°C. An internal machine is employed for heating purposes to provide the required active temperatures in the system. The electrodes are separated by a ceramic layer. Na-S batteries are extremely effective, with general effectiveness of nearly 90% and are made from low-cost components. However, owing to the extreme sodium reactivity when subjected to air and moisture, they present some safety danger. Na-S batteries are produced with the majority of projects situated in Japan and the United States in cylindrical and block-shaped settings. They are highly suitable and recommended for high power and long discharge applications.

1.6.2 Heat storage

The heat storage is classified into two types, namely, sensible and latent heat storage. The water is used as the medium for the storage of heat and by enhancing the temperature of the heat storage material, the objective

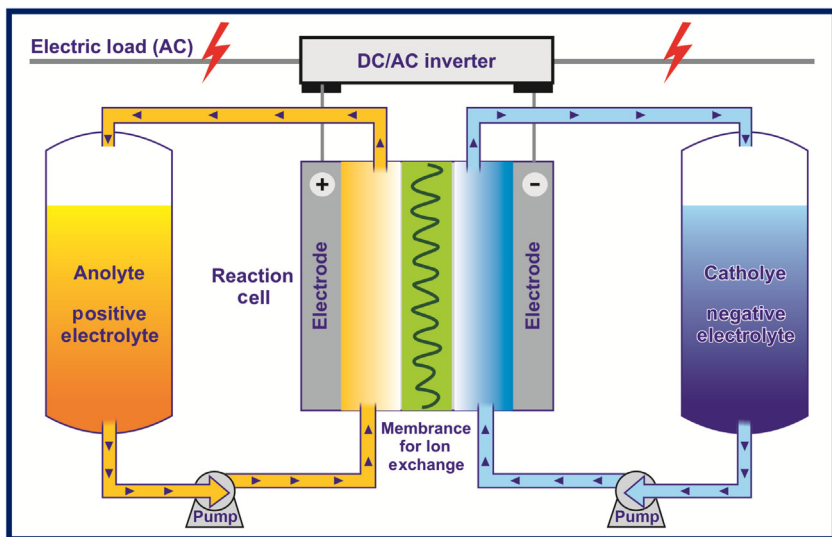


Figure 1.8 Traditional flow battery configuration with a membrane.

of the sensible material can be finished. Solar and thermal power plants employ the latent heat storage type which employs regenerative materials for operation. The required heat and the electricity generation is achieved by the photothermal system. For instance, in the winter season, a solar-only system is not suitable. Hence, the thermal (heat) comes into the picture [26,27]. The heat storage system's power storage effectiveness can reach 95%–97% [28], and the price of storing large batteries is only about 1/30. Molten salt storage technology is presently being introduced to the concentrated solar thermal power plant as a study hotspot. Some of the significant advantages are economic, the higher production of heat, and it is safe and secure. These kinds of systems are commercially available in Europe and North America. However, the issues are still very prominent in its practical implementation, in which one of its shortcomings is the corrosive nature. Additionally, the temperature of the molten salt solidification is high and it is simple to scrap machinery.

1.6.3 Electrochemical energy storage

There are different systems (devices) for electrical energy storage such as lead-acid batteries, lithium-ion batteries, sodium-sulfur batteries, redox flow batteries. Some of the significances of the conventional batteries are that they were economical and easy to handle, but they have limitations like their reduced capacitances and higher discharge of the power, lower energy density, and shorter life cycle, and they contributed to the pollution [29,30]. In recent years, Japan, the United States, and other nations have been dedicated to developing more sophisticated lead-acid batteries, and several kinds of batteries have been created including lead-carbon batteries, super batteries, etc. Some the lithium-based batteries are lithium-iron-phosphate batteries (Li-Fe-P), titanium-lithium batteries (Li-Ti), lithium-nickel-manganese-cobalt (Li-NMC) batteries and they are employed in the power industries. The significance of Li-Fe-P is enhanced stability and life cycle; Li-Ti is more economical, with secured safety, expanded life cycle, and satisfactory charge and discharge process. The higher energy density and the power density is attributed to the Li-NMC batteries. Some of the limitations of Li-NMC batteries are that they are costly and the availability of the cobalt salt is low. There are two types of redox flow batteries currently in research, which are vanadium and bromine-zinc redox flow battery. The vanadium redox flow battery has a long life and long cycle, but low energy and power density, and a

slow reaction. The flow battery of zinc-bromine has high energies, low prices, and regular deep discharges, but also a higher rate of self-discharge induced by a complicated electrode reaction. The sodium battery has the advantages of high energy density, outstanding performance, long life, etc. At the MW stage, it has become a well-developed, commercially operated, electrochemical energy storage technology. It utilizes the flammable metal sodium, however, and works under circumstances of elevated heat (300°C – 350°C), which presents a security risk.

1.6.4 Electromagnetic energy storage

Electromagnetic storage systems are made up of ultracapacitors that store energy in an electrical field. The advantages of ultracapacitors are that they have much faster than electrochemical battery-storage discharges and charges than battery-driven power densities, without relying on chemical reactions. They can also endure one million loading and discharge cycles and work with an output of approximately 100%. Lower and lighter than batteries are used with ultracapacitors and no toxic chemicals or metals are needed. Ultracapacitors are not suitable for long-term uses, but are more suitable for extremely short energy bursts. For various uses in electric vehicles, ultrasensors can also be used to permit renewables through firming power generation, and recent research has also been carried out to provide wind turbines with the power they need to adjust their pitch or angle to help harness wind energy. Ultracapacitors are expected to provide short-term power before battery system joins, and can be quickly recharged by the additional energy supply as a holding gear hybrid of longer-lasting battery schemes. The electromagnetic energy processing involves mainly supercapacitor and superconductive magnet energy storage. The supercapacitor has the benefits of the high density of energy, quick reaction, high effectiveness, lengthy cycle life, low maintenance, a wide variety of operating temperatures, etc. The supercapacitor, however, is appropriate for use in conjunction with other energy storage techniques because of the low power density [31,32]. The charge/discharge speed of superconductive magnetic energy storage is critical, with advantages of high power density and fast response, great efficiency in energy conversion, long lifetime, etc. It is suitable for high energy requirements. However, a high cost, low energy density, and complicated maintenance has many drawbacks [33].

1.6.5 Chemical energy storage

Chemical energy storage is secondary hydrogen or synthetic gas fuel carrier that electrolyzes hydrogen and can also be synthesized into natural gas (i.e., methane) with carbon dioxide. This green technology could lead to large-scale storage of more than 100 GWh of energy without any pollution. The conversion efficiency issue, however, is just 40%–50%, and there is a high cost requiring a big investment, and also low security. Hydrogen energy storage technologies have also been demonstrated in many countries [34]. The fuel cell is the primary method of using hydrogen. The fuel cell of the proton exchange membrane (PEM) is widely used as a backup energy source and increases the use of renewable energy in the electrical, thermal, transport, and other sectors. Today, the primary objective of the introduction of renewable energy and hydrogen as the main energy method is to increase cost, efficacy, and life span.

1.6.6 Other storage

For this study, technologies categorized as “other technologies” include fuel cells and metal-air batteries. Fuel cells, such as batteries, undergo an electrochemical reaction to supply energy, but vary in that electricity is produced through a source of hydrogen-containing fuel that reacts with oxygen, generally provided from the air. Fuel cells can provide energy output continually as long as they have both fuel and an air supply, and therefore do not fit in the traditional mold of charging and recharging cycles of the battery. Metal-air batteries are also a promising technology with a cathode-like anode made of metal and air (oxygen). Different metals are being investigated now, as this technology continues mainly in the R&D stage.



1.7 Challenges and prospects of energy storage technologies

1.7.1 Challenges of the energy storage application

In renewable energy generation grid integration, distributed generation, microgrid, transmission and distribution, intelligent grid and ancillary facilities, the energy storage technology has promising implementation prospects. China's 2050 growth scenario shows that the demand for energy

storage will range from 560 to 780 GW [35]. However, energy storage technology's large-scale implementation still faces difficulties in both the technical and economic facets. The cumulative installation distribution of global energy storage for various applications is shown in Fig. 1.9.

1.7.2 Prospects of energy storage technology development

A research project on renewable energy production and energy storage readiness was conducted by VLPGO (12 of the major energy grid operators). The United States, Japan, France, China, and other nations have taken the power of wind, solar, and other nonfossil energy into account for their long-term resources plans. With the trends of the fast expansion of the power scheme and large-scale renewable energy growth, each nation has conducted grid planning for the next 10–20 years, considering energy storage, evaluating multiple kinds of energy storage techniques, and planning or building many projects that can strongly encourage the growth and implementation of energy storage technology in the smart grid. Energy storage is implemented in many counties as a quick response

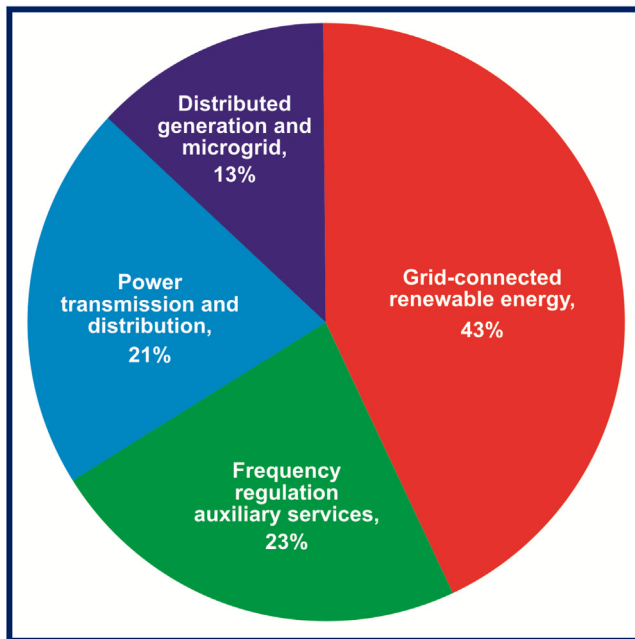


Figure 1.9 Cumulative installation distribution of global energy storage for various applications.

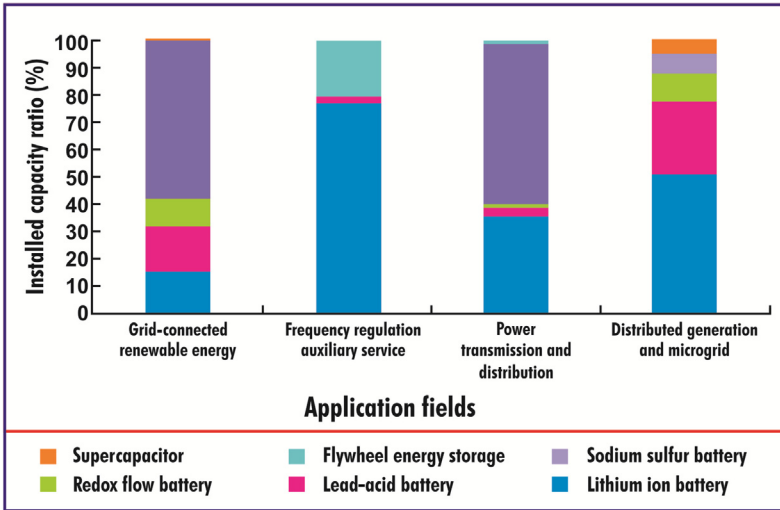


Figure 1.10 Cumulative installation distribution of different types of energy storage on various applications globally.

product for frequency regulatory service, according to the research outcomes, and the most powerful system businesses are prepared to buy this service. The Electric Power Research Institute (EPRI) identified 14 classes for energy storage applications [36] and defined them. Energy storage has important effects on the inclusion of large-scale renewable energy grids, moving loads, postponing construction of power grids, and enhancing the safety of power systems. These will also simultaneously generate a wonderful chance for the growth of energy storage. In the future, the worldwide energy storage price is projected to grow at a rate of 26% annually, based on Woori's prediction [37]. Although there is great potential for energy storage, the major problems are still the high costs, an ineffective incentive strategy, the infinite price mechanisms, and the business model. The cumulative distribution of multiple types of power storage systems worldwide for different applications is shown in Fig. 1.10.



1.8 Energy storage systems costs and values

Studies aimed at presenting benchmark numbers for the cost and value of energy storage systems are facing enormous difficulties.

Calculating the related expenses and service values for energy storage devices is a challenge not only because of the broad range of techniques but also because of many internal circumstances. One way to create an apple-to-apple comparison between storage technologies is by using the levelized energy cost (LCoS) where the technology per kWh is calculated as a function of the total project lifetime costs divided by the expected lifetime power output. For example, where a CAES system may have a higher initial investment in the capital than a Li-ion battery system, a lifetime power output of a CAES system is much higher than a Li-ion battery system (which usually only lasts 10 years) and thus lowers the LCoS. However, the LCoS formula fails to correctly represent other main points, including geographical limitations (vital to CAES and pumped hydro), battery fire safety issues, and more suitable technical characteristics for the various applications. Lazard, a global financial consulting company, tried to correct this by comparing LCoS only within specified categories of applications. However, the usefulness of the report is restricted, as real project planning would require a site-specific assessment considering soil, local electricity, climate, etc. Further complicating efforts to evaluate the economics of energy storage, is the difficulty of successfully evaluating storage equipment's value over its lifetime. The results of the metastudy reveal little consensus, further driving the point that the most appropriate way to calculate energy storage costs and values is on a case-by-case basis are shown in [Fig. 1.11](#).



1.9 Technology frontiers

Recently, costs have fallen across all kinds of storage along with improvements in battery activities and safety.

1.9.1 Improvements in traditional battery technology

1.9.1.1 Flow batteries

Breakthroughs include improvements in and choice of various solid and liquid electrolytes, manufacturing techniques with reduced toxicity, reduced cost, and greater flow batteries for energy density. Many study attempts were aimed toward various nonaqueous redox flow battery

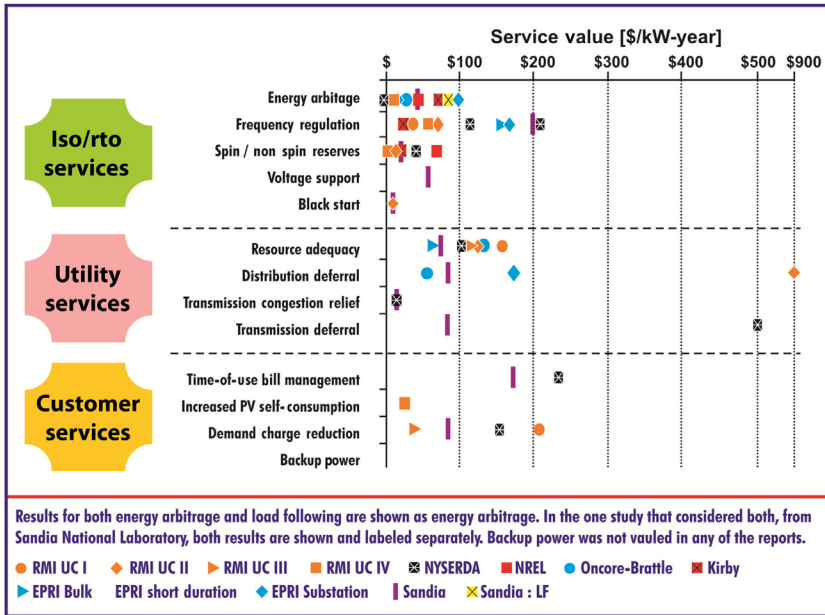


Figure 1.11 Service values of energy storage across application sectors according to several leading studies (US) show little consensus.

technologies, such as low-cost all-iron flow batteries and irrigated flow batteries of organic polymer electrolyte.

1.9.1.2 Molten salt batteries

Research attempts have been made to reduce battery operating temperatures and increase energy density in molten salt batteries, such as sodium-sulfur batteries and sodium nickel batteries.

1.9.1.3 Metal-air batteries

Research focused on the development of low-cost nonplatinum catalysts in zinc-air, lithium-air, and other metal-air batteries.

1.9.2 Lithium-ion battery safety research

Li-ion batteries are already commonly used in private electronics, electric vehicles, and storage devices on the grid-scale. Operational safety has become a significant problem for practical apps apart from battery efficiency and lifetime. Research instructions include the external direction of surveillance and heating and instead move toward the use of inner parts

(electrolytes, membranes, electrode materials, etc.) to control battery function and safety.

1.9.3 Solid-state battery R&D

Li-ion solid-state batteries are Li-ion batteries that use solid electrolyte materials. Solid-state batteries have excellent safety efficiency, high energy density, and a wide variety of operating temperatures. Many scientists are hoping to apply this technology to the next generation of Li-ion batteries, given these advantages. This has prompted research to create strong and quasi-solid electrolytes. Some study teams are working to enhance the compatibility of solid-state electrolytes, standard cathode materials, and metallic lithium anodes, all while inhibiting the development of lithium dendrites in these installations. Others focus on building high-quality energy and stable Li-ion battery systems for the solid-state cycle. Gel-type electrolyte materials have also become a significant topic of studies into materials science. Because solid-state batteries have shown promising outcomes, new study attempts are now moving away from the growth of electrolytes and moving toward complete battery structural design and industrial production processes, with battery samples and prototypes constantly rolling off the assembly lines.

1.9.4 Emerging battery systems

The limited reserves of the raw materials needed for Li-ion batteries and financial conditions drive attempts to find solutions to Li-ion such as metal-ion batteries, metal-air batteries, and metal-carbon batteries. With regard to ongoing studies into sodium-ion batteries and sodium-ion supercapacitors, developments in metal-ion battery technology are based on the design principles behind Li-ion batteries. Research has produced progress in the development of battery systems using other metals of elevated valence such as aluminium ion and calcium ion batteries. The metal acts as an anode in metal-carbon dioxide and metal-air batteries and uses the cathode of ambient air. These batteries have elevated energy density and are eco-friendly because the cathode does not need to be stored inside the battery. Lithium-air battery study is currently focused on choosing high-efficiency catalysts and protecting the metal lithium cathode. It will be some time before the widespread use of this technology becomes achievable.



1.10 Conclusion

We need an equally diverse portfolio of energy storage systems with the appropriate operational properties, just as we require a wide range of electrical power systems to meet our demands. Rapid expansion and installation of renewable energy sources are rapidly responsible for the pressing need for economical space on a large scale. It is hard to predict which of the strategies of energy storage will dominate the future, but it will be most likely a range of storing solutions to meet specific but flexible needs of the similarly sophisticated technology for the power generation we employ today and in the future. Fulfilling the demands of features of such a wide range of systems undoubtedly poses technical problems as stated in the chapter, but it also provides a sufficient array of storage applications, especially where these technologies can be used in synergistic combinations that complement each other and compensate for their shortcomings. It also provides innovation and progress in processing methods, tools, and processes where the scientific community has a significant role to play.

References

- [1] J. Hu, S.L. Yang, C.Y. Hou, et al., Present condition analysis on typical demonstration application of large-scale energy storage technology and its enlightenment, *Power Syst. Technol.* 39 (4) (2015) 879–885.
- [2] J.L. Li, L.T. Tian, X.K. Lai, Outlook of electrical energy storage technologies under energy internet background, *Autom. Electr. Power Syst.* 39 (23) (2015) 15–25.
- [3] C.S. Wang, D. Wang, Y. Zhou, Framework analysis and technical challenges to smart distribution system, *Autom. Electr. Power Syst.* 39 (9) (2015) 2–9.
- [4] C.S. Wang, Z. Wu, P. Li, Prospects and challenges of distributed electricity storage technology, *Autom. Electr. Power Syst.* 38 (16) (2014) 1–8.
- [5] Q.Y. Lu, W. Hu, Y. Min, et al., A multi-pattern coordinated optimization strategy of wind power and energy storage system considering temporal dependence, *Autom. Electr. Power Syst.* 39 (2) (2015) 6–12.
- [6] Y. Niu, F. Zhang, H. Zhang, et al., Optimal control strategy and capacity planning of hybrid energy storage system for improving AGC performance of thermal power units, *Autom. Electr. Power Syst.* 40 (10) (2016) 38–45.
- [7] H.J. Wang, Q.Y. Jiang, An overview of control and configuration of energy storage system used for wind power fluctuation mitigation, *Autom. Electr. Power Syst.* 38 (19) (2014) 126–135.
- [8] X.M. Yuan, S.J. Cheng, J.Y. Wen, Prospects analysis of energy storage application in grid integration of large-scale wind power, *Autom. Electr. Power Syst.* 37 (1) (2013) 14–18.
- [9] W.J. Liu, L. Sun, Z.Z. Lin, et al., Short-period restoration strategy in isolated electrical islands with intermittent energy sources, energy storage systems and electric vehicles, *Autom. Electr. Power Syst.* 39 (16) (2015) 49–58.

- [10] X.X. Zhou, Z.X. Lu, Y.M. Liu, et al., Development models and key technologies of future grid in China, *Proc. CSEE* 34 (29) (2014) 4999–5007.
- [11] B. Dunn, H. Kamath, J.M. Tarascon, Electrical energy storage for the grid: a battery of choices, *Science* 334 (2011) 928–935.
- [12] E.D. Wachsman, C.A. Marlowe, K.T. Lee, Role of solid oxide fuel cells in a balanced energy strategy, *Energy Environ. Sci.* 5 (2012) 5498–5509.
- [13] A.S. Arico, P. Bruce, B. Scrosati, J.-M. Tarascon, W.V. Schalkwijk, Nanostructured materials for advanced energy conversion and storage devices, *Nat. Mater.* 4 (2005) 366–377.
- [14] M. Armand, J.-M. Tarascon, Building better batteries, *Nature* 451 (2008) 652–657.
- [15] Z. Yang, J. Zhang, M.C.W. Kintner-Meyer, X. Lu, D. Choi, J.P. Lemmon, et al., Electrochemical energy storage for green grid, *Chem. Rev.* 111 (2011) 3577–3613.
- [16] M.S. Whittingham, Materials challenges facing electrical energy storage, *MRS Bull.* 33 (2008) 411–419.
- [17] C.J. Barnhart, S.M. Benson, On the importance of reducing the energetic and material demands of electrical energy storage, *Energy Environ. Sci.* 6 (2013) 1083–1092.
- [18] D.A.J. Rand, A journey on the electrochemical road to sustainability, *J. Solid. State Electrochem.* 15 (2011) 1579–1622.
- [19] M. Winter, R.J. Brodd, What are batteries, fuel cells, and supercapacitors? *Chem. Rev.* 104 (2004) 4245–4269.
- [20] O. Grogger, H.A. Gesteiger, J.-P. Suchsland, Review-electromobility: batteries or fuel cells? *J. Electrochem. Soc.* 162 (2015) A2605–A2622.
- [21] E.K. Yu, L.J. Chen, Characteristics and comparison of largescale electric energy storage technologies, *Zhejiang Electr. Power* 12 (2011) 4–8.
- [22] S. Mei, J. Wang, F. Tian, et al., Design and engineering implementation of non-supplementary fired compressed air energy storage system: TICC-500, *Sci. China Technol. Sci* 58 (4) (2015) 600–611.
- [23] X.D. Xue, S.W. Mei, Q.Y. Lin, et al., Energy inter-net oriented non-supplementary fired compressed air energy storage and prospective of application, *Power Syst. Technol.* 40 (1) (2016) 164–171.
- [24] Y.A. Chen, S.L. Gan, J.H. Zhou, et al., Energy storage technology of flywheel, *Chin. J. Power Source* 40 (8) (2016) 1718–1721.
- [25] X.B. Zhang, J.W. Chu, H.L. Li, et al., Key technologies of flywheel energy storage systems and current development status, *Energy Storage Sci. Technol.* 4 (1) (2015) 55–60.
- [26] A. Zahedi, Sustainable power supply using solar energy and wind power combined with energy storage, *Energy Procedia* 52 (2014) 642–650.
- [27] I.L. Garcia, J.L. Alvarez, D. Blanco, Performance model for parabolic trough solar thermal power plants with thermal storage: comparison to operating plant data, *Sol. Energy* 85 (10) (2011) 2443–2460.
- [28] B.D. Vick, T.A. Moss, Adding concentrated solar power plants to wind farms to achieve a good utility electrical load match, *Sol. Energy* 92 (2013) 298–312.
- [29] L.L. Jia, P. Liu, W.H. Zhang, Research progress of electrochemical technology of energy storage, *Chin. J. Power Sour* 40 (8) (2014) 1972–1974.
- [30] S.P. Xu, X.J. Li, D. Hui, A review of development and demonstration application of large-scale electrochemical energy storage, *Electr. Power Constr.* 34 (7) (2013) 73–80.
- [31] X.Y. Zhang, H.Z. Zhang, Z.Q. Lin, et al., Recent advances and challenges of stretchable supercapacitors based on carbon materials, *Sci. China Mater.* 59 (6) (2016) 475–494.
- [32] F. Béguin, V. Presser, A. Balducci, et al., Carbons and electrolytes for advanced supercapacitors, *Adv. Mater.* 26 (14) (2014) 2219–2251.

- [33] X. Luo, J. Wang, M. Dooner, et al., Overview of current development in electrical energy storage technologies and the application potential in power system operation, *Appl. Energy* 137 (2015) 511–536.
- [34] X.X. Huo, J. Wang, L. Jiang, et al., Review on key technologies and applications of hydrogen energy storage system, *Energy Storage Sci. Technol.* 5 (2) (2016) 197–203.
- [35] J.H. Bai, S.X. Xin, J. Liu, et al., Roadmap of realizing the high penetration renewable energy in China, *Proc. CSEE* 35 (14) (2015) 3699–3705.
- [36] D. Rastler, Electric energy storage technology options: A white paper primer on applications, *Costs, and Benefits*. EPRI, Palo Alto, CA, 2010. 1020676.
- [37] Woori Investment and Securities, Industry Analysis Rechargeable Battery Industry. [S. l.] (2011).

Fundamental electrochemical energy storage systems

Suresh Sagadevan¹, A.R. Marlinda¹, Zaira Zaman Chowdhury¹,
Yasmin Binti Abdal Wahab¹, Nor Aliya Hamizi¹, M.M. Shahid²,
Faruq Mohammad³, Jiban Podder⁴ and Mohd Rafie Johan¹

¹Nanotechnology & Catalysis Research Centre, University of Malaya, Kuala Lumpur, Malaysia

²Center of Micro-Nano System, School of Information Science and Technology, Fudan University, Shanghai, P.R. China

³Department of Chemistry, College of Science, King Saud University, Riyadh, Kingdom of Saudi Arabia

⁴Department of Physics, Bangladesh University of Engineering and Technology, Dhaka, Bangladesh

2.1 Introduction

Electrical dual layer capacitors (EDLCs) are known as supercapacitors that can be charged and discharged up to 10^6 times without power deficiency with a high-specific power density [1–7]. The EDLCs store electrical energy by adsorption of physical ionic species, not by electrochemical reactions on internal surfaces of high porosity electrodes. Meanwhile, recharging the batteries requires only a small energy density. Due to fast charging kinetics, high power densities, and longer cycling life, the EDLCs have more advantages compared to batteries [8]. The working principle of an ideal EDLC is supported by charging and discharging nearly $\sim 1000\text{--}2000\text{ m}^2/\text{g}$ electrochemical double-layer electrodes at the very large surface [9–11]. A wide selection of materials has been proposed for EDLCs electrodes over the last few decades. Among these materials, their complicated morphology, high micropore architecture, well-adjustable pore size distributions, and functionality, such as porous material electrodes, were a few important properties [12]. Many materials such as carbon, metal oxides, conducting polymers, and synthetic polymers have now been tested as EDLC elements. Yet carbon with a large surface has been used as an electrode and most porous electrodes are made of carbon [13]. Simple processability, nontoxicity, chemical stability, lower density, larger surface area, high electrical conductivity, and comparatively

cheaper materials are the main advantages that attract the porous carbons for practical applications. Also, electrolyte selection is important to enhance EDLC performance. Due to wide electrochemical windows, remarkable thermal stability, and nonvolatility [14,15], room temperature ionic liquids are commonly used as working electrolytes. The theoretical modeling for the investigation of EDLCs is based on the simplicity of the models corresponding to the geometry of tunable pores and the interaction of electrolyte and electrode [16]. For EDLC theoretical research three types of electrode architectures are typically used [17–19]. Several EDLC models, such as planar surfaces, cylindrical pores with concave internal surfaces, and cylindrical particles with convex external surfaces and spherical surfaces, were widely used in the investigation. This chapter is focused on electrochemical energy storage (EES) engineering on high energy density applications. Applications with high energy and high power densities for the same material are becoming more and more required in both current and near-future applications. Pseudocaps, a faradaic redox cycle on or near the surface, offers a way of obtaining high energy density at high load discharge rates.



2.2 Background of energy storage

EES is widely used to generate power. It is now used for portable electronics. It can be also applied to electrify the transport sector in the form of batteries and electrochemical capacitors (ECs). Global energy needs are expected to increase over the coming decades. Thus in many developed countries, EES technologies are combined with the power grid for combining it with renewable sources of energy such as solar and wind for electric grid power. Although there are a lot of opportunities for application of EES, these devices have to overcome several challenges and research should concentrate on identifying better materials for both storage and energy delivery. Basically, for consumer products and stationary power, plentiful, nontoxic materials should be used which would reduce the costs and improve the safety of EES devices. EES systems can be considered as a vital issue for the sustainable development of energy technology. Renewable resources like solar radiation or wind can be used to generate electricity to meet our energy needs sustainably.

Electricity generation from these renewable sources involves well-organized and consistent electrical energy storage methods. Electricity must continuously be obtainable for viable and residential end-uses on a reliable basis. Therefore in the use of large-scale solar or wind power generation, the development of new EES systems is critical. However, the use of hybrid electric vehicles (HEVs), plug-in hybrids, and all-electro-vehicles need meaningfully upgraded EES equipment. EES quality, reliability, and knowledge growth are required for modern mobile devices, including laptops and smartphones.



2.3 Electrochemical capacitors

ECs, which are also called supercapacitors, are of two kinds, based on their various mechanisms of energy storage, that is, EDLCs and pseudocapacitors. EDLCs initially store charges in double electrical layers formed near the electrode/electrolyte interfaces, as shown in Fig. 2.1.

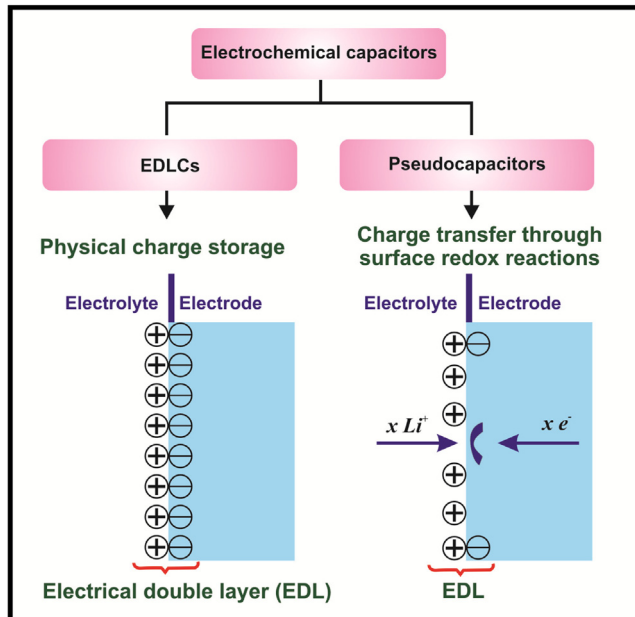


Figure 2.1 Classification of electrochemical capacitors. *EDL*, Electrical double layer; *EDLCs*, Electrical dual layer condensers.

Therefore the process is highly reversible and the life cycle is essentially unlimited. Nevertheless, pseudocapacitors do not only store energy in the EDLCs via the electrical double layer. This saves energy by fast oxidation–reduction reactions (redox) and conceivable intercalation of ion electrodes. The construction material of the electrode and the electrolyte regulate the electrochemical condenser performance jointly. The three primary electrode material groups used in ECs consist of (1) carbon-based materials, (2) metal transition oxides, and (3) conductive polymers. There are also three types of electrolyte compounds for ECs: (1) organic electrolytes, (2) ionic acid, and (3) aqueous electrolytes.

The output of ECs can be similar to different electrical storage devices. Fig. 2.2 displays the Ragone's map with its energy and power densities. These are similar to fuel cells and batteries, and the capacities indicate very large energy densities. Nonetheless, because of their mechanical loading ability, capacitors have low energy densities. Batteries and fuel cells are high in energy, but they have a low density due to their slower kinetic reactions. Electric condensers connect the distance between condensers and battery/fuel cells. Through maintaining a high power condenser capacity, electrochemical condensers will display the battery's high energy density.

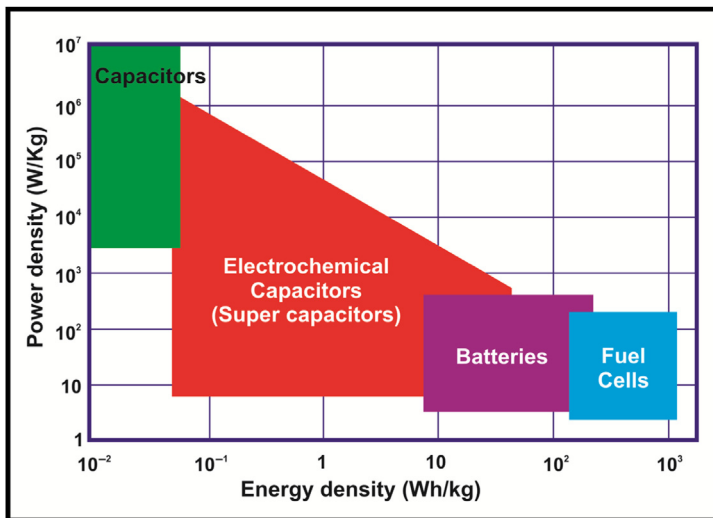


Figure 2.2 Power density versus energy density of various energy storage systems.

2.4 Principle of energy storage in electrochemical capacitors

EC devices have gained considerable interest as they have the unique features of a speedy rate of charging–discharging as well as a long life span. Charging–discharging can take place within a few seconds in EC devices. They have higher power densities than other energy storage devices. General Electric presented in 1957 the first EC-related patent. After that, they have been used in versatile fields of power supply and storage, backup power, and power quality improvement.

2.5 Charge storage mechanism in electrical dual layer condensers

EDLCs can be retained in energy without faradaic reactions [20,21] by means of load adsorption on the electrode surface. The configuration of the charges within the double layer of Helmholtz creates a displacement current during the charging and discharging process. The materials can quickly respond to the potential change as well as physical reactions. Thus it can quickly deliver the energy, as shown in Fig. 2.2. using the Ragone plot. Nevertheless, the quantity of stored energy is restricted and considerably lower than that of pseudocapacitors and batteries. This is basically for the containment of the electrode surface. It describes the EDL capacitance as follows [22].

$$C_{dl} = \frac{Q}{V} = \frac{\varepsilon_r \varepsilon_o A}{d} \quad (2.1)$$

where C_{dl} is the EDL capacitance of a single electrode, Q is the total charge transferred at potential V , ε_r is the dielectric constant of the electrolyte, ε_o is the dielectric constant of vacuum, d is the charge separation distance, and A is the electrode surface area. When C_{dl} is constant for EDLCs, the following equation describing the response current I can be derived from Eq. 2.2:

$$I = \frac{dQ}{dt} = C_{dl} \frac{dV}{dt} \quad (2.2)$$

where t is the charge time. If the applied voltage V varies with time t in a linear way, that is, $V = V_0 + \nu t$ (where V_0 is the initial voltage and ν is the sweep rate (Vs^{-1} or $mV s^{-1}$)), the relationship can be described as

$$I = C_{dl}\nu \quad (2.3)$$

Based on Eq. (2.3), the magnitude of current changes linearly with the sweep rate. A well-defined plot of rectangular current (I)–voltage (ν) or cyclic voltammogram is possible with the application of various sweep speeds. The voltage is increased (loaded) or reduced (discharged) constantly when the condenser is charged or discharged with the continuous current. This can be calculated by Eq. (2.3). It is anticipated that, in that case, a triangular load/discharge curve will be obtained. A lot of effort to understand and model electrode materials for energy storage applications has been made over the last few years. As EDLC supercapacitors, carbon-based materials, such as activated carbon [23] and graphene [24–27] carbon nanotubes, are used. In that case, the surface area of the electrode, surface functional state [28–30], pore texture, distribution of pores [31,32], and several carbon layers [33] are all significant variables. The energy efficiency of EDLCs can nevertheless be increased by combining carbon pore sizes to electrolyte ion sizes and carbon surface functionalization using oxygen [34] or by increasing oxygen content [35], using redox-active species-based electrolytes [36] and designing new forms of ionic iodide [37–39] or codoping [40,41]. In high energy density devices, the application of EDLC supercapacitors at larger scales is yet limited due to their intrinsic disadvantages.



2.6 Electrical double-layer capacitor

Two electrodes are divided into one cell by an electrolyte. An electrode and electrolyte interface stores a charge by electrostatic means. Opposite charges are placed on two different layers explaining the name's origin. One set resides on the electrode as shown in Fig. 2.3 and the other on the electrolyte.

The electrostatic and electrolytic capacitors do not have a dielectric medium. But the electrolyte's stability limits the operating voltage. Throughout the double layer, a potential difference develops. The

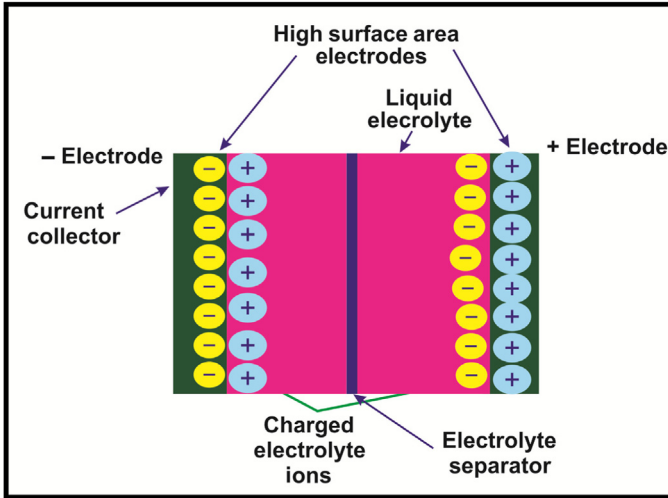


Figure 2.3 EDLC shown with the charge separation at both electrodes.

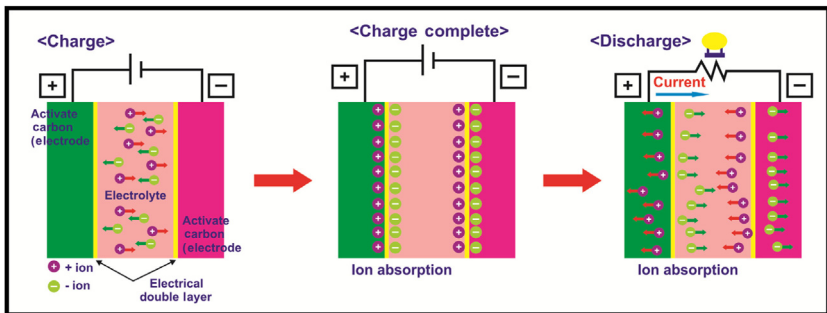


Figure 2.4 Charging and discharging phases of the EDLC.

separation of charges is in the range of a few Angstroms. Material with a large surface area is used as electrodes and from Eq. (2.4)

$$C = \frac{\epsilon A}{d} \quad (2.4)$$

surface area A is high on the numerator and the distance d on the denominator is very low, so the total value is small. Fig. 2.4 illustrates the charging process when the packed EDLC is fully charged and discharged.

When voltage is applied between two electrodes, electrolyte ions are absorbed onto the electrodes having opposite polarity. Thus a double layer at both the electrodes is developed. When a load is applied, it

substitutes the voltage source and the ions return back to the electrolyte. The electrolytes can be aqueous or organic. Fig. 2.5 illustrates the voltage distribution through a charged EDLC cell using the equivalent electrical circuit. The presence of load separation-related capacitance will make both the electrodes contribute to C_1 and C_2 as shown in Fig. 2.5 where they are connected in a series connection. The resistance exists due to the presence of R_1 and R_2 collectors and the internal R_i resistance generated from the movement of ions inside the electrolyte, there is also a series of resistance present here. The capacitance behavior of the double layer can be explained using Fig. 2.6.

This model has used different types of polar solvents like water or organic liquids such as methanol and acetonitrile. The interactions of the dipoles with the charged electrode surface in solvent molecules allow them to place themselves nearer to the electrode surface with the oppositely charged end. Explicitly, adsorbed electrolyte ions are present in this

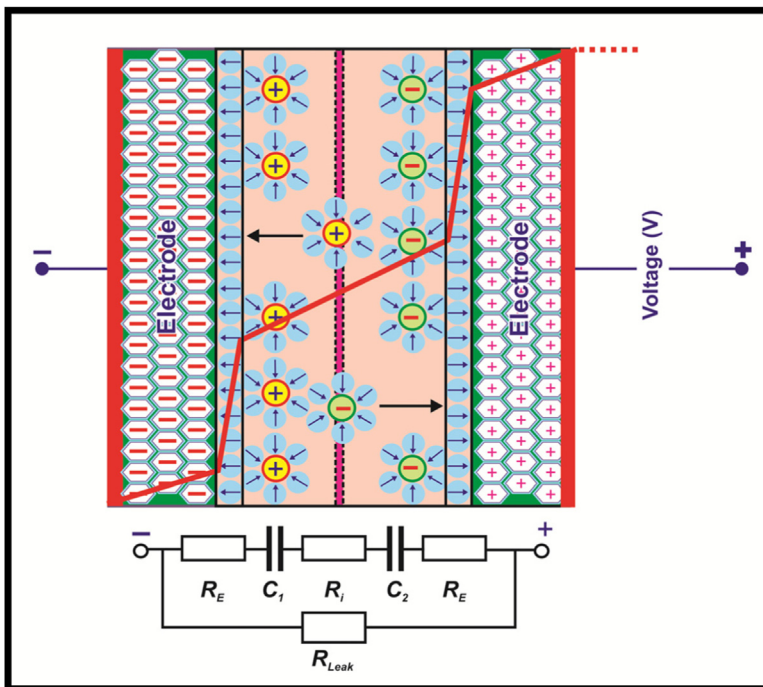


Figure 2.5 Voltage distribution across a charged EDLC and the equivalent electrical circuit.

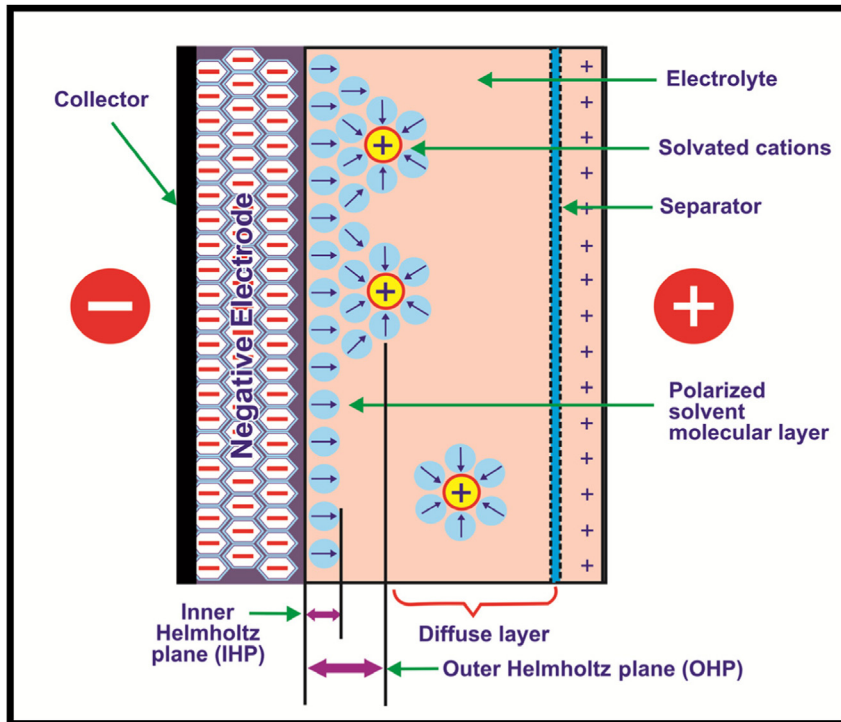


Figure 2.6 Model illustrating the double layer capacitance.

layer. As the surface of the electrode is covered by the other parts, the ions are enclosed partly by the solvent molecules. There is a rivalry between the water molecules and the electrolyte charged ions. Both the molecules and ions want to reside proximately to the layer associated with the surface of the electrode. The IHP is the monolayer of solvent molecules having a thickness of a single molecule of the electrolyte. This forms the dielectric medium between the opposite charges. The OHP extends from the electrolyte to form one layer of the double layer to the center of the charged ion. A linear disparity of the potential occurs along the Helmholtz plane with a change in distance. It becomes exponential outside of this region. Fig. 2.7 illustrates the potential variation across the dual-layer and in the diffuse layer of the bulk solution.

Also called the double layer, the Stern layer broadens to the OHP. Therefore the double-layer capacitance consists of the Helmholtz plane/Stern layer capacitance and the diffuse layer capacitance as a series connection also shown in Fig. 2.7.

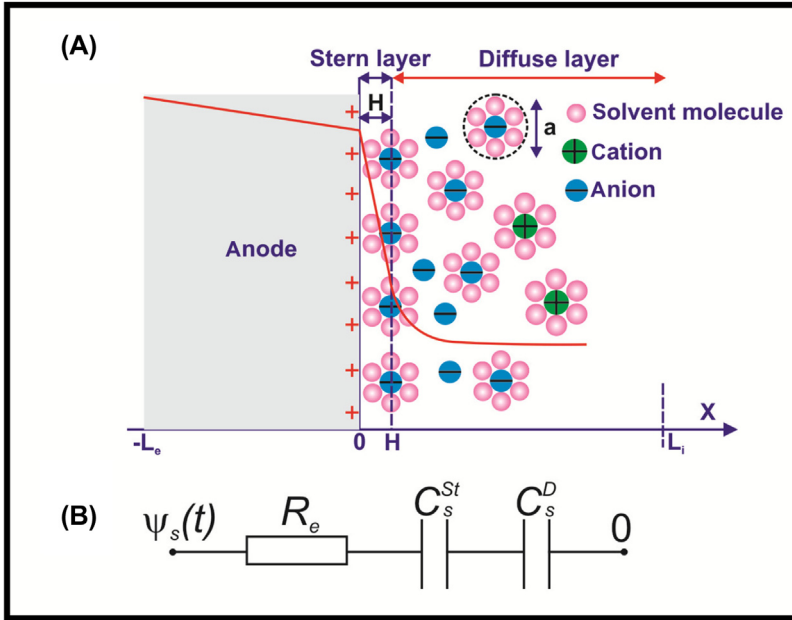


Figure 2.7 Electrical circuit describing the split in the capacitance between the Stern layer and the diffuse layer.

$$\frac{1}{C} = \frac{1}{C_s} + \frac{1}{C_D} \quad (2.5)$$

C_s is the capacitance of the Stern layer and C_D is the capacitance of the diffuse layer. As mentioned earlier, the formation of two parallel plate condenser at the electrodes were contributed to a single EDLC cell with two condensers connected in series. Thus a series of capacitance needs to be added to give the net capacitance in both the electrodes. Fig. 2.8 shows a different form of an EDLC cell's equivalent circuit. R_p is the isolating layer's resistance and is assumed to be sufficiently large. The circuit exhibits a parallel combination of C_{dl} and R_p due to the presence of a capacitance and a resistance across the double layer. However, both are kept at an identical voltage. Next, there is a resistance from the adjacent areas—electrolytes, electrodes, and current collectors, and this is shown as R_s .

Until recently, the best carbon materials showed approximately 150 Fg^{-1} double-layer capacities where the pore size of the carbon was optimized using the ionic liquid electrolytes [42]. Surface functionalization using nitrogen and oxygen can improve the energy densities of EDLCs

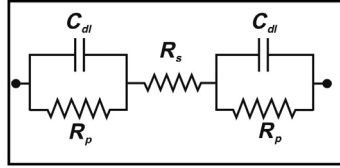


Figure 2.8 Equivalent electrical circuit of an EDLC cell.

[43]. Furthermore, if the pore sizes can correspond to the size of the electrolyte ion [44], the application of redox-active electrolyte species [45], as well as the development of ionic liquid mixtures can significantly improve the cell voltage and temperature range [46]. The application of 2D graphene for EDLCs has also become popular nowadays. The specific capacity can be enhanced up to $100\text{--}250\text{ Fg}^{-1}$ due to the application of graphene which has a high surface area [47,48]. However, the gravimetric-normalized capacitance may cause difficulties due to the nanoscale sheet-like morphological feature of graphene [49]. The flexible device architectures of EDLCs can be effectively developed using graphene.



2.7 Pseudocapacitor

The mechanism of a pseudocapacitor is due to the formation of electrical double layers. This is initiated by the insertion and adsorption of ions from the electrolyte into/on the surface of the electrode together with reduction–oxidation reactions from the load storage. The mechanism is nearly two-dimensional and therefore charging–discharge rates are comparable with the EDLCs. The magnitude of capacity increases due to the presence of chemical reactions. A pseudocapacitor is a hybrid between a battery and a dual-layer capacitor. It is also formulated due to the presence of an electrolyte in two separate electrodes. Charge storage is achieved by chemical and electrostatic ways. The chemical process includes the transmission of charges during the reduction–oxidation (redox) reaction. During charging of the battery, the transmission rate increases owing to the application of thinner redox substances over the surface of the electrode. This also happens due to the lower penetration of electrolyte ions. Multiple processes take place to store charge which

cause the increase of capacitance values in pseudocapacitors. Fig. 2.9 shows a cell with a pseudocapacitor.

As the equivalent electrical circuit is shown in Fig. 2.10, C_ϕ is the potential-dependent pseudo-capacitance, R_F is the electrode-electrolyte resistance, and R_D is the faradaic resistance that can act when the ions desorb. C_ϕ may well exceed the double-layer capacitance C_{dl} at certain potentials. Due to the additive law of capacitance, the parallel combination of the capacitors helps to build the capacitance of pseudocapacitors.

Faradaic energy storage can be represented by pseudocapacity. The reaction on the surface or close-surface region of the electrodes is primarily based on the fast redox reaction. In the course of charging [50,51], electrosorption/electrodesorption generally occurs through the electrode by transferring charges, but without any major phase transformation. The charge status (q) depends on the potential of the electrode and depends on the degree of colored charge/discharge transferred. The variation of Q values about potential increases the derivative values, dQ/dV . In turn, this changes the pseudocapacity (C_{pou}) values. Faradaic energy storage, in essence, is pseudocapacity, as opposed to EDL efficiency. However, the EDL capacity is related to the potential-dependent accumulation of electrostatic charges. Moreover, there are differences between pseudocapacity

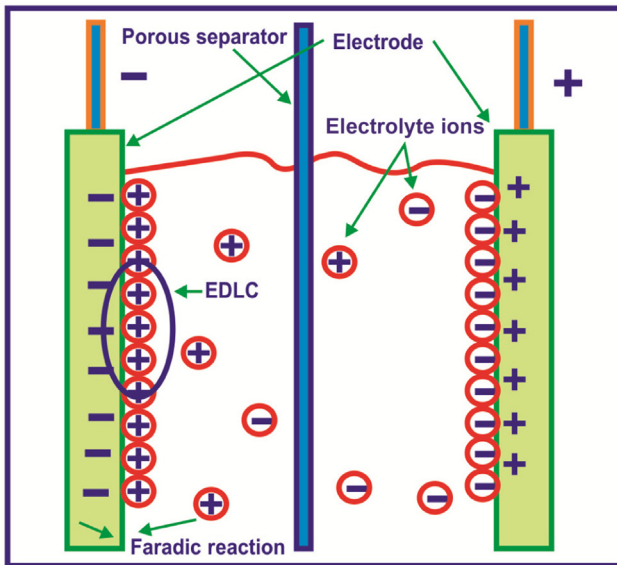


Figure 2.9 Pseudocapacitor exhibiting electric double layer and faradaic reactions.

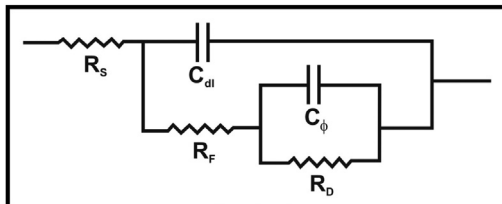


Figure 2.10 Equivalent electrical circuit of a pseudocapacitor.

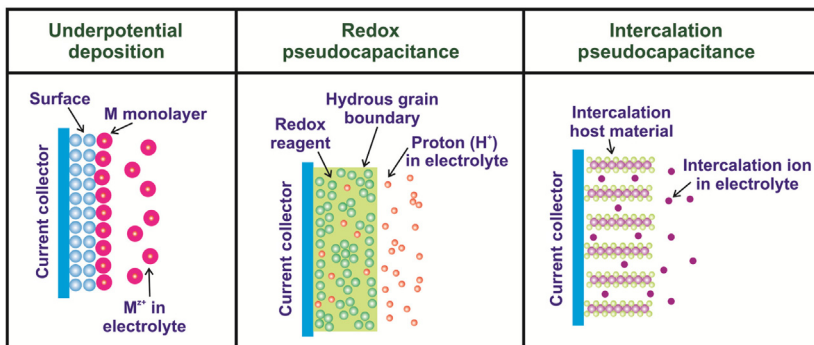


Figure 2.11 Schematic diagrams of the different faradaic processes.

and the ideal Nernstian process in battery-type materials in which the faradaic reactions take place at a constant potential. Pseudocapacity can be categorized into three main types: (1) low-potential deposition (UPD) (2D), (2) surface redox system (2D), and (3) intercalation system (quasi-2D) [52], as illustrated in Fig. 2.11.

2.8 Types of pseudocapacitance

Two-dimensionally or almost two-dimensional storage load processes are defined as pseudocapacity. There are three mechanisms of pseudocapacity: underpotential, redox, and intercalating.

2.8.1 Underpotential deposition

As the name implies, a positive potential is stored in addition to Nernst’s potential. Depositing a metal onto another metal’s electrode surface is

higher at a potential reduction than when deposited on itself. The deposit thickness normally does not exceed a monolayer. Over a continuous range of potential, fractional surface coverage occurs.

2.8.5 Redox pseudocapacitance

In the case of pseudo redox capability in the existence of faradaic reactions, the phenomenon of charge transfer occurs between electrodes and electrolytes through redox reactions. Redox reactions suggest reduction—oxidation reactions. These lead to a change in the oxidation state of species. Reduction happens when electrons are admitted and the oxidation state is reduced. Oxidation means that electrons are emitted and the state of oxidation decreases. Ruthenium redox was shown to demonstrate pseudocapacity by absorbing protons from electrolytes and transferring them back to the electrolyte in the case of hydrated ruthenium oxide. Fig. 2.12 shows the chemical process and the resulting reaction. Responses are limited to the surface of the electrode. Following a change in the oxidation state, ions are adsorbed to the electrode surface [53].

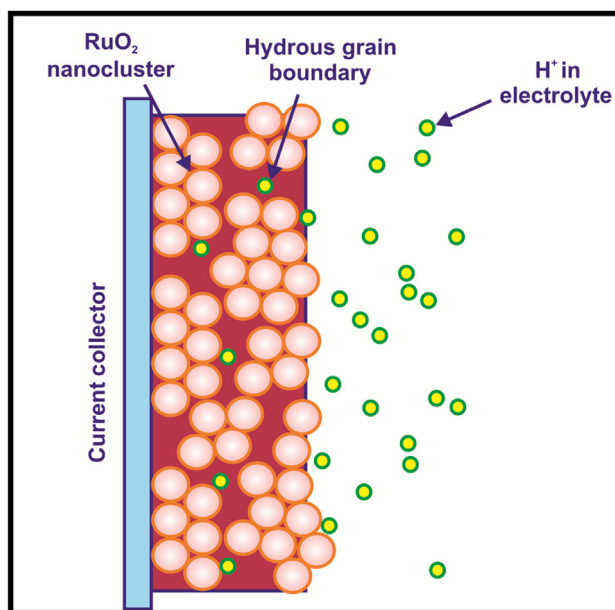



Figure 2.12 Redox pseudocapacitance for ruthenium oxide.

2.8.3 Intercalation pseudocapacitance

Inserting cations into a solid electrode's bulk lattice is called intercalation. During insertion, the electrode's electrical neutrality is maintained with an adequate number of electrons transferred to the host. Conditions to occur for intercalation include:

- The host is required to have an appropriate reduction agent to assist with the intercalation of the incoming cation from the electrolyte and the external circuit electron.
- Loss of metal host content in van der Waals (unpopulated areas).
- In the host above Fermi stage, low-lying bands are present. Electrons will quickly excite to the drive band if the energy difference at operating temperatures is low enough.
- The alignment of the elements in the grid array must be maintained during the insertion/removal process.

The ion's ability to propagate through the electrode surface is reduced in injection. In this case, with the square root of the sweeping frequency, the current stream rises at a certain voltage. The redox processes of the substrate are not regulated by diffusion. In a nanoscale substance, the size of the diffusion path is much shorter. The short track distances are perceived as good electronic and ionic transportation, which helps it also to work in less conductive fabrics.



2.9 Conclusion

In EDLC's electrochemical cells, energy is usually stored through electrostatic charging separation. Because of its porosity, its surface area improved and it enhances cell power. The rate at which ions travel inside the electrolyte has been somehow reduced. The electrolytes with high ionic conductivity can exhibit a faster capacity for load-discharge. The absence of chemical reactions as well as the addition of physical ions inside the electrode structure can ensure a long cycle life. However, it can be a disadvantage also for storing a large amount of energy. Thus compared to similar-dimensional batteries, EDLCs can exhibit high power densities with lower energy densities. They can show a longer cycle of life also. Capacitive storage can initiate a boost to the power which is needed for the distribution of power and storage while working in tandem with batteries.

References

- [1] B.E. Conway, *Electrochemical Supercapacitors, Scientific Fundamentals, and Technological Applications*, Kluwer/Plenum, New York, 1999.
- [2] M. Ue, Applications of ionic liquids to double layer capacitors, in: H. Ohno (Ed.), *Electrochemical Aspects of Ionic Liquids*, Wiley, Hoboken, 2005, pp. 205–223.
- [3] R. Koetz, M. Carlen, *Electrochim. Acta* 45 (15–16) (2000) 2483–2498.
- [4] P. Sharma, T.S. Bhatti, *Energy Convers. Manag.* 51 (2010) 2901–2912.
- [5] A. Burke, *J. Power Sources* 91 (2000) 37–50.
- [6] A. Lewandowski, M. Galinski, *J. Power Sources* 173 (2007) 822–828.
- [7] A. Burke, *Electrochim. Acta* 53 (2007) 1083–1091.
- [8] P. Simon, Y. Gogotsi, *Acc. Chem. Res.* 46 (2013) 1094–1103.
- [9] R. Kotz, M. Carlen, *Electrochim. Acta* 45 (1999) 2483–2498.
- [10] E. Bakhoun, *Ferroelectr. Freq. Control.* 56 (2009) 14–21.
- [11] J. Bard, L.R. Faulkner, *Electrochemical Methods, Fundamentals, and Applications*, second ed., John Wiley & Sons, Inc, 2001, pp. 12–13.
- [12] C. Merlet, B. Rotenberg, P.A. Madden, P.L. Taberna, P. Simon, Y. Gogotsi, et al., *Nat. Mater.* 11 (2012) 306–310.
- [13] E. Frackowiak, Q. Abbas, F. Beguin, *J. Energy Chem.* 22 (2013) 226–240.
- [14] M.V. Fedorov, A.A. Kornyshev, *Chem. Rev.* 114 (2014) 2978–3036.
- [15] R. Hayes, G.G. Warr, R. Atkin, *Chem. Rev.* 115 (2015) 6357–6426.
- [16] V. Meunier, J.S. Huang, G. Feng, R. Qiao, B.G. Sumpter, *ASME Int. Mech. Eng. Congr. Expo.* 11 (2010) 21–30.
- [17] J. Huang, B.G. Sumpter, V. Meunier, *Angew. Chem., Int. Ed.* 47 (2008) 520–524.
- [18] J. Huang, B.G. Sumpter, V. Meunier, G. Yushin, C. Portet, Y. Gogotsi, *J. Mater. Res.* 25 (2010) 1525–1531.
- [19] G. Feng, S. Li, V. Presser, P.T. Cummings, *J. Phys. Chem. Lett.* 4 (2013) 3367–3376.
- [20] B.E. Conway, *J. Electrochem. Soc.* 138 (1991) 1539.
- [21] M.D. Stoller, R.S. Ruoff, *Energy Environ. Sci.* 3 (2010) 1294.
- [22] L.L. Zhang, X.S. Zhao, *Chem. Soc. Rev.* 38 (2009) 2520.
- [23] E. Senokos, V. Reguero, J. Palma, J.J. Vilatela, R. Marcilla, *Nanoscale* 8 (2016) 3620.
- [24] X. Yang, C. Cheng, Y. Wang, L. Qiu, D. Li, *Science* 341 (2013) 534.
- [25] J.R. Miller, R.A. Outlaw, B.C. Holloway, *Electrochim. Acta* 56 (2011) 10443.
- [26] E. Raymundo-Piñero, K. Kierzek, J. Machnikowski, F. Béguin, *Carbon* 44 (2006) 2498.
- [27] A.B. Fuertes, M. Sevilla, *ChemSusChem* 8 (2015) 1049.
- [28] Y.J. Oh, J.J. Yoo, Y.I. Kim, J.K. Yoon, H.N. Yoon, J.-H. Kim, et al., *Electrochim. Acta* 116 (2014) 118.
- [29] Y.W. Zhu, S. Murali, M.D. Stoller, K.J. Ganesh, W.W. Cai, P.J. Ferreira, et al., *Science* 332 (2011) 1537.
- [30] C.T. Hsieh, H. Teng, *Carbon* 40 (2002) 667.
- [31] C. Largeot, C. Portet, J. Chmiola, P.-L. Taberna, Y. Gogotsi, P. Simon, *J. Am. Chem. Soc.* 130 (2008) 2730.
- [32] J. Chmiola, G. Yushin, Y. Gogotsi, C. Portet, P. Simon, P.L. Taberna, *Science* 313 (2006) 1760.
- [33] H. Ji, X. Zhao, Z. Qiao, J. Jung, Y. Zhu, Y. Lu, et al., *Nat. Commun.* (2014) 5.
- [34] C. Li, D. Wang, T. Liang, G. Li, X. Wang, M. Cao, et al., *Sci. China Ser. E: Technol. Sci.* 46, 349.
- [35] N. Morimoto, T. Kubo, Y. Nishina, *Sci. Rep.* 6 (2016) 21715.
- [36] K. Fic, E. Frackowiak, F. Beguin, *J. Mater. Chem.* 22 (2012) 24213.

- [37] D. Gueon, J.H. Moon, *ACS Appl. Mater. Interfaces* 7 (2015) 20083.
- [38] J.W. Jeon, R. Sharma, P. Meduri, B.W. Arey, H.T. Schaefer, J.L. Lutkenhaus, et al., *ACS Appl. Mater. Interfaces* 6 (2014) 7214.
- [39] H.C. Youn, S.M. Bak, M.S. Kim, C. Jaye, D.A. Fischer, C.W. Lee, et al., *ChemSusChem* 8 (2015) 1875.
- [40] S. Zhang, A. Ikoma, K. Ueno, Z. Chen, K. Dokko, M. Watanabe, *ChemSusChem* 8 (2015) 1608.
- [41] J. Zhou, J. Lian, L. Hou, J. Zhang, H. Gou, M. Xia, et al., *Nat. Commun.* (2015) 6.
- [42] P. Simon, Y. Gogotsi, *Nat. Mater.* 7 (2008) 845–854.
- [43] L. Hao, X. Li, L. Zhi, *Adv. Mater.* 25 (2013) 3899–3904.
- [44] J. Chmiola, G. Yushin, Y. Gogotsi, C. Portet, P. Simon, P.L. Taberna, *Science* 313 (2006) 1760–1763.
- [45] K. Fic, E. Frackowiak, F. Beguin, *J. Mater. Chem.* 22 (2012) 24213–24223.
- [46] R. Lin, P.-L. Taberna, S. Fantini, V. Presser, C.R. Perez, F. Malbosc, et al., *J. Phys. Chem. Lett.*, 2 (2011) 2396–2401.
- [47] Y. Huang, J. Liang, Y. Chen, *Small* 8 (2012) 1805–1834.
- [48] W.-Y. Tsai, R. Lin, S. Murali, L.L. Zhang, J.K. McDonough, R.S. Ruoff, et al., *Nano Energy* 2 (2013) 403–411.
- [49] Y. Gogotsi, P. Simon, *Science* 334 (2011) 917–918.
- [50] B.E. Conway, *Prog. Surf. Sci.* 16 (1984) 1.
- [51] B.E. Conway, *Prog. Surf. Sci.* 49 (1995) 331.
- [52] B.E. Conway, W.G. Pell, *J. Solid. State Electrochem.* 7 (2003) 637.
- [53] Arkady A. Karyakin, *Electroanalysis* 13 (10) (2001) 813–819.



Introduction to supercapattery

Arshid Numan^{1,2}, Yiqiang Zhan¹, Mohammad Khalid² and Mohammad Hatamvand¹

¹State Key Laboratory of ASIC and System, SIST, Fudan University, Shanghai, China

²Graphene & Advanced 2D Materials Research Group (GAMRG), School of Science and Technology, Sunway University, Selangor, Malaysia



3.1 Introduction

The latest developments in the renewable energy resources demand highly efficient and affordable energy storage systems. The intermittent harvesting of energy from renewable energy resources, such as wind, sunlight, and tides, cannot be utilized directly due to the unstable power supply [1]. Therefore the development of cost-effective energy storage technologies is highly important. Electrochemical energy storage systems (EES) are getting popular worldwide as they are capable of fulfilling the quest for energy demand and supply. Over the past two decades, there has been an exponential increase in the development of novel nanomaterials for EES [2,3]. Primarily, EES technologies are based on electrochemical reactions or electrostatic interactions to store energy and are mainly classified into rechargeable batteries and supercapacitors (also known as electrochemical capacitors), respectively. Although, a huge amount of research has been undertaken, and significant progress has been made for the development of both technologies (supercapacitors and rechargeable), the performance of the individual device is still lagging the commercial expectations [4]. The batteries are capable of delivering a high energy density while their power density is very low due to the faradaic reactions used for charge storage. In fact, intercalation or doping and dedoping of charge in the structure of the electrode material leads to slower charging and discharging of the battery, thus resulting in reduced power density. Therefore the deployment of batteries is limited to applications where high energy density is required. On the other hand, supercapacitors use physical adsorption/desorption or surface-based faradaic reactions (in the

case of pseudocapacitors), which provide a high power density but the energy density is compromised. The poor energy density of the supercapacitor is due to their smaller electrochemical potential window, especially in aqueous electrolytes using a symmetric electrode assembly. For example, an activated carbon-based symmetric supercapacitor can deliver one fourth of the specific capacitance value of an individual activated carbon electrode when measured in a three-electrode cell system.

This scenario opened up a new avenue of research, which proposed the hybridization of a rechargeable battery and supercapacitors in a single device [5]. This hybrid device is an intermediate device that can deliver high energy density and high power density of supercapacitors and batteries, respectively (Fig. 3.1). The operating potential window of the hybrid device also is enhanced due to the combined potential window of the capacitive and battery electrodes [7]. Fig. 3.2A depicts the cyclic voltammetry (CV) curves (showing the individual potential window) of cobalt phosphate (which is a well-known battery-grade electrode material) and activated carbon. The potential window of the hybrid device (using cobalt phosphate as a positive electrode and activated carbon as a negative electrode) can be extended to 1.5 V which is the sum of the potential window of both electrodes (Fig. 3.2B) [8].

The investigation of a hybrid energy storage device is quite old, but the first patented device was reported in the mid-1990s when Varakin et al. combined a nickel oxide-based battery electrode with a carbon fiber capacitive

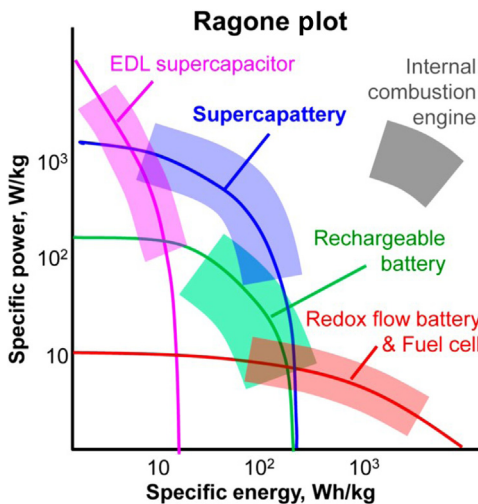


Figure 3.1 Ragone plot of different energy storage devices and the position of hybrid device (supercapattery) [6].

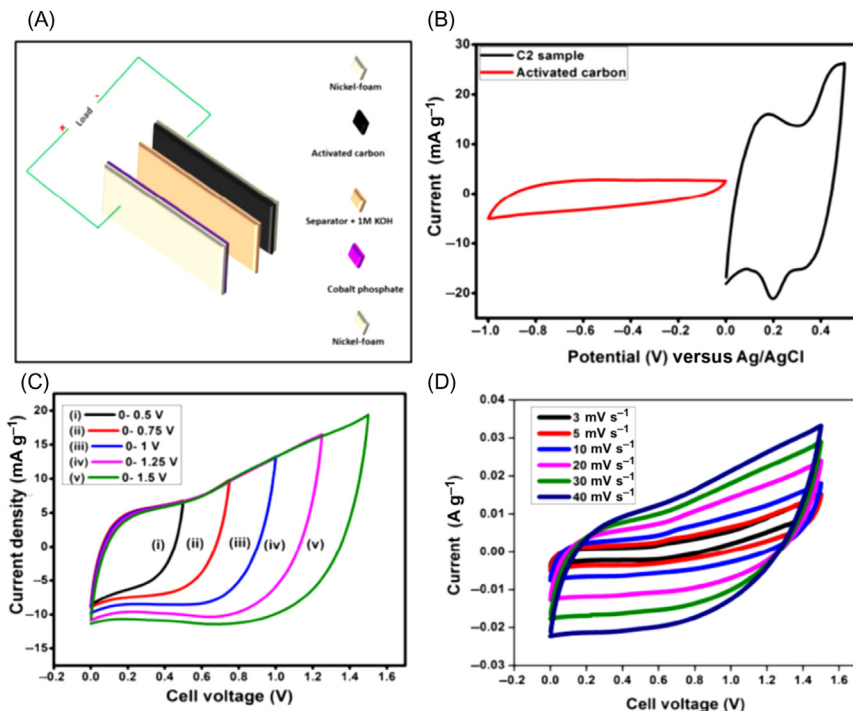


Figure 3.2 Schematic illustration of the assembled supercapattery device. (B) comparative CV curves of $\text{Co}_3(\text{PO}_4)_2$ as a positive electrode and activated carbon (AC) as a negative electrode examined in a three-electrode cell system using 1 M KOH as an electrolyte. (C) CV curves of $\text{Co}_3(\text{PO}_4)_2/\text{AC}$ supercapattery device measured at different potential windows at a scan rate of 10 mV s^{-1} . (D) CV curves of $\text{Co}_3(\text{PO}_4)_2/\text{AC}$ supercapattery device measured at different scan rates.

electrode in a single device [9]. Due to the combination of two kinds of charge storage mechanisms (electrical double layer and faradaic reactions), the inventors manage to improve the performance by 8–10 times. Further different combinations of capacitive and battery electrodes were used to fabricate the hybrid energy device which possessed a high cycle life and enhanced potential window leading to improved energy and power density [6].

The hybridization of energy storage devices can be of a different types based on the different types of electrode assembly. The combination could be the assembly of one type of capacitive electrode (electrical double layer) with other kinds of capacitive electrode (pseudocapacitive), and this device can be named as a hybrid supercapacitor. In the second case, one battery electrode with another capacitive electrode can be combined to form a two-terminal device which should be called a hybrid energy

storage device. However, in the literature, this device is also called a hybrid supercapacitor, which is misleading. Recently, a new name was proposed for the battery and capacitive-based electrode device as “Supercapattery” [6]. The term supercapattery is the combination of “supercapa” (from supercapacitor) and “ttery” (from the battery). Therefore it is suggested to use the term supercapattery for the hybrid energy storage systems formed by a battery and capacitive electrode.

The supercapattery is expected to achieve high performance and a durable cycle life as it utilizes both capacitive and battery-grade materials. The hybridization of the material could be at electrode materials level or device level. In the first approach, capacitive material could be combined with battery-grade material to make a composite. For example, activated carbon alone is a well-known capacitive material that stores charges electrostatically at its surface and pores. This activated carbon can be combined with battery-grade material such as nickel oxide (NiO) to form hybrid material. This hybrid material can offer a high specific capacity compared to activated carbon and high-power density and life cycle compared to NiO. In this approach, the focus is on the synthesis route, design, and nanoarchitecture of the hybrid material. In the device level approach, individual battery and capacitive electrodes are combined to form the hybrid device. This approach looks facile but practically is quite a challenging task to combine the unmatched performance electrodes in a single device. Only a few successful works are reported in the literature [10–12].

Several review articles have discussed the development of hybrid nanomaterials, but only a few were focused on the design and engineering of the device. This chapter will give a deep insight into the fundamentals of charge storage and the latest developments in supercapattery. The vague concepts about pseudocapacitive materials and battery-grade materials will be elaborated.



3.2 Charge storage mechanism in electrochemical energy storage systems

The charge storage capability of an EES depends upon many factors such as the charge storage mechanism (electrostatically or electrochemically), type of electrode and electrolyte, and the assembly of the device (symmetric or asymmetric). Since the charge is stored on electrodes, therefore, the indigenous properties of an electrode material, such as porosity, crystallinity,

electrical conductivity, thermal and electrochemical stability, and surface area, have a significant impact on the performance of the device.

The awareness of charge storage mechanism and its understanding provides a strong basis to evaluate the electrochemical performance of the EES. There are three different types of electrode material (based on their charge storage mechanism) which are used in EES: (1) capacitive, (2) pseudocapacitive, and (3) battery-grade electrode materials.

Capacitive materials employ the physical phenomenon of electrostatic attraction of charges without using any chemical reactions, which renders a high power density but the poor energy density of the electrode. The charges are stored physically at the electrode and electrolyte interface or deep inside the pores of the capacitive material, as shown in Fig. 3.3A. On the other hand, pseudocapacitive materials undergo faradaic reactions to store charges due to which they offer high energy density but with the compromise of low energy density. The charge storage in pseudocapacitive materials is by adsorption of electrolyte ions on the electrode surface accompanied by charge transfer between the electrode and electrolyte. The faradaic reactions are surface-based only, due to which reaction kinetics are rapid (Fig. 3.3B). Like pseudocapacitive materials, battery-grade materials also use faradaic reactions to store charges, but the faradaic reactions take place deep inside the electrode material altering the crystal structure of battery-grade electrode. Due to the deep faradaic reactions, the rate capability of the battery-grade electrode is

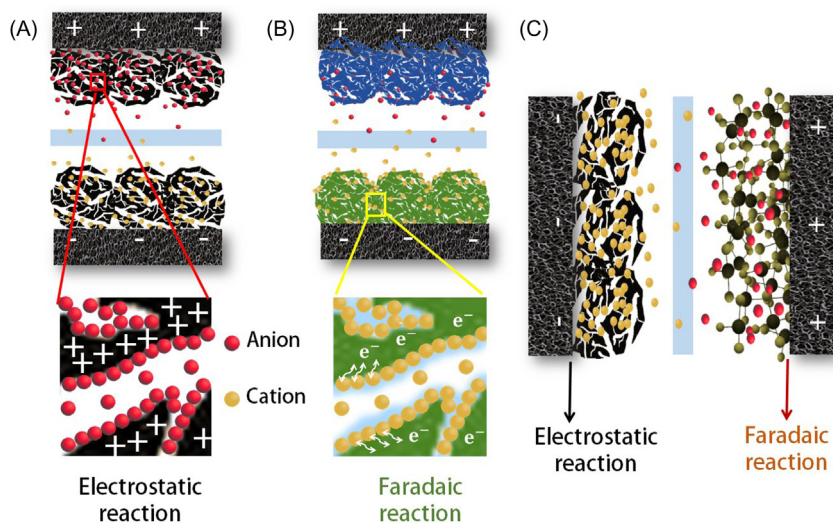


Figure 3.3 Schematic diagram of (A) ELDC, (B) pseudocapacitor, and (C) supercapattery.

poor compared to pseudocapacitive materials. The schematic illustration of charge storage in battery-grade material is shown in Fig. 3.3C. Herein, confusion arises between battery-grade and pseudocapacitive materials as both are using faradaic reactions. The full description of each type of electrode and the misleading concepts are explained in the following section.

3.2.1 Electrical double-layer capacitive electrode

Capacitive (more specifically, electrical double-layer capacitive) materials store charges physically by electrostatic adsorption of electrolyte ions on the surface of the electrode (Fig. 3.3A). During the charging process, the double layer of charges is formed at the interface of electrode and electrolyte due to which capacitors based on these materials are called electrical double-layer capacitors (EDLC). The carbonaceous materials with high surface area ($1000\text{--}2500\text{ m}^2\text{ g}^{-1}$), such as activated carbon, carbon nanotubes, graphene, and fullerene, are used as capacitive electrode material in EDLC. The specific capacitance of EDLC is far higher than conventional capacitors due to the high surface area of the EDLC electrodes as compared to conventional electrodes which use a metal plate as an electrode. The cyclic stability and power density of EDLC is higher than rechargeable batteries as the charge storage mechanism is physical by the adsorption of electrolyte ions rather than using electrochemical reactions.

The electrochemical characteristics such as CV and galvanostatic charge–discharge (GCD) demonstrate almost rectangular and triangular curve shapes, respectively (Fig. 3.4).

3.2.2 Pseudocapacitive electrode

Pseudocapacitive materials store charges by highly reversible surface faradaic reactions. The charges are stored by the physical transfer of electrons between electrodes and electrolyte instead of the physical adsorption of ions. Due to this, the capacitance of pseudocapacitive materials is higher than EDLC materials. Transition metal oxides such as RuO_2 and MnO_2 are the well-known pseudocapacitive materials. V_2O_5 , SbO_2 , and F_2O_3 conducting polymers (polyaniline, polypyrrole) are also categorized as pseudocapacitive materials in some cases [13]. The electrochemical signature of the pseudocapacitive material is the same as the EDL capacitive materials due to which it is named as “pseudocapacitive” (behaves like capacitive material). Both capacitive and pseudocapacitive materials demonstrate a leaf-like (almost rectangular) CV curve and almost triangular GCD curve,

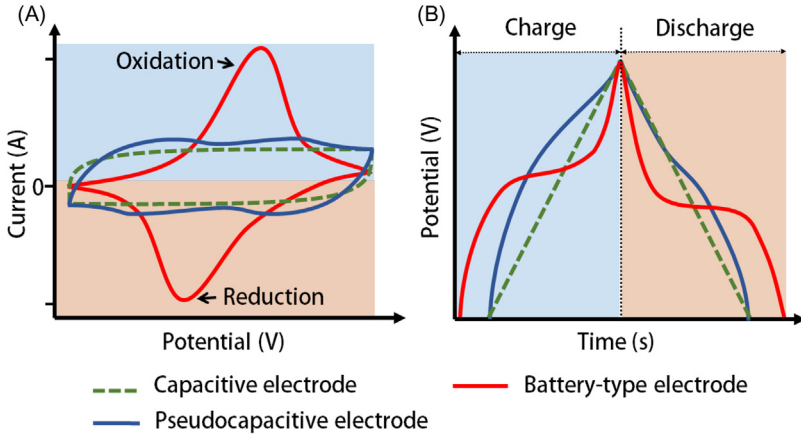


Figure 3.4 Electrochemical signature of (A) CV and (B) GCD capacitive and faradaic charge storage.

even in a three-electrode cell system (within a given potential window). Fig. 3.4 shows the CV and GCD curves of EDLC (green dotted line) and pseudocapacitive (blue line) materials. The electrochemical signature of both materials is similar, even the charge storage mechanism is different.

The capacitive behavior of the pseudocapacitive materials depends upon its nanoarchitecture, conductivity, and hydration properties. The charge storage mechanism in pseudocapacitive materials can be further categorized into three types depending upon the properties of the material. The first type is underpotential deposition, where electrolyte ions adsorb on the surface of the electrode, forming a monolayer of ions. In the second case, capacitive behavior is due to the faradaic reactions in which electrolyte ions adsorb on the electrode surface and at the same time undergo faradaic reactions. The third scenario is the intercalation where ions from the electrolyte intercalate into the layers of electrode materials associated with faradaic reactions without distorting the crystal structure of the material [13].

3.2.3 Battery electrode

Like pseudocapacitors materials, battery-grade materials also use faradaic reactions, due to which these materials are reported misleadingly as pseudocapacitive materials. Battery-grade materials use deep faradaic reactions to store the charges which are rarely reversible. The charge storage in battery-grade materials is due to the phase transformation of the materials, unlike pseudocapacitive materials where the phase of the crystal of the

materials remains constant [14]. Nickel and cobalt oxide are well-known battery-grade materials which form metal oxyhydroxide during charging (or during the forward scan in CV) and restore their original crystal phase during discharge (or reverse scan in CV) in alkaline electrolyte. The reaction mechanism is represented in the following equation [15].



where M is transition metal (Ni, Co, Zn, etc.) or a combination of metals. Due to the phase transformation of the material's crystal structure, battery-grade materials are capable of delivering high energy density compared to capacitive materials. Nevertheless, the rate capability and life cycle of the battery-grade materials are compromised.

The doping and dedoping process in the crystal structure of the battery-grade material during faradaic reactions renders a completely different electrochemical signature compared to capacitive and pseudocapacitive materials. Fig. 3.4 (red line) shows a typical CV and GCD curve of the battery-grade material. A couple of redox peaks in CV and the non-linear curve with a plateau at GCD reflect the pure faradaic reactions [6].

Electrochemical signature (CV and GCD curves) can give an obvious indication of battery-grade material. The capacitive terms, formulas, and units should not be used for battery-grade materials. Many publications reported false specific capacitance (rather should be specific capacity) for battery-grade materials [14,16–18]. Therefore it is very important to elaborate on the confusion between battery-grade and pseudocapacitive materials. The evaluation of the definition of pseudocapacitive materials, the confusion between battery-grade and pseudocapacitive materials are discussed in detail in the following section. Moreover, the cases where battery-grade material mimics pseudocapacitive materials by demonstrating a similar electrochemical signature are also elaborated upon.



3.3 Difference between pseudocapacitive and battery-grade materials

3.3.1 Why pseudocapacitive materials are considered capacitive?

Pseudocapacitive materials were first time defined in Conway's book "Electrochemical Supercapacitors: Scientific Fundamentals and Technological Applications" [19].

In this book, the capacitive effect of pseudocapacitive materials was proposed due to the rapid and reversible faradaic reactions which take place at the surface or near-surface of the pseudocapacitive electrode. The question arises, why are pseudocapacitive materials considered as capacitive materials? According to the basics of physics, capacitance is a ratio between charge accepted to the voltage. In other words, the ratio between the rate of charge acceptance and change in potential is a constant value which is called capacitance.

$$C = \frac{dQ}{dV} \quad (3.2)$$

where C is capacitance, dV is derivative of potential, and dQ is derivative charge. According to this equation, any material demonstrating an electrochemical signature in such a way that the ratio of charge stored in a given potential range is constant would be capacitive material. The electrochemical signature (quasirectangular CV and linear GCD) of pseudocapacitive and EDLC materials follows the equation of capacitance. However, the electrochemical signature of battery-grade materials does not fulfill the requirements of Eq. (3.1). This means that battery-grade materials should not be considered as capacitive material and the capacity formula, as well as units, should be used rather than the capacitance formula. Applying the formula of capacitance to the battery-grade materials leads to the false and higher values of specific capacitance compared to real capacity value. The formula to estimate the specific capacity of the battery-grade electrode using a CV curve is given as:

$$Q_s = \frac{1}{vm} \int_{V_i}^{V_f} I \times V dV \quad (3.3)$$

where Q_s is the specific capacity in coulomb per gram ($C g^{-1}$), v is scan rate in volt per second ($V s^{-1}$), and the integral term is the area under the CV curve. The following equation estimates the specific capacity through GCD:

$$Q_s = \frac{I \times \Delta t}{m} \quad (3.4)$$

where I is the discharge current in amperes (A), Δt is discharge time (after IR drop), and m is the mass loading of materials. The fact that charge storage is based on a faradaic process implies that the electrode material acts a bit like a battery; nevertheless, the electrochemical signatures are reflected

with the presence of (quasi)-rectangular CVs and the almost linear GCD curves similar to EDLC, indicative of rapid faradaic reactions that are not limited by solid-state diffusion [20].

3.3.2 Confusion between pseudocapacitive and battery-grade materials

With the development of nanomaterials, the surface area of the battery electrode was enhanced significantly. This led to shortening of the ion diffusion pathways, and bulk redox reactions were converted into surface redox reactions. Subsequently, a few battery-grade materials behave like pseudocapacitive materials by demonstrating an electrochemical signature (quasirectangular CV and linear GCD curves) like capacitive materials [21–23]. In other words, when the dimension of the electrode materials (powder or thin films) reaches a critical size, the material starts behaving like a pseudocapacitive material. These kinds of materials are proposed to be “extrinsic pseudocapacitive materials” [13]. However, in such cases, the pseudocapacitive behavior is only due to the nanoarchitecture or the design of the material but not due to the intrinsic behavior of the electrode material.

When the size and design of the electrode is engineered in such a way that charge storage sites dominate at the surface of the electrode material, then only interfacial faradaic reactions take place [13,24]. The phenomenon happens when the size of the electrode material is reduced to a critical size, which leads to a high surface area, dominating the surface charge storage sites and reduction in the diffusion lengths. This leads to fast charge/discharge kinetics by the surface redox reactions. Due to these reasons, the electrochemical signature of such material is similar to pseudocapacitive material. However, the electrochemical signature of the same material in bulk size is like battery-grade material. In short, a single material can show both battery-grade and pseudocapacitive behavior when the size is tuned from bulk to critical size, respectively.

LiCoO_2 is well-known battery-grade material which is used as a positive electrode to store Li-ions by an intercalation mechanism [22]. The electrochemical signature of bulk LiCoO_2 is similar to battery-grade material by showing a well-documented pair of redox peaks in CV and plateaus in GCD. However, when the size of LiCoO_2 is tuned from bulk to critical size, the plateaus at GCD disappear, which indicates the surface redox reactions (Fig. 3.5).

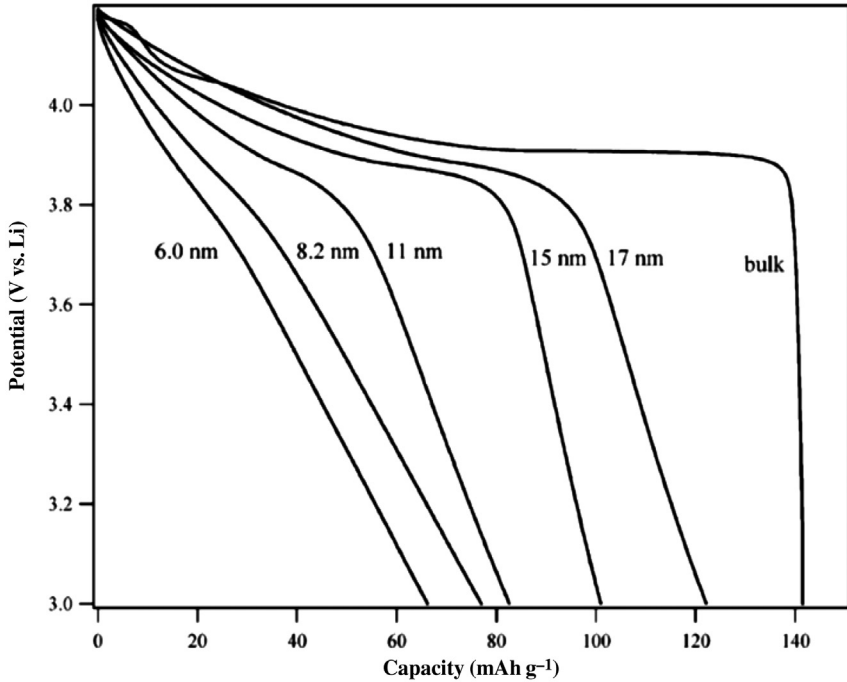


Figure 3.5 Crystallite size effect of LiCoO₂ electrode [22].

Similarly, thin (few nanometers) layered battery-grade materials also present pseudocapacitive behavior. For example, nanosized layered nickel hydroxide is also considered to be an extrinsic pseudocapacitive material to some of the researchers. In this case, the faradaic reactions are surface controlled, which provides rapid charge–discharge kinetics. Additionally, battery-grade transition metal oxides such as Nb₂O₅, TiO₂, and MoO₂ were also reported as intrinsic pseudocapacitive materials due to their higher charge storage kinetics which in some cases surpass the pseudocapacitive materials [25–27]. Although the rate capability of these materials is comparable or even superior (in some cases) to pseudocapacitive materials, still they cannot be categorized as pseudocapacitive materials. To further clarify the charge storage mechanism of these materials, Dunn et. al. introduced a new term of “intercalation pseudocapacitive materials” for such materials [14]. In this kind, ions from the electrolyte intercalate into the tunnels or the layers of electrode material along with faradaic charge transfer without altering the crystallographic phase of the electrode material [28].

The new terminology “intercalation or extrinsic pseudocapacitance” accommodated a wide range of materials from the past few years. However, in most the cases, the intercalation of pseudocapacitive materials shows obvious peaks in the CV, which is the behavior of battery materials. It is challenging to reveal that the charge storage in intercalation pseudocapacitors is not a diffusion-limited process. Therefore the quantitative determination of the charge storage kinetics in such kinds of materials is vitally important. Dunn et al. in 2007 proposed a formula to estimate the charge storage contribution from the surface-confined charge transfer and diffusion-controlled reactions using CV analysis [29]. The Dunn’s formula is as follows:

$$i(V) = k_1 v^{1/2} + k_2 v \quad (3.5)$$

Here, the term $k_2 v$ gives the amount of charge storage due to the surface-confined or nondiffusion-limited charge storage reactions (capacitive currents) from which current is proportional to the potential sweep rate. The term $k_1 v^{1/2}$ represents diffusion-controlled currents from which current is proportional to the square root of potential sweep rate. The formula can be simplified as follows:

$$i(V) = a v^b \quad (3.6)$$

By calculating the value of b , capacitive and diffusion control, the contribution can be estimated. For example, if the current is proportional to the sweep rate (over the wide range of sweep rates), the value of the b will be one. This means that charge storage is due to the nondiffusion control or surface-confined charge transfer reactions. However, when there is a case where current is proportional to the square root of the sweep scan, the value of b will be 0.5, which means it is a diffusion-controlled process. The peak current of the MnO_2 electrode is proportional to the sweep rate ($b = 1$) confirming the capacitive charge storage. However, LiFePO_4 demonstrated the battery-grade electrochemical signature as the value of b is 0.5. Dunn’s approach to identifying the charge storage kinetics is extensively used for different kinds of materials. Using this technique, TiO , MoO_3 and Nb_2O_5 were categorized as pseudocapacitive materials as the value of b is approximately 1.

Although, Dunn’s formula is enough to quantitatively estimate the contribution of capacitive and diffusion-controlled currents for intercalation pseudocapacitors, the application of this technique for deep faradaic reactions is not suitable. For instance, lithium storage was estimated at a

very low scan rate (2 mV s^{-1}) without considering ion diffusion limitations [30]. The result is shown in Fig. 3.6A, where the red line depicts the pseudocapacitive contribution. Surprisingly, pseudocapacitive current arose in the redox faradaic peaks. Similar behavior was also shown by the materials where storage is due to the conversion or alloying process rather than intercalation [31,32]. For example, when B-SnS₂ (Fig. 3.6B–D) is employed in sodium-ion batteries, the capacity contribution due to nondiffusion-controlled reaction was found to be 58%–77% at a sweep rate of 0.2 – 5 mA s^{-1} [31]. Similarly, VSe₂ (Fig. 3.6E,F) used as an anode in potassium ion batteries, and its capacitive contribution using a nondiffusion-controlled process was estimated to be up to 90.7% [32]. Many other battery-grade materials are reported as capacitive materials when they showed a higher capacitive contribution by applying Dunn's formula. This literature further confused the definition of battery and pseudocapacitive materials.

As mentioned earlier, the pseudocapacitive behavior of the battery-grade materials is either due to small size or a very thin layer. Therefore if the value of $b = 1$ in Dunn's formula, it means that there are surface-confined faradaic reactions that are taking place due to the small size or

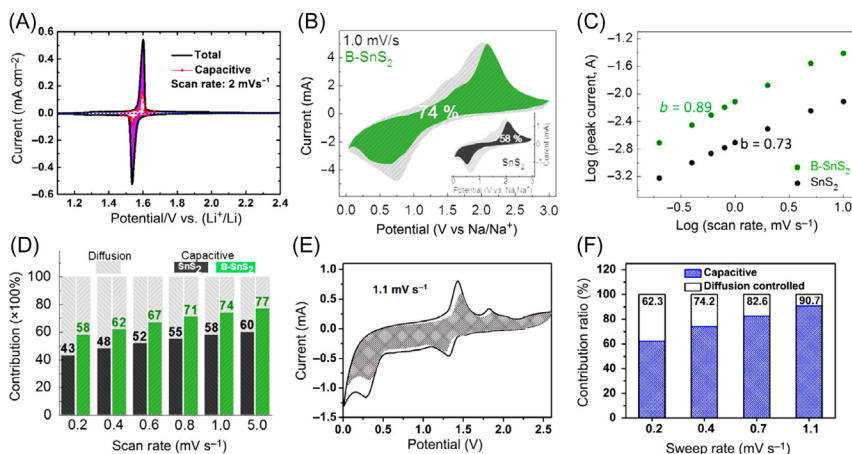


Figure 3.6 (A) Li^+ storage of $\text{Li}_4\text{Ti}_5\text{O}_{12}$ with capacitive currents (k1m) being plotted at certain potentials around redox peaks. (B) CV and capacitive contribution and diffusion contribution (gray) of SnS_2 electrode for Na^+ storage. (C) Relationship between logarithm cathodic peak current and logarithm scan rates. (D) Capacitive capacities contribution ratio at different scan rates. (E) K^+ storage of VSe_2 with the pseudocapacitive contribution. (F) The pseudocapacitive contributions at different sweep rates.

thin layer of the material. A similar explanation was provided by Conway [33]. Nevertheless, kinetics analysis is important to realize the faradaic reactions, but it cannot be solely used to recognize any materials as pseudocapacitive or battery-grade material. The fundamental criteria must be the electrochemical signature which should be taken into account in order to identify the type of material [6,34,35]. Therefore materials with an electrochemical signature of a constant ratio of dQ/dV within a fixed potential window should be considered to be capacitive materials. The materials with plateaus in GCD and peaks in the CV curve should be treated as battery-grade material with a physical unit of C or mAh.



3.4 Conclusions

The prodigious development of the electronic industry catalyzed the development of renewable energy resources and EES technology. The existing energy storage technology, such as battery and supercapacitors, are widely employed in different applications depending upon energy and power density demands. However, the stand-alone performance of each device (batteries and supercapacitors) is still not up to the mark. Therefore the hybridization of both device materials in a single device (supercapattery) has been done to bridge the performance gap between supercapacitors and batteries. The supercapattery combines the features of high energy and power density from the battery and supercapacitor. Recently, a vast range of nanomaterials have been investigated as electrode materials for energy storage devices. However, significant developments in nanoscience and nanotechnology led to a reduction in the size of electrode materials. The small size of nanomaterials (especially battery-grade materials) results in the reduction in diffusion lengths for ions for charge storage. Due to this, negligible ion diffusion and surface-confined faradaic reactions take place, which results in the electrochemical behavior of a battery-grade electrode like a capacitive electrode. However, this behavior is not intrinsic, rather it is due to the small size of the nanomaterial. Therefore numerous battery-grade electrodes are reported misleadingly as a capacitive electrode. One of the approaches for such materials to estimate the charge storage due to surface-confined faradaic reaction is to use quantitative kinetic analysis. However, due to the complex reaction kinetics in the composite electrode, simple

quantitative kinetic analysis is insufficient to identify the type of electrodes. In order to understand the reaction mechanism deeply, it is highly important to understand the electrochemical features based on Conway's definition first, and then apply the quantitative kinetic analysis using Dunn's equation. Therefore for pseudocapacitive material the electrochemical signature should possess almost rectangular CV and a linear GCD curve with the value of b close to 1 (using Eq. 3.6). On the contrary, battery-grade material demonstrates CV with prominent peaks and nonlinear GCD with the value of b almost equal to 0.5 for bulk size. The value of b can be higher than 0.5 if the nanosize battery materials are used, which means the process is no longer a diffusion-controlled process.

References

- [1] P.T. Moseley, J. Garche, *Electrochemical Energy Storage for Renewable Sources and Grid Balancing*, Newnes, 2014.
- [2] N. Liu, W. Li, M. Pasta, Y. Cui, *Nanomaterials for electrochemical energy storage*, *J. Front. Phys.* 9 (3) (2014) 323–350.
- [3] B.-M. Jun, S. Kim, J. Heo, C.M. Park, N. Her, M. Jang, et al., *Review of mxenes as new nanomaterials for energy storage/delivery and selected environmental applications*, *J. Nano Res.* 12 (3) (2019) 471–487.
- [4] W. Gu, G. Yushin, *Review of nanostructured carbon materials for electrochemical capacitor applications: Advantages and limitations of activated carbon, carbide-derived carbon, zeolite-templated carbon, carbon aerogels, carbon nanotubes, onion-like carbon, and graphene*, *Wiley Interdiscip. Rev. Energy* 3 (5) (2014) 424–473.
- [5] J. Iqbal, L. Li, A. Numan, S. Rafique, R. Jafer, S. Mohamad, et al., *Density functional theory simulation of cobalt oxide aggregation and facile synthesis of a cobalt oxide, gold and multiwalled carbon nanotube based ternary composite for a high performance supercapattery*, *New J. Chem.* 43 (33) (2019) 13183–13195.
- [6] G.Z. Chen, *Supercapacitor and supercapattery as emerging electrochemical energy stores*, *Int. Mater. Rev.* 62 (4) (2017) 173–202.
- [7] F.S. Omar, A. Numan, S. Bashir, N. Duraisamy, R. Vikneswaran, Y.-L. Loo, et al., *Enhancing rate capability of amorphous nickel phosphate supercapattery electrode via composition with crystalline silver phosphate*, *Electrochim. Acta* 273 (2018) 216–228.
- [8] N. Duraisamy, N. Arshid, K. Kandiah, J. Iqbal, P. Arunachalam, G. Dhanaraj, et al., *Development of asymmetric device using $\text{Co}_3(\text{PO}_4)_2$ as a positive electrode for energy storage application*, *J. Mater. Sci. Mater. Electron.* 30 (8) (2019) 7435–7446.
- [9] I. Varakin, A. Stepanov, V. Menukhov, *Capacitor with a double electrical layer*, *J. PCT/RU* (1995) 95–00171.
- [10] B. Akinwolemiwa, C. Peng, G.Z. Chen, *Redox electrolytes in supercapacitors*, *J. Electrochem. Soc.* 162 (5) (2015) A5054–A5059.
- [11] S. Makino, Y. Shinohara, T. Ban, W. Shimizu, K. Takahashi, N. Imanishi, et al., *4V class aqueous hybrid electrochemical capacitor with battery-like capacity*, *RSC Adv.* 2 (32) (2012) 12144–12147.
- [12] W. Shimizu, S. Makino, K. Takahashi, N. Imanishi, W. Sugimoto, *Development of a 4.2V aqueous hybrid electrochemical capacitor based on MnO_2 positive and protected Li negative electrodes*, *J. Power Sources* 241 (2013) 572–577.

- [13] Y. Jiang, J. Liu, Definitions of pseudocapacitive materials: a brief review, *Energy Environ. Mater.* 2 (1) (2019) 30–37.
- [14] V. Augustyn, P. Simon, B. Dunn, Pseudocapacitive oxide materials for high-rate electrochemical energy storage, *J. Energy Environ. Mater.* 2 (1) (2014) 30–37.
- [15] O. Fatin Saiha, Development of Metal Phosphate Incorporated Polyaniline Electrodes for Supercapattery/Fatin Saiha Omar, University of Malaya, 2018.
- [16] L.-Q. Mai, A. Minhas-Khan, X. Tian, K.M. Hercule, Y.-L. Zhao, X. Lin, et al., Synergistic interaction between redox-active electrolyte and binder-free functionalized carbon for ultrahigh supercapacitor performance, *Nat. Commun.* 4 (2013) 2923.
- [17] H. Wang, H.S. Casalongue, Y. Liang, H. Dai, Ni(OH)₂ nanoplates grown on graphene as advanced electrochemical pseudocapacitor materials, *J. Am. Chem. Soc.* 132 (21) (2010) 7472–7477.
- [18] K.C. Liu, M.A. Anderson, Porous nickel oxide/nickel films for electrochemical capacitors, *J. Electrochem. Soc.* 143 (1) (1996) 124–130.
- [19] B.E. Conway, *Electrochemical Supercapacitors: Scientific Fundamentals and Technological Applications*, Springer Science & Business Media, 2013.
- [20] P. Simon, T. Brousse, F. Favier, *Supercapacitors Based on Carbon or Pseudocapacitive Materials*, John Wiley & Sons, 2017.
- [21] V. Augustyn, J. Come, M.A. Lowe, J.W. Kim, P.-L. Taberna, S.H. Tolbert, et al., High-rate electrochemical energy storage through Li⁺ intercalation pseudocapacitance, *Nat. Mater.* 12 (6) (2013) 518.
- [22] M. Okubo, E. Hosono, J. Kim, M. Enomoto, N. Kojima, T. Kudo, et al., Nanosize effect on high-rate li-ion intercalation in LiCoO₂ electrode, *J. Am. Chem. Soc.* 129 (23) (2007) 7444–7452. Available from: <https://doi.org/10.1021/ja0681927>.
- [23] Y. Xia, T.S. Mathis, M.Q. Zhao, B. Anasori, A. Dang, Z. Zhou, et al., Thickness-independent capacitance of vertically aligned liquid-crystalline mxenes, *Nature* 557 (7705) (2018) 409–412.
- [24] M. Ghidui, M.R. Lukatskaya, M.-Q. Zhao, Y. Gogotsi, M.W. Barsoum, Conductive two-dimensional titanium carbide ‘clay’ with high volumetric capacitance, *Nature* 516 (7529) (2014) 78.
- [25] V. Augustyn, J. Come, M.A. Lowe, J.W. Kim, P.-L. Taberna, S.H. Tolbert, et al., High-rate electrochemical energy storage through Li⁺ intercalation pseudocapacitance, *Nat. Mater.* 12 (6) (2013) 518.
- [26] M. Zúcalová, M. Kalbác, L. Kavan, I. Exnar, M. Graetzel, Pseudocapacitive lithium storage in TiO₂ (b), *Chem. Mater.* 17 (5) (2005) 1248–1255.
- [27] T. Brezesinski, J. Wang, S.H. Tolbert, B. Dunn, Ordered mesoporous α -MoO₃ with iso-oriented nanocrystalline walls for thin-film pseudocapacitors, *Nat. Mater.* 9 (2) (2010) 146.
- [28] P. Simon, Y. Gogotsi, B. Dunn, Where do batteries end and supercapacitors begin? *Science* 343 (6176) (2014) 1210–1211.
- [29] J. Wang, J. Polleux, J. Lim, B. Dunn, Pseudocapacitive contributions to electrochemical energy storage in TiO₂ (anatase) nanoparticles, *J. Phys. Chem. C* 111 (40) (2007) 14925–14931.
- [30] P. Yu, C. Li, X. Guo, Sodium storage and pseudocapacitive charge in textured Li₄Ti₅O₁₂ thin films, *J. Phys. Chem. C* 118 (20) (2014) 10616–10624.
- [31] D. Chao, P. Liang, Z. Chen, L. Bai, H. Shen, X. Liu, et al., Pseudocapacitive na-ion storage boosts high rate and areal capacity of self-branched 2d layered metal chalcogenide nanoarrays, *ACS Nano* 10 (11) (2016) 10211–10219.
- [32] C. Yang, J. Feng, F. Lv, J. Zhou, C. Lin, K. Wang, et al., Metallic graphene-like VSe₂ ultrathin nanosheets: superior potassium-ion storage and their working mechanism, *J. Adv. Mater.* 30 (27) (2018) 1800036.

- [33] B. Conway, D. Kannangara, Zinc oxidation and redeposition processes in aqueous alkali and carbonate solutions ii. Distinction between dissolution and oxide film formation processes, *J. Electrochem. Soc.* 134 (4) (1987) 906–918.
- [34] T. Brousse, D. Bélanger, J.W. Long, To be or not to be pseudocapacitive? *J. Electrochem. Soc.* 162 (5) (2015) A5185–A5189.
- [35] Y. Gogotsi, R.M. Penner, *Energy Storage in Nanomaterials—Capacitive, Pseudocapacitive, or Battery-Like?* ACS Publications., 2018.

Conducting polymeric nanocomposite for supercapattery

Meenakshi Gusain¹, Irfan Ahmed^{1,2} and Yiqiang Zhan¹

¹State Key Laboratory of ASIC and System, Centre of Micro-Nano System, SIST, Fudan University, Shanghai, China

²Department of Physics, Government Postgraduate College, Mansehra, (Higher Education Department- HED) Khyber Pakhtunkhwa, Pakistan

4.1 Introduction to conducting polymers

Conducting polymers (C-polymers) are being fabricated and extensively investigated with the advancement in polymer science and related fields. By virtue of their high charge density and low-cost fabrication techniques, these materials have grabbed much research interest as well as the attention of industrialists around the globe. C-Polymers are organic moieties possessing alternate bonds (single and double) along the polymeric backbone chain forming delocalized electronic states, which are the origin of conduction in a polymer. These delocalized electronic states are advantageous for their best optoelectronic properties. However, conductivity in a polymer cannot arise only by conjugation, mostly doping is required for the appropriate and fast charge flow which enhances the charge transport properties. Similarly, other strategies like chemical manipulation, such as the nature of the dopant, degree of doping, and blending with various other polymers, are related modifications that are also employed [1]. The degree of doping is directly related to the main chain structure and varies from one polymer to another. The number of counteranions present per unit of monomer is termed as the doping degree. C-Polymers in their doped state are termed as intrinsically conducting polymers and their conductivity ranges from a few Scm^{-1} to 500Scm^{-1} [2]. These polymers undergo a redox reaction to accumulate charges which leads to an increase in energy storage capacity, and thus a reduction in self-discharge is observed [3]. The properties of C-polymers, such as

their fast charge–discharge kinetics, appropriate structural morphology, and quick doping and undoping methods, make them ideal candidate materials for use in various applications, such as electronics, optoelectronics, electromechanical devices, and chemical and biosensors [4–7]. C-Polymers with enhanced surface area and increased porosity offer good performances due to the presence of surface interactions along with high surface-to-volume contribution at nanoscale dimensions.

Shirakawa et al. discovered the first intrinsic C-polymers, named polyacetylene [8]. Since then the idea of implementing the properties of polymers with high electrical conductivity in the technological field increased exponentially. Following, the conductivity revealed by polyacetylene (PA), and other polymers like polythiophene (PTh), polypyrrole (PPy), and their related derivatives also confirmed conductivities even at higher temperatures [9]. C-Polymers, as mentioned earlier, are systems with highly pi-conjugated polymeric chains. Many structural moieties such as polyacetylene (PA), polyaniline (PANI), polyphenylene (PPh), and poly(phenylene) vinylene (PPV) have been explored with similar attributes of electrical conductivities [10,11]. The value of the band gap of C-polymers exists in the range of 1.5–3.0 eV, so these materials are termed as organic semiconductors as well. Methods used to measure the value of band gap using (1) the band edge wavelength of absorption spectra and (2) oxidation and reduction potentials measured from the study of electrochemical cyclic voltammetry. For electrode formations polymer need to dissolve and blend properly in some relevant solvent, however, the C-polymers are insoluble by nature. By linking appropriate substituents in the side chain of conjugated polymers their solubility in organic solvents can be increased. For example, polythiophene cannot be soluble in any solvent, however the hexyl-substituted derivative of polythiophene (P₃HT) can easily solubilize in organic solvents like dichlorobenzene, chlorobenzene, toluene, etc.



4.2 Types of C-polymers

The chain of the main structural backbone of C-polymers is formed with polymers mentioned in Fig. 4.1. The substitution of the side chain into the main structural backbone of C-polymers leads to the origin of various other derivatives, for example, poly(3-alkylthiophene) from thiophene, etc.

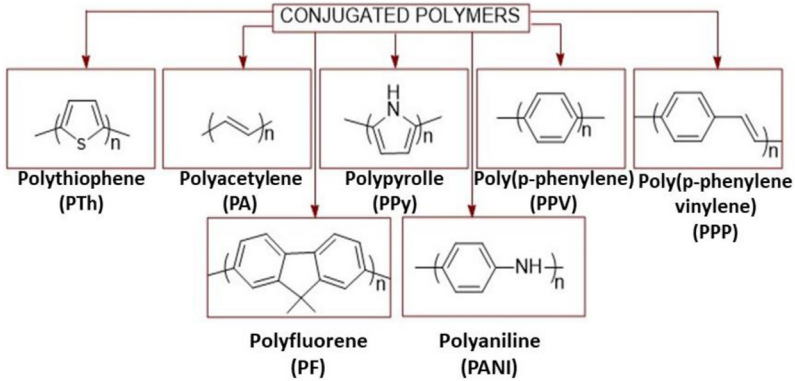


Figure 4.1 The chain of the main structural backbone conjugated polymer, which is divided into various types of distinct structures.

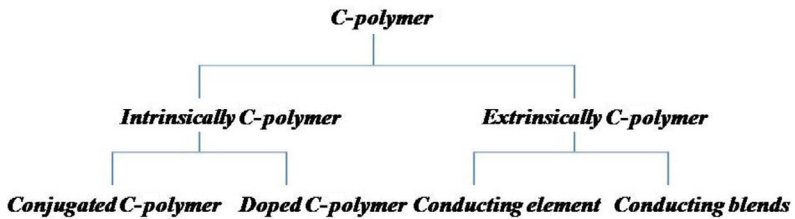


Figure 4.2 The diagram shows the classification of C-polymers into intrinsic and extrinsic conducting polymers.

Although various C-polymers were synthesized and investigated by researchers, polyaniline (PANI), polyacetylene (PA), polythiophene (PTh), and polypyrrole (PPy) have been explored enormously and are considered to show good combinations of properties like conductivity, ease of synthesis, and long-term stability.

These polymers can be categorized in various modes depending upon the approach used for their classification. The first approach is based on the reason for the conductivity and the second approach used for the classification of polymer is the nature of the structural backbone.

4.2.1 Based on conductivity

Based on the conductivity approach, C-polymers may be classified as intrinsically C-polymers and extrinsically C-polymers, as shown in Fig. 4.2.

4.2.1.1 Intrinsically conducted polymer

Conductivity in C-polymers is attributed to the presence of conjugation in the structural backbone of a polymer. The conjugation in polymer is attributed to π electrons as well as by doping with other elements. Intrinsically C-polymers consist of conjugated π electrons due to the presence of a double bond or lone-pair of electrons in their structure. These lone pairs are the origin of the formation of valance and conduction bands throughout the polymer backbone chain. The electrical conductivity in polymers requires absorption of activation energy either thermally or photochemically. These polymers can also be doped with a Lewis acid or Lewis base, developing positive and negative charge, respectively, and causes conductivity in the polymer known as a doped C-polymers. When a conjugated polymer is treated with a Lewis acid, oxidation occurs, creating a positive charge in the polymer. The delocalization of positive charge causes electrical conductivity and the polymer is termed as *p*-doped C-polymer. When a conjugated polymer is treated with a Lewis base, reduction occurs, creating negative charge in the polymer. The delocalization of negative charge causes electrical conductivity and the polymer is termed as *n*-doped C-polymers.

4.2.1.2 Extrinsically conducted polymer

Extrinsically conducted polymer achieves conductivity by the addition of an external element or by making blends. Similarly, to enhance their conductivity, the incorporation of carbon black, metal oxides, and metallic fibers into the polymer has been extensively studied [12]. This leads to an increase in surface area, more porosity, and creates a filamentous nature, hence the conducting properties of C-polymers are enhanced.

4.2.2 Based on structural backbone

Regarding this approach the classification of C-polymers is based on their monomer structure backbone and consists of:

4.2.2.1 Noncyclic C-polymers

In this category, polymer consists of only double bonds and no aromatic moieties in the chain, such as polyacetylene.

4.2.2.2 Aromatic C-polymers

This polymer has an aromatic ring in its backbone, such as poly(*p*-phenylene) and its derivatives.

4.2.2.3 Polyheterocyclic C-polymers

This type of polymer has a heterocyclic group in the polymer backbone, for example, polythiophene (PTh), polypyrrole (PPy), and their derivatives.

The employment of pure C-polymers opened a new era of research for the best electrochemical performances, especially in flexible type supercapacitors. Likewise, PANI, PPy, PTh, PEDOT, and other C-polymers have been extensively investigated in the last few decades [4]. These polymers have exhibited outstanding values for maximum theoretical specific capacitance (1000 Fg^{-1} ; $100\text{--}400 \mu\text{F cm}^{-2}$) that is higher (two times) than the value for electrical double layer capacitors (EDLC) [13]. During charging and discharging cycles the mechanism of energy storage in C-polymeric capacitors is of pseudo type where a quick and reversible redox reaction (faradaic) occurs not only at the surface but also in the bulk material of the electrode as well. However, in EDLC there is a mechanism of electrostatic ionic interaction of the electrode's surface when the electrolyte is present. Although the kinetics of pseudocapacitors are relatively slower, they still have the ability to store higher capacitance per unit gram of material compared to their counterpart (EDLC) [14]. The performance of a few C-polymeric supercapacitors is shown in Table 4.1 (interested readers please refer to the articles [14,15]).



4.3 Problems related to conducting polymers based electrodes

C-polymers are the most extensively employed material for electrodes in supercapacitors and capable of bringing new opportunities by introducing the synergistic effect when their composite is used. C-polymers attain excellent properties like good conductivity, are comparatively less costly, show good environmental stability, facile synthesis, and flexibility, which make them promising pseudocapacitive candidate materials for such electrodes [14]. However, there are some potential problems associated with C-polymers in their pure form such as: (1) poor cyclic stability after a few charge-discharge cycles [16]; (2) low charge-discharge rate (low power) due to suppressed ionic diffusion into bulk of electrode [17]; (3) lack of mechanical stability associated with shrinkage and swelling of structure during doping-undoping mechanism [18]; and (4) lower

Table 4.1 Electrochemical performance of electrode fabricated by C-polymers for supercapacitors. The representation of parameters like specific capacitance, cyclic stability, energy, and power density of various C-polymer electrodes used in supercapacitors.

C-polymers electrode materials		Specific capacitance	Cyclic stability	Energy density	Power density
PPy	PPy	100 Ah kg ⁻¹	—	—	—
	Columnar PPy	95 mF cm ⁻² & 60 F cm ⁻³	—	—	—
	PPy hydrogel	380 F g ⁻¹ & 6.4 F cm ⁻²	—	—	—
	PPy nanosheets	547 F g ⁻¹	—	—	—
	PPy nanowires	282 F g ⁻¹ at 1 A g ⁻¹	—	31.8 Wh kg ⁻¹ at 1 A g ⁻¹	—
PANI	PPy nanowires array	566 F g ⁻¹	70% retention after 300 cycles	—	—
	PANi nanowhiskers	—	5% loss after 3000 cycles at 5 A g ⁻¹	—	—
	Nanofibrous PANi	609 F g ⁻¹ at 1.5 mA cm ⁻²	1000 cycles	26.8 Wh kg ⁻¹ at 1.5 mA cm ⁻²	—
	PANi nanowires	818 F g ⁻¹ at 1 mA cm ⁻²	1500 cycles	68 Wh kg ⁻¹ at 1 mA cm ⁻²	—
	Aligned PANi nanowires arrays	Max 950 F g ⁻¹ & 780 F g ⁻¹ at 40 A g ⁻¹	—	—	—
	LiPF ₆ -PANi	—	5000 cycles at 2 mA cm ⁻²	—	—
PEDOT	DMS-PANi	115 F g ⁻¹	5000 cycles at 2.5 mA cm ⁻²	—	—
	PEDOT	56 F g ⁻¹	1000 cycles	—	—
	PEDOT nanotubes	150 F g ⁻¹	—	5.6 Wh kg ⁻¹	25 kW kg ⁻¹
	PEDOT nanofibers	—	10,000 cycles at 2 mA cm ⁻²	—	—

Other C-polymers	PFPT	—	8000 cycles at 3.3 Wh kg ⁻¹	48 Wh kg ⁻¹	9 kW kg ⁻¹
	PcDT	70 F g ⁻¹	—	6 Wh kg ⁻¹	1 kW kg ⁻¹
	PMeT	28 F g ⁻¹ at 40 mA cm ⁻²	—	30 Wh kg ⁻¹ at 5 mA cm ⁻²	0.5 kW kg ⁻¹ at 5 mA cm ⁻²
	p-PMeT	230–260 F g ⁻¹ at 24–8 mA cm ⁻²	—	—	—
	PDTT	—	1000 cycles	—	—
	PDTDA	270 mA h g ⁻¹ at 0.7 mA cm ⁻²	—	675 Wh kg ⁻¹ a 0.7 mA cm ⁻²	—
	PDAAQ	36–136 F g ⁻¹ (aq.) & 45–50 Ah kg ⁻¹ (PVA)	—	25–46 Wh kg ⁻¹ at 90–30 C	10.2–30.5 kW kg ⁻¹

The table is drawn with permission of Z. Wang, et al. Polymers for supercapacitors: boosting the development of the flexible and wearable energy storage, Mater. Sci. Eng. R: Rep. 139 (2020) 100520. <https://doi.org/10.1016/j.mser.2019.100520>.

conductivity in few C-polymers compared to their doped and composite form. These drawbacks have hindered their development to a fully commercialized form (Fig. 4.3). In order to enhance and uprate their employment as electrode material, researchers have focused on various aspects, such as increasing the porosity by surface modifications, introducing interconnected porous nanostructures that lead to their enhanced cyclic stability, and mechanical robustness with better flexibility and power density [14,19]. Likewise, with innovation in the field of flexible supercapacitors, free-standing C-polymeric, hydrogel, and doping methods are also used for enhanced conductivity and to achieve superior electrochemical performance [17,20].

In order to overcome the shortcomings in C-polymers, various modifications in terms of binary and ternary composites with carbon and metal oxide reinforcements have been extensively researched to improve their electrochemical performances along with enhanced stability in supercapacitors [21]. The process of synthesis of various C-polymeric composites electrodes and their related research progress for supercapacitors is discussed in Section 4.4. Fig. 4.4 details the comparison of various materials used as electrodes in supercapacitors with respect to their electrochemical parameters, like specific capacitance (Fg^{-1}), current density (mAg^{-1}), and cyclic stability [22]. The C-polymer-based electrodes showed better specific capacitance, which is increased when their carbon composite structures are used; this is a clear indication of a synergetic effect. Similarly, the composite materials, like MXene, showed superior current density with

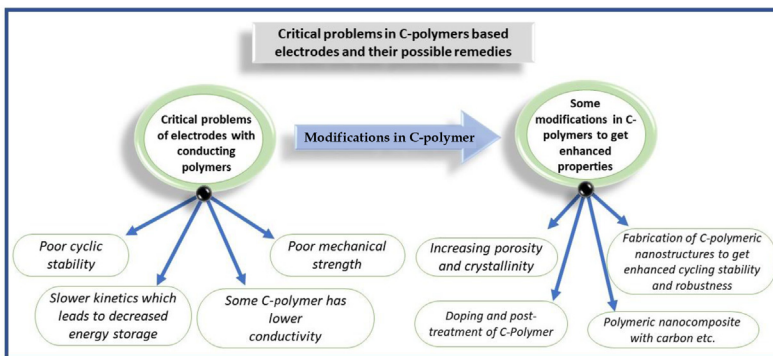


Figure 4.3 Some critical issues related to C-polymers in terms of their use as electrodes in supercapacitors. There are some modifications in C-polymers for possible solutions to related problems.

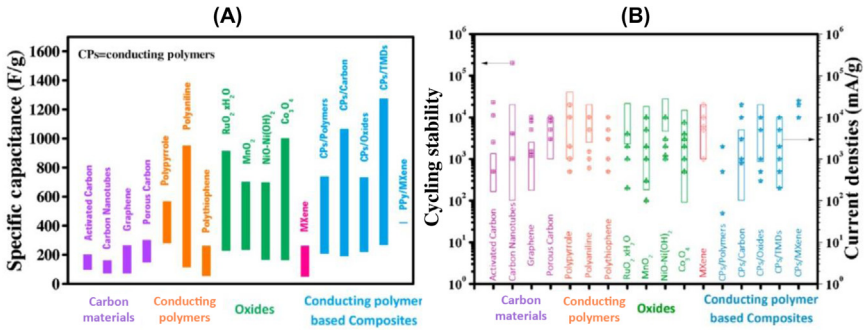


Figure 4.4 A detailed comparison of different electrode materials (carbon, C-polymers, oxide, and C-polymer composites) used for supercapacitors according to various parameters: (A) comparison in terms of specific capacitance; (B) a detailed comparison in terms of cyclic stability and current densities. *The figure is drawn with the permission of Z. Wang, et al., Polymers for supercapacitors: Boosting the development of the flexible and wearable energy storage, Mater. Sci. Eng. R: Rep. 139 (2020) 100520. <https://doi.org/10.1016/j.mser.2019.100520>.*

enhanced cyclic stability (Fig. 4.4), which is a clear evidence of a research direction where there is plenty of room available in terms of improvement in power density and stability.



4.4 Polymer nanocomposite

Nanocomposites are a unique category of composite formed by the combination of two or more constituents, in which one of the dispersed phases is found in the nanometer range. Because the dimension of the phases involved is in nanometer, so the term “nano” is included before the composite. Compared to conventional macrocomposite material, nanocomposites, due to their smaller size and enhanced surface-to-volume ratio, offer new behaviors and functionalities. The composites with nanoparticles dispersed in the polymeric matrix are termed polymer nanocomposites. The properties of polymer nanocomposites can be greatly improved by forming composites of C-polymers with other materials such as carbonaceous, chalcogenides, metal oxides, clays, etc. Inorganic nanoparticles with different sizes of various morphologies produce nanocomposites with extraordinary physical properties that are used

for various applications. Various synthetic methods have been introduced for synthesizing polymer nanocomposites. Depending on the process of fabrication and strategy of synthesis, the polymeric nanocomposites comprise two classes termed as (1) in situ synthesis and (2) ex situ synthesis.

4.4.1 In situ synthesis

In in situ synthesis, growth of one component is done in the presence of its counterpart leading to the formation of the nanocomposite. Therefore the in situ synthetic procedure for the synthesis of nanocomposites forms an efficient interfacial interaction between the components used. Polymerization by the in situ oxidative method of C-polymers using chemicals in the presence of metal chalcogenide is the best used method to form metal chalcogenides–polymer nanocomposites. In the typical procedure, monomers of polymer and other constituents are dispersed into the solvent followed by the addition of oxidant solution to the dispersion and the polymerization of the monomer initializes. The morphology of the nanocomposite can be controlled by tuning various conditions, such as (1) monomer concentration, (2) the temperature as well as total time of the reaction, (3) oxidant amount and dopant concentration, and (4) the molar ratio versus oxidant ratio to the monomer [23].

4.4.2 Ex situ synthesis

In the ex situ synthetic approach the component and its counterpart are synthesized separately, followed by dispersion in a solvent using mechanical stirring or ultrasonication, and then hybridization is achieved by a combination of the two components. This procedure requires a longer time duration and involves multiple steps to achieve the final nanocomposite. The structure of the monomer and the size and morphology of the constituent components are already defined. Electrophoretic deposition (EPD) is a famous method used to prepare these nanocomposite films [24].

Following are the three types of polymer nanocomposites discussed in this section:

1. Carbonaceous–polymer nanocomposite
2. Chalcogenide–polymer composite
3. Layered silicates–polymer nanocomposite

4.4.3 Carbonaceous–polymer nanocomposites

To date, much research work has been done on energy storage materials and related applications [25–27]. However, unlike traditional energy storage batteries which have drawbacks such as toxicity, low lifetime, explosion risk, and high cost, supercapacitors possessing large power densities have been successfully explored [27]. But there is a dire need to significantly improve the power density, cyclic-life stability, and safety of the present class of supercapacitors to fulfill their increasing demands in a broad range of electrical and electronic applications. Developments in new electrode materials along with new electrolyte with superior properties are highly essential. The performance of a supercapacitor depends primarily on five parameters: (1) work voltage; (2) specific energy; (3) specific capacitance; (4) power density; and (5) life cycle [28]. The preparation of efficient electrode materials with superior performance and good electrical conductivity is the focused research topic of various supercapacitor research groups [29,30]. The capacitance of a supercapacitor can be calculated from the mathematical relation:

$$C = (A\varepsilon_0)/d, \quad (4.1)$$

where A , ε_0 , d , and C represent the electrode area, material's dielectric constant in free space, the thickness of dielectric material, and the capacitance of final device, respectively. Increased surface area and long-term cyclic stability are the important parameters for the best performance of electrodes. As a result, for an easy and efficient movement of electrolyte ions through electrode material, pore size and specific porosity are the important factors that need to be addressed. To increase effective surface area and other related properties, various morphological nanostructures such as 0D, 1D, 2D, and 3D (D represents dimension) are widely used in electrodes for supercapacitors [31]. Mesoporous material with pore size ranging from 2–50 nm is considered as suitable for high double-layer capacitance. Being a suitable candidate for electrode material, mesoporous carbon has gained great interest for its excellent performance in supercapacitors [32]. The exceptional properties of carbon, such as its natural abundance, good electronic and thermal conductivity, electrochemical, chemical, and thermal resistance, low cost, and lightweight, etc. make it a promising electrode material for EDLC [33]. Various carbonaceous morphologies, such as activated porous carbon, single-walled carbon nanotubes, multiwalled carbon nanotubes, carbon nanofibers, carbon

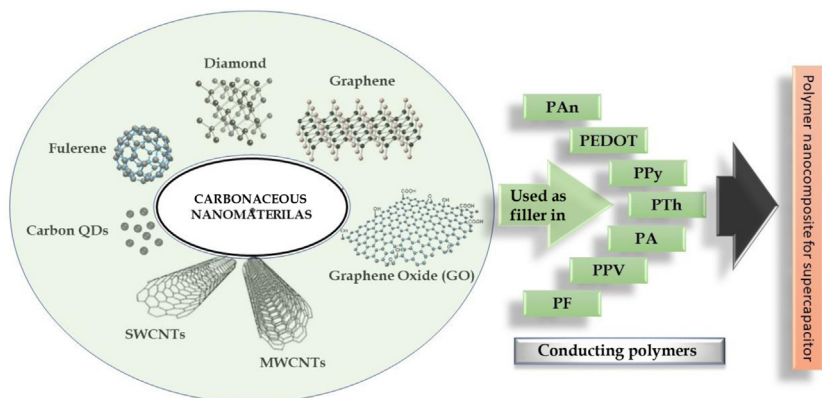


Figure 4.5 The representation of various morphologies of carbonaceous nanomaterials used as filler in matrices of different types of C-polymers to make nanocomposites. These nanocomposites are employed as electrode material for supercapacitors.

nanospheres, graphene, and graphene oxide are the novel materials of this century. Due to their intriguing properties such as high surface area, excellent environmental stability with long shelf-life and long cycle-life, exceptional electrochemical and thermal properties, these materials are mostly studied in supercapacitors [34,35]. Apart from the use of pure nanostructure material as an electrode, another approach for superior performance in supercapacitors is the employment of various nanocomposites where nanostructured material is used as filler in the C-polymeric matrix. A synergistic effect due to the overall combination of properties of constituent components is achieved. For example, C-polymers attain good mechanical and electrical properties and are used as a matrix for the incorporation of different carbonaceous nanomaterials which hold good electrical properties, so the properties of the overall composite is enhanced by the combination of both characteristics of the polymeric matrix and incorporated nanomaterial (Fig. 4.5) [36]. Carbonaceous C-polymer composite materials basically make improvements in the mechanical and electrical properties which are essential for the commercialization of these materials as electrodes in supercapacitors.

4.4.4 Chalcogenide–polymer nanocomposite

Metal chalcogenides have gained huge attention in the past few decades from researchers exploring their industrial applications. Properties of metal

chalcogenides can be altered either by quantum confinement effect or hybridization with other materials in order to improve their properties or incorporate some new attributes in them. The various approaches adopted are intercalation, composite fabrication, alloying, etc. to be exploited in diverse application such as electronics, optoelectronic devices, biosensors, energy storage, and biomedicines [37,38]. A composite of metal chalcogenides with C-polymers is always an interesting approach to engineer properties for electronic applications [39–41]. For application as an electrode material in an electrochemical cell, along with transition metal dichalcogenide, metal oxychalcogenides have also been explored. The nanocomposite of transition metal chalcogenides sheets with C-polymers overcomes the low electrical conductivity of chalcogenides, and similarly the sheet structure of chalcogenides provides space for ion storage and fast faradic redox reaction [42,43]. Polyaniline is one of the widely explored C-polymers and its modified nanocomposites with metal chalcogenides has been studied for the best electrochemical performance in supercapacitors. This composite showed enhanced electrochemical activity, improved electrical conductivity and long-term life cycle stability as compared to their pure counterpart (PANI) [34]. MoS₂/PANI has been very well explored in different ways in order to get enhanced supercapacitor performance [13,14,44,45]. A polymer has low thermal stability interrupting its use for higher temperature applications. However, their composite form showed enhanced thermal and mechanical stability [46]. Likewise, Ajibade et al. employed metal sulfide NPs in PMMA, and the particles retained their morphology and properties, as the retention of important properties reflects their positive synergic effect. A synergic effect between the matrix (PMMA) and incorporated NPs particles was observed, resulting in a combination of functionalities [47]. The major objective of the synthesis of these nanocomposites in terms of flexible energy storage devices, is to prepare a material that holds exceptional transparency and thermal stability with a retention of mechanical properties.

4.4.5 Polymer/layered silicates nanocomposite

Layered silicate nanocomposite has been studied by various researchers as a potential material for supercapacitors. Layered silicates have been known for the past 50 years following the study done by Bower

describing the absorption of DNA by montmorillonite [48]. The following years expanded the research of nanocomposites formed by montmorillonite with polymers such as polyvinyl and polyvinyl alcohol [49,50]. Phyllosilicates belong to the general class of (2:1) layered silicates and are famous for their common use in the preparation of nanocomposites. The structure of layered silicate consists of two-dimensional layers with alumina or magnesia in octahedral coordination sharing oxygen with two silica units in tetrahedron coordination [51]. These layers have inter-layer spacings where each layer stacks on one another through van der Waals forces. Ionic replacement within the layers by another ion of the same size without disturbing the structure generates a negative charge on the surface of these layers which is then counterbalanced by the alkali or alkaline earth metal cations that reside in the interlayer spacings. A layered silicate has two leading attributes which facilitate in building the nanocomposite. First, their capability of easy dispersion into constituent individual layers due to the presence of weak van der Waal forces in between the layers. Secondly, their tendency of varying surface chemistry by ion-exchange methods via organic as well as inorganic cations. The presence of hydrated Na^+ and K^+ ions in layered silicates make them readily soluble in hydrophilic polymers, such as poly(vinyl alcohol). Ion-exchange reactions with cations such as alkylammonium or alkyl phosphonium cation modify pristine layered silicates into organophilic silicate surface allowing them to be miscible with other polymer matrices [52–54].

The preparation method of the layered silicate/polymer nanocomposite can lead to three different situations depending upon the nature of silicates, cation, and polymer matrix as represented in Fig. 4.6 [55–57]. The blending of polymer in silicates may result in the separation of both the phases resulting in poor mechanical and thermal properties (Fig. 4.6(A)). Conversely, complete dispersion of polymer and silicate can also take place which results in unique properties that are not shared by their individual counterparts. The complete dispersion can cause either exfoliation of silicate layers losing the layering of the silicate structure dispersed uniformly in the polymer (Fig. 4.6(C)) or ordered morphology with polymer and layered silicate retaining layering in silicate structure (Fig. 4.6(B)).

The aim of incorporation of layered silicates in conducting polymer matrix leads to the highly porous structure boosting the electroactive surface in the resulting composite material. This makes smooth access for

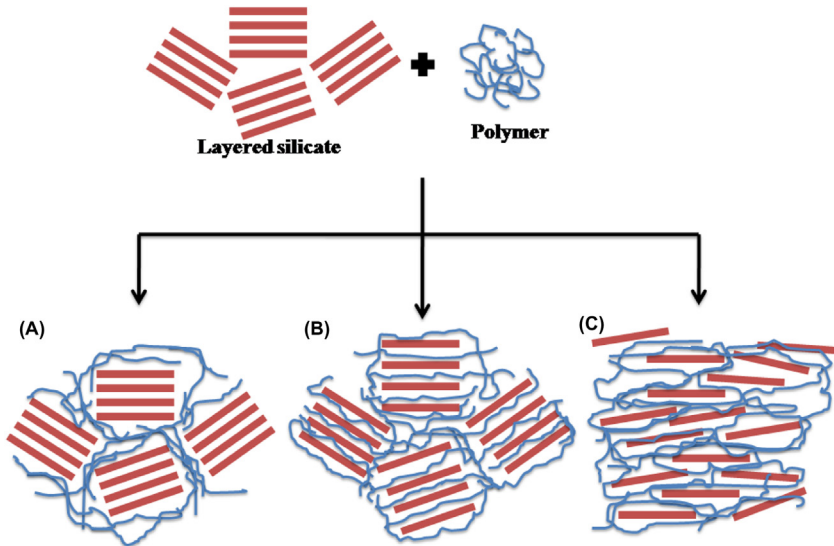


Figure 4.6 Schematic presentation of nanocomposite arises from interaction of layered silicates and polymers: (A) phase separated; (B) intercalated; and (C) exfoliated nanocomposites.

electrolytic ions facilitating the charge storage capacity of the electrode material used in the supercapacitor.

4.5 Nanocomposites of conducting polymer with various nanomaterials

4.5.1 Carbon-based nanocomposite materials

There is excellent proof of the synergetic effect showed by carbon-based nanocomposite materials when employed as an electrode in supercapacitor. These composites are composed of carbonaceous materials such as CNTs, graphene, carbon nanofillers, and activated carbons, which are incorporated in the matrix of the C-polymer [22,58–60]. To overcome the intrinsic drawbacks of C-polymers (refer to Section 4.3), carbon-based composites not only provide strong mechanical support by suppressing the degradation processes in the electrode but also increase their charge transport properties. The mechanical degradation process in the electrode is due to the volumetric change during the cyclic processes of the

charging–discharging state. Also, the carbon-based nanostructures such as 0D, 1D, and 2D morphologies provide nucleation sites for the growth of C-polymer which enhances the porosity of composites structure and improvement in ionic migration has been recorded as a result. Recently, Shiyu Ji et al. showed superior electrochemical performances of different types of electrodes prepared by the composite of PPy with carbon structures like carbon black, CNTs and electrochemical exfoliated graphene (EEG). Electrodes prepared by PPy/EEG nanocomposite showed superior behavior with the highest specific capacitance of 348.8 Fg^{-1} at a current density of 0.5 mAcm^{-2} . These electrodes retained their capacity of more than 90% after 5000 cycles [59]. Similarly, a free-standing architecture in the electrode was prepared by using PPy nanoparticles with functionalized CNTs that showed enhanced aerial capacitance (4585 mFcm^{-2}), aerial energy ($129.24 \text{ } \mu\text{hcm}^{-2}$), and power density (12.5 mWcm^{-2}). This free-standing composite electrode showed superior cyclic stability and retained its cycle-life stability up to $\sim 79\%$ after 10,000 charging–discharging cycles [61]. Flexible devices are of much importance in portable and wearable storage device applications. A directional electrospinning strategy was introduced in which CNTs and CNPs were first electrospun using PVA and PAA followed by a coating of C-polymer (PANI). This nanocomposite architecture, when used for flexible electrode, showed excellent tensile strength ($\sim 54.8 \text{ MPa}$) and the best specific capacitance (164.6 Fg^{-1}). This electrode retains its performance up to $\sim 90\%$ after 2000 cycles under various flexibility tests (bending, twisting, and deformation) [62]. The demonstration of the excellent electrical capacitance of PANI-CNT nanocomposite was recently shown by Wang Zhang et al., in which cyclodextrin polymer (CDP)-assisted CNTs were coated with a C-polymer, PANI (Fig. 4.7). The extraordinary specific capacitance (720 Fg^{-1} at 1 Ag^{-1}) with cyclic stability of retention up to 97% capacitance value at 5000 cycles has been achieved [63].

Other carbon-based nanostructures, like carbon sponges, carbon fibers, and mesoporous carbon, which attain high conductivity and increased surface area, are used with C-polymers resulting in composite materials with a synergic effect with enhanced mechanical and electrical characteristics. These research findings showed that the fabrication of electrodes for supercapacitors using carbon-based C-polymer composite is an effective approach to get good electrochemical and mechanical properties as well as good cycle stability.

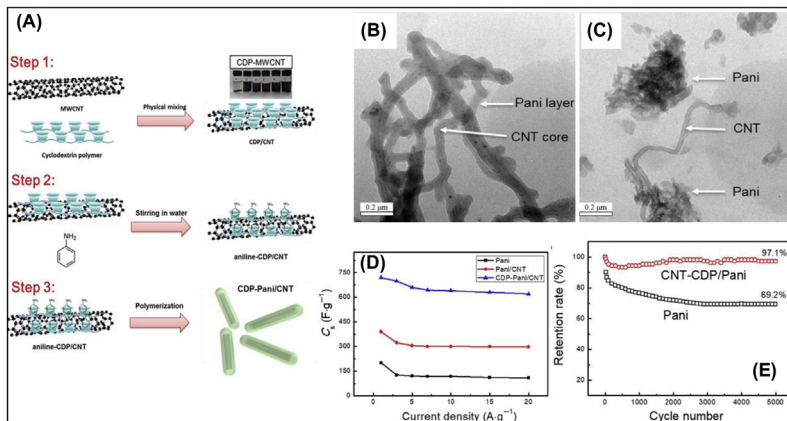


Figure 4.7 The representation of CDP-CNT/PANI nanocomposite showing superior electrochemical performance. (A) Fabrication steps of CDP-CNT/PANI nanocomposite; (B,C) the TEM images of CDP-PANI CNT and PANI CNT, respectively; (D) comparison of specific capacitance of three in which the CDP-PANI showed the highest value; (E) a comparison of the cyclic stability of CDP-PANI /CNT and pure PANI devices measured at constant current (0.5 Ag^{-1}) in which the former showed retention of 97% capacitance after 5000 cycles. The figure is drawn with permission of W. Zhang *et al.*, *Supramolecule-assisted synthesis of cyclodextrin polymer functionalized polyaniline/carbon nanotube with core-shell nanostructure as high-performance supercapacitor material. Electrochim. Acta* 331 (2020) 135345. <https://doi.org/10.1016/j.electacta.2019.135345>.

4.5.2 Metal oxide-based composites materials

Metal oxide composites with C-polymers have been explored extensively to exploit the advantages of both materials. Metal oxides have many unique properties which can be exploited for high-energy storage capacitors with long-term application. The composites of metal oxide with C-polymers enhances electrical conductivity, and good stability in the acidic environment can be achieved in composite form.

Holze *et al.* studied composite electrodes prepared with a wide range of metal oxides, such as MnO_2 , RuO_2 , TiO_2 , CuO , CoO , WO_3 and V_2O_5 in C-polymers [64]. To achieve better life-cycle stability and improved energy storage ability of electrode material, a ternary composite system has been investigated, in which, other than metal oxides and C-polymers, a third component, i.e., carbon, or its derivative forms have been studied. The ternary architecture explored by various researchers are PANI/ MnO_2 /graphene composites, PANI/GO/ MnO_2

nanocomposites and graphene/PEDOT/MnO₂ nanocomposites [65–67]. RuO₂/PEDOT composite was successfully studied by Liu et al., where increased active surface area and shorter ionic diffusion length are the possible reasons for enhancement in overall electrochemical performance. An increased specific capacitance of 1217 Fg⁻¹ for RuO₂/PEDOT composite was achieved [68]. Composite material of RuO₂ with PPy using a sputtering deposition method showed a specific capacitance of 302 Fg⁻¹ [69]. However, Cho et al. developed a screen-printed electrode system composed of RuO₂ with PEDOT:PSS by electrostatic stabilization resulting in the achievement of a large specific capacitance of ~820 Fg⁻¹ [70].

The most explored composites are of MnO₂, with different C-polymers such as PANI, polythiophene, and polypropylene exploited for supercapacitor electrode material. Thin-film composite of MnO₂ nanoparticle with PANI nanorods exhibited a specific capacitance of the value 415 Fg⁻¹ at 1000 cycle stability [71]. Coaxial nanofiber of PANi-MnO₂ exhibited a specific capacitance of 383 Fg⁻¹ with improved stability [72]. Polythiophene/MnO₂ nanocomposite studied by Lu et al. demonstrated a specific capacitance of value 290 Fg⁻¹, ascribed to its increased surface area [73]. Besides binary composites, ternary composites with three constituent materials are gaining much attention due to their outstanding performances. Especially C-polymer/carbon/metal oxide is considered as the most proven ternary composite due to their synergistic effect of best conductivity and pseudocapacitance rendering enhanced energy storage capacity. A ternary composite of PEDOT with graphene and MnO₂ extended the utility toward flexible supercapacitors, as designed by Moussa et al. [66]. The sponge pore surface of graphene platelets offers stretchability along with an enhanced specific capacitance of 802.99 Fg⁻¹ in the ternary composite (Fig. 4.8).

4.5.3 MXene and transition metal dichalcogenides composites

No doubt, to fulfill the requirements of modern development and technologies, the current research direction for energy storage devices is shifting toward more exceptional energy materials for efficient energy power density as compared to traditional materials, and 2D graphene used in electrodes for supercapacitors. These new emerging classes of materials are transition metal carbides (known as MXene) and transition metal

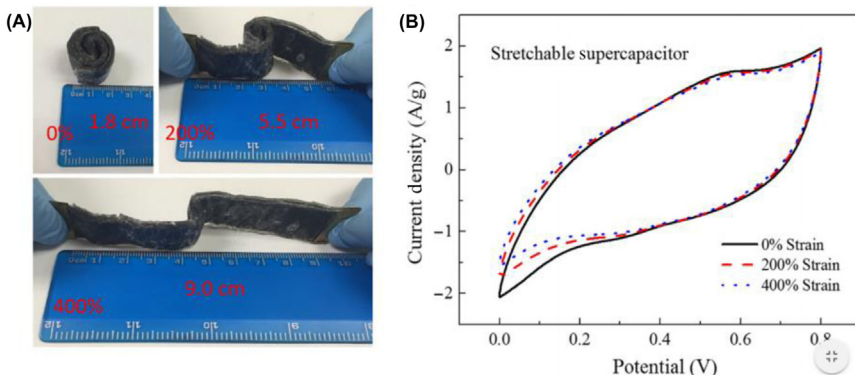


Figure 4.8 The stretchable supercapacitor of graphene/PEDOT/MnO₂ sponge ternary nanocomposite (A) at different values of strains, and (B) with corresponding cyclic voltammetry (CV) graphs at maximum 20 mV s⁻¹. The figure is drawn with permission by M. Moussa et al., 'Development of flexible supercapacitors using an inexpensive graphene/PEDOT/MnO₂ sponge composite', *Mater. Des.* 125 (2017) 1–10.

dichalcogenides (TMDs). MXene are 2D materials, with carbide and nitride first synthesized by US scientists at Drexel University in 2012 [74]. MXenes are a large family of materials represented by the formula of M_{n+1}AX_n, where M represents a transition metal, A represents a group of elements (Al, Si, P, S, Ga, Ge, As, Cd, Ln, Sn, Tl, Pb), and X represents C or N. Owing to their exceptional electronic properties these materials were also extensively investigated as composites with C-polymers for electrochemical energy storage devices [75,76]. For example, Jianjian Fu et al. reported that graphene-encapsulated MXene (Ti₂CT_x) with polyaniline composite (GMP) showed enhanced electrochemical performance [75]. The electrodes achieved capacitance of 635 Fg⁻¹ at the current density of 1 Ag⁻¹ with retention in its capacitance value up to ~98% after 10,000 cycles. This showed a superior cycle stability of these electrodes. The outstanding properties of materials incorporated like graphene with its robustness and chemically inert nature and highly conductive nature of both PANI and MXene material represented a synergic effect of all when used in combination for electrodes in supercapacitors. Similarly, Boota et al. reported the best cycle stability and electrochemical performance of MXene with PPy composite. In a typical process the author studied in situ polymerization of C-polymer (PPy) with MXene (Ti₃C₂T_x) that showed better nanostructure architecture of intercalated MXene

nanosheets with confined PPy polymeric chains that resulted in excellent ionic diffusion and charge transport properties, and hence delivered the best volumetric capacitance (1000 Fcm^{-3}). The electrode showed exceptional cycle stability after 25,000 cycles with the retention of 92% capacitance value [76]. A newly developed thin and optically transparent microsupercapacitor which has a color changing property, prepared using MXene/PEDOT nanocomposite, showed five-fold enhanced aerial capacitance compared to its pure counterpart (MXene). Direct fabrication of a MXene/PEDOT microsupercapacitor was done by an automated scalpel lithographic technique with an aerial capacitance of 2.4 mFcm^{-2} at a scanning rate of 10 mVs^{-1} which is a higher value as compared to its pure MXene counterpart (0.4 mFcm^{-2}) at the same scan rate [30] (Fig. 4.9). Although MXene showed superior electrochemical performance when used as material for electrodes in supercapacitor, there is still huge room for improvement available by altering the properties of surface terminated functional groups and also with more focus on their layered morphology along with the tuning of interlayer spacing of MXene. This modification will enhance their electrochemical performance as compared to pure MXene and other candidate materials.

Likewise, TMDs, including WS_2 , TiS_2 , MoSe_2 , MoS_2 , NbS_2 , and VS_2 , attain superior properties like more reactive surfaces and the presence of coordination sites [77]. These TMDs are a normally metallic and highly conductive class of materials generally represented by TMX_2 where transition metal and chalcogen are represented by TM and X, respectively [77]. Besides their use in various other applications like biomaterials, sensors, and electronics, TMDs are widely studied as emerging materials for electrochemical energy storage and conversion applications. TMDs attained much research focus due to the presence of 2D layered structures analogous to graphene and hold diverse electronic properties ranging from insulators, semiconductors, semimetals, and metals. Incorporation of chalcogenides in C-polymers increases the high electrical conductivity, and mechanical flexibility with tunable properties is observed [78]. Similarly, 2D TMDs have an exceptional edge with a surface for both Faradaic and non-Faradaic processes which are relatively faster than other conventional electrode materials like graphene and bulk TMDs [77]. The nanoporous morphology exhibits improved physical properties and electrochemical performance when used as electrode materials for a supercapacitor. Two electrodes

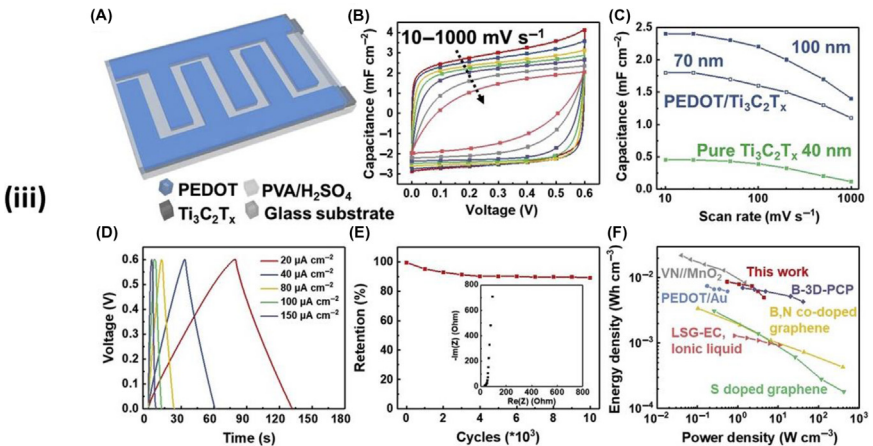
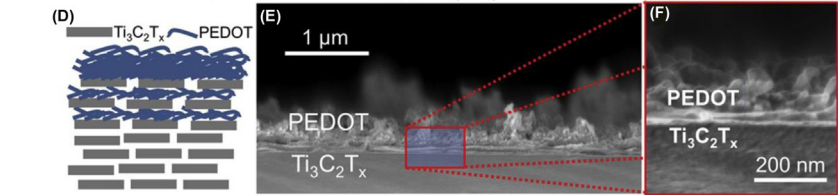
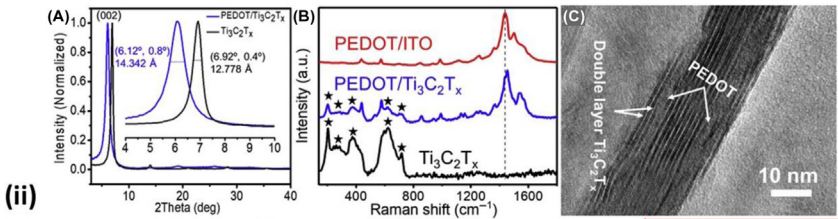
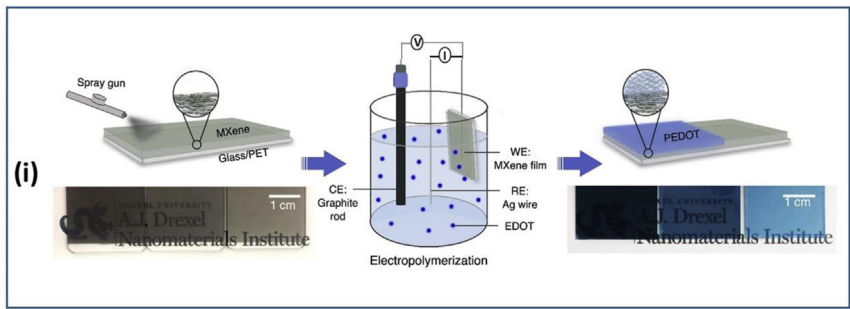


Figure 4.9 A direct fabrication electrode for microsupercapacitors prepared with MXene ($\text{Ti}_3\text{C}_2\text{T}_x$) with PEDOT and their various morphological characterizations and electrochemical performance. (i) schematics of deposition of this hybrid nanocomposite by sequential process of spraying MXene followed by electrochemical deposition of PEDOT; (ii) detailed structural and morphological characterizations of composite layers; (iii) electrochemical performances of the fabricated electrode including capacitance at various scan rate, cycle stability, Ragone plot, etc. *The figure is drawn with permission of J. Li, et al. MXene-conducting polymer electrochromic microsupercapacitors. Energy Storage Mater. 20 (2019): 455–461. <https://doi.org/10.1016/j.ensm.2019.04.028>.*

architecture was used by Kumar Das et al., where a positive electrode with nanoporous structure of NiSe prepared by selenization of already grown NiO nanoflower and negative electrode is made of WO_3/PPy nanocomposite. This new architecture showed outstanding performance of high-energy density (37.3 Whkg^{-1}) and power density of 1249 Wkg^{-1} (at 2 Ag^{-1}) when used as an electrode for all solid-state asymmetric supercapacitor devices [79]. The structure retained its capacitance value of 91% at 5000 charging–discharging cycles. In this device architecture, WO_3/PPy composite showed enhanced specific capacitance of 586 Fg^{-1} (at 2 Ag^{-1}) as compared to its pristine constituent components (WO_3 of 402 Fg^{-1} and PPy of 224 Fg^{-1}) at the same current measurements. Similarly, Lijun Ren et al., demonstrated MoS_2/PANI composite electrode for supercapacitor with different loading weight percentages of PANI, where 53 wt% of PANI showed the highest electrocapacitance performance [80]. The synergic effect of both component materials with excellent ionic and mechanical stability makes this architecture a suitable electrode material that achieved an energy density of 35 Whkg^{-1} and a power density of 335 Wkg^{-1} with 81% retention in capacitance value after 8000 cycles. Likewise, $\text{MoS}_2/\text{PPy}/\text{PANI}$ electrodes exhibited a specific capacitance of 1273 Fg^{-1} at a current density of 0.5 Ag^{-1} , which was relatively larger than those of constituted moieties [81]. The reason for such good capacitance is due to the shorter ionic diffusion pathways and good electrical conductivity. For all electrodes fabricated by $\text{MoS}_2/\text{PPy}/\text{PANI}$, the high-frequency region in Nyquist plots displayed no semicircles which is a clear evidence of sufficiently reduced charge transfer resistances [81]. TMDs have high surface area and thin dimensions which allow them to be successfully utilized as electrode material but suffer from low rate capability and cyclability. Their incorporation in polymer matrix overcomes the problem and extends its applicability to lithium-ion batteries and sensors [82,83]. These TMDs, due to their excellent surface morphology and facile synthesis route with the ease of incorporation in C-polymer, proved to be excellent electrode material in terms of increased energy density, long-term stability, and retention in energy storage. The electrochemical performances of various electrode materials in their composite form with C-polymers, when used for supercapacitors, are demonstrated in Table 4.2.

Table 4.2 Electrochemical performance in terms of two parameters specific capacitance and cyclic stability of various electrodes for supercapacitors prepared by conducting polymers (C-polymers) in their composite form with other materials.

Electrode materials	Specific capacitance	Cyclic stability
PPY		
PPy/PSF	500 F g ⁻¹ at 0.3 A g ⁻¹	15% loss after 800 cycles
PPy nanowires/graphene	165 F g ⁻¹ at 1 A g ⁻¹	1000 cycles
PPy nanotubes/MnO ₂	403 F g ⁻¹ at 1 A g ⁻¹	–
PPy nanocone/RuO ₂	15.1 m F cm ⁻² (302 F g ⁻¹) at 0.5 mA cm ⁻²	–
CuO/PPy core/shell	1275.5 F cm ⁻³	3000 cycles
PPy/CoO	Max 2223 F g ⁻¹	99.8% retention after 2000 cycles (electrode) & 20,000 cycles (supercapacitor)
PPy/V ₂ O ₅ nanofiber	172 F g ⁻¹ at 10 mV s ⁻¹	–
MnO ₂ /PPy/CNT	–	93.8% retention after 10,000 cycles
PPy/MoS ₂	695 F g ⁻¹ at 0.5 A g ⁻¹ & 500 F g ⁻¹ at 10 A g ⁻¹	85% retention after 4000 cycles at 1 A g ⁻¹
PPy/MXene	1000 F cm ⁻³ at 5 mV s ⁻¹	92% retention after 25,000 cycles
PPy/MXene film	406 F cm ⁻³	100% retention after 20,000 cycles
MWCNT/PPy	192 F g ⁻¹ & 1.0 F cm ⁻²	–
β-MnO ₂ nanocrystals/PPy	294 F g ⁻¹ at 1 A g ⁻¹	92.6% retention after 1000 cycles at 5 A g ⁻¹
PANI		
PANi nanorods/CNT	568 F g ⁻¹ at 10 A g ⁻¹	91.1% retention after 1000 cycles
CNT/PANi nanowires array	38 m F cm ⁻²	91% retention after 800 cycles
PANi/CF cloth	673 F g ⁻¹ & 3.5 F cm ⁻²	–
PANi/CF paper	638 F g ⁻¹ at 1 A g ⁻¹	Retained 580 F g ⁻¹ after 1000 cycles at 2 A g ⁻¹
r-GO/PANi film	385 F g ⁻¹ at 0.5 A g ⁻¹	90% retention after 5000 cycles
AC/PANi	587 F g ⁻¹ at 0.1 A g ⁻¹	Decrease from 415 to 385 F g ⁻¹ after 50 cycles
PANi/HPCM	Max 2200 F g ⁻¹ , 1270 F g ⁻¹ at 66.7 A g ⁻¹ (electrode) & 35 F g ⁻¹ (supercapacitor)	–
PANi/ND/MnO ₂ nanoparticles	415 F g ⁻¹ at 1.67 mA cm ⁻²	87 F g ⁻¹ for 1000 cycles at 2.36 mA
PANi/MnO ₂ coaxial nanofiber	383 F g ⁻¹ at 0.5 A g ⁻¹	75% retention after 2000 cycles at 10 A g ⁻¹
TiO ₂ nanotubes/PANi	732 F g ⁻¹ at 1 A g ⁻¹ & 543 F g ⁻¹ at 20 A g ⁻¹	86% retention after 2000 cycles
C/PANi/MoS ₂	678 F g ⁻¹ at 1 mV s ⁻¹	80% retention after 10,000 cycles
PANi-NF/CCG	210 F g ⁻¹ at 0.3 A g ⁻¹	800 cycles at 3 A g ⁻¹

(Continued)

Table 4.2 (Continued)

Electrode materials	Specific capacitance	Cyclic stability
Other C-polymers		
TiO ₂ nanotube/PTh	640 F g ⁻¹ at 5 mV s ⁻¹	—
PTh/MnO ₂	290 F g ⁻¹ at 1 A g ⁻¹ & 222 F g ⁻¹ at 10 A g ⁻¹	97.3% retention after 1000 cycles at 2 A g ⁻¹
RuO ₂ /PEDOT	664 F g ⁻¹	—
PEDOT/AC	158 F g ⁻¹ at 10 mV s ⁻¹ (electrode) & 90 F g ⁻¹ at 10 mV s ⁻¹ (supercapacitor)	60 cycles
PANi/CuO PEDOT/CuOPPy/CuO	286.35 F g ⁻¹ at 20 mV s ⁻¹ & 198.89 F g ⁻¹ at 5 mV s ⁻¹ & 20.78 F g ⁻¹ at 5 mV s ⁻¹	—
Mixed polymers		
PMeT/PVdF	616 F g ⁻¹	300 cycles, 16% loss after 150 cycles
PEDOT/PPy	260–290 F g ⁻¹	1000 cycles at 100 mV s ⁻¹
PANi/PPy nanograins	737 F g ⁻¹ at 5 mV s ⁻¹	2000 cycles
PMeT/PVdF	616 F g ⁻¹	300 cycles, 16% loss after 150 cycles
PPy/PANi coaxial nanoarrays	210 F g ⁻¹ at 0.5 A g ⁻¹ (electrode) & 64.5 F g ⁻¹ at 0.5 A g ⁻¹ (supercapacitor)	79.5% retention after 500 cycles
PEDOT-PSS/RuO ₂ ·XH ₂ O	653 F g ⁻¹	—
CF/PDMcT/PPy	1130 ± 100 F g ⁻¹	1000 cycles

The table is drawn with permission of Z. Wang, et al. *Polymers for supercapacitors: boosting the development of the flexible and wearable energy storage*, Mater. Sci. Eng. R: Rep. 139 (2020) 100520. <https://doi.org/10.1016/j.mser.2019.100520>.



4.6 Conclusion

The chapter has focused on various research investigations in terms of C-polymeric composites with other materials as electrodes. In order to overcome the drawbacks and limitations associated with C-polymers, the polymeric nanocomposite improves the overall electrochemical performance including specific capacitance, energy and power density, and increased cycle-life stability of the supercapattery device. The improvement in mechanical and structural properties of composite evidence their potential application toward high performance and flexible energy storage devices. Reports describing a well-defined behavior of composites of C-polymers with carbonaceous, metal oxide, carbon, MXene, and transition metal dichalcogenide. Their enhanced electrochemical performance in supercapacitors is a clear evidence of a reliable solution for further improvement that will lead a way toward commercialization.



4.7 Abbreviations

C-polymers	conducting polymers
PPy	polypyrrole
PA	polyacetylene
PANI	polyaniline
PTh	polythiophene
PPh	polyphenylene
PPV	poly(phenylene)vinylene
P₃HT	polythiophene
EDLC	electrical double layer capacitor
EPD	electrophoretic deposition
EEG	electrochemical exfoliated graphene
TMDs	Transition Metal Dichalcogenides.

References

- [1] M. Angelopoulos, Conducting polymers in microelectronics, *IBM J. Res. Dev.* 45 (1) (2001) 57–75.
- [2] G.A. Snook, P. Kao, A.S. Best, Conducting-polymer-based supercapacitor devices and electrodes, *J. Power Sources*. 196 (1) (2011) 1–12.
- [3] K. Lota, V. Khomeiko, E. Frackowiak, Capacitance properties of poly (3,4-ethylenedioxythiophene)/carbon nanotubes composites, *J. Phys. Chem. Solids* 65 (2–3) (2004) 295–301.
- [4] B.S. Dakshayini, et al., Role of conducting polymer and metal oxide-based hybrids for applications in amperometric sensors and biosensors, *Microchem. J.* 147 (2019) 7–24. Available from: <https://doi.org/10.1016/j.microc.2019.02.061>.
- [5] X. Lu, et al., One-dimensional conducting polymer nanocomposites: synthesis, properties and applications, *Prog. Polym. Sci.* 36 (5) (2011) 671–712. Available from: <https://doi.org/10.1016/j.progpolymsci.2010.07.010>.
- [6] A.G. MacDiarmid, et al., Polyaniline: electrochemistry and application to rechargeable batteries, *Synth. Met.* 18 (1–3) (1987) 393–398.
- [7] M.H. Naveen, N.G. Gurudatt, Y.-B. Shim, Applications of conducting polymer composites to electrochemical sensors: a review, *Appl. Mater. Today* 9 (2017) 419–433. Available from: <https://doi.org/10.1016/j.apmt.2017.09.001>.
- [8] H. Shirakawa, et al., Synthesis of electrically conducting organic polymers: halogen derivatives of polyacetylene, (CH), *J. Chem. Soc. Chem. Commun* (16)(1977) 578–580. Available from: <https://doi.org/10.1039/C39770000578>.
- [9] G. Heywang, F. Jonas, Poly (alkylenedioxythiophene) s—new, very stable conducting polymers, *Adv. Mater.* 4 (2) (1992) 116–118.
- [10] W.-S. Huang, B.D. Humphrey, A.G. MacDiarmid, Polyaniline, a novel conducting polymer. Morphology and chemistry of its oxidation and reduction in aqueous electrolytes, *J. Chem. Soc. Farad. Trans. 1: Phys. Chem. Condens. Phases* 82 (8) (1986) 2385–2400.
- [11] Y. Shi, et al., Nanostructured conductive polymers for advanced energy storage, *Chem. Soc. Rev.* 44 (19) (2015) 6684–6696.
- [12] S.A. Umoren, M.M. Solomon, Protective polymeric films for industrial substrates: a critical review on past and recent applications with conducting polymers and polymer composites/nanocomposites, *Prog. Mater. Sci.* 104 (2019) 380–450. Available from: <https://doi.org/10.1016/j.pmatsci.2019.04.002>.

- [13] M.A.A. Mohd Abdah, et al., Review of the use of transition–metal–oxide and conducting polymer–based fibres for high–performance supercapacitors, *Mater. Des.* 186 (2020) 108199. Available from: <https://doi.org/10.1016/j.matdes.2019.108199>.
- [14] Q. Meng, et al., Research progress on conducting polymer based supercapacitor electrode materials, *Nano Energy* 36 (2017) 268–285. Available from: <https://doi.org/10.1016/j.nanoen.2017.04.040>.
- [15] J. Wang, et al., Recent progress of biomass–derived carbon materials for supercapacitors, *J. Power Sources* 451 (2020) 227794. Available from: <https://doi.org/10.1016/j.jpowsour.2020.227794>.
- [16] H. Peng, et al., *Polymer Materials for Energy and Electronic Applications*, Academic Press, 2016.
- [17] G.A. Snook, P. Kao, A.S. Best, Conducting–polymer–based supercapacitor devices and electrodes, *J. Power Sources* 196 (1) (2011) 1–12. Available from: <https://doi.org/10.1016/j.jpowsour.2010.06.084>.
- [18] P. Asen, S. Shahrokhian, A.I. zad, Ternary nanostructures of Cr₂O₃/graphene oxide/ conducting polymers for supercapacitor application, *J. Electroanal. Chem.* 823 (2018) 505–516. Available from: <https://doi.org/10.1016/j.jelechem.2018.06.048>.
- [19] W. Teng, et al., Hierarchically interconnected conducting polymer hybrid fiber with high specific capacitance for flexible fiber–shaped supercapacitor, *Chem. Eng. J.* 390 (2020) 124569. Available from: <https://doi.org/10.1016/j.cej.2020.124569>.
- [20] Z. Yang, et al., Free–standing PEDOT/polyaniline conductive polymer hydrogel for flexible solid–state supercapacitors, *Electrochim. Acta* 322 (2019) 134769. Available from: <https://doi.org/10.1016/j.electacta.2019.134769>.
- [21] S. Iqbal, S. Ahmad, Recent development in hybrid conducting polymers: Synthesis, applications and future prospects, *J. Ind. Eng. Chem.* 60 (2018) 53–84. Available from: <https://doi.org/10.1016/j.jiec.2017.09.038>.
- [22] Z. Wang, et al., Polymers for supercapacitors: boosting the development of the flexible and wearable energy storage, *Mater. Sci. Eng. R: Rep.* 139 (2020) 100520. Available from: <https://doi.org/10.1016/j.mser.2019.100520>.
- [23] S. Komarneni, Nanocomposites, *J. Mater. Chem.* 2 (12) (1992) 1219–1230.
- [24] M.S. Nam, et al., A binder free synthesis of 1D PANI and 2D MoS₂ nanostructured hybrid composite electrodes by the electrophoretic deposition (EPD) method for supercapacitor application, *RSC Adv.* 6 (103) (2016) 101592–101601.
- [25] M.G. Junior, et al., in: E. Longo, FdeA. La Porta (Eds.), *Functional nanomaterials for applications in energy storage and conversion BT - recent advances in complex functional materials: from design to application*, Springer International Publishing, Cham, 2017, pp. 217–237.
- [26] N. Radenahmad, et al., Proton–conducting electrolytes for direct methanol and direct urea fuel cells – A state–of–the–art review, *Renew. Sustain. Energy Rev.* 57 (2016) 1347–1358. Available from: <https://doi.org/10.1016/j.rser.2015.12.103>.
- [27] M.O. Yanik, et al., Magnetic conductive polymer–graphene nanocomposites based supercapacitors for energy storage, *Energy* 138 (2017) 883–889. Available from: <https://doi.org/10.1016/j.energy.2017.07.022>.
- [28] Y. Li, et al., Review and prospect of NiCo₂O₄–based composite materials for supercapacitor electrodes, *J. Energy Chem.* 31 (2019) 54–78. Available from: <https://doi.org/10.1016/j.jechem.2018.05.010>.
- [29] J. Cherusseri, et al., Novel mesoporous electrode materials for symmetric, asymmetric and hybrid supercapacitors, *Nanotechnology* 30 (20) (2019) 202001. Available from: <https://doi.org/10.1088/1361-6528/ab0685>.
- [30] J. Li, et al., MXene–conducting polymer electrochromic microsupercapacitors, *Energy Storage Mater.* 20 (2019) 455–461. Available from: <https://doi.org/10.1016/j.ensm.2019.04.028>.

- [31] A. Hossain, et al., Recent developed different structural nanomaterials and their performance for supercapacitor application, *Appl. Mater. Today* 9 (2017) 300–313. Available from: <https://doi.org/10.1016/j.apmt.2017.08.010>.
- [32] C.-F. Liu, et al., Carbon materials for high-voltage supercapacitors, *Carbon* 145 (2019) 529–548. Available from: <https://doi.org/10.1016/j.carbon.2018.12.009>.
- [33] A.G. Pandolfo, A.F. Hollenkamp, Carbon properties and their role in supercapacitors, *J. Power Sources* 157 (1) (2006) 11–27. Available from: <https://doi.org/10.1016/j.jpowsour.2006.02.065>.
- [34] P. Liu, et al., Recent advancements of polyaniline-based nanocomposites for supercapacitors, *J. Power Sources* 424 (2019) 108–130. Available from: <https://doi.org/10.1016/j.jpowsour.2019.03.094>.
- [35] K. Sattler (Ed.), *Carbon Nanomaterials Sourcebook*, CRC Press, Boca Raton, 2016. Available from: <https://doi.org/10.1201/b19679>.
- [36] Y. Liu, S. Kumar, Polymer/carbon nanotube nano composite fibers—a review, *ACS Appl. Mater. Interfaces* 6 (9) (2014) 6069–6087. Available from: <https://doi.org/10.1021/am405136s>.
- [37] Y. Lattach, et al., Polypyrrole-Ru (2, 2'-bipyridine)₃²⁺/MoS_x structured composite film as a photocathode for the hydrogen evolution reaction, *ACS Appl. Mater. Interfaces* 7 (8) (2015) 4476–4480.
- [38] D.V. Talapin, et al., Synthesis of surface-modified colloidal semiconductor nanocrystals and study of photoinduced charge separation and transport in nanocrystal-polymer composites, *Physica E: Low Dimens. Syst. Nanostruct.* 14 (1–2) (2002) 237–241.
- [39] H.C. Leventis, et al., Nanostructured hybrid polymer – inorganic solar cell active layers formed by controllable in situ growth of semiconducting sulfide networks, *Nano Lett.* 10 (4) (2010) 1253–1258.
- [40] R. Narizzano, V. Erokhin, C. Nicolini, A heterostructure composed of conjugated polymer and copper sulfide nanoparticles, *J. Phys. Chem. B* 109 (33) (2005) 15798–15802.
- [41] T. Yamamoto, et al., Electrically conductive metal sulfide-polymer composites prepared by using organosols of metal sulfides, *Chem. Mater* 4 (3) (1992) 570–576.
- [42] H. Tang, et al., Growth of polypyrrole ultrathin films on MoS₂ monolayers as high-performance supercapacitor electrodes, *Adv. Mater.* 27 (6) (2015) 1117–1123.
- [43] C. Yang, et al., Rational synthesis of carbon shell coated polyaniline/MoS₂ monolayer composites for high-performance supercapacitors, *Nano Res.* 9 (4) (2016) 951–962.
- [44] G. Ma, et al., In situ intercalative polymerization of pyrrole in graphene analogue of MoS₂ as advanced electrode material in supercapacitor, *J. Power Sources* 229 (2013) 72–78.
- [45] J. Wang, et al., High conductivity graphene-like MoS₂/polyaniline nanocomposites and its application in supercapacitor, *J. Alloy. Compd.* 619 (2015) 38–43.
- [46] J. Osuntokun, P.A. Ajibade, Structural and thermal studies of ZnS and CdS nanoparticles in polymer matrices, *J. Nanomater.* 2016 (2016) 13.
- [47] P.A. Ajibade, J.Z. Mbese, Synthesis and characterization of metal sulfides nanoparticles/poly (methyl methacrylate) nanocomposites, *Int. J. Polym. Sci.* (2014) 2014.
- [48] C.A. Bower, Studies on the form and availability of organic soil phosphorous, *IOWA Agric. Exp. Stn. Res. Bull.* (1949) 339–362.
- [49] D.J. Greenland, Adsorption of polyvinyl alcohols by montmorillonite, *J. Colloid Sci.* 18 (7) (1963) 647–664.
- [50] A. Blumstein, Etude Des Polymerisations En Couche Adsorbee. 1, *Bull. Soc. Chim. Fr.* (5)(1961) 899.
- [51] E.P. Giannelis, R. Krishnamoorti, E. Manias, Polymer-silicate nanocomposites: model systems for confined polymers and polymer brushes, *Polymers in Confined Environments*, Springer, 1999, pp. 107–147.

- [52] X. Kornmann, H. Lindberg, L.A. Berglund, Synthesis of epoxy–clay nanocomposites: Influence of the nature of the clay on structure, *Polymer* 42 (4) (2001) 1303–1310.
- [53] E. Manias, et al., Polypropylene/montmorillonite nanocomposites. Review of the synthetic routes and materials properties, *Chem. Mater.* 13 (10) (2001) 3516–3523.
- [54] M. Zanetti, S. Lomakin, G. Camino, Polymer layered silicate nanocomposites, *Macromol. Mater. Eng.* 279 (1) (2000) 1–9.
- [55] M. Alexandre, P. Dubois, Polymer-layered silicate nanocomposites: preparation, properties and uses of a new class of materials, *Mater. Sci. Eng. R: Rep.* 28 (1–2) (2000) 1–63.
- [56] S. Pavlidou, C.D. Papaspyrides, A review on polymer–layered silicate nanocomposites, *Prog. Polym. Sci.* 33 (12) (2008) 1119–1198.
- [57] S.S. Ray, M. Okamoto, Polymer/layered silicate nanocomposites: a review from preparation to processing, *Prog. Polym. Sci.* 28 (11) (2003) 1539–1641.
- [58] Y. Hou, et al., Design and synthesis of hierarchical MnO₂ nanospheres/carbon nanotubes/conducting polymer ternary composite for high performance electrochemical electrodes, *Nano Lett.* 10 (7) (2010) 2727–2733. Available from: <https://doi.org/10.1021/nl101723g>.
- [59] S. Ji, et al., A universal electrolyte formulation for the electrodeposition of pristine carbon and polypyrrole composites for supercapacitors, *ACS Appl. Mater. Interfaces* 12 (11) (2020) 13386–13399. Available from: <https://doi.org/10.1021/acsami.0c01216>.
- [60] X. Cheng, et al., Design of a hierarchical ternary hybrid for a fiber-shaped asymmetric supercapacitor with high volumetric energy density, *J. Phys. Chem. C. Am. Chem. Soc.* 120 (18) (2016) 9685–9691. Available from: <https://doi.org/10.1021/acs.jpcc.6b02794>.
- [61] J. Parayangattil Jyothibasu, M.-Z. Chen, R.-H. Lee, Polypyrrole/carbon nanotube freestanding electrode with excellent electrochemical properties for high-performance all-solid-state supercapacitors, *ACS Omega.* (2020). Available from: <https://doi.org/10.1021/acsomega.9b04029>.
- [62] J. Han, et al., Electrospun core–shell nanofibrous membranes with nanocellulose-stabilized carbon nanotubes for use as high-performance flexible supercapacitor electrodes with enhanced water resistance, thermal stability, and mechanical toughness, *ACS Appl. Mater. Interfaces* 11 (47) (2019) 44624–44635. Available from: <https://doi.org/10.1021/acsami.9b16458>.
- [63] W. Zhang, et al., Supramolecule-assisted synthesis of cyclodextrin polymer functionalized polyaniline/carbon nanotube with core-shell nanostructure as high-performance supercapacitor material, *Electrochim. Acta* 331 (2020) 135345. Available from: <https://doi.org/10.1016/j.electacta.2019.135345>.
- [64] R. Holze, 9 - Metal oxide/conducting polymer hybrids for application in supercapacitors, in: D.P. Dubal, P.B.T.-M.O. Gomez-Romero (Eds.), *Metal Oxides*, Elsevier, 2017, pp. 219–245. S. Available from: <https://doi.org/10.1016/B978-0-12-810464-4.00009-7>.
- [65] W. Kai, et al., Electrodeposition synthesis of PANI/MnO₂/graphene composite materials and its electrochemical performance, *Int. J. Electrochem. Sci.* 12 (2017) 8306–8314.
- [66] M. Moussa, et al., Development of flexible supercapacitors using an inexpensive graphene/PEDOT/MnO₂ sponge composite, *Mater. Des.* 125 (2017) 1–10.
- [67] S. Palsaniya, H.B. Nemade, A.K. Dasmahapatra, Graphene based PANI/MnO₂ nanocomposites with enhanced dielectric properties for high energy density materials, *Carbon* 150 (2019) 179–190. Available from: <https://doi.org/10.1016/j.carbon.2019.05.006>.

- [68] R. Liu, et al., Synthesis and characterization of RuO₂/poly(3,4-ethylenedioxythiophene) composite nanotubes for supercapacitors, *Phys. Chem. Chem. Phys.* 12 (17) (2010) 4309–4316. Available from: <https://doi.org/10.1039/B918589P>.
- [69] J. Zang, et al., Well-aligned cone-shaped nanostructure of polypyrrole/RuO₂ and its electrochemical supercapacitor, *J. Phys. Chem. C*. 112 (38) (2008) 14843–14847.
- [70] S. Cho, M. Kim, J. Jang, Screen-printable and flexible RuO₂ nanoparticle-decorated PEDOT: PSS/graphene nanocomposite with enhanced electrical and electrochemical performances for high-capacity supercapacitor, *ACS Appl. Mater. Interfaces* 7 (19) (2015) 10213–10227.
- [71] L. Chen, et al., Synthesis and pseudocapacitive studies of composite films of polyaniline and manganese oxide nanoparticles, *J. Power Sources* 195 (11) (2010) 3742–3747.
- [72] H. Jiang, J. Ma, C. Li, Polyaniline–MnO₂ coaxial nanofiber with hierarchical structure for high-performance supercapacitors, *J. Mater. Chem.* 22 (33) (2012) 16939–16942.
- [73] L.U. Qing, Y. Zhou, Synthesis of mesoporous polythiophene/MnO₂ nanocomposite and its enhanced pseudocapacitive properties, *J. Power Sources* 196 (8) (2011) 4088–4094.
- [74] M. Naguib, et al., Two-dimensional transition metal carbides, *ACS Nano* 6 (2) (2012) 1322–1331. Available from: <https://doi.org/10.1021/nn204153h>.
- [75] J. Fu, et al., Architecturally robust graphene-encapsulated MXene Ti₂CTx@polyaniline composite for high-performance pouch-type asymmetric supercapacitor, *ACS Appl. Mater. Interfaces* 10 (40) (2018) 34212–34221. Available from: <https://doi.org/10.1021/acami.8b10195>.
- [76] M. Boota, et al., Pseudocapacitive electrodes produced by oxidant-free polymerization of pyrrole between the layers of 2D titanium carbide (MXene), *Adv. Mater.* 28 (7) (2016) 1517–1522. Available from: <https://doi.org/10.1002/adma.201504705>.
- [77] L. Lin, et al., Two-dimensional transition metal dichalcogenides in supercapacitors and secondary batteries, *Energy Storage Mater.* 19 (2019) 408–423. Available from: <https://doi.org/10.1016/j.ensm.2019.02.023>.
- [78] A. Sajedi-Moghaddam, E. Saievar-Iranizad, M. Pumera, Two-dimensional transition metal dichalcogenide/conducting polymer composites: synthesis and applications, *Nanoscale* 9 (24) (2017) 8052–8065.
- [79] A.K. Das, et al., Highly rate capable nanoflower-like NiSe and WO₃@PPy composite electrode materials toward high energy density flexible all-solid-state asymmetric supercapacitor, *ACS Appl. Electron. Mater.* 1 (6) (2019) 977–990. Available from: <https://doi.org/10.1021/acsaelm.9b00164>.
- [80] L. Ren, et al., Growth of PANI thin layer on MoS₂ nanosheet with high electrocapacitive property for symmetric supercapacitor, *J. Alloy. Compd.* 798 (2019) 227–234. Available from: <https://doi.org/10.1016/j.jallcom.2019.05.240>.
- [81] K. Wang, et al., Constructing a “Pizza-Like” MoS₂/polypyrrole/polyaniline ternary architecture with high energy density and superior cycling stability for supercapacitors, *Adv. Mater. Interfaces* 3 (19) (2016) 1600665.
- [82] K.-J. Huang, et al., Novel electrochemical sensing platform based on molybdenum disulfide nanosheets-polyaniline composites and Au nanoparticles, *Sens. Actuators B: Chem.* 194 (2014) 303–310.
- [83] A.P. Nayak, et al., Pressure-induced semiconducting to metallic transition in multi-layered molybdenum disulfide, *Nat. Commun.* 5 (2014) 3731.



Carbonaceous nanocomposites for supercapattery

Andrews Nirmala Grace, Sandhya Venkateshalu
and Subashini Gnanasekar

Centre for Nanotechnology Research, Vellore Institute of Technology (VIT), Vellore, India



5.1 Introduction

In order to cater for the energy demand considering the foreseeable exhaustion of fossil fuels, research is being focused on electrochemical energy storage technologies and in developing new efficient electrode materials [1]. A new energy storage device supercapattery possesses an improved capacity with its nature being similar to that of a supercapacitor [2]. The ideally polarized “supercapacitor-type” electrode generally stores charge with the formation of an electric double layer (EDL) at the electrode surface and the weakly polarized “battery-type” electrode stores charges based on redox reactions happening at the electrode interface [3]. Thus supercapattery is a hybrid energy storage device with carbonaceous materials as the negative electrode (negatrod) and battery grade materials as the positive electrode (positrod) [4].

The electrical conductivity of the battery type metal complexes and polymers (LiFePO_4 , $\text{Li}_2\text{MnSiO}_4/\text{Al}_2\text{O}_3$, poly(3,4-ethylenedioxythiophene), polyaniline, etc.) is quite poor which leads to an increase in the resistance of the electrode. This increase in resistance in turn leads to low power density compared to that of electrolytic capacitors and EDL capacitors [4–7]. In order to overcome the difficulty in the easy transport of ions and electrons to all active sites of an electrode, research is being focused on developing various nanomaterials with porous structures [8].

Various carbonaceous materials such as activated carbon (AC), reduced graphene oxide (rGO), graphene oxide (GO), and carbon nanotubes (CNT) are the materials used for the ideally polarized electrode [3]. Carbonaceous materials are known to possess low electrical resistance, large surface area,

high porosity, and good electrochemical stability. With their high porous nature they allow rapid ion access thereby improving the rate capability significantly [9]. Fig. 5.1 shows the comparison of different carbonaceous materials as electrodes for supercapattery. It is well-known that AC is a widely reported material as a supercapattery electrode to date. Though they exhibit high surface area, the electrolyte ions cannot access all the carbon atoms (as shown in Fig. 5.1A) available in it, thus limiting its electrochemical performance. Another important carbon material, CNT exhibits enhanced electrical conductivity but single-walled carbon nanotubes (SWCNTs) get agglomerated to stack into bundles (shown in Fig. 5.1B) and thus only the outermost CNTs are accessible by the electrolyte ions and all the innermost carbon atoms go unused, leading to poor capacitance. One of the widely researched carbon nanomaterials is graphene. As shown in Fig. 5.1C, the graphene sheets are held together through the van der Waals forces and the sheets might get agglomerated due to these weak forces acting between them, thereby making it difficult for the electrolyte ions to access the pores. To overcome the difficulty found in graphene, CNTs can be made as a composite with graphene, as shown in Fig. 5.1D. CNTs help in the separation of graphene sheets,

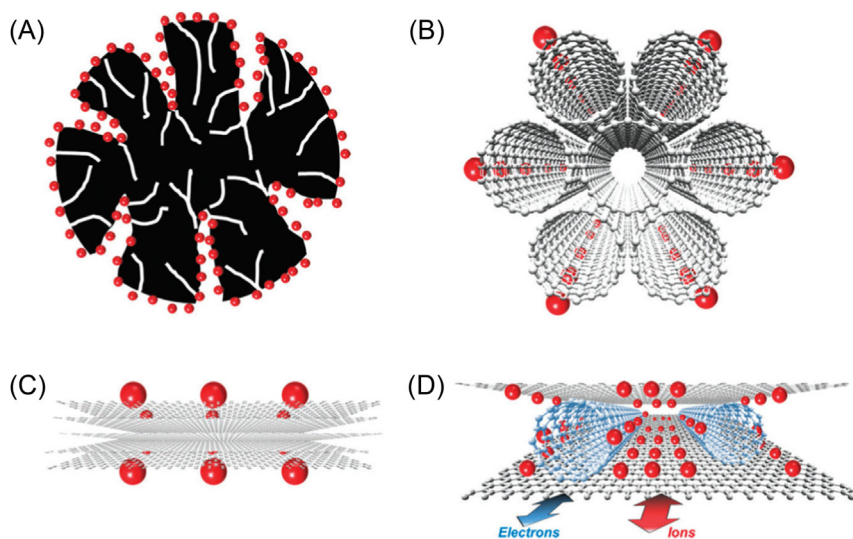


Figure 5.1 Different carbonaceous materials (A) activated carbon, (B) CNT, (C) graphene, and (D) graphene–CNT composite as supercapattery electrodes. *Reproduced with permission from Q. Cheng, J. Tang, J. Ma, H. Zhang, N. Shinya, L.-C. Qin, Graphene and carbon nanotube composite electrodes for supercapacitors with ultra-high energy density, Phys. Chem. Chem. Phys.* 13 (2011) 17615–17624. Copyright 2011, Royal Society of Chemistry.

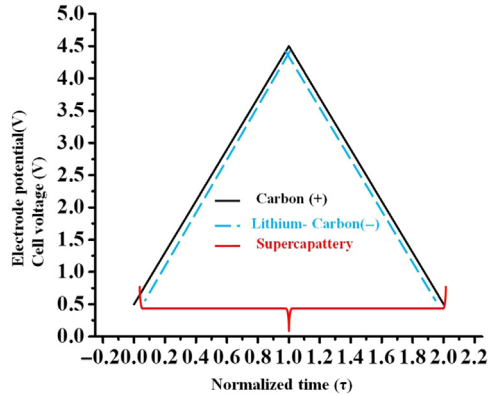


Figure 5.2 Charge–discharge curve of a supercapattery with activated carbon as the positrode and lithium metal or lithiated carbon as the negatrode. Black and red lines indicate the calculated electrode potential while the blue dashed line indicates the cell voltage [11].

thereby providing the electrolyte ions with rapid diffusion pathways [10]. A detailed description of these individual carbon materials with their composites as electrodes in supercapattery will be discussed in the following sections of this chapter.

Chen predicted the performance of a supercapattery device with lithium or lithiated carbide as the negative electrode and carbon as the positive electrode, as given in Fig. 5.2. It can be seen that the system is highly capacitive with a minimum potential on carbon vs. lithium of 0.5 V. This prevents the carbon electrode from undergoing lithiation during discharge. In order to achieve this capacitive performance, it is necessary to balance the electrode masses or charges [11].



5.2 Carbonaceous electrode materials

5.2.1 Graphene and its composites

With the discovery of graphene—the wonder material—by Geim et al., most of the limitations observed in carbonaceous materials were removed [12]. Graphene-based materials exhibit outstanding electronic, mechanical, and chemical properties which enable them to be most suitable to be used in storage devices [13]. A freshly exfoliated sheet of graphene will have a surface area of $2630 \text{ m}^2 \text{ g}^{-1}$ with a theoretical capacitance of 550 F g^{-1} , but

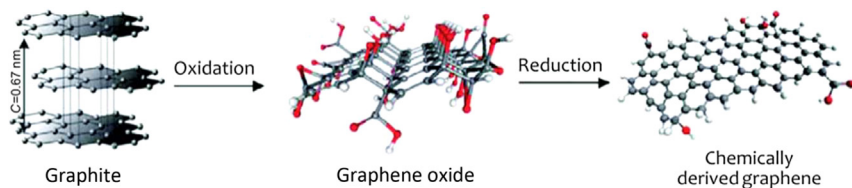


Figure 5.3 Synthesis of graphene from graphite [25].

this value of capacitance is usually not observed practically due to the agglomeration of graphene sheets that happen during the synthesis process [14]. Thus enhancing the electrochemical performance of the graphene-based electrode materials is still a major focus of research [15,16]. Graphene is a two-dimensional structured material (a monolayer of graphite) which consists of tunable interlayer spacing and accessible pores with a very large surface area, making it suitable for energy storage applications [17–19]. Graphene synthesized through various methods, such as mechanical exfoliation, electrochemical exfoliation, arc discharge, chemical vapor deposition etc., is expected to exhibit different specific capacitances due to the changes in the process parameters [20–24]. GO is an important derivative of graphene which also consists of a layered structure with surface terminated oxygen containing functional groups such as hydroxyl (C–OH), carboxyl (C=O), and epoxy groups (C–O). These groups attached to the edges of the graphene sheets (shown in Fig. 5.3) help in the stabilization of sheets and also in the redox reactions, thus exhibiting both EDLC as well as pseudocapacitance [26,27]. By reducing GO, reduced graphene (rGO) can be obtained; thus GO acts as a precursor in producing reduced graphene [28]. Graphene sheets help in anchoring various conducting polymers and transition metal oxides thereby enhancing their electrochemical performance [29].

Graphene, with its 2D nature, exhibits properties such as high tunable surface area, good chemical stability, excellent mechanical behavior, and electrical conductivity [30]. Graphene acts as a highly conducting network to support the faradaic reactions of other pseudomaterials [25]. In this regard, various metal oxides, carbonaceous materials, and conducting polymers are made into composites with graphene to form supercapattery electrodes. The 2D layered structure of graphene helps in the easy intercalation of electrolyte ions, thereby enhancing the electrochemical performance [10].

Peng et al. reported the use of rGO as a negative electrode with hydration nickel phosphate ($\text{Ni}_3(\text{PO}_4)_2 \cdot 8\text{H}_2\text{O}$) synthesized through a microwave-assisted method as the positive electrode in a supercapattery device. A specific capacity of 122.3 C g^{-1} at a current density of 1 A g^{-1}

was obtained. An energy density of 25.48 Wh kg^{-1} at a power density of 750.02 W kg^{-1} was exhibited by the hybrid supercapattery with a stability of 84.23% after 1000 charge–discharge cycles [31].

In the work reported by Athika et al., a solution combustion process was implemented to synthesize $\text{Ni/NiFe}_2\text{O}_4@\text{C}$ nanocomposite which was tested for its electrochemical behavior. $\text{Ni/NiFe}_2\text{O}_4@\text{C}$ was used as the positive electrode with rGO as the negative electrode in the construction of the supercapattery device. From the cyclic voltammetry (CV) curves, as shown in Fig. 5.4, it can be seen that at lower potential windows (0–0.5 V and 0–0.6 V), the supercapattery device exhibits EDLC behavior as the CV curves are rectangular in shape. As the potential window was increased (0–0.8, 1, and 1.2 V) a

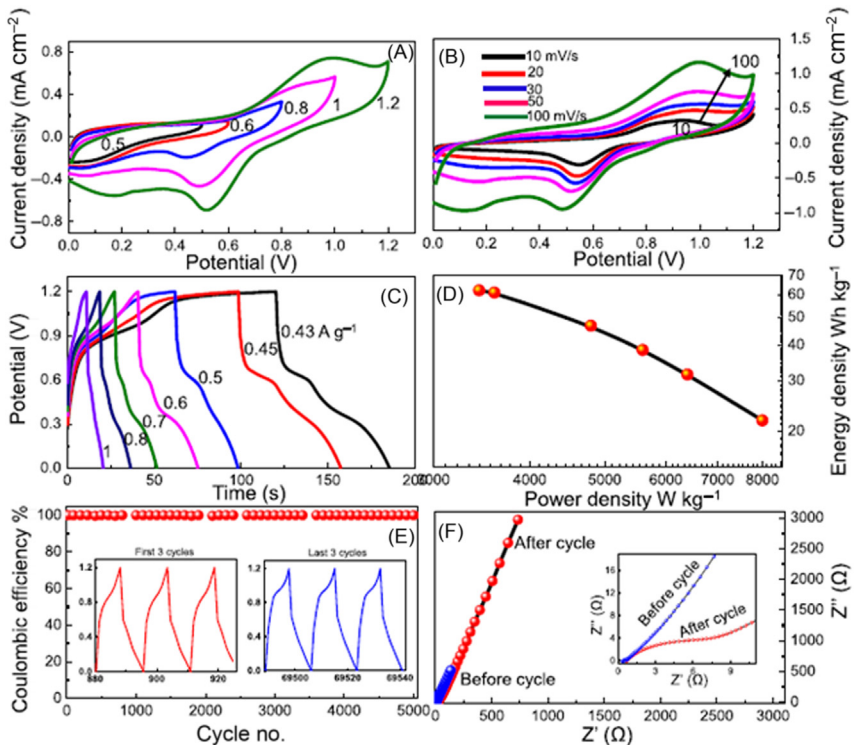


Figure 5.4 (A) CV curves recorded at a scan rate of 50 mV s^{-1} with different voltage windows; (B) CV curves recorded at various scan rates; (C) galvanostatic charge–discharge (GCD) profiles at different current densities; (D) Ragone plot; (E) coulombic efficiency; and (f) Nyquist plots. Reproduced with permission from A. Mattath, A. Prasath, A. Selva Sharma, V. Devi, E. Duraisamy, P. Elumalai, $\text{Ni/NiFe}_2\text{O}_4@\text{carbon}$ nanocomposite involving synergistic effect for high-energy density and high-power density supercapattery, *Mater. Res. Express* 6 (2019). Copyright 2019, IOP Publishing Ltd.

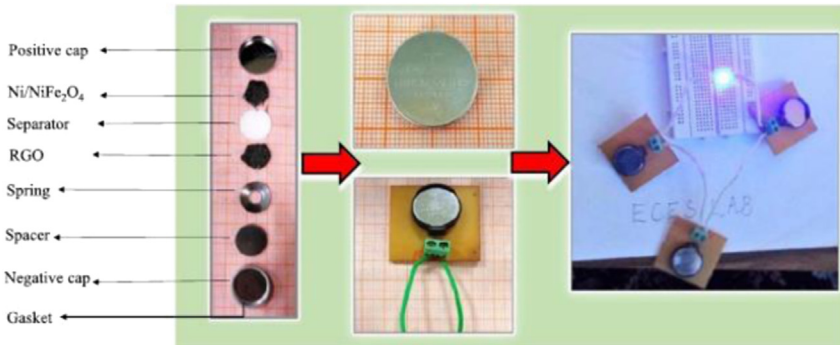


Figure 5.5 Assembly of three series connected CR2032 coin cells to power up the LED. Reproduced with permission from A. Mattath, A. Prasath, A. Selva Sharma, V. Devi, E. Duraisamy, P. Elumalai, Ni/NiFe₂O₄@carbon nanocomposite involving synergistic effect for high-energy density and high-power density supercapattery, *Mater. Res. Express* 6 (2019). Copyright 2019, IOP publishing Ltd.

quasirectangular shape was obtained. This implies that both EDLC and battery type behaviors were exhibited by the device. The rGO electrode contributes to the EDLC behavior while Ni/NiFe₂O₄@C contributes to the redox behavior of the device. Further, they demonstrated the potential applicability of the device by powering a LED using three CR2032 coin cells. The three fabricated coin cells provided a potential of 3.6 V that could glow the LED for more than 15 minutes as shown in Fig. 5.5 [32].

In the work reported by Heng et al., a supercapattery device was tested with GO/titanium dioxide (rGO/TiO₂) as the positive electrode and AC as the negative electrode. TiO₂ was loaded with different mass ratios of rGO and tested for its electrochemical behavior. For a mass ratio of 10 Wt% of rGO, a specific capacity of 116.70 mAh g⁻¹ at 0.2 A g⁻¹ was obtained. The large surface of rGO acts as a template in holding the TiO₂ nanocrystals and thereby helps in avoiding aggregation and promoting charge transfer [33].

5.2.2 Carbon nanotube and its composites

CNTs were first discovered by Iijima in 1991, and received remarkable attention in the field of novel electronic and electrochemical materials [34]. A single graphene sheet rolled up with *sp*² hybridization in nanoscale to form a nanotube is called a single-walled carbon nanotube (SWNT), and when multiple graphene sheets are rolled up they form multiwalled carbon nanotubes (MWCNTs). When two graphene sheets are rolled up, they form a special case of MWCNTs called double-walled carbon

nanotubes (DWCNTs). DWCNTs exhibit similar morphology and properties to SWCNTs. Fig. 5.6 depicts the formation of CNT from graphene and different types of CNTs [35]. These nanotubes are elongated in the nanoscale with a length of several micrometers up to centimeters and a diameter in the range of a few angstroms to tens of nanometers. The tubes are capped with fullerenes-like structures containing pentagons [36]. CNTs exhibit unique properties such as small size with high aspect ratio, light weight, good conductivity and tensile strength which enable them to be used as fillers in polymers, ceramics, and metallic surfaces [37]. Due to their excellent electrical, mechanical, and optical properties, they stand out as potential candidates for electrode materials in energy generation, conversion, and storage applications [38]. The carbon nanotube possess an extraordinary electronic property in that it can be metallic or semiconducting. This behavior is due to the symmetry of the planar system which varies according to the rolling action [39,40]. The orientation, dispersion, and contact with the electrode and electrolyte decides the electrochemical performance of the CNTs in the particular application. Among different carbon nanostructures, CNTs are unique due to their remarkable properties with micro- and nanometer-sized interconnected porous networks that

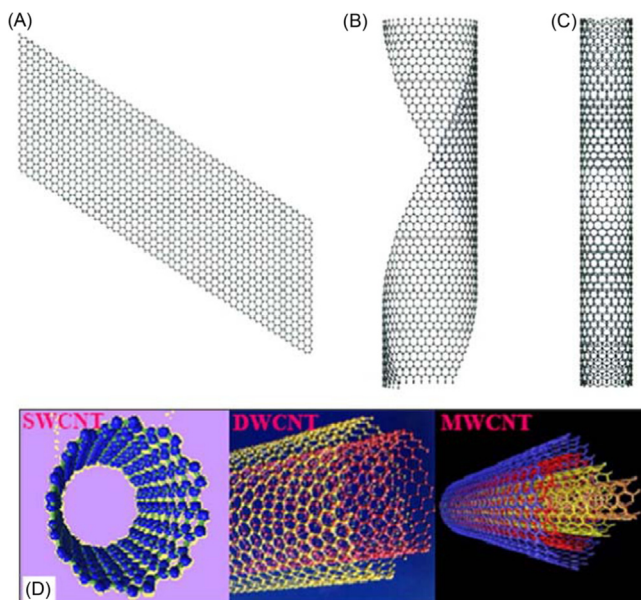


Figure 5.6 (A, B and C) Schematic of a graphene sheet rolled up to form a SWCNT, (D) three types of CNTs [35].

help in the passing of charge balancing ions. Also, the high electronic conductivity of CNTs is useful for the rapid movement of electrons within the electrode [41]. The characteristic features, such as high electrical and ionic conductivity of CNTs, enable them to be used as active electrode material for high-speed charging and discharging. The CNTs are highly stable in chemical and electrochemical environments, thus making them one of the best choices for electrodes of supercapattery. CNTs and their composites are receiving particular interest as they can be introduced in various reaction media with the desirable redox active materials [11].

Iqbal et al. prepared a ternary nanocomposite (MWCNT-Co₃O₄-Ag) through a facile hydrothermal technique (Fig. 5.7). The ternary nanocomposite exhibited a maximum specific capacity of 83.88 C g⁻¹ at 0.6 A g⁻¹. This specific capacity exhibited by the ternary composite is appreciably higher than that exhibited by MWCNT-Co₃O₄ and Co₃O₄ nanograins. The

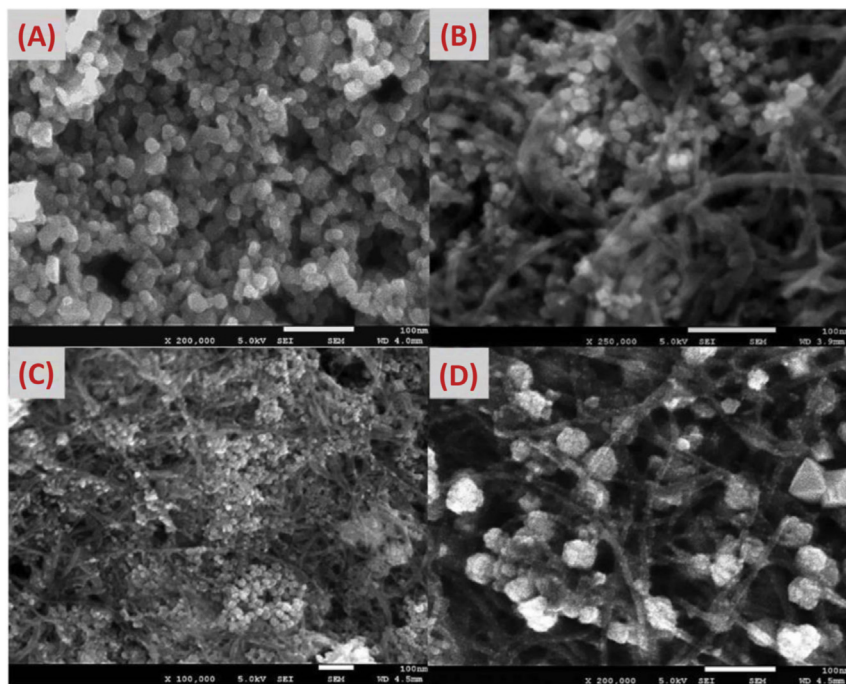


Figure 5.7 FESEM images of (A) Co₃O₄, (B) MWCNT-Co₃O₄ nanocomposite (C and D) MWCNT-Co₃O₄-Ag nanocomposite at different magnifications. Reproduced with permission from J. Iqbal, A. Numan, S. Rafique, R. Jafer, S. Mohamad, K. Ramesh, et al., High performance supercapattery incorporating ternary nanocomposite of multiwalled carbon nanotubes decorated with Co₃O₄ nanograins and silver nanoparticles as electrode material, *Electrochim. Acta* 278 (2018) 72–82. Copyright 2018, Elsevier Ltd.

increase in performance was attributed to the combined synergistic effect of conductive MWCNT, Co_3O_4 nanograins, and the Ag nanoparticles. The supercapattery device fabricated exhibited an energy and power density of 16.5 Wh kg^{-1} and 297.5 Wkg , respectively. The supercapattery device exhibited a high stable performance with 6.4% loss of its initial capacity after 3000 charge–discharge cycles [4].

A nozzle electrospinning technique followed by pyrolysis was used in the synthesis of NiCoP/CNF nanofibers. A NiCoP/CNF || NiCoP/CNF symmetric supercapattery device was fabricated and the charge/discharge mechanism in it is depicted in Fig. 5.8. When the device is applied with a low

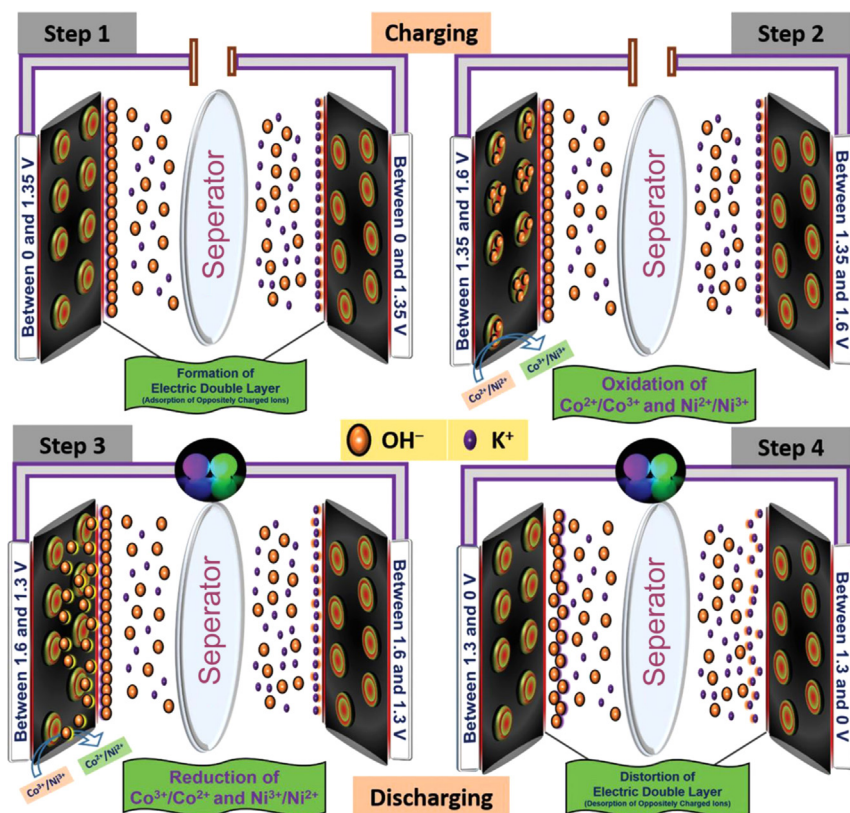


Figure 5.8 Charge–discharge mechanism in the symmetric supercapattery device with respect to the applied cell voltage. *Reproduced with permission from S. Surendran, S. Shanmugapriya, A. Sivanantham, S. Shanmugam, R. Kalai Selvan, Electrospun carbon nanofibers encapsulated with nicop: a multifunctional electrode for supercapattery and oxygen reduction, oxygen evolution, and hydrogen evolution reactions, Adv. Energy Mater. 8 (2018) 1800555. Copyright 2018, Wiley-VCH Verlag GmbH & Co. KGaA, Weinheim.*

potential, oppositely charged ions get attracted toward the NiCoP/CNF forming an EDL (shown in step 1 of Fig. 5.8). The larger the number of ions getting attracted to the electrode, the larger the storage capacity of the symmetric device. Co and Ni elements present on the CNF (positrode) get oxidized by the OH^- ions with the increase in potential at the positive electrode (step 2). This not only enhances the amount of charge stored but also helps the device reach higher potentials. The OH^- ions and the positive ions dissolve from the positive and negative electrode during the discharging process (step 3 and step 4). Thus a high capacity symmetric device was accomplished. A NiCoP/CNF electrode exhibits a specific capacitance of 333 F g^{-1} at 2 A g^{-1} and a supercapattery device provides an energy density of 36 Wh kg^{-1} with a power density of 4000 W kg^{-1} [42].

Vadiyar et al. reported a supercapattery device fabricated with Ag on CNTs wrapped with CuCo_2O_4 nanoflowers and thermocol-derived AC as the positive and negative electrodes, respectively. The schematic of the fabrication of supercapattery device with its electrochemical behavior is shown in Fig. 5.9. It also exhibited an energy density of 91 Wh kg^{-1} at the power density of 0.42 kW kg^{-1} with an excellent capacity retention of 98% after 20,000 cycles at a current density of 10 A g^{-1} [43].

5.2.3 Activated carbon and its composites

AC possess unique features such as high surface area, low cost, abundance, less corrosive, and wide operating temperature. The porosity and the AC framework is highly dependent on the activation process [44,45]. The AC used for electrodes in supercapattery is mostly the commercially available one. Among the carbonaceous materials used as electrodes in supercapattery, AC electrodes are the widely used ones in literature due to the high porous nature which facilitates easy ion access, thereby improving the electrochemical performance [46–48]. Manoharan et al. showed that the high surface area and porous nature of the AC (Fig. 5.10) is helpful in improving the energy storage capabilities of the AC electrode in proton-conducting electrolytes [49].

AC was used as the positrode with a lithium negatrode in an ionic electrolyte, 1-butyl-1-methylpyrrolidinium tri(pentafluoroethyl)trifluorophosphate (BMPyrFAP) containing gamma butyrolactone (γ -GBL) and LiClO_4 in a supercapattery cell. When AC electrodes were used in a symmetrical device, the equivalent series resistance (ESR) was 30 times higher than the value obtained for the supercapattery device with AC and lithium electrodes. The total resistance of the supercapattery device was about 180Ω with an ESR of $35 \Omega \text{ cm}^2$. With such a supercapattery working with ionic electrolytes, the

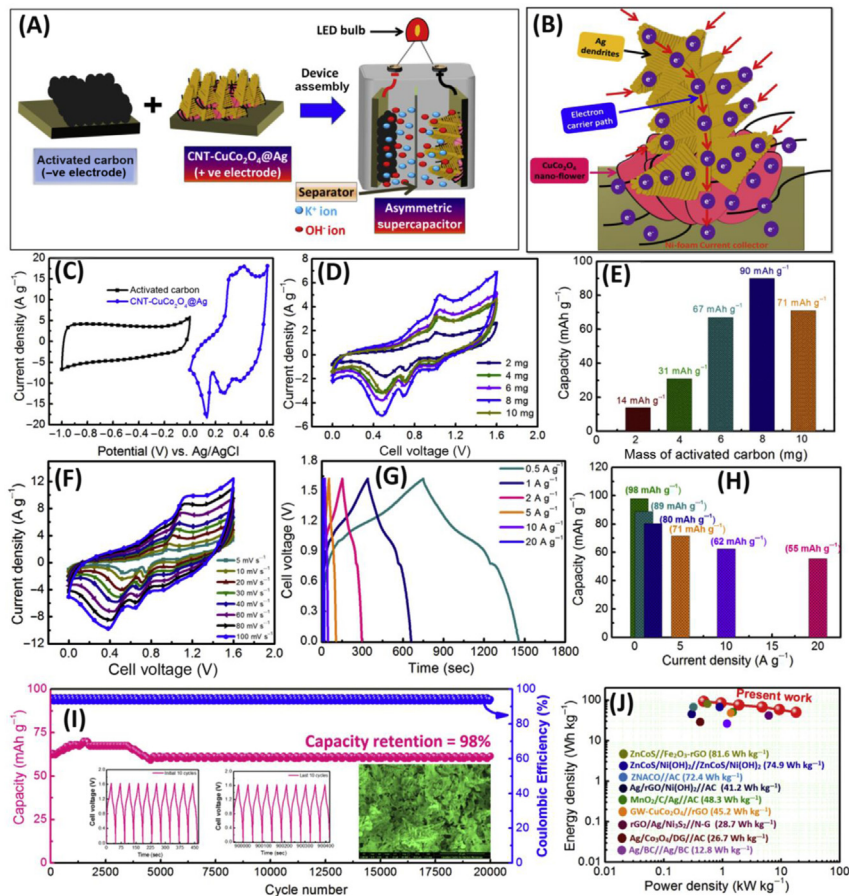


Figure 5.9 (A and B) Schematic of the fabrication of the CNT-CuCo₂O₄@Ag||AC supercapattery device with electron transport mechanism respectively, (C–J) electrochemical performances of the device. Reproduced with permission from M.M. Vadiyar, X. Liu, Z. Ye, Highly porous silver dendrites on carbon nanotube wrapped copper cobaltite nano-flowers for boosting energy density and cycle stability of asymmetric supercapattery, *J. Power Sources* 415 (2019) 154–164. Copyright 2019, Elsevier Ltd.

operating window can be greatly increased while maintaining the high power density [50].

A simple facile hydrothermal route was used in the synthesis of cobalt phosphate hydrate (Co₃(PO₄)₂ · 8H₂O) on a nickel foam (NF). A supercapattery device was assembled with Co₃(PO₄)₂ · 8H₂O/NF as the positrode and AC/NF as the negatrode. Such a device showed excellent capacity and stability when compared to those exhibited by the monometallic

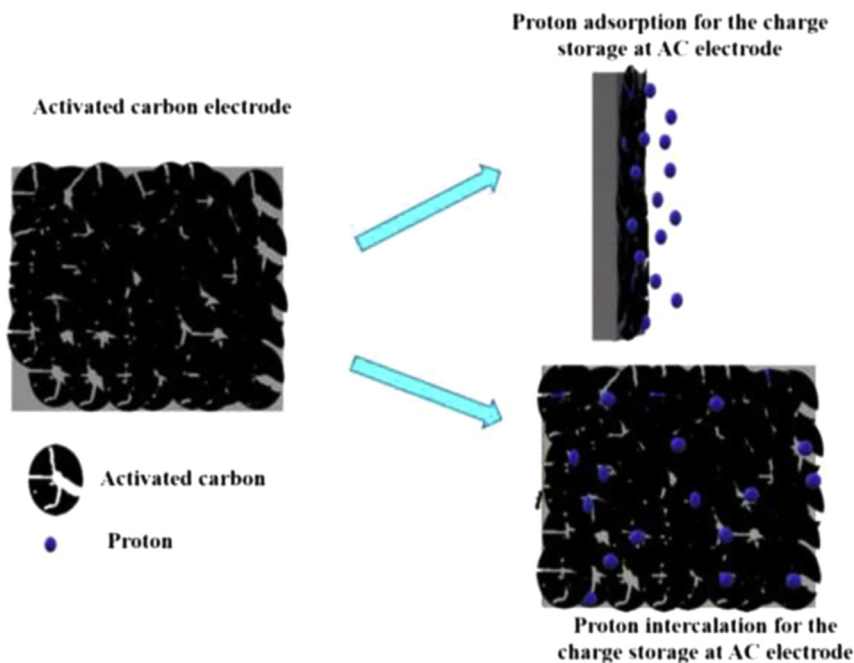


Figure 5.10 Schematic of proton adsorption and intercalation at the activated carbon electrode. Reproduced with permission from S. Manoharan, S. Sahoo, P. Pazhamalai, S.J. Kim, *Supercapacitive properties of activated carbon electrode using ammonium based proton conducting electrolytes*, *Int. J. Hydrog. Energy* 43 (2018) 1667–1674. Copyright 2017, Elsevier Ltd.

phosphate-based electrodes. $\text{Co}_3(\text{PO}_4)_2 \cdot 8\text{H}_2\text{O}/\text{NF}/\text{separator}/\text{AC}/\text{NF}$ delivers a high specific capacitance of 111.2 F g^{-1} with energy and power densities of 29.29 Wh kg^{-1} and 4687 W kg^{-1} , respectively. The device also exhibited a cyclic stability of 77.9% after 1000 charge–discharge cycles [51]. Omar et al. reported the preparation of a nickel phosphate–silver phosphate ($\text{Ni}_3(\text{PO}_4)_2\text{-Ag}_3\text{PO}_4$) nanocomposite through a sonochemical method. This composite was used as the positive electrode with AC as the negative electrode in a supercapattery cell. AC when used as a negative electrode can absorb more ions from the electrolyte with its porous nature. $\text{Ni}_3(\text{PO}_4)_2\text{-Ag}_3\text{PO}_4/\text{AC}$ exhibited a high energy density of 32.4 Wh kg^{-1} and power density of 6382 W kg^{-1} . A capacitance retention of about 82% was obtained even after 5000 cycles [52].

Manikandan et al. reported the fabrication of supercapattery with N, O-AC-coated Ni foam as the negative electrode and $\text{NiS}_2@\text{NiV}_2\text{S}_4$ (NS@NVS) as the positive electrode. Fig. 5.11 demonstrates the electrochemical behavior of

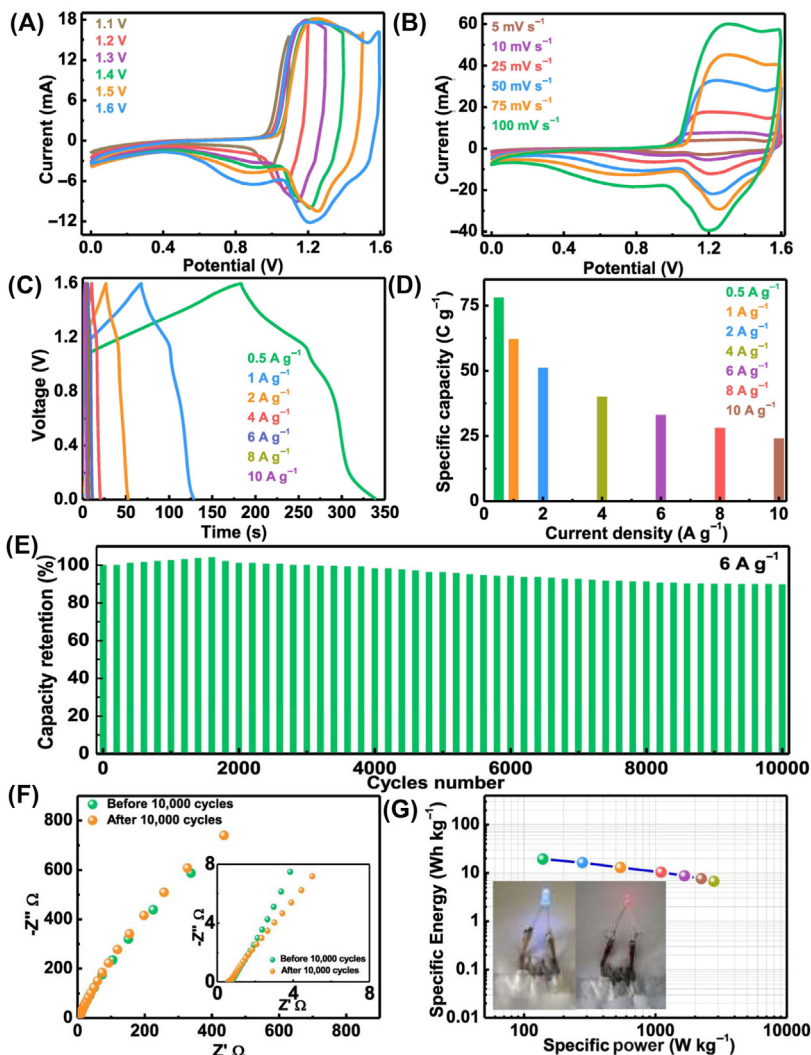


Figure 5.11 Electrochemical performance of NS@NVS//N,O-AC supercapattery. (A) CVs of the supercapattery measured at various potential range, (B) CVs of supercapattery at various scan rates, (C) galvanostatic discharge curves, (D) specific capacity of the supercapattery for various specific currents, (E) The specific capacity retention as a function of 10,000 charge/discharge cycles for the device at a specific current of 6 A g⁻¹, (F) The Nyquist plots before and after cycling stability of the device (inset shows the high-frequency region of the plots), and (G) Ragone plot of the NS@NVS//N,O-AC supercapattery displaying the correlation between energy and power densities (inset displays the glowing LED's (red and blue) using supercapattery). *Reproduced with permission from R. Manikandan, C.J. Raj, K.H. Yu, B.C. Kim, Self-coupled nickel sulfide @ nickel vanadium sulfide nanostructure as a novel high capacity electrode material for supercapattery, Appl. Surf. Sci. 497 (2019) 143778. Copyright 2019, Elsevier Ltd.*

Table 5.1 Comparison of different carbonaceous materials and their composites as electrodes in supercapattery.

Supercapattery	Specific capacity	Cell voltage	Capacity retention	Specific energy and power density	References
Ni ₃ (PO ₄) ₂ ·8H ₂ O rGO	122.3 C g ⁻¹ at 1 A g ⁻¹	1.5 V	83.59% after 1000 cycles	25.48 Wh kg ⁻¹ at 750.02 W kg ⁻¹	[31]
Ni/NiFe ₂ O ₄ @C rGO	–	1.2 V	100% after 5000 cycles	62 Wh kg ⁻¹ at 3440 Wh kg ⁻¹	[32]
rGO/TiO ₂ AC	186.2 mAh g ⁻¹ at 0.4 A g ⁻¹	1.45 V	92% after 3000 cycles	54.37 Wh kg ⁻¹ at 420.48 Wh kg ⁻¹	[33]
MWCNT-Co ₃ O ₄ -Ag AC	–	1.5 V	93.1% after 3000 cycles	16.5 Wh kg ⁻¹ at 297.5 Wh kg ⁻¹	[4]
NiCoP/CNF NiCoP/CNF	269 F g ⁻¹ at 1.5 A g ⁻¹	1.6 V	73% after 25000 cycles	36 Wh kg ⁻¹ at 1200 W kg ⁻¹	[42]
CNT-CuCo ₂ O ₄ @Ag AC	98 mAh g ⁻¹ at 0.5 A g ⁻¹	1.6 V	98% after 20000 cycles	91 Wh kg ⁻¹ at 0.42 kW kg ⁻¹	[43]
CoMoO ₄ AC	64 C g ⁻¹ at 1 A g ⁻¹	1.6 V	93% after 5000 cycles	18.89 Wh kg ⁻¹ at 1.06 kW kg ⁻¹	[48]
Co ₃ (PO ₄) ₂ ·8H ₂ O AC	111.2 F g ⁻¹ at 5 mA cm ⁻²	1.5 V	77.9% after 1000 cycles	29.29 Wh kg ⁻¹ at 468.75 W kg ⁻¹	[51]
LiMnPO ₄ AC	110 F g ⁻¹ at 1 mV s ⁻¹	1.5 V	88% after 5000 cycles	31 Wh kg ⁻¹ at 288 W kg ⁻¹	[47]

such a device. The CV curves plotted at varying potential windows indicate both EDLC and battery type behavior. Even at high scan rates, the shape of the CV curves and the redox peaks were retained indicating the faradic behavior of the supercapattery. The device could operate at a wide potential window of 1.6 V with a specific capacity, energy density, and power density of 78 C g^{-1} , 19.4 Wh kg^{-1} , and 140 W kg^{-1} respectively. The hybrid cell was stable up to 10,000 cycles with a capacitance retention of 90%. This improved stability can be attributed to the synergistic effect between the N,O enriched-AC negative electrode and NS@NVS positive electrode [53] (Table 5.1).



5.3 Summary and outlook

Supercapattery is a new hybrid energy storage system combining the benefits of both supercapacitors (fast charge–discharge rate) and batteries (energy storage capacity). Such a system combines the EDL capacitance and the capacitance obtained due to the redox reactions in the same cell. The type of electrode materials used in the construction of supercapattery is crucial in obtaining improved performance. Metal oxides and polymer complexes have been the most commonly used materials for battery type electrodes, whereas carbonaceous materials such as rGO, CNTs, and AC have been used in the construction of the supercapacitor-type electrode. The materials used in the construction of battery type electrodes possess a pseudocapacitive behavior but have a low surface area. Carbonaceous materials have porous structures with a high surface area which enable electrolyte ions to easily diffuse through them, thereby improving the storage capacity. Carbonaceous electrodes when made composites with battery type electrodes help in improving the overall energy and power capacities. Further innovations in the synthesis of electrode materials and fabrication techniques for supercapatteries will enable them to be used practically as hybrid energy storage devices in a myriad of applications.

References

- [1] D. Larcher, J.M. Tarascon, Towards greener and more sustainable batteries for electrical energy storage, *Nat. Chem.* 7 (2014) 19.
- [2] G.Z. Chen, Perception of supercapacitor and supercapattery, *Meet. Abstr. MA2011-02* (2011) 559.

- [3] A.J. Stevenson, D.G. Gromadskyi, D. Hu, J. Chae, L. Guan, L. Yu and G.Z. Chen, Supercapatteries with hybrids of redox active polymers and nanostructured carbons, *Nanocarbons for Advanced Energy Storage*, Vol 1, Wiley-VCH, 2015, 179–210.
- [4] J. Iqbal, A. Numan, S. Rafique, R. Jafer, S. Mohamad, K. Ramesh, et al., High performance supercapattery incorporating ternary nanocomposite of multiwalled carbon nanotubes decorated with Co_3O_4 nanograins and silver nanoparticles as electrode material, *Electrochim. Acta* 278 (2018) 72–82.
- [5] K.C. Ng, S. Zhang, C. Peng, G.Z. Chen, Individual and bipolarly stacked asymmetrical aqueous supercapacitors of CNTs / SnO_2 and CNTs / MnO_2 nanocomposites, *J. Electrochem. Soc.* 156 (2009) A846–A853.
- [6] G.A. Snook, P. Kao, A.S. Best, Conducting-polymer-based supercapacitor devices and electrodes, *J. Power Sources* 196 (2011) 1–12.
- [7] M. Ndipingwi, C. Ikpo, N. Hlongwa, N. Ross, M. Masikini, S.V. John, et al., Orthorhombic (Pmn21) nanostructured $\text{Li}_2\text{MnSiO}_4/\text{Al}_2\text{O}_3$ supercapattery electrode with efficient Li ion migratory pathway, *Batteries Supercaps* (2018).
- [8] Z. Fang, W. Xu, T. Huang, M. Li, W. Wang, Y. Liu, et al., Facile scalable synthesis of Co_3O_4 /carbon nanotube hybrids as superior anode materials for lithium-ion batteries, *Mater. Res. Bull.* 48 (2013) 4419–4423.
- [9] L. Hao, X. Li, L. Zhi, Carbonaceous electrode materials for supercapacitors, *Adv. Mater.* 25 (2013) 3899–3904.
- [10] Q. Cheng, J. Tang, J. Ma, H. Zhang, N. Shinya, L.-C. Qin, Graphene and carbon nanotube composite electrodes for supercapacitors with ultra-high energy density, *Phys. Chem. Chem. Phys.* 13 (2011) 17615–17624.
- [11] G.Z. Chen, Supercapacitor and supercapattery as emerging electrochemical energy stores, *Int. Mater. Rev.* 62 (2017) 173–202.
- [12] K. Novoselov, A. Geim, S. Morozov, D. Jiang, Y. Zhang, S. Dubonos, et al., Electric field effect in atomically thin carbon films, *Nat. Mater.* 6 (2004).
- [13] P. Simon, Y. Gogotsi, Materials for electrochemical capacitors, *Nat. Mater.* 7 (2008) 845–854.
- [14] R.S. Dey, H.A. Hjuler, Q. Chi, Approaching the theoretical capacitance of graphene through copper foam integrated three-dimensional graphene networks, *J. Mater. Chem. A* 3 (2015) 6324–6329.
- [15] Z. Yu, L. Tetard, L. Zhai, J. Thomas, Supercapacitor electrode materials: nanostructures from 0 to 3 dimensions, *Energy Environ. Sci.* 8 (2015) 702–730.
- [16] Y. Zhao, J. Liu, B. Wang, J. Sha, Y. Li, D. Zheng, et al., Supercapacitor electrodes with remarkable specific capacitance converted from hybrid graphene oxide/ NaCl /urea films, *ACS Appl. Mater. Interfaces* 9 (2017) 22588–22596.
- [17] M.D. Stoller, S. Park, Y. Zhu, J. An, R.S. Ruoff, Graphene-based ultracapacitors, *Nano Lett.* 8 (2008) 3498–3502.
- [18] Q. Qu, S. Yang, X. Feng, 2D sandwich-like sheets of iron oxide grown on graphene as high energy anode material for supercapacitors, *Adv. Mater.* 23 (2011) 5574–5580.
- [19] C. Liu, Z. Yu, D. Neff, A. Zhamu, B.Z. Jang, Graphene-based supercapacitor with an ultrahigh energy density, *Nano Lett.* 10 (2010) 4863–4868.
- [20] K.S. Novoselov, A.K. Geim, S.V. Morozov, D. Jiang, Y. Zhang, S.V. Dubonos, et al., Electric field effect in atomically thin carbon films, *Science* 306 (2004) 666–669.
- [21] C.-Y. Su, A.-Y. Lu, Y. Xu, F.-R. Chen, A.N. Khlobystov, L.-J. Li, High-quality thin graphene films from fast electrochemical exfoliation, *ACS Nano* 5 (2011) 2332–2339.
- [22] K.S. Subrahmanyam, L.S. Panchakarla, A. Govindaraj, C.N.R. Rao, Simple method of preparing graphene flakes by an arc-discharge method, *J. Phys. Chem. C* 113 (2009) 4257–4259.

- [23] Y. Chen, H. Zhao, L. Sheng, L. Yu, K. An, J. Xu, et al., Mass-production of highly-crystalline few-layer graphene sheets by arc discharge in various H₂–inert gas mixtures, *Chem. Phys. Lett.* 538 (2012) 72–76.
- [24] J.J. Yoo, K. Balakrishnan, J. Huang, V. Meunier, B.G. Sumpter, A. Srivastava, et al., Ultrathin planar graphene supercapacitors, *Nano Lett.* 11 (2011) 1423–1427.
- [25] Q. Ke, J. Wang, Graphene-based materials for supercapacitor electrodes – A review, *J. Materiomics* 2 (2016) 37–54.
- [26] S. Stankovich, D.A. Dikin, G.H.B. Dommett, K.M. Kohlhaas, E.J. Zimney, E.A. Stach, et al., Graphene-based composite materials, *Nature* 442 (2006) 282–286.
- [27] Q. Ke, Y. Liu, H. Liu, Y. Zhang, Y. Hu, J. Wang, Surfactant-modified chemically reduced graphene oxide for electrochemical supercapacitors, *RSC Adv.* 4 (2014) 26398–26406.
- [28] S. Mao, K. Yu, S. Cui, Z. Bo, G. Lu, J. Chen, A new reducing agent to prepare single-layer, high-quality reduced graphene oxide for device applications, *Nanoscale* 3 (2011) 2849–2853.
- [29] D. Nandi, V.B. Mohan, A.K. Bhowmick, D. Bhattacharyya, Metal/metal oxide decorated graphene synthesis and application as supercapacitor: a review, *J. Mater. Sci.* 55 (2020) 6375–6400.
- [30] A.C. Lokhande, I.A. Qattan, C.D. Lokhande, S.P. Patole, Holey graphene: an emerging versatile material, *J. Mater. Chem. A* 8 (2020) 918–977.
- [31] X. Peng, H. Chai, Y. Cao, Y. Wang, H. Dong, D. Jia, et al., Facile synthesis of cost-effective Ni₃(PO₄)₂·8H₂O microstructures as a supercapattery electrode material, *Mater. Today Energy* 7 (2018) 129–135.
- [32] A. Mattath, A. Prasath, A. Selva Sharma, V. Devi, E. Duraisamy, P. Elumalai, Ni/NiFe₂O₄@carbon nanocomposite involving synergistic effect for high-energy density and high-power density supercapattery, *Mater. Res. Express* 6 (2019).
- [33] I. Heng, F.W. Low, C.W. Lai, J.C. Juan, N. Amin, S.K. Tiong, High performance supercapattery with rGO/TiO₂ nanocomposites anode and activated carbon cathode, *J. Alloy. Compd.* 796 (2019) 13–24.
- [34] S. Iijima, Helical microtubules of graphitic carbon, *Nature* 354 (1991) 56–58.
- [35] A. Aqel, K.M.M.A. El-Nour, R.A.A. Ammar, A. Al-Warthan, Carbon nanotubes, science and technology part (I) structure, synthesis and characterisation, *Arab. J. Chem.* 5 (2012) 1–23.
- [36] R.H. Baughman, A.A. Zakhidov, W.A. de Heer, Carbon nanotubes—the route toward applications, *Science* 297 (2002) 787–792.
- [37] K. Saeed, I. Khan, Carbon nanotubes-properties and applications: a review, *Carbon Lett.* 14 (2013).
- [38] S. Kumar, M. Nehra, D. Kedia, N. Dilbaghi, K. Tankeshwar, K.-H. Kim, Carbon nanotubes: A potential material for energy conversion and storage, *Prog. Energy Combust. Sci.* 64 (2017).
- [39] V.N. Popov, Carbon nanotubes: properties and application, *Mater. Sci. Eng. R. Rep.* 43 (2004) 61–102.
- [40] N.M. Saifuddin, A.Z. Raziah, A.R. Junizah, Carbon nanotubes: a review on structure and their interaction with proteins, *J. Chem.* 2013 (2012).
- [41] H. Pan, J. Li, Y.P. Feng, Carbon nanotubes for supercapacitor, *Nanoscale Res. Lett.* 5 (2010) 654–668.
- [42] S. Surendran, S. Shanmugapriya, A. Sivanantham, S. Shanmugam, R. Kalai Selvan, Electrospun carbon nanofibers encapsulated with NiCoP: a multifunctional electrode for supercapattery and oxygen reduction, oxygen evolution, and hydrogen evolution reactions, *Adv. Energy Mater.* 8 (2018) 1800555.

- [43] M.M. Vadiyar, X. Liu, Z. Ye, Highly porous silver dendrites on carbon nanotube wrapped copper cobaltite nano-flowers for boosting energy density and cycle stability of asymmetric supercapattery, *J. Power Sources* 415 (2019) 154–164.
- [44] M. Kaman, K. Subramani, N. Sudhan, N. Ilayaraja, M. Sathish, Aloe vera derived activated high-surface-area carbon for flexible and high-energy supercapacitors, *ACS Appl. Mater. Interfaces* 8 (2016) 35191–35202.
- [45] Z. Hu, M. Srinivasan, Mesoporous high-surface-area activated carbon, *Microporous Mesoporous Mater.* 43 (2001) 267–275.
- [46] I.M. Babu, J.J. William, G. Muralidharan, Hierarchical β -Co(OH)₂/CoO nanosheets: an additive-free synthesis approach for supercapattery applications, *Ionics* 25 (2019) 2437–2444.
- [47] N. Priyadharsini, A. Shanmugavani, S. Surendran, B. Senthilkumar, L. Vasylechko, R. Kalai Selvan, Improved electrochemical performances of LiMnPO₄ synthesized by a hydrothermal method for Li-ion supercapatteries, *J. Mater. Sci. Mater. Electron.* 29 (2018) 18553–18565.
- [48] B.C. Kim, R. Manikandan, K.H. Yu, M.-S. Park, D.-W. Kim, S.Y. Park, et al., Efficient supercapattery behavior of mesoporous hydrous and anhydrous cobalt molybdate nanostructures, *J. Alloy. Compd.* 789 (2019) 256–265.
- [49] S. Manoharan, S. Sahoo, P. Pazhamalai, S.J. Kim, Supercapacitive properties of activated carbon electrode using ammonium based proton conducting electrolytes, *Int. J. Hydrog. Energy* 43 (2018) 1667–1674.
- [50] L. Yu, G.Z. Chen, High energy supercapattery with an ionic liquid solution of LiClO₄, *Faraday Discuss.* 190 (2016) 231–240.
- [51] H. Shao, N. Padmanathan, D. McNulty, C. O'Dwyer, K.M. Razeeb, Supercapattery based on binder-free Co₃(PO₄)₂·8H₂O multilayer nano/microflakes on nickel foam, *ACS Appl. Mater. Interfaces* 8 (2016) 28592–28598.
- [52] F.S. Omar, A. Numan, S. Bashir, N. Duraisamy, R. Vikneswaran, Y.-L. Loo, et al., Enhancing rate capability of amorphous nickel phosphate supercapattery electrode via composition with crystalline silver phosphate, *Electrochim. Acta* 273 (2018) 216–228.
- [53] R. Manikandan, C.J. Raj, K.H. Yu, B.C. Kim, Self-coupled nickel sulfide @ nickel vanadium sulfide nanostructure as a novel high capacity electrode material for supercapattery, *Appl. Surf. Sci.* 497 (2019) 143778.



Binary metal oxides for supercapattery devices

Muhammad Zahir Iqbal and Abbas Khan

Nanotechnology Research Laboratory, Faculty of Engineering Sciences, GIK Institute of Engineering Sciences and Technology, Topi, Pakistan



6.1 Introduction

The rapid increase in the concerns and challenges of electrochemical energy storage has made the supercapacitors and batteries a viable choice for fulfilling the energy needs of modern society [1]. As a prospective power source, electrochemical supercapacitors have gained considerable research interest due to their excellent power density and long cycling stability [2,3]. In order to meet the requirements of practical applications, tremendous research has been carried out to explore high-performance active electrode materials for equipping the supercapacitor in novel device architectures. The charge storage processes typically follow two mechanisms: (1) electric double-layer effect (EDLE), where charge is stored electrostatically at the electrode–electrolyte interface following the formation of a Helmholtz double-layer during polarization; and (2) Faradaic charge storage mechanism which is based on the contribution of electrochemical reactions [3,4]. The former most often occurs in carbon-based materials that exhibit electrostatic charge storage at the electrode interface. The latter generally require metal oxides and conductive polymers to be used as an electrode material which gives high capacitance and energy density compared to electric double-layer capacitors (EDLC). The materials with Faradaic charge storage abilities are used for electrodes of a battery device. EDLC is the most representative and basic system in this classification which is based on the electric double-layer effect and allows the charges to be stored electrostatically on its electrode surfaces [5,6]. The charge storage mechanisms of supercapacitors are depicted in Fig. 6.1. As a third option in the category of supercapacitors, the idea of asymmetric and

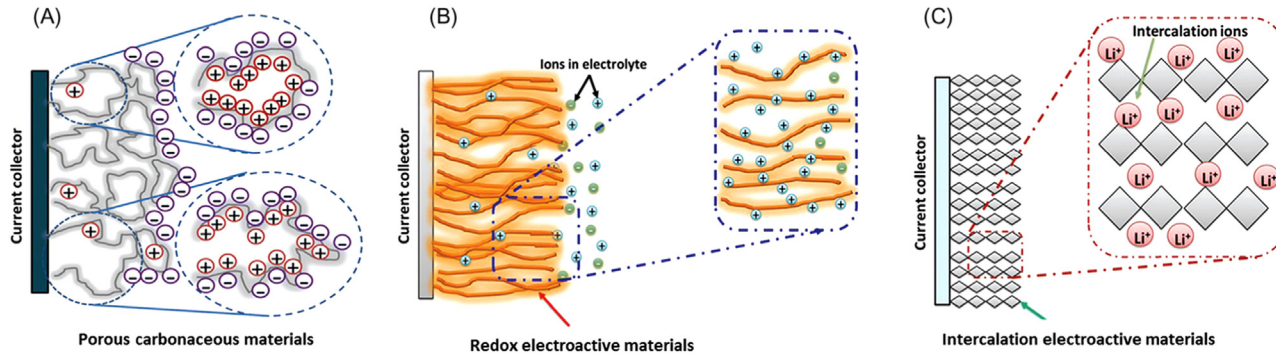


Figure 6.1 Charge storage mechanism of supercapacitor materials. (A) Electric double-layer capacitors store the charges at its electrode surface of porous carbonaceous materials. The charges are confined onto the electrode surface by electrostatic adsorption of negative ions. Charge storage mechanism of pseudocapacitive materials: (B) redox behavior as found in RuO_2 and (C) intercalation behavior wherein insertion and desertion of Li^+ ions take place in the active material. Reprinted with permission from S. Balasubramaniam, et al., *Comprehensive insight into the mechanism, material selection and performance evaluation of supercapatteries*. *Nano-Micro Lett.* 12 (2020) 1–46 [7]. Copyright 2020 Springer Nature.

hybrid supercapacitors came into being, with the intention to improve the energy density up to a range of 20–30 Wh kg⁻¹ [4]. This type of supercapacitor has features of both the abovementioned configurations, as indicated by the name “hybrid.”

During the charge/discharge of the hybrid type of supercapacitive devices, electrostatic surface adsorption/desorption, as well as oxidation/reduction reactions, simultaneously occur at the electrode–electrolyte contact zone. Due to performance enhancement and more inclination of such devices toward real applications, the concept has been extended to develop the battery-type hybrid SCs. Such architectures can be developed by combining a SC electrode with a battery electrode. This unique configuration is taken into account with a label of either high energy SCs or high power batteries, as it merges the energy features of batteries to the power capabilities of SCs. In the recent literature, this unique battery–supercapacitor hybridization is termed as “supercapattery” [6,8]. This provides an opportunity for exploring the full potential of hybrid devices, which will help to overcome the individual problems and fill up the gap between batteries and supercapacitors [9,10]. The general guidance for the behavior of hybrid devices during electrochemical measurements is shown in Fig. 6.2. The shaded area shows the probability for the output curves of a supercapattery to exist between these two limiting cases.

In practice, any type of battery material in an appropriate electrolyte can be used for the development of supercapattery. Still, recent research

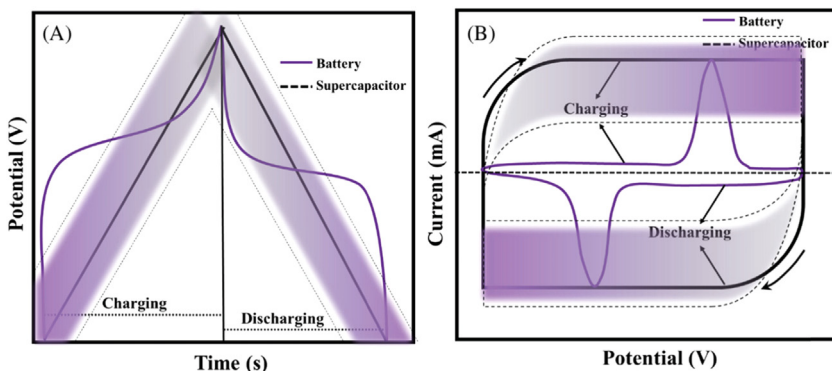


Figure 6.2 Schematic diagram for battery and supercapacitor comparison and possible outputs for hybrid devices. (A) Galvanostatic charge discharge curves. (B) Cyclic voltammogram curves. The shaded area shows that the curves for a supercapattery lies between these two limiting cases.

has been focused on the utilization of transition metal oxides/hydroxide [Co_3O_4 or $\text{Co}(\text{OH})_2$, NiO or $\text{Ni}(\text{OH})_2$, MnO_2 , V_2O_5 , etc.] as electrode materials for hybrid energy storage devices. Despite their excellent performance in electrochemical energy storage, these materials face some challenges in their commercial utilization, such as the toxic nature and high price of RuO_2 , low electronic and ionic conductivity as well as instability of NiO or Co_3O_4 , or the structural degradation of MnO_2 in electrolyte [11–13]. In order to further improve the storage performance and to overcome the challenges of single metal-based oxides, the concept of dual metallic component-based oxides, called binary metal oxides (BMOs), have been introduced. The electrochemical output of BMOs follows the battery-like signatures (deviation from rectangular CV and triangular GCD curves which are attributes of capacitive materials) [14,15]. Therefore these materials are regarded to be supercapattery electrode materials with a high energy density like batteries and a high power density comparable to supercapacitors [16]. This chapter gives an overview of the charge storage behavior of various BMOs with a detailed summary of the latest research in the field of supercapattery.



6.2 Binary metal oxides

BMOs are the class of nanomaterials possessing properties of high charge storage capacity, better electronic conductivities, and stability in structural arrangements. These features make them good contenders as an electrode material for supercapacitors. The basic atomic structure of BMOs comprises redox active ions which are connected with one or more transition metal ions. As an electrode material, the metallic entities in binary architecture play a synergistic role in enhancing the cationic substitutions within the material. In addition, due to the binary metallic correlation in BMOs, the issues of conventional unitary metal oxides such as low electronic conductivity and limited stability have improved dramatically.

Furthermore, the BMO platform causes strengthening of the active sites, which enhances the reversible storage capability compared to their unitary metallic oxides [17–19]. In this context, nickel-based BMOs showed remarkable improvements, for example, in recent reports, Ni-Co-O and Ni-Mn-O showed a considerably high capacitive performance compared with unitary nickel oxide [20,21]. In the same way, the incorporation of

copper with nickel oxide in a BMO configuration has been reported to give an increase of 30% capacitive performance over pure nickel oxide [22]. Following this strategy, several other types of interesting BMOs with various choices of metallic components have been developed in recent research which have confirmed the superior performance of these materials in hybrid energy storage devices [23,24]. These materials, as electrodes in supercapattery, exhibit the synergistic effect for enhancing the performance of the device in terms of a wider potential window, enriched reaction sites, outstanding electronic conductivities, and upgraded stability.

6.2.1 Synthesis of binary metal oxides

Several routes may be employed for the synthesis of BMOs which are shown in Fig. 6.3 and discussed below in detail:

6.2.1.1 Hydrothermal/solvothermal technique

The simplest, low cost and widely used technique for the synthesis of BMOs is the solvothermal technique which is sometimes also referred to as the hydrothermal method. This is a one-pot synthesis method that involves the recrystallization of materials by the provision of high temperature and pressure in a closed system [25]. In order to achieve a saturation

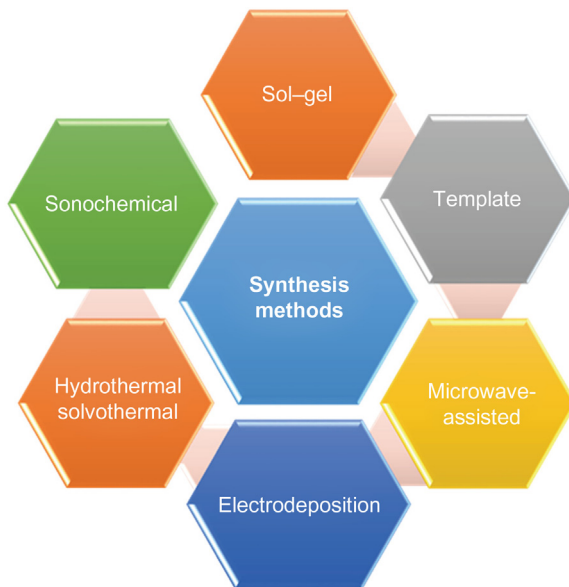


Figure 6.3 Synthesis methods for different types of binary metal oxides.

pressure, the temperature is kept mostly higher than 100°C. Instead of temperature, several other factors, such as the amount of solvent and dissolved precursors significantly affect the output product. A variety of metal oxides and their multicomponent nanostructures and transition metal-based compounds with multiple oxidation states can be synthesized by adopting this technique [3,24]. This method is advantageous in terms of its purity in output product, the involvement of chemicals with no toxic or harmful effects, easily achievable reaction conditions, and the formation of highly pure and large-sized crystals. Furthermore, by varying the reaction conditions in this route, a reasonable control over the particle size, distribution, and morphology of materials can be achieved [26]. The reaction conditions for the preparation of BMOs by the solvothermal method and the formation of different types of nanostructured materials are summarized in Table 6.1.

6.2.1.2 Microwave-assisted technique

Microwave-assisted synthesis of nanostructures was reported for the first time in 1986. It involves the utilization of microwaves which results in a heat-driven fast chemical reaction of organic and inorganic precursors in the solution. For the synthesis of BMOs, although the solvothermal method can be adopted, it requires a long reaction time ranging from hours to days [38]. The microwave-assisted technique dramatically reduces the reaction time to minutes and seconds and thus becomes an appealing route for the synthesis of BMOs. This route is advantageous for the growth of highly sensitive nanomaterials that require controlled reaction conditions. In particular, for the growth of BMOs, the reaction follows a heat-controlled mechanism which causes the elimination of the side reactions and offers a rapid crystallization. A variety of BMOs, such as XFe_2O_4 ($X = Zn, Ni, Mg, Co, Mn$), $Fe_2(MoO_4)_3$, $FeVO_4$, and $NiCo_2O_4$, etc., have been synthesized by a microwave-assisted method [39]. Wang et al. developed well crystalline XFe_2O_3 ($X = Mn, Co$) nanostructures (diameter >10 nm) by adopting a microwave-assisted synthesis route in which microwave heating was provided for 10 min without involving a calcination process [29]. High crystallinity can be attained by this method, whereas the control over the morphology and phase of BMOs is challenging to achieve [38]. The combined microwave–solvothermal route has summed up the benefits of individual conditions as it effectively decreases the reaction time and gives control over the phase and morphology of BMOs.

Table 6.1 Synthesis of binary metal oxides (BMOs) materials by several routes.

BMO materials	Synthesis method	Conditions	References
Urchin-like NiCo ₂ O ₄	Solvothermal method	H ₂ O, 100°C, 48 h	[27]
CoMoO ₄ nanoplate arrays on Ni-foam	Solvothermal method	H ₂ O, 180°C, 12 h	[25]
NiMnO ₃ -N-doped-graphene nanocomposite	Solvothermal method	H ₂ O, 180°C, 12 h	[28]
MgFe ₂ O ₄ nanoparticles	Microwave-assisted ball milling	1 kW, 15 min milling, 15 min MW, 60 h	[29]
Fe ₂ (MoO ₄) ₃ Pancake-like structures consists of nanosheets	Microwave-assisted hydrothermal synthesis	2.45 GHz, 200 W, 150°C, 1 min	[30]
NiCo ₂ O ₄ 3D hierarchical flower shaped	Microwave-assisted synthesis	320 W, 100°C, 15 min	[31]
Nano-Ni/Co(OH) ₂ nanoflake composite film	Electrodeposition method	25°C, current of 1.0 mA cm ⁻² for 200 s	[32]
Na _x MnO ₂ nanoflakes on nickle foam	Electrodeposition method	Current density of 350–500 μA cm ⁻² for 20, 100, and 200 min	[33]
Binary Mn–Co oxides	Electrodeposition method	25°C, potential of 0.8 V yield a total passed charge of 1.5 C cm ⁻²	[34]
Mesoporous crystalline CuCo ₂ O ₄	Hard template (nanocasting strategy)	400°C for 5 h, KIT-6 mesoporous template	[35]
ZnMn ₂ O ₄ ball-in-ball hollow microspheres	Thermally driven contraction process	170°C for 90 min, PVP	[36]
NiCo ₂ O ₄ hollow spheres with complex interior structures	Self-template hydrothermal method	180°C for 6 h in autoclave, glycerol	[37]

6.2.1.3 Sonochemical method

The sonochemical method is the most convenient and adaptable approach which can be used for the formation of materials in nanoscale dimensions. It utilizes the ultrasonic energy for decomposition of materials into small particles and the subsequent formation of a variety of nanomaterials like metal oxides, hydroxides, phosphates, and composites, etc. [40–42]. It is also a recommended technique for the dispersion of suspensions into the

solvents. A typical synthesis is carried out either by direct contact of ultrasonic source to the precursor solution (by dipping an ultrasonic probe into the solution) or by providing ultrasonic radiation in an indirect way (using a bath sonicator). Direct sonication is favorable for the applications where a high amount of ultrasonic energy is required. The ultrasonic waves travel through the solution in the form of compression–rarefaction coupling (generated due to a pressure gradient) and initiate a reaction known as a sonochemical reaction. During the reaction process, the formation and evolution of bubbles in the solution increases due to the continuous transfer of ultrasonic energy from the probe to the liquid medium. The fast growth (around 5–20 μm) and implosive collision of the bubbles causes them to liberate their stored potential energy in the liquid medium [43,44]. The involvement of high particle collision rates, rapid temperature and pressure variations (about 5000 K and 1000 atm), and extreme cooling rates (1010 K s^{-1}) during the reaction process effectively modify the dimensions and morphology of nanoparticles [45,46].

6.2.1.4 Electrodeposition method

Electrodeposition is also a one-pot synthesis method used for the development of BMOs nanostructures. The underlying mechanism in this process involves electrochemical Faradaic reactions. An electric current is allowed to pass through the solution containing metal salts which results in the deposition of metal ions on the surface of the cathode/anode [24]. Therefore this technique is widely used for metal/hydroxide coatings and the growth of BMOs nanomaterials. During the synthesis process of BMOs, various parameters, such as deposition potential, type and nature of anion, and pH of the solution are taken into account for controlling the reaction [32]. The method is favorable for BMOs growth because it directly grows the material on the surface of the current collector which results in a decrease in the electrical contact resistance up to 20% as compared to conventional two-step (material synthesis and electrode deposition) methods. Therefore the direct growth of BMOs on electrically conducting substrate effectively increases the gravimetric and volumetric energy density [47]. Furthermore, this process can take place even at room temperature to achieve the required product.

The best practice of this method is growth of NiCo_2O_4 by electrical reduction in nitrate salt solution of both metals. This results in the formation of a material with hydroxide phases that turns into BMOs by an annealing process. Additionally, different types of conducting platforms

like stainless steel, nickel foam, or carbon cloth/fiber can be used as a substrate for electrodeposition. One such synthesis has been reported by Du's group in which nanosheets of NiCo_2O_4 were deposited on carbon fiber for the fabrication of flexible supercapacitor devices [48]. Besides single BMOs, a microwave-assisted method for synthesis of composite/hybrid materials like $\text{NiCo}_2\text{S}_4@\text{MnO}_2$ and $\text{Ni}(\text{OH})_2@\text{NiCo}_2\text{O}_4$ has also been reported [49,50]. Despite its advantages, the low yield of this process is the main problem that limits its practical applicability.

6.2.1.5 Template method

The mesoporous structure of BMOs has highly advantageous features like a large active surface area, pore size tunability, and controlled morphology. These attributes of an electrochemically active material offer a unique structure to the material which is an essential requirement for the enhancement of interfacial contact between the electrode and electrolyte. This allows the easy diffusion of ionic electrolytes into the mesopores. Therefore mesoporous structures are the appropriate choice for their utilization in catalysis, sensors, and energy storage devices [51,52]. Initially, the synthesis of mesoporous materials was unsuccessful because of thermal instability. Consequently, novel routes were developed for the synthesis of mesoporous structures by coupling a template method with conventional methods (solvothermal or hydrothermal). A template method is further categorized into two types, hard and soft template method. In the hard template method, silica is considered to be an ideal template for the development of mesostructured BMOs. Mesoporous silica with strong interconnected four covalent bonds exhibits uniformity in pore size distribution and possesses a structure with a high degree of order at the nano-scale level. For instance, Yuan's group reported the fabrication of mesoporous microstructures of NiCo_2O_4 by employing a silica template [53]. They achieve highly uniform size distribution and good structural stability after removing the template and the material showed remarkable performance as a supercapacitor electrode. In hard templating, mesoporous carbon or silica KIT-6 is also used as a template to obtain highly ordered structures of BMOs. Several other BMOs structures like ZnCo_2O_4 , CoFe_2O_4 , and CuFe_2O_4 , etc. have also been developed by adopting hard template method [54–56].

On the other hand, the soft template method involves the use of surfactants, organic molecules, or block copolymers, which play the role of structure-controlling agents during the material growth process. The soft

template method is relatively low cost and has the ability to synthesize a variety of BMOs structures without the need for sophisticated facilities. Jan et al. adopted the soft template technique (using polymer) for the synthesis of 3D nanocrystalline NiMoO_4 thin-film electrodes [57]. The material exhibits enhanced storage capacity when used for batteries. Similarly, polyvinylpyrrolivone (PVP) was also used as a capping agent during the formation of NiCo_2O_4 mesoporous structures. The nitrogen and $\text{C}=\text{O}$ functional groups in the ring structure of PVP perform an act of coordination with metallic ions and greatly assist the development of a mesoporous structure. Thus this template method is an adoptable technique for the synthesis of a variety of BMOs with diverse morphologies. In combination with conventional synthesis routes, the template method could be more advantageous and have a prospect for future research in the field.

6.2.1.6 Other synthesis methods

There are several other modified and novel synthesis techniques that could be adopted for the growth and synthesis of 1D, 2D, or 3D BMOs, like the electrospinning method adopted for the synthesis of BMO nanofibers, the molten salt route for cobaltites, solution combustion synthesis of ferrites nanomaterial, the hot injection method for magnetates nanoparticles, and the microemulsion route for the growth of nanowires of BMOs [58–61].

6.2.2 Binary metal oxides for supercapattery applications

6.2.2.1 Cobaltites

Cobaltates (MCo_2O_4) are the compounds of cobalt oxide (Co_3O_4), which itself has been considered a good contender as an anode material for lithium-ion batteries due to its reversible capacity [62]. On the other hand, the toxic nature and high cost of cobalt species are the main obstacles in the way of their utilization in batteries and supercapatteries devices [24]. Therefore recent research has been devoted toward the development of environment-friendly and low cost spinel structures of MCo_2O_4 ($\text{M} = \text{Ni}, \text{Mn}, \text{Fe}, \text{Zn}$ and Cu , etc.) for energy storage applications [35,63–65]. Among them, zinc cobaltite has been reported as the most promising material for energy storage [66,67]. In the cubic spinel compounds of ZnCo_2O_4 , the zinc ions reside over the tetrahedral sites of the structure and contribute to capacity enhancement due to the alloying process [68]. During the charge storage process, the complex electrochemical mechanism is followed due to the involvement of multistep redox reactions as reported by Reddy's group [69]. In the CV results, a shift in cathodic

peak potential from 0.67 to 1.1 V was observed, which represents the decaying process of the ZnCo_2O_4 compound. The appearance of two peaks corresponds to the reactions that occur due to the transition of oxidation states of zinc (Zn to Zn^{+2}) and cobalt (Co to Co^{3+}) [69]. Several other cobaltites like nickel cobaltite, manganese cobaltite, and iron cobaltite showed a similarity in electrochemical charge storage mechanism to that of zinc cobaltite [70–72]. Nickel cobaltite (NiCo_2O_4) has also been considered a promising material of the cobaltite series. The interesting inverse spinel structure of NiCo_2O_4 consists of Ni-ions occupied at octahedral sites and Co-ions equally occupied by both tetrahedral and octahedral sites as shown in Fig. 6.4 [73].

In addition, a variety of designs and structures of cobaltite nanomaterials in different dimensions have been reported. These include 1D structures such as ZnCo_2O_4 nanowires and internally hollow porous nanotubes (200–300 nm), which offer a large surface-to-volume ratio and superior electronic transport [68,74]. Pendashteh et al. fabricated highly ordered mesoporous CuCo_2O_4 nanowires via a template method which exhibits remarkable performance as a supercapacitor electrode (specific capacitance of 1210 Fg^{-1}) [75]. These ordered mesoporous structures increase the accessibility of an electrolyte ion into the electrode by providing more diffusion channels (as represented in Fig. 6.5A which resulted in

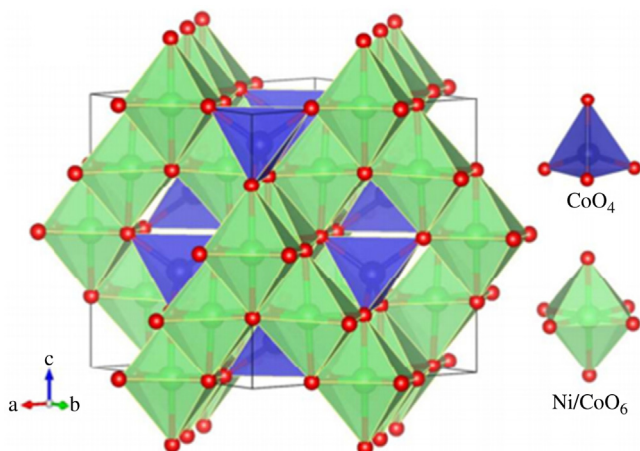


Figure 6.4 Structural arrangements of spinel NiCo_2O_4 . Reprinted with permission from L. Shen, et al., Self-templated formation of uniform NiCo_2O_4 hollow spheres with complex interior structures for lithium-ion batteries and supercapacitors. *Angew. Chem. Int. Ed.* 54 (6) (2015) 1868–1872. Copyright 2015 Royal Society of Chemistry.

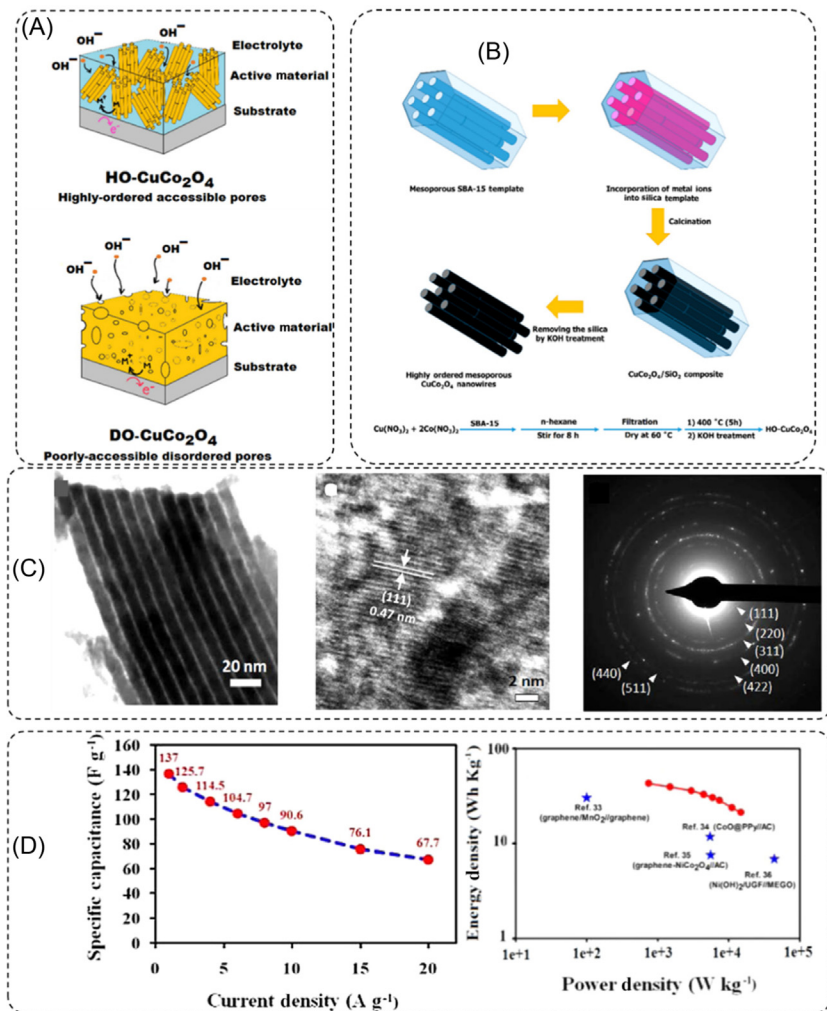


Figure 6.5 (A) Comparison model for pore access in highly ordered and disordered CuCo_2O_4 mesoporous materials. (B) Schematic representation of steps involved during synthesis of mesoporous CuCo_2O_4 nanowires by template method. (C) Surface characterizations of CuCo_2O_4 nanowires (TEM, HRTEM images). (D) Electrochemical characterizations of $\text{CuCo}_2\text{O}_4//\text{AC}$ asymmetric device (specific capacitance and Ragone plot at different current densities). Reprinted with permission from A., Pendashteh, et al., Highly ordered mesoporous CuCo_2O_4 nanowires, a promising solution for high-performance supercapacitors. *Chem. Mater.* 27 (11) (2015) 3919–3926. Copyright 2015 American Chemical Society.

an ultrahigh performance (42.8 Wh kg^{-1} at 15 kW kg^{-1}) when the material was used for the development of an asymmetric supercapacitor. The material preparation process is shown in Fig. 6.5B, while surface and electrochemical characterizations are depicted in Fig. 6.5C–D. Besides, the highly ordered structure gives rise to an excellent rate capability of 64% even at a larger current density value of 20 Ag^{-1} due to the sufficient transport of charged species from interconnected pathways in the electrode. Similarly, 3D mesoporous ZnCo_2O_4 microspheres have been synthesized by Wang's group (Fig. 6.6A–K) [76]. Due to uniform pores distribution and high specific surface area the material exhibits high specific capacitance of 953.2 Fg^{-1} at 4 Ag^{-1} with cyclic stability of 97.8% after 3000 cycles. The high capacitive performance results from the porous nature of the structure which helps in reducing the pathways for electronic and ionic pathways and enhancing the contact area between electrode and electrolyte.

Vijayakumar et al. developed an interesting layered architecture of ZnCo_2O_4 nanosheets by its direct growth on the Ni-foam (Fig. 6.7A–I) [63]. The layered structure not only provides a high surface-to-volume ratio but irregular arrangements of nanosheets offer enough porosity and active electrochemical sites, which were reported to be an ultimate reason for the enhanced performance. Other cobaltite nanostructures, for instance, FeCo_2O_4 nanoflakes, nanoporous double-shelled CuCo_2O_4 hollow spheres, mesoporous $\text{Ni}_{0.3}\text{Co}_{2.7}\text{O}_4$ hierarchical structures, and flower-like morphology $\text{Cu}_{0.27}\text{Co}_{2.73}\text{O}_4$; and composites of cobaltite with other conductive platforms like porous NiCo_2O_4 nanosheet composites grown on graphene and carbon nanotubes, nanocomposite of ZnCo_2O_4 intercalated with polyaniline, and 3D $\text{ZnCo}_2\text{O}_4/\text{N}$ -doped reduced graphene oxide composite, etc. have recently been reported to be high-performance materials for supercapatteries [65,66,77–80]. Despite their advantages, the major concern related to electronic conductivity rate capability still needs to be focused upon by developing novel designs and structures of cobaltites nanostructures.

6.2.2.2 Ferrites

Ferrites (MFe_2O_4) are the compounds of iron oxides (Fe_2O_4) with M representing other metallic species, for example, Zn, Ni, Cu, or Co. The exciting electrochemical features and other advantages including the abundant occurrence, low cost, and eco-friendly nature of Fe_2O_4 make it a suitable choice for electrochemical supercapacitors and batteries. Its

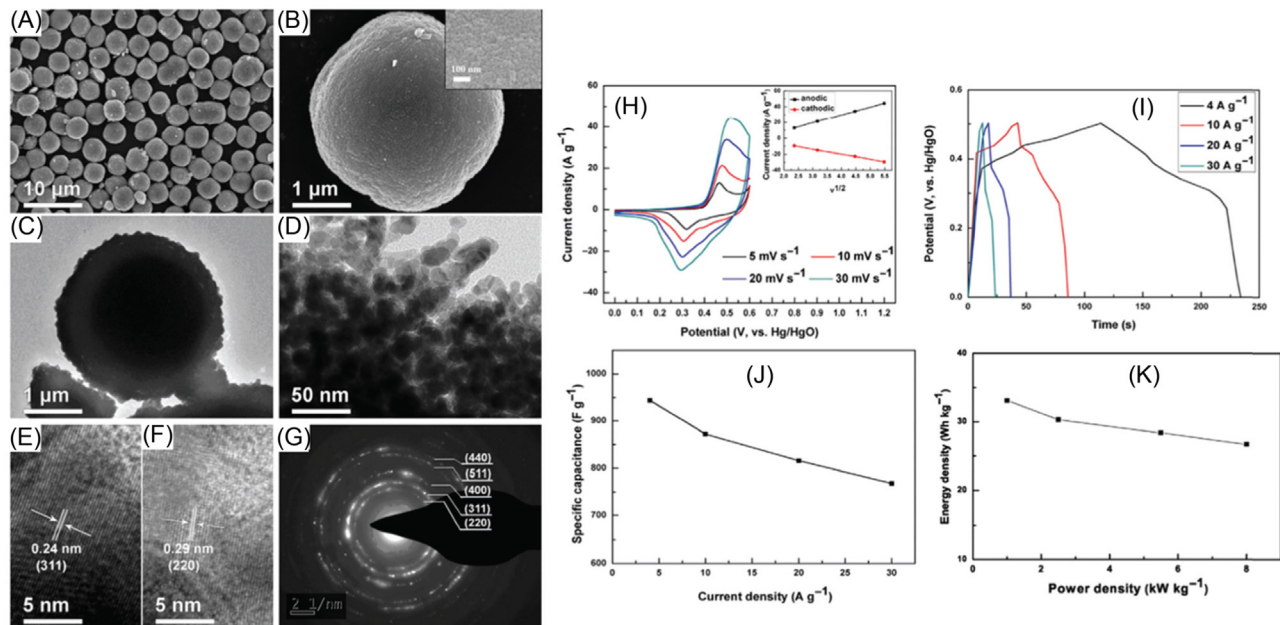


Figure 6.6 Surface characterization of mesoporous ZnCo_2O_4 microspheres: (A, B) SEM photographs; (C, D) TEM images at low resolution; (E, F) HRTEM photographs; and (G) SAED pattern. Electrochemical results of mesoporous ZnCo_2O_4 microspheres; (H) CVs results at different scan rates (inset: anodic and cathodic peak current density trend w.r.t inverse scan rates); (I) GCD at different current density values. (J) Specific capacitance versus current density; (K) Ragone plot at different current densities. *Reprinted with permission from Q., Wang, et al., Facile fabrication and supercapacitive properties of mesoporous zinc cobaltite microspheres. J. Power Sources 284 (2015) 138–145. Copyright 2015 Elsevier.*

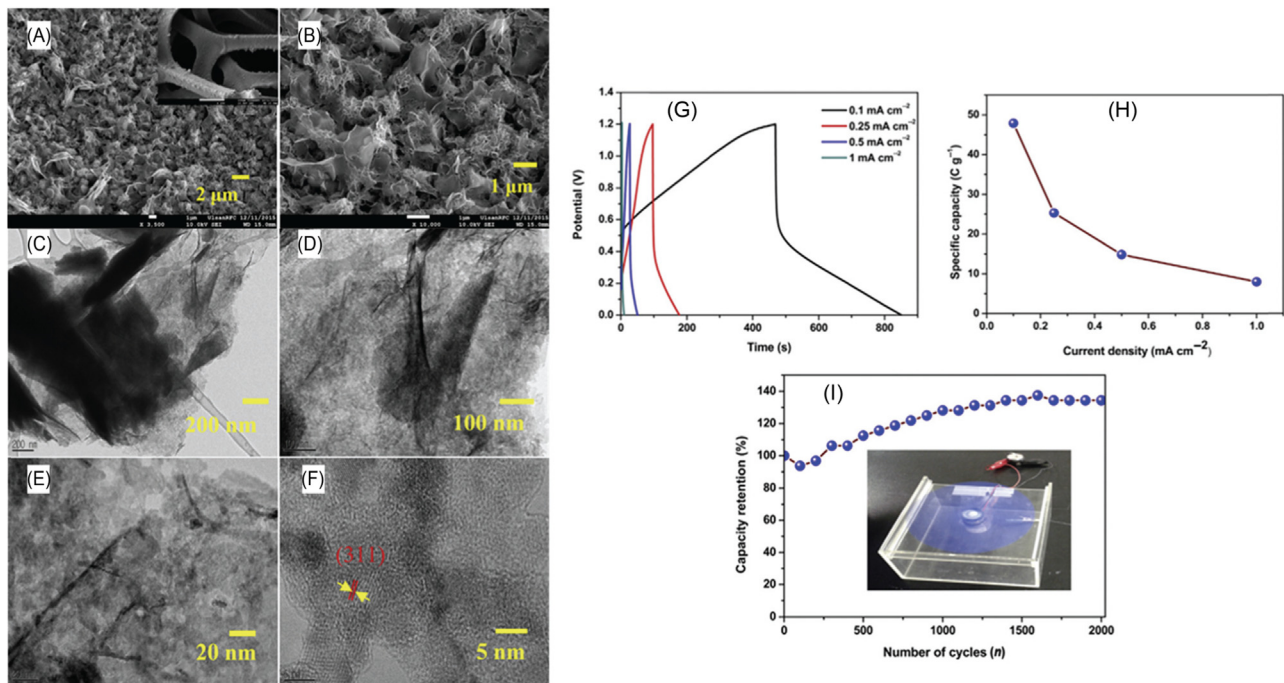


Figure 6.7 Surface studies of thin layered nanosheets of ZnCo₂O₄ (A, B) FESEM images (C–F) HRTEM photographs. Electrochemical results of ZnCo₂O₄ symmetric device; (G) GCD output trends at various current densities; (H) specific capacitance versus current density; (I) results of life cycle test (inset: photograph of coupled devices for mini fan operation). Reprinted with permission from S. Vijayakumar, et al., Porous thin layered nanosheets assembled ZnCo₂O₄ grown on Ni-foam as an efficient electrode material for hybrid supercapacitor applications. *Int. J. Hydrogen Energy* 42 (5) (2017) 3122–3129. Copyright 2016 Elsevier.

reversible capacity is estimated theoretically to be 926 mAhg^{-1} for lithium-ion storage [81]. However, Fe_2O_4 suffers from low conductivity and high oxidation potential which diversely affect the energy density and also cause a reduction in the capacity retention of the system due to reaction kinetics [82,83]. Therefore to overcome these issues, several strategies were adopted to design the novel spinal structures in the form of MFe_2O_4 for their utilization in hybrid energy storage devices [24,84–86]. The various dimensional spinal nanostructures exhibit high capacity, improved cycling stability, and enhanced rate capability compared to Fe_2O_4 . Similar to ZnCo_2O_4 , ZnFe_2O_4 grabbed much attention as an anode material for batteries not only due to its general attributes, such as being less toxic, cost-effective, and allowing easy synthesis, but specifically due to working at a much lower working potential as compared to cobaltite and other dimensional nanostructures of Fe_2O_4 [82,83,87]. However, in full cell configuration, the improved output voltage is expected due to their coupling with other electrode materials in a hybrid configuration. ZnFe_2O_4 nanostructures were mostly reported for anode material in lithium-ion batteries because of its high theoretically calculated specific capacity of 1072 mAhg^{-1} , due to the process of conversion and alloying reactions for reversible storage in nonaqueous electrolytes.

Javed et al. reported the development of mesoporous ZnFe_2O_4 nanowall arrays on carbon textiles for flexible supercapacitors and studied the lithium-ion hopping mechanism and energy barrier in prepared material by DFT calculations (Fig. 6.8A–E) [88]. The material exhibited good electrochemical behavior with a high specific capacity of 162.7 mAhg^{-1} at 3.35 Ag^{-1} which is retained 96.4% after 8000 cycles. The flexible supercapacitor showed specific energy up to 85 Wh kg^{-1} at a specific power of 1000 W kg^{-1} with a cyclic stability of 97.3% after 10,000 cycles. The charge storage mechanism in ZnFe_2O_4 nanowall arrays is followed by the redox process (Fe^{3+} to Fe^{2+} reactions) as well as an intercalation process of electrolyte ions into the electrode surface. DFT results showed that the low energy barrier value (0.37 eV) caused an easy diffusion of Li^+ ions into the electrode material. Similarly, ZnFe_2O_4 nanoparticles prepared by an aspartic acid-assisted combustion method also showed good performance as an electrode material for asymmetric supercapacitors (Fig. 6.8F–I) [89]. The highest specific capacitance for ZnFe_2O_4 nanoparticles was achieved 1235 Fg^{-1} at 1 mA cm^{-2} , while in asymmetric combination (ZnFe_2O_4 negative and $\text{Ni}(\text{OH})_2$ positive electrode), the device delivered a specific energy of 33 W h kg^{-1} and specific power of 68 W kg^{-1} , respectively.

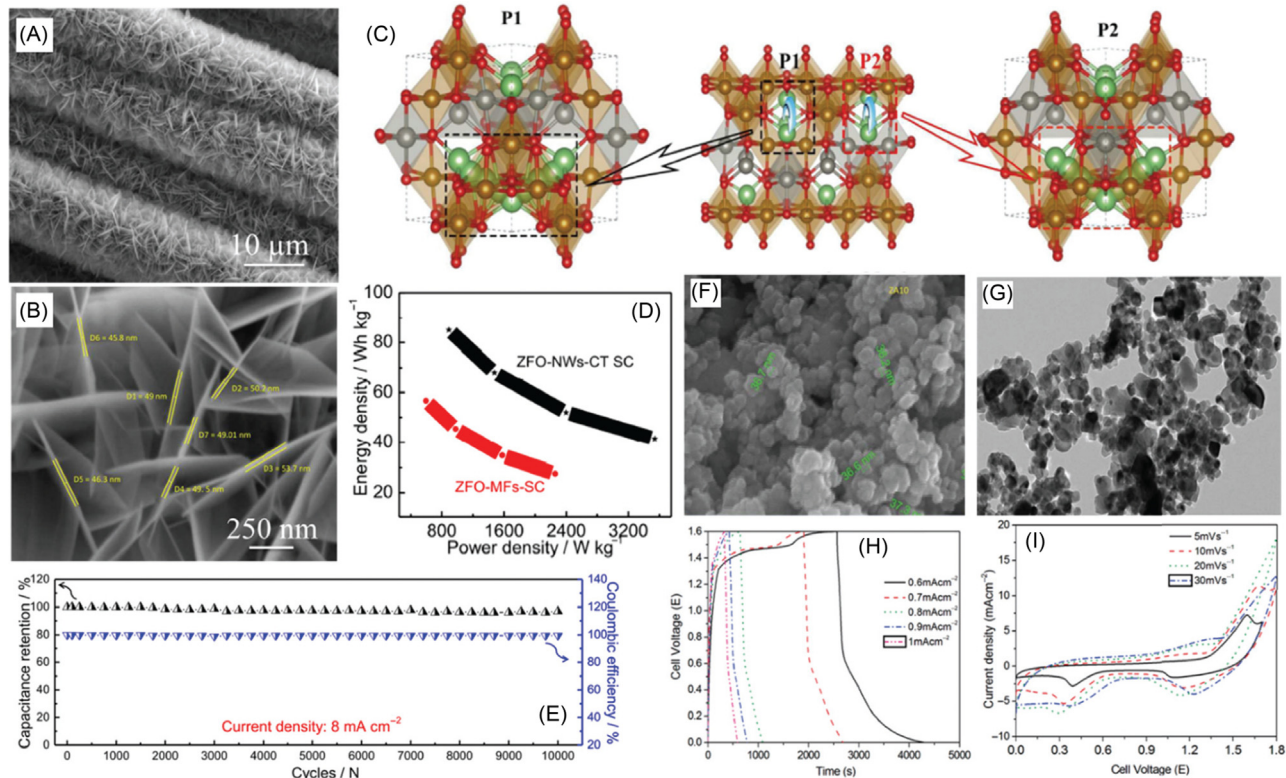


Figure 6.8 (A, B) SEM results of ZnFe₂O₄ nanowall arrays on carbon textile fibers. (C) DFT measurements of diffusion paths (P1, P2) for lithium-ion hopping in Li₆Zn₆Fe₁₂O₃₂ spinel architectures. The energy barrier for Li⁺ hopping in P1 and P2 was 0.37 and 0.69 eV, respectively. (D) Performance comparison of (E) cyclic stability results of ZnFe₂O₄ nanowalls on carbon textile fibers-based symmetric solid-state supercapacitor. Surface characterization of ZnFe₂O₄ nanoparticles: (F) HRSEM image; (G) TEM image. Electrochemical results of asymmetric supercapacitor fabricated by ZnFe₂O₄ nanoparticles (negative electrode) and Ni(OH)₂ (positive electrode): (H) CV curves at different scan rates and (I) GCD results at different current densities in 2M NaOH. (E) Reprinted with permission from M.S. Javed, et al., *Exploring Li-ion hopping behavior in zinc ferrite and promoting performance for flexible solid-state supercapacitor. Electrochim. Acta* 295 (2019) 558–568. Copyright 2018 Elsevier. Reprinted with permission from A. Shanmugavani, R.K. Selvan, *Synthesis of ZnFe₂O₄ nanoparticles and their asymmetric configuration with Ni (OH) 2 for a pseudocapacitor. RSC Adv.* 4 (51) (2014) 27022–27029. Copyright 2011 Royal Society of Chemistry.

Similarly, manganese ferrites (MnFe_2O_4) and cobalt ferrites (CoFe_2O_4) in different dimensional structures have been extensively studied for their utilization in hybrid supercapacitors. Guo's group presented MnFe_2O_4 colloidal nanocrystal assemblies (diameter ranges from 230 to 950 nm) as a supercapacitor electrodes material [90].

Similarly, diverse morphology of ferrite nanostructures such as CoFe_2O_4 nanotube arrays, NiFe_2O_4 nanowires, spinel MnFe_2O_4 nanorods, CoFe_2O_4 nanoparticles, and mixed-phase bismuth ferrite nanoflakes, etc. have been achieved by novel synthesis routes (Fig. 6.9A–L) [91–95].

Zhang et al. reported an interesting structure comprised of CoFe_2O_4 nanomesh arrays synthesized via by modified hydrothermal method followed by annealing process for supercapacitor electrodes and oxygen evolution reactions [96]. They achieve ultrahigh specific capacitance of 1426 Fg^{-1} at 1 Ag^{-1} which retained to 1024 Fg^{-1} even at 20 Ag^{-1} and notable cyclic stability of 92.6% was obtained after 3000 cycles (Fig. 6.10A–I). The ultrahigh capacity was due to the complete accessibility of active sites of the porous and high surface area nanomesh array structures. Besides ferrites in binary architectures (MFe_2O_4), ternary ferrites compounds ($\text{M}'\text{MFe}_2\text{O}_4$), and composites of ferrites with highly conductive carbonaceous materials have grabbed the recent research attention and been reported as an emerging material for supercapattery devices [84,97–99].

6.2.2.3 Manganites

Although cobaltites and ferrites are attractive materials among the BMOs, a manganite series of nanostructures with the general formula XMn_2O_4 ($\text{X} = \text{Ni}, \text{Cu}, \text{Co}$ or Fe , etc.) has also been reported as a promising energy storage material. The size occupied by Mn^{3+} in XMn_2O_4 is greater (with a radius of 0.79 \AA) than that of Co^{3+} in XCo_2O_4 (with a radius of 0.75 \AA), which considerably alters the properties of the material [100]. For instance, in ZnMn_2O_4 and ZnCo_2O_4 , both spinel nanostructures contained bivalent Zn -ions at tetrahedral sites and trivalent $\text{Mn}^{3+}/\text{Co}^{3+}$ at octahedral sites but ZnMn_2O_4 has relatively low bandgap of 1.23 eV [101]. However, among the manganites, CuMn_2O_4 with an inverted cubic spinel structure gives a higher bandgap value (1.40 eV) and superior conductivity ($6 \times 10^5 \Omega \text{ cm}$) compared to ZnMn_2O_4 ($2.5 \times 10^5 \Omega \text{ cm}$) [102]. Other manganites such as CoMn_2O_4 exhibit a tetrahedral structure, while NiMn_2O_4 shows cubic spinel structures and the bandgap increases in the sequence: $\text{CoMn}_2\text{O}_4 < \text{NiMn}_2\text{O}_4 < \text{CuMn}_2\text{O}_4$ [103]. The

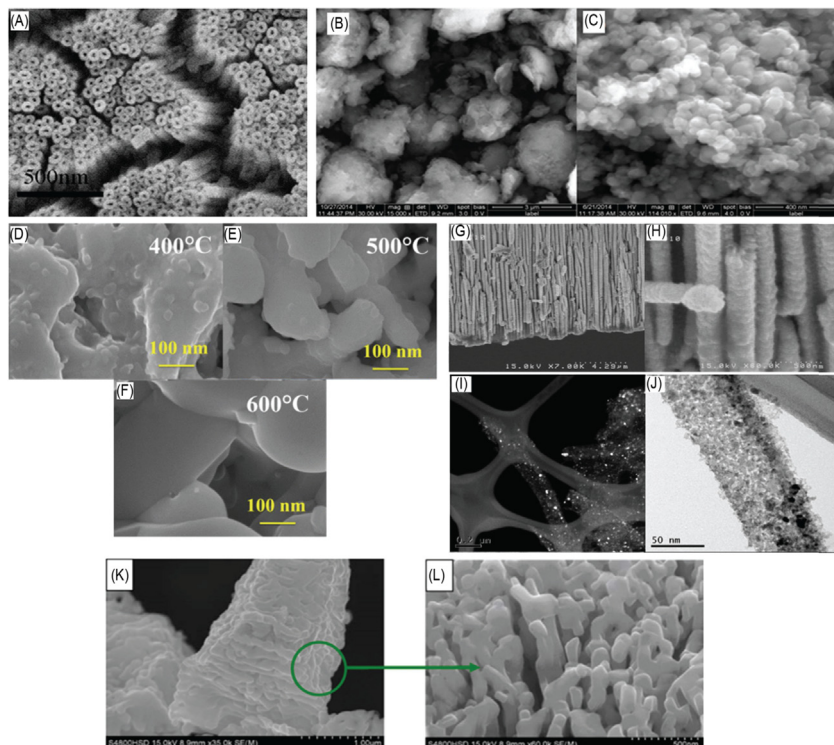


Figure 6.9 (A) SEM image of CoFe_2O_4 nanotube arrays synthesized by sol–gel template method. (B, C) FESEM image of $\text{Co}(\text{OH})_2$ and $\text{Co}_2\text{Fe}(\text{CN})_6$ particles, respectively. FESEM images of bismuth ferrite thin-film electrodes annealed at (D) 400°C (E) 500°C (F) 600°C . (G–H) Cross-section FESEM images of NiFe_2O_4 nanowires. TEM images of NiFe_2O_4 nanowires: (I) dark field; (J) bright field. (K, L) SEM images of spinel MnFe_2O_4 nanorods. (A) Reprinted with permission from Y. Xu et al., *Synthesis of CoFe_2O_4 nanotube arrays through an improved sol–gel template approach*. *Mater. Lett.* 62 (8–9) (2008) 1403–1405. (B, C) Reprinted with permission from A. Shanmugavani, D. Kalpana, R.K. Selvan, *Electrochemical properties of CoFe_2O_4 nanoparticles as negative and $\text{Co}(\text{OH})_2$ and $\text{Co}_2\text{Fe}(\text{CN})_6$ as positive electrodes for supercapacitors*. *Mater. Res. Bull.* 71 (2015) 133–141. Copyright 2015 Elsevier. Copyright 2007 Elsevier. (E) Reprinted with permission from V.V. Jadhav, et al., *Mixed-phase bismuth ferrite nanoflake electrodes for supercapacitor application*. *Appl. Nanosci.* 6 (4) (2016) 511–519. Copyright 2015 Springer Nature. (J) Reprinted with permission from A. Mehri, S.S. Ebrahimi, S. Masoudpanah, *Synthesis and characterization of high aspect ratio NiFe_2O_4 nanowire*. *J. Anal. Appl. Pyrolysis* 110 (2014) 235–238. Copyright 2014 Elsevier. (K, L) Reprinted with permission from X. Hou, et al., *Synthesis and characterizations of spinel MnFe_2O_4 nanorod by seed–hydrothermal route*. *J. Alloy. Compd.* 491(1–2) (2010) 258–263. Copyright 2009 Elsevier.

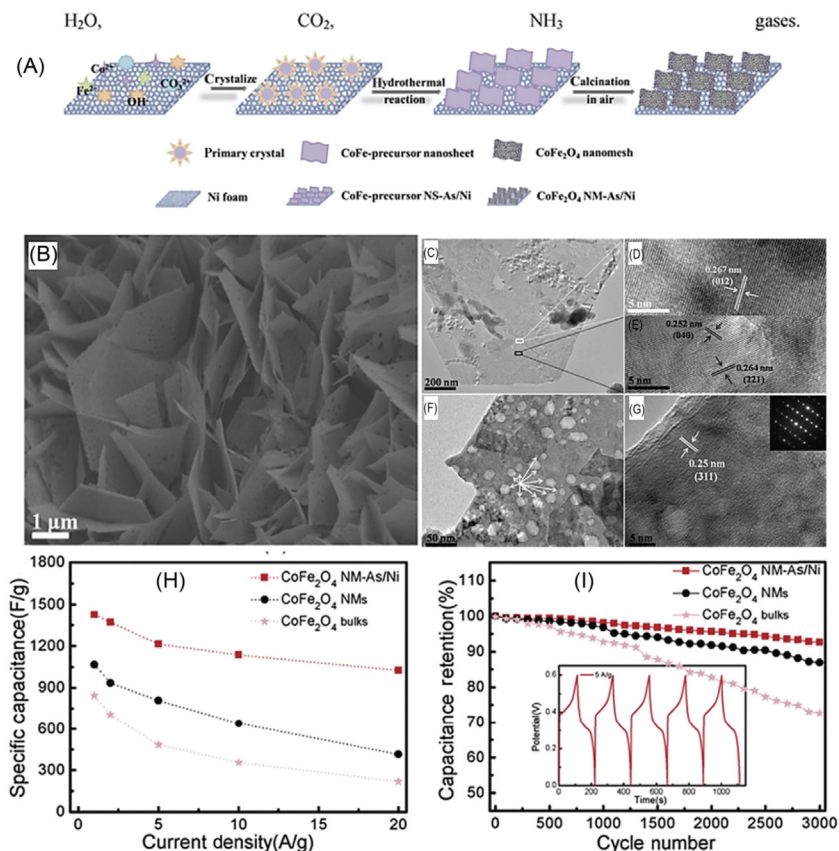


Figure 6.10 (A) Schematic representation of synthesis process of porous CoFe_2O_4 nanomesh arrays on nickel foam (B) SEM image of CoFe_2O_4 nanomesh arrays on nickel foam. (C) TEM image of CoFe precursor NS-As/Ni. HRTEM images of (D) $\text{Fe}_2(\text{CO}_3)(\text{OH})$; (E) $\text{Co}(\text{CO}_3)_{0.5}(\text{OH})_2 \cdot 0.11\text{H}_2\text{O}$; (F) TEM image of CoFe_2O_4 nanomesh arrays on nickel foam; (G) HRTEM image of CoFe_2O_4 nanomesh arrays on nickel foam (inset: corresponding SAED images). Electrochemical characteristics of CoFe_2O_4 nanomesh arrays on nickel foam, CoFe_2O_4 nanomesh and CoFe_2O_4 bulks electrodes (H) Specific capacitance variations w.r.t current densities. (I) Cyclic stability test for 3000 cycles at 5 Ag^{-1} (inset: last five cycles for CoFe_2O_4 nanomesh arrays on nickel foam). Reprinted with permission from L. Liu, et al., Binary cobalt ferrite nanomesh arrays as the advanced binder-free electrode for applications in oxygen evolution reaction and supercapacitors. *J. Power Sources* 327 (2016) 599–609. Copyright 2009 Elsevier.

XMn_2O_4 nanomaterial has attracted huge research attention because of the accumulating advantages, such as being less hazardous, cost-effective, and requiring operating voltages at lower values comparative to Co and Fe [104–107]. Owing to the high electrochemical performance and

better redox activities of XMn_2O_4 , these nanostructures have been studied widely as anode materials for lithium-ion batteries [108]. Various dimensional nanostructures of manganites, like 1D porous nanowires and hollow nanotube structures, exhibit better performance because of the provision of enriched electronic pathways, a large active surface area, and a shielding field for the mechanical stresses induced during electrochemical phenomena [109,110]. The unique XMn_2O_4 nanomaterials in the 1D configuration demonstrated a high storage capacity, better rate performance, and excellent cyclic stability for lithium-ion batteries. However, the utilization of manganites and their composites for electrochemical supercapacitors and hybrid energy storage devices have also been reported [111,112]. The individual performances of various BMOs is systematically presented in Table 6.2.

Similarly, when BMO-based materials are utilized for the development of supercapattery devices (two-electrode configuration), their performance is evaluated in terms of energy density, power density, and cyclic stability. For comparison, the performances of various BMO-based supercapattery devices is presented in Table 6.3.



6.3 Summary and future outlook

In this chapter, the characteristics of various BMOs and their recent advances for hybrid energy storage applications have been discussed. The structural and chemical properties of BMOs greatly affect their electrochemical performance. Thus to improve the storage performances of BMOs, different unique dimensional nanostructures have been synthesized by employing novel routes. Besides considerable advancement in the development of rational BMOs electrode designs during recent years, some hurdles and challenges still need to be addressed for future supercapattery devices. These include the synthesis of dimensional structures with precisely controlled morphologies, novel strategies for enhancing the surface area of material by mounting unique structures, new methods for large-scale material production, high mass-loaded electrode architectures for commercialization purposes, optimization of electrode engineering issues, and developing an in-depth understanding of the complex electrochemical mechanisms involved during device operation. It provides an

Table 6.2 Comparison of performance of various binary metal oxide (BMOs) in three-electrode configuration.

BMO materials	Synthesis method	Specific capacitance	Rate capability	Life cycles	References
Flower-like $\text{Co}_3\text{O}_4\text{-NiO}$	Cathodic electrodeposition	687.5 Fg^{-1} at 0.5 Ag^{-1}	94% retained from 0.5 to 10 Ag^{-1}	92% retained after 2500 cycles	[113]
Hierarchical porous NiCo_2O_4	Polyethylene glycol-directed technique	743 Fg^{-1} at 1 Ag^{-1}	78.6% retention at 40 Ag^{-1}	6.2% loss after 3000 cycles	[114]
Hierarchical porous spinel NiCo_2O_4	Chemical precipitation method	1270 Fg^{-1} at 1 Ag^{-1}	81% retention at 10 Ag^{-1}	4.8% loss after 5000 cycles	[115]
Nickel copper oxide on carbon fiber paper	Hydrothermal synthesis	1711 Fg^{-1} at 5 Ag^{-1}	—	15% capacitance reduction after 5000 cycles	[116]
Spinel MnCo_2O_4	Sol-gel method	405 Fg^{-1} at 5 mAcm^{-2}	67.9% retention at 40 mA cm^{-2}	95.1% over 1000 cycles	[117]
CoMn_2O_4 nanowires	Hydrothermal synthesis	2108 Fg^{-1} at 1 Ag^{-1}	$\sim 62\%$ retention at 20 Ag^{-1}	$\sim 100\%$ Coulombic efficiency	[118]
MnCo_2O_4 nanowires	Hydrothermal synthesis	1342 Fg^{-1} at 1 Ag^{-1}	$\sim 76\%$ retention at 20 Ag^{-1}	$\sim 100\%$ Coulombic efficiency	[118]
Highly ordered Mesoporous CuCo_2O_4 nanowires	SBA-15 nanocasting	1210 Fg^{-1} at 2 Ag^{-1}	64% retention at 20 Ag^{-1}	93.5% retention at varying current densities during 4250 cycles	[75]
Highly porous ZnCo_2O_4 nanotubes	Electrospinning method	770 Fg^{-1} at 10 Ag^{-1}	84% retention at 60 Ag^{-1}	10.5% capacitance reduction after 3000 cycles	[119]
MgCo_2O_4	Molten salt method	$\sim 320 \text{ Fg}^{-1}$ at 0.5 Ag^{-1}	—	93% Coulombic efficiency after 2000 cycles	[58]
3D hierarchical CuCo_2O_4 nanourchin architecture	Hydrothermal synthesis	1569.9 Fg^{-1} at 0.6 Ag^{-1}	71.1% retention at 20 Ag^{-1} for 1000 cycles	98.0% capacitance retention after 4000 cycles	[120]

Table 6.3 Comparison of various binary metal oxide (BMOs) in supercapattery configurations.

BMOs supercapattery	Energy density (Wh kg ⁻¹)	Power density (W kg ⁻¹)	Potential window(V)	Life cycles	References
MnCo ₂ O ₄ //AC	33.8	318.9	1.7	~ 85% after 10,000 cycles	[121]
Binary nickel – cobalt oxides//AC	34.9	875	1.75	86.4% after 10,000 cycles	[122]
FeCo ₂ O ₄ //AC	23	3780	1.6	91% after 5000 cycles	[123]
ZnCo ₂ O ₄ //AC	41	384	1.6	78% after 7000 cycles	[124]
CuCo ₂ O ₄ //AC	42.81	15.0	1.5	85.8% after 5000 cycles	[75]
Anhydrous CoMoO ₄ //AC	18.89	1.06	1.6	~ 93% after 5000 cycles	[125]

opportunity and direction to enhance the research in this field to overcome these issues and will result in directing the BMO-based supercapattery devices toward practical applications.

References

- [1] G. Wang, L. Zhang, J. Zhang, A review of electrode materials for electrochemical supercapacitors, *Chem. Soc. Rev.* 41 (2) (2012) 797–828.
- [2] B.E. Conway, Transition from “supercapacitor” to “battery” behavior in electrochemical energy storage, *J. Electrochem. Soc.* 138 (6) (1991) 1539.
- [3] Y. Wang, Y. Song, Y. Xia, Electrochemical capacitors: mechanism, materials, systems, characterization and applications, *Chem. Soc. Rev.* 45 (21) (2016) 5925–5950.
- [4] Y. Shao, et al., Design and mechanisms of asymmetric supercapacitors, *Chem. Rev.* 118 (18) (2018) 9233–9280.
- [5] Y. Gogotsi, R.M. Penner, *Energy Storage in Nanomaterials—Capacitive, Pseudocapacitive, or Battery-Like?* ACS Publications, 2018.
- [6] B. Akinwolemiwa, C. Peng, G.Z. Chen, Redox electrolytes in supercapacitors, *J. Electrochem. Soc.* 162 (5) (2015) A5054–A5059.
- [7] S. Balasubramaniam, et al., Comprehensive insight into the mechanism, material selection and performance evaluation of supercapatteries, *Nano-Micro Lett.* 12 (2020) 1–46.
- [8] G.Z. Chen, Supercapacitor and supercapattery as emerging electrochemical energy stores, *Int. Mater. Rev.* 62 (4) (2017) 173–202.
- [9] A. Du Pasquier, et al., A comparative study of Li-ion battery, supercapacitor and non-aqueous asymmetric hybrid devices for automotive applications, *J. Power Sources* 115 (1) (2003) 171–178.
- [10] M.S. Halper, J.C. Ellenbogen, *Supercapacitors: A Brief Overview*, The MITRE Corporation, McLean, Virginia, 2006, pp. 1–34.
- [11] H. Xia, et al., Hierarchically structured Co₃O₄@ Pt@ MnO₂ nanowire arrays for high-performance supercapacitors, *Sci. Rep.* 3 (1) (2013) 1–8.
- [12] Y.-T. Wang, et al., Synthesis of nanostructured mesoporous manganese oxides with three-dimensional frameworks and their application in supercapacitors, *J. Phys. Chem. C.* 115 (13) (2011) 5413–5421.

- [13] M. Zhi, et al., Nanostructured carbon–metal oxide composite electrodes for supercapacitors: a review, *Nanoscale* 5 (1) (2013) 72–88.
- [14] L. Yu, G.Z. Chen, Redox electrode materials for supercapatteries, *J. Power Sources* 326 (2016) 604–612.
- [15] L. Guan, L. Yu, G.Z. Chen, Capacitive and non-capacitive faradaic charge storage, *Electrochim. Acta* 206 (2016) 464–478.
- [16] K. Chen, D. Xue, Colloidal supercapattery: redox ions in electrode and electrolyte, *Chem. Rec.* 18 (3) (2018) 282–292.
- [17] M.-C. Liu, et al., Design and synthesis of $\text{CoMoO}_4\text{--NiMoO}_4 \cdot x \text{H}_2\text{O}$ bundles with improved electrochemical properties for supercapacitors, *J. Mater. Chem. A* 1 (4) (2013) 1380–1387.
- [18] D. Guo, et al., NiMoO_4 nanowires supported on Ni foam as novel advanced electrodes for supercapacitors, *J. Mater. Chem. A* 1 (32) (2013) 9024–9027.
- [19] Y. Yang, D. Kim, P. Schmuki, Anodic formation of Ti–V binary oxide mesosponge layers for supercapacitor applications, *Chem. Asian J.* 6 (11) (2011) 2916–2919.
- [20] T.Y. Wei, et al., A cost-effective supercapacitor material of ultrahigh specific capacitances: spinel nickel cobaltite aerogels from an epoxide-driven sol–gel process, *Adv. Mater.* 22 (3) (2010) 347–351.
- [21] H. Chen, et al., One-step fabrication of ultrathin porous nickel hydroxide–manganese dioxide hybrid nanosheets for supercapacitor electrodes with excellent capacitive performance, *Adv. Energy Mater.* 3 (12) (2013) 1636–1646.
- [22] L. Zhang, C. Tang, H. Gong, Temperature effect on the binder-free nickel copper oxide nanowires with superior supercapacitor performance, *Nanoscale* 6 (21) (2014) 12981–12989.
- [23] X. Zheng, et al., Ultrafine nickel–copper carbonate hydroxide hierarchical nanowire networks for high-performance supercapacitor electrodes, *Chem. Eng. J.* 290 (2016) 353–360.
- [24] C. Yuan, et al., Mixed transition–metal oxides: design, synthesis, and energy-related applications, *Angew. Chem. Int. Ed.* 53 (6) (2014) 1488–1504.
- [25] D. Guo, et al., *Facile synthesis and excellent electrochemical properties of CoMoO_4 nanoplate arrays as supercapacitors*, *J. Mater. Chem. A* 1 (24) (2013) 7247–7254.
- [26] C. German, K. Von Damm, Hydrothermal processes, *Treatise Geochem.* 6 (2006) 181–222.
- [27] P. Taheri, S. Hsieh, M. Bahrami, Investigating electrical contact resistance losses in lithium-ion battery assemblies for hybrid and electric vehicles, *J. Power Sources* 196 (15) (2011) 6525–6533.
- [28] S. Giri, D. Ghosh, C.K. Das, *One pot synthesis of ilmenite-type NiMnO_3 –“nitrogen-doped” graphene nanocomposite as next generation supercapacitors*, *Dalton Trans.* 42 (40) (2013) 14361–14364.
- [29] D. Chen, Y. Zhang, C. Tu, *Preparation of high saturation magnetic MgFe_2O_4 nanoparticles by microwave-assisted ball milling*, *Mater. Lett.* 82 (2012) 10–12.
- [30] L. Zhang, et al., *Pancake-like $\text{Fe}_2(\text{MoO}_4)_3$ microstructures: microwave-assisted hydrothermal synthesis, magnetic and photocatalytic properties*, *N. J. Chem.* 34 (9) (2010) 2027–2033.
- [31] Y. Lei, et al., *Rapid microwave-assisted green synthesis of 3D hierarchical flower-shaped NiCo_2O_4 microspheres for high-performance supercapacitor*, *ACS Appl. Mater. Interfaces* 6 (3) (2014) 1773–1780.
- [32] X. Xia, et al., *Three-dimensional porous nano-Ni/Co(OH) $_2$ nanoflake composite film: a pseudocapacitive material with superior performance*, *J. Phys. Chem. C.* 115 (45) (2011) 22662–22668.
- [33] L. Mai, et al., Fast ionic diffusion-enabled nanoflake electrode by spontaneous electrochemical pre-intercalation for high-performance supercapacitor, *Sci. Rep.* 3 (2013) 1718.

- [34] J.-K. Chang, et al., Physicochemical properties and electrochemical behavior of binary manganese–cobalt oxide electrodes for supercapacitor applications, *Mater. Chem. Phys.* 108 (1) (2008) 124–131.
- [35] S. Sun, et al., *Synthesis of ordered mesoporous CuCo_2O_4 with different textures as anode material for lithium ion battery*, *Microporous Mesoporous Mater.* 169 (2013) 242–247.
- [36] G. Zhang, et al., *Formation of ZnMn_2O_4 ball-in-ball hollow microspheres as a high-performance anode for lithium-ion batteries*, *Adv. Mater.* 24 (34) (2012) 4609–4613.
- [37] L. Shen, et al., *Self-templated formation of uniform NiCo_2O_4 hollow spheres with complex interior structures for lithium-ion batteries and supercapacitors*, *Angew. Chem. Int. Ed.* 54 (6) (2015) 1868–1872.
- [38] M. Nüchter, et al., Microwave assisted synthesis—a critical technology overview, *Green. Chem.* 6 (3) (2004) 128–141.
- [39] X. Gu, et al., *Synthesis and microwave absorbing properties of highly ordered mesoporous crystalline NiFe_2O_4* , *Chem. Commun.* 47 (18) (2011) 5337–5339.
- [40] R.V. Kumar, Y. Diamant, A. Gedanken, Sonochemical synthesis and characterization of nanometer-size transition metal oxides from metal acetates, *Chem. Mater.* 12 (8) (2000) 2301–2305.
- [41] P. Jeevanandam, Y. Koltypin, A. Gedanken, Synthesis of nanosized α -nickel hydroxide by a sonochemical method, *Nano Lett.* 1 (5) (2001) 263–266.
- [42] F.S. Omar, et al., Enhancing rate capability of amorphous nickel phosphate supercapattery electrode via composition with crystalline silver phosphate, *Electrochim. Acta* 273 (2018) 216–228.
- [43] C. Deng, et al., One-pot sonochemical fabrication of hierarchical hollow CuO sub-microspheres, *Ultrason. Sonochem.* 18 (5) (2011) 932–937.
- [44] J.J. Hinman, K.S. Suslick, *Nanostructured materials synthesis using ultrasound*, *Sonochemistry*, Springer, 2017, pp. 59–94.
- [45] K. Krishnamoorthy, G.-S. Kim, S.J. Kim, Graphene nanosheets: ultrasound assisted synthesis and characterization, *Ultrason. Sonochem.* 20 (2) (2013) 644–649.
- [46] H. Xu, B.W. Zeiger, K.S. Suslick, Sonochemical synthesis of nanomaterials, *Chem. Soc. Rev.* 42 (7) (2013) 2555–2567.
- [47] L. Mai, et al., Fast ionic diffusion-enabled nanoflake electrode by spontaneous electrochemical pre-intercalation for high-performance supercapacitor, *Sci. Rep.* 3 (1) (2013) 1–8.
- [48] J. Du, et al., *Ultrathin porous NiCo_2O_4 nanosheet arrays on flexible carbon fabric for high-performance supercapacitors*, *ACS Appl. Mater. Interfaces* 5 (15) (2013) 7405–7409.
- [49] J. Yang, et al., *Hybrid $\text{NiCo}_2\text{S}_4@ \text{MnO}_2$ heterostructures for high-performance supercapacitor electrodes*, *J. Mater. Chem. A* 3 (3) (2015) 1258–1264.
- [50] L. Huang, et al., *Hybrid composite $\text{Ni}(\text{OH})_2@ \text{NiCo}_2\text{O}_4$ grown on carbon fiber paper for high-performance supercapacitors*, *ACS Appl. Mater. Interfaces* 5 (21) (2013) 11159–11162.
- [51] J. Zhang, A. Yu, Nanostructured transition metal oxides as advanced anodes for lithium-ion batteries, *Sci. Bull.* 60 (9) (2015) 823–838.
- [52] M. Yang, et al., Preparation of multi-metal oxide hollow sphere using layered double hydroxide precursors, *Chin. J. Chem.* 30 (9) (2012) 2183–2188.
- [53] Y. Bai, et al., *Template method to controllable synthesis 3D porous NiCo_2O_4 with enhanced capacitance and stability for supercapacitors*, *J. Colloid Interface Sci.* 468 (2016) 1–9.
- [54] L. Hu, et al., *Facile synthesis of uniform mesoporous ZnCo_2O_4 microspheres as a high-performance anode material for Li-ion batteries*, *J. Mater. Chem. A* 1 (18) (2013) 5596–5602.
- [55] Q. Cao, Z. Liu, R. Che, *Ordered mesoporous CoFe_2O_4 nanoparticles: molten-salt-assisted rapid nanocasting synthesis and the effects of calcining heating rate*, *N. J. Chem.* 38 (7) (2014) 3193–3198.

- [56] M. Li, et al., *Mesoporous silica KIT-6 supported superparamagnetic CuFe₂O₄ nanoparticles for catalytic asymmetric hydrosilylation of ketones in air*, Green. Chem. 16 (5) (2014) 2680–2688.
- [57] J. Haetge, I. Djerdj, T. Brezesinski, *Nanocrystalline NiMoO₄ with an ordered mesoporous morphology as potential material for rechargeable thin film lithium batteries*, Chem. Commun. 48 (53) (2012) 6726–6728.
- [58] S.G. Krishnan, et al., *Characterization of MgCo₂O₄ as an electrode for high performance supercapacitors*, Electrochim. Acta 161 (2015) 312–321.
- [59] S.D. Perera, et al., *Enhanced supercapacitor performance for equal Co–Mn stoichiometry in colloidal Co_{3-x}MnxO₄ nanoparticles, in additive-free electrodes*, Chem. Mater. 27 (23) (2015) 7861–7873.
- [60] K.V. Sankar, R.K. Selvan, *The ternary MnFe₂O₄/graphene/polyaniline hybrid composite as negative electrode for supercapacitors*, J. Power Sources 275 (2015) 399–407.
- [61] C. An, et al., *Porous NiCo₂O₄ nanostructures for high performance supercapacitors via a microemulsion technique*, Nano Energy 10 (2014) 125–134.
- [62] X. Su, et al., *Silicon-based nanomaterials for lithium-ion batteries: a review*, Adv. Energy Mater. 4 (1) (2014) 1300882.
- [63] S. Vijayakumar, et al., *Porous thin layered nanosheets assembled ZnCo₂O₄ grown on Ni-foam as an efficient electrode material for hybrid supercapacitor applications*, Int. J. Hydrogen Energy 42 (5) (2017) 3122–3129.
- [64] Y. Sharma, et al., *Studies on spinel cobaltites, FeCo₂O₄ and MgCo₂O₄ as anodes for Li-ion batteries*, Solid. State Ion. 179 (15–16) (2008) 587–597.
- [65] S.G. Mohamed, et al., *High-performance lithium-ion battery and symmetric supercapacitors based on FeCo₂O₄ nanoflakes electrodes*, ACS Appl. Mater. Interfaces 6 (24) (2014) 22701–22708.
- [66] F.S. Omar, et al., *A promising binary nanocomposite of zinc cobaltite intercalated with polyaniline for supercapacitor and hydrazine sensor*, J. Alloy. Compd. 716 (2017) 96–105.
- [67] S.G. Mohamed, S.Y. Attia, N.K. Allam, *One-step, calcination-free synthesis of zinc cobaltite nanospheres for high-performance supercapacitors*, Mater. Today Energy 4 (2017) 97–104.
- [68] W. Luo, et al., *Electrospun porous ZnCo₂O₄ nanotubes as a high-performance anode material for lithium-ion batteries*, J. Mater. Chem. 22 (18) (2012) 8916–8921.
- [69] M. Reddy, et al., *Nano-ZnCo₂O₄ material preparation by molten salt method and its electrochemical properties for lithium batteries*, J. Electrochem. Soc. 158 (12) (2011) A1423–A1430.
- [70] J. Li, et al., *High electrochemical performance of monodisperse NiCo₂O₄ mesoporous microspheres as an anode material for Li-ion batteries*, ACS Appl. Mater. Interfaces 5 (3) (2013) 981–988.
- [71] G. Huang, et al., *Core–shell ellipsoidal MnCo₂O₄ anode with micro-/nano-structure and concentration gradient for lithium-ion batteries*, ACS Appl. Mater. Interfaces 6 (23) (2014) 21325–21334.
- [72] S.G. Mohamed, et al., *Ternary spinel MCo₂O₄ (M = Mn, Fe, Ni, and Zn) porous nanorods as bifunctional cathode materials for lithium–O₂ batteries*, ACS Appl. Mater. Interfaces 7 (22) (2015) 12038–12046.
- [73] J. Wu, et al., *Ultrathin NiCo₂O₄ nanosheets grown on three-dimensional interwoven nitrogen-doped carbon nanotubes as binder-free electrodes for high-performance supercapacitors*, J. Mater. Chem. A 3 (29) (2015) 15331–15338.
- [74] N. Du, et al., *Porous ZnCo₂O₄ nanowires synthesis via sacrificial templates: high-performance anode materials of Li-ion batteries*, Inorg. Chem. 50 (8) (2011) 3320–3324.
- [75] A. Pendashteh, et al., *Highly ordered mesoporous CuCo₂O₄ nanowires, a promising solution for high-performance supercapacitors*, Chem. Mater. 27 (11) (2015) 3919–3926.
- [76] Q. Wang, et al., *Facile fabrication and supercapacitive properties of mesoporous zinc cobaltite microspheres*, J. Power Sources 284 (2015) 138–145.

- [77] H.B. Wu, H. Pang, X.W.D. Lou, Facile synthesis of mesoporous Ni_{0.3}Co_{2.7}O₄ hierarchical structures for high-performance supercapacitors, *Energy Environ. Sci.* 6 (12) (2013) 3619–3626.
- [78] F. Saleki, et al., *MOF assistance synthesis of nanoporous double-shelled CuCo₂O₄ hollow spheres for hybrid supercapacitors*, *J. Colloid Interface Sci.* 556 (2019) 83–91.
- [79] S. Raj, P. Kar, P. Roy, Facile synthesis of flower-like morphology Cu_{0.27}Co_{2.73}O₄ for a high-performance supercapattery with extraordinary cycling stability, *Chem. Commun.* 54 (87) (2018) 12400–12403.
- [80] L. Zhang, et al., *Ultra-high-rate, ultra-long-life asymmetric supercapacitors based on few-crystalline, porous NiCo₂O₄ nanosheet composites*, *J. Mater. Chem. A* 6 (4) (2018) 1412–1422.
- [81] D. Bresser, et al., *Carbon coated ZnFe₂O₄ nanoparticles for advanced lithium-ion anodes*, *Adv. Energy Mater.* 3 (4) (2013) 513–523.
- [82] J. Liu, et al., Iron oxide-based nanotube arrays derived from sacrificial template-accelerated hydrolysis: large-area design and reversible lithium storage, *Chem. Mater.* 22 (1) (2009) 212–217.
- [83] M. Reddy, et al., *α -Fe₂O₃ nanoflakes as an anode material for Li-ion batteries*, *Adv. Funct. Mater.* 17 (15) (2007) 2792–2799.
- [84] K.V. Sankar, et al., Facile hydrothermal synthesis of carbon-coated cobalt ferrite spherical nanoparticles as a potential negative electrode for flexible supercapattery, *J. Colloid Interface Sci.* 513 (2018) 480–488.
- [85] B. Jang, et al., Direct synthesis of self-assembled ferrite/carbon hybrid nanosheets for high performance lithium-ion battery anodes, *J. Am. Chem. Soc.* 134 (36) (2012) 15010–15015.
- [86] P.F. Teh, et al., *Nanoweb anodes composed of one-dimensional, high aspect ratio, size tunable electrospun ZnFe₂O₄ nanofibers for lithium ion batteries*, *J. Mater. Chem.* 21 (38) (2011) 14999–15008.
- [87] X.W. Lou, et al., *Self-supported formation of needlelike Co₃O₄ nanotubes and their application as lithium-ion battery electrodes*, *Adv. Mater.* 20 (2) (2008) 258–262.
- [88] M.S. Javed, et al., Exploring Li-ion hopping behavior in zinc ferrite and promoting performance for flexible solid-state supercapacitor, *Electrochim. Acta* 295 (2019) 558–568.
- [89] A. Shanmugavani, R.K. Selvan, *Synthesis of ZnFe₂O₄ nanoparticles and their asymmetric configuration with Ni(OH)₂ for a pseudocapacitor*, *RSC Adv.* 4 (51) (2014) 27022–27029.
- [90] P. Guo, et al., Electrochemical properties of colloidal nanocrystal assemblies of manganese ferrite as the electrode materials for supercapacitors, *J. Mater. Sci.* 52 (9) (2017) 5359–5365.
- [91] Y. Xu, et al., *Synthesis of CoFe₂O₄ nanotube arrays through an improved sol–gel template approach*, *Mater. Lett.* 62 (8–9) (2008) 1403–1405.
- [92] A. Shanmugavani, D. Kalpana, R.K. Selvan, *Electrochemical properties of CoFe₂O₄ nanoparticles as negative and Co(OH)₂ and Co₂Fe(CN)₆ as positive electrodes for supercapacitors*, *Mater. Res. Bull.* 71 (2015) 133–141.
- [93] V.V. Jadhav, et al., Mixed-phase bismuth ferrite nanoflake electrodes for supercapacitor application, *Appl. Nanosci.* 6 (4) (2016) 511–519.
- [94] A. Mehri, S.S. Ebrahimi, S. Masoudpanah, Synthesis and characterization of high aspect ratio NiFe₂O₄ nanowire, *J. Anal. Appl. Pyrolysis* 110 (2014) 235–238.
- [95] X. Hou, et al., *Synthesis and characterizations of spinel MnFe₂O₄ nanorod by seed–hydrothermal route*, *J. Alloy. Compd.* 491 (1–2) (2010) 258–263.
- [96] L. Liu, et al., Binary cobalt ferrite nanomesh arrays as the advanced binder-free electrode for applications in oxygen evolution reaction and supercapacitors, *J. Power Sources* 327 (2016) 599–609.

- [97] M. Athika, et al., Ni/NiFe₂O₄@ Carbon Nanocomposite Involving Synergistic Effect for High-Energy Density and High-Power Density Supercapattery, *Materials Research Express*, 2019.
- [98] L. Geng, et al., *Design and regulation of novel MnFe₂O₄@ C nanowires as high performance electrode for supercapacitor*, *Nanomaterials* 9 (5) (2019) 777.
- [99] K. Song, et al., *Hierarchical structure of CoFe₂O₄ core-shell microsphere coating on carbon fiber cloth for high-performance asymmetric flexible supercapacitor applications*, *Ionics* 25 (10) (2019) 4905–4914.
- [100] T. Nishikawa, T. Nakajima, Y. Shinohara, *An exploratory study on effect of the isomorphic replacement of Ti⁴⁺ ions by various metal ions on the light absorption character of TiO₂*, *J. Mol. Struct. Theochem.* 545 (1–3) (2001) 67–74.
- [101] C. Yuan, et al., *Template-free fabrication of mesoporous hollow ZnMn₂O₄ sub-microspheres with enhanced lithium storage capability towards high-performance li-ion batteries*, *Part. Part. Syst. Charact.* 31 (6) (2014) 657–663.
- [102] Y. Bessekhouad, M. Trari, *Photocatalytic hydrogen production from suspension of spinel powders AMn₂O₄ (A = Cu and Zn)*, *Int. J. Hydrogen Energy* 27 (4) (2002) 357–362.
- [103] S. Hosseini, et al., *Nanocrystalline AMn₂O₄ (A = Co, Ni, Cu) spinels for remediation of volatile organic compounds—synthesis, characterization and catalytic performance*, *Ceram. Int.* 38 (2) (2012) 1655–1661.
- [104] Y. Yang, et al., *Nanocrystalline ZnMn₂O₄ as a novel lithium-storage material*, *Electrochem. Commun.* 10 (8) (2008) 1117–1120.
- [105] Y. Deng, et al., *Controllable synthesis of spinel nano-ZnMn₂O₄ via a single source precursor route and its high capacity retention as anode material for lithium ion batteries*, *J. Mater. Chem.* 21 (32) (2011) 11987–11995.
- [106] S. Wang, N. Wu, *Operating characteristics of aqueous magnetite electrochemical capacitors*, *J. Appl. Electrochem.* 33 (3–4) (2003) 345–348.
- [107] C. Lokhande, D. Dubal, O.-S. Joo, *Metal oxide thin film based supercapacitors*, *Curr. Appl. Phys.* 11 (3) (2011) 255–270.
- [108] Y. Zhao, et al., *Recent developments and understanding of novel mixed transition-metal oxides as anodes in lithium ion batteries*, *Adv. Energy Mater.* 6 (8) (2016) 1502175.
- [109] Y. Zhang, et al., *Porous ZnMn₂O₄ nanowires as an advanced anode material for lithium ion battery*, *Electrochim. Acta* 182 (2015) 1140–1144.
- [110] L. Zhang, et al., *Hierarchical porous ZnMn₂O₄ hollow nanotubes with enhanced lithium storage toward lithium-ion batteries*, *Chem.—A Eur. J.* 21 (30) (2015) 10771–10777.
- [111] J. Cheng, et al., *Influence of component content on the capacitance of magnetite/reduced graphene oxide composite*, *J. Electroanal. Chem.* 698 (2013) 1–8.
- [112] H. Wei, et al., *Significantly enhanced energy density of magnetite/polypyrrole nanocomposite capacitors at high rates by low magnetic fields*, *Adv. Compos. Hybrid. Mater.* 1 (1) (2018) 127–134.
- [113] Z. Zeng, et al., *Flower-like binary cobalt-nickel oxide with high performance for supercapacitor electrode via cathodic electrodeposition*, *Ceram. Int.* 43 (2017) S633–S638.
- [114] H. Jiang, J. Ma, C. Li, *Hierarchical porous NiCo₂O₄ nanowires for high-rate supercapacitors*, *Chem. Commun.* 48 (37) (2012) 4465–4467.
- [115] I. Shakir, et al., *Synthesis of hierarchical porous spinel nickel cobaltite nanoflakes for high performance electrochemical energy storage supercapacitors*, *RSC Adv.* 3 (44) (2013) 21386–21389.
- [116] L. Zhang, H. Gong, *Unravelling the correlation between nickel to copper ratio of binary oxides and their superior supercapacitor performance*, *Electrochim. Acta* 234 (2017) 82–92.
- [117] L.-B. Kong, et al., *The specific capacitance of sol-gel synthesised spinel MnCo₂O₄ in an alkaline electrolyte*, *Electrochim. Acta* 115 (2014) 22–27.

- [118] Y. Xu, et al., *Facile synthesis route of porous $MnCo_2O_4$ and $CoMn_2O_4$ nanowires and their excellent electrochemical properties in supercapacitors*, *J. Mater. Chem. A* 2 (39) (2014) 16480–16488.
- [119] G. Zhou, et al., *Simple method for the preparation of highly porous $ZnCo_2O_4$ nanotubes with enhanced electrochemical property for supercapacitor*, *Electrochim. Acta* 123 (2014) 450–455.
- [120] W. Liu, et al., *Hierarchical $CuCo_2O_4$ nanourchin supported by Ni foam with superior electrochemical performance*, *J. Alloy. Compd.* 756 (2018) 68–75.
- [121] B. Saravanakumar, et al., *Holey two dimensional manganese cobalt oxide nanosheets as a high-performance electrode for supercapattery*, *Chem. Eng. J.* 373 (2019) 547–555.
- [122] J. Zhang, et al., *Binary nickel–cobalt oxides electrode materials for high-performance supercapacitors: influence of its composition and porous nature*, *ACS Appl. Mater. Interfaces* 7 (32) (2015) 17630–17640.
- [123] A. Pendashteh, et al., *Nanostructured porous wires of iron cobaltite: novel positive electrode for high-performance hybrid energy storage devices*, *J. Mater. Chem. A* 3 (32) (2015) 16849–16859.
- [124] B. Guan, et al., *Facile synthesis of $ZnCo_2O_4$ nanowire cluster arrays on Ni foam for high-performance asymmetric supercapacitors*, *J. Mater. Chem. A* 2 (38) (2014) 16116–16123.
- [125] B.C. Kim, et al., *Efficient supercapattery behavior of mesoporous hydrous and anhydrous cobalt molybdate nanostructures*, *J. Alloy. Compd.* 789 (2019) 256–265.



Ternary nanocomposites for supercapattery

Javed Iqbal^{1,2}, Shahid Bashir³, Mohammad Omaish Ansari², Rashida Jafer⁴, Asim Jilani², Sharifah Mohammad¹, K. Ramesh³ and S. Ramesh³

¹Department of Chemistry, Faculty of Science, University of Malaya, Kuala Lumpur, Malaysia

²Center of Nanotechnology, King Abdulaziz University, Jeddah, Saudi Arabia

³Center for Ionics University of Malaya, Department of Physics, Faculty of Science, University of Malaya, Kuala Lumpur, Malaysia

⁴Department of Physics, Faculty of Science, King Abdulaziz University, Jeddah, Saudi Arabia



7.1 Introduction

Several redox active metal oxides, for instance, NiO, MnO₂, MoO₂, Fe₂O₃, and Co₃O₄, etc., have been utilized in the past as electrode materials for energy storage devices with improved performance [1]. With the evolving technology in the 21st century that needs better electrochemical performance, pristine metal oxides as electrode materials are unable to manage the current energy demand because of their underrated performance. The metal oxide nanostructures as standalone material experience increased particle aggregation which substantially reduces its active sites, causing fast capacity diminishing and structural falsification in charge–discharge reactions [2]. Therefore it is required to integrate nanostructures with extremely conductive bases. Carbon materials, like multiwalled carbon nanotubes (MWCNTs), graphene (GN), and conducting polymers (CPs) like polypyrrole (PPy), polyaniline (PANI), poly(3,4-ethylenedioxythiophene) (PEDOT), polythiophene (PTh), and poly(p-phenylenevinylene) (PPV) are proved to be accurate platforms which do not only enable the mechanism of charge transfer but also avoid the accumulation of nanoparticles (NPs), heading to an increment of electrochemical surface area and the cycling stability [3].

The MWCNTs hold an exclusive structure and extraordinary physiochemical properties like the electronic structure of sp^2 hybridized carbon

[4]. The metal oxides are usually reactive towards sp^2 hybridized carbons of the MWCNTs, and so their nanostructures can be engrafted on the MWCNTs with a reaction between the sidewalls of MWCNTs and metal ions. The MWCNTs are considered to be tremendously narrow conductors and have diameters of many atomic distances, to show ballistic electron transport, with a large porosity with hollow structures. Due to all these special characteristics, they have become a very suitable platform to back metal oxide NPs to clearly decrease the particles' accumulation and enhance the electron transportation for the deposition of the metal oxide nanostructures onto the MWCNTs network, particularly, in electrochemical enforcements. So the metal oxide nanostructure intercalation on the top of the MWCNTs network can stop fast capacity decline, structural falsification, and particle accumulation [5]. Additionally, the synergic outcome can be presented by metal oxide nanostructures hybridization along with carbon matrices to fully optimize the electrochemical functioning.

Another carbon material, GN is an ideal matrix with many distinctive characteristics, for example theoretically a huge surface area ($2630 \text{ m}^2 \text{ g}^{-1}$), enhanced electrical conductivity (106 S cm^{-2}), remarkable mechanical flexibility, thermal and chemical stability [6]. GN is a top drawer host material for growing nanostructures for superior performance electrochemical applications. The GN is a two-dimensional honeycomb structured thin sheet of atoms where every carbon atom is sp^2 hybridized. The three hybridized orbitals ($2s$, $2p_x$, and $2p_y$) form sigma bonds with the adjacent carbon atoms and unhybridized ($2p_z$) orbitals form a conjugated π -bond perpendicular to the GN lattice in which delocalized electrons are responsible for the distinctive electronic charge carrier mobility property of the GN [7]. This is a well-understood fact that metal oxides intercalation with GN materials provide conducting networks along with the advantage of diminishing the danger of large volume changes during the course of a charge–discharge mechanism. Its unique 2D nanostructures are remarkably favorable in order to provide more electrochemically active sites for the rapid redox process. Besides that, it supports a decrease in the diffusion length of the charge carriers

The finding of electrically “metal-like” CPs has brought forward the field of electrochemically active polymer research field and appeared as a powerful choice for utilizing them as electrode materials in pseudocapacitive devices. CPs are the second group of the entrant materials for redox pseudocapacitors because they bear quick and alterable oxidation/reduction procedures, good electrical conductivity, and low cost. Commonly

used CPs are PPy, PANI, PEDOT, PTh, and PPV and can be exploited for various applications. CPs offer more compensations in the comparison of transition metal oxides, which are also a family of pseudocapacitors. The energy density and capacitance of CPs is much greater than what is offered by electric double-layer capacitors (EDLC) because the CPs do not just have the capability of storing the charge in the electrical double layer but can undergo rapid Faradaic redox reactions. Furthermore, the decreased cost of manufacturing and low ESR has led to huge curiosity in the associated research. They are classically synthesized through chemical or electrochemical oxidation of the monomer and rendered conductive via a conjugated bond system along with polymer backbone [8]. The general edifice of all CPs comprises recurrently alternating single and double (C-C, C = C) bonds, creating an overlapping area of p -orbitals, and linking the successive single bonds. That permits a delocalization of π -electrons transversely at all the successively aligned p -orbitals, introducing a π -conjugated backbone thoroughly in the chains of polymer. The introduced π -conjugated backbone controls the formation and circulation of the charge carriers, consequently making the intrinsic CPs. This type of polymer building could affect the electrochemical performance critically through the mobility of ion and pores accessibility. Consequently, the structural design of the polymer becomes very important for higher efficiency and stability for charge storage. There are two types of charging process, that is, p -doped in anions during oxidation and n -doped in cations during reduction. Early studies of n -doped materials were achieved on polyacetylene and later on poly- p -phenylene. The polymers constructed in this way show high impedances when having gone through n -doping and hence are not fit for use as negative electrodes [9]. A few CPs, such as PPy and PANI, would be p -doped only because of a requirement for very negative potentials for n -doped, when compared with the potential limit of reduction of molecular solvent-based electrolytes [10]. It was reported that p -doped polymers show more stability against degradation when compared with n -doped polymers; for this reason, investigating the p -doped polymers are more promising [11]. Nevertheless, the key downside of CPs is based upon their deprived stability of cycling while being used as bulk materials and hence show a restricted cycle life. Shrinking, swelling, breaking, or cracking in the doping/dedoping procedure of nonstop charge–discharge methods are associated with CPs films and so regularly worsen their conducting behavior [12,13]. The composites of nanostructured CPs with different materials

are advised for stabilizing the cycling. The deposition of Poly(tri(4-(thiophen-2-yl)phenyl)amine) on greatly porous films or templated nanotube structures returned a much higher capacitance of about 950 F g^{-1} in 100 mM tetrabutylammonium tetrafluoroborate in acetonitrile [14]. A ternary nanocomposite of rGO/PPy/Cu₂O-Cu(OH)₂ was prepared by another group for use as an electrode material of supercapacitors (SCs). This ternary composite showed a remarkable gravimetric specific capacitance (997 F g^{-1} at a current density of 10 A g^{-1}) in three electrode systems. The GN EDLC, composed with the pseudocapacitive properties of PPy and Cu₂O-Cu(OH)₂, increased the power and energy densities up to individual values of 20 Wh kg^{-1} and 8000 W kg^{-1} . For the rGO/PPy/Cu₂O-Cu(OH)₂ SCs, the highest power density was recorded as $19,998.5 \text{ W kg}^{-1}$ at an energy density of 5.8 Wh kg^{-1} , with a retaining capacitance of about 90% after an operation of 2000 cycles [15]. The CPs are usually acknowledged to be weak mechanically, hence the composites can be considered to help avoid mechanical breaking of the polymers in the extended cycling [12].

The noble metals (Ag, Au, Pt, Pd, etc.) could be utilized to augment the conductivity of the ternary nanocomposite through extended channels of electron transfer that can establish the redox reaction. It is well-known that conducting platform, such as MWCNTs, rGO, and CPs, forming ternary nanocomposites with metal oxide and noble metals possess improved performance as an electrode material compared to pristine metal oxide or binary nanocomposites of metal oxides with some conducting matrices, such as MWCNTs, rGO, and CPs.



7.2 Noble metals

The precious metals, for example, silver (Ag), gold (Au), platinum (Pt), and palladium (Pd), have been greatly understood and used for myriad applications. The metals and their rare occurrences are clearly noticed from their names. Au and Ag have been known noble metals since prehistoric times. The first metal known to man was Au with Ag and copper. Au was recognized readily by the ancient civilizations as a valuable metal. A special interest in Au was expressed by folk tales, numerous legends, and even the bible. In the middle ages, several attempts were made to

make Au out of different chemical elements. The Latin word “aurum,” meaning “shining dawn,” is the source of the word Au.

Ag in its pure form is almost white, soft, lustrous, very ductile, and malleable. Ag has excellent heat and electrical conductivity properties. Its symbol Ag is derived from the Latin word “argentum.” Ag is one of the scarcest elements in the known metals. Mostly, Ag used nowadays is gained from the Ag ores, together with argentite. Due to its very high conductivity, it is in high demand, but the huge cost makes it nonviable to use in electrical drives. Ag is highly applicable in the electrical industries, printed circuits, and electrical contacts in the computer keyboards. In oxidation reactions, it is also used as a catalyst because of its catalytic nature.

Pt is largely used in microelectronics because it possesses distinctive features such as good resistivity against oxidation, excellent catalytic performance, and 5.6 eV work function. The Pt NPs promote the propagation mechanism of ions and electrons which consequently offers more eminent reversible capacitance at high scan rates. Pd has rarely been used in the application of SCs, so this may come into the limelight in the future. The composites of Pd with C₆₀, PANI, MWCNTs and GN in the form of binary or ternary nanocomposites have been utilized for supercapacitor applications [16,17].

The optimized use of a small amount of precious metal in the form of a nanostructure with different combinations in the form of nanocomposites play a pivotal role to enhance the electrochemical activity in the binary or ternary nanocomposites. The transition metal oxides decorated with noble metal NPs are greatly beneficial for many applications. Therefore for an improved rate performance of pseudocapacitors, metal oxides doped with precious metals have been studied broadly [18,19].



7.3 Metal oxides

In the area of energy storage research, an electrochemical supercapacitor is looked at as the most promising candidate because of an ample power density, higher stable cycling, and reversibility [20]. SCs are thought to have a great supply of eminent power as well as high capacity retentions [21]. The exploration of novel materials for improved functions of the supercapacitor is of prime importance. SCs fall into different

categories such as electrochemical capacitors made up of carbon containing double-layered electrodes and pseudocapacitors in which the electrodes are constituted of transition metal oxides. Also the CPs [4–6] and the transition metals are considered super materials for electrochemical SCs because of their faster faradaic and nonfaradaic activity that helps the ions and electrons to be involved in the mechanism of charge storage [22–26].

Over the years, transition metals such as MnO_2 , FeO , Fe_2O_3 , Co_3O_4 , ZnO , V_2O_5 , NiO , CuO , TiO_2 , etc. have been promising electrode materials in energy storage devices due to their high surface area, high theoretical capacitance, diverse constituents and morphologies, abundant reserves, etc. [27]. Metal oxides can be fabricated into different novel morphologies, as shown is in Fig. 7.1, varied electroconductivity, and different oxygen vacancies which can result in high conductivity, enhanced surface area, electroactive sites, and chemical stability [28]. Metal oxides generally offer pseudocapacitance and on doping with another metal can afford additional redox reactions with reduced charge transfer impedance for electrochemical SCs and the specific capacitance is much larger than that of single metal oxides [29,30]. Composite of metal oxides with CPs, carbonaceous materials, and noble metals have been lately reported to possess improved electroconductivity, high specific capacitance, and improved cyclic stability [31,32].

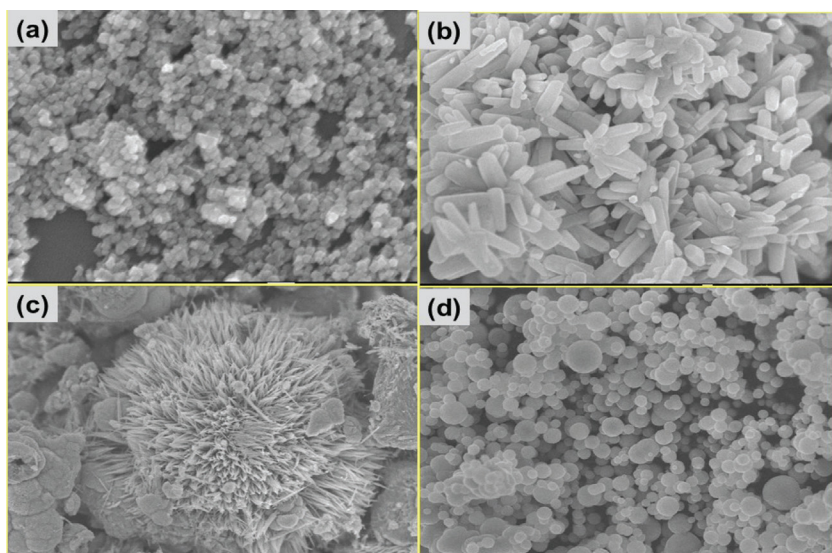


Figure 7.1 SEM micrographs of various transition metal oxides (A) Co_3O_4 nanograins, (B) ZnO_2 rods, (C) TiO_2 flower, and (D) Fe_2O_3 spherical nanostructures.

7.3.1 Gold-containing ternary nanocomposites

Zhang and his coworkers prepared a hierarchical ternary heterostructure of $\text{MoO}_2/\text{Au}/\text{MnO}_2$ by electrodeposition method [33]. After coating an Au layer, the diffusion of ions and capacity of collecting charge were remarkably enhanced. They observed that the electrochemical activity in relation to a real specific capacitance of $\text{MoO}_2/\text{Au}/\text{MnO}_2$ increased to 112 mF cm^{-2} at 5 mV s^{-1} low scan rate. In another approach, Zheng's group prepared a nanocomposite by incorporating Au nanostructures into ZnO/NiO for supercapacitor active electrode materials. The $\text{ZnO}-\text{Au}-\text{NiO}$ composites presented an extreme specific capacitance of 4.1 F cm^{-2} at a current density of 5 mA cm^{-2} and exceptional stability (about 19.7% loss after 4000 cycles) [34].

Wang's research group synthesized core-shell nanowires of hybrid $\text{WO}_{3-x}@\text{Au}@\text{MnO}_2$ on a carbon fabric. They reported that the newly developed $\text{WO}_{3-x}@\text{Au}@\text{MnO}_2$ core-shell NWs produced specific capacitance of 588 F g^{-1} at 10 mV s^{-1} scanning rate and 1195 F g^{-1} at a current density of 0.75 A g^{-1} [19]. The synthesized ternary composite, $\text{WO}_{3-x}@\text{Au}@\text{MnO}_2$ showed remarkable good retention capacity, power density of 30.6 kW kg^{-1} at 78.1 Wh kg^{-1} energy density, and high energy density of 106.4 Wh kg^{-1} at power density of 23.6 kW kg^{-1} . Wang and his coworkers published another report in which they used solvothermal and a redox method for the synthesis of RuO_2 -nanocomposites. The assembled SCs using RuO_2 -nanocomposites produced enhanced specific capacitances of 537.7 F g^{-1} and 558.2 F g^{-1} , at a current density of 50 mA g^{-1} in H_2SO_4 electrolyte. The reported values of specific capacitance are 350.1 F g^{-1} for the RuO_2/C nanocomposites and 478.5 F g^{-1} for the $\text{RuO}_2-\text{Au}/\text{C}$ nanocomposites at 200 mA g^{-1} current density with excellent capacity retention [35].

Zhu et al. prepared novel $\text{NiCo}_2\text{O}_4@\text{Au}$ nanotubes (NTs) with a porous and hollow interiors structure. The specific capacitance of the prepared ternary nanocomposite, $\text{NiCo}_2\text{O}_4@\text{Au}$ produced 1013.5 F g^{-1} and after 10,000 cycles maintained 85.13% capacity retention [36]. Fig. 7.2 illustrates the electrochemical results of the $\text{NiCo}_2\text{O}_4@\text{Au}$ and NiCo_2O_4 and their comparison.

7.3.2 Platinum-containing ternary nanocomposites

Xia et al. prepared novel active material for enhanced-performance SCs with the idea of graded $\text{Co}_3\text{O}_4@\text{Pt}@\text{MnO}_2$ core-shell-shell structure. Fig. 7.3 shows the prepared active material, $\text{Co}_3\text{O}_4@\text{Pt}@\text{MnO}_2$, and

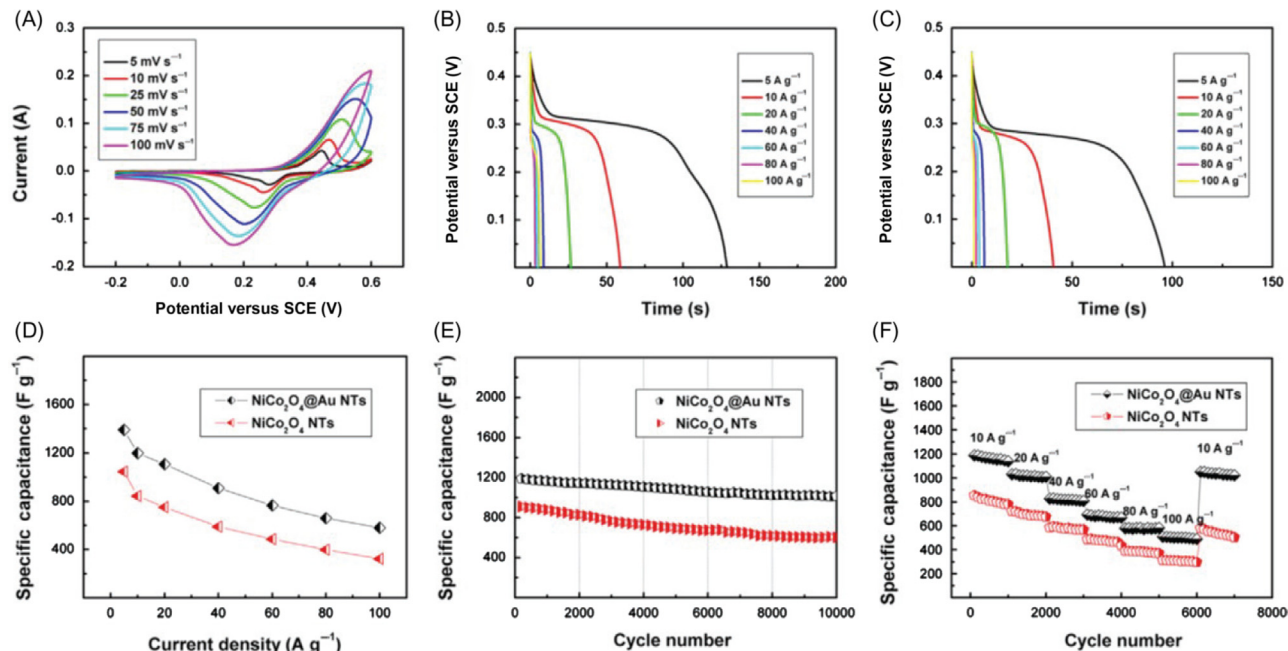
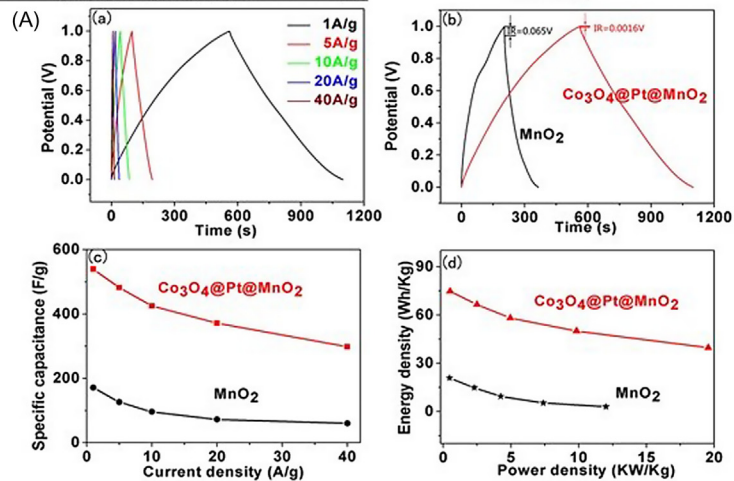
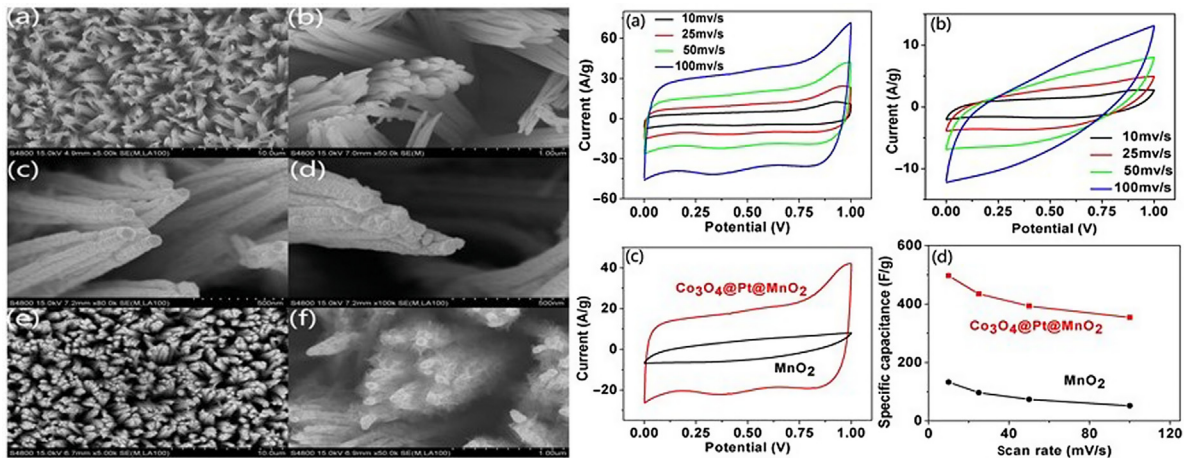


Figure 7.2 (A) CVs of the NiCo₂O₄@Au at various scan rates ranging from 5 to 100 mV s⁻¹; (B,C) charge–discharge curves of the NiCo₂O₄@Au and NiCo₂O₄ various current densities; (D) the specific capacitance of NiCo₂O₄@Au and NiCo₂O₄ at various current densities; (E) cycling performance of the NiCo₂O₄@Au and NiCo₂O₄ and (F) Cycling stability of the NiCo₂O₄@Au and NiCo₂O₄ NTs at varied high current densities. Taken from reference J. Zhu, Z. Xu, B. Lu, *Ultrafine Au nanoparticles decorated NiCo₂O₄ nanotubes as anode material for high-performance supercapacitor and lithium-ion battery applications*, *Nano Energy* 7 (2014) 114–123.



(C)

(Continued)

◀ **Figure 7.3** (A) SEM images of (a, b) Co_3O_4 , (c, d) $\text{Co}_3\text{O}_4@\text{Pt}$, and (e, f) $\text{Co}_3\text{O}_4@\text{Pt}@\text{MnO}_2$; (B) CVs of (a) $\text{Co}_3\text{O}_4@\text{Pt}@\text{MnO}_2$ electrode and (b) MnO_2 thin film electrode at different scan rates in an aqueous solution of Na_2SO_4 (1 M). (c) Comparison of the CV curves of $\text{Co}_3\text{O}_4@\text{Pt}@\text{MnO}_2$ electrode (*red*) and MnO_2 thin film electrode (*black*) at a scan rate of 50 mV/s. (d) Specific capacitances of $\text{Co}_3\text{O}_4@\text{Pt}@\text{MnO}_2$ electrode (*red*) and MnO_2 thin film electrode (*black*) at different scan rates. (C) (a) Charge–discharge curves of $\text{Co}_3\text{O}_4@\text{Pt}@\text{MnO}_2$ electrode at different current densities. (b) Comparison of charge-discharge curves of $\text{Co}_3\text{O}_4@\text{Pt}@\text{MnO}_2$ electrode (*red*) and MnO_2 thin film electrode (*black*) at a current density of 1 A/g. (c) Specific capacitances of $\text{Co}_3\text{O}_4@\text{Pt}@\text{MnO}_2$ NA electrode (*red*) and MnO_2 thin film electrode (*black*) at different scan rates. (d) Ragone plots of $\text{Co}_3\text{O}_4@\text{Pt}@\text{MnO}_2$ electrode (*red*) and MnO_2 thin film electrode (*black*). Taken from reference H. Xia, D. Zhu, Z. Luo, Y. Yu, X. Shi, G. Yuan, et al., *Hierarchically structured $\text{Co}_3\text{O}_4@\text{Pt}@\text{MnO}_2$ nanowire arrays for high-performance supercapacitors*, *Sci. Rep.* 3 (2013) 2978.

promising results when utilized for SCs. They reported 497 F g^{-1} and 539 F g^{-1} specific capacitances through cyclic voltammetry (CV) and by GCD at current density of 1 A g^{-1} respectively and excellent rate performance, that is, 39.6 Wh kg^{-1} at 40 A g^{-1} . Also, no capacitance loss even after 5000 cycles was observed which shows its excellent cycling performance [37].



7.4 Carbonaceous materials

SC are leading in research related to energy storage devices and are at the cutting edge to replace some conventional batteries because of their higher values of supercapacitance, extremely enhanced power density, and extended life cycle. The quick release of stored energy puts them in the list of outstanding candidates for many advance applications, such as in advanced optical systems. In this regard, electrodes made by combining two or three different materials are being used and respectively termed as binary and ternary composite electrodes. Carbon in its various forms like activated carbon, carbon nanotubes (CNTs) (single and multiwall), carbon aerogels, and GN are preferred to be utilized as an electrode material for their large specific surface area, good electrical conductivity, ability to interact with other materials (metal, metal oxide and polymer), ease of synthesis, and low cost. However, the efficiencies and properties of the carbon-based SCs also depend on the synthetic method and source of carbon such as in the case of activated carbon.

Carbon materials have been commonly utilized as electrode materials because of their low cost and ease of fabrication into different shapes such as cloth, wire, mats, foil, etc. The highly porous structure of these materials and pores matching the size of the ions ensure the efficient charging of the electrical double layer. The size of the pores can be adjusted by altering the synthesis conditions, that is, changing the precursor, time of reaction, or other physical or chemical conditions [38]. Activated carbon, CNT, and GN have been widely used carbonaceous materials lately owing to their high conductive properties and ease of fabrication into other shapes or composites with different materials [39–41]. GN made up of sp^2 -hybridized carbon atoms composed of a hexagonal lattice and is the basis of bucky balls, CNTs, and graphite. CNT can be composed by the

cylindrical roll of a single sheet of GN (single-walled carbon nanotubes or SWCNTs) or by many sheets of GN (MWCNTs). These carbonaceous materials can be fabricated into materials possessing high surface area, conductivity, and mechanical and optical properties which can be used in high performance electrochemical systems [42]. Capacitors involving carbon materials are EDLCs that store energy at the electrolyte/carbon interface through alterable ion adsorption on top of the carbon surface, consequently charging the so called “double-layer capacitance” and charge storage mechanism occurs in the absence of redox reaction [43].

7.4.1 Carbon nanotubes

There was another breakthrough for SCs in 1991, when Iijima discovered a carbon containing material named as CNTs. This material was further graded into SWCNTs and MWCNTs, as shown in Fig. 7.4. CNTs are a form of graphite with a hollow cylindrical shape with high stability, high specific surface area, and low resistivity, and this material serves as an excellent support as a conductive additive for pseudocapacitance properties due to the following three reasons: (1) CNTs-based materials are categorized by a high rebounding and thus the composite electrodes can simply take the volumetric deviations in charge and discharge analysis, which ultimately enhance their life cycle; (2) the porosity of CNTs eases the diffusion properties of ions in composites electrode; and (3) lastly the CNTs have a higher percolation of charge particles in comparison to other activated carbon-based electrode materials [44].

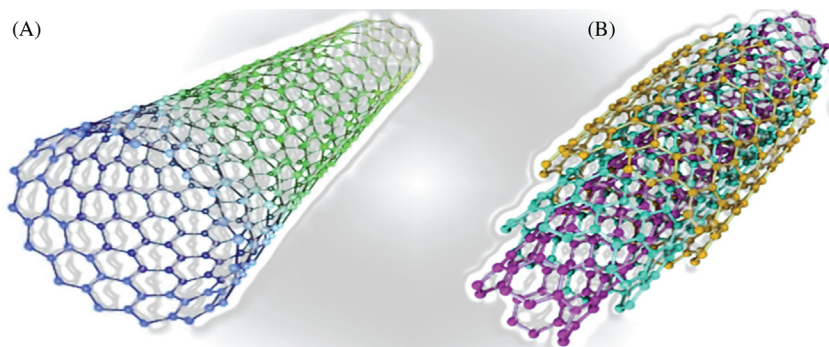


Figure 7.4 Graphical illustration of (A) SWCNTs and (B) MWCNTs.

7.4.1.1 Silver-containing ternary nanocomposites

Cobalt oxide (Co_3O_4) ternary nanocomposite with silver (Ag) NPs and chemically activated MWCNTs were prepared by a simple single step hydrothermal method at low temperature to produce ternary nanocomposite, MWCNTs- Co_3O_4 -Ag by Iqbal and his coworkers [45]. Fig. 7.5 shows the formation of the prepared ternary nanocomposite and its utilization in supercapattery assembly. The electrochemical studies, such as CV, galvanostatic charge-discharge (GCD), and electrochemical impedance spectroscopy (EIS), were performed in 1 M KOH media to evaluate the as-synthesized samples as electrode materials for energy storage devices. The MWCNTs- Co_3O_4 -Ag nanocomposite produced the highest specific capacity (Q_s) of 83.88 C g^{-1} at a current density of 0.6 A g^{-1} , which is remarkably higher than the binary nanocomposite MWCNTs- Co_3O_4 (55.33 C g^{-1}) and pure Co_3O_4 (39.24 C g^{-1}) in three electrode cells. The improved results of the prepared ternary nanocomposite were linked with the deaggregation phenomena of Co_3O_4 nanograins due to their growth on porous and highly conductive platform offered by the MWCNTs and synergistic effect of good conducting Ag NPs. Therefore three of the components of ternary nanocomposite collectively produced the combined effect to achieve the excellent performance. The assembled device comprising the active electrode prepared with ternary nanocomposite was able to run in a wide potential window of 1.5 V. They reported

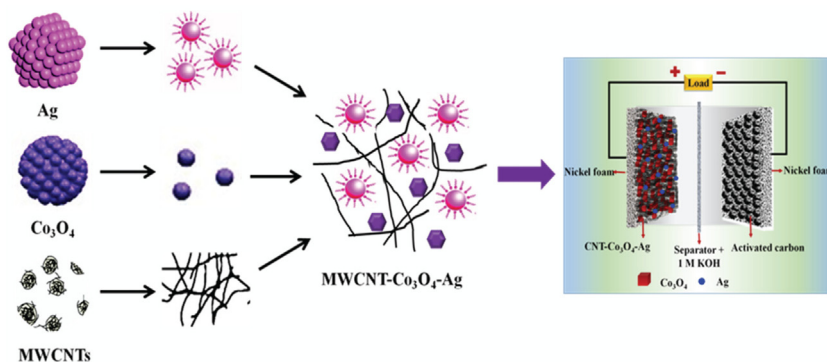


Figure 7.5 Formation of the ternary nanocomposite MWCNTs- Co_3O_4 -Ag and assembled supercapattery incorporating MWCNTs- Co_3O_4 -Ag as a positive electrode material. Taken from reference J. Iqbal, A. Numan, S. Rafique, R. Jafer, S. Mohamad, K. Ramesh, et al., High performance supercapattery incorporating ternary nanocomposite of multiwalled carbon nanotubes decorated with Co_3O_4 nanograins and silver nanoparticles as electrode material, *Electrochim. Acta* 278 (2018) 72–82.

the energy density value of 16.5 Wh kg^{-1} against the power density of 297.5 W kg^{-1} at a current density of 0.2 A g^{-1} . Moreover, the assembled device showed the loss of only 6.4% of its initial value even after 3000 cycles, thereby showing excellent capacity retention.

7.4.1.2 Gold-containing ternary nanocomposites

Reddy et al. prepared hybrid coaxial nanotube arrays of Au–MnO₂/CNT applying three techniques using porous alumina templates, that is, electrodeposition, vacuum infiltration, and CVD techniques [46]. The prepared electrodes with hybrid coaxial nanotube arrays, Au–MnO₂/CNT, produced specific capacitance of 68 F g^{-1} and power density and energy density of 33 kW kg^{-1} and 4.5 Wh kg^{-1} , respectively. These are promising results reported by Reddy's group.

Iqbal et al. synthesized a novel ternary material (Co₃O₄/Au@MWCNTs) with Co₃O₄ NPs, MWCNTs, and Au NPs through a facile single-step hydrothermal route [47]. Initially, the density functional theory simulations were performed to describe the aggregation phenomena in Co₃O₄ NPs, and then proved further with the experimental studies. To overcome the aggregation phenomena of Co₃O₄ NPs, MWCNTs with Au NPs were incorporated which substantially reduced the particle aggregations. The standard three electrodes cell studies revealed that Co₃O₄/Au@MWCNTs composite possesses an excellent energy density, rate capability, and very good cyclic stability compared to unsupported Co₃O₄ or the binary Co₃O₄@MWCNTs. The promising electrochemical performance compared to the single Co₃O₄ or the binary Co₃O₄@MWCNTs materials is assigned to the synergetic effects of MWCNTs and Au to disaggregate the Co₃O₄ NPs and to enhance the overall conductivity, respectively. In order to get insight into the evaluation performance, the two electrodes devices were assembled employing activated carbon as a negative electrode and Co₃O₄/Au@MWCNTs composite as a positive electrode material. The two electrodes supercapattery device demonstrated splendid cycling stability with a retention value of 91.70% in 1 M KOH for over 3500 cycles. Additionally, it exhibited an excellent energy density of 18.80 Wh Kg^{-1} at a power density of 302.00 W Kg^{-1} . These encouraging outcomes can be associated with the distinctive morphology, outstanding conductive networks, increased electroactive sites, and emergence of strong networking of Co₃O₄, MWCNT, and Au in the ternary composite.

7.4.2 Graphene

GN, after its first discovery by Novoselov et al. in 2004 [48], has been of interest globally for its possible applications in numerous areas, such as electrical, electrochemicals, SCs, photocatalytic, optics, and biomedicine [49,50]. GN comprises sp^2 -hybridized, single-layered, two-dimensional carbon atoms arranged in an array of hexagonal honeycomb lattice [51]. Its planar orbitals are energetically stable comprising the localized sigma bonds arranged at three adjacent carbon atoms in this lattice [52]. This structure of GN give it its enhanced surface area and good electrical conductivity, as well as some of its exceptional properties like breaking and tensile strength (Young's modulus), which respectively have benchmark values of $\sim 42 \text{ N m}^{-1}$ and 1.0 T Pa [53]. Furthermore, the large surface area ($2630 \text{ m}^2 \text{ g}^{-1}$), electronic transportation, that is, high intrinsic mobility of ($200,000 \text{ cm}^2 \text{ v}^{-1} \text{ s}^{-1}$), thermal conductivity ($\sim 5000 \text{ W m}^{-1} \text{ K}^{-1}$), and extraordinary mechanical characteristics make it a prospective material for its applications in aforementioned fields [54]. Zhon et al. [55] used an in situ polymerization process to prepared $\text{MoS}_2/\text{rGO}/\text{PANI}$ ternary nanocomposites for supercapacitor application. The prepared nanocomposites have 570 F g^{-1} specific capacitance, due to extraordinary properties of GN. The oxidized form of GN is graphene oxide (GO) which is obtained by the oxidation of the graphite and results in the extended interlayer parting as well as the functionalization of the basal planes of the graphite (Fig. 7.6). The process of reduction of GO eliminates the functional groups from its edges and the basal planes thereby resulting in the formation of conjugated double bond along the chain. In parallel, the

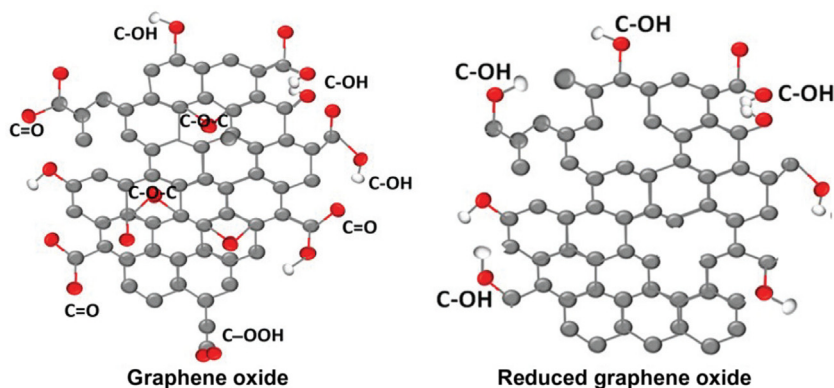


Figure 7.6 GO containing functional groups on its honeycomb matrix, whereas rGO containing fewer functional groups compared to GO.

repulsion created by the electronegativity of the functional group is also reduced which puts the GN sheets back in stacking. In general, incomplete reduction takes place and the resulting rGO retains some properties of GO and pristine GN. The conductivity of rGO is more than GO but lesser than pristine GN. Whereas, the interlayers parting of the GN sheets in rGO is less than GO and more than that in graphite.

7.4.2.1 Silver-containing ternary nanocomposites

Reduced graphene oxide (rGO) has commonly been used to prepare composites with various materials, such as metal and metal oxides, by utilizing different techniques to improve the supercapacitor performance. Ma and coworkers synthesized rGO nanocomposite by using a two-step synthesis with Ag and MnO₂ NPs with a high degree of uniformly distributed NPs over the rGO sheets surface. The two-step method in which first Ag and MnO₂ NPs were uniformly decorated on RGO sheets was prepared by an in situ development of MnO₂ nanostructures on GO sheets and then in a second step reduction of GO and Ag⁺ to produce Ag/MnO₂/rGO. The prepared material revealed a specific capacitance of 467.5 F g⁻¹ at 5 mV s⁻¹ sweep scan rate [56].

A simple one-step hydrothermal process was followed for the synthesis of rGO-Co₃O₄-Ag, rGO-Co₃O₄, and Co₃O₄ for electrochemical storage application (Fig. 7.6) [57]. The confirmation of the successful synthesis and characterizations were performed by various analytical techniques. The nanograins (Co₃O₄) grown on the rGO framework decorated with Ag NPs showed the superior electrochemical performance when tested by CV, GCD, and EIS techniques compared with the other samples (rGO-Co₃O₄ and Co₃O₄). The superior performance is due to the reduced aggregations of nanograins and decoration of Ag NPs which ultimately increase the active sites of the ternary nanocomposite. The assembled supercapattery (rGO-Co₃O₄-Ag//AC) demonstrated a high energy density, 23.63 Wh kg⁻¹ at a power density of 440 Wkg⁻¹ which was described due to the combination of rGO-Co₃O₄-Ag with AC. Moreover, it showed the high specific capacity (115.8 Cg⁻¹) at 0.6 Ag⁻¹, fantabulous reversibility with a cycling efficiency of ~85.5% after 3000 cycles in an alkaline media (1 M KOH) foreground the efficacy of the utilized synthesis protocol. The as-synthesized ternary nanocomposite may act as a replacement electrode material for applications in supercapattery and could open the door for the development of superior performance electrochemical storage devices (Fig. 7.7).

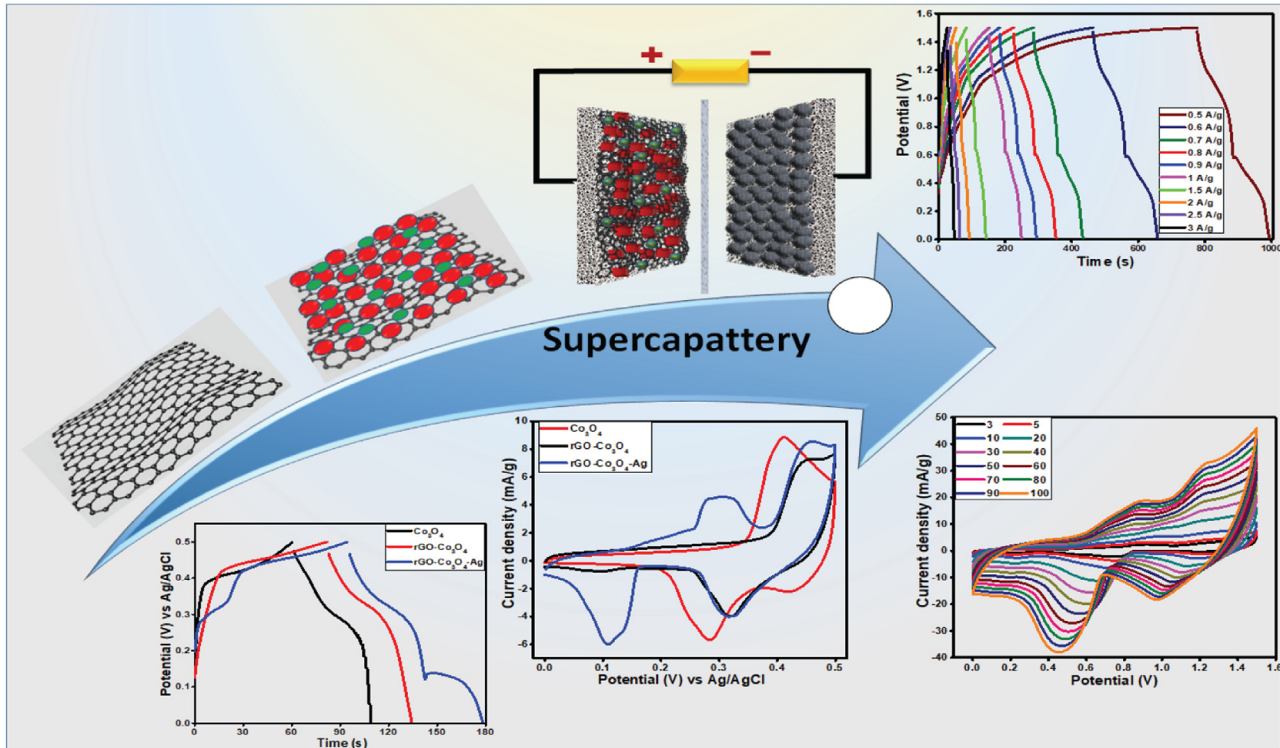


Figure 7.7 Showing the development of ternary nanocomposite, $rGO-Co_3O_4-Ag$ and its subsequent utilization as an electrode material in supercapattery. Also the results obtained from the assembled device are presented. Taken from reference J. Iqbal, A. Numan, R. Jafer, S. Bashir, A. Jilani, S. Mohammad, et al., Ternary nanocomposite of cobalt oxide nanograins and silver nanoparticles grown on reduced graphene oxide conducting platform for high-performance supercapattery electrode material, *J. Alloy. Compd.* 821 (2020) 153452.

7.4.2.2 Gold-containing ternary nanocomposites

Veeramani et al. prepared a GN-based ternary nanocomposite in which they utilized a two-step method, electrophoretic, and electrochemical deposition methods. The developed Au–MnO₂–GN nanocomposite film was utilized in supercapacitor assembly. The assembled device produced specific capacitance of 575 F g⁻¹ at a current density of 2.5 A g⁻¹ in a galvanostatic charge discharge process, which are excellent results [58].



7.5 Conducting polymers

CPs have π bonded configurations and can be oxidized or reduced by chemical or electrochemical means. Thus the chemical and physical properties like electrical conductivity and optical characteristics of these polymers can be easily tuned by monitoring the degree of oxidation/reduction, using different media for oxidation/reduction, controlling temperature, moisture content, etc. [59]. So, CPs can be described as macromolecules with a conjugated arrangement of bonds along the backbone and attains positive or negative charges by the oxidation or reduction process, respectively. Among all CPs, PANI, PTh, PPy, their derivatives, have been widely studied owing to their peculiar properties such as low cost, ease of synthesis, long shelf life and tunable electrical conductivity [60,61].

These conductive polymers are promising pseudocapacitive materials and the supercapacitor electrodes fabricated from them are economical, easy to process, have good conductivity and a long shelf life [62,63]. Despite being widely explored materials, the cycling stability of CPs doesn't meet the desirable necessities yet. Poor cyclic stability conduces a rapid fall of specific capacitance thereby resulting in a poor life cycle [64,65]. Thus in order to enhance life cycle, the CPs are often fabricated with carbonaceous materials, metal oxides, metals, etc. [66].

7.5.1 Ternary composites of polyaniline

The initial exploration of electrochemical characteristics of PANI can be attributed to Diaz and coworkers [67]. In 1984, Feldberg studied the electrochemistry of CPs and reported the possible contribution of capacitive

current which was also later supported by the voltammetric and impedance spectroscopic studies [68–70]. These findings established CPs as an anticipating entrant for electrochemical research carrying pseudocapacitive behaviors. Yet, the major limitation of CPs is their meagre cyclic stability due to the mechanical swelling and shrinking while doping/dedoping, thereby resulting in the degradation of electrode [71,72]. To overcome this, composites of CPs with carbonaceous materials, metals, metal oxides, noble metals, etc., have been fabricated [73–75]. Owing to their good conductivity, the incorporation of noble metals into bulk materials have gained much attention in the area of active electrode materials development for electrochemical energy storage devices. The noble metals can facilitate a fast charge transport mechanism resulting from the redox process of pseudocapacitors to the current collectors [76].

7.5.1.1 Silver-containing ternary nanocomposites

The incorporation of noble metals can intercede the efficient charge propagation through the PANI. Ternary composites of PANI containing noble metals and carbonaceous materials or metal salts have been widely reported. Metal salts, such as MnO_2 , in spite of high theoretical capacitance have a densely packed structure and low conductivity which limits their application for supercapacitor applications. The incorporation of PANI and Ag separately have seen the rise in electrical conductivity and the specific capacitance of the final binary composite [77,78]. Kim et al. observed enhanced electrochemical characteristics of $\text{Ag-MnO}_2@\text{PANI}$ in comparison to $\text{MnO}_2@\text{PANI}$ and PANI. $\text{MnO}_2@\text{PANI}$ showed much higher current density than PANI owing to its huge surface area and the contributory effect of MnO_2 [79]. The addition of Ag to $\text{MnO}_2@\text{PANI}$ in $\text{Ag-MnO}_2@\text{PANI}$ further enhanced the current density which can be accredited to its enhanced surface area and electrical conductivity with faster ion transport. Similarly, $\text{Ag-Ce}(\text{NO}_3)_3@\text{PANI}$ also showed higher electrical conductivity and capacitance owing to the well distributed Ag in the PANI matrix. The addition of Ce ions and Ag caused the resistivity to drop from 1.02Ω for PANI and 0.67Ω for $\text{Ce}(\text{NO}_3)_3@\text{PANI}$ to final 0.34Ω for $\text{Ag-Ce}(\text{NO}_3)_3@\text{PANI}$. This led to high charge transfer, hence enhanced electrochemical characteristics [80].

Ag-containing carbonaceous materials like GN or CNT in pure or modified forms have also been widely reported. The report of Dhibar et al. showed uniformly coated PANI on MWCNTs surface with Ag NPs decorated over it [81]. The $\text{Ag-MWCNTs}@\text{PANI}$ nanocomposite was

reported to have the maximum value of capacitance, that is, 528 F g^{-1} in comparison to PANI and Ag-PANI which presented much lower values of 376 and 475 F g^{-1} at 5 mV s^{-1} scan rate, respectively. The enhanced capacitance was related to the high electrical conductivity, that is, 4.24 S cm^{-1} of Ag-MWCNTs@PANI, high surface area provided by the MWCNTs, as well as the presence of Ag NPs. Similarly, multilayer supershort CNTs prepared by tailoring raw MWCNTs in combination with Ag and PANI displayed very enhanced electrical conductivity of 18.5 cm^{-1} and specific capacitance of 615 F g^{-1} at 1 A g^{-1} . The CNTs not only provided added transport paths and curtail the transmission distance for the electrolyte ions/electrons but also have more open pores than MWCNTs and these properties are further enhanced on addition of Ag which leads to better conductivity and electrochemical characteristics [82].

GN, owing to its higher conductivity than CNTs, has shown much improved electrochemical characteristics. Sawangphruk et al. showed that Ag NPs can assist the dispersion of GN by preventing its restacking [83]. The Ag-GN@PANI nanocomposite also showed much higher surface area of $545 \text{ m}^2 \text{ g}^{-1}$ in comparison to 505 and $93 \text{ m}^2 \text{ g}^{-1}$ of GN and PANI, respectively. The specific capacitance of Ag-GN@PANI was reported to be 830 F g^{-1} at a scan rate of 5 A g^{-1} that is far greater than what was earlier discussed in CNTs reported composites. Graphite nanofibers, when used instead of GN, and combined with Ag and PANI showed 212 F g^{-1} specific capacitance, in contrast to 153 and 80 F g^{-1} reported for graphite nanofibers@PANI and PANI, respectively. The Ag NPs were interpreted to act as bridges between the graphitic fibers and PANI which led to decreased contact resistance and hence an improved charge transfer [84]. Activated carbon has been an extensively exploited electrode material for SCs. Ag-activated carbon@PANI was prepared by Patil et al. by simple oxidative polymerization of aniline in the presence of activated carbon, and later reaction with AgNO_3 to incorporate Ag particles. The electrodes of Ag-activated carbon@PANI on a stainless steel metal sheet, made using the dip-coating methodology, showed specific capacitance of 567 F g^{-1} at 5 mV s^{-1} and energy density of 86.30 Wh kg^{-1} at 1 mA cm^{-2} which is much higher than values reported for pure PANI and other binary combinations [85].

7.5.1.2 Gold-containing ternary nanocomposites

Au NPs have also been reported with PANI in ternary composites for electrochemical applications. Shayeh et al. [86] interpreted that Au NPs can improve the electrical characteristics of rGO sheets. On account of this, Ag-rGO@PANI composite was proposed as an electrode material. PANI and Ag-rGO@PANI nanocomposite was prepared by electrochemical polymerization and the Ag-rGO@PANI nanocomposite showed specific capacitance of 340 and 110 F g^{-1} at the scan rate of 2 and 100 mV s^{-1} , respectively, while PANI showed much decreased specific capacitance of 190 to 60 F g^{-1} at the same scan rates. High values of specific capacitance even at higher scan rates in comparison to PANI show that Au NPs do not block the pores. The Nyquist plots (Fig. 7.8A) also showed that the magnitude of contact resistance is much smaller in Ag-rGO@PANI than in Pure PANI, which suggests that Au-rGO improves the charge transfer phenomenon of PANI composite electrode. Fig. 7.8B shows the variation with the specific capacitance of Ag-rGO@PANI at diverse scan rates while Fig. 7.8C displays the cyclic stabilities of the PANI and Ag-rGO@PANI electrodes. Another report of similar composite by in situ oxidative polymerization methodology showed highly dispersed Au and well exfoliated PANI sheets. It was interpreted that PANI acts as spacers between the rGO sheets, thereby avoiding the restacking of sheets. The ternary composite showed specific capacitance of 572 F g^{-1} at a current density of 0.1 A g^{-1} by a three-electrode system and 88.54 retention after 10,000 cycles [87].

7.5.1.3 Palladium-containing ternary nanocomposites

Pd NPs have also been used to fabricate PANI-based ternary composites. Gobal et al. [16] showed that changes in the morphology of PANI to improve the charge transfer can be done by sonochemical loading of Pd NPs on TiO_2 NTs followed by galvanostatic electropolymerization of aniline. The morphological studies showed that PANI was deposited uniformly on the Pd- TiO_2 , therefore exposing the high surface area of PANI. It is assumed that Pd NPs help in aligned and ordered growth of PANI, thereby leading to porous morphology of Pd- TiO_2 @PANI which is highly desirable for electrochemical studies [88]. The ternary composite showed much higher specific capacitance of 1060 F g^{-1} in 1 M H_2SO_4 electrolyte at a current of 2 A g^{-1} in comparison to 210 F g^{-1} obtained for PANI electrode. The cyclic stability was also observed to be exceptionally high and the ternary composite maintained 94% of initial capacity

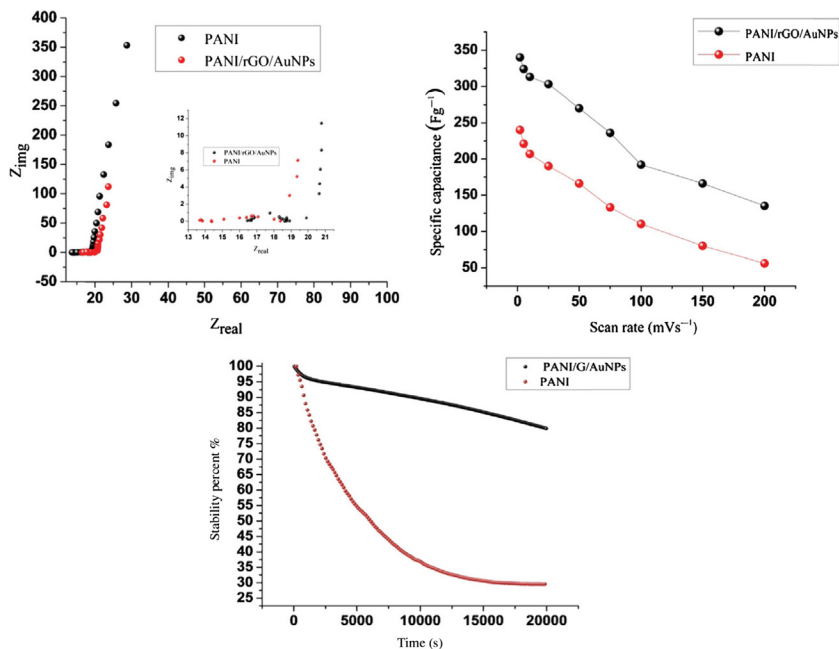


Figure 7.8 Nyquist plots logged from 10 kHz to 0.01 Hz with an ac amplitude of 5 mV for PANI and PANI/rGO/AuNPs electrode. (A) Variations of the specific capacitance for PANI/rGO/AuNPs electrode as a function of the scan rate in 1 M H_2SO_4 solution; (B) and stability of two PANI and Ag-rGO@PANI electrodes after successive cycles at 50 mVs^{-1} for 20,000 s. Taken from reference J. Shabani Shayah, A. Ehsani, M. R. Ganjali, P. Norouzi, B. Jaleh, *Conductive polymer/reduced graphene oxide/Au nano particles as efficient composite materials in electrochemical supercapacitors*, *Appl. Surf. Sci.* 353 (2015) 594–599.

in 1.0 M H_2SO_4 electrolyte after 10 days of repeated use. Pd NPs in combination with GN and CNT also showed high charge transfer properties and the resultant ternary composite with PANI showed coordinative interactions of the Pd NPs with CNT/GN and PANI chains, higher number of ion-accessible sites, an interconnected porous network, and high mechanical strength, thereby providing a better synergism [89,90].

7.5.1.4 Platinum-containing ternary nanocomposites

Pt reinforced CNT composite yarn coated with PANI has also been studied to develop wearable next-generation electronic textiles. Pt-CNT@PANI yarn capacitor showed longer charge discharge time than CNT@PANI capacitor and the areal capacitance reached to 97.670 mF cm^{-2} , which is 27 times the value reported for rGO@CNT

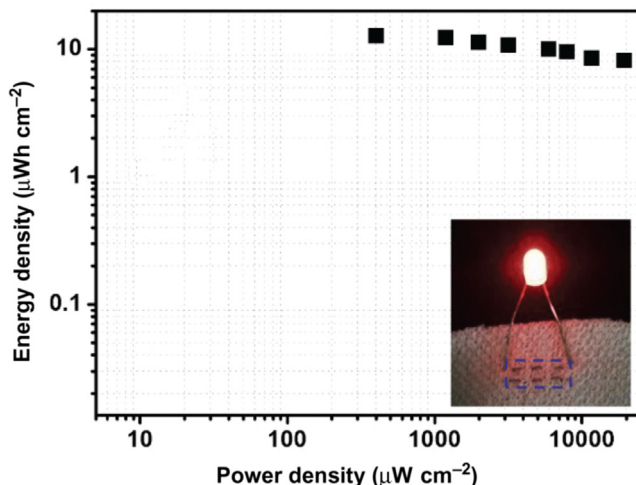


Figure 7.9 Ragone plots of the linear device fabricated according to the method in this paper in comparison with recently reported linear devices. Inset picture shows a LED indicator powered by two Pt/CNT@PANI nanocomposite yarn supercapacitors connected in series. Taken from reference Q. Wang, Y. Wu, T. Li, D. Zhang, M. Miao and A. Zhang, High performance two-ply carbon nanocomposite yarn supercapacitors enhanced with a platinum filament and in situ polymerized polyaniline nanowires, *J. Mater. Chem. A* 4, 2016, 3828–3834.

yarn and seven times that reported for CNT@PANI yarn [91,92]. The Ragone plot (Fig. 7.9) was calculated from the GCD curves. The areal energy density of the device varied from 12.68 to 8.13 $\mu\text{Wh cm}^{-2}$ at power densities from 399 to 19,381 $\mu\text{W cm}^{-2}$ respectively, which is much higher than other reported yarns [93,94]. The inset in Fig. 7.9 shows that two small SCs in series can light a LED indicator, which is a hugely promising prospect for electronic devices.

7.5.2 Ternary nanocomposites of polypyrrole containing noble metals

Like PANI, the Ag-GN@PPy composite reported by Kalambate et al. [95] showed high electrochemical characteristics. The morphological analysis showed PPy embedded into GN sheets and Ag NPs on PPy (Fig. 7.10). This structure reduces the diffusion resistance of electrolyte into the electrode matrix. The authors proposed that synergistic effect of GN, Ag, and PPy led to a high cyclic stability of 92% after 1000 cycles and the ternary composite showed much higher specific capacitance of 450 F g^{-1} at a current density of 0.9 mA g^{-1} in comparison to single or

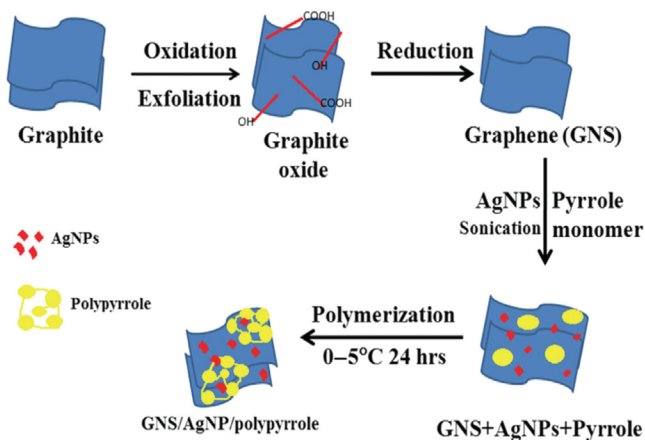


Figure 7.10 Illustration of the preparation procedure for GNS/AgNPs/PPY nanocomposites. Taken from reference J. Shabani Shayeh, A. Ehsani, M.R. Ganjali, P. Norouzi, B. Jaleh, *Conductive polymer/reduced graphene oxide/Au nano particles as efficient composite materials in electrochemical supercapacitors*, *Appl. Surf. Sci.*, 353 (2015) 594–599.

binary composites (Fig. 7.11). Another report of epoxide-functionalized bucky paper combined with PPy and Ag NPs for supercapacitor electrode material showed improved electrochemical performance due to the interactions between the constituents which led to improved charge transfer. The hydrogen bonding occurred between PPy and the epoxide group of bucky paper and a coordinate bonded structure was formed between PPy and Ag NPs, thereby leading to improved electrochemical performance [96].

7.5.3 Ternary nanocomposites of polythiophene or other polymers containing noble metals

PTh and noble metal ternary composite when employed as an electrode material also showed promising results. Ag-rGO@PTh prepared by in situ polymerization and chemical reduction of GO in the presence of Ag NPs showed a high specific capacitance of 953.13 F g^{-1} at a scan rate of 4 mV s^{-1} with up to 91.88% retention after 1000 charge/discharge cycles. Ates et al. [97] interpreted that Ag NPs form a good conductive network and the interaction of PTh and Ag on rGO synergistically improves specific capacitance. PTh derivatives such as 3,4-ethylenedioxythiophene): poly(styrenesulfonate) (PEDOT:PSS) in combination with Ag and MnO_2 was utilized as flexible high performance supercapacitor materials by Yu et al. [98]. The Ag NPs and PEDOT:PSS acted as current collectors.

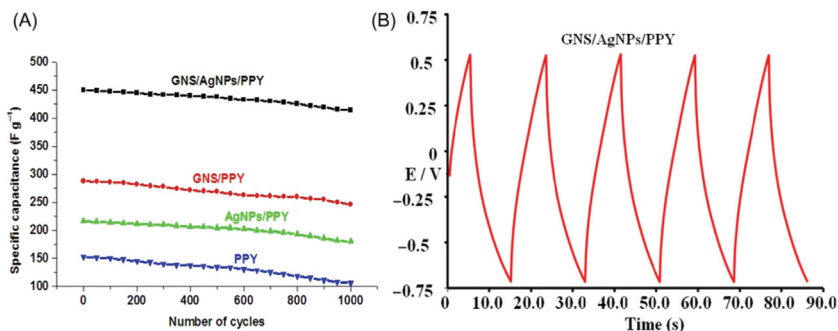


Figure 7.11 (A) Capacitance cycling performance of the as-prepared GNS/AgNPs/PPY, GNS/PPY, AgNPs/PPY and PPY electrodes at a current density of 0.9 mA g^{-1} ; (B) first five charge–discharge cycles for GNS/AgNPs/PPY electrode. Taken from reference J. Shabani Shayeh, A. Ehsani, M.R. Ganjali, P. Norouzi, B. Jaleh, *Conductive polymer/reduced graphene oxide/Au nano particles as efficient composite materials in electrochemical supercapacitors*, *Appl. Surf. Sci.* 353 (2015) 594–599.

A high specific capacitance of 862 F g^{-1} at a current density of 2.5 A g^{-1} was achieved which suggests fast electron transport from Ag nanowires to PEDOT:PSS and finally to MnO_2 layer. The flexible supercapacitor also showed 98% capacitance retention even after 100 bends of 180 degrees (Fig. 7.12). Similarly, Au-GO@poly(p-phenylenediamine) composite showed specific capacitance of 238 F g^{-1} which was much higher than that of poly(p-phenylenediamine) and GO@poly(p-phenylenediamine) as the latter showed much lower values of 11 and 176 F g^{-1} , respectively.

7.6 Conclusions and future work

The demand of high-energy storage systems is growing at a rapid pace due to the trend toward miniature and smart technology. The ternary nanocomposites based on noble metals can enhance the electrochemical signature of the electrode materials and demonstrate a higher specific capacity by providing transfer channels or by contributing in a redox reaction. Furthermore, the combination in the ternary nanocomposites of CPs, metal oxides, and noble metals substantially enhances the electrochemical performance through the conductivity and charge–discharge ability. It is crucial to utilize the noble metals economically in order to enhance the performance of supercapattery because they are quite costly.

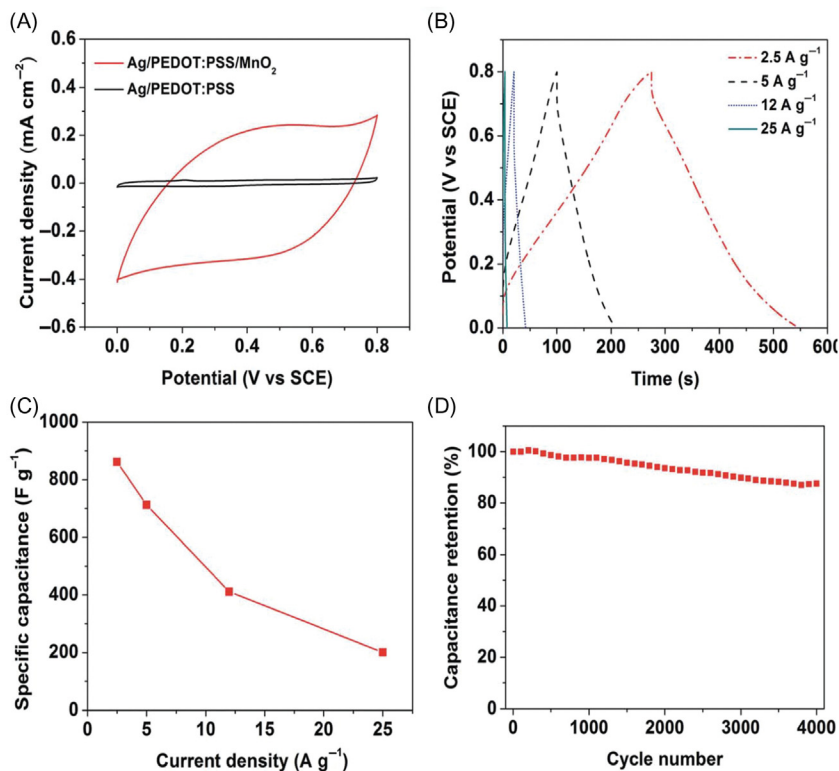


Figure 7.12 (A) CV curves of Ag-NW/PEDOT:PSS-NP and Ag-NW/PEDOT:PSS-NP/MnO₂ at a scan rate of 20 mV s⁻¹. (B) GCD curves of Ag-NW/PEDOT:PSS-NP/MnO₂ at different current densities (2.5–25 A g⁻¹). (C) Specific capacitances of Ag-NW/PEDOT:PSS-NP/MnO₂ as a function of the current density. (D) Cycle performance of Ag-NW/PEDOT:PSS-NP/MnO₂ at a scan rate of 100 mV s⁻¹. Taken from reference J. Shabani Shayeh, A. Ehsani, M.R. Ganjali, P. Norouzi, B. Jaleh, *Conductive polymer/reduced graphene oxide/Au nano particles as efficient composite materials in electrochemical supercapacitors*, *Appl. Surf. Sci.* 353 (2015) 594–599.

In the future, to achieve the target of assembling the superior performance supercapattery, two kinds of noble metals-based nanocomposites could be utilized by overcoming some of the problems which hindered their use at a commercial scale. Even though excellent performance has been demonstrated by single noble metals-based ternary nanocomposites, their applications are limited to the laboratory scale. Thus extensive research is required to explore a general, cost-effective and facile procedure for developing two kinds of noble metals-based nanocomposites material which could be utilized at an industrial scale. These challenges could be

addressed by developing the trend of using two kinds of noble metal-based composites in high-performance supercapattery to meet the demand for efficient technologies that can help to develop two kinds of noble metal-based nanocomposites at the nanoscale range, so as to increase the overall surface to volume ratio, and hence reduce the noble metals loading. If we can address these issues well, the two kinds of noble metal-based nanocomposites will have prospects of very wide application in supercapattery.

Acknowledgments

This work was financially supported by the Fundamental Research Grant Scheme (FRGS) from the Ministry of Education, Malaysia (FP062-2018A) and Impact-Oriented Interdisciplinary Research Grant (IIRG007A-19IISS), University of Malaya, Malaysia.

References

- [1] E. Iwama, K. Kisu, W. Naoi, P. Simon, K. Naoi, 10 – Enhanced hybrid supercapacitors utilizing nanostructured metal oxides A2 - Dubal, Deepak P, in: P. Gomez-Romero (Ed.), *Metal Oxides in Supercapacitors*, Elsevier, 2017, pp. 247–264.
- [2] Z. Fang, W. Xu, T. Huang, M. Li, W. Wang, Y. Liu, et al., Facile scalable synthesis of Co_3O_4 /carbon nanotube hybrids as superior anode materials for lithium-ion batteries, *Mater. Res. Bull.* 48 (2013) 4419–4423.
- [3] M.M. Shahid, A.H. Ismail, A.M.A.A. AL-Mokaram, R. Vikneswaran, S. Ahmad, A. Hamza, et al., A single-step synthesis of nitrogen-doped graphene sheets decorated with cobalt hydroxide nanoflakes for the determination of dopamine, *Prog. Nat. Sci.: Mater. Int.* 27 (2017) 582–587.
- [4] V.N. Popov, Carbon nanotubes: properties and application, *Mater. Sci. Eng. R Rep.* 43 (2004) 61–102.
- [5] K.I. Ozoemena, S. Chen, *Nanomaterials in Advanced Batteries and Supercapacitors*, Springer, 2016.
- [6] H. Wang, X. Yuan, G. Zeng, Y. Wu, Y. Liu, Q. Jiang, et al., Three dimensional graphene based materials: synthesis and applications from energy storage and conversion to electrochemical sensor and environmental remediation, *Adv. Colloid Interface Sci.* 221 (2015) 41–59.
- [7] M.J. Allen, V.C. Tung, R.B. Kaner, Honeycomb carbon: a review of graphene, *Chem. Rev.* 110 (2009) 132–145.
- [8] H. Shirakawa, E.J. Louis, A.G. MacDiarmid, C.K. Chiang, A.J. Heeger, Synthesis of electrically conducting organic polymers: halogen derivatives of polyacetylene, (CH)_x, *J. Chem. Soc. Chem. Commun.* (1977) 578–580.
- [9] R. Friend, R. Gymer, A. Holmes, J. Burroughes, R. Marks, C. Taliani, et al., Electroluminescence in conjugated polymers, *Nature* 397 (1999) 121.
- [10] P. Wan, X. Wen, C. Sun, B.K. Chandran, H. Zhang, X. Sun, et al., Flexible transparent films based on nanocomposite networks of polyaniline and carbon nanotubes for high-performance gas sensing, *Small* 11 (2015) 5409–5415.
- [11] G.M. Spinks, V. Mottaghitalab, M. Bahrami-Samani, P.G. Whitten, G.G. Wallace, Carbon-nanotube-reinforced polyaniline fibers for high-strength artificial muscles, *Adv. Mater.* 18 (2006) 637–640.

- [12] E. Frackowiak, V. Khomenko, K. Jurewicz, K. Lota, F. Béguin, Supercapacitors based on conducting polymers/nanotubes composites, *J. Power Sources* 153 (2006) 413–418.
- [13] P. Simon, Y. Gogotsi, Materials for electrochemical capacitors, *Nature Materials*, 7 (2008) 845–854.
- [14] M.E. Roberts, D.R. Wheeler, B.B. McKenzie, B.C. Bunker, High specific capacitance conducting polymer supercapacitor electrodes based on poly (tris (thiophenylphenyl) amine), *J. Mater. Chem.* 19 (2009) 6977–6979.
- [15] P. Asen, S. Shahrokhian, A high performance supercapacitor based on graphene/polypyrrole/Cu₂O–Cu(OH)₂ ternary nanocomposite coated on nickel foam, *J. Phys. Chem. C* 121 (2017) 6508–6519.
- [16] F. Gobal, M. Faraji, Electrodeposited polyaniline on Pd-loaded TiO₂ nanotubes as active material for electrochemical supercapacitor, *J. Electroanal. Chem.* 691 (2013) 51–56.
- [17] R.A. Dar, L. Giri, S.P. Karna, A.K. Srivastava, Performance of palladium nanoparticle–graphene composite as an efficient electrode material for electrochemical double layer capacitors, *Electrochim. Acta* 196 (2016) 547–557.
- [18] J. Kang, A. Hirata, L. Kang, X. Zhang, Y. Hou, L. Chen, et al., Enhanced supercapacitor performance of MnO₂ by atomic doping, *Angew. Chem. Int. Ed.* 52 (2013) 1664–1667.
- [19] X. Lu, T. Zhai, X. Zhang, Y. Shen, L. Yuan, B. Hu, et al., WO_{3-x}@Au@MnO₂ core–shell nanowires on carbon fabric for high-performance flexible supercapacitors, *Adv. Mater.* 24 (2012) 938–944.
- [20] Y. Hou, Y. Cheng, T. Hobson, J. Liu, Design and synthesis of hierarchical MnO₂ nanospheres/carbon nanotubes/conducting polymer ternary composite for high performance electrochemical electrodes, *Nano Lett.* 10 (2010) 2727–2733.
- [21] B.E. Conway, *Electrochemical Supercapacitors: Scientific Fundamentals and Technological Applications*, Springer Science & Business Media, 2013.
- [22] S.K. Meher, P. Justin, G. Ranga Rao, Microwave-mediated synthesis for improved morphology and pseudocapacitance performance of nickel oxide, *ACS Appl. Mater. Interfaces* 3 (2011) 2063–2073.
- [23] G.M. Suppes, B.A. Deore, M.S. Freund, Porous conducting polymer/heteropolyoxometalate hybrid material for electrochemical supercapacitor applications, *Langmuir* 24 (2008) 1064–1069.
- [24] Y.-B. He, G.-R. Li, Z.-L. Wang, C.-Y. Su, Y.-X. Tong, Single-crystal ZnO nanorod/amorphous and nanoporous metal oxide shell composites: controllable electrochemical synthesis and enhanced supercapacitor performances, *Energy Environ. Sci.* 4 (2011) 1288–1292.
- [25] R. Tummala, R.K. Guduru, P.S. Mohanty, Nanostructured Co₃O₄ electrodes for supercapacitor applications from plasma spray technique, *J. Power Sources* 209 (2012) 44–51.
- [26] Q. Qu, Y. Shi, L. Li, W. Guo, Y. Wu, H. Zhang, et al., V₂O₅ · 0.6 H₂O nanoribbons as cathode material for asymmetric supercapacitor in K₂SO₄ solution, *Electrochem. Commun.* 11 (2009) 1325–1328.
- [27] G. Yu, L. Hu, N. Liu, H. Wang, M. Vosgueritchian, Y. Yang, et al., Enhancing the supercapacitor performance of graphene/MnO₂ nanostructured electrodes by conductive wrapping, *Nano Lett.* 11 (2011) 4438–4442.
- [28] C. An, Y. Zhang, H. Guo, Y. Wang, Metal oxide-based supercapacitors: progress and perspectives, *Nanoscale Adv.* (2019).
- [29] F. Wang, X. Wu, X. Yuan, Z. Liu, Y. Zhang, L. Fu, et al., Latest advances in supercapacitors: from new electrode materials to novel device designs, *Chem. Soc. Rev.* 46 (2017) 6816–6854.

- [30] R.R. Salunkhe, Y.V. Kaneti, Y. Yamauchi, Metal–organic framework-derived nanoporous metal oxides toward supercapacitor applications: progress and prospects, *ACS Nano* 11 (2017) 5293–5308.
- [31] Y. Yan, T. Wang, X. Li, H. Pang, H. Xue, Noble metal-based materials in high-performance supercapacitors, *Inorg. Chem. Front.* 4 (2017) 33–51.
- [32] S. Shahabuddin, A. Pandey, J. Kaur, R. Saidur, N.A. Mazlan, S.N.A. Baharin, The metal oxide nanoparticles doped polyaniline based nanocomposite as stable electrode material for supercapacitors, in: 2018 International Conference and Utility Exhibition on Green Energy for Sustainable Development (ICUE), IEEE, 2018, pp. 1–7.
- [33] X. Zhang, Y. Xu, Y. Ma, M. Yang, Y. Qi, A hierarchical $\text{MoO}_2/\text{Au}/\text{MnO}_2$ heterostructure with enhanced electrochemical performance for application as supercapacitor, *Eur. J. Inorg. Chem.* 2015 (2015) 3764–3768.
- [34] X. Zheng, X. Yan, Y. Sun, Z. Bai, G. Zhang, Y. Shen, et al., Au-embedded ZnO/NiO hybrid with excellent electrochemical performance as advanced electrode materials for supercapacitor, *ACS Appl. Mater. Interfaces* 7 (2015) 2480–2485.
- [35] P. Wang, H. Liu, Q. Tan, J. Yang, Ruthenium oxide-based nanocomposites with high specific surface area and improved capacitance as a supercapacitor, *RSC Adv.* 4 (2014) 42839–42845.
- [36] J. Zhu, Z. Xu, B. Lu, Ultrafine Au nanoparticles decorated NiCo_2O_4 nanotubes as anode material for high-performance supercapacitor and lithium-ion battery applications, *Nano Energy* 7 (2014) 114–123.
- [37] H. Xia, D. Zhu, Z. Luo, Y. Yu, X. Shi, G. Yuan, et al., Hierarchically structured $\text{Co}_3\text{O}_4@ \text{Pt} @ \text{MnO}_2$ nanowire arrays for high-performance supercapacitors, *Sci. Rep.* 3 (2013) 2978.
- [38] E. Frackowiak, Carbon materials for supercapacitor application, *Phys. Chem. Chem. Phys.* 9 (2007) 1774–1785.
- [39] S. Ahmed, A. Ahmed, M. Rafat, Supercapacitor performance of activated carbon derived from rotten carrot in aqueous, organic and ionic liquid based electrolytes, *J. Saudi Chem. Soc.* 22 (2018) 993–1002.
- [40] G. Wu, P. Tan, D. Wang, Z. Li, L. Peng, Y. Hu, et al., High-performance supercapacitors based on electrochemical-induced vertical-aligned carbon nanotubes and polyaniline nanocomposite electrodes, *Sci. Rep.* 7 (2017) 43676.
- [41] M. Horn, B. Gupta, J. MacLeod, J. Liu, N. Motta, Graphene-based supercapacitor electrodes: addressing challenges in mechanisms and materials, *Curr. Opin. Green. Sustain. Chem.* 17 (2019) 42–48.
- [42] M. Zhi, F. Yang, F. Meng, M. Li, A. Manivannan, N. Wu, Effects of pore structure on performance of an activated-carbon supercapacitor electrode recycled from scrap waste tires, *ACS Sustain. Chem. Eng.* 2 (2014) 1592–1598.
- [43] P. Simon, A. Burke, Nanostructured carbons: double-layer capacitance and more, *Electrochem. Soc. Interface* 17 (2008) 38.
- [44] H. Pan, J. Li, Y. Feng, Carbon nanotubes for supercapacitor, *Nanoscale Res. Lett.* 5 (2010) 654.
- [45] J. Iqbal, A. Numan, S. Rafique, R. Jafer, S. Mohamad, K. Ramesh, et al., High performance supercapattery incorporating ternary nanocomposite of multiwalled carbon nanotubes decorated with Co_3O_4 nanograins and silver nanoparticles as electrode material, *Electrochim. Acta* 278 (2018) 72–82.
- [46] A.L.M. Reddy, M.M. Shaijumon, S.R. Gowda, P.M. Ajayan, Multisegmented Au-MnO_2 /carbon nanotube hybrid coaxial arrays for high-power supercapacitor applications, *J. Phys. Chem. C* 114 (2009) 658–663.
- [47] J. Iqbal, L. Li, A. Numan, S. Rafique, R. Jafer, S. Mohamad, et al., Density functional theory simulation of cobalt oxide aggregation and facile synthesis of a cobalt

- oxide, gold and multiwalled carbon nanotube based ternary composite for a high performance supercapattery, *N. J. Chem.* 43 (2019) 13183–13195.
- [48] A. Jilani, M.H.D. Othman, M.O. Ansari, S.Z. Hussain, A.F. Ismail, I.U. Khan, Inamuddin, Graphene and its derivatives: synthesis, modifications, and applications in wastewater treatment, *Environ. Chem. Lett.* 16 (2018) 1301–1323.
- [49] A. Jilani, M.H.D. Othman, M.O. Ansari, R. Kumar, A. Alshahrie, A.F. Ismail, et al., Facile spectroscopic approach to obtain the optoelectronic properties of few-layered graphene oxide thin films and their role in photocatalysis, *N. J. Chem.* 41 (2017) 14217–14227.
- [50] A. Jilani, M.H.D. Othman, M.O. Ansari, R. Kumar, I.U. Khan, M.S. Abdel-wahab, et al., Structural, optical, and photocatalytic investigation of nickel oxide@ graphene oxide nanocomposite thin films by RF magnetron sputtering, *J. Mater. Sci.* 53 (2018) 15034–15050.
- [51] A. Jilani, M.H.D. Othman, M.O. Ansari, I. Ullah Khan, S.Z. Hussain, Linear /non-linear optical susceptibility spectroscopic constants of polyaniline@graphene oxide nanocomposite thin films, *Synth. Met.* 251 (2019) 30–39.
- [52] I. Yahia, A. Jilani, M.S. Abdel-wahab, H. Zahran, M.S. Ansari, A.A. Al-Ghamdi, et al., The photocatalytic activity of graphene oxide/Ag₃PO₄ nano-composite: loading effect, *Optik* 127 (2016) 10746–10757.
- [53] A. Jilani, M.H.D. Othman, M.O. Ansari, M. Oves, A. Alshahrie, I.U. Khan, et al., A simple route to layer-by-layer assembled few layered graphene oxide nanosheets: optical, dielectric and antibacterial aspects, *J. Mol. Liq.* 253 (2018) 284–296.
- [54] A. Jilani, M.H.D. Othman, M.O. Ansari, M. Oves, S.Z. Hussain, I.U. Khan, et al., Structural and optical characteristics, and bacterial decolonization studies on non-reactive RF sputtered Cu–ZnO@ graphene based nanoparticles thin films, *J. Mater. Sci.* (2019).
- [55] L.-Z. Bai, Y.-H. Wang, S.-S. Cheng, F. Li, Z.-Y. Zhang, Y.-Q. Liu, Synthesis and electrochemical performance of molybdenum disulfide-reduced graphene oxide-polyaniline ternary composites for supercapacitors, *Front. Chem.* 6 (2018). 218–218.
- [56] L. Ma, X. Shen, Z. Ji, G. Zhu, H. Zhou, Ag nanoparticles decorated MnO₂/reduced graphene oxide as advanced electrode materials for supercapacitors, *Chem. Eng. J.* 252 (2014) 95–103.
- [57] J. Iqbal, A. Numan, R. Jafer, S. Bashir, A. Jilani, S. Mohammad, et al., Ternary nanocomposite of cobalt oxide nanograins and silver nanoparticles grown on reduced graphene oxide conducting platform for high-performance supercapattery electrode material, *J. Alloy. Compd.* 821 (2020) 153452.
- [58] V. Veeramani, B. Dinesh, S.-M. Chen, R. Saraswathi, Electrochemical synthesis of Au–MnO₂ on electrophoretically prepared graphene nanocomposite for high performance supercapacitor and biosensor applications, *J. Mater. Chem. A* 4 (2016) 3304–3315.
- [59] N. Parveen, N. Mahato, M.O. Ansari, M.H. Cho, Enhanced electrochemical behavior and hydrophobicity of crystalline polyaniline@graphene nanocomposite synthesized at elevated temperature, *Compos. Part. B: Eng.* 87 (2016) 281–290.
- [60] M.O. Ansari, R. Kumar, S.A. Ansari, S.P. Ansari, M.A. Barakat, A. Alshahrie, et al., Anion selective pTSA doped polyaniline@graphene oxide-multiwalled carbon nanotube composite for Cr(VI) and Congo red adsorption, *J. Colloid Interface Sci.* 496 (2017) 407–415.
- [61] T. Bashir, A. Shakoor, E. Ahmed, N.A. Niaz, S. Iqbal, M.S. Akhtar, et al., Magnetic, electrical and thermal studies of polypyrrole–Fe₃O₄ nanocomposites, *Polym. Sci. Ser. A* 59 (2017) 902–908.
- [62] A. Alshahrie, M.O. Ansari, High performance supercapacitor applications and DC electrical conductivity retention on surfactant immobilized macroporous ternary

- polypyrrole/graphitic- C_3N_4 @graphene nanocomposite, *Electron. Mater. Lett.* 15 (2019) 238–246.
- [63] M.O. Ansari, A. Alshahrie, S.A. Ansari, Facile route to porous polyaniline@nanodiamond-graphene based nanohybrid structures for DC electrical conductivity retention and supercapacitor applications, *J. Polym. Res.* 26 (2019) 76.
- [64] J. Xu, K. Wang, S.-Z. Zu, B.-H. Han, Z. Wei, Hierarchical nanocomposites of polyaniline nanowire arrays on graphene oxide sheets with synergistic effect for energy storage, *ACS Nano* 4 (2010) 5019–5026.
- [65] C. Meng, C. Liu, L. Chen, C. Hu, S. Fan, Highly flexible and all-solid-state paper-like polymer supercapacitors, *Nano Lett.* 10 (2010) 4025–4031.
- [66] Q. Meng, K. Cai, Y. Chen, L. Chen, Research progress on conducting polymer based supercapacitor electrode materials, *Nano Energy* 36 (2017) 268–285.
- [67] A.F. Diaz, J.A. Logan, Electroactive polyaniline films, *J. Electroanal. Chem. Interfacial Electrochem.* 111 (1980) 111–114.
- [68] S.W. Feldberg, Reinterpretation of polypyrrole electrochemistry. Consideration of capacitive currents in redox switching of conducting polymers, *J. Am. Chem. Soc.* 106 (1984) 4671–4674.
- [69] J.P. Ferraris, M.M. Eissa, I.D. Brotherston, D.C. Loveday, A.A. Moxey, Preparation and electrochemical evaluation of poly (3-phenylthiophene) derivatives: potential materials for electrochemical capacitors, *J. Electroanal. Chem.* 459 (1998) 57–69.
- [70] B.E. Conway, Transition from “supercapacitor” to “battery” behavior in electrochemical energy storage, *J. Electrochem. Soc.* 138 (1991) 1539–1548.
- [71] V. Khomenko, E. Frackowiak, F. Béguin, Determination of the specific capacitance of conducting polymer/nanotubes composite electrodes using different cell configurations, *Electrochim. Acta* 50 (2005) 2499–2506.
- [72] L. Li, H. Song, Q. Zhang, J. Yao, X. Chen, Effect of compounding process on the structure and electrochemical properties of ordered mesoporous carbon/polyaniline composites as electrodes for supercapacitors, *J. Power Sources* 187 (2009) 268–274.
- [73] A. Afzal, F.A. Abuilwaiwi, A. Habib, M. Awais, S.B. Waje, M.A. Atieh, Polypyrrole/carbon nanotube supercapacitors: technological advances and challenges, *J. Power Sources* 352 (2017) 174–186.
- [74] K.-U. Lee, J.Y. Byun, H.-J. Shin, S.H. Kim, A high-performance supercapacitor based on polyaniline-nanoporous gold, *J. Alloy. Compd.* 779 (2019) 74–80.
- [75] J. Arjomandi, J.Y. Lee, R. Movafagh, H. Moghanni-Bavil-Olyaei, M.H. Parvin, Polyaniline/aluminum and iron oxide nanocomposites supercapacitor electrodes with high specific capacitance and surface area, *J. Electroanal. Chem.* 810 (2018) 100–108.
- [76] H. Xia, C. Hong, X. Shi, B. Li, G. Yuan, Q. Yao, et al., Hierarchical heterostructures of Ag nanoparticles decorated MnO_2 nanowires as promising electrodes for supercapacitors, *J. Mater. Chem. A* 3 (2015) 1216–1221.
- [77] J.M. Sieben, E. Morallón, D. Cazorla-Amorós, Flexible ruthenium oxide-activated carbon cloth composites prepared by simple electrodeposition methods, *Energy* 58 (2013) 519–526.
- [78] H. Jiang, J. Ma, C. Li, Polyaniline- MnO_2 coaxial nanofiber with hierarchical structure for high-performance supercapacitors, *J. Mater. Chem.* 22 (2012) 16939–16942.
- [79] J. Kim, H. Ju, A.I. Inamdar, Y. Jo, J. Han, H. Kim, et al., Synthesis and enhanced electrochemical supercapacitor properties of Ag- MnO_2 -polyaniline nanocomposite electrodes, *Energy* 70 (2014) 473–477.
- [80] Y. Li, Z. Li, F. Zheng, Polyaniline/silver/cerium nitrate ternary composite: synthesis, characterization and enhanced electrochemical properties, *J. Appl. Polym. Sci.* 132 (2015).

- [81] S. Dhibar, C.K. Das, Silver nanoparticles decorated polyaniline/multiwalled carbon nanotubes nanocomposite for high-performance supercapacitor electrode, *Ind. Eng. Chem. Res.* 53 (2014) 3495–3508.
- [82] L. Tang, F. Duan, M. Chen, Silver nanoparticle decorated polyaniline/multiwalled super-short carbon nanotube nanocomposites for supercapacitor applications, *RSC Adv.* 6 (2016) 65012–65019.
- [83] M. Sawangphruk, M. Suksomboon, K. Kongsupornsak, J. Khuntilo, P. Srimuk, Y. Sanguansak, et al., High-performance supercapacitors based on silver nanoparticle–polyaniline–graphene nanocomposites coated on flexible carbon fiber paper, *J. Mater. Chem. A* 1 (2013) 9630–9636.
- [84] K.-S. Kim, S.-J. Park, Bridge effect of silver nanoparticles on electrochemical performance of graphite nanofiber/polyaniline for supercapacitor, *Synth. Met.* 162 (2012) 2107–2111.
- [85] D.S. Patil, S.A. Pawar, R.S. Devan, S.S. Mali, M.G. Gang, Y.R. Ma, et al., Polyaniline based electrodes for electrochemical supercapacitor: synergistic effect of silver, activated carbon and polyaniline, *J. Electroanal. Chem.* 724 (2014) 21–28.
- [86] J. Shabani Shayeh, A. Ehsani, M.R. Ganjali, P. Norouzi, B. Jaleh, Conductive polymer/reduced graphene oxide/Au nano particles as efficient composite materials in electrochemical supercapacitors, *Appl. Surf. Sci.* 353 (2015) 594–599.
- [87] L. Wang, T. Wu, S. Du, M. Pei, W. Guo, S. Wei, High performance supercapacitors based on ternary graphene/Au/polyaniline (PANI) hierarchical nanocomposites, *RSC Adv.* 6 (2016) 1004–1011.
- [88] D. Ibrahim Abouelamaiem, M.J. Mostazo-López, G. He, D. Patel, T.P. Neville, I.P. Parkin, et al., New insights into the electrochemical behaviour of porous carbon electrodes for supercapacitors, *J. Energy Storage* 19 (2018) 337–347.
- [89] S. Giri, D. Ghosh, A. Malas, C.K. Das, A facile synthesis of a palladium-doped polyaniline-modified carbon nanotube composites for supercapacitors, *J. Electron. Mater.* 42 (2013) 2595–2605.
- [90] P.K. Kalambate, C.R. Rawool, S.P. Karna, A.K. Srivastava, Nitrogen-doped graphene/palladium nanoparticles/porous polyaniline ternary composite as an efficient electrode material for high performance supercapacitor, *Mater. Sci. Energy Technol.* 2 (2019) 246–257.
- [91] Q. Wang, Y. Wu, T. Li, D. Zhang, M. Miao, A. Zhang, High performance two-ply carbon nanocomposite yarn supercapacitors enhanced with a platinum filament and in situ polymerized polyaniline nanowires, *J. Mater. Chem. A* 4 (2016) 3828–3834.
- [92] J. Ren, L. Li, C. Chen, X. Chen, Z. Cai, L. Qiu, et al., Twisting carbon nanotube fibers for both wire-shaped micro-supercapacitor and micro-battery, *Adv. Mater.* 25 (2013) 1155–1159.
- [93] L. Kou, T. Huang, B. Zheng, Y. Han, X. Zhao, K. Gopalsamy, et al., Coaxial wet-spun yarn supercapacitors for high-energy density and safe wearable electronics, *Nat. Commun.* 5 (2014) 3754.
- [94] F. Su, X. Lv, M. Miao, High-performance two-ply yarn supercapacitors based on carbon nanotube yarns dotted with Co_3O_4 and NiO nanoparticles, *Small* 11 (2015) 854–861.
- [95] P.K. Kalambate, R.A. Dar, S.P. Karna, A.K. Srivastava, High performance supercapacitor based on graphene-silver nanoparticles-polypyrrole nanocomposite coated on glassy carbon electrode, *J. Power Sources* 276 (2015) 262–270.
- [96] H. Kim, M. Ramalingam, V. Balakumar, X. Zhang, W. Gao, Y.-A. Son, et al., Chemically interconnected ternary AgNP/polypyrrole/functionalized buckypaper composites as high-energy-density supercapacitor electrodes, *Chem. Phys. Lett.* (2019) 136957.

- [97] M. Ates, S. Caliskan, E. Ozten, A ternary nanocomposite of reduced graphene oxide, Ag nanoparticle and polythiophene used for supercapacitors, Fuller. Nanotub. Carbon Nanostructures 26 (2018) 360–369.
- [98] Z. Yu, C. Li, D. Abbitt, J. Thomas, Flexible, sandwich-like Ag-nanowire/PEDOT:PSS-nanopillar/MnO₂ high performance supercapacitors, J. Mater. Chem. A 2 (2014) 10923–10929.



Metal/metal oxide thin film electrodes for supercapatteries

Mohammad Islam¹, Sofia Javed², Muhammad Aftab Akram² and Muhammad Usman²

¹Center of Excellence for Research in Engineering Materials, Deanship of Scientific Research, King Saud University, Riyadh, Saudi Arabia

²Department of Materials Engineering, School of Chemical and Materials Engineering, National University of Sciences and Technology, Islamabad, Pakistan



8.1 Hybrid supercapacitors or supercapatteries

A typical supercapacitor or ultracapacitor may be classified based on the electrode material type and the surface charge storage mechanism. The three main capacitor types are (1) electric double layer capacitor (EDLC), (2) pseudocapacitor, and (3) hybrid supercapacitor. The EDLC have electrostatic attraction forces that are responsible for the separation of the electronic and ionic charges at the electrolyte/electrode interfacial region. There are no chemical reactions involved, but the charge storage is by means of noncapacitive faradaic storage (NCFS). On the other hand, capacitive faradaic storage (CFS) is induced in pseudocapacitors by means of reduction/oxidation chemical reactions, also referred to as charge transfer reactions at the electrode surface. In a hybrid supercapacitor, both capacitive (CFS) as well as NCFS mechanisms are active. The EES devices may, therefore, be categorized as shown in Fig. 8.1.

The charge storage in hybrid supercapacitors occurs through both electrostatic charge separation (NCFS) and surface redox reactions (CFS) [1]. A hybrid supercapacitor or supercapattery, therefore, combines the merits of supercapacitor (high output power) and the battery (high energy density). The galvanostatic charging and discharging (GCD) measurements during electrochemical testing correspond to linear plots in the case of pseudocapacitance and nonlinear behavior for electrode materials in batteries. The cyclic voltammetry (CV) studies show a continuous redox reaction within the potential range as represented by a rectangular shape

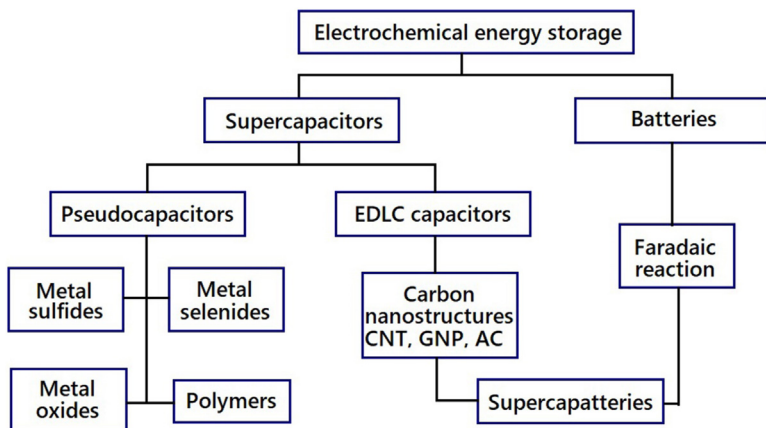


Figure 8.1 Classification of the electrochemical energy storage devices.

for pseudocapacitive behavior, whereas redox reaction at particular potentials as peaks shaped CV corresponds to the electrode materials in batteries [2,3].

The key differences between supercapacitor and supercapattery have been illustrated in Fig. 8.2A,B [4]. While ruthenium dioxide is considered to be the first redox active material that exhibits a rectangular CV shape (Fig. 8.2A1), similar observations were reported for transition metal oxides (TMO) and conductive polymers [5–8]. Unlike a supercapacitor, the CFS behavior in a supercapattery produces a voltammogram with distinct peaks and nonlinear GCD owing to Nernstian behavior, as showcased in Fig. 8.2B1. The comparison of various EES devices on the basis of energy and power output is summarized by the Ragone plot in Fig. 8.2C [9]. Depending on the electrolyte type—aqueous or organic—the supercapatteries may output higher specific power or energy. The electrode material may be either pseudocapacitive or battery type depending on whether the redox reactions occur continuously or at a particular position within the range of electrode potential. The electrode materials used in batteries offer advantages of superior intercalation charge storage, longer discharge times, and greater operational safety.

8.1.1 Prerequisites for a supercapattery

A typical supercapattery device incorporates two different types of electrodes: a battery-type electrode to store high energy density by involving the faradic reactions and a second electrode consisting of a supercapacitor type

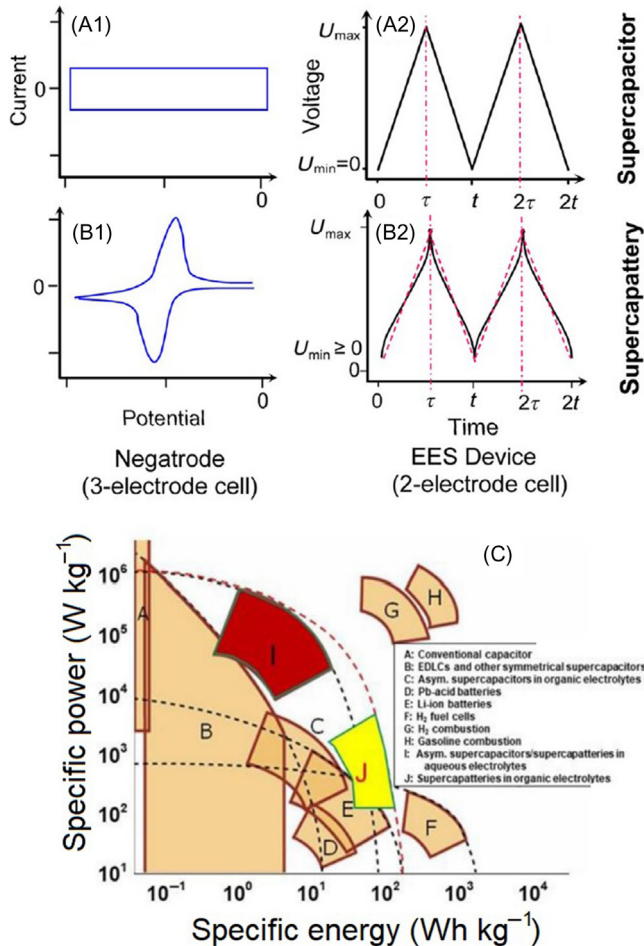


Figure 8.2 Comparison of CV and GCD behavior of a typical (A) supercapacitor and (B) supercapattery. (C) Ragone plot showing supercapattery technology development with reference to other EES devices [4,9].

material with high porosity, greater specific surface area, and relatively shorter path length to sustain high power density. The synergetic effects of both electrodes result in a device with high output power and energy densities. This type of device is highly desirable for an efficient energy storage device. Such devices are, therefore, able to charge and discharge rapidly like supercapacitors and store high energy like batteries.

Ideally, a supercapattery should have combination of highly polarizable capacitor-like and battery-like electrodes. In such hybrid device configuration, the capacitor-like electrode having a wide potential window will

generate EDLC and/or pseudocapacitance, whereas the battery-like electrode will contribute either via pseudocapacitance (surface redox reaction) or NCFS. It is noteworthy that a pseudocapacitor consisting of two identical or different pseudocapacitive electrodes may also be referred to as a supercapattery. In case of a hypothetical supercapattery that is made up of a lithium metal negatrod and a 400 F g^{-1} positrod, the theoretical specific energy produced upon discharging from 3.5 to 1.0 V will be 625 Wh kg^{-1} [9]. Thus, although the supercapattery design essentially incorporates metal oxides-based redox electrode materials, their low conductivity makes their practical use quite a challenge.



8.2 Metal oxides as electrode materials

Although represented by the general chemical formula MO_x , metal oxides may be monoxides (MO , where $\text{M}=\text{Ni}$, Ti , Co , Cu , etc.), dioxides (MO_2 , $\text{M}=\text{Ti}$, Cr , V , Zr , Pd , etc.), or trioxides (MO_3) that are quite rare. In general, the oxygen anions form lattice structures of face centered cubic (fcc) or hexagonal closed packed (hcp) structures, whereas metal cations occupy octahedral or tetrahedral interstitial sites. The monoxides such as NiO and TiO have Rocksalt crystal structure with oxygen anions forming the fcc lattice and the metal cations filling the octahedral sites. On the other hand, most of the dioxides possess rutile structure with hcp anions lattice and the metal cations occupying half of the octahedral sites. The fcc and hcp crystal structures along with octahedral and tetrahedral sites are schematically illustrated in Fig. 8.3. Transition metal monoxides (MO_x) including CoO , NiO , TiO , and VO have NaCl or rock salt structure. In a typical fcc lattice, the number of sites per unit cell is four and eight for octahedral and tetrahedral sites, respectively.

8.2.1 Promising metal oxides

Some of the extensively investigated electrode materials in nanostructured form are oxides of cobalt (Co_3O_4), copper (CuO), manganese (MnO_2), nickel (NiO), ruthenium (RuO_2), and vanadium (V_2O_5). The TMO including Fe_2O_3 , MnO_2 , RuO_2 , SnO_2 , and V_2O_5 exhibit a CFS mechanism by means of multiple surface successive redox reactions [10–13]. In a recent work, RuO_2 with a 2D nanosheet morphology displayed

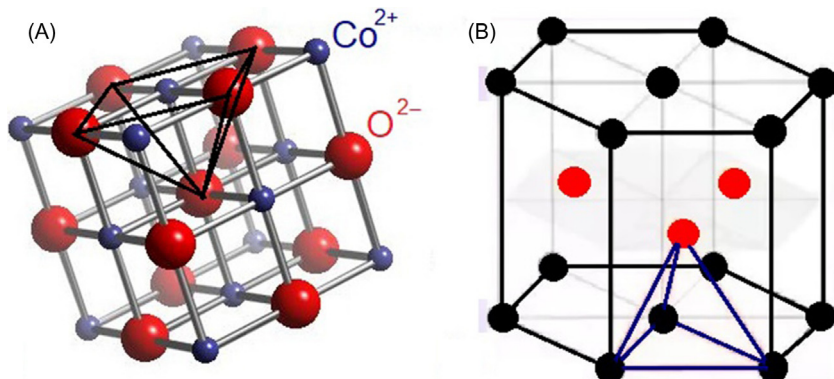
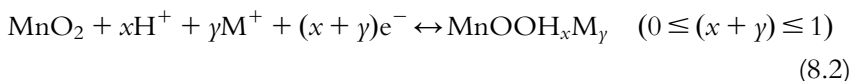


Figure 8.3 Schematic representation of (A) rock salt (CoO) unit cell, showing fcc crystal structure and octahedral site, and (B) hcp crystal structure with tetrahedral site.

$\sim 900 \text{ mAh g}^{-1}$ specific capacity and charge/discharge cyclic stability after 50 cycles of overpotential. Having a similar 2D morphology, V_2O_5 nanosheets demonstrated specific capacitance of 117 mAh g^{-1} at 59 mA g^{-1} and high temperature (50°C) cycle stability after 200 cycles. Molybdenum trioxide (MoO_3), when explored in nanosheet morphology for Li- O_2 batteries, indicated elevated cyclic stability with less overpotential due to increased density of oxygen vacancies [14,15].

The surface redox reactions in TMO involve protons or cations attachment as well as substoichiometric variations in the electrode composite. For RuO_2 and MnO_2 -based electrode materials, these chemical reactions can be presented as follows [13]:



While hydrous ruthenium oxide ($\text{RuO}_2 \cdot n\text{H}_2\text{O}$) with amorphous structure was found to produce large specific capacitance ($\sim 103 \text{ F g}^{-1}$) and great reversibility [16,17], its commercial viability was restrained by ruthenium's high cost and low abundance.

8.2.2 Technical issues with pure metal oxides

Although these composites are promising for improved EES performance, several issues, such as structural instability in electrolytes, poor cyclic stability, low electron and ion transport abilities, poor conductivity, toxicity

and high cost, that are associated with these oxides constrict the commercial use of these materials [18–26]. This fact makes it mandatory to pursue alternative materials and/or morphological/compositional tailoring of the existing materials by adopting approaches such as doping, hybridization, and nanocomposites processing. The EES capabilities of the TMO in supercapacitors may be increased by: (1) fine tuning the composite, for example, using carbonates and/or hydrides; (2) incorporating conductive additives, e.g. carbon nanotubes (CNT), graphene, conductive polymers, etc. for enhanced electron transport properties; and (3) tailoring surface morphology to maximize surface area and porosity in order to make available more active sites for electrolytic ion adsorption [27–29].



8.3 Performance of metal oxide electrodes

8.3.1 Nickel oxide

In nanostructured form, NiO is extensively used in EES due to its stability and efficient redox reactions for energy storage. It has been incorporated mostly in supercapacitors as zero-, one-, two- or three-dimensional nanostructures. Such structures may be obtained from diverse processing techniques including the sol–gel method, coprecipitate process, hydrothermal synthesis, solvothermal process, and electrodeposition. The electrochemical properties of NiO-based electrodes are derived from high thermal and chemical stability that, in turn, depends on specific surface area, morphology, and porosity level.

NiO with both layered and porous layer configurations has been proven to be an efficient material for supercapacitor applications. Wai Cai et al. [30] synthesized NiO hollow spheres with 770 F g^{-1} specific capacitance at 2 A g^{-1} current density. Another study reported that NiO with nanoflower morphology is a promising electrode material for supercapacitors with measured specific capacitance of 1678 F g^{-1} [31]. Upon comparison of different morphologies, it was found that NiO nanoplatelets produced via microwave-assisted synthesis recorded 1361 F g^{-1} specific capacitance as compared to that for NiO nanoslices (685 F g^{-1}) at 1 mV s^{-1} scan rate. Such an improvement in output performance was attributed to higher surface area of $161 \text{ m}^2 \text{ g}^{-1}$ [32]. Yet another work reported the synthesis of NiO nanoflakes through the tuning of processing

conditions during the hydrothermal method. The nanoflakes comprised homogeneous pores made by interconnection of flakes with each other and demonstrated high charge conductivity. The interconnected arrays showed a little polarization and high specific capacitance of 400 F g^{-1} at 2 A g^{-1} current density and excellent cyclic stability [33].

Another group produced NiO nanowires-based electrode materials with ribbon-like morphology to make supercapacitors with superior performance, namely a specific capacitance of 1200 F g^{-1} at 1 A g^{-1} and 95% capacitance retention after 5000 cycles [34]. A binder-free electrode for electrochemical testing was quite a novel approach adopted by Yao et al. [35] who produced NiO fibers directly over nickel foam with an average diameter of 280–400 nm. The supercapacitor incorporating this electrode recorded a specific capacitance of 725 F g^{-1} at 2 A g^{-1} and excellent capacitance retention after 8000 charge/discharge cycles. A relatively better performance of 919 F g^{-1} specific capacitance (at 1 A g^{-1}) and 97% capacitance retention was reported when employing self-assembled NiO nanowires with average diameter and length values of 350 nm and 2–4 μm , respectively, obtained from nanosheets via the solvothermal route [36].

8.3.2 Copper oxide

Although copper oxide has been explored for use in catalysis, sensors, photovoltaics, photoelectrochemical cells, lithium ion batteries, and supercapacitors [37–42], it is mostly investigated for electrochemical applications due to high charge transportation, low cost, and high charge sustainability. All these attributes have made it beneficial as electrode material for supercapacitors. Although copper oxide exists as CuO and Cu_2O , the former is mainly used in energy storage applications due to its high stability, charge storage ability, and more reactive sites for redox reactions in the electrolyte. The compound CuO has been investigated in several nanoscale morphologies including sheets, rods, flakes, and flowers as an electrode material in supercapacitors [43–47].

A 150-nm-thick CuO film consisting of CuO nanosheets was prepared on nickel foam via a template-free growth method. When used as an electrode material, the specific capacitance was determined to be 569 F g^{-1} at a current density of 5 mA cm^{-2} [48]. A different approach involving fabrication of binder-free electrode based on CuO nanosheets and nanorods over ITO glass yielded similar performance attributes with

no degradation after 1000 cycles [49]. Heng et al. [50] investigated the morphology effect of CuO nanoribbons and nanoflowers made using the chemical bath deposition process. It was found that the surface area of the former increased almost by twofold (from 37 to 71 m² g⁻¹) with an associated increase in the specific capacitance due to greater density of active sites for redox reaction. In another article, a facile, robust method to fabricate binder-free CuO electrode materials with nanosheets, microroses, and microwoolen-like nanostructures via chemical bath deposition was reported. Although all the electrodes were of uniform thickness with homogeneous porosity, the specific capacitance value was the maximum for microwoolen-like arranged CuO nanosheets owing to the interconnected network making it efficient for charge mobility [51].

8.3.2.1 CuO-based mixed oxides and nanocomposites

An approach toward making more efficient EES devices, the researchers have resorted to tailoring the morphology of material composites at the nanometer scale. The CuO nanoparticles embedded in a three-dimensional graphene network were reportedly produced over carbon cloth as the electrode material of a supercapacitor, with remarkable charge storage efficiency and specific capacitance of 1539 F g⁻¹ [52]. In another study, the electrochemical properties of a CuO-based electrode were enhanced by mixing it with CeO₂. The CeO₂-CuO composite showed a specific capacitance value of 396 F g⁻¹ [53].

Carbon-based materials exhibit tremendous attributes when decorated with nanomaterials [54,55]. An approach is used to improve the supercapacitive properties of CuO by making its composite with Co₃O₄ and CNTs. In this work, CuO and Co₃O₄ nanoparticles were synthesized by a simple hydrothermal method and decorated on CNTs. The specific capacitance for this electrode material was calculated at 279 F g⁻¹. The main purpose of CNTs in this composite was to improve the cyclic stability of electrode material. The composite exhibited remarkable capacitance retention of 89% after 5000 cycles [56].

8.3.3 Vanadium pentoxide (V₂O₅)

Vanadium oxides have attracted much attention in recent years due to their unique electronic, optoelectronic, and chemical characteristics. Several oxides of vanadium have been reported due to different oxidation states of vanadium and possess unique structure-dependent properties. Among these oxides, vanadium pentoxide has been explored as a negative

electrode in EES applications for its higher capacitance, cyclability, and broader working potential window. Lee et al. [57] synthesized amorphous vanadium pentoxide by rapidly quenching the heated powder and evaluated its capacitance in aqueous KCl, which turn out to be 350 F g^{-1} [46]. A few nanometers-thick hydrated vanadium oxide thin film was deposited on 3D porous CNT substrate by Kim et al. [58]. This structure showed a remarkable capacitance of 910 F g^{-1} and associated high specific capacity of 540 mAh g^{-1} .

8.3.4 Ruthenium oxide (RuO_2)

Ruthenium oxide (RuO_2) is the most widely used electrode material for supercapacitors due to its high theoretical capacitance value and the advantages of high cyclability, reversibility, wide working potential window, compatibility with charge/discharge rates, and reasonable conductivity. There are three oxidation states of Ru in the working potential window of 1.2 V. The practical capacitance of RuO_2 is less than the theoretical value of 2000 F g^{-1} due to its dependence on water uptake, crystallite size, morphology, and crystallinity. Also, intercalation capacitance is not possible due to compact crystalline nature, although there are a few reports of better performance by amorphous RuO_2 with bulk capacitance. Park et al. prepared the RuO_2 electrode on a titanium substrate by the electrodeposition method. The electrode characteristics depended on the morphology of the thin film formed with uniform thickness achieved by optimizing the cathode potential and the deposition time. The specific capacitance for this work was found to be 788 F g^{-1} [59]. Patake and Lokhande [60] synthesized RuO_2 thin films by anodic deposition of the method. They achieved a specific capacitance of 1190 F g^{-1} with uniform thickness.

8.3.5 Manganese dioxide (MnO_2)

Manganese dioxide (MnO_2) is a promising pseudocapacitive material with advantages of low cost and industrial scalability [61–64] that can be produced using facile, low cost, synthesis routes such as electrochemical deposition. Nanostructured MnO_2 with different morphologies (rods, sheets, spheres, and flowers) were fabricated through electrodeposition and tested as electrode materials in ECs [65,66]. Furthermore, MnO_2 exists as different polymorphs, including α , β , γ , λ , and δ types [67–69], with capacitance behavior dependent on the particular polymorphic type,

as reported by Yin et al. [70]. The specific capacitance of MnO_2 strongly depends on its crystal structure with values in descending order of $\alpha\text{-MnO}_2 > \delta\text{-MnO}_2 > \beta\text{-MnO}_2$.

Beside morphology and polymorph type, the surface chemistry of MnO_2 also affects its capacitance, as is the case with most of the ECs [71]. For instance, Zhai et al. [72] demonstrated the beneficial effect of the surface oxygen vacancies toward enhancement in the MnO_2 capacitance. Another study by Gao et al. [73] revealed the effect of Mn vacancies in $\delta\text{-MnO}_2$ nanosheets for an increase in the specific capacitance and cycling stability. Sun et al. [29] synthesized the MnO_2 nanowires on Ni dendrites support by electrodeposition technique. It was a quite efficient approach to fabricate electrodes for supercapacitors. This fabricated electrode showed the specific capacitance of 1110 F g^{-1} with excellent cyclic stability. The morphology like trees made it highly reactive with electrolyte for redox reactions.

8.3.5.1 Manganese dioxide based nanocomposites

Research on the core-shell structure of MnO_2 on $\alpha\text{-Fe}_2\text{O}_3$ involved coating the Fe_2O_3 nanowires with MnO_2 using a wet chemical process. The thin film of the heterogeneous structure was fabricated to exhibit high specific capacitance. The backbone of ferrites gives the charge stability to the composite. After 1000 cycles, 98% specific capacitance of this composite was retained, which is excellent for electrode materials in supercapacitors [74]. The efficient supercapacitive properties of the material have been attributed to the core-shell structure of TiO_2 and MnO_2 [75]. Hierarchical TiO_2 nanobelts on MnO_2 were synthesized by a facile hydrothermal approach with a resulting specific capacitance of 518 F g^{-1} [76]. A recent study explored the effect of hydrothermal synthesis time on the resulting morphology of MnO_2 nanostructures and compared EC properties of $\alpha\text{-MnO}_2$ and $\alpha\text{-MnO}_2/\text{activated carbon (AC)}$ nanocomposites. The largest specific capacitance value for the MnO_2 in K_2SO_4 electrolyte was 629.2 C g^{-1} , which was increased to 977.4 C g^{-1} (up by 55%) upon AC incorporation. The capacity retention was also higher (81.3 vs 53.2%) after 3000 cycles at 0.2 A g^{-1} due to larger carrier concentration and low charge transfer resistance [77].

A MnO_x/CNT nanocomposite electrode having $\sim 65 \text{ wt.}\%$ MnO_2 recorded a specific capacitance of 144 F g^{-1} and capacitance retention for the device to be 91% after 9000 cycles. The SEM microstructure of the MnO_x/CNT nanocomposite and the CVs recording after a certain

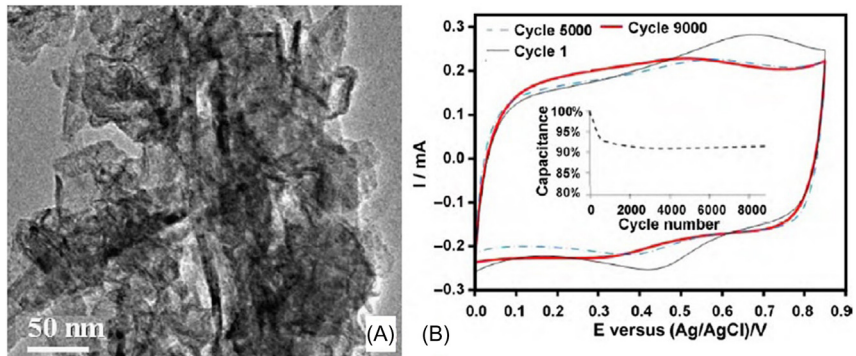


Figure 8.4 (A) TEM microstructure of 80 wt.% MnO_x/CNT , and (B) CV curves of the 60 wt.% MnO_x/CNTs after continuous potential cycling for 1000, 5000, and 9000 cycles. The inset shows capacitance loss after 8000 cycles [78].

number of cycles during continuous potential cycling are shown in Fig. 8.4. The device experienced a rapid decrease in the potential range of 0.0–0.85 V, possibly due to morphological changes in the MnO_x during the first 200 charging–discharging cycles and associated absorption–desorption of the H^+ and/or K^+ counterions [78].

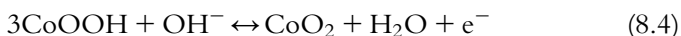
8.3.6 Cobalt oxide (Co_3O_4)

Although different oxides of cobalt such as Co_3O_4 , CuCo_2O_4 , FeCo_2O_4 , and NiCo_2O_4 have been explored for supercapatteries, these cobalt-based composites yield lower than theoretical specific capacitance value. It is believed that the specific capacitance can be enhanced through the development of some appropriate cobalt-based material structure. Co_3O_4 possesses a cubic spinel crystal structure and is a p-type semiconductor at low temperature. It has a direct band gap (2.10 eV) as well as an indirect band gap (1.6 eV). The cobalt ions in Co_3O_4 exist in two oxidation states Co^{2+} and Co^{3+} that are located at the interstitial tetrahedral and octahedral sites of the closed packed f.c.c. structure formed by the O^{2-} , respectively. In the Co_3O_4 structure, Co^{2+} and Co^{3+} ions are distributed on the tetrahedral and octahedral sites, respectively, with a high surface-to-volume ratio and significant catalytic activity. The tendency of Co_3O_4 nanocrystals, however, leads to a reduction in the density of active sites with subsequent fast capacity fading and structural distortion during cyclic charging [79,80]. Also, low scan rate, high resistivity, low charge transfer kinetics, toxicity, and low charge

ionic conductivity of Co_3O_4 are the main obstacles toward the use of Co_3O_4 in practical applications [81].

8.3.6.1 Cobalt oxide-based nanocomposites

The addition of graphene or multiwalled CNT into Co_3O_4 nanostructures inhibits the tendency of Co_3O_4 nanocrystals to agglomerate as well as causing an increase in the active sites for the redox reactions, thus aiding faradaic reactions through a rapid charge transfer at the graphene/CNT walls and edges. The excellent electronic conductivity of the Ag nanoparticles, on the other hand, enables rapid electron transfer during the redox process through extended channels. CV studies of the nano-grain Co_3O_4 displayed asymmetric shoulder redox peaks owing to multiple Co_3O_4 phases and redox transitions to different oxidation states including Co(II), Co(III), and Co(IV) due to faradaic behavior. The composite Co_3O_4 , therefore, exhibits typical battery-type behavior in which electrolyte dispersion in the material gives rise to redox peaks. In a 1 M KOH alkaline solution, two sequential steps represent the oxidation reduction process, as given by the following equations:



The SEM microstructure depicting homogeneous dispersion of Ag and Co_3O_4 nanoparticles along with CNT, the supercapattery device configuration, and the cyclic stability up to 3000 cycles are presented in Fig. 8.5. The specific capacity value increased during the first 250 cycles exhibiting gradual activation of the nanocomposite surface, followed by a drop by 6.9%. The maximum specific capacity values for Co_3O_4 nano-grains and CNT- Co_3O_4 -Ag nanocomposite were 39.24 and 83.88 C g^{-1} , respectively, demonstrating excellent synergistic effects of Ag nanoparticles and CNT [82].

Using nickel foam, carbonate hydroxide $\text{Co}_2(\text{CO}_3)(\text{OH})_2$ with nano-flakes or polyhedron flowers morphology, depending on the use of water or ethanol as solvent, were produced from hydrothermal synthesis at 120°C for 4 hours. As shown in Fig. 8.6a, the vertically aligned, mutually interconnected nanoflakes with high surface area offered easy access to the electrolyte ions. The polyhedron flowers, presented in Fig. 8.6b, were found to have an average particle size of 0.3–1.13 μm . The cyclic voltammogram (CV) curves, obtained at 5 mVs^{-1} scan rate, revealed greater

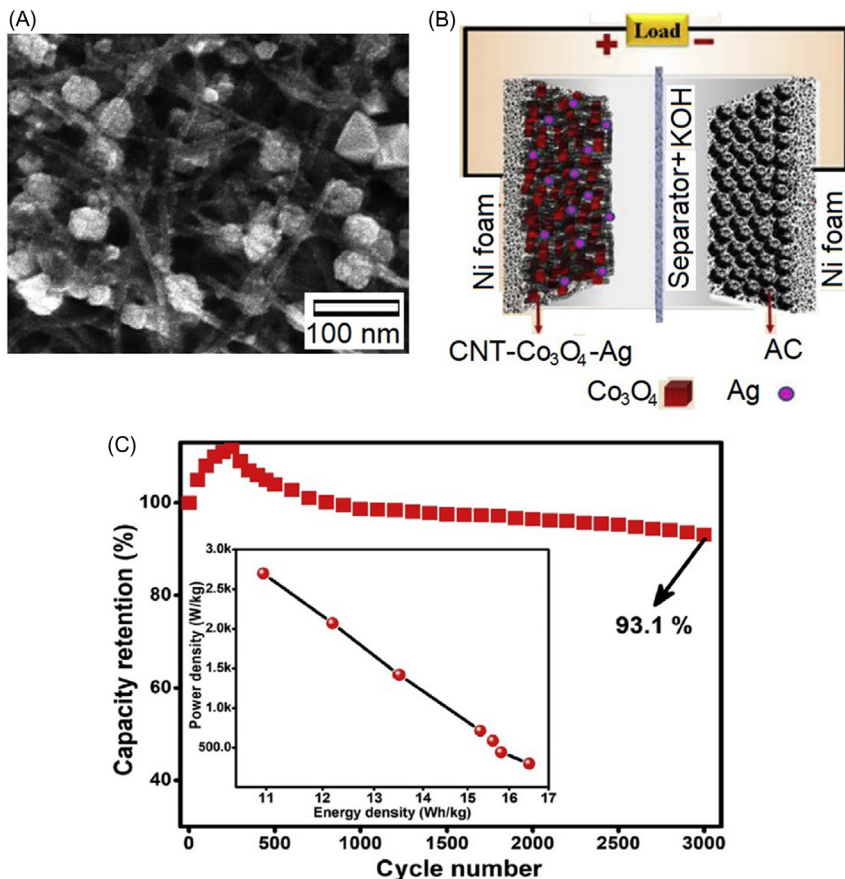


Figure 8.5 (A) SEM microstructure of the CNT-Co₃O₄-Ag nanocomposite; (B) AC//CNT-Co₃O₄-Ag supercapattery device configuration; and (C) charging/discharging cyclic stability with inset showing power density as a function of energy density [82].

charge storage capability and better electrochemical utilization of the nanoflakes when compared with the Co₂(CO₃)(OH)₂ polyhedron flowers. Also, both capacitive and battery-type mechanisms were noticed from the two potential-independent and -dependent current regions. The supercapattery offered a long cycle life with specific capacitance retention of 85% over 4000 cycles, along with greater values of specific capacitance (91 F g⁻¹) and energy density (26.22 Wh kg⁻¹ at power density 828 W kg⁻¹) [83].

Another supercapattery device based on spinel cobalt oxide (Co₃O₄) and reduced graphene oxide (rGO) as positive and negative electrodes,

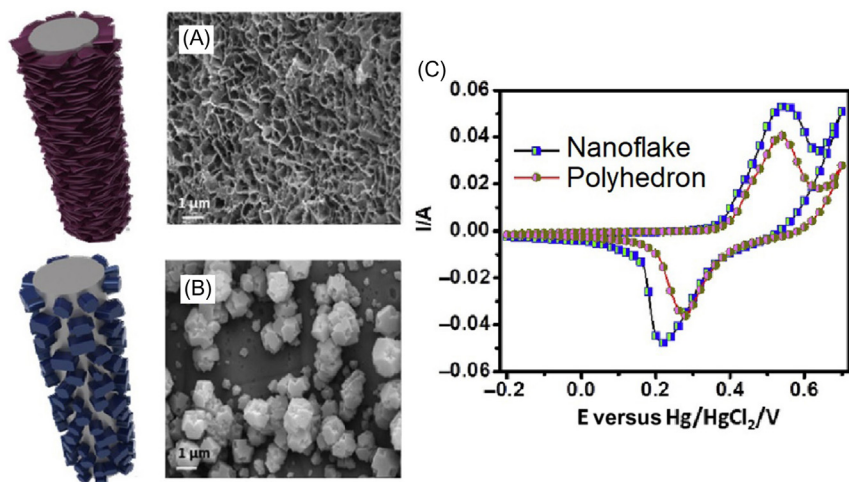


Figure 8.6 (A, B) Schematic illustration and FE-SEM microstructures of the $\text{Co}_2(\text{CO}_3)(\text{OH})_2$ nanoflakes and polyhedron flowers and (C) CV curves at 5 mVs^{-1} [83].

respectively, delivered high energy density and coulombic efficiency [84]. The mechanical stability and charge transport to the metal current collector was further enhanced through Co_3O_4 nanoflakes deposition, via ammonia evaporation and thermal treatment, over rGO wrapped nickel foam. The supercapattery exhibited high specific capacitance of 80 F g^{-1} and stability. In this case, the ion diffusion during the charging/discharging process is facilitated by the 3D open structure, thus resulting in a very high specific capacity [85].

8.3.6.2 Cobalt oxide-based mixed oxides

The inherent issues related to the use of cobalt oxide may be addressed by employing binary metal oxides for higher electrical conductivity and more rapid redox reactions. One such material composite may be bimetallic Cu-Co oxide (CuCo_2O_4) that has shown improved electrochemical performance and excellent activity in hybrid supercapacitors. Recently, double-shell CuCo_2O_4 hollow spheres were produced via a self-templated method using metal-organic frameworks (MOFs). The phase pure composite CuCo_2O_4 formation was confirmed from X-ray diffraction and X-ray photoelectron spectroscopy analyses, whereas both BET and BJH methods indicated a reasonably high surface area of $93 \text{ m}^2 \text{ g}^{-1}$ and porosity. When used as an electrode, an ultrahigh specific capacitance

of 701 C g^{-1} was recorded at 2 A g^{-1} with capacitance retention of $>93.6\%$ after 6000 charge/discharge cycles [55].

In yet another innovative approach, a binary transition metal oxide of the composite MnCo_2O_4 and holey 2D nanosheets configuration was synthesized using graphene oxide as a sacrificial template. Electrochemical testing of the pouch-like supercapattery employing MnCo_2O_4 nanosheets and AC as positive and negative electrodes, respectively, delivered improved performance due to higher surface area of $132 \text{ m}^2 \text{ g}^{-1}$ and nanosize holes. The electrode material displayed a specific capacity of 774 mAh g^{-1} at 1 A g^{-1} , a maximum specific energy of 33.8 Wh kg^{-1} at 318.9 W kg^{-1} , and capacity retention of 84.8% after 10,000 cycles [86].

The synthesis of binary metal oxides of cobalt with other metals has therefore enabled an increase in the electrochemical properties of Co_3O_4 . The synergistic effect of two metals enhances the performance of the supercapacitor as compared to the unitary metal oxide [87]. Chang et al. [88] produced NiCo_2O_4 electrode composites for supercapacitors applications. On the other hand, ultralayered, mesoporous nickel cobaltite nanosheets (NiCo_2O_4) were prepared without using any template and exhibited $>80\%$ capacitance retention after 5000 charge–discharge cycles [89]. A hierarchical array of $\text{Co}_3\text{O}_4@ \text{NiCo}_2\text{O}_4$ nanowires, when used as electrode material, displayed high aerial capacitance of 2.04 F cm^{-2} at 5 mV s^{-1} and 83.7% capacitance retention after 1500 cycles [90]. ZnCo_2O_4 with nanoflowers morphology were obtained over nickel foam and produced a specific capacitance of 684.9 Fg^{-1} at 1 A g^{-1} with capacitance loss of 4.38% only after 3000 cycles [91].



8.4 Hybridization of metal oxides

The limitations of the metal oxides may be overcome by integrating them with other composites in a physical or chemical manner. This approach can yield mixed oxides, heterostructures, or nanocomposites with superior electrochemical properties of the resulting electrode material due to synergistic effect of the constituent phases. For example, the advantages of low cost, abundance, and high theoretical capacity exhibited by MnO_2 were combined with good conductivity and specific capacity, catalytic activity, and more electrochemical active sites offered by CoS

nanosheets were explored by coating CoS on the MnO_{2-x} arrays in a core/shell configuration. The composite electrode displayed a high specific capacitance of 781.1 C g^{-1} at 2 mA cm^{-2} . The supercapattery device made by using $\text{MnO}_{2-x}@\text{CoS}$ and nitrogen–oxygen codoped porous carbon (NOPC) as positive and negative electrodes, respectively, exhibited high values of energy density (34.72 Wh kg^{-1}) and power density (597.24 W kg^{-1}) besides excellent capacitance retention of 89.6% after 9000 cycles [92].

As compared to ternary transition metal hydroxides, a stable ternary composite NiCo-MnO_2 , produced via a simple wet chemical precipitation method followed by annealing, exhibited better cyclic stability. When investigated as an electrode in a hybrid asymmetric supercapattery, the device revealed specific capacitance, energy density, and power density values of 130.67 F g^{-1} , 48.83 Wh kg^{-1} , and 896.88 W kg^{-1} at 1 A g^{-1} , respectively. The device also showed excellent capacitance retention of 96.78% after 10,000 cycles [93]. In yet another study, amorphous nickel–cobalt–manganese hydride (NiCoMn-OH) was made using a mixed solvent strategy during hydrothermal synthesis. When used as a positive electrode against rGO as a negative electrode, the assembled supercapattery yielded a specific energy of 19.9 Wh kg^{-1} at 20.9 kW kg^{-1} specific power, demonstrating potential for utilization as an electroactive material [94]. A novel nanocomposite comprising Ru-RuO₂ nanoparticles and activated carbon (Ru-RuO₂/AC) with a large surface area indicated a high specific capacitance of 1460 F g^{-1} at 10 A g^{-1} and an excellent charging/discharging rate capability in terms of 94% capacitance retention after 10,000 cycles at 50 A g^{-1} [95]. An integrated composite of RuO₂ and electrochemically reduced graphene exhibited a high energy density of 43.8 Wh kg^{-1} at 0.75 kW kg^{-1} and 92.8% retention of initial specific capacitance value after 10,000 cycles [96].

The electrochemical performance of supercapatteries incorporating certain metal oxide-based electrode materials have been showcased in Table 8.1. In the case of asymmetric supercapatteries, the negative electrodes are the carbon-based materials such as CNT, graphene, and AC. It is interesting to note that diverse solution processing routes as well as nano-scale morphologies were explored. The key performance attributes including specific capacitance, energy and power densities, and cyclic stability in terms of capacitance retention after a certain number of charge/discharge cycles are given in Table 8.1.

Table 8.1 The metal oxide-based electrode composites used as positive electrodes in supercapatteries and their electrochemical properties.

Supercapattery configuration	Electrode synthesis; morphology	C_s (F g ⁻¹)	E_d (Wh kg ⁻¹)	P_d (W kg ⁻¹)	C_R (%)	N	References
rGO//CuCo ₂ O ₄	Self-template chemical; hollow spheres	701 C g ⁻¹	38.4 Wh kg ⁻¹ , 16 kW kg ⁻¹		93.6	6000	[55]
AC//Co ₂ (CO ₃)(OH) ₂	Hydrothermal; nanoflakes	91 F g ⁻¹	26.2 Wh kg ⁻¹ at 828 W kg ⁻¹		85	4000	[83]
AC//Co ₃ O ₄ -rGO/NF	NH ₃ evaporation + thermal treatment; nanoflakes	80 F g ⁻¹	20 Wh kg ⁻¹ at 1200 Wkg ⁻¹		94.5	10,000	[85]
AC//MnCo ₂ O ₄	Polyol process; holey 2D nanosheets		34 Wh kg ⁻¹ at 319 Wkg ⁻¹		85	10,000	[86]
CNT-Co ₃ O ₄ -Ag	Hydrothermal; nanoparticles, nanotubes		16.5 Wh kg ⁻¹ at 297 W kg ⁻¹		93.6	3000	[82]
AC//CMO-aH	Coprecipitate; anhydrous, mesoporous CoMoO ₄	177 C g ⁻¹	18.9 Wh kg ⁻¹ at 1060 W kg ⁻¹		93	5000	[97]
RuO ₂ -GNS//RuO ₂ -GNS	Electrodeposition; ultrafine nanoparticles	480 F g ⁻¹	30.9 Wh kg ⁻¹ at 14000 W kg ⁻¹		92.7	10,000	[98]
C-FP//Ti ₃ C ₂ -Mn ₃ O ₄	Solvothermal process; Ti ₃ C ₂ -Mn ₃ O ₄ nanocomposite		28.3 Wh kg ⁻¹ at 463.4Wkg ⁻¹		92.6	10,000	[99]
rGO//Co ₃ O ₄	Sol-gel; nanoparticles		40 Wh kg ⁻¹ at 742 W kg ⁻¹				[84]

C_s , Specific capacitance (F g⁻¹); E_d , energy density (Wh kg⁻¹); P_d , power density (W kg⁻¹); C_R , capacitance retention (%); No. charge/discharge cycles (N); C-FP, iron cations on PANI film.



8.5 Summary

Continuous efforts are being made to develop supercapatteries with reasonably high levels of energy and power densities and device stability. The positive electrode of such energy storage device exhibits pseudocapacitive behavior through surface redox reactions for capacitive faradaic storage. The performance of the device depends on the cations present in the electrode as well as their chemistry matching with electrolyte reactions.

Metal oxides are an important contender for application as electrode materials in supercapatteries. While material composites including ruthenium oxide (RuO_2), cobalt oxide (Co_3O_4), and manganese oxide (MnO_x) offer strong potential, issues related to cost, availability, and toxicity limit their scope for commercial viability. There are several factors that are sought for faster surface redox reactions, including (1) greater electroactive surface area; (2) favorable surface composition, chemistry, and defect density; (3) hydrous or anhydrous state; (4) chemical toxicity or environmental issues; and (5) the desire to scale up retaining superior device performance and stability, that catalyze further development of this technology. The global research community has therefore been prompted to employ novel approaches toward the development of electrode compositions. Some of these are (1) doping/codoping and/or binary or ternary oxides; (2) tuning and investigating different nanoscale morphologies; (3) hybridization with other nanostructures to produce, e.g., core/shell heterostructures; and (4) nanocomposites fabrication.

References

- [1] L. Yu, G.Z. Chen, Ionic liquid-based electrolytes for supercapacitor and supercapattery, *Front. Chem.* 7 (2019) 272 (8 pages).
- [2] A.J. Stevenson, D.G. Gromadskyi, D. Hu, J. Chae, L. Guan, L. Yu, et al., Supercapatteries with hybrids of redox active polymers and nanostructured carbons, *Nanocarbons for Advanced Energy Storage*, Wiley-VCH Verlag GmbH & Co. KGaA, 2015, pp. 179–210.
- [3] C. Klumpner, G. Asher, G.Z. Chen, *Selecting the Power Electronic Interface for a Supercapattery Based Energy Storage System*, IEEE, New York, 2009.
- [4] G.Z. Chen, Supercapacitor and supercapattery as emerging electrochemical energy stores, *Int. Mater. Rev.* 62 (4) (2017) 173–202.
- [5] S. Trasatti, G. Buzzanca, Ruthenium dioxide: a new interesting electrode material. Solid state structure and electrochemical behavior, *J. Electroanal. Chem. Int. Electrochem.* 29 (1971) A1–A5.

- [6] S.H. Glarum, J.H. Marshall, The in situ ESR and electrochemical behavior of poly (aniline) electrode films, *J. Electrochem. Soc.* 134 (1987) 2160–2165.
- [7] E.M. Genies, C. Tsintavis, Redoxmechanism and electrochemical behaviour of polyaniline deposits, *J. Electroanal. Chem. Int. Electrochem.* 195 (1985) 109–128.
- [8] A. Rudge, J. Davey, I. Raistrick, Conducting polymers as active materials in electrochemical capacitors, *J. Power Sources* 47 (1994) 89–107.
- [9] L. Yu, G.Z. Chen, Redox electrode materials for supercapacities, *J. Power Sources* 326 (2016) 604–612.
- [10] V. Augustyn, P. Simon, B. Dunn, Pseudocapacitive oxide materials for high-rate electrochemical energy storage, *Energy Environ. Sci.* 7 (2014) 1597–1614.
- [11] T. Brousse, D. Belanger, J.W. Long, To be or not to be pseudocapacitive? *J. Electrochem. Soc.* 162 (2015) A5185–A5189.
- [12] G.P. Wang, L. Zhang, J.J. Zhang, A review of electrode materials for electrochemical supercapacitors, *Chem. Soc. Rev.* 41 (2012) 797–828.
- [13] P. Simon, Y. Gogotsi, Materials for electrochemical capacitors, *Nat. Mater.* 7 (2008) 845–854.
- [14] M.M. Alsaif, et al., High-performance field effect transistors using electronic inks of 2D molybdenum oxide nanoflakes, *Adv. Funct. Mater.* 26 (2016) 91–100.
- [15] K. Khan, A.K. Tareen, M. Aslam, A. Mahmood, Q. Khan, Y. Zhang, et al., Going green with batteries and supercapacitor: two dimensional materials and their nanocomposites based energy storage applications, *Prog. Solid. State Chem* 58 (2020), 100254.
- [16] J. Chae, K.C. Ng, G.Z. Chen, Nanostructured materials for the construction of asymmetrical supercapacitors, *Proc. Inst. Mech. Eng. Part. A J. Power Energy* 224 (2010) 479–503.
- [17] J. Chae, G.Z. Chen, 1.9 V aqueous carbon–carbon supercapacitors with unequal electrode capacitances, *Electrochim. Acta* 86 (2012) 248–254.
- [18] H. Xia, D. Zhu, Z. Luo, Y. Yu, X. Shi, G. Yuan, et al., Hierarchically structured $\text{Co}_3\text{O}_4/\text{Pt}/\text{MnO}_2$ nanowire arrays for high-performance supercapacitors, *Sci. Rep.* 3 (2013) 2978.
- [19] C.-C. Hu, K.-H. Chang, M.-C. Lin, Y.-T. Wu, Design and tailoring of the nanotubular arrayed architecture of hydrous RuO_2 for next generation supercapacitors, *Nano Lett.* 6 (2006) 2690–2695.
- [20] W.-G. Lee, H.S. Jang, C. Justin Raj, M. Rajesh, B.C. Kim, W.-J. Cho, et al., Effect of proton irradiation on the structural and electrochemical properties of MnO_2 nanosheets, *J. Electroanal. Chem.* 811 (2018) 16–25.
- [21] J. Huang, J. Zhu, K. Cheng, Y. Xu, D. Cao, G. Wang, Preparation of Co_3O_4 nanowires grown on nickel foam with superior electrochemical capacitance, *Electrochim. Acta* 75 (2012) 273–278.
- [22] S. Vijayakumar, S. Nagamuthu, G. Muralidharan, Supercapacitor studies on NiO nanoflakes synthesized through a microwave route, *ACS Appl. Mater. Interfaces* 5 (2013) 2188–2196.
- [23] R. Manikandan, C. Justin Raj, M. Rajesh, B.C. Kim, G. Nagaraju, W.-G. Lee, et al., Rationally designed spider web-like trivanadium heptaoxide nanowires on carbon cloth as a new class of pseudocapacitive electrode for symmetric supercapacitors with high energy density and ultra-long cyclic stability, *J. Mater. Chem. A* 6 (2018) 11390–11404.
- [24] Y.-T. Wang, A.-H. Lu, H.-L. Zhang, W.-C. Li, Synthesis of nanostructured mesoporous manganese oxides with three-dimensional frameworks and their application in supercapacitors, *J. Phys. Chem. C.* 115 (2011) 5413–5421.
- [25] M. Zhi, C. Xiang, J. Li, M. Li, N. Wu, Nanostructured carbon-metal oxide composite electrodes for supercapacitors: a review, *Nanoscale* 5 (2013) 72–88.

- [26] Y. Bai, M. Du, J. Chang, J. Sun, L. Gao, Supercapacitors with high capacitance based on reduced graphene oxide/carbon nanotubes/NiO composite electrodes, *J. Mater. Chem. A* 2 (2014) 3834–3840.
- [27] O.A. Vargas, A. Caballero, L. Hernan, J. Morales, Improved capacitive properties of layered manganese dioxide grown as nanowires, *J. Power Sources* 196 (2011) 3350–3354.
- [28] W. Hong, J. Wang, P. Gong, J. Sun, L. Niu, Z. Yang, et al., Rational construction of three dimensional hybrid $\text{Co}_3\text{O}_4/\text{NiMoO}_4$ nanosheets array for energy storage application, *J. Power Sources* 270 (2014) 516–525.
- [29] Z. Sun, S. Firdoz, E.Y. Yap, L. Li, X. Lu, Hierarchically structured MnO_2 nanowires supported on hollow Ni dendrites for high-performance supercapacitors, *Nanoscale* 5 (10) (2013) 4379–4387.
- [30] C.-Y. Cao, W. Guo, Z.-M. Cui, W.-G. Song, W. Cai, Microwave-assisted gas/liquid interfacial synthesis of flowerlike NiO hollow nanosphere precursors and their application as supercapacitor electrodes, *J. Mater. Chem.* 21 (9) (2011).
- [31] H. Pang, Y. Shi, J. Du, Y. Ma, G. Li, J. Chen, et al., Porous nickel oxide microflowers synthesized by calcination of coordination microflowers and their applications as glutathione electrochemical sensor and supercapacitors, *Electrochim. Acta* 85 (2012) 256–262.
- [32] M. Khairy, S.A. El-Safy, Mesoporous NiO nanoarchitectures for electrochemical energy storage: influence of size, porosity, and morphology, *RSC Adv.* 3 (45) (2013).
- [33] X. Yan, X. Tong, J. Wang, C. Gong, M. Zhang, L. Liang, Synthesis of mesoporous NiO nanoflake array and its enhanced electrochemical performance for supercapacitor application, *J. Alloy. Compounds* 593 (2014) 184–189.
- [34] M. Yao, Z. Hu, Z. Xu, Y. Liu, P. Liu, Q. Zhang, Template synthesis and characterization of nanostructured hierarchical mesoporous ribbon-like NiO as high performance electrode material for supercapacitor, *Electrochim. Acta* 158 (2015) 96–104.
- [35] M. Kundu, L. Liu, Binder-free electrodes consisting of porous NiO nanofibers directly electrospun on nickel foam for high-rate supercapacitors, *Mater. Lett.* 144 (2015) 114–118.
- [36] A. Liu, H. Che, Y. Mao, Y. Wang, J. Mu, C. Wu, et al., Template-free synthesis of one-dimensional hierarchical NiO nanotubes self-assembled by nanosheets for high-performance supercapacitors, *Ceram. Int.* 42 (9) (2016) 11435–11441.
- [37] J. Azevedo, L. Steier, P. Dias, M. Stefik, C.T. Sousa, J.P. Araújo, et al., On the stability enhancement of cuprous oxide water splitting photocathodes by low temperature steam annealing, *Energy Environ. Sci.* 7 (12) (2014) 4044–4052.
- [38] S. Gao, Y. Sun, F. Lei, J. Liu, L. Liang, T. Li, et al., Freestanding atomically-thin cuprous oxide sheets for improved visible-light photoelectrochemical water splitting, *Nano Energy* 8 (2014) 205–213.
- [39] Y.S. Lee, D. Chua, R.E. Brandt, S.C. Siah, J.V. Li, J.P. Mailoa, et al., Atomic layer deposited gallium oxide buffer layer enables 1.2 V open-circuit voltage in cuprous oxide solar cells, *Adv. Mater.* 26 (27) (2014) 4704–4710.
- [40] S. Masudy-Panah, K. Radhakrishnan, H.R. Tan, R. Yi, T.I. Wong, G.K. Dalapati, Titanium doped cupric oxide for photovoltaic application, *Sol. Energy Mater. Sol. Cell* 140 (2015) 266–274.
- [41] C.G. Morales-Guio, S.D. Tilley, H. Vrubel, M. Gratzel, X. Hu, Hydrogen evolution from a copper(I) oxide photocathode coated with an amorphous molybdenum sulfide catalyst, *Nat. Commun.* 5 (2014) 3059.
- [42] L. Zhu, M. Hong, G.W. Ho, Fabrication of wheat grain textured TiO_2/CuO composite nanofibers for enhanced solar H_2 generation and degradation performance, *Nano Energy* 11 (2015) 28–37.

- [43] J. Wang, W.-D. Zhang, Fabrication of CuO nanoplatelets for highly sensitive enzyme-free determination of glucose, *Electrochim. Acta* 56 (22) (2011) 7510–7516.
- [44] W. Zhang, H. Wang, Y. Zhang, Z. Yang, Q. Wang, J. Xia, et al., Facile microemulsion synthesis of porous CuO nanosphere film and its application in lithium ion batteries, *Electrochim. Acta* 113 (2013) 63–68.
- [45] Y. Ma, H. Wang, J. Key, S. Ji, W. Lv, R. Wang, Control of CuO nanocrystal morphology from ultrathin “willow-leaf” to “flower-shaped” for increased hydrazine oxidation activity, *J. Power Sources* 300 (2015) 344–350.
- [46] H. Li, S. Yu, X. Han, Fabrication of CuO hierarchical flower-like structures with biomimetic superamphiphobic, self-cleaning and corrosion resistance properties, *Chem. Eng. J.* 283 (2016) 1443–1454.
- [47] M.-J. Deng, C.-C. Wang, P.-J. Ho, C.-M. Lin, J.-M. Chen, K.-T. Lu, Facile electrochemical synthesis of 3D nano-architected CuO electrodes for high-performance supercapacitors, *J. Mater. Chem. A* 2 (32) (2014) 12857–12865.
- [48] G. Wang, J. Huang, S. Chen, Y. Gao, D. Cao, Preparation and supercapacitance of CuO nanosheet arrays grown on nickel foam, *J. Power Sources* 196 (13) (2011) 5756–5760.
- [49] A.C. Nwanya, D. Obi, K.I. Ozoemena, R.U. Osuji, C. Awada, A. Ruediger, et al., Facile synthesis of nanosheet-like CuO film and its potential application as a high-performance pseudocapacitor electrode, *Electrochim. Acta* 198 (2016) 220–230.
- [50] B. Heng, C. Qing, D. Sun, B. Wang, H. Wang, Y. Tang, Rapid synthesis of CuO nanoribbons and nanoflowers from the same reaction system, and a comparison of their supercapacitor performance, *RSC Adv.* 3 (36) (2013).
- [51] D.P. Dubal, G.S. Gungor, R. Holze, C.D. Lokhande, Mild chemical strategy to grow micro-roses and micro-woolen like arranged CuO nanosheets for high performance supercapacitors, *J. Power Sources* 242 (2013) 687–698.
- [52] Y. Li, X. Wang, Q. Yang, M.S. Javed, Q. Liu, W. Xu, et al., Ultra-fine CuO nanoparticles embedded in three-dimensional graphene network nano-structure for high-performance flexible supercapacitors, *Electrochim. Acta* 234 (2017) 63–70.
- [53] G. Manibalan, G. Murugadoss, R. Thangamuthu, P. Ragupathy, R. Mohan Kumar, R. Jayavel, Enhanced electrochemical supercapacitor and excellent amperometric sensor performance of heterostructure CeO₂-CuO nanocomposites via chemical route, *Appl. Surf. Sci.* 456 (2018) 104–113.
- [54] M. Sheikhzadeh, S. Sanjabi, M. Gorji, S. Khabazian, Nano composite foam layer of CuO/graphene oxide (GO) for high performance supercapacitor, *Synth. Met.* 244 (2018) 10–14.
- [55] F. Saleki, A. Mohammadi, S.E. Moosavifard, A. Hafizi, M.R. Rahimpour, MOF assistance synthesis of nanoporous double-shelled CuCo₂O₄ hollow spheres for hybrid supercapacitors, *J. Colloid Interface Sci.* 556 (2019) 83–91.
- [56] S. Ramesh, A. Kathalingam, K. Karuppasamy, H.-S. Kim, H.S. Kim, Nanostructured CuO/Co₂O₄@ nitrogen doped MWCNT hybrid composite electrode for high-performance supercapacitors, *Compos. Part. B: Eng.* 166 (2019) 74–85.
- [57] H.Y. Lee, J.B. Goodenough, Ideal supercapacitor behavior of amorphous V₂O₅ · nH₂O in potassium chloride (KCl) aqueous solution, *J. Solid. State Chem.* 148 (1) (1999) 81–84.
- [58] I.-H. Kim, J.-H. Kim, B.-W. Cho, Y.-H. Lee, K.-B. Kim, Synthesis and electrochemical characterization of vanadium oxide on carbon nanotube film substrate for pseudocapacitor applications, *J. Electrochem. Soc.* 153 (6) (2006).
- [59] H.-S. Park, K.-D. Jung, O.-S. Joo, Performance of supercapacitor with electrodeposited ruthenium oxide film electrodes—effect of film thickness, *J. Power Sources* 134 (1) (2004) 148–152.
- [60] B.-O. Park, C.D. Lokhande, Chemical synthesis of nano-porous ruthenium oxide (RuO₂) thin films for supercapacitor application, *Appl. Surf. Sci.* 254 (2008) 2820–2824.

- [61] M. Toupin, T. Brousse, D. Bélanger, Charge storage mechanism of MnO_2 electrode used in aqueous electrochemical capacitor, *Chem. Mater.* 16 (2004) 3184–3190.
- [62] T. Brousse, M. Toupin, R. Dugas, L. Athouël, O. Crosnier, D. Bélanger, Crystalline MnO_2 as possible alternatives to amorphous compounds in electrochemical supercapacitors, *J. Electrochem. Soc.* 153 (2006) A2171–A2180.
- [63] O. Ghodbane, J.-L. Pascal, B. Fraisse, F. Favier, Structural in situ study of the thermal behavior of manganese dioxide materials: toward selected electrode materials for supercapacitors, *ACS Appl. Mater. Interfaces* 2 (2010) 3493–3505.
- [64] Y. Sun, N. Huang, X. Sun, D. Wang, J. Zhang, S. Qiao, et al., An improvement on capacitive properties of clew-like MnO_2 by thermal treatment under nitrogen, *Int. J. Hydrog. Energy* 42 (2017) 20016–20025.
- [65] Z. Ye, T. Li, G. Ma, X. Peng, J. Zhao, Morphology controlled MnO_2 electrodeposited on carbon fiber paper for high-performance supercapacitors, *J. Power Sources* 351 (2017) 51–57.
- [66] H. Xia, W. Xiao, M.O. Lai, L. Lu, Improved capacitive behaviour of MnO_2 thin film prepared by electrodeposition on Pt substrate with a MnO_x buffer, *Funct. Mater. Lett.* 2 (2009) 13–18.
- [67] Y.-L. Chan, S.-Y. Pung, S. Sreekantan, F.-Y. Yeoh, Photocatalytic activity of β - MnO_2 nanotubes grown on PET fibre under visible light irradiation, *J. Exp. Nanosci.* 11 (2016) 603–618.
- [68] Z. Ai, L. Zhang, F. Kong, H. Liu, W. Xing, J. Qiu, Microwave assisted green synthesis of MnO_2 nanoplates with environmental catalytic activity, *Mater. Chem. Phys.* 111 (2008) 162–167.
- [69] A. Baral, D.P. Das, M. Minakshi, M.K. Ghosh, D.K. Padhi, Probing environmental remediation of RhB organic dye using α - MnO_2 under visible-light irradiation: structural, photocatalytic and mineralization studies, *Chem. Sel.* 1 (2016) 4277–4285.
- [70] B. Yin, S. Zhang, H. Jiang, F. Qu, X. Wu, Phase-controlled synthesis of polymorphic MnO_2 structures for electrochemical energy storage, *J. Mater. Chem. A* 3 (2015) 5722–5729.
- [71] D.A. Tompsett, S.C. Parker, M. Saiful Islam, Surface properties of α - MnO_2 : relevance to catalytic and supercapacitor behaviour, *J. Mater. Chem. A* 2 (2014) 15509–15518.
- [72] T. Zhai, S. Xie, M. Yu, P. Fang, C. Liang, X. Lu, et al., Oxygen vacancies enhancing capacitive properties of MnO_2 nanorods for wearable asymmetric supercapacitors, *Nano Energy* 8 (2014) 255–263.
- [73] P. Gao, P. Metz, T. Hey, Y. Gong, D. Liu, D.D. Edwards, et al., The critical role of point defects in improving the specific capacitance of δ - MnO_2 nanosheets, *Nat. Commun.* 8 (2017) 14559–14569.
- [74] D. Sarkar, G.G. Khan, A.K. Singh, K. Mandal, High-performance pseudocapacitor electrodes based on α - $\text{Fe}_2\text{O}_3/\text{MnO}_2$ core-shell nanowire heterostructure arrays, *J. Phys. Chem. C*. 117 (30) (2013) 15523–15531.
- [75] X. Lu, M. Yu, G. Wang, T. Zhai, S. Xie, Y. Ling, et al., H-TiO₂@MnO₂//H-TiO₂@C core-shell nanowires for high performance and flexible asymmetric supercapacitors, *Adv. Mater.* 25 (2) (2013) 267–272.
- [76] Y. Luo, D. Kong, J. Luo, S. Chen, D. Zhang, K. Qiu, et al., Hierarchical TiO₂ nanobelts@MnO₂ ultrathin nanoflakes core-shell array electrode materials for supercapacitors, *RSC Adv.* 3 (34) (2013).
- [77] H. Shen, Y. Zhang, X. Song, Y. Liu, H. Wang, H. Duan, et al., Facile hydrothermal synthesis of actinaria-shaped α - MnO_2 /activated carbon and its electrochemical performances of supercapacitor, *J. Alloys. Compd.* 770 (2019) 926–933.
- [78] S.W. Zhang, C. Peng, K.C. Ng, G.Z. Chen, Nanocomposites of manganese oxides and carbon nanotubes for aqueous supercapacitor stacks, *Electrochim. Acta* 55 (2010) 7447–7453.

- [79] X. Wang, M. Li, Z. Chang, Y. Yang, Y. Wu, X. Liu, $\text{Co}_3\text{O}_4@$ MWCNT nanocable as cathode with superior electrochemical performance for supercapacitors, *ACS Appl. Mater. Interfaces* 7 (2015) 2280–2285.
- [80] Z. Fang, W. Xu, T. Huang, M. Li, W. Wang, Y. Liu, et al., Facile scalable synthesis of Co_3O_4 /carbon nanotube hybrids as superior anode materials for lithium-ion batteries, *Mater. Res. Bull.* 48 (2013) 4419–4423.
- [81] H.-J. Qiu, L. Liu, Y.-P. Mu, H.-J. Zhang, Y. Wang, Designed synthesis of cobalt-oxide-based nanomaterials for superior electrochemical energy storage devices, *Nano Res.* 8 (2) (2015) 321–339.
- [82] J. Iqbal, A. Numan, S. Rafique, R. Jafer, S. Mohamad, K. Ramesh, et al., High performance supercapattery incorporating ternary nanocomposite of multiwalled carbon nanotubes decorated with Co_3O_4 nanograins and silver nanoparticles as electrode material, *Electrochim. Acta* 278 (2018) 72–82.
- [83] K.V. Sankar, Y. Seo, S.C. Lee, S. Liu, A. Kundu, C. Ray, et al., Cobalt carbonate hydroxides as advanced battery-type materials for supercapacities: influence of morphology on performance, *Electrochim. Acta* 259 (2018) 1037–1044.
- [84] V.S. Devi, M. Athika, E. Duraisamy, A. Prasath, A.S. Sharma, P. Elumalai, Facile sol-gel derived nanostructured spinel Co_3O_4 as electrode material for high-performance supercapattery and lithium-ion storage, *J. Energy Storage* 25 (2019) 100815.
- [85] S. Raj, S.K. Srivastava, P. Kar, P. Roy, In situ growth of Co_3O_4 nanoflakes on reduced graphene oxide-wrapped Ni-foam as high performance asymmetric supercapacitor, *Electrochim. Acta* 302 (2019) 327–337.
- [86] B. Saravanakumara, X. Wanga, W. Zhanga, L. Xinga, W. Lia, Holey two dimensional manganese cobalt oxide nanosheets as a high performance electrode for supercapattery, *Chem. Eng. J.* 373 (2019) 547–555.
- [87] Q. Wang, B. Liu, X. Wang, S. Ran, L. Wang, D. Chen, et al., Morphology evolution of urchin-like NiCo_2O_4 nanostructures and their applications as pseudocapacitors and photoelectrochemical cells, *J. Mater. Chem.* 22 (40) (2012) 21647–21653.
- [88] S.-K. Chang, K.-T. Lee, Z. Zainal, K.-B. Tan, N.A. Yusof, W.M.D.W. Yusoff, et al., Structural and electrochemical properties of manganese substituted nickel cobaltite for supercapacitor application, *Electrochim. Acta* 67 (2012) 67–72.
- [89] C. Yuan, J. Li, L. Hou, L. Yang, L. Shen, X. Zhang, Facile template-free synthesis of ultralayered mesoporous nickel cobaltite nanowires towards high-performance electrochemical capacitors, *J. Mater. Chem.* 22 (31) (2012) 16084–16090.
- [90] G. Zhang, T. Wang, X. Yu, H. Zhang, H. Duan, B. Lu, Nanoforest of hierarchical $\text{Co}_3\text{O}_4@$ NiCo_2O_4 nanowire arrays for high-performance supercapacitors, *Nano Energy* 2 (5) (2013) 586–594.
- [91] T. Huang, C. Zhao, R. Zheng, Y. Zhang, Z. Hu, Facilely synthesized porous ZnCo_2O_4 rodlike nanostructure for high-rate supercapacitors, *Ionics* 21 (11) (2015) 3109–3115.
- [92] Q. Hu, M. Tang, M. He, N. Jiang, C. Xu, D. Lin, et al., Core-shell $\text{MnO}_2@$ CoS nanosheets with oxygen vacancies for high-performance supercapattery, *J. Power Sour* 446 (2020) 227335.
- [93] K.O. Oyedotun, M.J. Madito, D.Y. Momodu, A.A. Mirghni, T.M. Masikhwa, N. Manyala, Synthesis of ternary NiCo-MnO_2 nanocomposite and its application as a novel high energy supercapattery device, *Chem. Eng. J.* 335 (2018) 416–433.
- [94] H.C. Chen, Y. Qin, H. Cao, X. Song, C. Huang, H. Feng, et al., Synthesis of amorphous nickel-cobalt-manganese hydroxides for supercapacitor-battery hybrid energy storage system, *Energy Storage Mater.* 17 (2019) 194–203.
- [95] M.N. Hossain, S. Chen, A. Chen, Fabrication and electrochemical study of ruthenium-ruthenium oxide/activated carbon nanocomposites for enhanced energy storage, *J. Alloy. Compd.* 751 (2018) 138e147.

- [96] M. Li, H. He, Nickel-foam-supported ruthenium oxide/graphene sandwich composite constructed via one-step electrodeposition route for high-performance aqueous supercapacitors, *Appl. Surf. Sci.* 439 (2018) 612–622.
- [97] B.C. Kim, R. Manikandan, K.H. Yu, M.-S. Park, D.-W. Kim, S.Y. Park, et al., Efficient supercapattery behavior of mesoporous hydrous and anhydrous cobalt molybdate nanostructures, *J. Alloy. Compd.* 789 (2019) 256–265.
- [98] S. Kong, K. Cheng, T. Ouyang, Y. Gao, K. Ye, G. Wang, et al., Facile electrodepositing processed of RuO₂-graphene nanosheets-CNT composites as a binder-free electrode for electrochemical supercapacitors, *Electrochim. Acta* 246 (2017) 433–442.
- [99] K.O. Oyedotun, D.Y. Momodu, M. Naguib, A.A. Mirghni, T.M. Masikhwa, A.A. Khaleed, et al., Electrochemical performance of two-dimensional Ti₃C₂-Mn₃O₄ nanocomposites and carbonized iron cations for hybrid supercapacitor electrodes, *Electrochim. Acta* 301 (2019) 487–499.

Layered double hydroxide as electrode material for high-performance supercapattery

Aruni Shajkumar¹, Sarbani Sahu¹, Navaneethan Duraisamy²,
Lukas Schmidt-Mende³ and Ananthakumar Ramadoss¹

¹School for Advanced Research in Polymers: Laboratory for Advanced Research in Polymeric Materials, Central Institute of Plastics Engineering and Technology, Bhubaneswar, India

²Department of Chemistry, J.K.K. Nataraja College of Arts and Science, TN, India

³Department of Physics, University of Konstanz, Konstanz, Germany

9.1 Introduction

The fast-growing population and drastically depleting fossil fuels are creating a rising demand for sustainable, eco-friendly, and cost-effective methods to harvest energy as well as to efficiently store it. Even though a lot of technological innovations are being established in the field of energy storage assemblies, such as capacitors, batteries, supercapacitors, and hybrid battery–supercapacitors (supercapattery), their lower theoretical efficiency drive the researchers to develop novel efficient materials for such hybrid storage devices. With the advent of nanostructures, the conventional capacitors have been replaced by supercapacitors and hybrid supercapacitors that can perform both the functions of a battery and a supercapacitor (supercapattery). However, the efficiency of these assemblies strongly varies with regard to the electrode materials used, structural characteristics, synthesis routes, and morphology.

Lately, layered double hydroxides (LDH) are gaining a great deal of interest for use in supercapacitors owing to their distinctive two-dimensional (2D) ionic lamellar structure which demonstrates an anionic exchange property [1], consistency in optimum conditions, and resistance to alkalis. They are a type of anionic clay which are also known as hydro-talcite due to their similar structure as hydro-talcite mineral ($[\text{Mg}_6\text{Al}_2(\text{OH})_{16}](\text{CO}_3) \cdot 4(\text{H}_2\text{O})$). LDHs can be represented generally as

$[M_{1-n}^{2+}M_n^{3+}(\text{OH})_2]^{n+}[A^{z-}]_{n/z} \cdot m\text{H}_2\text{O}$, in which M^{2+} corresponds to divalent cations (e.g., iron, copper, magnesium, nickel, zinc, cobalt, etc.) whereas M^{3+} represents trivalent ions (e.g., aluminum, chromium, iron, manganese, gallium, etc.); n is the molar ratio of divalent metal cations to the total number of cations present in the structure $\left[n = \frac{M^{2+}}{(M^{2+} + M^{3+})} \right]$ which usually falls between 0.2 and 0.33. A^{z-} represents an anion (Fig. 9.1). Being versatile, the main feature of LDH is its fine-tunability, that is, by varying the molar proportion and characteristics of the metal cations and the kind of interlamellar anions, the properties of LDHs can be varied widely [2].

These anionic clays or hydrotalcite, otherwise known as LDHs, have unique properties like chemical stability, biocompatibility, pH-dependent solubility, etc. Hydrotalcite exhibits a layered structure constituted of positively charged hydroxide layers with an interlayer of negatively charged ions and water molecules. Their compositional flexibility makes them interesting as different metal ions can be isomorphously substituted into their structure without disturbing the original layered structure. LDHs contain positively charged layers with negatively charged ions and water molecules in the interlayer region. These positively charged layers are hydroxide layers, where divalent metal cations are isomorphously substituted with trivalent metal cations. The interlayer anions act as charged balancing species and water molecules occupy the free space between the layers. One of the

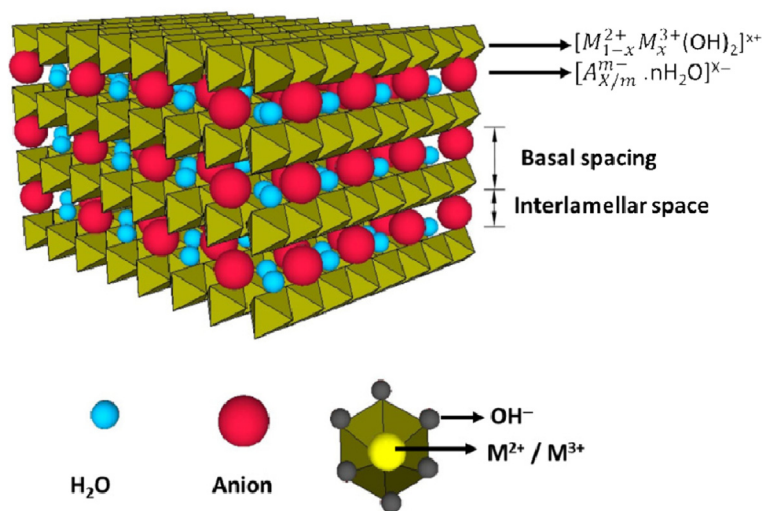


Figure 9.1 Schematic representation of layered double hydroxides structures.

major benefits of this layered structure is its stability. This stability of the structure is due to the presence of hydrogen bonds from water molecules combining a hydroxyl layer with anions and also the electrostatic force between them. Owing to their unique structural arrangement, easy tunability of metal ions, and chemical modification without changing its layered morphology, LDH can be used as a potential structure not only in preparing efficient electrode materials for charge storage assemblies but also in fields, such as biomedicine, sensors, catalysis, and several more [3–6].

This chapter focuses on the recent developments in LDH for the preparation of electrodes for supercapattery, charge storage mechanism, synthesis routes, and recent trends in LDH. Transition metal hydroxides, owing to the layered structure and good conductivity, are widely used as LDH materials in energy storage. To overcome the disadvantages of conventional LDHs, the basic units of LDHs can have different structural arrangements, such as core–shell, hollow–spheres, and different 3D nano- and microporous structures, which are discussed in this chapter. In addition to this, to improve the electrochemical performance of the LDH-based electrodes, LDH is used in combination with different active materials like carbon nanotubes (CNTs) and graphene (1D and 2D structures). Such composites are gaining a lot of interest nowadays. Some of the important developments in this area are also covered in the present chapter. However, as most of the papers report specific capacitance values, we focus on the Farad per gram (F g^{-1}) values in this chapter instead of specific capacity due to the mislabeling of the charge storage mechanism.



9.2 Energy storage mechanism

A supercapacitor material has two types of charge storage mechanism: (1) electric double layer capacitance (EDLC); and (2) pseudocapacitive material. Mechanisms like surface adsorption/desorption and intercalation/deintercalation are shown in supercapacitor and battery-type materials [7,8].

In a more classified manner, it can be stated that EDLC-type materials like activated carbon or CNT undergo reversible electrolyte ion adsorption or desorption at the electrode–electrolyte interface. This surface of the interaction is known as the electric double layer region [9,10]. So, in short, EDLC-type material undergoes reversible ion distribution upon

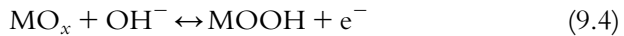
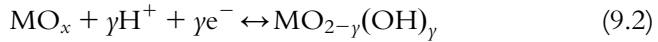
application of external voltage. As this process is entirely dependent on the active surface area of the electrode (charge is stored on the thin layer of the external surface of electrode material) the higher the active surface area of the electrode, the better is the interaction. Hence, the amount of energy storage is through the physical process only and is lower compared to other supercapacitor or battery-type materials with no involvement of chemical reactions in the process.

The charge storage mechanism of pseudocapacitive material can be divided into two categories. One type is surface redox reaction controlled pseudocapacitance and the other is intercalation and deintercalation [11]. In the process of a surface redox reaction, the electrolyte cations and anions undergo adsorption and desorption over the electrode surface. Thus in this process, a faradaic redox reaction is observed. Although these types of pseudocapacitive materials undergo a faradaic redox reaction, their behavior is like EDLC-type materials. They show nearly rectangular cyclic voltammetry (CV) and linear and triangular galvanostatic charge–discharge (GCD) curves.

On the other hand, the pseudocapacitance dominated by ion intercalation/deintercalation includes a reversible process of electrolyte cation (like K^+ , Li^+ , H^+ , Na^+) intercalation and deintercalation through the electrode material crystal structure. The materials that encounter phase transitions during the charge/discharge process are called battery type [12–14]. Typically, the oxidation and reduction process occurs throughout the process. In detail, during the process of charging, the transition metals with low valence get oxidized to a high valence state. Whereas during the discharging process the higher valence transition metal undergoes reduction to come back to its original state. So the entire process of charge storage mechanism inside a battery is reversible [15]. The oxidation and reduction peaks in CV and plateaus regions in GCD curves can prominently identify the battery-type behavior. As compared to supercapacitor type materials, battery-type materials show better charge storage ability but poor rate capability. The major cause of this poor rate performance is their sluggish kinetics arising from slow phase transformations during the charge/discharge process. For a better understanding of the reaction mechanism of battery-type material, some of the examples of transition metal oxides and hydroxides can be considered.

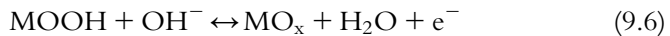
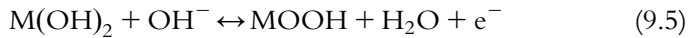
Primarily, in metal hydroxides and oxides electrodes different types of charge storage processes like ion intercalation/deintercalation, surface redox reactions with anions, or surface adsorption/desorption etc. The

reversible reaction that occurs between metal oxides and different alkali ions of the electrolyte can be generalized as:[16–18]



where M indicates the metal ion and C^+ refers to alkali ion of the electrolyte.

Similarly, through protonation/deprotonation, the transition metal hydroxides react with the hydroxyl ions of the electrolyte. This can be symbolized through the following reaction:



It can be inferred that the transition metals with high valency can give better battery-type mechanism.

Transition metal hydroxides can have two phases of crystal structures: α -phase and β -phase. The α -phase contains a hydrotalcite-like structure consisting of cationic layers $M(OH)_{2-x}$ intercalated by anions. The β -phase have a brucite-like structure consisting of a layered hexagonal structure along with a stoichiometry composition of metal cations and hydroxide anions. The interlayer spacing of α -phase (7.0 Å) is higher compared to the interlayer spacing of β -phase (4.6 Å) due to anion intercalation. Therefore the α -phase shows better electroactivity [18,19].



9.3 Synthesis of layered double hydroxides nanostructures

Synthesis routes lay the foundation in determining the property, morphology, and final efficiency of a material/structure. Therefore establishing an optimized synthesis route with controlled parameters is inevitable in any application. In addition to property tuning, the adopted method should also be economical, eco-friendly, and easy to upgrade. A lot of studies have been

focused on developing an optimum method for synthesizing LDH structures. The first reported synthesis of LDH was done by Miyata and Okada [20] via the direct hydrolysis of an inorganic salt in the presence of a strong base. The common synthesis routes to prepare LDHs can be generally classified into three: direct synthesis, indirect synthesis, and memory effect method. The schematic illustration for the fabrication methods of LDH nanostructures is shown in Fig. 9.2. The direct synthesis routes involve coprecipitation, sol–gel synthesis, urea hydrolysis, and hydrothermal/solvothermal synthesis, whereas the indirect routes comprise ionic exchange.

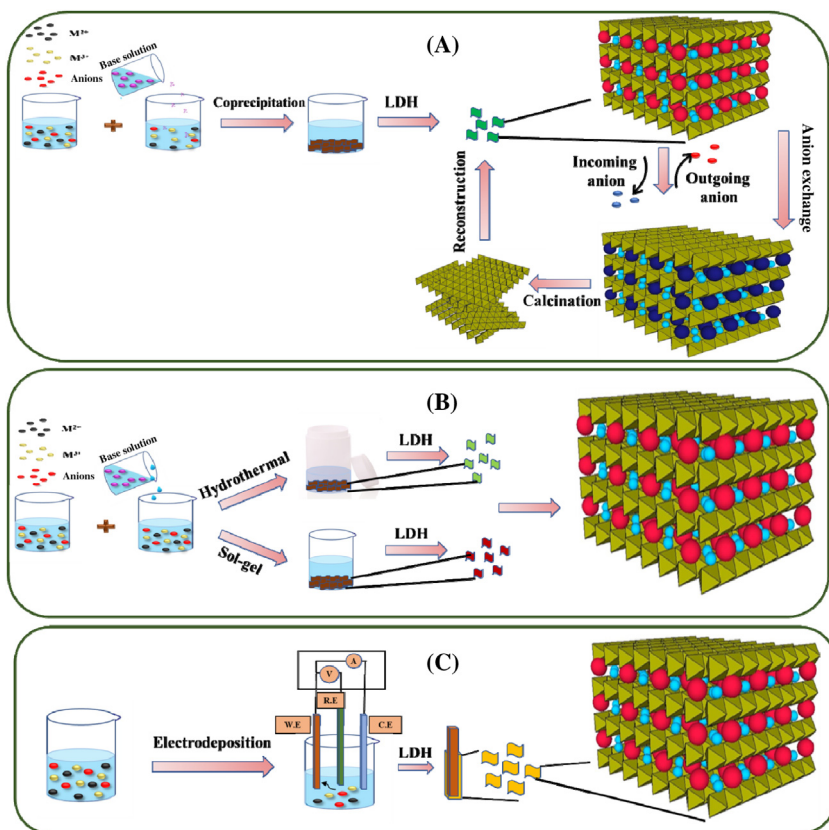


Figure 9.2 Schematic illustration for the fabrication methods of LDH nanostructures: (A) coprecipitation, anion exchange, reconstruction; (B) hydrothermal, sol–gel; and (C) electrodeposition.

9.3.1 Direct synthesis

a. Coprecipitation

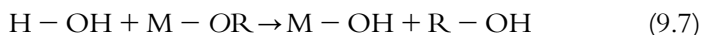
It is the most widely practiced synthesis route for the preparation of LDHs owing to the ease of synthesis, higher output, economic viability, and large scale-up gradation [2,21,22]. This method includes the coprecipitation of inorganic salts in a basic medium under controlled pH. Moreover, this synthetic route can be adapted for a broad variety of cations and anions (inorganic and organic) and larger molecules, such as biomolecules can be intercalated. In this method, an anionic solution which needs to be intercalated is added slowly to a solution containing M^{2+} and M^{3+} at a predetermined ratio under stirring. This step is followed by increasing the pH (6–11) of the reaction medium either by the addition of a base or urea due to which the metal hydroxides will be precipitated [21]. The precipitate will be further subjected to thermal treatment, that is, aging to improve the crystallinity of the attained structure. The aging usually prolongs from a few hours to several days. The theory behind coprecipitation is based on the condensation of hexa-aqua metal complexes in solution that results in the formation of a brucite-like structure with uniformly distributed cations and interlamellar anions. The critical parameter that determines the formation of hydroxalite is the pH of the reaction media. An optimum pH value needs to be maintained for the precipitation of the metal hydroxide. Too low or too high pH may obstruct the formation of a precipitate. Moreover, the precipitation pH may take part in deciding the properties as well as the characteristic nature of the final product [2]. For instance, the crystallite size can be varied by changing the pH [23]. The studies conducted by Valim et al. [23] showed that at constant pH, the end product possessed an increased crystallinity and pore size, higher specific surface area, and smaller particle size when compared to the material prepared at a varying pH. When urea is used as a pH controller, the resulting material demonstrated an improved crystallinity and homogenous particle size distribution owing to the slow hydrolysis process of urea [24].

Thus, in short, pH, temperature, route adopted for precipitation, nature and ratio of the negative and positively charged ions, and aging have a pivotal role in controlling the properties and morphology of the obtained hydroxalite [2].

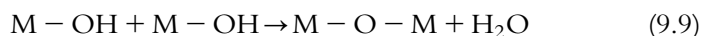
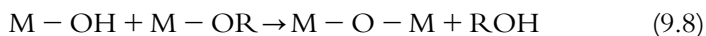
b. Sol–gel synthesis

As the name indicates sol–gel synthesis involves a hydrolysis condensation reaction in which the metallic precursor forms the sol by

undergoing hydrolysis and partial condensation which is often followed by its gelation by condensation. The commonly used precursors are metallic alkoxides, acetates or acetylacetonate, and inorganic salts [21]. The most commonly used metal precursor is metal alkoxides, $M(OR)_n$, where M is the metal, n is the valency of the metal, and R represents the alcohol group. The mechanism of LDH synthesis via sol–gel involves the formation of a reactive hydroxyl group by the hydrolysis of a metal alkoxide.



This step is followed by the nucleation–substitution followed by condensation



The condensation step is further followed by gelation resulting in the formation of a three-dimensional (3D) network comprising oxygen and metal with water and alcohol trapped in the mesoscopic pores [2].



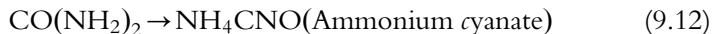
The properties of the obtained structure can be tuned by varying the hydrolysis condensation rate which in turn can be varied by varying the reaction parameters, such as pH, concentration, and characteristics of the precursors, nature of solvent, and temperature of the reaction. Even though, the LDH obtained via sol–gel exhibits better features in terms of pore-size control, high specific area, and high purity when compared to material obtained via coprecipitation, this method is less explored when compared to the latter.

c. Urea hydrolysis

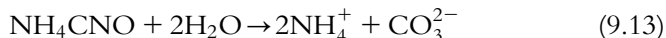
It is already well-known that when urea is used as a precipitating agent the attained LDH possesses better crystallinity [24]. Thus urea hydrolysis is commonly used to produce LDHs with high crystallinity because of its ability to attain a lower level of supersaturation [2]. The rate of hydrolysis of urea can be controlled by simply varying the reaction temperature, which is directly related to the crystallinity and particle size of the final product acquired. For instance, when a lower temperature is used, the hydrolysis

rate will be slower which results in the formation of considerably larger particles [25]. Mainly two steps are involved in urea hydrolysis out of which step 1 is the rate-determining step [2].

Step I (Rate-determining step)



Step II (Hydrolysis of ammonium cyanate)



Step II results in the increase of pH in the reaction medium, which leads to the precipitation of a large number of metal hydroxides. The urea hydrolysis method is very much practiced in synthesizing high charge density compounds which are tedious to prepare with other methods.

d. *Hydrothermal/solvothermal synthesis*

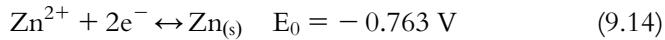
The main difference between the hydrothermal synthesis and solvothermal synthesis routes is the nature of the reaction medium. A hydrothermal reaction proceeds in an aqueous medium whereas solvothermal uses a nonaqueous solvent [21,26,27]. Among the different synthetic routes, this is one of the most widely adopted synthetic methods for preparing well-crystallized LDHs with intercalated organic guest species that is having a low affinity toward LDHs. The general procedure for hydrothermal/solvothermal synthesis involves the addition of a suitable salt or acid to a suspension of metal cations (M^{2+} and M^{3+}). This reaction mixture will be further subjected to high pressure and high temperature in an autoclave. This synthetic procedure involves no or little waste when compared to coprecipitation which makes it a preferred method over coprecipitation. Moreover, hydrothermal/solvothermal synthesis is very much opted to prepare fine-tuned LDHs with controlled particle sizes and morphologies with improved crystallinity [21].

e. *Electrodeposition*

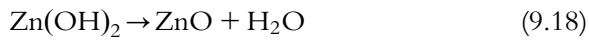
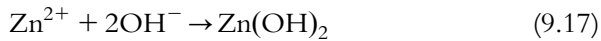
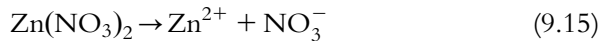
Electrodeposition is a commonly used method to prepare in situ metallic coatings on a conductive material in the presence of a precursor salt solution of the metal to be deposited using an electric current. For LDH synthesis, this method is adopted to acquire pure films [28]. This method is used in the preparation of Ni–Al LDHs, Ni–Mn LDHs, Mg–Al LDHs, Mg–Cr LDHs [29], Ni–Al LDHs [30], Ni–Fe LDH [31], and Zn–Al LDH [28].

An aqueous solution of the metal salts (M^{2+} and M^{3+}) to be electrodeposited is used as a source. For example, in the case of Zn–Al LDHs,

an aqueous solution of zinc and aluminum salts are used as a source of Zn^{2+} and Al^{3+} , respectively [28]. OH^- and NO_3^- ions are used to control the pH. An increased local pH at the working electrode facilitates the formation of LDH only on the working electrode. The reference electrode is made of Ag/AgCl and the counter electrode used is platinum [28,31]. The cathodic deposition of zinc metal is explained as follows:



Generation of OH^- ions is a mandate for the deposition of LDH which is achieved through the reduction of nitrate ions (NO_3^-). Deposition of pure Zn–Al LDH is attained by choosing a potential that is enough to reduce NO_3^- ions but not sufficient for the Zn^{2+} ions to undergo reduction.



When LDH synthesis is carried out by electrodeposition, the deposition potential must be chosen in accordance with the concentration of metal ions (M^{2+}) and NO_3^- ions and the solution pH must be maintained at an optimum value.

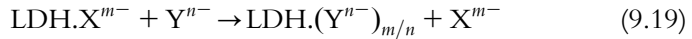
9.3.2 Indirect synthesis

a. Anion exchange

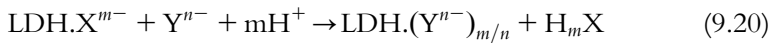
This synthetic route is most widely used for materials where coprecipitation is not possible, specifically when the chosen metal ions cannot withstand high pH or when there is a chance for plausible interaction between the metal ion and the guest species [21]. This procedure can be used for the intercalation of a multitude of anions particularly monovalent ions, such as Cl^- and NO_3^- because monovalent ions are less selective ($OH < F < Cl < Br < NO_3^-$) than the bivalent ions (SO_4^{2-} , CO_3^{2-}) in terms of exchange complexity. Among all the anions used, nitrate ions are found to be the most suitable precursors for anionic exchanges as they can be easily displaced in the interlamellar spaces [2].

This route is classified as an indirect method because here the LDH is first synthesized via coprecipitation and later exchanged with target anions by stirring the LDH precursor in an inert atmosphere in the presence of

excess anions which need to be intercalated. The anion exchange between the LDH precursor and the solution is usually based on the electrostatic forces between the positive layers of LDH and the substituting anions. There are two possible ways for the target anions to be intercalated which are explained in the form of equations [22]:



or



The anions present in the interlamellar spaces of LDH have a weak electrostatic interaction with the LDH layers which facilitate their exchange with anions having higher electrostatic interaction with the layers. The prerequisites to facilitate an anion exchange reaction are the following [22]:

1. Choice of an appropriate solvent.
2. Chemical composition of the brucite type layers.
3. High temperatures favor anion exchange.
4. A pH of 4 or above should be maintained, as lower pH will lead to the rupture of hydroxyl layers.

b. Reconstruction method (memory effect)

LDH disintegrates to a mixture of metal oxide at a temperature of 400°C–500°C, which upon exposure to water regenerates back into its older LDH structure. The reconstruction method utilizes this memory effect of LDHs [21,22]. This method is generally used to intercalate bigger anions or when the target anions cannot be intercalated into the LDH lamella using the anion exchange method and is rarely used in the synthesis of LDH material for supercapattery.

In short, upon comparing the aforementioned synthesis route, coprecipitation results in a higher yield and various parameters can be controlled during the synthesis. The sol–gel synthesis route gives an LDH structure with better pore-size control, high specific surface area, and purity and is typically used in synthesizing core–shell LDHs [32]. Urea hydrolysis results in a highly crystalline structure, whereas the hydrothermal route results in a higher crystalline product with better pore and size distribution. Electrodeposition is used to attain extra pure LDH films on different conducting substrates. The anion exchange route is found to be better for intercalating larger anions. The product obtained via the reconstruction method delivers a poorly crystallized structure with partial intercalation when compared to other methods.



9.4 Transition metal layered double hydroxides for supercapattery

The increasing need for sustainable and clean energy leads to the birth of energy storage devices. With electrochemical energy being the most environmentally viable source for producing energy, electrochemical energy storage devices such as supercapacitors have been in high demand recently. Among the different supercapacitors developed, those that are based on LDH electrodes are gaining a lot of interest due to their multitude of properties as discussed previously. Different metal hydroxides are used as the building blocks for LDH to possess superior properties. Transition metal hydroxides owing to their high energy densities and specific capacity is commonly used as an active material for the synthesis of LDH structures. They have a higher valence state which results in increased interfacial redox reaction. Some of the commonly used transition metals in supercapacitors comprise monometallic transition metal hydroxides of nickel (Ni), cobalt (Co), manganese (Mn), ruthenium (Ru), etc. Even though transition metals are preferred widely in LDH-based supercapacitors, most of the aforementioned monometallic transition metal hydroxides possess low conductivity and low specific capacitance [33]. Therefore they are often used as a combination of two transition metal hydroxides.

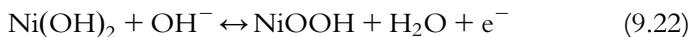
Herein some of the commonly used transition metal hydroxide combination: nickel–cobalt LDH, nickel–manganese LDH, cobalt–manganese LDH, and cobalt–aluminum LDH are briefly discussed.

9.4.1 Nickel–Cobalt layered double hydroxides (Ni–Co LDH)

Electrodes made from nickel hydroxide, due to their considerable energy and power density as well as proton recyclability, are widely used in electrochemical energy storage devices. However, these electrodes exhibit poor conductivity (10^{-5} – 10^{-9} S cm⁻¹) upon cycling due to the increased resistance of the nickel hydroxide [33,34]. This leads to their limited use in fabricating energy storage devices. One of the prominent ways to overcome this hurdle is to use a combination of nickel hydroxide (Ni(OH)₂) with other potent material such as cobalt hydroxide (Co(OH)₂). Co(OH)₂ is well-known to possess excellent electrical conductivity compared with Ni(OH)₂, but due to its low supercapacitive behavior in comparison with Ni(OH)₂ the former has limited use in supercapacitor applications [35]. But a combination of nickel hydroxide and cobalt hydroxide at a specific mixing/doping ratio can improve the supercapacitive behavior of both the materials to a

great extent. Thus a mixed metal hydroxide is greatly preferred over single hydroxides due to the combined properties of the independent constituents of the former.

The faradaic reactions during the energy storage mechanism of Ni–Co LDHs are explained as follows:



As aforementioned, the conductivity of cobalt hydroxide is superior to that of nickel hydroxide which enables the electrodes made from this composition to exhibit better performance in terms of electrochemical energy storage. However, a further enhancement of conductivity can be achieved by the addition of a conductive binder or a conductive substrate, as conductivity is the key parameter in determining the performance efficiency.

a. Nickel–cobalt layered double hydroxides electrodes prepared with binders

In this method, the Ni–Co LDH is prepared via a hydrothermal or coprecipitation method. The as-prepared LDH is then mixed with a conductive binder material such as carbon black, polymer, etc. along with a solvent under an appropriate ratio to get a slurry which will be then layered on a substrate via doctor blading or drop-casting. These composites (Ni–Co/binder) considerably improve the surface area (Fig. 9.3) and specific capacitance (1911.1 F g^{-1} at current density of 2 A g^{-1}) when compared to the Ni–Co LDH alone [26]. Even though the Ni–Co LDH/binder composites give enhanced properties, the binder acts only as filler which in some cases

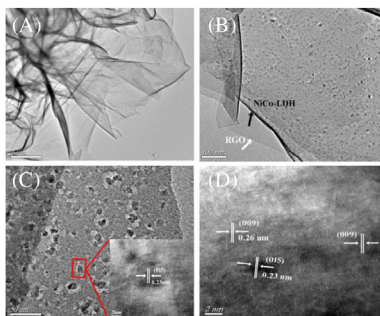


Figure 9.3 (A–C) TEM and (D) HR-TEM images of NiCo-LDH/RGO-3 composite [26].

adversely influence the performance efficiency of the electrode. Thus to minimize the consequence of binders the nickel–cobalt LDH can be directly deposited/grown on an appropriate substrate.

b. Binder-free nickel–cobalt layered double hydroxides electrode

In binder-free Ni–Co LDH electrodes, the LDH is deposited directly or grown on a substrate via common methods such as hydrothermal method [36,37], precipitation [33], chemical bath deposition [38], and electrochemical deposition [39]. Huang et al. [36]. prepared an assembly with Ni–Co LDH deposited on a carbon fiber paper with NiCo₂O₄ nanowires which exhibited a specific capacitance of 2682 F g⁻¹ at 3 A g⁻¹ current density with a 63.6% capacitance retentiveness at 20 A g⁻¹. Another substrate involved ZnO nanoflakes and nanowires for depositing nickel–cobalt LDH where the electrode with nanoflake substrate exhibited 1624 F g⁻¹ specific capacitance which was 1.6 times higher when compared to the nanowire. The main reason for this is higher surface area and low internal resistance of the nanoflake when compared to the nanowire [37]. For improving the rate capability, Yue et al. [40] used electrochemically activated graphite fibers and prepared NiCo-LDH nanoflakes and FeOOH nanosheets. Electrochemically activated graphite fibres (EAGFs) are used as a support in this case. Ni–Co LDH nanoflakes and FeOOH nanosheets can be anchored on electrochemically activated graphene fibers via electrodeposition. The high-performance hybrid supercapacitor device comprising NiCo-LDH/EAGFs as the negative electrode and FeOOH/EAGFs as the positive electrode attains a wide voltage window of 0–1.8 V. The electrode prepared using this assembly exhibited a 130 W h kg⁻¹ energy density with a power density of 10.8 kW kg⁻¹. In this method due to the formation of C–O–Metal bonding, the oxygen-functionalized carbon on electrochemically activated graphite fibers can bind strongly with NiCo-LDH and FeOOH, which supports in establishing the fast electron transfer routes and fluent ion transport avenues.

Nickel sheet can also be used as a substrate to deposit Ni–Co LDH. Zheng et al. [41] fabricated ultrathin porous Ni–Co LDH hybrid nanosheets on metal Ni sheet via a facile hydrothermal method without any adsorptive surfactant. The prepared Ni–Co LDH hybrid nanosheet-based electrodes for supercapacitors in aqueous electrolyte displayed a significantly improved specific capacitance of 2184 F g⁻¹ at 1 A g⁻¹ and energy density of 91.76 Wh kg⁻¹ at 825.84 W kg⁻¹, due to the distinct synergistic effect between Ni²⁺ and Co²⁺. Electrode materials achieved

excellent long-term cycling stability, withholding 88.5% of the original capacitance after 2000 cycles.

Another binder-free NiCo-LDH was prepared on Ni-coated textile for flexible and wearable supercapacitors via a hydrothermal route by Jeong et al. [42]. They have studied the specific capacitance for different ratios of Ni:Co and found out that an increased cobalt ratio, when compared to nickel (3:7 ratio of Ni:Co), gave high specific capacitance values (1050 F g^{-1} at 1 A g^{-1}) which is due to the redox behavior of highly conductive $\text{Co}(\text{OH})_2$ and the increased interlayer spacing with intercalation of NO_3^- . And the supercapacitor assembled using this electrode demonstrated a maximum volumetric energy density of 1.25 mWh cm^{-3} at a power density of 47.4 mW cm^{-3} . Lan et al. [43] followed a hydrothermal route to synthesize a free-standing electrode by the intercalation of vertically aligned sodium dodecylbenzene sulfonate (SDBS) into nickel–cobalt LDH nanosheets and carbon fiber cloth (CFC) [Fig. 9.4]. The asymmetric supercapacitor (ASC) fabricated using the aforementioned electrode demonstrated an increased energy density of 70.94 Wh kg^{-1} at power density of 400 W kg^{-1} with capacitance retention of 89.96% at a current density of 10 A g^{-1} for 1000 cycles.

A study conducted by Han and coworkers [44] dealt with the synthesis of Ni–Co LDH on a nickel foam using PVP as a structure-directing agent. This binder-free assembly exhibited a high specific capacity of 724.9 C g^{-1} at 1 A g^{-1} current density. The hybrid supercapacitor (HSC) assembled using this electrode possessed 32.3 Wh kg^{-1} energy density at 387.1 W kg^{-1} power density [Fig. 9.5].

Along with nickel foam [44,45], carbon fabric [46], stainless-steel [38], titanium nitride nanotube (TiN) [47] are also used as a substrate to deposit Ni–Co LDH. Warsi and coworkers [46] fabricated a conformal coating

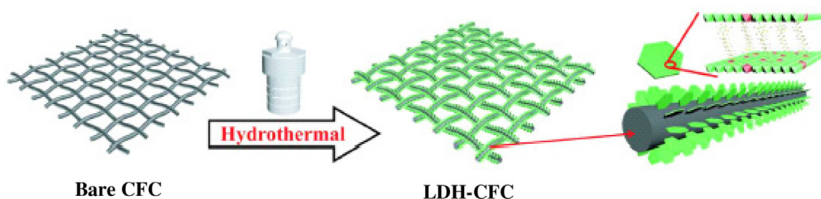


Figure 9.4 Synthetic route showing NiCo-SDBS-LDH@CFC. Reprinted from Ref Y. Lan, M. Li, W. Fan, Q. Deng, Z. Zeng, J. Wang, et al., *Functional molecules regulated and intercalated nickel–cobalt LDH nano-sheets on carbon fiber cloths as an advanced free-standing electrode for high-performance asymmetric supercapacitors*, *Electrochim. Acta* 321 (2019) 134708.

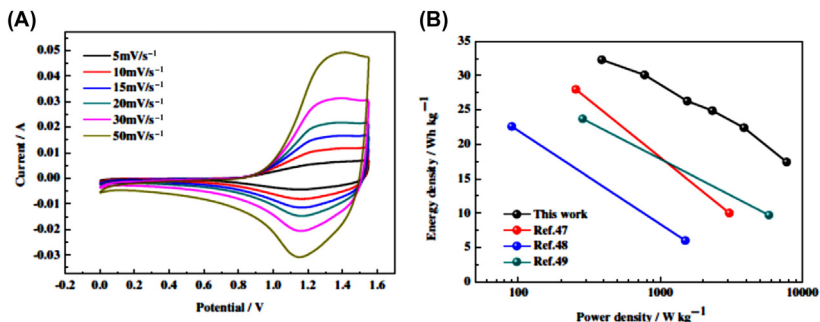


Figure 9.5 (A) Cyclic voltammetry curves of the hybrid supercapacitor fabricated using nickel–cobalt LDH//AC at varying scan rates. (B) Ragone plot of the hybrid supercapacitor. *Reproduced from E. Han, Y. Han, L. Zhu, P. Yang, X. Du, Polyvinyl pyrrolidone-assisted synthesis of flower-like nickel–cobalt layered double hydroxide on Ni foam for high-performance hybrid supercapacitor, Ionics 24 (2018) 2705–2715.*

of cobalt–nickel LDH nanoflakes on a carbon fabric which demonstrated an increased specific capacitance of 1938 F g^{-1} when compared to NiCo-LDH on carbon fiber deposited via drop-casting (1292 F g^{-1}). Shang et al. [47] fabricated a $\text{Ni}_x\text{Co}_{2-x}(\text{OH})_{6x}$ deposited on to a self-standing TiN nanotube which showed a specific capacitance of 2543 F g^{-1} at a scan rate of 5 mV s^{-1} .

3D porous nickel arrays/conductive cloth is also used to deposit NiCo-LDH nanosheets (NiCo-LDH@3D Ni/CC) to prepare high-performance supercapacitors as shown in Fig. 9.6A [39]. The electrodes fabricated using this structure exhibited an increased mass capacitance of 2248 F g^{-1} and areal capacitance of 3260 mF cm^{-2} . The symmetric solid-state supercapacitor assembly using NiCo-LDH@3D Ni/CC electrodes showed an increased areal capacitance of 116.7 mF cm^{-2} at 5 mA cm^{-2} with full retention of capacitance after 10,000 cycles at 10 mA cm^{-2} [Fig. 9.6B–E].

Mehrabimatin et al. [48] fabricated lightweight, flexible ASCs using NiCo-LDHs with 3D nitrogen-doped graphene (NG) as support that exhibited high performance. One of the main advantages is the presence of highly conductive nitrogen-doped graphene that facilitates quick charge transfer and (dis)charging of the deposited nickel–cobalt LDH. The electrode prepared using the aforementioned LDH assembly exhibited an improved specific capacitance of 1397 F g^{-1} at current density of 10 A g^{-1} . The as-prepared ASC had shown superior performance efficiency to the previously reported analogs with a high specific capacitance

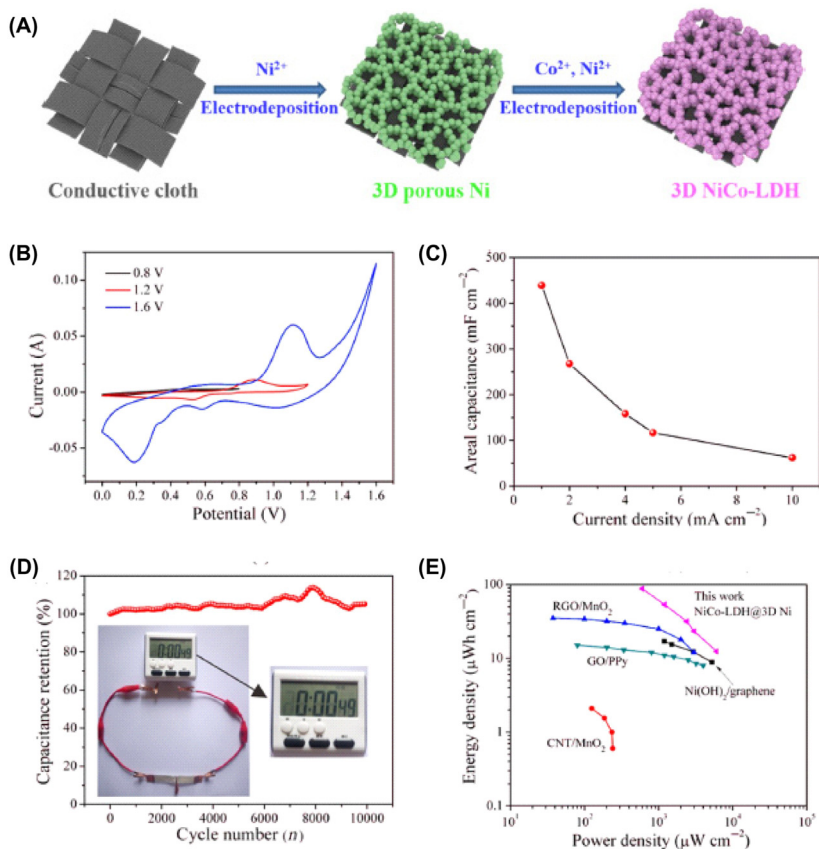


Figure 9.6 (A) Fabrication of NiCo-LDH on 3D porous Ni arrays; Performance efficiency of all SC symmetric supercapacitors from 3D Ni/LDH; (B) Cyclic voltammograms curves at the varying potential at 50 mV s^{-1} scan rate; (C) Areal capacitance vs current density plot; (D) Cycling stability for 10,000 cycles at 10 mA cm^{-2} . Inset shows the digital LCD clock powered by two devices in series connection; and (E) Ragone plots that compare current assembly with analogous devices. *Reprinted from Y. Li, J. Chen, H. Ye, F. Zhang, X.-Z. Fu, R. Sun, et al., Hierarchical NiCo hydroxide nanosheets deposited on 3D porous Ni arrays for cost-effective high-performance supercapacitors, J. Mater. Sci. Mater. Electron. 30 (2019) 2552–2562.*

of 109 F g^{-1} at current density of 0.5 A g^{-1} with a maximum energy density of 49 W h kg^{-1} [Fig. 9.7].

Qin et al. [49] have studied the fabrication of hybrid supercapacitors (HSC) using flower-like NiCo-LDHs and activated carbon (AC) in KOH (NiCo-LDH//AC) in which the NiCo-LDH exhibited a high specific capacitance of 777 C g^{-1} . The assembled device exhibited specific energy

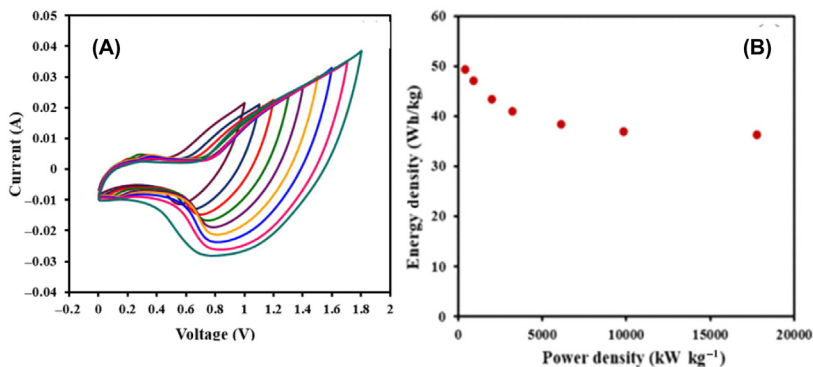


Figure 9.7 (A) Cyclic voltammograms of NiCo-LDH@NG/CC//NG/CC ASC device at 50 mV s^{-1} scan rate at different voltage. (B) Ragone plots of the ASC device [48].

of 69.5 Wh kg^{-1} with a specific power of 450 W kg^{-1} with cycling stability up to 5000 cycles. Electrodeposition is also widely used to prepare Ni–Co LDH. Wang and coworkers [50] synthesized Ni–Co LDH nanosheets using unipolar pulse electrodeposition on a carbon paper. By varying the feeding molar ratio of Ni and Co at a proportion of 9:1 LDH structure exhibited a high specific capacitance of 2189.8 F g^{-1} at current density of 1 A g^{-1} and good cycle stability, retaining 70.3% of the initial capacitance after 20000 charge and discharge cycles at 50 A g^{-1} owing to the charge transfer between Co and Ni cations, porous microstructure and uniform configuration [50]. The ASC assembled using this LDH assembly exhibited an energy density of 4.1 Wh kg^{-1} with 4000 W kg^{-1} power density with outstanding capacitance retention (82.7%) after 2000 cycles. Zhou et al. [51] adopted a microwave-assisted synthetic route to prepare a flower-on-sheet Ni–Co LDH structure with controlled morphology. The as-obtained LDH exhibited a high capacitance of 1187.2 F g^{-1} at a current density of 1 A g^{-1} . The assembled device with the commercial activated carbon as the negative electrode that exhibited an energy density of 36.2 Wh kg^{-1} at a power density of 150 W kg^{-1} .

c. Nickel–cobalt layered double hydroxides directly grown on electroactive substrates

In this method, the LDHs is directly grown on an electroactive current collector to improve the efficiency of the electrodes while device fabrication. The LDHs can be grown via general synthesis methods such as precipitation [52], chemical bath deposition [53,54], and electrodeposition

[55]. The commonly used current collectors are graphene [56], graphene foam [53,55], CNT [54], etc. Cheng and coworkers [52] assembled a free-standing composite of Ni–Co LDH by their direct growth on a mixture of graphene oxide and CNT which exhibited an increased specific capacitance of 2360 F g^{-1} at 0.5 A g^{-1} . In another work done by Patil et al. [53], Ni–Co LDH grown on to graphene foam substrate demonstrated a specific capacitance of 1847 F g^{-1} at a current density of 5 A g^{-1} [Fig. 9.8]. Chen et al. [54] studied the development of nickel–cobalt LDH on MWCNT paper which has nanoflake morphology. The electrode composed of this assembly exhibited a specific capacitance of 2633 F g^{-1} at current density of 0.5 A g^{-1} .

A solvothermal method was adopted to synthesize NiCo-LDH nanosheets (Fig. 9.9) which were directly grown on carbon fiber cloth (NiCo-LDH/CFC) by Wang and coworkers [16]. By varying the Ni/Co ratio, they have studied the varying specific capacitance values and for an optimal Ni/Co ratio of 1:1, the electrode demonstrated a specific capacitance of 2242.9 F g^{-1} (1009.3 C g^{-1}) at 1 A g^{-1} with an outstanding rate capability of 61% at a current density of 60 A g^{-1} . The capacitor fabricated using this assembly demonstrated an energy density of 59.2 Wh kg^{-1} with a

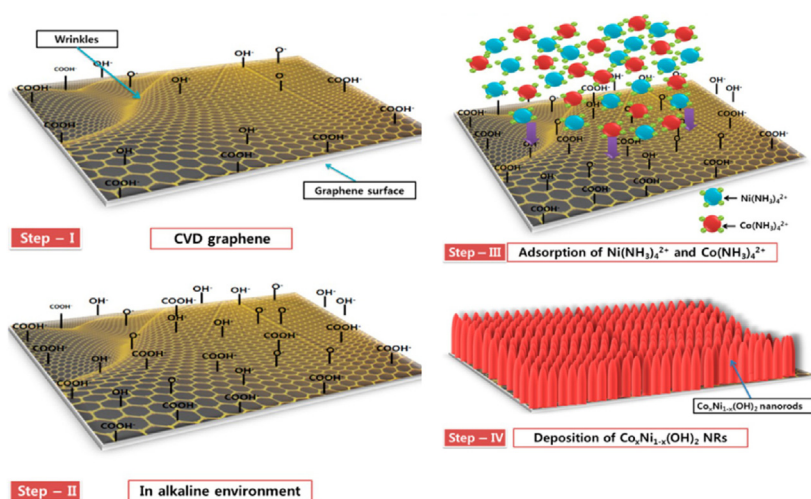


Figure 9.8 Pictorial depiction showing the step-by-step growth of $\text{Co}_x\text{Ni}_{1-x}(\text{OH})_2$ nanorods on graphene foam (GF). Reprinted from S.C. Jun, U. Patil, J. Sohn, S. Kulkarni, S. Lee, H. Park, et al., *Enhanced supercapacitive performance of chemically grown cobalt–nickel hydroxides on three-dimensional graphene foam electrodes*, *ACS Appl. Mater. Interfaces* 6 (2014) 2450–2458.

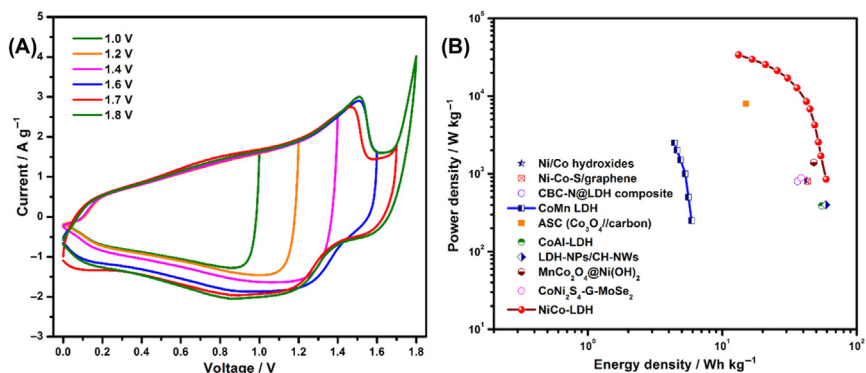


Figure 9.9 (A) Cyclic voltammograms of the fabricated HSC at different voltages at scan rate of 10 mV s^{-1} . (B) Ragone plot of HSC. *Reprinted from T. Wang, S. Zhang, X. Yan, M. Lyu, L. Wang, J. Bell, et al., 2-Methylimidazole-derived Ni–Co layered double hydroxide nanosheets as high rate capability and high energy density storage material in hybrid supercapacitors, ACS Appl. Mater. Interfaces 9 (2017) 15510–15524.*

power density of 34 kW kg^{-1} . A longstanding stability test shows that 82% of the initial capacitance of the hybrid device remains after 5000 cycles. Fig. 9.9A represents the CV of the fabricated HSC at various voltages with a scan rate of 10 mV s^{-1} followed by a Ragone plot of HSC (Fig. 9.9B.)

The work done by Xing et al. [57] dealt with the direct growth of vertically aligned 3D ultrathin Ni–Co LDHs on nickel foam using a facile single-step hydrothermal method. By varying the volume ratio of the solvent they have fine-tuned the Ni–Co phase from a single α phase to multiphase (α and β). The authors have observed that the multiphase Ni–Co LDH exhibited an increased specific capacitance of 2617 F g^{-1} at 1 A g^{-1} . This can be related to the mixed crystal phase and the distinguishable multilayers present in the structure. Following the high specific capacitance of the multiphase LDHs, the poly-phase NiCo-LDH/NF supercapacitor electrodes retained 70% of its capacitance after 1300 cycles at 10 A g^{-1} . The device fabricated (Fig. 9.10) using this electrode demonstrated a high specific capacitance of 439.5 mF cm^{-2} at 2 mA cm^{-2} .

Yang et al. [58] fabricated ultrathin and sinuous nickel–cobalt LDH nanosheet structures grown on the exterior of graphene oxide (Ni–Co LDH-G) via a surface-confined strategy. These electrodes demonstrated a high specific capacitance of 1489 F g^{-1} at current density of 1 A g^{-1} with 68% retention of the initial capacitance. Another study conducted by Dong et al. [59] dealt with the synthesis of opening flower-like porous

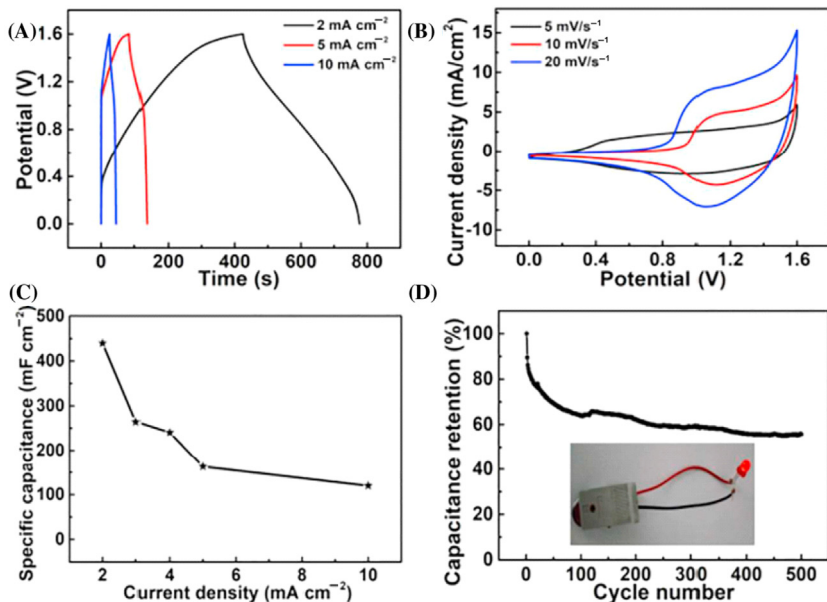


Figure 9.10 Electrochemical performance of Ni–Co LDH/NF//AC ASC: (A) GCD curves at varying current densities; (B) cyclic voltammetry curve at varying sweep rates; (C) specific capacitance at varying current density; and (D) charging/discharging cycle efficiency at 2 mA cm⁻² for 500 cycles. Inset LED test. Reprinted from H. Xing, Y. Lan, Y. Zong, Y. Sun, X. Zhu, X. Li, et al., *Ultrathin NiCo-layered double hydroxide nanosheets arrays vertically grown on Ni foam as binder-free high-performance supercapacitors*, *Inorg. Chem. Commun.* 101 (2019) 125–129.

nickel–cobalt LDH nanosheets. They varied the ratio of Ni and Co to vary the interlamellar distance, structural characteristics, and electrochemical properties. A ratio of Ni and Co in 1:2 revealed a high specific capacitance of 3168.3 F g⁻¹ at a current density of 1 A g⁻¹. A one-step hydrothermal self-assembly was adopted to prepare 3D sea urchin structured Ni–Co LDH which demonstrated a capacity of 808.4 C g⁻¹ at a current density of 1 A g⁻¹ [60]. This improved efficiency is plausibly due to the increased surface area, porosity of the urchin-like LDHs, and the large interlamellar spacing. Further, the ASC device was fabricated with Ni–Co LDH as positive electrode and activated carbon as negative electrode and displayed a high energy density of 41.46 Wh kg⁻¹ at a power density of 212.68 W kg⁻¹ at 1 A g⁻¹. In a similar study that used a hydrothermal method for the synthesis of Ni–Co LDHs, they were grown on a diatomite biotemplate where the structural characteristics and properties are optimized by varying the Ni–Co ratios [61]. In this study it

is revealed that an increased proportion of nickel not only improves the performance efficiency of the biotemplate but also results in a change of morphology of Ni–Co LDHs from nanowires to nanosheets (Fig. 9.11). These composites demonstrated an outstanding specific capacitance of 514 F g^{-1} at 1 A g^{-1} . The ASC fabricated using the self-assembled nickel–cobalt LDH@diatomite@nickel foam//AG showed a high energy density of 56 Wh kg^{-1} at a current density of 1 A g^{-1} .

Another type of structural modification for Ni–Co LDH involves structural alteration of Ni–Co LDH to hollow microspheres. For instance, Li et al. [62] did structural alteration of Ni–Co LDHs to hollow microspheres. They are prepared via a coprecipitation method using SiO_2 microspheres as a sacrificial template. This structural assembly demonstrated a specific capacitance of 1766.4 F g^{-1} at current density of 1 A g^{-1} . Using this microsphere and activated carbon, the prepared hybrid supercapacitor gave a 44.3 Wh kg^{-1} energy density at a power

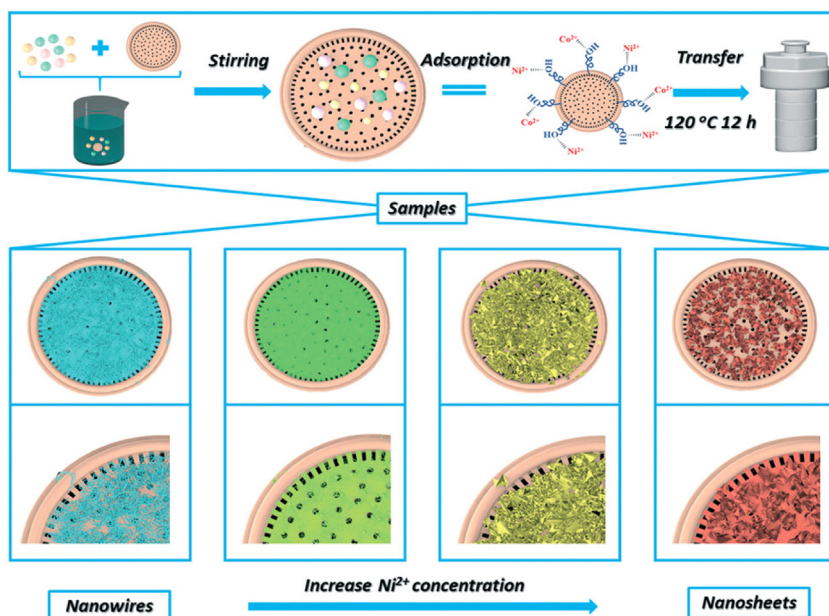


Figure 9.11 Schematic showing the fabrication process for the synthesis of nickel–cobalt LDH prepared on diatomite biotemplate. Reproduced from C. Jing, X. Liu, X. Liu, D. Jiang, B. Dong, F. Dong, et al., *Crystal morphology evolution of Ni–Co layered double hydroxide nanostructure towards high-performance biotemplate asymmetric supercapacitors*, *CrystEngComm* 20 (2018) 7428–7434.

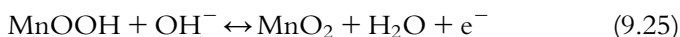
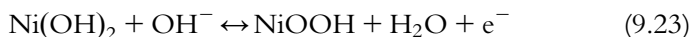
density of 0.425 kW kg^{-1} . A similar study conducted by Li and coworkers [63] dealt with the preparation of hollow nanostructured LDH nanosheets composed of multianions. This structure exhibited a large surface area and better properties. A xerogel of Ni–Co LDH is prepared by adopting a sol–gel route [64]. This assembly demonstrated a high specific capacity of 1170 C g^{-1} at a current density of 2 A g^{-1} . The ASC fabricated using this assembly demonstrated an increased energy density of 74.37 Wh kg^{-1} at 492 Wh kg^{-1} power density and maintained comparatively high energy density of 15.99 Wh kg^{-1} at a high power density of 6395 Wh kg^{-1} . Xing et al. [65] adopted a modified synthetic route to attain Ni–Co LDH. They have employed varying concentrations of ammonium fluoride to grow the nickel–cobalt LDHs on nickel foam with controlled surface morphology. This LDH exhibited an improved surface area and conductivity with a high electrochemical performance demonstrating a specific capacitance of 1445 F g^{-1} at 2 A g^{-1} .

Apart from the components and conductivity of the electrode materials, other factors that influence the efficiency of these electrode materials are crystallinity, morphology, surface area and conductivity of the mixed metal hydroxide LDHs. For instance, a highly crystalline structure exhibits high conductivity and cycling stability, whereas different morphologies of the LDH electrode such as nanosheets [66], nanowires [45], nanorods [67] etc. exhibit different electrochemical performances. The increased surface area, on the other hand, provides more active sites resulting in improved ionic diffusion and electron conduction which enhance the efficiency of the electrode.

9.4.2 Nickel–Manganese layered double heterostructures (Ni–Mn LDH)

Along with cobalt, manganese is also used in combination with nickel due to the reported effectiveness in terms of low cost, multiple oxidation states, and abundance [2]. Substituting cobalt(II) with manganese(II) will result in the better dispersion of nickel ions on the host layers resulting in the extensive use of nickel ions [68]. Moreover, similar to Ni–Co, Ni–Mn LDH also can undergo redox reactions. Thus along with Ni–Co LDH, Ni–Mn LDH is also receiving a lot of interest. In addition to the conventional coprecipitation and hydrothermal method, the reverse micelle method can also be adapted to attain Ni–Mn LDH nanosheets in the colloidal form [69].

The faradaic reaction during an energy storage mechanism for Ni–Mn electrodes when applied in supercapattery is explained as follows:



As Ni–Mn LDHs get dissolved in acidic medium, an alkaline medium is commonly used as an electrolyte for Ni–Mn electrode-based SCs. To improve the efficiency of Ni–Mn LDHs, it is often deposited/grown on conductive substrates.

Shi et al. [70] synthesized a honeycomb-like nickel–manganese LDH grafted on a carbon cloth (Fig. 9.12). They achieved a specific capacitance of 2239 F g^{-1} at a current density of 5 mA cm^{-2} . Elements forming Ni–Mn-LDH, that is, nickel and manganese both can provide richer ion for redox reactions in a similar way as other binary metal compounds. Zhang et al. [71] fabricated Ni–Mn-LDH@CuO/CF electrode with an extraordinary areal capacitance of 2430.8 F g^{-1} at current density of 0.8 A g^{-1} . They reported that the current intensity of Ni–Mn-LDH@CuO is much larger than individual Ni–Mn-LDH and CuO

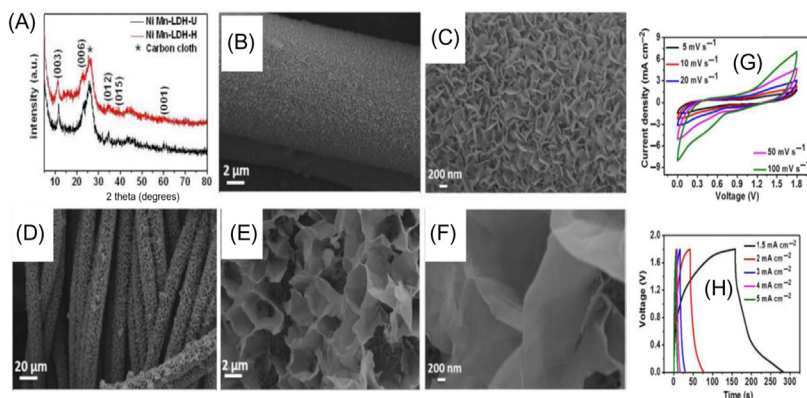


Figure 9.12 (A) XRD spectra obtained from Ni–Mn-LDH-H and Ni–Mn-LDH-U on carbon cloth; scanning electron microscope images of (B–C) Ni–Mn-LDH-U and (D–F) Ni–Mn-LDH-H. (G) Cyclic voltammety. (H) Galvanostatic charge–discharge curves of the device at different scan rates and current densities. *Reproduced from L. Shi, P. Sun, L. Du, R. Xu, H. He, S. Tan, et al., Flexible honeycomb-like NiMn layered double hydroxide/carbon cloth architecture for electrochemical energy storage, Mater. Lett. 175 (2016) 275–278.*

electrode under the same scan rates. Here Ni–Mn-LDH offers a higher surface area with an increased number of active sites for fast intercalation of electrolyte resulting in improved electrochemical kinetics. Cu, on the other hand, is used to deliver excellent electronic conductivity; hence by combining both, they achieved such a high-performance electrode. Lin et al. [72] prepared a three-dimensional $\text{CuCo}_2\text{S}_4@\text{NiMn-LDH}$ core-shell heterostructures on a nickel foam without using any organic binders. The resultant $\text{CuCo}_2\text{S}_4@\text{Ni-Mn-LDH}$ exhibited a high specific capacitance of 2520 F g^{-1} at 2 A g^{-1} .

For example, Yu and coworkers [73] prepared nickel–manganese LDH using a solvothermal procedure on nickel foam which exhibited a specific capacitance of 2703 F g^{-1} . In a similar work, Jingwen et al. [74] grew nickel–manganese LDHs on CNT support. This assembly showed a specific capacitance of 2960 F g^{-1} at 1.5 A g^{-1} . Wan and coworkers [75] studied the working efficiency of a flexible ASC prepared using the in situ grown nickel–manganese LDH arrays on a 3D graphene sponge which exhibited a high power density and energy density. Due to their structure, NiMn-LDH radically increases the contact area with electrolytes and provides more active points for reduction–oxidation reactions. The synergistic effect of Mn with Ni can highly improve the electrochemical activity of Ni in LDH.

9.4.3 Cobalt–Manganese (Co–Mn LDH) and Cobalt–Aluminum (Co–Al LDH) layered double hydroxides

Co–Mn LDH: As discussed already the oxides and hydroxides of cobalt (Co) demonstrate a considerably higher conductivity than those of nickel (Ni). In addition, environmental viability, cost-effectiveness, and good thermal conductivity also improve the attractiveness of cobalt to be used as an electrode material. This encourages researchers to widely focus on LDHs based on cobalt. One such combination is cobalt and manganese (Co–Mn LDH) owing to the unique redox combination of Co^{2+} and Mn^{2+} . However, there is still a limited number of research works going on in the field of LDH based on Co–Mn for supercapattery application. Ochai-Ejeh [76] prepared Co–Mn LDH nanoflakes via a solvothermal procedure. The device fabricated using this assembly showed a specific capacitance of 65 F g^{-1} with an energy density of 20.3 Wh Kg^{-1} at a current density of 0.5 A g^{-1} . To improve the performance efficiency of Co–Mn LDHs they are used in combination with other conductive materials such as carbon. For instance, Zhao et al. [77] grew Co–Mn

LDH on flexible carbon fibers using an in situ method and the SC fabricated using this electrode exhibited a high specific capacitance of 1079 F g^{-1} at a current density of 2.1 A g^{-1} . Further, Wang et al. [78] fabricated the Co–Mn LDH flakes on carbon cloth. This electrode demonstrated a specific capacitance of 633.4 F g^{-1} at 1 A g^{-1} . Apart from morphology, another prime factor in enhancing the performance is the interlayer spacing which is discussed previously. For example, Lui et al. [79] produced CoMn-LDH by using three different manganese solutions. A schematic representation is shown in Fig. 9.13. They used $\text{Mn}(\text{NO}_3)_2$, $\text{Mn}(\text{SO}_4)_4$, and MnCl_2 as a precursor and concluded that manganese sulfate possesses the highest interlayer spacing with enhanced electrochemical performance compare with the other two. Hence, it is also important to tailor the interlayer spacing of layered structures for the enhancement of energy storage properties.

Co–Al LDH: Another commonly studied cobalt-based LDH is cobalt–aluminum layered double heterostructures (Co–Al LDH). The first Co–Al LDH electrode for supercapacitor application was communicated by Wang and coworkers [80]. The synthesized Co–Al LDH nanosheets were deposited on to ITO and the electrodes demonstrated a specific capacitance of 667 F g^{-1} . Wang and coworkers also demonstrated

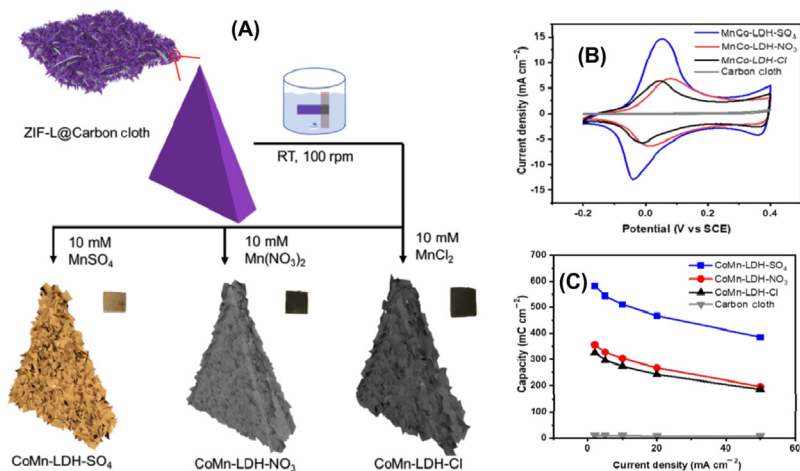


Figure 9.13 (A) Image representing the synthesis process for Co–Mn layered double hydroxides. (B) CV and specific capacity of Co–Mn LDHs. Reproduced from X. Liu, L. Zhang, X. Gao, C. Guan, Y. Hu, J. Wang, *Enlarged interlayer spacing in cobalt–manganese layered double hydroxide guiding transformation to layered structure for high supercapacitance*, *ACS Appl. Mater. Interfaces* 11 (2019) 23236–23243.

that the capacitance of the electrodes can be improved by changing the ratio between cobalt and aluminum to 3:1 [81]. In Co–Al LDH, the efficiency of the electrode is determined by the isomorphous substitution of cobalt ions by aluminum ions. Another parameter that determines the performance of the electrode is the maximum exploitation of Co sites in Co–Al LDH. Further, Guoxiang et al. [82] synthesized Co–Al LDH nanoflakes on nickel foam that exhibited a high specific capacitance of 930 F g^{-1} at 2 A g^{-1} with capacitance retention of 88.9%. The fabricated assembly showed an energy density of 44.6 Wh kg^{-1} with 799.6 W kg^{-1} power density (Fig. 9.14).

Dong and his coworkers [83] synthesized a multilayer film composed of cobalt–aluminum LDH nanosheets and graphene oxide via a layer-by-layer assembly which showed a specific capacitance of 880 F g^{-1} and areal capacitance of 70 F m^{-2} at a scan rate of 5 mV s^{-1} . They have also shown the plausible future application of the Co–Al LDH as electrodes for flexible supercapacitors by depositing the multilayer Co–Al LDH/GO nanosheets on

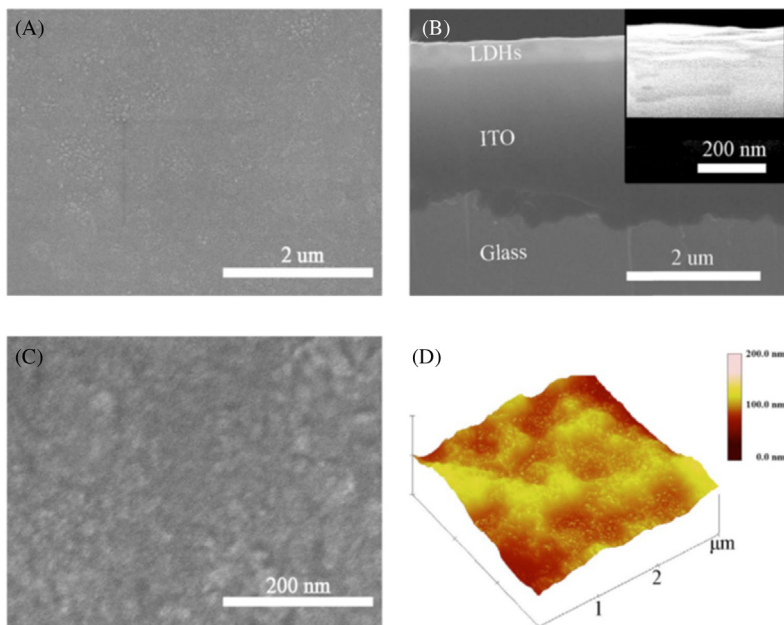


Figure 9.14 (A–C) FE-SEM. (D) AFM images of Co–Al LDHS. Reproduced from Y. Wang, W. Yang, J. Yang, A Co–Al layered double hydroxides nanosheets thin-film electrode: Fabrication and electrochemical study, *Electrochem. Solid-State Lett.* 10 (2007) A233–A236.

to a PET substrate. Further development in this field involves the assembly of Co–Al LDH in conjunction with other active materials such as nanowires or nanorods into different hierarchical 3D structures [2,84] which will be discussed in the later sections of this chapter.

9.5 Core–shell layered double hydroxides

Even though, LDH occupies a superior position in the energy storage world, like any other material it also has drawbacks such as inability to reach the theoretical capacity, aggregation of the active species, low electrical conductivity, and slow ion transfer rate that adversely affects the overall performance of the device itself [85,86]. These drawbacks can be overcome by altering the structural design to facilitate increased accessibility of active sites and electrochemical performance of LDHs. To attain this, efforts are being put greatly towards developing nanostructured LDH-based materials. It is well-known that nanostructures improve the properties of a material by providing improved surface area and the synergistic effects of its constituents when they are composed of multiple components. In the case of energy storage applications, nanostructures play a pivotal position in ion transport during the charging–discharging process. This directly affects the efficiency of the electrodes. The LDH-derived nanostructures can be generally categorized into four (Fig. 9.15); one-dimensional (1D) structure [87,88], 2D structure [89,90], 3D structures [91], and core–shell structures [32,92,93]. One-dimensional LDH structure is prepared by combining LDH with 1D substrates such as CNTs [87,88], nanowires [94], carbon nanofibers [95,96], etc., whereas 2D LDH is achieved by the use of a 2D substrate such as graphene [89,90]. 3D LDHs, on the other hand, are self-assembled structures, for instance, where LDH nanosheets are self-assembled into a 3D flower-like structure [91]. All the aforementioned hierarchical assemblies are a promising approach to ensure an increased efficiency when compared to the conventional LDH structure. However, the agglomeration of individual nanosheets in LDH still causes hindrance to the complete exploitation of LDH-based energy devices. The fourth category of LDH-derived nanostructures, the core–shell structures, offer an effective solution to increase the efficiency of LDH-based devices by the combinatorial properties of different pseudocapacitive materials. These structures are also proved to prevent the agglomeration of nanosheets in LDH, which is directly related

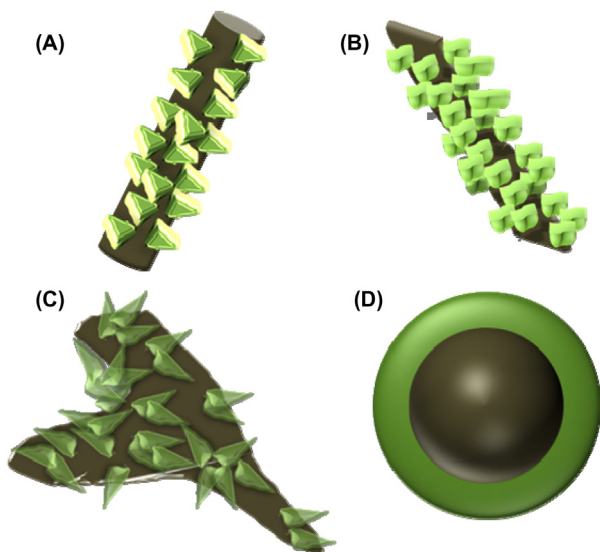


Figure 9.15 Representative images of different LDH-derived nanostructures: (A) 1D LDH; (B) 2D LDH; (C) 3D LDH; and (D) core-shell LDH.

to the accessibility of active sites, which in turn is directly proportional to the performance efficiency of the whole assembly.

Core-shell (core@shell), as the name indicates, is composed of a core which is surrounded by a shell material. A huge advantage of these structures is the ability to tune their properties and multifunctionalities by varying the composition, shape, and alignment/order of the building blocks. The most common type of core-shell LDHs is the one where a 1D material such as nanowires and nanorods is used as a core, which facilitates an effective pathway for transporting ions. The shell, in this case, is often a 2D material (LDH) due to which the core-shell structure possesses a larger surface area and increased number of electroactive sites. Moreover, by tuning the synthetic procedures one can tune the core-shell architecture to attain different hierarchical assemblies. Commonly discussed LDH-derived architectures/assemblies are shown in Fig. 9.16.

In core@LDH core-shell particles, the core is often comprised of SiO_2 , TiO_2 , Fe_3O_4 , and carbon. The synthetic pathway of the aforementioned structure does not vary much from the conventional synthesis routes used to prepare core-shell structures. This involves direct deposition, sol-gel method [32], and coprecipitation [92]. In the direct

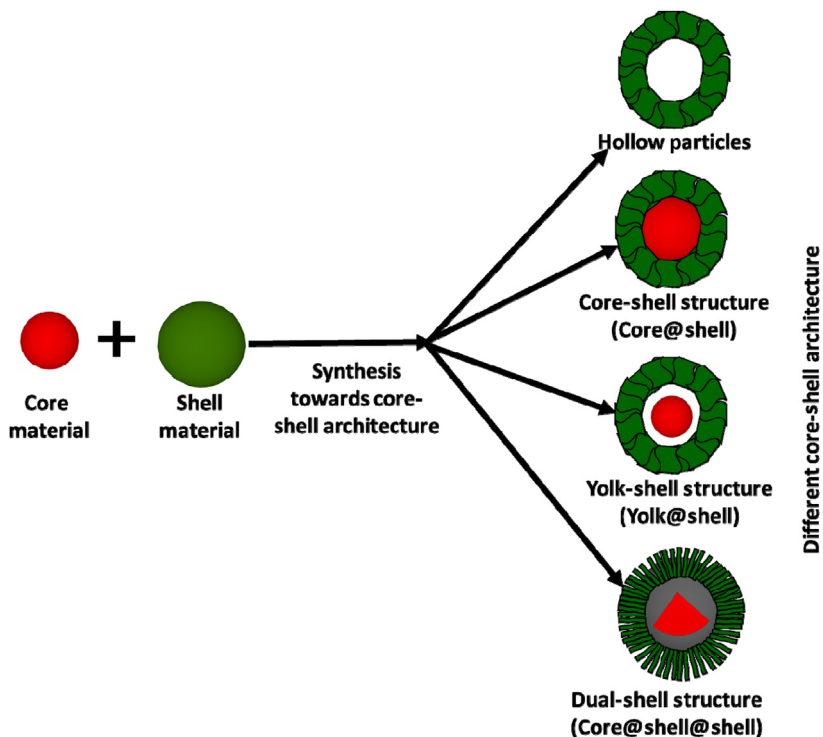


Figure 9.16 Schematic illustration of different LDH-derived core–shell architectures.

deposition, both the LDH and the core materials are synthesized separately and then combined to attain the required structure. The sol–gel method, on the contrary, involves the introduction of the core material to a primer solution which facilitates the formation of a double hydroxide layer on top of the core surface which will be further deposited with the desired LDH material. For instance, Tao et al. demonstrated a sol–gel route to synthesize nickel–cobalt double hydroxides microspheres (Ni/Co-DHM) core–shell particles by first dispersing the synthesized monodisperse silica spheres to AlOOH primer solution under vigorous stirring, followed by washing and drying. Repeated cycles of this procedure resulted in the formation of a layer-by-layer assembly of AlOOH on SiO₂ (SiO₂@AlOOH) particles which was later converted to Ni/Co-DHM by reacting the SiO₂–AlOOH with an alkaline solution containing Ni²⁺ and Co²⁺ ions via hydrothermal route. They have observed that the obtained structure possesses a 3D architecture with a hollow interior surrounded by a hedgehog-like shell which demonstrated an improved

faradaic redox reaction and mass transfer. This, in turn, improved the pseudocapacitance performance of the structure.

Coprecipitation is widely adopted as a synthesis route for the preparation of core–shell LDHs due to its ease of operation [92]. This method particularly involves the adsorption of metal cations on to the surface of the core followed by the crystal growth on the core which is initiated by the addition of a precipitating agent (e.g., base). Kwok et al. [92] adopted a similar route to attain core–shell $\text{SiO}_2@\text{Mg}_2\text{Al-CO}_3\text{-AMO-LDHs}$ by reacting magnesium and aluminum salts in the presence of a silica particle suspension in an alkaline medium at room temperature. This was followed by AMO treatment to attain the final core–shell LDH with the aforementioned structural composition which demonstrated superior properties. Irrespective of the synthesis routes, the properties of the resulting LDH-derived structures depend on the various synthetic parameters such as reaction temperature, pH, and aging temperature. Since the electrochemical performance efficiency of LDH-derived materials are directly related to their morphology, the microstructure, and degree of integration of the constituent materials, it is crucial to maintain a strict synthesis regime. Other methods also include simple hydrothermal synthesis, electrocatalysis, etc.

The work done by Liu et al. [93] has demonstrated the preparation of manganese cobalt-LDHs@Ni(OH)₂ core–shells on a conductive nickel foam via a two-stage hydrothermal process. Due to the presence of multiple components, the obtained structure demonstrated an increased specific capacitance in the range of 2320 F g^{-1} at a current density of 3 A g^{-1} and a capacitance of 1308 F g^{-1} at a high current density of 30 A g^{-1} with excellent cycling stability that paves the way toward the development of high energy, high power density supercapacitors.

The work done by Li et al. [97] dealt with the synthesis of a flower-like $\text{Fe}_3\text{O}_4@\text{C}@\text{LDH}$ structure (Fig. 9.17) by the combination of a hydrothermal and in situ growth process. They chose Fe_3O_4 as a core material owing to its high theoretical Li storage capacity. Even though Fe_3O_4 possesses a significant aerial capacity, it has limited application in energy storage because of its lower specific surface area and lower gravimetric capacitance. The authors have managed to overcome the existing drawbacks of the Fe_3O_4 electrode by employing the flower-like core–shell structure where the presence of a carbon coating significantly improves the surface area which facilitates more reactive locations for charge storage, improves chemical stability of the electrode material, and

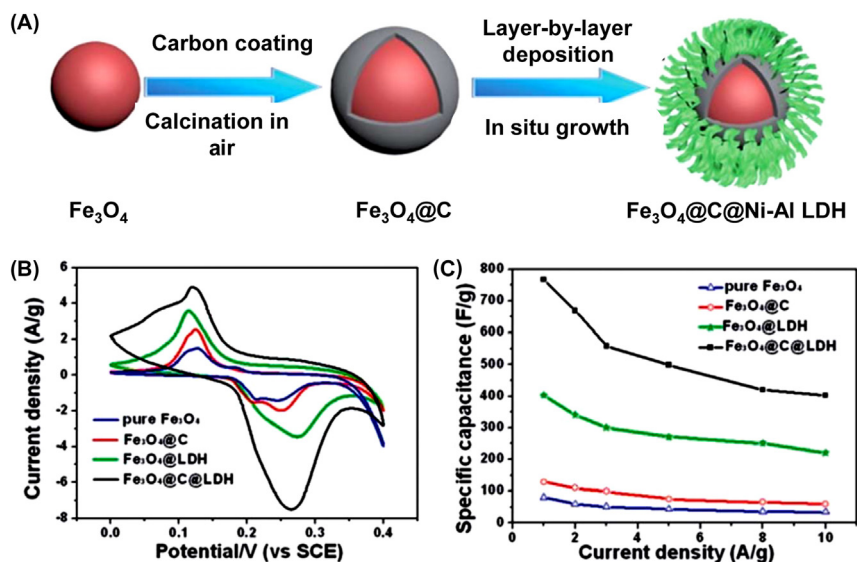


Figure 9.17 (A) Image showing the preparation of $\text{Fe}_3\text{O}_4@\text{C}@\text{Ni-Al-LDH}$ core–shells; (B) CV curve of the core–shell electrode; and (C) plots showing specific capacitance versus current density of the electrode. Reproduced from L. Li, R. Li, S. Gai, F. He, P. Yang, *Facile fabrication and electrochemical performance of flower-like $\text{Fe}_3\text{O}_4@\text{C}@\text{layered double hydroxide (LDH)}$ composite*, *J. Mater. Chem. A*, 2 (2014) 8758–8765.

enhances the electronic conductivity. In the meantime, the large specific surface area of Ni–Al double hydroxide layer further improved the pseudocapacitance by providing effective diffusion channels to the electrolyte. The porous nature of the hydroxide films acts as an ion reservoir. Thus the synergistic effect of multifunctional constituents of the core–shell resulted in an increased specific capacitance (767.6 F g^{-1}), improved cycling stability (92% after 1000 cycles), reduced resistance toward charge transfer and ion diffusion, and improved stability when compared to pure Fe_3O_4 or pure Fe_3O_4 -coated systems.

Zhao et al. [91] investigated the enhancement of supercapacitance properties of complex transition metal oxides, such as binary manganese cobalt oxide (MnCo_2O_4). Irrespective of their low specific capacitance and low operating voltage, these complex metal oxides exhibit better electrical conductivity and higher electrochemical activity, taking into account their single counterparts. To improve the properties of these metal oxides Zhao and coworkers developed a core–shell structure which is ordered in a nanoflower-like assembly where the MnCo_2O_4 is the core and a pseudocapacitive hydroxide, nickel hydroxide, is shell as shown in Fig. 9.18. This

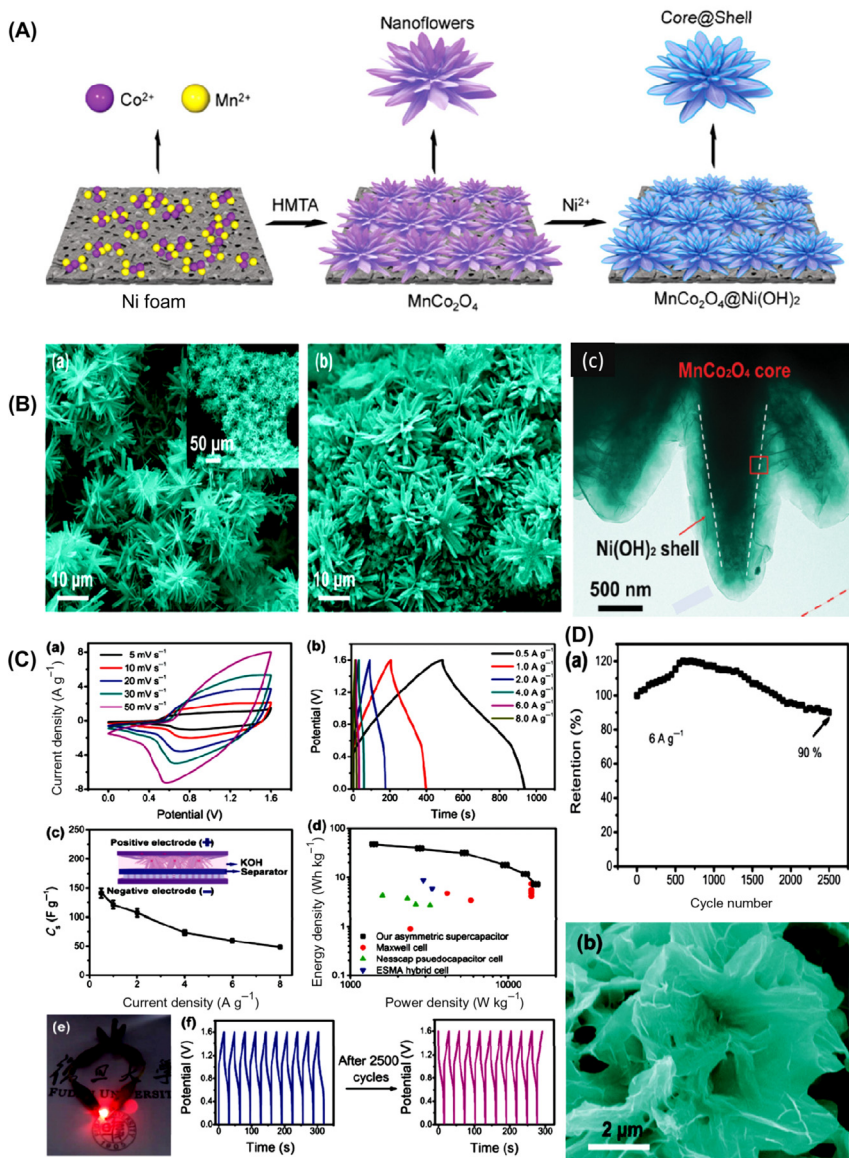


Figure 9.18 (A) Preparation of $\text{MnCo}_2\text{O}_4@Ni(\text{OH})_2$ nanoflowers. (B) (a) Scanning electron microscope image of MnCo_2O_4 belt-based nanoflowers, (b, c) Scanning electron microscope and transmission electron microscope images of $\text{MnCo}_2\text{O}_4@Ni(\text{OH})_2$ belt-based core-shell nanoflowers. (C) (a) CV curves of ASC at varying scan rates, (b) GCD curves, (c) C_s curves of ASC at varying current densities with inset depicting the ASC configuration, (d) Comparison Ragone plots of the fabricated ASC with other commercial supercapacitors, (e) Real-time performance showing the working of a red LED indicator using two supercapacitors connected in series, and (f) Cycle stability (first and last ten cycles) at 6 A g^{-1} current density. (D) (a) Cycling performance of ASC and (b) SEM image of the nanoflowers structure after 2500 charging/discharging cycles at 6 A g^{-1} . Reproduced from Y. Zhao, L. Hu, S. Zhao, L. Wu, Preparation of $\text{MnCo}_2\text{O}_4@Ni(\text{OH})_2$ core-shell flowers for asymmetric supercapacitor materials with ultrahigh specific capacitance, *Adv. Funct. Mater.* 26 (2016) 4085–4093.

unique assembly not only enables the structure to effectively utilize the synergistic properties of both the pseudocapacitive materials but also facilitate effective diffusion channels for the electrolyte ions to migrate during the charging/discharging process resulting in superior electrochemical performance with a specific capacitance of 2154 F g^{-1} at current density of 5 A g^{-1} [91].

The ASC devised using the aforementioned assembly demonstrated superior electrochemical performance for the energy density of 48 Wh Kg^{-1} at 1.4 kW kg^{-1} and a power density of 14.9 kW kg^{-1} at 7.26 Wh kg^{-1} . In addition to enhanced electrochemical performance, the device showed improved stability with a 90% capacitance retention even after 2500 cycles with a stable structural morphology (Fig. 9.18D) [91].

In a study conducted by Liang and coworkers [98], they have developed a core–hybrid structure constituting two hydroxides, nickel–cobalt LDHs nanowires, and nickel hydroxide nanosheets, using a carbon cloth fiber substrate (Fig. 9.19A). Owing to their synergistic properties, the

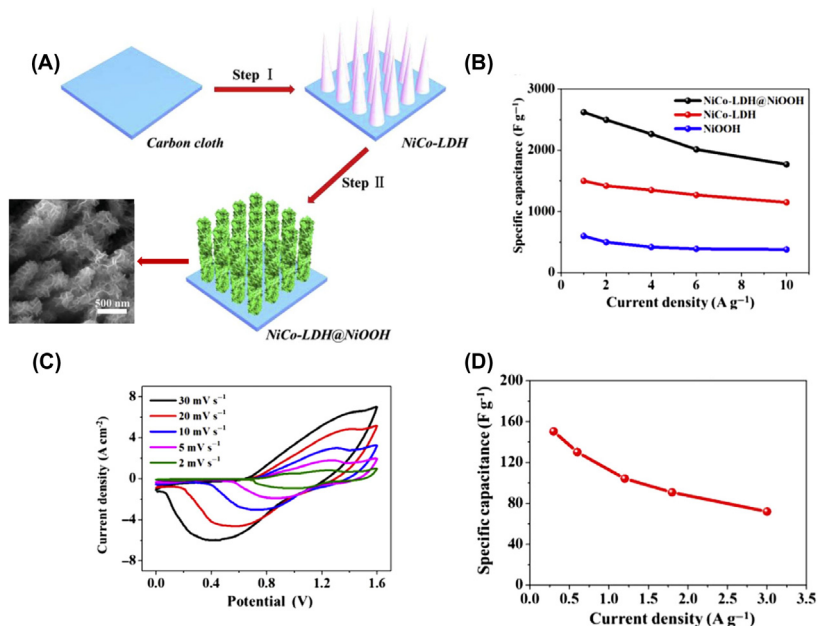


Figure 9.19 (A) Image representing the synthesis of NiCo-LDH@NiOOH core–shell heterostructures and the corresponding SEM image. (B) Specific capacitance of nickel–cobalt LDHs@NiOOH, nickel–cobalt-LDHs, and nickel hydroxide under varying current densities. (C) CV of NiCo-LDH@NiOOH//AC ASC. (D) Specific capacitance of the fabricated ASC. Reproduced from H. Liang, J. Lin, H. Jia, S. Chen, J. Qi, J. Cao, et al., Hierarchical NiCo-LDH@NiOOH core–shell heterostructure on carbon fiber cloth as battery-like electrode for supercapacitor, *J. Power Sources* 378 (2018) 248–254.

obtained electrode exhibited superior properties in terms of high specific capacitance (2622 F g^{-1} at 1 A g^{-1} current density; Fig. 9.19B), cycle stability and capacitance retention (88.5%). The ASC (Fig. 9.19C) fabricated using the aforementioned assembly exhibited a high specific capacitance (Fig. 9.19D) and high energy density and power density.

Li et al. [99] developed a combination of $(\text{Ni},\text{Co})\text{Se}_2/\text{NiCo-LDH}$ core–shells which can be used potentially as ASCs. In this, they have developed a $(\text{Ni},\text{Co})\text{Se}_2$ core which possesses a cactus-like structure with NiCo-LDH as a shell. They have found that the unique cactus-like structure enabled the electrode to possess a high capacity (1224 F g^{-1}), good performance rate, and extended stability. This study paves the way toward fabrication of advanced storage electrodes including electrodes for flexible ASCs (Fig. 9.20A–B). The ASC fabricated using the $(\text{Ni},\text{Co})\text{Se}_2/\text{NiCo-LDH}/\text{PC}$ exhibited a high energy density of 39 Wh kg^{-1} and a power density of 1650 W kg^{-1} at 1.65 V with a 90% capacitance retention after 3000 cycles.

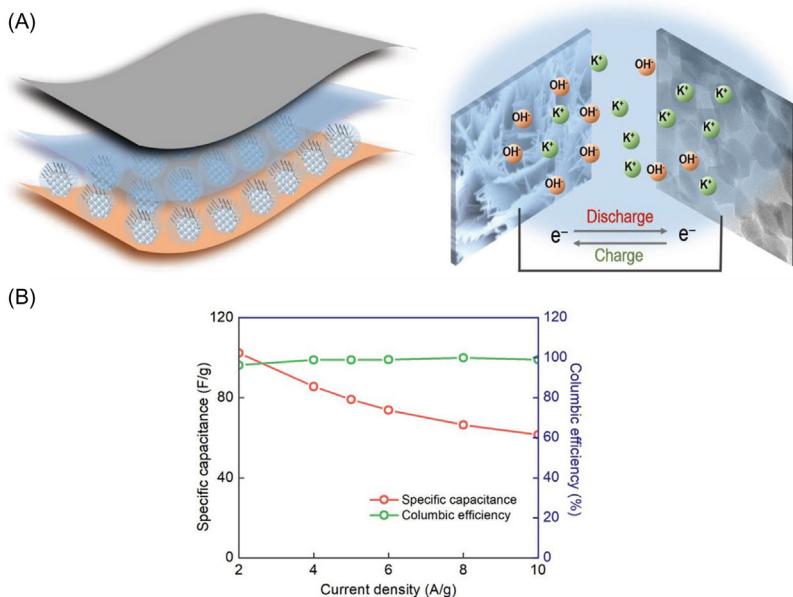


Figure 9.20 (A) Schematic illustration showing the ASC assembly prepared using $(\text{Ni},\text{Co})\text{Se}_2/\text{NiCo-LDH}$ arrays grown on carbon cloth (positive electrode) and ZIF-derived porous carbon (cathode). (B) Curve showing specific capacitance and coulombic efficiency. Reprinted from X. Li, H. Wu, C. Guan, A.M. Elshahawy, Y. Dong, S.J. Pennycook, et al., $(\text{Ni},\text{Co})\text{Se}_2/\text{NiCo-LDH}$ core/shell structural electrode with the cactus-like $(\text{Ni},\text{Co})\text{Se}_2$ core for asymmetric supercapacitors, *Small* 15 (2019) 1803895.

Chen et al. [100] have synthesized a $\text{NiCo}_2\text{O}_4@\text{Co-Fe LDHs}$ core-shell nanowires arranged on nickel foam via hydrothermal and calcination methods. This structure demonstrated an improved specific capacitance of 1557.5 F g^{-1} and the devised two-electrode hybrid device ($\text{NiCo}_2\text{O}_4@\text{Co-Fe LDH}/\text{activated carbon}$) exhibited an energy density of 28.94 Wh kg^{-1} with a power density of 950 W kg^{-1} . In a similar study done by Zhang et al. [101], they developed a 3D heterostructured $\text{Co}_3\text{O}_4@\text{LDH}$ nanowire core-shell electrode grown on nickel foam (Fig. 9.21). The synergistic properties of the individual components showed superior properties. They have devised a hybrid supercapacitor (HSC) using the aforementioned structure as a positive electrode and

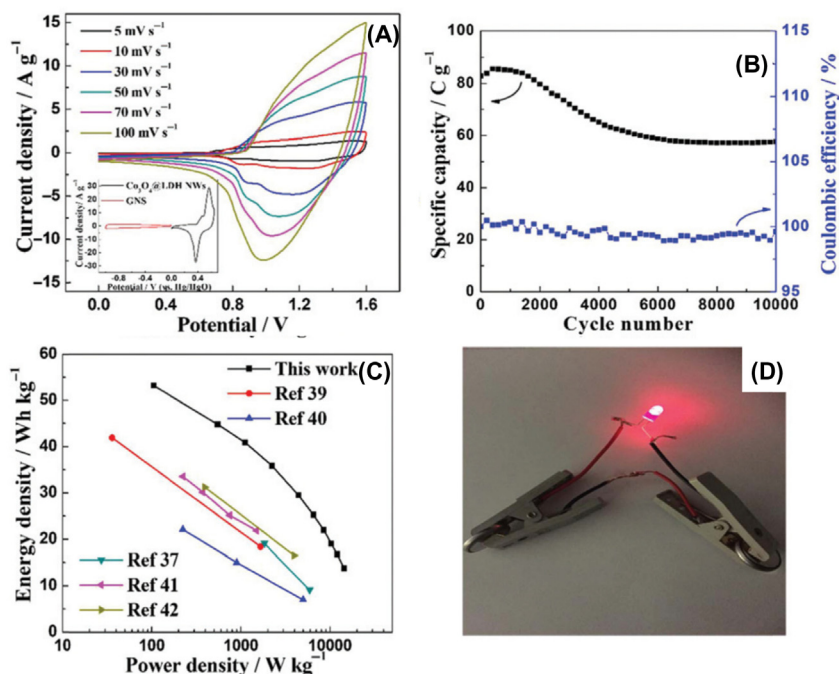


Figure 9.21 (A) CV for the $\text{Co}_3\text{O}_4@\text{LDH}/\text{GNS}$ hybrid supercapacitor device (inset: CV profiles of $\text{Co}_3\text{O}_4@\text{LDH}$ and GNS at 5 mV s^{-1}). (B) Curve showing the charging/discharging cycles of the HSC at 6 A g^{-1} at 10,000 cycles. (C) Ragone plot for the hybrid supercapacitor showing energy density vs. power density at different charge/discharge rates. (D) Real-time working of an HSC. Reproduced from L. Zhang, K.N. Hui, K.S. Hui, S.W. Or, 3D heterostructured cobalt oxide@layered double hydroxide core-shell networks on nickel foam for high-performance hybrid supercapacitor, Dalton Trans. 48 (2019) 150–157.

graphene nanosheets as a negative electrode. This assembly showed an energy density of 53.2 Wh kg^{-1} and a power density of 16.4 kW kg^{-1} .

Zhao and coworkers [102] prepared $\text{Co}_3\text{O}_4@\text{CoNi-LDH}$ core/shell nanosheet array on Ni foam as a battery-type electrode. Here Co_3O_4 acted as the core and CoNi acted as the shell which exhibited a specific capacitance of 2676.9 F g^{-1} at 0.5 A g^{-1} . The synergic effect of the core and shell structure is an effective method to minimize the hurdles involved in LDHs. This combines the inimitable characteristics of various components resulting in improved surface area and capacitance. Li et al. [103] fabricated a $\text{CuO}@\text{LDH}$ core-shell nanowire array on a gracile copper wire substrate via a three-step procedure. The hierarchical structure of LDH shell enables the effective revelation of surface active sites for faradaic redox reaction and therefore benefits the interfacial charge transport. Zhou et al. [104] designed a 3D hierarchical carbon cloth@ $\text{CoMoO}_4@\text{NiCo-LDH}$ core-shell nanowire arrays supported specific capacitance of 2024 F g^{-1} at 1 A g^{-1} . The mesoporous structure of LDH helps as an ion-buffering reservoir to accommodate volume variation during charge-discharge processes. The ASC delivered a maximum energy density of 59.5 Wh kg^{-1} at a power density of 800 W kg^{-1} . Liang et al. [98] fabricated a $\text{NiCo-LDH}@\text{NiOOH}//\text{AC}$ device that resulted in a high energy density of 51.7 Wh kg^{-1} while the power density is 599 W kg^{-1} . They have grown nickel-cobalt LDHs nanowires directly eliminating the binders and additives, resulting in good electrical interaction between material and substrate.

Apart from transition metal complexes and simple metal oxide, polymers are also used as an electroactive material in developing LDH-derived core-shell structures. Among the many conductive polymers, polyaniline (PANI) is generally employed in energy-related applications due to its pseudocapacitive characteristics, such as high conductivity, good chemical stability, and reversible redox behavior [86]. Even though PANI is a promising source of electroactive material in energy storage applications, its poor cycle life and mechanical properties limit wide use in electrochemical applications. The work done by Ge et al. [86] demonstrated an effective way to overcome the drawbacks of PANI by combining it with LDHs and developing a hybrid core-shell structure via in situ polymerization and electrodeposition. This assembly comprises a PANI nanofiber core and a nickel-cobalt LDHs nanosheets shell on carbon cloth as shown in Fig. 9.22.

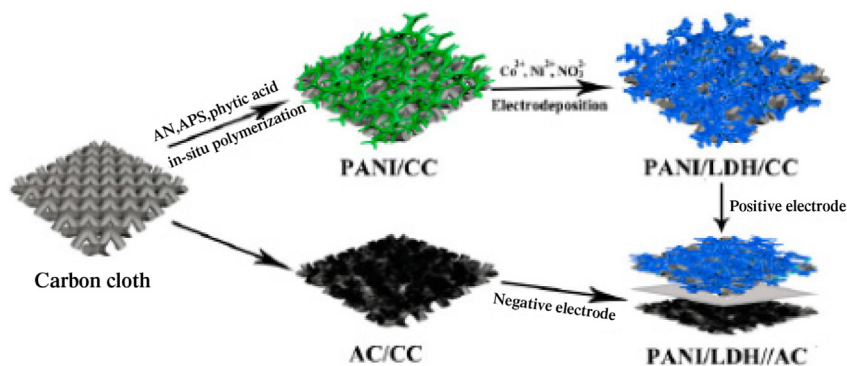


Figure 9.22 Step by step representation showing the synthetic route of polyaniline/layered double hydroxides/carbon cloth core–shell structures and ASCs. *Reproduced from X. Ge, Y. He, T. Plachy, N. Kazantseva, P. Saha, Q. Cheng, Hierarchical PANI/NiCo-LDH core–shell composite networks on carbon cloth for high performance asymmetric supercapacitor, Nanomaterials 9 (2019) 527.*

The conductive PANI fibers in the form of a 3D network provide enough surface area for the deposition of NiCo-LDHs. The porous channels in the network not only act as electrolyte reservoirs which shorten the electron–electrolyte ion transport distance but also facilitate easy diffusion channels for the electrolyte to access the active sites resulting in an accelerated redox reaction. In their work Ge et al. [86] employed this unique structure to develop an ASC which demonstrated an improved specific capacitance (147.2 F g^{-1}), an improved energy density of 46.0 Wh kg^{-1} at 351.6 W kg^{-1} power density, and good rate capability with enhanced capacitance retention.

In addition to the multifunctionalities a core–shell LDH can possess, tunable interior architecture is one of its salient features. For example, different structural designs, varying from hollow particles to yolk–shell nanostructures, can be architected using a core–shell particle by varying the synthetic parameters (Fig. 9.23). The work done by Shao et al. [105] demonstrates the fine-tuning of the interior design of a core–shell to obtain different hybrid structures. They have synthesized a core–shell LDH with SiO_2 as the core and Ni–Al-LDH as the shell via the sol–gel technique followed by in situ growth (as mentioned at the beginning of this section). The interior structure of the $\text{SiO}_2@\text{AlOOH}$ microspheres was tuned by varying the pH of the reaction media during the in situ growth of the LDH. The obtained particles showed different internal

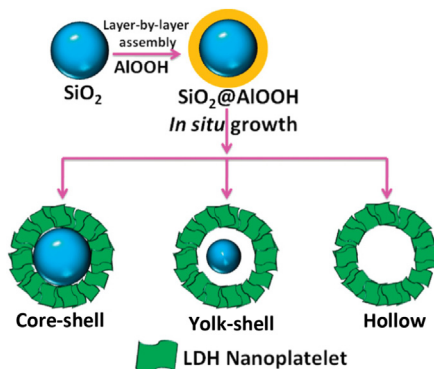


Figure 9.23 Synthesis of layered double hydroxides microspheres with variable structural morphologies. Reprinted from M. Shao, F. Ning, Y. Zhao, J. Zhao, M. Wei, D.G. Evans, et al., Core-shell layered double hydroxide microspheres with tunable interior architecture for supercapacitors, *Chem. Mater.* 24 (2012) 1192–1197.

morphologies such as core-shell particles, yolk-shell particles, and hollow particles, as shown in Fig. 9.23. When compared to the core-shell and yolk-shell particles obtained, the hollow particles showed an outstanding pseudocapacitance. This improved pseudocapacitance can be directly ascribed to the improved surface area and improved mesoporosity present in the hollow shell which in turn improves the faradaic redox reactions and mass transfer of electrolytes.

Thus it is evident that hierarchical structures such as core-shells due to the amalgamated properties of its individual components exhibit superior properties which lead to the overall increase of performance efficiency in terms of electrochemical storage devices. This property enhancement makes these structures an unavoidable topic in LDH-derived assemblies. However, it is not easy to list all the structural assemblies in this direction. Therefore the authors have carefully picked unique structural assemblies to give a brief idea about the broad topic under discussion. A detailed description of similar hierarchical structural assemblies is currently beyond the scope of this chapter and will be discussed elsewhere.

9.6 Carbon material/layered double hydroxide composites for supercapattery

Carbon is the most abundant material in nature, and is easily recovered from several accessible sources such as landscape, industries, transports, biomass, and coal. Hence, carbon materials are employed in the fabrication of low-cost electrodes for energy device applications. All carbons do not have

similar physicochemical properties due to their variation on the structural arrangement of a carbon atom, for example, diamond and graphite. Diamond has a sigma bond between sp^3 hybridized carbon atom, where all carbons are involved for bonding and there are no free electrons, but in graphite (layered structure) each carbon atom (sp^2 hybridization) is bonded with three other carbons and has one free electron, which is responsible for the good conductivity. In this aspect, nanotechnology has developed pioneering research on carbon materials via the creation of carbon with multidimensions. Among these, 1D (CNTs) and 2D (graphene) have played an important role in energy storage devices owing to their large surface area, excellent electrical conductivity, feasible tunability, good mechanical stability, and efficient electrochemical activity. Both CNTs and graphene-based electrodes and their electrochemical performance are explained in this section.

a. Carbon nanotubes/Layered double hydroxides

CNTs or 1D carbon comprises a cylindrical structure with length and diameter in the range of a few microns and nanometer scales. CNTs are particularly divided into single-walled (SW), double-walled (DW), and multiwalled (MW) corresponding to several graphene sheets. The very first CNTs were discovered by Iijima in 1991 [106]. CNTs possess sp^2 bonded carbon atoms of graphene with a hexagonal lattice structure, that exhibits good electrical and thermal conductivities with excellent mechanical and chemical stabilities [107]. In terms of electrical conductivity, MWCNTs have metallic behavior and SWCNTs possess the behavior of both metal and semiconductors with respect to their chirality and diameter size. As synthesized CTNs exhibit a high specific surface area of $1600 \text{ m}^2 \text{ g}^{-1}$ and a good carrier mobility of $15,000 \text{ cm}^2 \text{ Vs}^{-1}$ (both ions and holes) [108]. The porous structure of CTNs provides an easy pathway for ion transportation between electrolytes and electrodes in electrochemical energy storage applications. An et al. reported a specific capacitance of CNTs of around 180 F g^{-1} with an energy and power densities of 7 Wh Kg^{-1} and 20 kW Kg^{-1} [109]. Hate et al. reported CNTs using $1 \text{ M Et}_4\text{NBF}_4$ /propylene carbonate (organic) electrolyte possessing a voltage of 4 V and an energy density of 94 Wh Kg^{-1} at the power density of 210 kW Kg^{-1} [110]. Further, CNTs are considered to be a filler to be used in composites to enhance electrical conductivity. Zhao et al. developed nickel–manganese LDH by directly developing nickel–manganese LDHs nanosheets onto the exterior of CNT and achieved a high specific capacitance of 2960 F g^{-1} at 1.5 A g^{-1} and excellent cycling performance [74]. Wang and coworkers [111] developed hierarchical nickel–aluminum

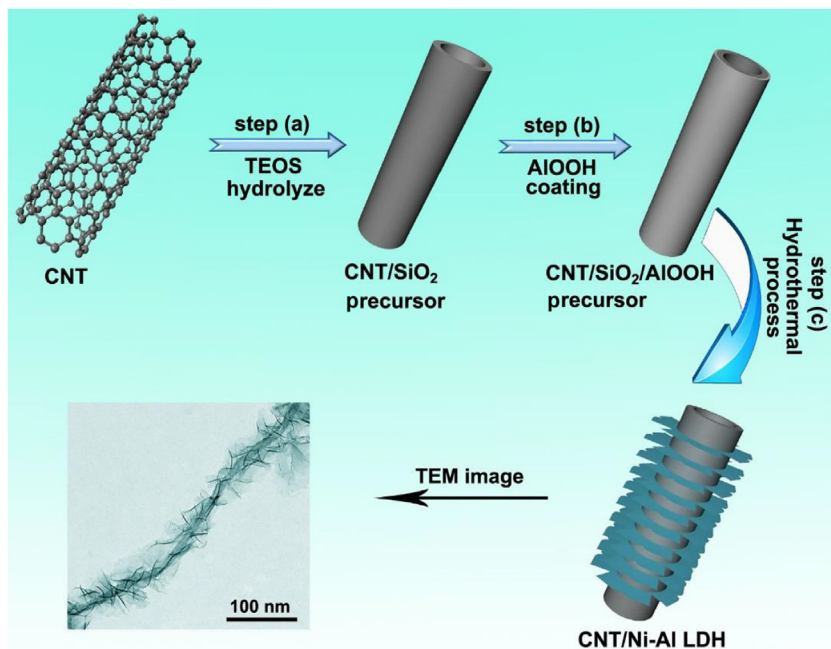


Figure 9.24 Schematic representation for the step-by-step growth of nickel–aluminum layered double hydroxide composite. Reproduced from Y. Wang, Z. Chen, H. Li, J. Zhang, X. Yan, K. Jiang, et al., *The synthesis and electrochemical performance of core–shell structured Ni–Al layered double hydroxide/carbon nanotubes composites*, *Electrochim. Acta* 222 (2016) 185–193.

LDHs CNTs by the hydrothermal method (Fig. 9.24). CNTs functioned as backbones in this design to form a 3D core–shell nanostructure with a high electrochemical performance of 1017 C g^{-1} .

Yu et al. explained the sandwich structured chemically modified CNTs between exfoliated Co–Al LDH nanosheets via electrostatic assembly. CNTs provide a wide contact area of the composite electrode with the electrolyte and also admirable conductivity. The as-synthesized composite electrode demonstrated a specific capacitance of 884 F g^{-1} with cyclic retention of about 88% after 2000 cycles [112]. Li et al. reported a composite Ni–Al LDH and CNTs electrode synthesized by a simple solution method (Fig. 9.25). EDLC behavior of CNTs dramatically support the electrical conductivity and reduce the electrochemical polarization. A binary composite demonstrated a specific capacitance of 1500 F g^{-1} at a current density of 1 A g^{-1} . The as-prepared electrode was used as the anode and activated carbon as a cathode in an ASC, which

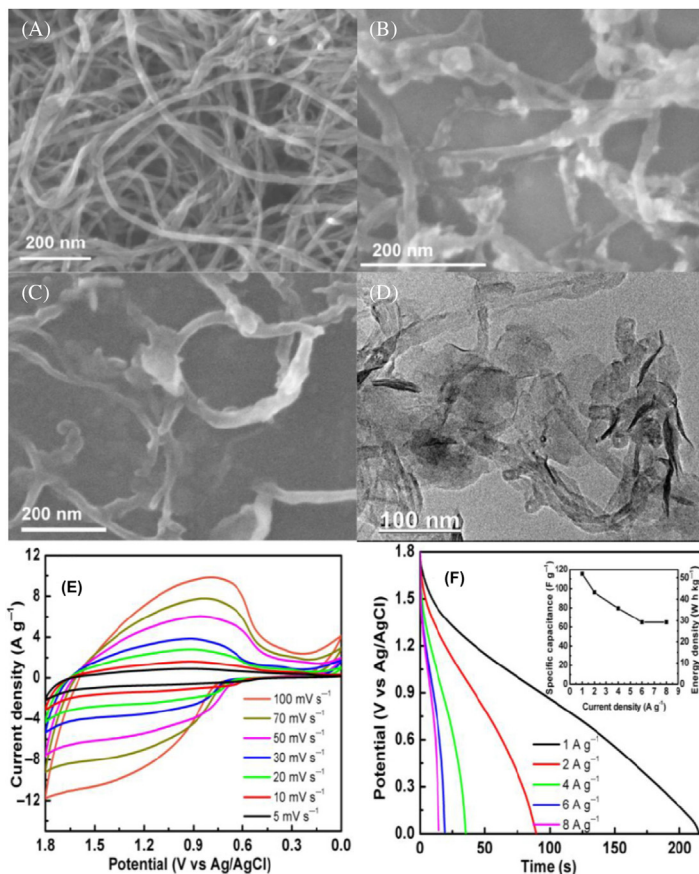


Figure 9.25 Scanning electron microscope images of (A) acid-treated CNTs, (B) $\text{Al}_2\text{O}_3/\text{CNTs}$, (C) Ni–Al-LDHs/CNTs, and (D) transmission electron microscope image of Ni–Al-LDHs/CNTs. (E) CV and (F) discharging profiles of Ni–Al-LDHs/CNT//SC. Inset shows the specific capacitance and energy density of the full cell. *Reproduced from M. Li, F. Liu, J.P. Cheng, J. Ying, X.B. Zhang, Enhanced performance of nickel–aluminum layered double hydroxide nanosheets/carbon nanotubes composite for supercapacitor and asymmetric capacitor, J. Alloy. Compd. 635 (2015) 225–232.*

exhibited a potential window of about 1.8 V with appropriate energy density (52 Wh Kg^{-1}) and excellent cyclic stability [113]. Niu et al. fabricated an ASC using porous Ni–Co LDH nanosheets on CNTs and nitrogen-doped carbon nanosheets as positive and negative electrodes. The device revealed a maximum energy and power densities of 37.4 Wh Kg^{-1} and 750 W Kg^{-1} , respectively, and also excellent cyclic retention of around 94.5% after 5000 cycles [114]. Yang et al. reported an

interesting work on a 3D architecture-based ternary composite of flower-like Ni–Al LDH intercalated CNTs which were self-assembled on graphene nanosheets, providing an increased specific capacitance of 1562 F g^{-1} and outstanding cyclic retention [115].

b. Graphene/Layered double hydroxides

Graphene is considered a well-known 2D layer and all carbons are arranged in a honeycomb structure. A monolayer of graphene sheet possesses a large theoretical surface area of $2620 \text{ m}^2 \text{ g}^{-1}$, the high mechanical strength of $\sim 1 \text{ TPa}$. Graphene is widely used for electrochemical energy storage systems owing to its unique benefits of admirable physicochemical properties and excellent cyclic and rate capability. Graphene is synthesized via two ways: (1) mechanical exfoliation and (2) chemical method. Of the above two methods, the chemical method is widely used to synthesize graphene via graphene oxide mediation. A first chemical method (Hummer's method) was developed in 1958 as a very safe, easy, faster, and more efficient method to produce graphite oxide. Later in 2004 (after the discovery of single-layer graphene), most of the researchers turned toward single-layer graphene from graphite due to the superior characteristics (physicochemical properties) and performance of graphene. Therefore the same method has been slightly modified to produce graphene oxide via the addition of persulfate and an exfoliation process, called the modified Hummer's method [116]. A synthesized graphene oxide is composed of a multitude of oxygenic functional groups such as hydroxyl and carboxyl group. This makes graphene oxide suitable for efficient photocatalytic or chemical catalytic application but not for energy storage due to its poor electrochemical conductivity. This can be overcome by reducing the graphene oxide using a strong reducing agent (hydrazine or any other reducing agent) to produce chemical-derived graphene (reduced graphene oxide—rGO), which possesses high electrical and electrochemical conductivity [117]. However, rGO or graphene sheets exhibit a major drawback of quick restacking or agglomeration of single layers to form graphite due to the effect of van der Waals interactions between adjacent sheets. This leads to severely reduced coulombic efficiency [117]. These issues can be overcome by introducing supporting materials with graphene sheet-like metal oxide, conducting polymers, metal sulfides, layer double hydroxides, etc. Amongst these, graphene-LDH has received significant attention in terms of performance efficiency owing to the combined effect of both graphene and LDH.

LDHs and graphene show exceptional electrochemical properties that are closely complementary with each other. Hence combining LDH with

graphene can enhance the electrochemical performance. Yan and coworkers noted the preparation of LDHs/graphene nanocomposites using a layer-by-layer self-assembly technique. Initially, the substrate was modified with a polymer poly(diallyl dimethylammonium chloride) (PDDA). The treated substrate was then dipped in graphene oxide, deionized water, and LDH solutions, followed by rinsing in DI water which resulted in a nacre-like LDH–graphene nanocomposite [118]. Wang and coworkers [89] prepared nickel–aluminum LDHs/graphene composites which prevented the agglomeration of LDH and graphene nanosheet. This provided an unrestricted pathway for hydrated ions to the interior surface, which is more helpful to improve the exploitation of active materials for improved efficiency of the supercapacitor. Memon et al. [119] and Cai et al. [26] prepared LDHs/graphene composites with urea as a basic source. Urea could induce slow nucleation of OH^- ions and the growth of LDHs during the hydrothermal process. Dong et al. designed multilayer films of cobalt–aluminum LDHs nanosheets and graphene oxide and found that specific capacitance per unit surface area increased linearly with the increase of layer number [83]. In LDHs/graphene composites, graphene helps to improve the conductivity and LDH renders agglomeration of excess graphene in the composite (Fig. 9.26). The synergetic effects enhance the specific capacitance. For example, Wu and coworkers prepared a porous cobalt–aluminum LDHs/graphene film with a specific capacitance of 1043 F g^{-1} at 1 A g^{-1} [120]. Porosity may tremendously increase the ionic transportation in CoAl-LDH/graphene films.

Xu and coworkers reported a simple in situ vertical growth of nickel–aluminum LDHs nanosheets on the surface of graphene to build a hierarchical hybrid composite using aluminum hydroxide colloids as an aluminum source [121]. The hierarchical 3D nanocomposite with sandwich structure has a specific surface area of $184.7 \text{ m}^2 \text{ g}^{-1}$, achieving a specific capacitance of 1329 F g^{-1} at a current density of 3.57 A g^{-1} [121]. Jiang et al. studied nickel–cobalt-loaded carbon fiber covered with mesoporous NiMoO_4 nanosheet when intercalated with graphene oxide as a sandwich flexible electrode material. The aforementioned structure demonstrated good electrochemical performance with a specific capacitance of 2100 F g^{-1} at a current density of 1 A g^{-1} and capacitance was retained at about 91% after 5000 cycles. Carbon fiber/Ni–Co LDH@ NiMoO_4 /GO as the positive electrode and activated carbon as the negative electrode was assembled as an ASC and exhibited high energy density of 538.3 Wh Kg^{-1} at a power density of 2.522 kW kg^{-1} with a cell voltage about 1.6 V and

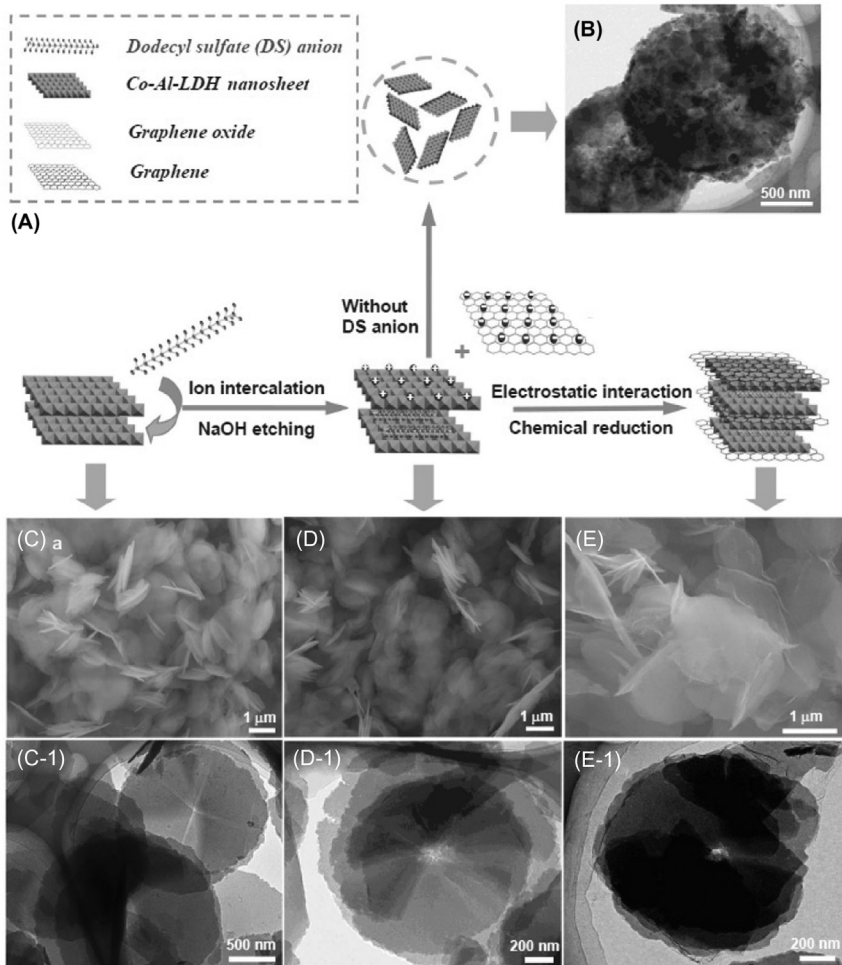


Figure 9.26 Image showing the formation process and structure of layered double hydroxides/graphene composite with an increased amount mesopores through a dual support system. (B) Scanning electron and transmission electron microscope images of P-LDH, (C, C-1) LDH, (D, D-1) SP-LDH, and (E, E-1) GSP-LDH. *Reproduced from X. Wu, L. Jiang, C. Long, T. Wei, Z. Fan, Energy Storage: Dual support system ensuring porous Co–Al hydroxide nanosheets with ultrahigh rate performance and high energy density for supercapacitors, Adv. Funct. Mater. 25 (2015) 1648–1655.*

cyclic retention of 80.3% up to 5000 cycles [122]. Li and coworkers reported a solid-phase exfoliation method for the exfoliation of Co–Al LDH, followed by intercalation with GO nanosheet. The entire composite was reduced into Co–Al LDH/rGO nanocomposite. The obtained composite provides a specific capacitance of 1492 F g^{-1} at 1 A g^{-1} and

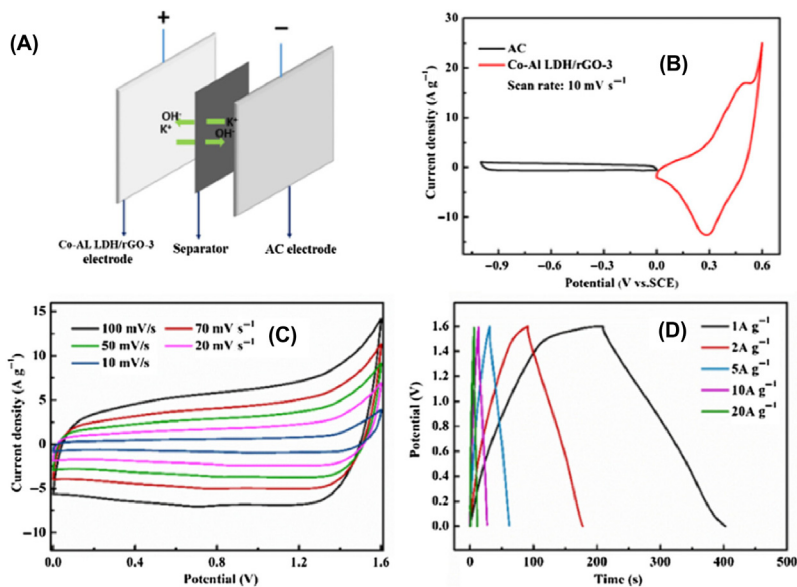


Figure 9.27 (A) Schematic representation of the Co–Al LDH/rGO-3//AC ASC; (B) CV profiles of electrodes in the three-electrode system at a scan rate of 10 mV s^{-1} ; (C) cyclic voltammetry; and (D) galvanostatic charge–discharge curves at various scanning rates and current densities. Reproduced from J. Li, P. Zhang, X. Zhao, L. Chen, J. Shen, M. Li, et al., Structure-controlled Co–Al layered double hydroxides/reduced graphene oxide nanomaterials based on solid-phase exfoliation technique for supercapacitors, *J. Colloid Interface Sci.* 549 (2019) 236–245.

capacitance retention of 94.3% after 5000 cycles with an energy density of 44.6 Wh Kg^{-1} at a power density of 799.6 W Kg^{-1} [Fig. 9.27] [123]. Bandyopadhyay et al. reported proton-functionalized graphitic carbon nitride modified graphene/Ni–Al LDH and 3D protonated graphitic carbon nitride-functionalized graphene as the positive and negative electrodes, and KOH/PVA gel was used as an electrolyte to assemble an asymmetric device. There was a cell potential window of 1.6 V with an excellent cyclic life of 91% after 7000 cycles [124]. Wang et al. described hydrothermally prepared Ni–Fe–LDH/rGO/carbon fibers as an electrode for a supercapacitor. It exhibited an improved specific capacitance of 1330.2 F g^{-1} at 1 A g^{-1} . Further, it was used as the positive electrode and activated carbon as the negative electrode to assemble an ASC. The device exhibited a high energy density of 33.7 Wh Kg^{-1} at a power density of 785.8 W Kg^{-1} and cyclic stability of around 97.1% of the initial capacitance after 2500 cycles [125]. Shahrokhian and coworkers reported Ni–Co LDH/rGO on nickel foam

synthesized via a two-step electrochemical method, where CTAB was a cationic surfactant. It exhibited a specific capacitance of 2133.3 F g^{-1} at a current density of 4 A g^{-1} [126]. Wang and his coworkers reported that the one-pot hydrothermal method of vertically aligned Co–Ni LDH and rGO sheet on carbon cloth exhibited excellent electrochemical performance with the addition of rGO. A fabricated symmetric device achieved an energy density of 30.29 Wh Kg^{-1} at a power density of 1500 W Kg^{-1} with remarkable cyclic retention after 3000 cycles [127]. Therefore the rGO and CNTs intercalated LDH provides an outstanding energy and power density with longer cyclic stability due to superior electrochemical conductivity and expansion of the contact area between electrode and electrolytes. It will play a significant role in forthcoming energy storage applications.

9.7 Summary

LDHs are 2D lamellar structures that possess characteristics such as flexibility, chemical stability, biocompatibility, pH-dependent solubility, etc. Owing to their unique structure and the easy tunability of their constituent metal ions they have found a place not only in catalysis and biomedicine but also in energy storage devices (e.g., supercapattery). To fine-tune the properties of the LDH, a well-defined synthetic procedure is necessary. By altering their molar ratio, the nature of the metal cations, and type of interlayer anions, a broad diversity of physicochemical properties can be achieved. Among the different methods available, coprecipitation and hydrothermal methods are the most commonly adopted techniques for the synthesis of LDH for supercapattery. Generally, transition metal hydroxides, due to their superior conductivity, high specific capacitance, and high energy densities often have been chosen as the best candidates for LDH. Instead of a single metal hydroxide, a bimetallic combination of transition metal hydroxides is used to improve the performance efficiency of the fabricated device. The most widely studied LDHs that are included in this chapter include Ni–Co LDH, Ni–Mn LDH, Co–Mn LDH, and Co–Al LDH. In the reported research works, a considerable increase of specific capacitance can be observed when a combination of metal hydroxides is used for electrode fabrication owing to the synergistic properties from the individual components. However, these combinations still possess problems such as agglomeration of the active species, low electrical conductivity, slow ion transfer, and inability to reach low theoretical capacity.

To minimize these drawbacks and improve the performance efficiency of LDHs-based electrodes, structural modifications such as mixing LDH with active materials (with a binder and binder-free composites), the fabrication of hierarchical structures such as 1D, 2D, 3D, and core–shell structures is adopted nowadays. These modifications can provide improved accessibility of active sites and increase the performance efficiency by utilizing the combined properties of its constituents. One-dimensional LDH nanostructures generally involve a combination of LDH with other active materials such as CNTs, nanowires, nanofibers etc. Two-dimensional nanostructures involve a combination of LDH with 2D structures such as graphene, whereas 3D LDH includes self-assembled structures. Another widely studied hierarchical assembly of LDH is a core–shell structure where often an active material acts as a core and the shell is made of LDHs. These hierarchical structures exhibit improved characteristics in terms of high specific capacitance and performance efficiency owing to their increased surface area, little agglomeration, and faster ion exchange channels. From the various research works reported here, it is clear that these structural alterations resulted in increased performance efficiency when compared to the conventional LDH assemblies. These merits are attracting a great deal of attention toward improving the properties of existing nanostructures and developing new hierarchical nanostructures. To attain the required properties one must be careful to choose the appropriate combination of active materials and the LDH material. However, despite the advances in this area and various hierarchical structures, still there is a large room for improvement to attain high-performance LDH electrodes for supercapattery applications.

Acknowledgments

The authors wish to thank for the financial support by the Indo–German joint project (DST Project No: INT/FRG/DAAD/P-09/2018 and DAAD Project No: 57389570) and also Technology Mission Division (TMD), Department of Science and Technology (DST), New Delhi, India, for a research Grant under Materials for Energy Storage (MES) Scheme No. DST/TMD/ MES/2K17/29.

References

- [1] F. Li, X. Duan, Applications of layered double hydroxides, in: X. Duan, D.G. Evans (Eds.), Layered Double Hydroxides, Springer, Berlin, Heidelberg, 2006, pp. 193–223.
- [2] M. Sarfraz, I. Shakir, Recent advances in layered double hydroxides as electrode materials for high-performance electrochemical energy storage devices, *J. Energy Storage* 13 (2017) 103–122.

- [3] L. Li, Z. Gu, W. Gu, J. Liu, Z.P. Xu, Efficient drug delivery using SiO₂-layered double hydroxide nanocomposites, *J. Colloid Interface Sci.* 470 (2016) 47–55.
- [4] M. Herrero, A.M. Martos, A. Varez, J.C. Galván, B. Levenfeld, Synthesis and characterization of polysulfone/layered double hydroxides nanocomposite membranes for fuel cell application, *Int. J. Hydrogen Energy* 39 (2014) 4016–4022.
- [5] J. Gong, X. Han, X. Zhu, Z. Guan, Layer-by-layer assembled multilayer films of exfoliated layered double hydroxide and carboxymethyl- β -cyclodextrin for selective capacitive sensing of acephatemet, *Biosens. Bioelectron.* 61 (2014) 379–385.
- [6] S. Barkhordari, M. Yadollahi, Carboxymethyl cellulose capsulated layered double hydroxides/drug nanohybrids for cephalexin oral delivery, *Appl. Clay Sci.* 121–122 (2016) 77–85.
- [7] V. Srinivasan, J.W. Weidner, Capacitance studies of cobalt oxide films formed via electrochemical precipitation, *J. Power Sources* 108 (2002) 15–20.
- [8] F.L. Tye, Manganese dioxide electrode—X. A theoretical treatment based on the concept of two solid solutions in the range γ -MnO₂ to δ -MnOOH, *Electrochim. Acta* 30 (1985) 17–23.
- [9] A. Laheäär, A. Arenillas, F. Beguin, Change of self-discharge mechanism as a fast tool for estimating long-term stability of ionic liquid based supercapacitors, *J. Power Sources* 396 (2018) 220–229.
- [10] J. Zhang, X.S. Zhao, On the configuration of supercapacitors for maximizing electrochemical performance, *ChemSusChem* 5 (2012) 818–841.
- [11] V. Augustyn, P. Simon, B. Dunn, Pseudocapacitive oxide materials for high-rate electrochemical energy storage, *Energy Environ. Sci.* 7 (2014) 1597–1614.
- [12] T. Wang, H.C. Chen, F. Yu, X.S. Zhao, H. Wang, Boosting the cycling stability of transition metal compounds-based supercapacitors, *Energy Storage Mater.* 16 (2019) 545–573.
- [13] P. Simon, Y. Gogotsi, B. Dunn, Where do batteries end and supercapacitors begin? *Science* 343 (2014) 1210.
- [14] T. Brousse, D. Bélanger, J. Long, To be or not to be pseudocapacitive? *J. Electrochem. Soc.* 162 (2015) A5185–A5189.
- [15] Y. Wang, Y. Song, Y. Xia, Electrochemical capacitors: mechanism, materials, systems, characterization and applications, *Chem. Soc. Rev.* 45 (2016) 5925–5950.
- [16] T. Wang, S. Zhang, X. Yan, M. Lyu, L. Wang, J. Bell, et al., 2-Methylimidazole-derived Ni–Co layered double hydroxide nanosheets as high rate capability and high energy density storage material in hybrid supercapacitors, *ACS Appl. Mater. Interfaces* 9 (2017) 15510–15524.
- [17] H.T. Tan, W. Sun, L. Wang, Q. Yan, 2D transition metal oxides/hydroxides for energy-storage applications, *ChemNanoMat* 2 (2016) 562–577.
- [18] H. Wang, H.S. Casalongue, Y. Liang, H. Dai, Ni(OH)₂ nanoplates grown on graphene as advanced electrochemical pseudocapacitor materials, *J. Am. Chem. Soc.* 132 (2010) 7472–7477.
- [19] T. Nguyen, Md.F. Montemor, Metal oxide and hydroxide-based aqueous supercapacitors: from charge storage mechanisms and functional electrode engineering to need-tailored devices, *Adv. Sci.* 6 (2019) 1801797.
- [20] S. Miyata, A. Okada, Synthesis of hydrotalcite-like compounds and their physico-chemical properties—the systems Mg²⁺-Al³⁺-SO₄²⁻ and Mg²⁺-Al³⁺-CrO₄²⁻, *Clays Clay Miner.* 25 (1977) 14–18.
- [21] M. Bini, F. Monteforte, Layered double hydroxides (LDHs): versatile and powerful hosts for different applications, *J. Anal. Pharm. Res.* 7 (2018) 00206.
- [22] G. Mishra, B. Dash, S. Pandey, Layered double hydroxides: a brief review from fundamentals to application as evolving biomaterials, *Appl. Clay Sci.* 153 (2018) 172–186.

- [23] E.L. Crepaldi, P.C. Pavan, J.B. Valim, Anion exchange in layered double hydroxides by surfactant salt formation, *J. Mater. Chem.* 10 (2000) 1337–1343.
- [24] U. Costantino, F. Marmottini, M. Nocchetti, R. Vivani, New synthetic routes to hydrotalcite-like compounds – characterisation and properties of the obtained materials, *Eur. J. Inorg. Chem.* 1998 (1998) 1439–1446.
- [25] M. Ogawa, H. Kaiho, Homogeneous precipitation of uniform hydrotalcite particles, *Langmuir* 18 (2002) 4240–4242.
- [26] X. Cai, X. Shen, L. Ma, Z. Ji, C. Xu, A. Yuan, Solvothermal synthesis of NiCo-layered double hydroxide nanosheets decorated on RGO sheets for high performance supercapacitor, *Chem. Eng. J.* 268 (2015) 251–259.
- [27] J. Wei, Z. Gao, Y. Song, W. Yang, J. Wang, Z. Li, et al., Solvothermal synthesis of Li–Al layered double hydroxides and their electrochemical performance, *Mater. Chem. Phys.* 139 (2013) 395–402.
- [28] M.S. Yarger, E.M.P. Steinmiller, K.-S. Choi, Electrochemical synthesis of Zn – Al layered double hydroxide (LDH) films, *Inorg. Chem.* 47 (2008) 5859–5865.
- [29] L. Indira, P.V. Kamath, Electrogeneration of base by cathodic reduction of anions: novel one-step route to unary and layered double hydroxides (LDHs), *J. Mater. Chem.* 4 (1994) 1487–1490.
- [30] E. Scavetta, A. Mignani, D. Prandstraller, D. Tonelli, Electrosynthesis of thin films of Ni, Al hydrotalcite like compounds, *Chem. Mater.* 19 (2007) 4523–4529.
- [31] H. Yang, S. Luo, Y. Bao, Y. Luo, J. Jin, J. Ma, In situ growth of ultrathin Ni–Fe LDH nanosheets for high performance oxygen evolution reaction, *Inorg. Chem. Front.* 4 (2017) 1173–1181.
- [32] Y. Tao, L. Zaijun, L. Ruiyi, N. Qi, K. Hui, N. Yulian, et al., Nickel–cobalt double hydroxides microspheres with hollow interior and hedgehog-like exterior structures for supercapacitors, *J. Mater. Chem.* 22 (2012) 23587–23592.
- [33] R. Patel, J.T. Park, M. Patel, J.K. Dash, E.B. Gowd, R. Karpoomath, et al., Transition-metal-based layered double hydroxides tailored for energy conversion and storage, *J. Mater. Chem. A* 6 (2018) 12–29.
- [34] A.M. Elshahawy, K.H. Ho, Y. Hu, Z. Fan, Y.W.B. Hsu, C. Guan, et al., Microwave – assisted hydrothermal synthesis of nanocrystal β -Ni(OH)₂ for supercapacitor applications, *CrystEngComm* 18 (2016) 3256–3264.
- [35] V. Pralong, A. Delahaye-Vidal, B. Beaudoin, J.B. Leriche, J.M. Tarascon, Electrochemical behavior of cobalt hydroxide used as additive in the nickel hydroxide electrode, *J. Electrochem. Soc.* 147 (2000) 1306–1313.
- [36] L. Huang, D. Chen, Y. Ding, S. Feng, Z.L. Wang, M. Liu, Nickel–cobalt hydroxide nanosheets coated on NiCo₂O₄ nanowires grown on carbon fiber paper for high-performance pseudocapacitors, *Nano Lett.* 13 (2013) 3135–3139.
- [37] N.T.H. Trang, H.V. Ngoc, N. Lingappan, D.J. Kang, A comparative study of supercapacitive performances of nickel cobalt layered double hydroxides coated on ZnO nanostructured arrays on textile fibre as electrodes for wearable energy storage devices, *Nanoscale* 6 (2014) 2434–2439.
- [38] R.R. Salunkhe, K. Jang, S.-w Lee, S. Yu, H. Ahn, Binary metal hydroxide nanorods and multi-walled carbon nanotube composites for electrochemical energy storage applications, *J. Mater. Chem.* 22 (2012) 21630–21635.
- [39] Y. Li, J. Chen, H. Ye, F. Zhang, X.-Z. Fu, R. Sun, et al., Hierarchical NiCo hydroxide nanosheets deposited on 3D porous Ni arrays for cost-effective high-performance supercapacitors, *J. Mater. Sci.: Mater. Electron.* 30 (2019) 2552–2562.
- [40] B.L. Yue, D. Jia, J. Tang, A. Zhang, F. Liu, T. Chen, et al., Improving the rate capability of ultrathin NiCo-LDH nanoflakes and FeOOH nanosheets on surface electrochemically modified graphite fibers for flexible asymmetric supercapacitors, *J. Colloid Interface Sci.* 560 (2020) 237–246.

- [41] X. Zheng, Z. Gu, Q. Hu, B. Geng, X. Zhang, Ultrathin porous nickel–cobalt hydroxide nanosheets for high-performance supercapacitor electrodes, *RSC Adv.* 5 (2015) 17007–17013.
- [42] Y.-M. Jeong, I. Son, S.-H. Baek, Binder-free of NiCo–layered double hydroxides on Ni-coated textile for wearable and flexible supercapacitors, *Appl. Surf. Sci.* 467–468 (2019) 963–967.
- [43] Y. Lan, M. Li, W. Fan, Q. Deng, Z. Zeng, J. Wang, et al., Functional molecules regulated and intercalated nickel-cobalt LDH nano-sheets on carbon fiber cloths as an advanced free-standing electrode for high-performance asymmetric supercapacitors, *Electrochim. Acta* 321 (2019) 134708.
- [44] E. Han, Y. Han, L. Zhu, P. Yang, X. Du, Polyvinyl pyrrolidone-assisted synthesis of flower-like nickel-cobalt layered double hydroxide on Ni foam for high-performance hybrid supercapacitor, *Ionics* 24 (2018) 2705–2715.
- [45] W. Zhu, Z. Lu, G. Zhang, X. Lei, Z. Chang, J. Liu, et al., Hierarchical Ni_{0.25}Co_{0.75}(OH)₂ nanoarrays for a high-performance supercapacitor electrode prepared by an in situ conversion process, *J. Mater. Chem. A* 1 (2013) 8327–8331.
- [46] M.F. Warsi, I. Shakir, M. Shahid, M. Sarfraz, M. Nadeem, Z.A. Gilani, Conformal coating of cobalt-nickel layered double hydroxides nanoflakes on carbon fibers for high-performance electrochemical energy storage supercapacitor devices, *Electrochim. Acta* 135 (2014) 513–518.
- [47] C. Shang, S. Dong, S. Wang, D. Xiao, P. Han, X. Wang, et al., Coaxial Ni_xCo_{2x}(OH)_{6x}/TiN nanotube arrays as supercapacitor electrodes, *ACS Nano* 7 (2013) 5430–5436.
- [48] B. Mehrabimatin, E.P. Gilshteyn, M.E. Melandsø Buan, O. Sorsa, H. Jiang, A. Irajizad, et al., Flexible and mechanically durable asymmetric supercapacitor based on NiCo-Layered double hydroxide and nitrogen-doped graphene using a simple fabrication method, *Energy Technol.* 7 (2019) 1801002.
- [49] Q. Qin, D. Ou, C. Ye, L. Chen, B. Lan, J. Yan, et al., Systematic study on hybrid supercapacitor of Ni-Co layered double hydroxide//activated carbons, *Electrochim. Acta* 305 (2019) 403–415.
- [50] X. Wang, X. Li, X. Du, X. Ma, X. Hao, C. Xue, et al., Controllable synthesis of NiCo LDH nanosheets for fabrication of high-performance supercapacitor electrodes, *Electroanalysis* 29 (2017) 1286–1293.
- [51] Y. Zhou, J. Li, Y. Yang, B. Luo, X. Zhang, E. Fong, et al., Unique 3D flower-on-sheet nanostructure of NiCo LDHs: controllable microwave-assisted synthesis and its application for advanced supercapacitors, *J. Alloy. Compd.* 788 (2019) 1029–1036.
- [52] Y. Cheng, H. Zhang, C.V. Varanasi, J. Liu, Improving the performance of cobalt–nickel hydroxide-based self-supporting electrodes for supercapacitors using accumulative approaches, *Energy Environ. Sci.* 6 (2013) 3314–3321.
- [53] S.C. Jun, U. Patil, J. Sohn, S. Kulkarni, S. Lee, H. Park, et al., Enhanced supercapacitive performance of chemically grown cobalt-nickel hydroxides on three-dimensional graphene foam electrodes, *ACS Appl. Mater. Interfaces* 6 (2014) 2450–2458.
- [54] H. Chen, F. Cai, Y. Kang, S. Zeng, M. Chen, Q. Li, Facile assembly of Ni–Co hydroxide nanoflakes on carbon nanotube network with highly electrochemical capacitive performance, *ACS Appl. Mater. Interfaces* 6 (2014) 19630–19637.
- [55] G. Xiong, P. He, D. Wang, Q. Zhang, T. Chen, T.S. Fisher, Hierarchical Ni–Co hydroxide petals on mechanically robust graphene petal foam for high-energy asymmetric supercapacitors, *Adv. Funct. Mater.* 26 (2016) 5460–5470.
- [56] Y. Song, X. Cai, X. Xu, X.-X. Liu, Integration of nickel–cobalt double hydroxide nanosheets and polypyrrole films with functionalized partially exfoliated graphite for

- asymmetric supercapacitors with improved rate capability, *J. Mater. Chem. A* 3 (2015) 14712–14720.
- [57] H. Xing, Y. Lan, Y. Zong, Y. Sun, X. Zhu, X. Li, et al., Ultrathin NiCo-layered double hydroxide nanosheets arrays vertically grown on Ni foam as binder-free high-performance supercapacitors, *Inorg. Chem. Commun.* 101 (2019) 125–129.
- [58] J. Yang, C. Yu, C. Hu, M. Wang, S. Li, H. Huang, et al., Surface-confined fabrication of ultrathin nickel cobalt-layered double hydroxide nanosheets for high-performance supercapacitors, *Adv. Funct. Mater.* 28 (2018) 1803272.
- [59] T. Dong, X. Zhang, M. Li, P. Wang, P. Yang, Hierarchical flower-like Ni–Co layered double hydroxide nanostructures: synthesis and super performance, *Inorg. Chem. Front.* 5 (2018) 3033–3041.
- [60] L. Hou, Q. Du, L. Su, S. Di, Z. Ma, L. Chen, et al., Ni–Co layered double hydroxide with self-assembled urchin like morphology for asymmetric supercapacitors, *Mater. Lett.* 237 (2019) 262–265.
- [61] C. Jing, X. Liu, X. Liu, D. Jiang, B. Dong, F. Dong, et al., Crystal morphology evolution of Ni–Co layered double hydroxide nanostructure towards high-performance biotemplate asymmetric supercapacitors, *CrystEngComm* 20 (2018) 7428–7434.
- [62] M. Li, P. Yuan, S. Guo, F. Liu, J.P. Cheng, Design and synthesis of Ni–Co and Ni–Mn layered double hydroxides hollow microspheres for supercapacitor, *Int. J. Hydrogen Energy* 42 (2017) 28797–28806.
- [63] Z. Li, F. Han, C. Li, X. Jiao, D. Chen, Multi-anion intercalated layered double hydroxide nanosheet-assembled hollow nanoprisms with improved pseudocapacitive and electrocatalytic properties, *Chem. – An. Asian J.* 13 (2018) 1129–1137.
- [64] H. Liu, J. Li, M. Wang, Y. Liu, J. Liu, H. Cui, Controlled microstructure in two dimensional Ni–Co LDH nanosheets-crosslinked network for high performance supercapacitors, *Adv. Powder Technol.* 30 (2019) 1239–1246.
- [65] C. Xing, F. Musharavati, H. Li, E. Zalezhad, O.K.S. Hui, S. Bae, et al., Synthesis, characterization, and properties of nickel–cobalt layered double hydroxide nanostructures, *RSC Adv.* 7 (2017) 38945–38950.
- [66] H. Chen, L. Hu, M. Chen, Y. Yan, L. Wu, Nickel–cobalt layered double hydroxide nanosheets for high-performance supercapacitor electrode materials, *Adv. Funct. Mater.* 24 (2014) 934–942.
- [67] X. Sun, G. Wang, H. Sun, F. Lu, M. Yu, J. Lian, Morphology controlled high performance supercapacitor behaviour of the Ni–Co binary hydroxide system, *J. Power Sources* 238 (2013) 150–156.
- [68] A.-L. Yan, X.-C. Wang, J.-P. Cheng, Research progress of NiMn layered double hydroxides for supercapacitors: a review, *Nanomaterials* 8 (2018) 747.
- [69] H. Sim, C. Jo, T. Yu, E. Lim, S. Yoon, J.H. Lee, et al., Reverse micelle synthesis of colloidal nickel–manganese layered double hydroxide nanosheets and their pseudocapacitive properties, *Chem.—Eur. J.* 20 (2014) 14880–14884.
- [70] L. Shi, P. Sun, L. Du, R. Xu, H. He, S. Tan, et al., Flexible honeycomb-like NiMn layered double hydroxide/carbon cloth architecture for electrochemical energy storage, *Mater. Lett.* 175 (2016) 275–278.
- [71] A. Zhang, W. Zheng, Z. Yuan, J. Tian, L. Yue, R. Zheng, et al., Hierarchical NiMn-layered double hydroxides@CuO core-shell heterostructure in-situ generated on Cu(OH)₂ nanorod arrays for high performance supercapacitors, *Chem. Eng. J.* 380 (2020) 122486.
- [72] J. Lin, H. Jia, H. Liang, S. Chen, Y. Cai, J. Qi, et al., Hierarchical CuCo₂S₄@NiMn-layered double hydroxide core-shell hybrid arrays as electrodes for supercapacitors, *Chem. Eng. J.* 336 (2018) 562–569.
- [73] S. Yu, Y. Zhang, G. Lou, Y. Wu, X. Zhu, H. Chen, et al., Synthesis of NiMn-LDH nanosheet@Ni₃S₂ nanorod hybrid structures for supercapacitor electrode materials with ultrahigh specific capacitance, *Sci. Rep.* 8 (2018) 5246.

- [74] J. Zhao, J. Chen, S. Xu, M. Shao, Q. Zhang, F. Wei, et al., Hierarchical NiMn layered double hydroxide/carbon nanotubes architecture with superb energy density for flexible supercapacitors, *Adv. Funct. Mater.* 24 (2014) 2938–2946.
- [75] H. Wan, J. Liu, Y. Ruan, L. Lv, L. Peng, X. Ji, et al., Hierarchical configuration of NiCo₂S₄ nanotube@Ni–Mn layered double hydroxide arrays/three-dimensional graphene sponge as electrode materials for high-capacitance supercapacitors, *ACS Appl. Mater. Interfaces* 7 (2015) 15840–15847.
- [76] F.O. Ochai-Ejeh, M.J. Madito, D.Y. Momodu, A.A. Khaleed, O. Olaniyan, N. Manyala, High performance hybrid supercapacitor device based on cobalt manganese layered double hydroxide and activated carbon derived from cork (*Quercus Suber*), *Electrochim. Acta* 252 (2017) 41–54.
- [77] J. Zhao, J. Chen, S. Xu, M. Shao, D. Yan, M. Wei, et al., CoMn-layered double hydroxide nanowalls supported on carbon fibers for high-performance flexible energy storage devices, *J. Mater. Chem. A* 1 (2013) 8836–8843.
- [78] D. Wang, J. Li, D. Zhang, T. Liu, N. Zhang, L. Chen, et al., Layered Co–Mn hydroxide nanoflakes grown on carbon cloth as binder-free flexible electrodes for supercapacitors, *J. Mater. Sci.* 51 (2016) 3784–3792.
- [79] X. Liu, L. Zhang, X. Gao, C. Guan, Y. Hu, J. Wang, Enlarged interlayer spacing in cobalt–manganese layered double hydroxide guiding transformation to layered structure for high supercapacitance, *ACS Appl. Mater. Interfaces* 11 (2019) 23236–23243.
- [80] Y. Wang, W. Yang, J. Yang, A Co–Al layered double hydroxides nanosheets thin-film electrode: fabrication and electrochemical study, *Electrochem. Solid-State Lett.* 10 (2007) A233–A236.
- [81] Y. Wang, W. Yang, C. Chen, D.G. Evans, Fabrication and electrochemical characterization of cobalt-based layered double hydroxide nanosheet thin-film electrodes, *J. Power Sources* 184 (2008) 682–690.
- [82] P. Guoxiang, X. Xinhui, L. Jingshan, C. Feng, Y. Zhihong, F. Hongjin, Preparation of CoAl layered double hydroxide nanoflake arrays and their high supercapacitance performance, *Appl. Clay Sci.* 102 (2014) 28–32.
- [83] X. Dong, L. Wang, D. Wang, C. Li, J. Jin, Layer-by-layer engineered Co–Al hydroxide nanosheets/graphene multilayer films as flexible electrode for supercapacitor, *Langmuir* 28 (2012) 293–298.
- [84] J. Han, Y. Dou, J. Zhao, M. Wei, D. Evans, X. Duan, Flexible CoAl LDH@PEDOT core/shell nanoplatelet array for high-performance energy storage, *Small* 9 (2013) 98–106.
- [85] X. Li, D. Du, Y. Zhang, W. Xing, Q. Xue, Z. Yan, Layered double hydroxides toward high-performance supercapacitors, *J. Mater. Chem. A* 5 (2017) 15460–15485.
- [86] X. Ge, Y. He, T. Plachy, N. Kazantseva, P. Saha, Q. Cheng, Hierarchical PANI/NiCo-LDH core-shell composite networks on carbon cloth for high performance asymmetric supercapacitor, *Nanomaterials* 9 (2019) 527.
- [87] J. Zhao, J. Chen, S. Xu, M. Shao, Q. Zhang, F. Wei, et al., Flexible electronics: hierarchical NiMn layered double hydroxide/carbon nanotubes architecture with superb energy density for flexible supercapacitors (*Adv. Funct. Mater.* 20/2014), *Adv. Funct. Mater.* 24 (2014). 2921–2921.
- [88] J. Yang, C. Yu, X. Fan, Z. Ling, J. Qiu, Y. Gogotsi, Facile fabrication of MWCNT-doped NiCoAl-layered double hydroxide nanosheets with enhanced electrochemical performances, *J. Mater. Chem. A* 1 (2013) 1963–1968.
- [89] Z. Wang, X. Zhang, J. Wang, L. Zou, Z. Liu, Z. Hao, Preparation and capacitance properties of graphene/NiAl layered double-hydroxide nanocomposite, *J. Colloid Interface Sci.* 396 (2013) 251–257.

- [90] C. Yu, J. Yang, C. Zhao, X. Fan, G. Wang, J. Qiu, Nanohybrids from NiCoAl-LDH coupled with carbon for pseudocapacitors: understanding the role of nanostructured carbon, *Nanoscale* 6 (2014) 3097–3104.
- [91] Y. Zhao, L. Hu, S. Zhao, L. Wu, Preparation of $\text{MnCo}_2\text{O}_4@\text{Ni}(\text{OH})_2$ core-shell flowers for asymmetric supercapacitor materials with ultrahigh specific capacitance, *Adv. Funct. Mater.* 26 (2016) 4085–4093.
- [92] W.L.J. Kwok, D.-G. Crivoi, C. Chen, J.-C. Buffet, D. O'Hare, Silica@layered double hydroxide core-shell hybrid materials, *Dalton Trans.* 47 (2018) 143–149.
- [93] S. Liu, S.C. Lee, U. Patil, I. Shackery, S. Kang, K. Zhang, et al., Hierarchical MnCo-layered double hydroxides@Ni(OH)₂ core-shell heterostructures as advanced electrodes for supercapacitors, *J. Mater. Chem. A* 5 (2017) 1043–1049.
- [94] L. Yu, H. Zhou, J. Sun, F. Qin, F. Yu, J. Bao, et al., Cu nanowires shelled with NiFe layered double hydroxide nanosheets as bifunctional electrocatalysts for overall water splitting, *Energy Environ. Sci.* 10 (2017) 1820–1827.
- [95] I. Shakir, M. Shahid, U.A. Rana, I.M.A. Nashef, R. Hussain, Nickel–Cobalt layered double hydroxide anchored zinc oxide nanowires grown on carbon fiber cloth for high-performance flexible pseudocapacitive energy storage devices, *Electrochim. Acta* 129 (2014) 28–32.
- [96] K. Gopalsamy, Z. Xu, B. Zheng, T. Huang, L. Kou, X. Zhao, et al., Bismuth oxide nanotubes–graphene fiber-based flexible supercapacitors, *Nanoscale* 6 (2014) 8595–8600.
- [97] L. Li, R. Li, S. Gai, F. He, P. Yang, Facile fabrication and electrochemical performance of flower-like $\text{Fe}_3\text{O}_4@\text{C}@\text{layered double hydroxide (LDH)}$ composite, *J. Mater. Chem. A* 2 (2014) 8758–8765.
- [98] H. Liang, J. Lin, H. Jia, S. Chen, J. Qi, J. Cao, et al., Hierarchical NiCo-LDH@NiOOH core-shell heterostructure on carbon fiber cloth as battery-like electrode for supercapacitor, *J. Power Sources* 378 (2018) 248–254.
- [99] X. Li, H. Wu, C. Guan, A.M. Elshahawy, Y. Dong, S.J. Pennycook, et al., Ni₂CoSe₂/NiCo-LDH core/shell structural electrode with the cactus-like (Ni₂Co)Se₂ core for asymmetric supercapacitors, *Small* 15 (2019) 1803895.
- [100] W. Chen, J. Wang, K.Y. Ma, M. Li, S.H. Guo, F. Liu, et al., Hierarchical NiCo₂O₄@Co-Fe LDH core-shell nanowire arrays for high-performance supercapacitor, *Appl. Surf. Sci.* 451 (2018) 280–288.
- [101] L. Zhang, K.N. Hui, K.S. Hui, S.W. Or, 3D heterostructured cobalt oxide@layered double hydroxide core-shell networks on nickel foam for high-performance hybrid supercapacitor, *Dalton Trans.* 48 (2019) 150–157.
- [102] J.-J. Zhou, Q. Li, C. Chen, Y.-L. Li, K. Tao, L. Han, Co₃O₄@CoNi-LDH core/shell nanosheet arrays for high-performance battery-type supercapacitors, *Chem. Eng. J.* 350 (2018) 551–558.
- [103] Z. Li, M. Shao, L. Zhou, R. Zhang, C. Zhang, J. Han, et al., A flexible all-solid-state micro-supercapacitor based on hierarchical CuO@layered double hydroxide core-shell nanoarrays, *Nano Energy* 20 (2016) 294–304.
- [104] Y. Zhao, X. He, R. Chen, Q. Liu, J. Liu, J. Yu, et al., A flexible all-solid-state asymmetric supercapacitors based on hierarchical carbon cloth@CoMoO₄@NiCo layered double hydroxide core-shell heterostructures, *Chem. Eng. J.* 352 (2018) 29–38.
- [105] M. Shao, F. Ning, Y. Zhao, J. Zhao, M. Wei, D.G. Evans, et al., Core-shell layered double hydroxide microspheres with tunable interior architecture for supercapacitors, *Chem. Mater.* 24 (2012) 1192–1197.
- [106] S. Iijima, Helical microtubules of graphitic carbon, *Nature* 354 (1991) 56–58.
- [107] H. Dai, Carbon nanotubes: opportunities and challenges, *Surf. Sci.* 500 (2002) 218–241.

- [108] G. Wang, R. Liang, L. Liu, B. Zhong, Improving the specific capacitance of carbon nanotubes-based supercapacitors by combining introducing functional groups on carbon nanotubes with using redox-active electrolyte, *Electrochim. Acta* 115 (2014) 183–188.
- [109] K.H. An, K. Jeon, W. Kim, Y. Park, S.C. Lim, D.J. Bae, et al., Characterization of supercapacitors using singlewalled carbon nanotube electrodes, *J. Korean Phys. Soc.* 39 (2001) S511–S517.
- [110] A. Izadi-Najafabadi, S. Yasuda, K. Kobashi, T. Yamada, D.N. Futaba, H. Hatori, et al., Extracting the full potential of single-walled carbon nanotubes as durable supercapacitor electrodes operable at 4 V with high power and energy density, *Adv. Mater.* 22 (2010) E235–E241.
- [111] Y. Wang, Z. Chen, H. Li, J. Zhang, X. Yan, K. Jiang, et al., The synthesis and electrochemical performance of core-shell structured Ni-Al layered double hydroxide/carbon nanotubes composites, *Electrochim. Acta* 222 (2016) 185–193.
- [112] L. Yu, N. Shi, Q. Liu, J. Wang, B. Yang, B. Wang, et al., Facile synthesis of exfoliated Co–Al LDH–carbon nanotube composites with high performance as supercapacitor electrodes, *Phys. Chem. Chem. Phys.* 16 (2014) 17936–17942.
- [113] M. Li, F. Liu, J.P. Cheng, J. Ying, X.B. Zhang, Enhanced performance of nickel–aluminum layered double hydroxide nanosheets/carbon nanotubes composite for supercapacitor and asymmetric capacitor, *J. Alloy. Compd.* 635 (2015) 225–232.
- [114] H. Niu, Y. Zhang, Y. Liu, N. Xin, W. Shi, NiCo-layered double-hydroxide and carbon nanosheets microarray derived from MOFs for high performance hybrid supercapacitors, *J. Colloid Interface Sci.* 539 (2019) 545–552.
- [115] W. Yang, Z. Gao, J. Wang, J. Ma, M. Zhang, L. Liu, Solvothermal one-step synthesis of Ni–Al layered double hydroxide/carbon nanotube/reduced graphene oxide sheet ternary nanocomposite with ultrahigh capacitance for supercapacitors, *ACS Appl. Mater. Interfaces* 5 (2013) 5443–5454.
- [116] N.I. Kovtyukhova, P.J. Ollivier, B.R. Martin, T.E. Mallouk, S.A. Chizhik, E.V. Buzaneva, et al., Layer-by-layer assembly of ultrathin composite films from micron-sized graphite oxide sheets and polycations, *Chem. Mater.* 11 (1999) 771–778.
- [117] R. Dubey, V. Guruviah, Review of carbon-based electrode materials for supercapacitor energy storage, *Ionics* 25 (2019) 1419–1445.
- [118] Y.-X. Yan, H.-B. Yao, L.-B. Mao, A.M. Asiri, K.A. Alamry, H.M. Marwani, et al., Micrometer-thick graphene oxide-layered double hydroxide nacre-inspired coatings and their properties, *Small* 12 (2016) 745–755.
- [119] J. Memon, J. Sun, D. Meng, W. Ouyang, M.A. Memon, Y. Huang, et al., Synthesis of graphene/Ni–Al layered double hydroxide nanowires and their application as an electrode material for supercapacitors, *J. Mater. Chem. A* 2 (2014) 5060–5067.
- [120] X. Wu, L. Jiang, C. Long, T. Wei, Z. Fan, Energy Storage: dual support system ensuring porous Co–Al hydroxide nanosheets with ultrahigh rate performance and high energy density for supercapacitors, *Adv. Funct. Mater.* 25 (2015) 1648–1655.
- [121] J. Xu, S. Gai, F. He, N. Niu, P. Gao, Y. Chen, et al., A sandwich-type three-dimensional layered double hydroxide nanosheet array/graphene composite: fabrication and high supercapacitor performance, *J. Mater. Chem. A* 2 (2014) 1022–1031.
- [122] M. Jiang, X. Zhang, Carbon fiber/Ni–Co layered double hydroxide@NiMoO₄/graphene oxide sandwich structure flexible electrode materials: facile synthesis and high supercapacitor performance, *J. Alloy. Compd.* 794 (2019) 13–20.
- [123] J. Li, P. Zhang, X. Zhao, L. Chen, J. Shen, M. Li, et al., Structure-controlled Co–Al layered double hydroxides/reduced graphene oxide nanomaterials based on solid-phase exfoliation technique for supercapacitors, *J. Colloid Interface Sci.* 549 (2019) 236–245.

- [124] P. Bandyopadhyay, X. Li, N.H. Kim, J.H. Lee, Graphitic carbon nitride modified graphene/NiAl layered double hydroxide and 3D functionalized graphene for solid-state asymmetric supercapacitors, *Chem. Eng. J.* 353 (2018) 824–838.
- [125] F. Wang, T. Wang, S. Sun, Y. Xu, R. Yu, H. Li, One-step synthesis of nickel iron-layered double hydroxide/reduced graphene oxide/carbon nanofibres composite as electrode materials for asymmetric supercapacitor, *Sci. Rep.* 8 (2018) 8908.
- [126] S. Shahrokhian, S. Rahimi, R. Mohammadi, Nickel-cobalt layered double hydroxide ultrathin nanosheets coated on reduced graphene oxide nonosheets/nickel foam for high performance asymmetric supercapacitors, *Int. J. Hydrogen Energy* 43 (2018) 2256–2267.
- [127] D. Wang, A. Wei, L. Tian, A. Mensah, D. Li, Y. Xu, et al., Nickel-cobalt layered double hydroxide nanosheets with reduced graphene oxide grown on carbon cloth for symmetric supercapacitor, *Appl. Surf. Sci.* 483 (2019) 593–600.



MXene

Ghulam Ali¹, Muhammad Zahir Iqbal² and Faiza Jan Iftikhar³

¹U.S.–Pakistan Center for Advanced Studies in Energy, National University of Sciences and Technology, H-12, Islamabad, Pakistan

²Faculty of Engineering Sciences, GIK Institute of Engineering Sciences and Technology, Topi, Pakistan

³NUTECH School of Applied Sciences and Humanities, National University of Technology, Islamabad, Pakistan



10.1 MXene

The development and rational design of new types of materials over the past two decades have played a key role in adopting and developing new technologies that are interlinked with the growth of the economy of a nation. The discovery of the two-dimensional (2D) graphene, which is usually up to a few atomic layers thick, has opened up new research vistas in diverse applications. Such 2D materials have garnered a lot of attention as a result of their advantages over their bulk counterparts that include mechanical, electronic, and optical properties that can be tuned according to their applications [1,2]. Several other materials such as silicene, germanene, and phosphorene have also been prepared with a 2D structure and have revealed unusual properties due to their unique chemistries. Thus the addition of novel materials in the 2D family structure can find a wider scope for future applications by adopting a rational approach toward their design with a better understanding of the structure. In this vein, transition metal carbides, nitrides, and carbonitrides as layered structures have been extensively researched and have been coined as MXene in the same fashion as graphene. The general formula for MXene is designated as $M_{n+1}X_nT_n$ ($n = 1-3$) where M signifies the transition metals, such as V, Ti, Cr, Zr, Nb, Mo, etc.; X is carbon and/or nitrogen; and T is oxygen, fluorine, or hydroxyl. The MXenes are derived from MAX phase where M and X stand for the usual notations and A is an IIIA or IVA element.

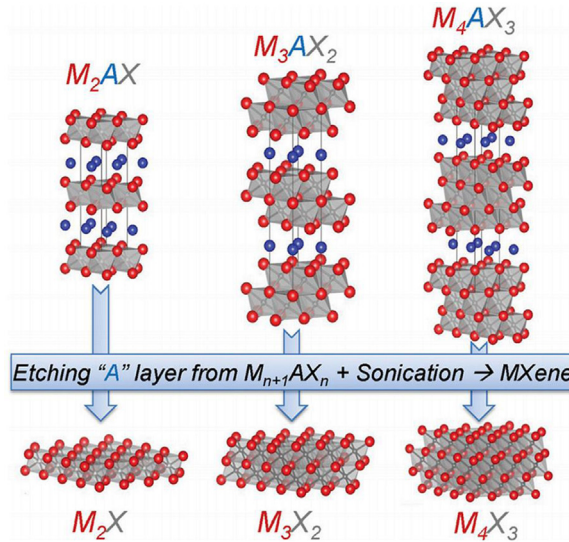


Figure 10.1 Preparation route of MXenes from MAX phase [3].

10.2 Structure and types of MXene

The crystal structure of MXene is hexagonal closed-packed where M atoms fill up the closed-packed structure while atoms of X are located at the interstitial sites of the octahedral geometry. The arrangement of M atoms in the crystal lattice alters with its composition, for example, M_2X has close-packed ordering with ABABAB stacking, while M_3X_2 and M_4X_3 have face-centered cubic ordering with ABCABC stacking (Fig. 10.1). The atomic ordering of elements is important for the synthesis of MXene, which involves etching of the layers from their MAX phase precursors [3]. The "A" from MAX is etched using fluoride-containing acids to prepare MXene. MXene can also be prepared by non-MAX precursors such as Mo_2CT , $\text{Mo}_2\text{Ga}_2\text{C}$, etc., as well as chemical vapor deposition.

10.3 MXene in supercapacitors

Supercapacitors (SCs) or electric double-layer capacitors (EDLCs) are energy storage (ES) devices known to provide high power density and long shelf life. However they are troubled by issues of low energy density, which

is mainly due to the electrostatic charge storage caused by the electrical double layer (EDL) formation. The energy density of EDLCs can be amplified by utilizing the edge sites of 2D materials which are chemically more active sites for electrolyte ion insertion compared to van der Waals gaps in bulk materials. MXene, as one of the most investigated families and an emerging class for SCs, has remained at the forefront of scientific interest and research in the past decades due to its fascinating structure, such as high surface area and mechanical properties. MXene boasts high intrinsic electrical conductivity making it a promising material for ES over conventionally investigated metal oxides/sulfides, where the latter makes use of the reasonably large amount of conductive agents in the fabrication of the electrode. Usually, the surface structure of electrode materials is pivotal for the electrochemical performance of SCs and hence a lot of attention has been focused on that area of development. Additionally, the terminal groups such as $-\text{OH}$ and $-\text{F}$ at the surface of the electrode have a role to play by blocking electrolyte ion transport in MXene and hence result in reduced capacitance. Gogotsi's group have demonstrated the charge storage mechanism in $\text{Ti}_3\text{C}_2\text{T}_x$ MXene by using synchrotron-based X-ray absorption spectroscopy (XAS). Both the XAS and electrochemical results revealed that the ES in $\text{Ti}_3\text{C}_2\text{T}_x$ MXene is mainly due to the Ti atoms undergoing redox reactions in the structure. It was revealed that the capacitance can be increased by lowering the concentration of terminal groups so that more Ti atoms are exposed to electrochemical reactions and lead to enhancing the inter-layer spacing of $\text{Ti}_3\text{C}_2\text{T}_x$ MXene [4].

MXene offers several advantages, such as its hydrophilic nature, due to the presence of $-\text{O}$ or $-\text{OH}$ terminal groups, the layered structure based on transition metals capable of redox reactions, and fast transport of ions in contrast to graphene, which possesses a hydrophobic nature and its preparation requires surfactants or polymers. Furthermore, MXene has successfully been demonstrated as an efficient electrode in symmetric microSCs. Li et al. showed that surface group modified and cation intercalated 2D $\text{Ti}_3\text{C}_2\text{T}_x$ MXenes electrodes displayed a specific capacitance of 500 F g^{-1} at a scan rate of 1 mV s^{-1} and cycling stability of 99% after 10,000 cycles. When used as electrodes in symmetric SC, 2D $\text{Ti}_3\text{C}_2\text{T}_x$ MXenes delivered an energy density of 27.4 Wh kg^{-1} at a current density of 1 A g^{-1} which was greater than the energy density of carbon-based EDLCs (19.5 Wh kg^{-1}) [5]. Due to the highly crystalline nature, the fabricated MXenes electrode are expected to facilitate the cation de/intercalation and can withstand high rate cycling. Majid et al. demonstrated that

cation driven V_2CT_x electrodes showed high electrochemical properties and exhibited stability over one million cycles with a capacitance retention of 77% [6].

The porous structure of MXene material-based electrodes provides the composite with excellent absorption sites for high capacitance that can be used for electrochemical SCs. As MXenes' nature is exceptionally hydrophilic, the cylindrical $Ti_3C_2T_x$ swiftly absorbs large amounts of water in a very few seconds. The porous $Ti_3C_2T_x$ has a specific surface area of $230 \text{ m}^2/\text{g}$ and absorbs around 22 times its weight in deionized (DI) water. Other scientists and researchers have also reported the absorption of porous 2D materials like graphene. Zhang et al. fabricated $g\text{-C}_3\text{N}_4/\text{graphene}$ oxide enveloped sponge with an absorption capacity of 49.8 g g^{-1} for n-hexane [7]. The density of $Ti_3C_2T_x$ is exceptionally greater than graphene. The absorption capacities obtained for porous $Ti_3C_2T_x$ and its composites are 72.6 g cm^{-3} . The electrochemical dependence of such MXene $Ti_3C_2T_x$ and NiO composite material at different ratios can be observed in Fig. 10.2, which shows a slower rate of ion transport at high scan rates [8] and a higher specific capacitance at 1:1 ratio than other prepared sample ratios. This concludes that the addition of NiO improves the electrochemical performance of $Ti_3C_2T_x$, thus presenting a roadmap to select different morphological possibilities for economical and high-performance SCs.

Aqueous electrolytes have mostly been used to investigate MXenes rendering a narrow operating voltage window as a result of water electrolysis that results in low energy and power densities. Thus to enhance the operating voltage window, organic or ionic liquid (IL) electrolytes have been proven as potential candidates for the MXenes electrode. Simon et al. reported the use

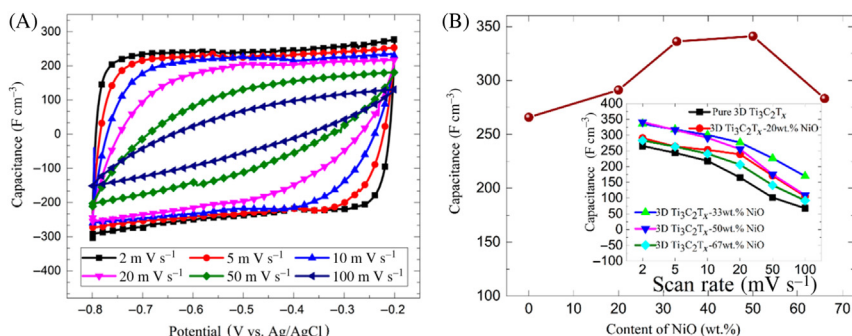


Figure 10.2 Scan rate dependence on specific capacitance [8].

of organic electrolytes such as 1-ethyl-3-methylimidazolium bis(trifluoromethyl sulfonyl)imide (EMITFSI), tetraethylammonium tetrafluoroborate (TEABF₄) and 1-ethyl-3-methylimidazolium tetrafluoroborate (EMIBF₄) in acetonitrile. MXenes in EMITFSI organic electrolyte showed a threefold increased capacitance with the addition of carbon nanotubes (CNTs) to increase the accessibility of ions to the active material [9].

One of the most prominent features of MXene in SCs is that the electrodes can be prepared without a costly nickel foam current collector and can be used as free-standing electrodes. This can reduce the cost and increase the energy density of SCs by utilizing more surface of the material. Moreover, the free-standing structure of MXenes can offer diverse applications in flexible, portable, and wearable electronics.



10.4 MXene in rechargeable batteries

Rechargeable batteries require reversible de/intercalation of alkali ions such as Li⁺, Na⁺, and K⁺ into the host material. The materials which offer redox reactions to occur can be used as electrodes for batteries. MXene offers redox reactions at the surface of the transition metals used as the electrode material. Further, the outstanding electrical conductivity of MXene is beneficial for fast electron transfer and large interlayer spacing resulting in a smaller volume change upon alkali ion de/intercalation.

Lithium-ion batteries (LIBs) are already ruling the portable electronic industry with the advantage of delivering high energy and power densities, and no memory loss along with excellent cycling performance. These unique properties of LIBs have made it possible to use them for commercial applications such as electric vehicles (EVs) and stationary storage devices. The proper selection of electrode material is very important for the efficient performance of LIBs. To develop high-performance LIBs, especially for high-performance EVs, extensive research is being carried out to develop unique materials with unprecedented power and energy densities. 2D MXenes have been employed as electrode materials in LIBs where they undergo redox reaction and fast ion transport at the surface, causing high power density. The charge storage mechanism of MXene was investigated using DFT calculations and the calculated results showed that Li ions occupy vacant sites of Al atoms. The theoretical capacity of Ti₃C₂T_x was determined to be 320 mAh g⁻¹, marginally less than

graphite's theoretical capacity, which is 372 mAh g^{-1} . The capacity of $\text{Ti}_3\text{C}_2\text{T}_x$ can be increased by the intercalation of different molecules and ions between the layers. Gogotsi et al. have achieved an outstanding capacity of 410 mAh g^{-1} by intercalation of ions which is shown to be fourfold higher than the as-synthesized material after 100 cycles. The capacity can be increased by enhancing the O-terminated and surface functional groups of MXene that offer to adsorb extra lithium in the electrode material [10]. Further increase in the capacity is possible by introducing conductive polymers and carbon materials in the interlayer spacing which helps to diffuse the guest ions in 3D, that is, perpendicular-to-layer direction. High capacity of 1250 mAh g^{-1} is reported by incorporating CNTs in free-standing $\text{Ti}_3\text{C}_2\text{T}_x$ as the anode [11].

The high electrochemical performance of MXene electrodes was obtained by synthesizing the composites with other compounds, such as metallic and metal oxides. In this regard, MXene composites with Sn, Ag, SnO_2 , TiO_2 , Co_3O_4 , NiCo_2O_4 , and MoS_2 were synthesized and used as anodes for LIBs. Amongst these, $\text{Ti}_3\text{C}_2\text{T}_x/\text{NiCo}_2\text{O}_4$ composite electrode delivered an extraordinary capacity of 1200 mAh g^{-1} at a high rate of 1 C during the 100th cycle [12]. This strategy was found to be useful in other metallic and metal oxide-based composites where the composite electrode delivered high capacities, long cycle life, and high coulombic efficiencies.

Because of large interlayer spacing, the MXene structure is favorable for the de/intercalation of other alkali ions such as Na^+ and K^+ . The commonly used graphite anode in LIBs shows limited de/intercalation of sodium ions because of the large ionic radius of sodium compared to the lesser interlayer spacing. Thus MXene could be a potential candidate as an anode material for sodium-ion batteries (SIBs). $\text{Ti}_3\text{C}_2\text{T}_x$ nanosheets showed an increased discharge capacity of 370 mAh g^{-1} , suggesting the feasibility of MXenes as potential anodes for SIBs [13]. The sodium insertion/extraction mechanism demonstrated by the solid-state Na magic angle spinning nuclear magnetic resonance suggests that the structure remains stable during the dis/charge process. The structure shows less volume expansion during the de/sodiation process and results in fast sodium diffusion. [14] The nanotechnology industry, based on material engineering, has constructed architecture/configuration of ES devices with notable and unique features. Thus MXene was prepared in 3D hollow spheres as the anode in SIB and showed high conductivity, good cycling stability, and rate capability as shown in Fig. 10.3A. The 3D $\text{Ti}_3\text{C}_2\text{T}_x$ macroporous anode (Fig. 10.3B) showed a high reversible specific capacity

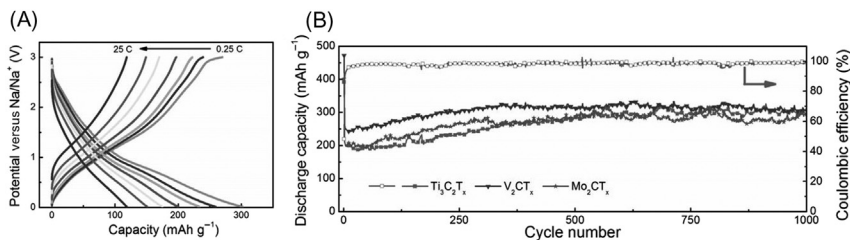


Figure 10.3 (A) Charge–discharge curves of 3D $\text{Ti}_3\text{C}_2\text{T}_x$ film electrode at different current rates. (B) Cycle tests of different MXene electrodes at a rate of 2.5 C. [15].

of 295 mAh g^{-1} after 1000 cycles at a rate of 2.5 C [15]. 2D sulfur-based Ti_3C_2 has been reported as a positive electrode for SIBs and has shown the outstanding capacity of 135 mAh g^{-1} at 2 A g^{-1} with a high retention capacity of 99.96% after 1000 cycles. The properties are attributed to pseudocapacitive sulfur decorated MXene sheets rendering intercalation and surface controlled ES mechanisms [16]. MXenes have shown high performance in SIBs when prepared as composites with CNTs and metal oxides/sulfides.

An MXene electrode has been used in potassium-ion batteries in the form of the 3D porous structure where it showed high reversible capacity. Because of high conductivity and large interlayer spacing, MXenes have been proven as promising candidates for multi-ion batteries such as Mg, Ca, and Al. However, more effort is required in the preparation of suitable structures and optimum electrolytes for outstanding performance.

10.5 MXene in supercapattery

Both high power and energy density are desired to be achieved in ES devices for the development of portable electronics and EVs [17]. In electrochemical energy storage (EES) devices, batteries possess high energy density and low power densities, while SCs, on the other hand, provide high power but low energy density [18,19]. The merging of SCs and batteries in a single device provides the opportunity to harness both high energy and -power density in a single device fulfilling the requirements of the high-performance storage devices. One of the successful implementations of this type of integration of the most desired features has been the lithium-ion–capacitor electrode materials as a class of hybrid metal ion

capacitor (MIC) that have demonstrated characteristics of both battery and SCs. Thus these materials possess energy density higher than that of battery and output power density as high as that of SCs [20–22]. This merged device possessing a high energy density along with a high power density is referred to as a supercapattery, as is shown in Fig. 10.4.

Thus to enhance the energy density and power density in supercapatteries the major focus has been on developing electrode materials. The electrode material should be chosen by keeping in mind the chemistries of the electrode material along with the electrolyte used. The selection of material is dependent on the presence of redox ion formation and active site availability of that material, as processes like electron transfer, ion diffusion, and electrochemical activities directly rely on the presence of redox ions [23,24]. Owing to MXenes' excellent conductivity, they have been pursued as the material of choice in the field of electrochemical supercapattery devices, as shown in Fig. 10.5.

MXene is utilized as transparent conductors because of their high conductivity, that is, up to 2140 S cm^{-1} . There are many other applications of MXenes in EES and conversion devices related to its properties and characteristics [26]. The techniques to synthesize MXenes including exfoliation and

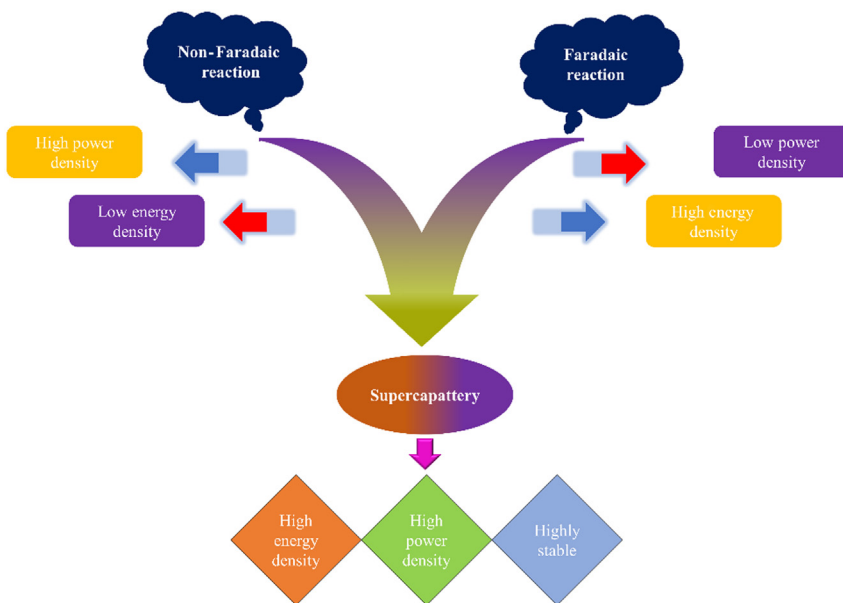


Figure 10.4 Merging of battery and supercapacitor.

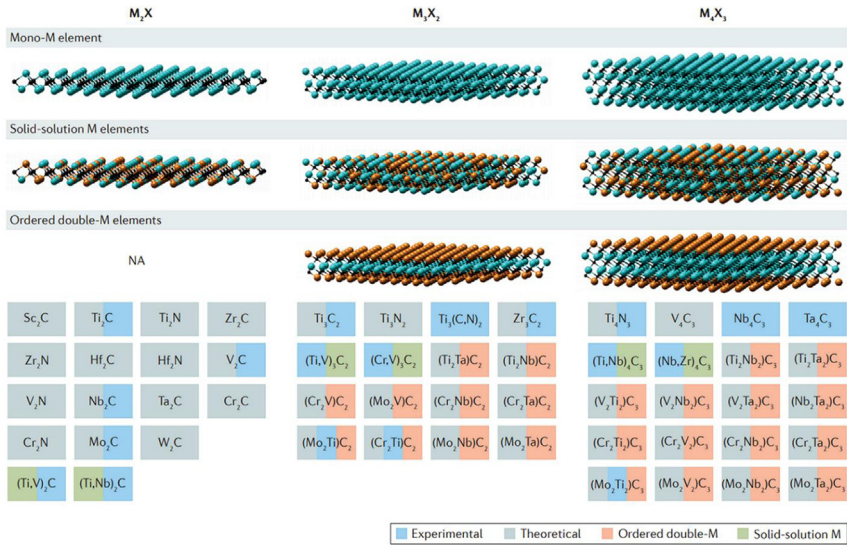


Figure 10.5 Types of MXenes used for energy storage applications Reproduced from [25].

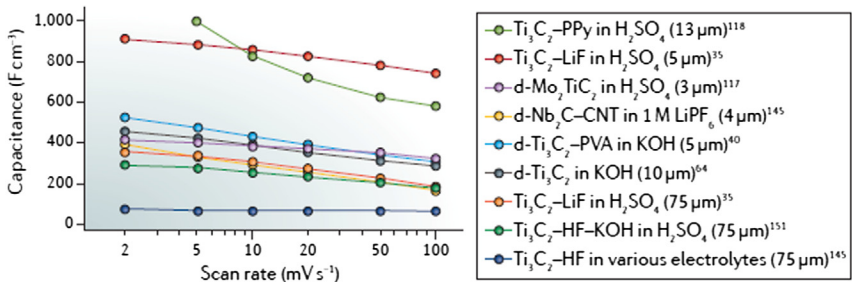


Figure 10.6 Capacitance performance comparison of MXene electrode [25].

delamination introduce various new functional groups, provide steric configuration and microstructures that have a profound effect on the electrochemical response from these materials. MXenes in different electrolytes and thickness for supercapattery applications are highlighted [25], as is evident from the capacitance graph of different MXene materials in Fig. 10.6.

After passing through the HF exfoliation process MXenes are generally added to with functional groups such as F, OH, and O groups [27]. These are known to be the active groups in these materials and the ES processes in supercapatteries are believed to occur in these active groups present at the surface interface.

For supercapacitors, charge storage occurs predominantly in the EDL formed at the surface of the electrode and the electrolyte and also on the active shallow sites [28]. In the case of rechargeable batteries, MXene generally stores energy by the processes of adsorption and desorption. Hence, MICs as a compromise between SC and batteries, have demonstrated high power and energy densities when MXene as the pseudocapacitive electrode along with a metal intercalation electrode was employed for its practical applications [29–31]. Hence, 2D Ti_2CT_x acting as the pseudocapacitive negative electrode for electrochemical transport of ions in Li-ion hybrid capacitors was reported to increase the interlayer distance between the Ti_2CT_x units due to chloride termination which added favorably to the electrochemical behavior of the cell (refer to Fig. 10.7) [32]. The electrode was coupled to a positive electrode as $\text{LiNi}_{1/3}\text{Co}_{1/3}\text{Mn}_{1/3}\text{O}_2$. The cell demonstrated a high capacity of 206 mAh g^{-1} at a voltage of 2.5 V and a 160 Wh kg^{-1} of specific energy density based on weight employed for both electrode materials. Additionally, Li-ion-based capacitors prepared by engaging MXene-based composites have shown remarkable specific energy and power density, such as when cetyltrimethylammonium bromide-Sn(IV)-based Ti_3C_2 was used as the pseudocapacitor electrode [33]. Similarly Na^+ ion hybrid capacitors have shown faster rates as compared to Na^+ ion batteries. It is, however, relevant to mention here that the sluggish kinetics due to size considerations of Na^+ ion and small capacitance due to the material used for Na^+ ion intercalation offers a bottleneck for the advancement of Na^+ ion hybrid capacitors which could be overcome by using Ti_2C MXene as the negative electrode and $\text{Na}_2\text{Fe}_2(\text{SO}_4)_3$ as

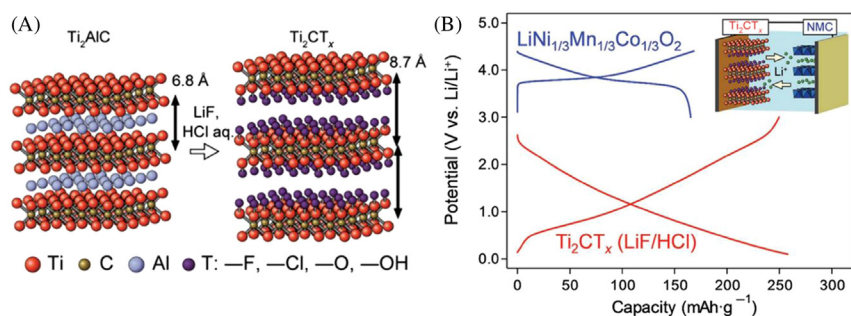


Figure 10.7 (A) Graphical representation of the fabrication by LiF-HCl treatment of MAX phase of Ti_2AlC to MXene Ti_2CT_x . (B) Charge/discharge curves for Ti_2CT_x and $\text{LiNi}_{1/3}\text{Co}_{1/3}\text{Mn}_{1/3}\text{O}_2$ versus Li/Li^+ . The inset shows a full Li-ion hybrid capacitor for Ti_2CT_x and $\text{LiNi}_{1/3}\text{Co}_{1/3}\text{Mn}_{1/3}\text{O}_2$ Reproduced from [32].

the positive electrode exhibiting higher reversible specific capacity of 102.7 mAh g⁻¹ at 600 mA g⁻¹ for 100 cycles with an energy and power density of 260 Wh kg⁻¹ and 1440 W kg⁻¹, respectively, attributed to an increase in interlayer distance of MXene layer due to de/sodiation [22]. Similarly, the mechanistic elucidation of de/intercalation of Na⁺ ion in V₂CT_x was conducted which exhibited a specific capacity of 50 mAh g⁻¹ at an operational voltage of 3.5 V. The structural/compositional flexibility offered by MXenes is an attractive choice for use to further enhance the performance of electrodes for supercapattery devised cells [34].

Similarly employing composites based on 2D MXene offers the design of hybrid EES devices with promising efficiencies. An asymmetric hybrid SC device was assembled using a composite of Ti₃C₂ MXene with nanostructured Mn₃O₄ as the anode and carbonized Fe cation as the cathode and it offered excellent power and energy density at 1 A g⁻¹. The accordion-like structure of Ti₃C₂ was able to boost the permeability of the electrolyte into the electrode, which resulted in increased transport of ions and electrochemical performance. Mn₃O₄ were found evenly lodged in the interlayer spacing of the Ti₃C₂ sheets with some found on the surface of it. This resulted in a specific capacity of 128 mAh g⁻¹ higher than either of the pristine materials [35–37] and also resulted in extenuating the changes in volume due to the insertion of cations [38]. Moreover, layered double hydroxide (LDH) have been used as positive electrodes in hybrid capacitors due to their low cost, environment-friendliness, and excellent electrochemical performance. In NiMn-LDH, the Mn is linked to increased electrochemical behavior of Ni in LDH [39,40]. However, adding conductive material improves the energy density and helps to overcome restricted redox kinetics. Thus a 3D highly porous nanosheet architecture based on Ti₃C₂ MXene-derived carbon of the same fashion as graphene nanosheets and NiMn-LDH nanocomposite was employed as the positive electrode. This has been shown to deliver fast electron transport with the shortest pathway for the transport of ions and electrons along with highly exposed active sites for electrochemical reactions to happen at NiMn-LDH. The nanocomposite is reported to provide a specific capacity of 228 mAh g⁻¹ at 1 A g⁻¹ with excellent rate capability and cycling stability. The negative electrode was a porous carbon and the assembly manifested high power and energy density of 802 W kg⁻¹ and 45.2 Wh kg⁻¹ [41].

Additionally, many theoretical studies have been conducted on the MXene family for the application of the materials in the field of ES

devices. DFT (density functional theory) suggested that for Ti_3C_2 MXene material, ions occupied the most favorable sites preferably at the top of the carbon atoms and delivered a theoretical specific capacity of 320 mAh g^{-1} [42]. Theoretical studies have shown a storage capacity of 413.0 mAh g^{-1} in interlayer expanded bare Ti_3C_2 MXenes [43]. Instinctive point defects are considered to be mobile and are reported to affect the surface chemistry for TiO_x , [44]. All the known storage mechanisms, including insertion, reversible conversion reactions, stripping, extraction, and plating can be found in MXenes [13]. Layered MXenes were interpolated and merged with an organic small molecule with a polar nature, such as *N*-dimethylformamide (DMF), hydrazine, and urea, intercalated in its layers [10]. Consequently, materials containing N groups were embedded onto MXene [28,45]. However, it was observed that *N*-doped 2D MXene $\text{Ti}_3\text{C}_2\text{T}_x$ obtained by a postetch annealing process displayed much improved electrochemical capacitance compared with solution-processed *N*-doped MXene [46]. In brief, the development of further inorganic materials as electrode materials for supercapattery devices with enhanced layer spacing, the formation of intercalated cations, and conversion of functional groups are the most significant factors for the electrochemical performance of MXenes.



10.6 Conclusion

MXene has opened up a new vista to employ free-standing electrodes in SCs without the use of Ni foam as a current collector, while increasing the energy density at the same time. Large interlayer spacing in MXene layers have been found to be promising for de/intercalation of ions such as Na^+ , Li^+ , etc. Thus different composites of MXenes with metallic oxides demonstrating extraordinary capacity and cycling stability have been reported as anodes for LIBs. Furthermore, owing to MXenes' excellent conductivity, they have been pursued as the material of choice in the field of electrochemical supercapattery and research has been focused on enhancing interlayer spacing and the conversion of functional groups to manifest high energy and power density. Thus the MXene family has been proven to be promising electrode material for ES applications. Their unique features, including outstanding biocompatibility, extraordinarily high interlayer spacing and conductivity, and environment-friendliness, are the reasons

behind the massive attraction to these materials [47,48]. Hence, MXene has the ability to dis/charge at quite rapid rates and also the capability to store a large amount of charge per unit volume or mass [49]. It is worth mentioning that the chemical and physical properties of the MXene materials, including ion mobility, mechanical and structural characteristics, and electronic transport properties play a major role in the storage of charges, and must be considered while employing such materials.

References

- [1] S. Wu, et al., Graphene-containing nanomaterials for lithium-ion batteries, *Adv. Energy Mater.* 5 (21) (2015) 1500400.
- [2] X. Guo, et al., Nanostructured graphene-based materials for flexible energy storage, *Energy Storage Mater.* 9 (2017) 150–169.
- [3] M. Naguib, et al., 25th anniversary article: MXenes: a new family of two-dimensional materials, *Adv. Mater.* 26 (7) (2014) 992–1005.
- [4] M.R. Lukatskaya, et al., Probing the mechanism of high capacitance in 2D titanium carbide using in situ X-ray absorption spectroscopy, *Adv. Energy Mater.* 5 (15) (2015) 1500589.
- [5] J. Li, et al., Achieving high pseudocapitance of 2D titanium carbide (MXene) by cation intercalation and surface modification, *Adv. Energy Mater.* 7 (15) (2017) 1602725.
- [6] A. VahidMohammadi, et al., Assembling 2D MXenes into highly stable pseudocapacitive electrodes with high power and energy densities, *Adv. Mater.* 31 (8) (2019) 1806931.
- [7] R. Zhang, et al., Multifunctional *g*-C₃N₄/graphene oxide wrapped sponge monoliths as highly efficient adsorbent and photocatalyst, *Appl. Catal. B: Environ.* 235 (2018) 17–25.
- [8] K. Zhang, et al., Three-dimensional porous Ti₃C₂T_x-NiO composite electrodes with enhanced electrochemical performance for supercapacitors, *Materials* 12 (1) (2019) 188.
- [9] Y. Dall’Agnese, et al., Capacitance of two-dimensional titanium carbide (MXene) and MXene/carbon nanotube composites in organic electrolytes, *J. Power Sources* 306 (2016) 510–515.
- [10] O. Mashtalir, et al., *Intercalation and delamination of layered carbides and carbonitrides.*, *Nat. Commun.* 4 (2013) 1716.
- [11] C.E. Ren, et al., Porous two-dimensional transition metal carbide (MXene) flakes for high-performance Li-ion storage, *ChemElectroChem* 3 (5) (2016) 689–693.
- [12] M.-Q. Zhao, et al., 2D titanium carbide and transition metal oxides hybrid electrodes for Li-ion storage, *Nano Energy* 30 (2016) 603–613.
- [13] Y. Xie, et al., Prediction and characterization of MXene nanosheet anodes for non-lithium-ion batteries, *ACS Nano* 8 (9) (2014) 9606–9615.
- [14] S. Kajiyama, et al., Sodium-ion intercalation mechanism in MXene nanosheets, *ACS Nano* 10 (3) (2016) 3334–3341.
- [15] M.Q. Zhao, et al., Hollow MXene spheres and 3D macroporous mxene frameworks for Na-ion storage, *Adv. Mater.* 29 (37) (2017) 1702410.
- [16] S. Sun, et al., Hybrid energy storage mechanisms for sulfur-decorated Ti₃C₂ MXene anode material for high-rate and long-life sodium-ion batteries, *Chem. Eng. J.* 366 (2019) 460–467.
- [17] H.-S. Kim, et al., *Oxygen vacancies enhance pseudocapacitive charge storage properties of MoO_{3-x}.*, *Nat. Mater.* 16 (4) (2017) 454.
- [18] M. Yu, et al., Dual-doped molybdenum trioxide nanowires: a bifunctional anode for fiber-shaped asymmetric supercapacitors and microbial fuel cells, *Angew. Chem. Int. Ed.* 55 (23) (2016) 6762–6766.

- [19] D. Larcher, J.-M. Tarascon, Towards greener and more sustainable batteries for electrical energy storage, *Nat. Chem.* 7 (1) (2015) 19.
- [20] K. Naoi, P. Simon, New materials and new configurations for advanced electrochemical capacitors, *J. Electrochem. Soc.* 17 (1) (2008) 34–37.
- [21] W.H. Shin, et al., Nitrogen-doped multiwall carbon nanotubes for lithium storage with extremely high capacity, *Nano Lett.* 12 (5) (2012) 2283–2288.
- [22] X. Wang, et al., Pseudocapacitance of MXene nanosheets for high-power sodium-ion hybrid capacitors, *Nat. Commun.* 6 (2015) 6544.
- [23] M.-K. Song, et al., Anomalous pseudocapacitive behavior of a nanostructured, mixed-valent manganese oxide film for electrical energy storage, *Nano Lett.* 12 (7) (2012) 3483–3490.
- [24] W. Gao, Electrochemical and electromechanical studies on nanostructured electrodes for supercapacitors, *Analytical chemistry*. Sorbonne Université / Université Pierre et Marie Curie - Paris VI, (2018).
- [25] B. Anasori, M.R. Lukatskaya, Y. Gogotsi, 2D metal carbides and nitrides (MXenes) for energy storage, *Nat. Rev. Mater.* 2 (2) (2017) 16098.
- [26] Z. Guo, et al., Strain-mediated type-I/type-II transition in MXene/Blue phosphorene van der Waals heterostructures for flexible optical/electronic devices, *J. Mater. Chem. C* 5 (4) (2017) 978–984.
- [27] Y. Xie, et al., Role of surface structure on Li-ion energy storage capacity of two-dimensional transition-metal carbides, *J. Am. Chem. Soc.* 136 (17) (2014) 6385–6394.
- [28] M. Ghidui, et al., Alkylammonium cation intercalation into Ti_3C_2 (MXene): effects on properties and ion-exchange capacity estimation, *Chem. Mater.* 29 (3) (2017) 1099–1106.
- [29] Y. Zhong, et al., Transition metal carbides and nitrides in energy storage and conversion, *Adv. Sci.* 3 (5) (2016) 1500286.
- [30] H. Wang, et al., Nonaqueous hybrid lithium-ion and sodium-ion capacitors, *Adv. Mater.* 29 (46) (2017) 1702093.
- [31] H. Tang, et al., MXene–2D layered electrode materials for energy storage, *Prog. Nat. Sci.: Mater. Int.* 28 (2) (2018) 133–147.
- [32] S. Kajiyama, et al., Enhanced Li-ion accessibility in MXene titanium carbide by steric chloride termination, *Adv. Energy Mater.* 7 (9) (2017) 1601873.
- [33] J. Luo, et al., Pillared structure design of MXene with ultralarge interlayer spacing for high-performance lithium-ion capacitors, *ACS Nano* 11 (3) (2017) 2459–2469.
- [34] Y. Dall’Agnese, et al., Two-dimensional vanadium carbide (MXene) as positive electrode for sodium-ion capacitors, *J. Phys. Chem. Lett.* 6 (12) (2015) 2305–2309.
- [35] A.G. Dylla, G. Henkelman, K.J. Stevenson, *Lithium insertion in nanostructured TiO_2 (B) architectures*, *Acc. Chem. Res.* 46 (5) (2013) 1104–1112.
- [36] J. Zhu, et al., *Composites of TiO_2 nanoparticles deposited on Ti_3C_2 MXene nanosheets with enhanced electrochemical performance*, *J. Electrochem. Soc.* 163 (5) (2016) A785–A791.
- [37] F. Davar, et al., *Thermal decomposition route for synthesis of Mn_3O_4 nanoparticles in presence of a novel precursor*, *Polyhedron* 29 (7) (2010) 1747–1753.
- [38] K. Oyedotun, et al., Investigation of graphene oxide nanogel and carbon nanorods as electrode for electrochemical supercapacitor, *Electrochim. Acta* 245 (2017) 268–278.
- [39] H. Sim, et al., Reverse micelle synthesis of colloidal nickel–manganese layered double hydroxide nanosheets and their pseudocapacitive properties, *Chem. Eur. J.* 20 (45) (2014) 14880–14884.
- [40] J. Zhao, et al., Hierarchical NiMn layered double hydroxide/carbon nanotubes architecture with superb energy density for flexible supercapacitors, *Adv. Funct. Mater.* 24 (20) (2014) 2938–2946.

- [41] J. Zhu, et al., Three-dimensional porous MXene-derived carbon/nickel-manganese double hydroxide composite for high-performance hybrid capacitor, *J. Electroanal. Chem.* 836 (2019) 118–124.
- [42] Q. Tang, Z. Zhou, P. Shen, *Are MXenes promising anode materials for Li ion batteries? Computational studies on electronic properties and Li storage capability of Ti_3C_2 and $Ti_3C_2X_2$ ($X = F, OH$) monolayer*, *J. Am. Chem. Soc.* 134 (40) (2012) 16909–16916.
- [43] Y.-X. Yu, *Prediction of mobility, enhanced storage capacity, and volume change during sodiation on interlayer-expanded functionalized Ti_3C_2 MXene anode materials for sodium-ion batteries*, *J. Phys. Chem. C.* 120 (10) (2016) 5288–5296.
- [44] L.H. Karlsson, et al., Atomically resolved structural and chemical investigation of single MXene sheets, *Nano Lett.* 15 (8) (2015) 4955–4960.
- [45] M. Ghidui, et al., *Ion-exchange and cation solvation reactions in Ti_3C_2 MXene*, *Chem. Mater.* 28 (10) (2016) 3507–3514.
- [46] Y. Wen, et al., *Nitrogen-doped $Ti_3C_2T_x$ MXene electrodes for high-performance supercapacitors*, *Nano Energy* 38 (2017) 368–376.
- [47] F. Wang, et al., *TiO_2 nanoparticle modified organ-like Ti_3C_2 MXene nanocomposite encapsulating hemoglobin for a mediator-free biosensor with excellent performances*, *Biosens. Bioelectron.* 74 (2015) 1022–1028.
- [48] H. Liu, et al., *A novel nitrite biosensor based on the direct electrochemistry of hemoglobin immobilized on MXene- Ti_3C_2* , *Sens. Actuators B: Chem.* 218 (2015) 60–66.
- [49] M.D. Levi, et al., *Solving the capacitive paradox of 2D MXene using electrochemical quartz-crystal admittance and in situ electronic conductance measurements*, *Adv. Energy Mater.* 5 (1) (2015) 1400815.

Aqueous solid and gel electrolytes for supercapattery

Shahid Bashir¹, Mee Yoke Chong², Maryam Hina¹, Kashif Kamran³, S. Ramesh¹ and K. Ramesh¹

¹Centre for Ionics University of Malaya, Department of Physics, Faculty of Science, University of Malaya, Kuala Lumpur, Malaysia

²Centre for American Education, INTI International University, Persiaran Bandar Baru Nilai, Malaysia

³Department of Physics, University of Agriculture, Faisalabad, Pakistan

11.1 Introduction

The humble beginnings of the concept of the supercapacitor in the 1800s become a technical reality after 150 years and it took 20 years more to become commercially available [1]. An electric double-layer charge storage device was reported first time in 1957 by H.I. Becker [2]. They fabricated the device using two porous carbon electrodes. Later on, Becker patented this electrolytic capacitor with porous carbon electrodes after discovering its exceptionally high capacitance without understanding its energy storage principle. However, the works were not pursued until Standard Oil of Ohia (SOHIO) invented the first supercapacitor. Unfortunately, SOHIO failed to market the technology and licensed it to Nippon Electric Company (NEC) and they eventually commercialized the invention under the name of “supercapacitor” in 1978.

The commercialized supercapacitors were rated at 5.5 V (with the capacitance maximum of 1 F g^{-1}) and were used as power backup for computer memories. In 1980 ELIT, a Russian company, designed the ever first asymmetric supercapacitor and the symmetric supercapacitor in the following year. From 1975 to 1980, B.E. Conway worked on the application of ruthenium oxide (RuO_2) for supercapacitors and found that the electrochemical storage mechanism was different in supercapacitors and batteries [3]. The history of the supercapacitor is illustrated in Fig. 11.1.

Recently, the supercapacitor has been an auspicious energy storage device owing to significant features like high power density (P_d),

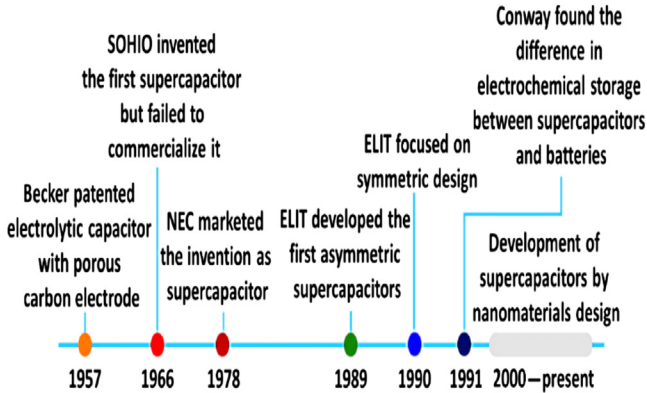


Figure 11.1 History of development of supercapacitors [1].

promising cyclic stability, and fast charge/discharge rate [4,5]. However, most commercialized supercapacitors possess very low energy density that limits them for exploitation in high energy and long-term applications [6]. Recent works reported that superconductors are incorporated with different types of electrolytes such as liquid, solid, and gel for electronic applications. These have different charge storage mechanism and are classified into three different types, that is, electric double-layer capacitor, pseudocapacitor, and hybrid supercapacitor or supercapattery. Electric double-layer capacitor is a two-electrode electrochemical device in which current collectors are coated with porous carbon materials and immersed in liquid electrolyte or a thin layer of solid or gel polymer electrolyte (GPE) is sandwiched between two electrodes. It works on the principle of separation of electronic and ionic charges at the electrode/electrolyte interface. The second type of electrochemical cell is the pseudocapacitor in which fast faradaic reactions occurring due to electrode materials are dominant [7]. Third is the supercapattery, an asymmetric device where faradaic (battery type) and capacitive electrodes are combined and energy is stored and delivered based on faradaic redox reaction on one electrode and nonfaradaic (ion adsorption) on the other electrode, respectively [8]. It is a bitter fact that the commercialization of supercapacitors is not feasible due to the lower energy density compared to a battery. This scenario brings the idea of a new hybrid device to meet the energy requirements worldwide which can combine the characteristics of supercapacitors and batteries, which is now known as supercapattery. Hence, this supercapattery emerges as a significant solution in

electrochemical energy storage devices that possesses the distinctive features of the battery (high energy density) and supercapacitor (high power density). Currently, research has been carried out on a large scale to improve the supercapattery performance [9,10].

There are three type of electrolytes used in the supercapacitors and supercapattery. These electrolytes are aqueous and organic liquids, polymer solids, and polymer gels. Liquid electrolytes are prone to leakage and toxic in nature while the solid polymer electrolytes have poor ionic conductivity and limited interfacial contact with the electrode. GPEs have no problem of leakage and possess free volume for movement of ions, but these electrolytes contain toxic organic solvents. Presently, hydrogels are emerging as a pivotal group of functional material [11]. These functional hydrogels are very significant as electrolytes for supercapacitors and supercapattery [12]. Hydrogels have a porous microstructure, free volume, large specific surface area, modifiable physical/chemical characteristics, short pathways for charge/mass transfer, and so forth [13]. These hydrogels are highly flexible and their mechanical strength is tunable [13,14].



11.2 Polymer electrolytes

Polymer electrolytes were discovered in 1973 by Fenton and his coworkers. The polymer electrolytes gained their popularity among researchers because they have potential in overwriting the role of the classical electrolytes (i.e., organic and aqueous electrolytes) [15]. Moreover, they have distinguished features to overcome the shortcomings of classical electrolytes that possess a narrow potential window due to the electrolysis of water, and being toxic, highly volatile, and highly flammable [16]. A polymer is a long-chain large molecule consisting of multiple monomers. The salt is an ionic compound with its own distinctive lattice energy value and dissociates into ions (cations and anions) when it dissolves into the solvent. When the polymer is dissolved into a suitable solvent and salt, a polymer electrolyte is formed. The ions bind to the functional groups of the polymer chain via various intermolecular forces such as ion–dipole force, permanent dipole, dispersion, or hydrogen bonding. The polymer serves as the backbone to facilitate the transportation of ions. In general, the nature of the developed polymer electrolyte (i.e., amorphous, crystalline, and semicrystalline) affects the mode of transportation of ions.

Nevertheless, it is worth mentioning that the techniques to associate polymer and salt classify the polymer electrolytes into various types, that are:

1. solid polymer electrolyte.
2. GPE.
3. hydrogel polymer electrolyte.

11.2.1 Ion conduction pattern in polymer electrolytes

11.2.1.1 Free volume theory

Vogel–Tamman–Fulcher (VTF) or William–Landel–Ferry (WLF) models are used to demonstrate the transportation of ions along the elastomeric host polymer via the space (free volume). The theory is not influenced by the surrounding temperature, but dependent on the glass transition temperature, T_g , of a host polymer. At the temperature above T_g of a host polymer, the host polymer exhibits a rubbery property, the particles are arranged randomly with high entropy. Subsequently, the host polymer possesses high average kinetic energy which causes great breaking and forming of interactions among the solvated ions. Hence, more free volume is generated to facilitate ions transportation. On the other hand, at the temperature below T_g of a host polymer, the host polymer exhibits a glassy property, the particles are highly ordered with low entropy. It hinders the motion of the host polymer and therefore less free volume is available to facilitate the transportation of ions [17]. In other words, this theory is suitable for amorphous materials [18]. There are two equations related to the free volume theory:

1. VTF equation is expressed as Eq. (11.1) [19]:

$$\sigma = AT^{-\frac{1}{2}}e^{-\frac{E_a}{k_B(T-T_0)}} \quad (11.1)$$

where σ is the conductivity of the polymer electrolyte at absolute temperature T , A is the constant related to the number of charge carriers in the electrolyte system, E_a is the pseudo activation energy, k_B is the Boltzmann constant, and T_0 is the ideal glass transition temperature (Vogel temperature), a temperature at which the free volume disappears [19]. When the empirical VTF equation rearranges, a linear graph of $\ln \sigma T^{\frac{1}{2}}$ against $\frac{1000}{T-T_0}$ is obtained. The gradient and intercept of the graph represent the $-\frac{E_a}{k_B}$ and $\ln A$, respectively. Fig. 11.2 explains the relationship between $\ln \sigma T^{\frac{1}{2}}$ and $\frac{1000}{T-T_0}$ [19].

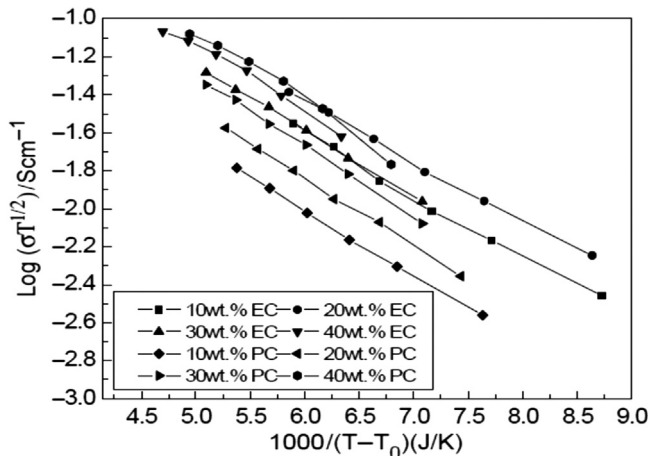


Figure 11.2 The plot of $\ln \sigma T^{\frac{1}{2}}$ against the $\frac{1000}{T-T_0}$ [19].

2. WLF equation is expressed in Eq. (11.2) [20]:

$$\log_{10} \frac{\sigma_T}{\sigma_{T_g}} = \frac{C_1(T - T_g)}{C_2(T + T_g)} \quad (11.2)$$

where σ_T , σ_{T_g} are the values of conductivity at given temperature T and T_g . On the other hand, the C_1 and C_2 are temperature-dependent ionic conductivity VTF parameters. The ideal values of C_1 and C_2 used to indicate the complete synthesis of polymer electrolytes are 17.4K and 51.6K [21]. WLF equation is employed to evaluate the ion conduction mechanism in host polymer along the segmental motion of the polymer chain via ion–dipole interactions at a temperature above T_g [20].

Polymer electrolytes that fitted the VTF equation for the application of batteries are poly(vinyl chloride) incorporated with lithium difluoro (oxalate)borate and a mixture of poly(ethylene oxide)/poly(dimethyl siloxane) (PEO/PDMS) blend and lithium perchlorate [22,23]. Meanwhile, the polymer electrolytes that obeyed the VTF equation for the application of supercapacitor are prepared by mixing ionic liquid 1-ethyl-3-methylimidazolium tetrafluoroborate and hexagonal boron nitride salt in sulfonated polysulfone (SPSU) as a host polymer by Gunday et al. [24] and potato starch/methyl cellulose blend fused with ammonium nitrate and glycerol by Hamsan et al. [25,24,25].

11.2.1.2 Arrhenius theory

Arrhenius theory which is also known as hopping mechanism states that ions' conduction along the host polymer is stable toward phase transition and relies solely on the surrounding temperature. As the temperature increases, the polymer expands and creates segmental translation owing to the rotation and vibration of polymer. On top of that, the ions receive more kinetic energy to overcome the energy of activation, hereafter, it hopped to the vacant sites either via intrachain or interchain interactions of the host polymer. The relationship between the absolute temperature and conduction of ions along the host polymer can be expressed in Eq. (11.3) [26]:

$$\sigma = \sigma_0 e^{-\frac{E_a}{k_B T}} \quad (11.3)$$

where σ is the conductivity at temperature T , σ_0 is the preexponential factor, E_a is the energy of activation, and k_B is the Boltzmann constant. When the Arrhenius theory equation rearranges, a linear graph of $\ln \sigma$ against $\frac{1000}{T}$ is plotted. The gradient and intercept of the graph represents the $-\frac{E_a}{k_B}$ and $\ln \sigma_0$, respectively [27].

Numerous charge carriers are thermally activated along the host polymer for the application of electrochemical devices such as conduction of sodium iodide along the poly(acrylamide-co-acrylic acid) assisted with propylene carbonate [28], chitosan thin film doped with sodium triflate [29], and poly(ethylene oxide) (PEO) incorporated with alumina nanofillers and tetrapropyl ammonium iodide [30]. Likewise, Jinisha et al. prepared solid polymer electrolyte by incorporating PEO/PVP with lithium nitrate, for use in lithium-ion batteries, that obeyed Arrhenius equation [31]. In addition, Zhu et al. [32] and Bao et al. [33] prepared PEO/lithium bis(tri-fluoromethane) sulfonamide/ceramic $\text{Li}_{0.33}\text{La}_{0.557}\text{TiO}_3$ nanofibers and comb-like nonionic waterborne polyurethane/lithium perchlorate solid polymer electrolytes, respectively, for lithium batteries. These electrolytes showed temperature-dependent behavior [32,33].

11.2.2 Classification of polymer electrolytes

Polymer electrolytes are classified as solid and GPEs. Solid and GPEs are briefly discussed in the given sections.

11.2.2.1 Solid polymer electrolytes

The first solid polymer electrolyte based on PEO was discovered by Fenton et al. in 1973. Conducting solid polymer electrolytes are formed

in lieu to the integration of salt, acids, or alkalis into the polymer matrix. The polymer matrix serves as a backbone, whereas the solvent dissociation of low lattice energy salts, acids, and alkalis serve as the mobile carriers. The mobile carriers are transported along the polymer matrix via the available space and intermolecular interactions (i.e., ion dipole, dispersion, permanent dipole, and hydrogen bonding) within the polymer network. The solid polymer electrolytes have been a suitable choice over their counterparts owing to their distinguished features that are light weight, easy to handle, flexible, leakage free, excellent dimensional and electrochemical stability, safe to use, and long cyclic life [34–38]. Solid polymer electrolytes are usually sandwiched between the capacitive electrode and battery electrode of the supercapattery. However, their low ionic conductivity at room temperature $\sim 10^{-7} \text{ S cm}^{-1}$ is one of the crucial reasons that hinders the use in supercapattery and significantly reduces its performance. Solid polymer electrolytes must fulfill three basic requirements prior to the construction of the supercapattery. They are as follows:

1. Performance—the polymer electrolyte used must have high ionic conductivity, an amorphous nature, excellent electrode/electrolyte interfacial contact, and a wide potential window, which leads to a higher power output from the device [39].
2. Durability—the polymer electrolyte must possess optimum mechanical strength along with outstanding chemical and electrochemical stability in order to sustain its performance when it is under operating conditions (i.e., operating temperature and electrochemical potential) [40].
3. Safety—the choice of polymer electrolyte and the methods to fabricate various devices have to be taken into account to prevent harm, such as spillage free, internal short circuit, use of corrosive solvent, and production of hazardous gases [41].

11.2.3 Classifications of solid polymer electrolytes

11.2.3.1 Types of host polymer in the solid polymer electrolyte

11.2.3.1.1 Biodegradable host polymer

According to Swift [42], the fragments that are produced via partially or completely breaking down the biomolecules/biomass by the enzymatic process is known as biodegradable polymers [42]. The biodegradable polymer has been used widely owing to its merits, which are [43–45]:

1. Cheap.
2. Easily accessible.
3. Biocompatibility.

4. Renewable source.
5. Environmentally friendly by releasing minimal hazardous products.

The biopolymers such as chitosan [46], cellulose acetate [46], κ -carrageenan [46], agar-agar [46], cellulose and its derivatives [21], corn starch [46], and poly(vinyl alcohol) (PVA) [47] have been explored by researchers for energy storage devices. Among natural polymers, chitosan and starch gained the most popularity as the host polymer for electric double-layer capacitor (EDLC) because they are capable of forming a mechanically stable thin film with good solubility and electrolytic properties [48,49]. As a result, in early 2016, the most outperform supercapacitor was fabricated by using biodegradable blend polymer of chitosan and chitin sponge. The EDLC can endure 10,000 cycles without any change in capacitance (97 F g^{-1}), energy density (8.91 Wh kg^{-1}), and power density (563 W kg^{-1}) at 5 mA current and working voltage of 0.8 V [45].

11.2.3.2 Synthetic host polymer

The polymer that is able to withstand all forms of degradation is known as a synthetic or nonbiodegradable polymer [42]. The synthetic host polymers are expensive, create the hassle of disposal, and cause severe depletion of petroleum resources [50]. Nevertheless, numerous synthetic polymers such as polyacrylonitrile (PAN), polyethylene glycol (PEG), polyaniline (PANI), polypyrrole (PPy), PEO, poly(methylmethacrylate) (PMMA), polyacrylamide, poly(vinyl pyrrolidone) (PVP), poly(vinylidene fluoride- ω -hexafluoropropylene) (PVdF-HFP), poly(2-hydroxyethyl methacrylate- ω -methyl methacrylate), etc. have been used to prepare solid polymer electrolytes for energy storage devices [51–53].

11.2.3.3 Methods to prepare solid polymer electrolytes

11.2.3.3.1 Solution casting technique

The solution casting technique is a two-step method to prepare solid polymer electrolytes. The first step is to form a homogeneous mixture by adding the appropriate amount of salt and polymer into the solvent. Following this, in the second step, the miscible solution prepared via magnetic stirring is poured onto the petri dish and allowed to dry for thin film formation. Although the classical technique has existed for decades, it is still being adopted by many researchers to prepare solid polymer electrolyte for the application of batteries and supercapacitors owing to its hassle-free steps. Perumal et al. [54] prepared a solid biopolymer electrolyte of tamarind seed polysaccharide and magnesium

perchlorate as charge carriers for magnesium ion batteries [54]. Sasikumar et al. fabricated lithium-ion batteries using PVAc/P (VdF-HFP)/ lithium trifluoromethanesulfonate solid polymer electrolyte. This showed very high ionic conductivity at room temperature ($1.1 \times 10^{-3} \text{ S cm}^{-1}$) [55]. On the other hand, Farhana et al. (2018) and Aziz et al. [56] prepared magnesium-based and proton-based EDLCs which were held strongly by the iota-carrageenan and chitosan/PEO blend as the backbone, respectively [56,57]. However, the solution casting technique has been innovated with the assistance of ultrasonic-microwave irradiation (US–MW) to improve ionic conductivity and dielectric polarizations of the ethylene carbonate (EC) plasticized solid polymer electrolyte of PEO/PMMA/lithium tetrafluoroborate. The newly invented technique is an extension of the conventional solution casting technique in which the homogenized solution will be sonicated by using an ultrasonicator for 10 minutes. Following this, the sonicated solution is subjected to microwave electromagnetic energy in a domestic oven for 10 minutes, as reported by Priyanka and Sengwa [58]. Conventional and modified solution casting techniques are shown in Figs. 11.3 and 11.4.

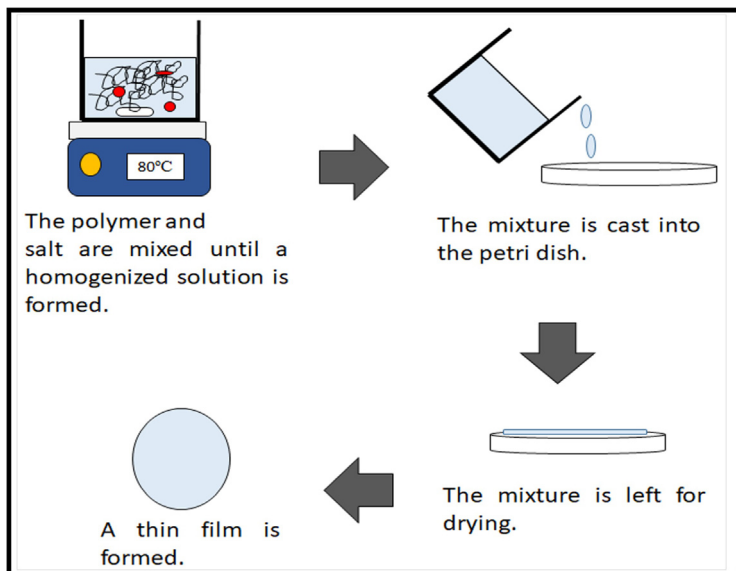


Figure 11.3 Conventional solution casting technique.

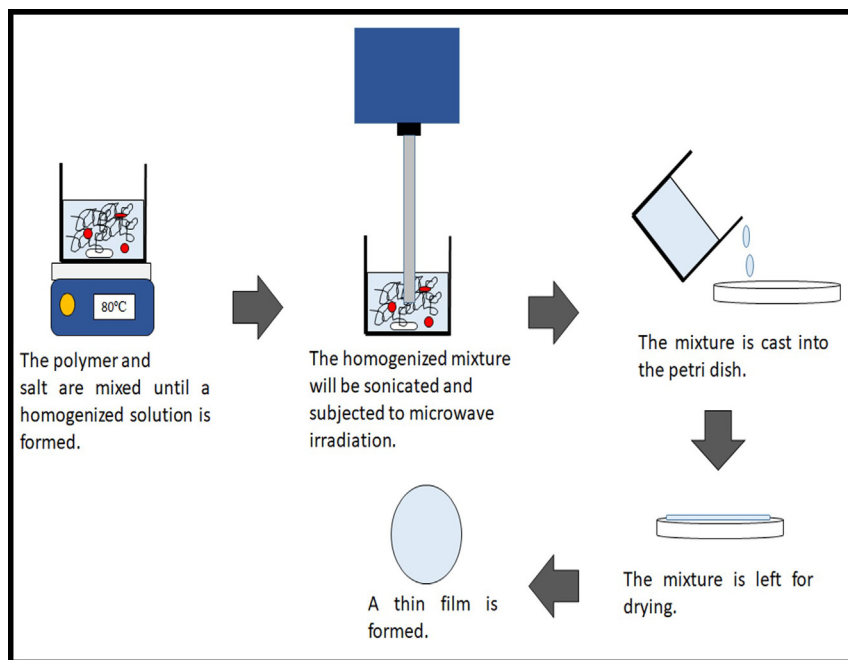


Figure 11.4 Modified solution casting technique.

11.2.3.3.2 Hot-press technique

The hot-press technique is a two-step process to prepare solid polymer electrolytes. This technique is novel to create good interfacial contact between the electrodes and electrolyte [59]. The first step in the hot-press technique involves the melting of the mixture, which contains an appropriate amount of salt and polymer, at the melting point of polymer, to form a slurry. Following this, in the second step, the slurry obtained is pressed between two cold metal blocks to form a uniform thin film. This technique possesses several advantages, which are as follows [60]:

1. Inexpensive.
2. Less cumbersome/fast/dry technique.
3. Forms a uniform thickness of thin film.
4. Solvent free.

This solvent-free technique improves the morphology of the solid polymer electrolyte compared to the solution casting technique because it does not involve the evaporation of a solvent [61]. The result is in good agreement in terms of the morphology of the solid polymer electrolyte of PEO/NaBr/silica nanofiller prepared via the same method [62].

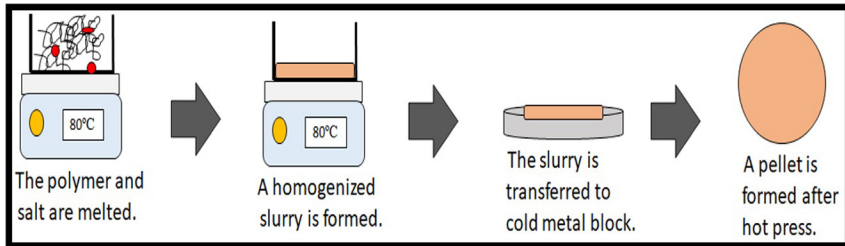


Figure 11.5 Hot-press technique.

Unfortunately, the ionic conductivity of solid polymer electrolyte prepared via hot-press technique is low at room temperature while the crystallinity is slightly increased [61]. In short, the attempt to prepare SPE for EDLC by using the hot-press method needs to be polished because it achieves low specific capacitance, as proven in the work by Verma et al. [53] using PEO, silver iodide, and activated carbon for the fabrication of EDLC [53]. As a result, EDLC obtained low specific capacitance (5 F g^{-1}) and high ionic conductivity at room temperature ($1.92 \times 10^{-3} \text{ S cm}^{-1}$). The block diagram of the hot-press technique is shown in Fig. 11.5.

11.2.4 Methods to improve the performance of the solid polymer electrolyte

11.2.4.1 Plasticizers

Plasticizers, known as high dielectric constant polar solvents or both low and high molecular organic liquids, have been explored to enhance the ion conduction in the system. The conduction of ion is higher when the dielectric constant of the plasticizer is greater than that of the host polymer and vice versa [63]. Various conventional plasticizers are used for supercapacitors and supercapattery. Commonly used plasticizers are EC ($\epsilon = 89.78$), propylene carbonate (PC) ($\epsilon = 66.14$), PEG [64], tetra ethylene glycol, diethyl carbonate, dimethyl carbonate (DMC) ($\epsilon = 3.10$), and glycerol [46] [65]. These plasticizers improve the ionic conductivity by increasing;

1. Degree of salt dissolution [66].
2. Amorphous phase [46].

Unfortunately, the plasticization effect ruptures the mechanical stability of the solid polymer electrolyte owing to its high vapor pressure and flammability [67]. Subsequently, oligoether-based plasticizer can be used to overcome its shortcomings [68]. Instead, oligoether-based plasticizers are

susceptible toward the nucleophilic attack by superoxide and reduced oxygen radicals during cyclic charge/discharge in lithium-ion batteries compared to conventional plasticizers [69]. The research is not stagnant as a novel solid plasticizer, succinonitrile (SN), has been employed by Zhang et al. [70]. They prepared a ceramic-based solid polymer electrolyte (PEO/LiTFSI/LiAlO₂) to enhance ionic conductivity and mechanical strength for fabrication of lithium batteries. This plasticizer has outstanding features (i.e., high polarity, excellent solvent for lithium salts, and enhanced ionic conductivities and mechanical strength) [70].

11.2.4.2 Nanofillers (passive and active/ceramic nanofillers)

Nanoparticles are used to integrate the mechanical strength, thermal, electrochemical, and interfacial stability of the polymer matrix. Nanofillers also enhance the conductivity of solid polymer electrolytes via the double-percolation-threshold model. The nanoparticles maintain the porous network of the host polymer which enables it to trap the ions [71]. The nanoparticles incorporated into the polymer matrix are classified into various categories:

1. Inert/passive/ceramic—ceramic or inert nanoparticles (i.e., aluminum oxide (Al₂O₃), silicon(IV) oxide (SiO₂), copper(II) oxide (CuO), stibnium(III) oxide (Sb₂O₃), zirconium(IV) oxide (ZrO₂), titanium(IV) oxide (TiO₂), and yttrium(III) oxide (Y₂O₃) in the solid polymer electrolyte improve the ionic conductivity and the mechanic/thermal strength. Generally, the ceramic nanoparticles exhibit their role on the surface of the polymer matrix very well because it creates a more amorphous region, provides a larger surface area, and builds up a good rapport between the electron—pair acceptor and electron—pair donor. Moreover, the high dielectric constant of ceramic nanoparticles such as ZrO₂ and TiO₂ decreases the viscosity of the polymer electrolyte and lattice energy of the salt [72].
2. Inorganic/active ceramic—most of the inorganic ceramic fillers like NASICON-structured LATP (Li_{1+x}Al_xTi_{2-x}(PO₄)₃), lithium lanthanum zirconium garnet (LLZO) (Li₇La₃Zr₂O₁₂), lithium-nitrogen (Li₂N) and lithium-alumina (LiAl₂O₃) portray excellent ionic conductivity of $\sim 10^{-4}$ S cm⁻¹ via the conduction process. Also, it enhances the chemical stability at room temperature along with a wide electrochemical window. Nevertheless, the huge interfacial resistance between the rigid and brittle ceramic electrolytes and the electrodes obstructs their practical applications.

3. Ferroelectric nanoparticles—the fillers (i.e., barium titanate (BaTiO_3), lithium niobate (LiNbO_3), and lead titanate (PbTiO_3)) have been used for transducers and actuators because of their high dielectric constant.
4. Carbon-based nanoparticles (carbon nanotubes, graphene sheets, and carbon black)—the fillers are surface functionalized to adsorb more charge carriers. In addition, they are highly conducting.

11.2.4.3 Room temperature ionic liquids

Ionic liquids are very useful to improve the characteristics of electrolytes, such as thermal stability and ionic conductivity, as well as possessing significant advantages for use in supercapacitors and supercapattery. They are helpful to increase the electrode/electrolyte interaction and electrochemical potential window. Therefore ionic liquids have been widely used electrolytes for organic synthesis, biochemical processes, extraction of solvent for chelate and metal, polymer electrolytes for energy storage devices and dye-sensitized solar cells (DSSC), biological applications (i.e., drug delivery and activating agent for enzymes), and biomass processing applications (i.e., conversion of biomass for biofuel and bio-oil). Generally, the cations in the ionic liquid are predominantly nitrogen heterocycles and can be categorized into pyrrolidinium, imidazolium, and piperidinium. Pyrrolidinium and piperidinium are saturated alicyclics, whereas imidazolium is an unsaturated alicyclic. Both pyrrolidinium and piperidinium are stronger Lewis bases than imidazolium. As a result, pyrrolidinium and piperidinium create stronger interactions with their counterions than imidazolium. Thus the dissociation of imidazolium from its counterion is easier [73].

The futuristic room temperature ionic liquids have been modified and synthesized by incorporation of polyhedral oligomeric silsesquioxane (POSS) to acquire marvelous thermal stability for the application of lithium batteries [74]. Apart from this, the superiority of ionic liquid has been adopted to synthesize poly(ionic liquid) (PIL). The poly(ionic liquid) can be prepared through the assimilation of two ionic liquids or between an ionic liquid and a polymer via covalent bond. Yang and coworkers integrate two ionic liquids of triethylmethylammonium bromide and lithium bis(fluorosulfonyl)imide, which have the ability to conquer the dendrite growth in the lithium battery as well as high cycling stability at 40°C [75]. On the other hand, Qi and coworkers polymerize the vinyl imidazolium monomer prior to the embedment into the polymeric POSS and it gives outstanding electrochemical stability up to 5 V with excellent capacity retention after 100 cycles. Consequently, the use of poly(ionic

liquid) gained interest among the researchers owing to its overwhelming thermal, mechanical, and electrochemical stability and higher ionic conductivity [76].

11.2.4.4 Polymer blends

Blending is a process of mixing two or more polymers physically to prepare a new type of material. In 1846 Parkes developed and patented the first polymer blend between natural rubber and gutta-percha (Khan et al., 2019). The selection of polymers for blending depends on the desired application. The benefits of polymer blends are:

1. to create materials with combinations of better mechanical, chemical, and versatile properties than the individual polymer;
2. cheaper to modify the existing polymer rather than to invent a new monomer or polymer; and
3. it creates more space for the adsorption of charge carriers by decreasing the crystalline structure

In addition to this, there are assorted polymer blends developed by the researchers for energy storage devices, such as chitosan/PVA, chitosan/PEO, chitosan/ κ -carrageenan, chitosan/iota (ι)-carrageenan, chitosan/starch, chitosan/sponge chitin, PVA/polystyrene sulfonic acid, PVdF-HFP/PVP, perfluorosulfonic acid/PTFE, PEG diacrylate/PVdF/PMMA, PVC/PMMA, PVC/PEO, etc. In order to reduce the environmental problem and to maintain the superior performance of EDLC simultaneously, some researchers prepared a polymer electrolyte by blending nonbiodegradable and biodegradable polymers such as PEO/chitosan blend.

11.2.4.5 Copolymerization

Copolymerization is a chemical process to combine two or more monomers. According to Mayo and Walling (1950), the reaction of copolymerization was first described in 1914 by Klatté using vinyl esters as a monomer (Mayo and Walling, 1950). This method portrays all the advantages as preparing blend polymers. The most durable supercapacitor was fabricated using a copolymer of PAN-*b*-PEG-*b*-PAN as polymer electrolyte. The supercapacitor demonstrated excellent cyclic stability (30,000 cycles) at a current density of 12.5 A g^{-1} at a potential window of 2 V and retained the capacitance with negligible loss. It achieved a maximum specific capacitance of 101 F g^{-1} , energy density of 11.5 Wh kg^{-1} , and power density of 10 kW kg^{-1} at 0.125 A g^{-1} . The most frequently used

copolymer as polymer electrolyte for EDLC is PVdF-HFP because it has mediocre crystalline and amorphous properties from PVdF and HFP, respectively. The use of PVdF-HFP as a host polymer in polymer electrolyte has been widespread because it contains seven fluorine atoms per monomer for the adsorption of charge carriers, which is believed to improve the ionic conductivity, large porosity, low T_g (-62°C), and high dielectric constant (~ 8.4) [77]. The performance comparison of solid polymer electrolytes is given in Table 11.1.

11.2.5 Gel polymer electrolytes

Solid polymer electrolytes are promising alternatives to liquid electrolytes and tackle the leakage issues. However, solid polymer electrolytes have low ionic conductivity (10^{-8} – 10^{-5} S cm $^{-1}$), improper contact with the electrode, and inferior mechanical strength. Due to poor ionic conductivity and electrode interaction, solid polymer electrolytes result in deteriorated cyclic performance. The limited mechanical strength prohibits the development of flexible and smart electronic devices. Therefore, to overcome these shortcomings, the combination of liquid and solid electrolytes is the most ideal substitute, known as GPE. GPEs gained significant attention as they play the role of electrolyte as well as separator. GPEs are highly flexible materials, so they can allow supercapacitors with adjustable shapes and portable and wearable devices. In addition, the elasticity and flexibility properties of GPEs are also prone to tolerating the volume change of electrode materials. Consequently, GPEs are the most desirable alternatives of liquid and solid electrolytes for supercapacitors and supercapattery.

11.2.6 Hydrogel electrolytes

GPEs possess promising characteristics. However, they have some disadvantages such as the involvement of toxic organic solvents which are harmful to human health and stability. The removal of organic solvents and the introduction of water is crucial. The substitution of GPEs are the hydrogel electrolytes. These hydrogels have significant potential advantages such as 3D networks, microstructures, controlled pore structure, porous morphology, self-healability, and an environment-friendly and nontoxic nature [100,101]. These hydrogels are unique combinations of conventional polymers and organic conductors. Furthermore, hydrogels improve the specific capacitance, rate capability, and cyclic life [102]. In

Table 11.1 Performance comparison of solid polymer electrolytes.

Method	Polymer	Salt	Solvent	Conductivity (S cm ⁻¹)	References
(A) Plasticizers					
Ethylene carbonate	Agar–agar	Ammonium bromide	Dimethylformamide	3.73×10^{-4}	[78]
Propylene carbonate	Poly(methyl methacrylate)	Lithium tetraborate	Tetrahydrofuran	5.14×10^{-6}	[79]
Polyethylene glycol	Carboxymethyl cellulose	Ammonium fluoride	Distilled water	6.62×10^{-7}	[80]
Dimethyl carbonate	Poly(vinylpyrrolidone)	Methanesulfonic acid	Dimethylformamide	3.27×10^{-5}	[81]
Glycerol	Hydroxylethyl cellulose	Lithium tetraborate	Deionized water	4.6×10^{-3}	[82]
Nitrile groups terminated oligoether	Poly(ethylene oxide)	Lithium bis (trifluoromethylsulfonyl) imide	Acetonitrile	1.11×10^{-4}	[67]
Succinonitrile	Poly(ethylene oxide)	Lithium bis (trifluoromethylsulfonyl) imide	Acetonitrile	1.36×10^{-5} at 30°C	[70]
(B) Nanofillers					
<i>i. Inert/passive/ceramic</i>					
Aluminum oxide	Poly(methyl methacrylate)	Lithium triflate	Tetrahydrofuran	1.52×10^{-4}	[83]
Silicon(IV) oxide	Hydroxylethyl cellulose	Magnesium triflate	Deionized water	2.7×10^{-4}	[84]
Zirconium(IV) oxide	Poly(vinyl pyrrolidone)	Sodium metaphosphate	Deionized water	1.03×10^{-3}	[85]
Copper(II) oxide	Polyindole	Lithium perchlorate	Acetonitrile	1.03×10^{-5}	[86]
Yttrium(III) oxide	Hydroxylethyl cellulose	Magnesium triflate	Deionized water	3.08×10^{-4}	[87]
Titanium(IV) oxide	Poly(ethylene oxide)	Lithium 2-trifluoromethyl- 4,5-dicyanoimidazole	Acetonitrile	2.11×10^{-5}	[88]

ii. Inorganic/active ceramic

NASICON-structured LATP ($\text{Li}_{1+x}\text{Al}_x\text{Ti}_{2-x}(\text{PO}_4)_3$)	Poly(vinylidene fluoride- hexafluoropropylene)	Lithium bis (trifluoromethanesulfonyl) imide	NMP (<i>N</i> -methyl-2- pyrrolidone)	1.02×10^{-4}	[89]
Lithium lanthanum zirconium garnet (LLZO) ($\text{Li}_7\text{La}_3\text{Zr}_2\text{O}_{12}$)	Poly(ethylene oxide)	Lithium bis (trifluoromethanesulfonyl) imide	Acetonitrile	5.5×10^{-4} at 30°C	[90]

iii. Ferroelectric

Barium titanate	Chitosan	Ammonium triflate	1% Acetic acid	NIL	[91]
Lead titanate	Pristine poly(vinylidene fluoride- hexafluoropropylene)	Lithium bis (perfluoroethanesulfonyl) imide	Tetrahydrofuran	4.6×10^{-5}	[92]

iv. Carbon-based

Graphene oxide sheets	Poly(acrylonitrile)	Lithium perchlorate	Dimethylformamide	4×10^{-4}	[18]
Carbon nanotubes	Poly(ethylene oxide)	Lithium hexafluorophosphate	Acetonitrile	1.3×10^{-3}	[93]

(C) Room temperature ionic liquids

Poly(ionic liquid) of Poly (diallyldimethyl- ammonium) bis (trifluoromethanesulfonyl) imide		Lithium bis (trifluoromethylsulfonyl) imide	Acetonitrile	2.0×10^{-4}	[75]
Imidazolium-based polyhedral oligomeric silsesquioxane ionic liquids	Poly(ethylene oxide)/ poly (vinylidene fluoride- hexafluoropropylene)	Lithium bis (trifluoromethanesulfonyl) imide	Dimethylformamide	8.0×10^{-4}	[74]

(Continued)

Table 11.1 (Continued)

Method	Polymer	Salt	Solvent	Conductivity (S cm ⁻¹)	References
(D) Polymer blend					
	Poly(vinylalcohol)/gum Arabic	Lithium perchlorate	Distilled water	1.6×10^{-4}	[94]
	Chitosan/methyl cellulose	Ammonium iodide	1% acetic acid	1.93×10^{-4}	[95]
	Poly(ethylene oxide)/poly(vinyl pyrrolidone)	Lithium nitrate	Methanol	1.13×10^{-3}	[31]
	Poly(ethylene oxide)/poly(vinylidene fluoride)	Ammonium iodide	Dimethylformamide	1.01×10^{-3}	[96]
	Poly(methylhydrogen-siloxane)/ poly(ethylene oxide)	Lithium bis(trifluoromethylsulfonyl)imide	Anhydrous acetonitrile	2×10^{-2} at 80°C	[97]
	Dextran/chitosan	Ammonium thiocyanate	1% acetic acid	1.28×10^{-4}	[98]
	Chitosan/iota (<i>I</i>)-carrageenan	Orthophosphoric acid	1% acetic acid	6.29×10^{-4}	[48]
	Poly(vinyl alcohol)/poly(acrylonitrile)	Magnesium perchlorate	Dimethylformamide	2.96×10^{-4}	[99]
(E) Copolymerization					
	Poly(acrylamide-co-acrylic acid)	Sodium iodide	NIL	1.88×10^{-5}	[28]

recent times, polymer hydrogels as functional materials gave a new direction to the development of environment-friendly supercapattery. There is an increasing drift in fabricating flexible supercapacitors using hydrogel polymers as electrodes and electrolytes due to the striking mechanical characteristics [103,104].

11.2.6.1 Graphene-based hydrogels

A self-assembled 3D-interconnected porous network of graphene hydrogels leads to a higher electrical conductivity, improved mechanical strength, smooth ion transportation, and integrated surface area. Due to the van der Waals interactions, the graphene sheets restack together by $\pi-\pi$ interactions, and reduce the accessible surface area and ions diffusion, which affect charge storage ability [105]. Duan et al. fabricated supercapattery by combining a negative graphene hydrogel electrode and a positive manganese dioxide (MnO_2) nanoplate nickel foam electrode in a single device. To prevent the aggregation of graphene nanosheets, an ecological reagent of L-glutathione was used to synthesize graphene hydrogel. This method is more advantageous than hydrothermal methods. This MnO_2 and graphene hydrogel-based reversible asymmetric high-performance supercapattery exhibits an energy density of 23.2 Wh Kg^{-1} in the potential range of 0 to 2 V [106].

Wang et al. reported three-dimensional graphene/vanadium oxide (VO_2) nanocomposite hydrogels and used them to fabricate a pseudocapacitor. The synthesized hydrogels resulted in smooth electronic and ionic transport, increased capacitance (426 F g^{-1} at 1 A g^{-1}), outstanding rate capability, and exceptional cyclic stability of the pseudocapacitor within a potential range of -0.6 to $+0.6 \text{ V}$ for 3D graphene/ VO_2 nanocomposite hydrogel. The hybrid electrodes showed enhanced electrochemical performance and positive synergistic effect [107].

11.2.6.2 Polyaniline hydrogels

PANI is a conducting polymer which got striking attention for numerous applications due to its simple synthesis, low cost, stable, and highly conducting nature. Therefore PANI is widely used in supercapattery. However, disadvantages were also observed when exploited in supercapattery. These disadvantages include poor cyclic stability, poor rate capability due to low charge transfer reaction, mechanical degradation, and swelling of conjugated polymer chain during charge/discharge phenomena. Therefore PANI hydrogels were synthesized to overwhelm these disadvantages. PANI hydrogels are

capable candidates owing to the 3D network, porous morphology, continuous conductive framework, large surface area, and quick charge transportation. For this, different strategies were adopted to synthesize PANI hydrogels. Firstly, PANI was embedded into the nonconducting polymer network or carbon matrix and homogeneously dispersed. However, the efficiency of the resulting hydrogels was limited by distinct conjugated backbones. On the other hand, PANI hydrogels were synthesized using numerous cross-linking agents, such as phytic acid, poly(styrene sulfonate), and poly(ethylene glycol)-diglycerol ether, to cross-link PANI. Hydrogels formed through this method also have disadvantages due to the presence of nonconducting cross-linking agents.

Polyaniline hydrogels using phytic acid were synthesized by the protonation of the nitrogen group on the main chain of PANI and hydrogels showed remarkable results. Phytic acid molecules cross-linked more than one PANI chain at a time to form mesh-like hydrogels. Hydrogels established high-performance supercapattery having 480 F g^{-1} specific capacitance and retained 83% capacitance after 10,000 cycles. These results are very promising in terms of capacitance and cyclic stability [108].

In other work, core-shell 3D conducting hydrogels were prepared using phytic acid where multiwalled carbon nanotubes (MWNTs) were used as core and PANI as shell. Aniline and MWNTs were dissolved in phytic acid solution followed by addition of an initiator into the mixture. The phytic acid formed H-bonds with MWNT-PANI to form a composite conductive network. MWNTs increased the surface area of mesoporous network which effectively promoted the electron transport and increased the electrical conductivity from 0.21 to 1.54 S cm^{-1} . The supercapacitor formed using these hydrogels had a specific capacitance of 609 F g^{-1} . These hydrogels opened a new pathway for the fabrication of supercapacitors with enhanced performance [109].

Nandi et al. synthesized PANI hydrogels using folic acid as a cross-linker. They grew silver nanoparticles inside the hydrogel matrix to improve the electrical conductivity. Silver nanoparticles enhanced the electrical properties up to 0.04 S cm^{-1} . The supercapacitor formed using these hydrogels had 295 F g^{-1} specific capacitance at 1 A g^{-1} . Silver nanoparticles significantly improved the specific capacitance (646 F g^{-1}) at 1 A g^{-1} and rate capability (403 F g^{-1} at 20 A g^{-1}). Furthermore, the supercapacitor retained 74% capacitance after 5000 cycles [110].

Carbon cloth is a carbon-based conducting substrate and it is cheap source of current collector. It is chemically stable, highly conductive, and flexible which is useful for portable electronic equipment. Horng et al.

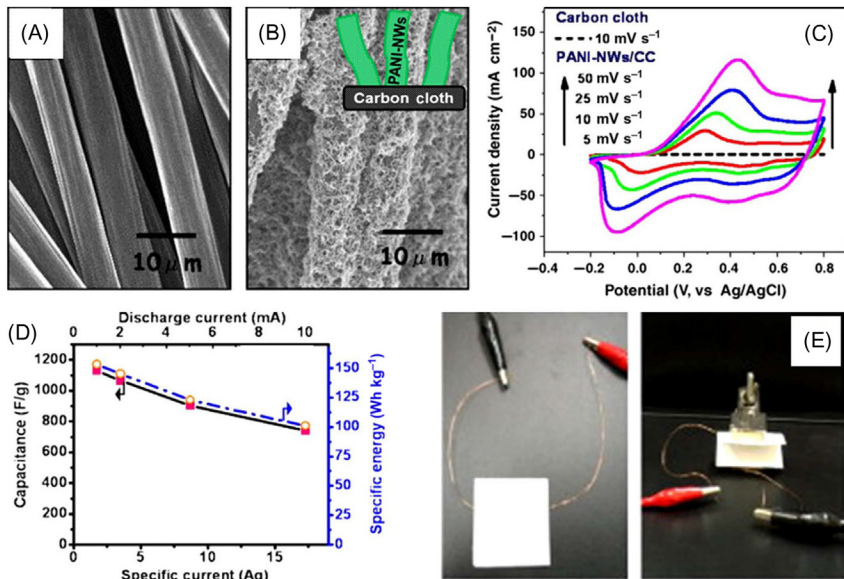


Figure 11.6 (A) Surface morphology of carbon cloth, (B) polyaniline nanowire electrode, (C) cyclic voltammetry, (D) capacitance versus current density, and (E) mechanical flexibility of fabricated device (flat and bent) [111].

used a direct growth electrochemical polymerization method to synthesize PANI nanowires on carbon cloth. They fabricated supercapattery using nanowires and performed electrochemical studies and found 1079 F g^{-1} specific capacitance. Fig. 11.6A and B represents surface morphology of bare carbon cloth and PANI nanowires. The device was fabricated by separating two symmetric electrodes using cellulose films and immersed in $1 \text{ M H}_2\text{SO}_4$. Fig. 11.6C & D signifies the cyclic voltammetry analysis of the fabricated device and results revealed faradaic redox reaction. Galvanic charge/discharge study investigated the decrease in capacitance with the increase in current density. Fig. 11.6E reveals the mechanical flexibility of the device and its electrochemical performance during bending [111].

11.2.6.3 Polypyrrole hydrogels

Polypyrrole is a conducting polymer. It achieved significant importance in supercapacitors and supercapattery due to its excellent electrical conductivity, large surface area, environmental friendliness, and ease of synthesis. However, there are certain limitations, such as mechanical stress and limited mass transportation, which hinder its electrochemical performance. To overcome these limitations, bacterial cellulose–PPy hydrogel composites

were prepared. They used FeCl_3 as an ionic cross-linker. These composites had a large specific surface area. This large surface area improved the specific charge capacity (459.5 F g^{-1} at 0.16 A g^{-1}) of the supercapacitor [112]. Wang et al. prepared a three-dimensional nanostructured cellulose–PPy network and free-standing paper-like films were prepared using phytic acid. The free-standing films were used to fabricate a device. The fabricated device obtained 46 F g^{-1} specific capacitance and retained 92% capacitance after 3000 cycles [113]. In other work, PPy–nanocellulose composite hydrogels were synthesized using phytic acid as a cross-linking agent. Phytic acid cross-linked PPy chains and formed a three-dimensional network through cross-linking. Furthermore, PPy was coated on the surface of nanocellulose through the hydrogen bonding of NH (PPy) and OH of cellulose [113].

11.2.6.4 Flexible hydrogel electrolytes

Flexible supercapacitors were fabricated using PVA-based gel electrolytes due to their cheap raw materials, nontoxicity, and physicochemical stability. But the hydroxyl group in PVA limits their practical use because it weakens the polymer and water molecule interaction. Therefore there is poor water retention, instability, insufficient ionic conductivity, mechanical rigidity, and a rapid charge/discharge rate [114]. Therefore PVA hydrogels were developed by adding a cross-linking agent, such as glutaraldehyde (GA), to improve mechanical flexible and ionic conductivity for supercapacitors [115].

Shih et al. fabricated a highly flexible, conductive, and air-stable pseudocapacitor based on poly(3,4 ethylenedioxythiophene):poly(styrenesulfonate)/poly(vinyl alcohol)/poly(methacrylic acid) hydrogel electrode and poly(vinyl alcohol)/poly(methacrylic acid)/phosphoric acid. The pseudocapacitor has excellent mechanical strength, fascinating ionic conductivity (3.1 S cm^{-1}) and outstanding electrochemical performance with areal capacitance of 7.38 mF cm^{-2} at 10 mV s^{-1} . The device maintained its electrochemical performance even after stretching up to 100%. Fig. 11.7A, B, C, and D shows the structure of hydrogel formation, electrode/electrolyte preparation, mechanical strength of electrode/electrolyte, and electrochemical cell fabrication [116].

Wang et al. synthesized chemically cross-linked PVA– H_2SO_4 hydrogel film for fabrication of PANI (PANI) supercapacitor (SCs). This cross-linked PVA– H_2SO_4 electrolyte exhibited the good ionic conductivity of 0.082 S cm^{-1} due to its ability to retain 90% of water in the polymer

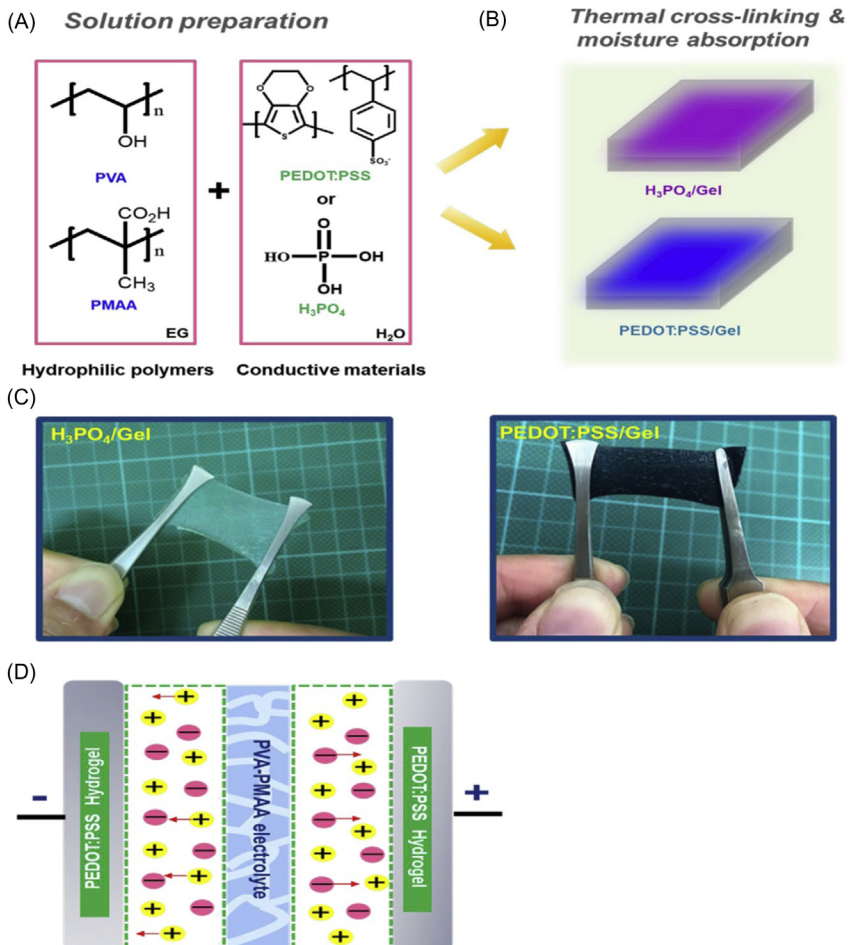


Figure 11.7 (A) structure of conducting hydrogel, (B) casting of prepared solution on teflon, (C) stretching of hydrogels electrode and electrolyte, and (D) sandwiching of hydrogel electrolyte between two electrodes [116].

network. The PANI supercapacitor with this electrolyte showed capacitance of 488 mF cm^{-2} with 90% stability after 7000 cycles [117].

Polyvinyl alcohol-based hydrogel electrolytes have been used for the fabrication of self-healable and flexible supercapacitors. PVA is low cost, nontoxic, and chemically stable in nature. However, it has some intrinsic properties to limit its application in supercapacitors. For example, the long carbon chain and inadequate hydrophilic groups on the main chain may deteriorate the interaction with water molecules as compared to other

hydrogels. This weak interaction leads to poor water retainability of PVA-based hydrogels and insufficient ionic conductivity which affects long-term stability. PVA-based hydrogels have been immersed in acids such as H_2SO_4 and H_3PO_4 and in bases such as KOH to improve the ionic conductivity. However, rapid water evaporation results in the reduction of ionic conductivity [114]. Some efforts were made to enhance the electrical conductivity and flexibility of PVA hydrogels for flexible supercapacitors. One such approach was to prepare PVA hydrogels using glutaraldehyde as a cross-linking agent to improve mechanical and electrochemical properties [115,117–119].

Polypyrrole was developed on film of chemically cross-linked PVA- H_2SO_4 for the synthesis of flexible hybrid materials and used to fabricate supercapacitors (SCs). The fabricated device delivered volumetric capacitance of 13.06 F cm^{-3} and energy density of $1160.9 \times 10^{-6} \text{ Wh cm}^{-3}$ and retained 97.9% capacitance after 10,000 cycles [119].

Apart from PVA, polyacrylamide hydrogels have also been exploited in flexible supercapacitors owing to their higher hydrophilicity, high ionic conductivity, and consistent performance at different pH conditions. Li et al. reported polyacrylamide-LiCl hydrogel with higher ionic conductivity ranging from 3.8 to 8.1 S cm^{-1} . Furthermore, carbon nanotubes have been embedded in the polyacrylamide-LiCl hydrogel to form composites. These polyacrylamide composite hydrogels were used to fabricate a supercapacitor that showed a specific capacitance of 99.3 F cm^{-3} . The fabricated device retained its performance during bending, kneading, and knotting. The supercapacitor showed 10 hours discharge time before dropping half of the open circuit voltage [120]. In other work, Tang et al. reported a flexible supercapacitor of sodium sulfate–anionic polyurethane acrylates/polyacrylamide (Na_2SO_4 -aPUA/PAAM) hydrogel electrolyte with high conductivity (0.036 S cm^{-1}), ultrahigh stretchability $>1000\%$, and stickiness. aPUA acts as a cross-linking agent which endows the hydrogel with high swell-ability even after absorbing 500% water. Furthermore, CNTs@manganese dioxide (MnO_2) was prepared as a hybrid electrode material. The supercapacitor was fabricated by sandwiching the hydrogel electrolyte between hybrid materials and electrochemical studies were investigated. The device exhibited enhanced specific capacitance of 478.6 mF cm^{-2} at 0.5 mA cm^{-1} and no significant change in performance was observed after 150% strain [121].

Huang et al. synthesized PAAM hydrogels cross-linked through vinyl hybrid silica nanoparticles (VSNPs). The VSNPs improved the mechanical

properties of hydrogels owing to their energy dissipating center. The flexible supercapacitor was fabricated using hydrogel electrolyte. The supercapacitor was fabricated using PAAM hydrogel electrolyte that showed 2.6-fold enhancement of capacitance over stretchability of 1000% and retained 99.4% capacitance at compressibility of 50% [122].

Similarly, Huang et al. reported polyacrylic acid (PPA) hydrogels using VSNPs as cross-linking agent. PAA-based hydrogel electrolytes had excellent stretchability and self-healability, as shown in Fig. 11.8. The flexible supercapacitor performed electrochemically better than PVA-based hydrogel electrolytes [123].

Na et al. reported hydrophobic-associated hydrogel polymer electrolyte of alcohol ethoxylate–acryloyl chloride (AEO-AC) modified poly(acrylamide) through UV radiation method. Hydrophobic alky chains associated with acrylamide main chain as a physical cross-linking agent to form micelles. Transmission electron microscopy (TEM) revealed the spherical shape of the nanoparticles. The spherical shape of the nanoparticles is due to the good dispersion of the physical cross-linking agent. The hydrogel poly(acrylamide) (HA-GPE) was prepared using lithium perchlorate (LiClO_4) which provided dissociative ions and assured diffusion of

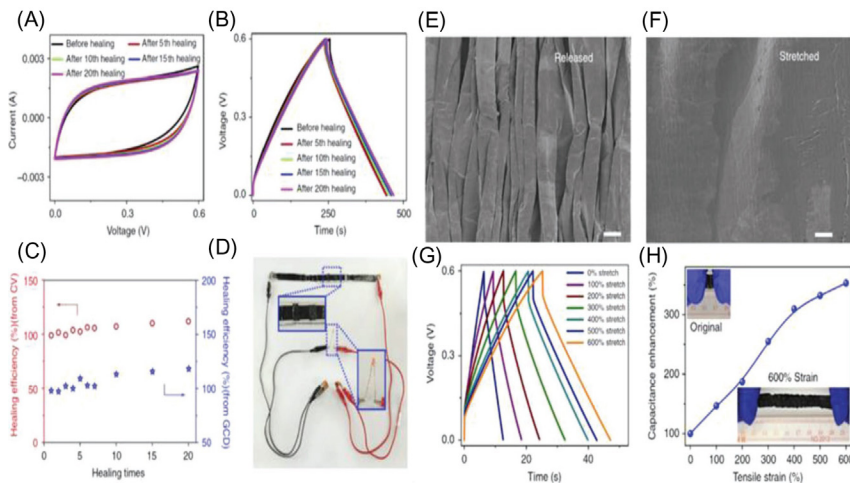


Figure 11.8 (A) Cyclic voltammety analysis before and after self-healing, (B) galvanic charge/discharge curves analysis before and after self-healing, (C) healing efficiency, (D) prototype performance, (E) morphology study of fabricated supercapacitor in free state, (F) morphology study of fabricated supercapacitor during stretching, (G) galvanic charge/discharge curves during stretching, and (H) capacitance versus tensile strain [123].

ions through activated porous carbon electrode. Lithium perchlorate was selected because of its stability, high dissociation property, and high ionic mobility. Fig. 11.9A–D shows the synthesis route of hydrogel electrolyte and TEM images.

In an ionic conductivity study, the mechanical properties and electrochemical performance of the HA-GPE was observed and are shown in Fig. 11.10A–H. The ionic conductivity improved with the increase in salt concentration from 0 to 5 mol L⁻¹. This ionic conductivity was due to the presence of free ions of Li⁺ and ClO₄⁻. The ionic conductivity increased with the concentration of LiClO₄ up to 5 mol L⁻¹ (Fig. 11.10A and B). However, the concentration of LiClO₄ affected the mechanical properties of the hydrogel electrolyte. The results revealed that mechanical strength increased with the concentration from 0 to 1 mol L⁻¹. The increment in the mechanical strength is due to the dispersion of Li⁺ ions in the hydrogel network which coordinate with the ethylene oxide units to make the movement of alkyl chains easier. A further increase in concentration reduced the mechanical strength and can be seen from

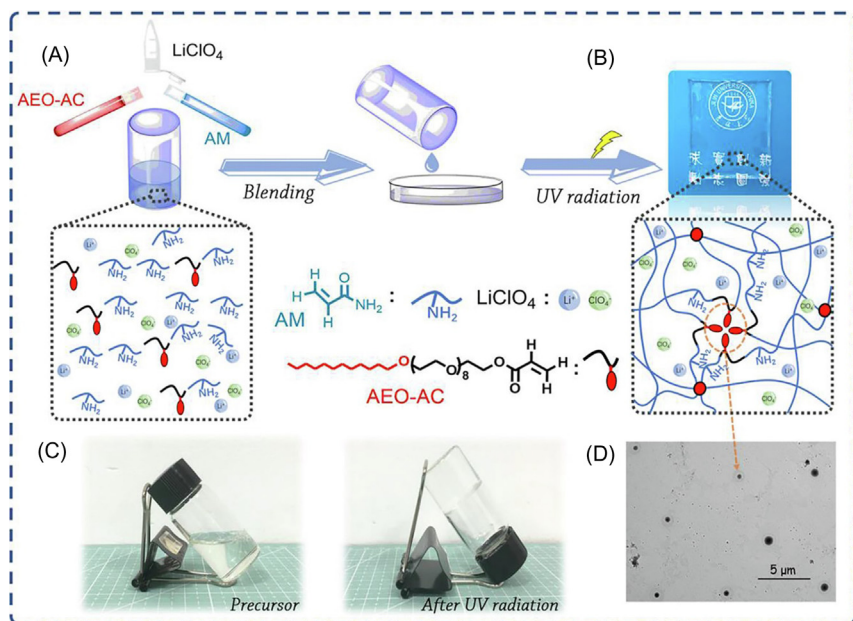


Figure 11.9 (A) UV radiation induced polymerization, (B) HA-GPE micelle membrane, (C) images of solution mixture and hydrogel after UV radiation, and (D) TEM image of HA-GPE micelle [124].

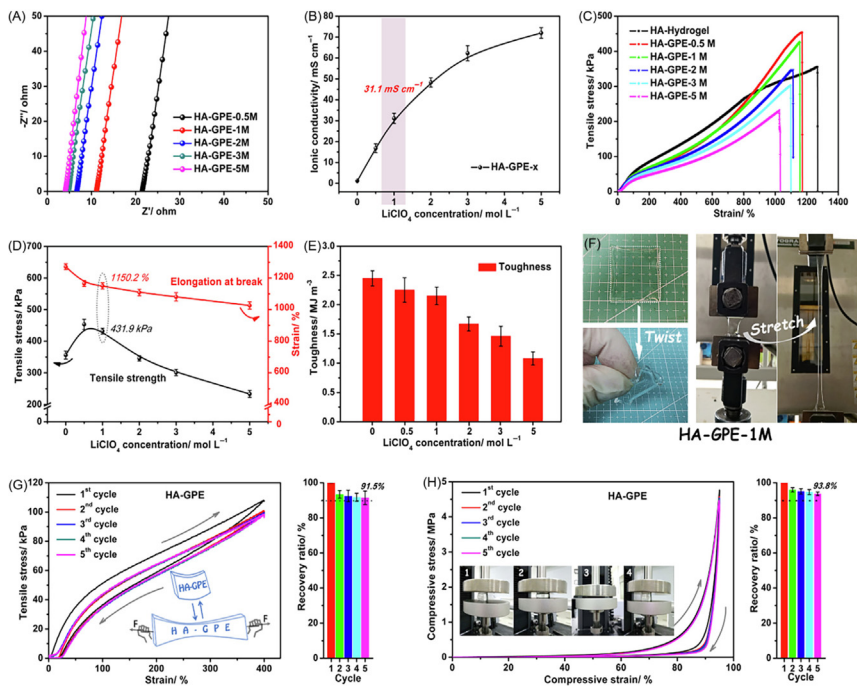


Figure 11.10 (A) Nyquist plot at room temperature, (B) ionic conductivity versus concentration of LiClO_4 , (C) stress–strain curves, (D) tensile stress versus salt concentration, (E) effect of salt concentration on toughness, (F) images of stretching (*right*) and twisting (*left*), (G) stress–strain curves after healing cycles and recovery ratio, and (H) compressive stress–compressive strain curves and recovery ratio [124].

Fig. 11.10C, D, and E. The optical images (Fig. 11.10F) showed the transparent, ultrastretchable, and flexible hydrogels.

The cyclic mechanical strength of the HA-GPE was investigated via cyclic stretching and compressive tests, and results show the low hysteresis during strain cycling. The recovery ratio was 91.5% after five successive cycles and HA-GPE exhibited excellent fatigue resistant characteristics with strength of 4.8 MPa and could recover immediately after unloading. This association–dissociation and reassociation owing to the physical cross-linking point led to hydrogel recovery (Fig. 11.10G and H). These studies suggested the possible fabrication of stretchable supercapacitors [124].

Despite of stretchability and flexibility, researchers introduced the polymer hydrogels in supercapacitors that work at low temperature. Usually, it become problematic when the supercapacitor worked at the

temperature below the freezing point of water. The formation of ice takes place which hinders the movement of water molecules and causes the salt precipitation. The ionic conductivity of the aqueous electrolytes depends on these two factors. In addition, the loss of solvent also results in inhibition of the rheological property of the polymer, from which polymer chains are correlated to charge hopping between polymer chains during charging/discharging. Due to these problems, supercapacitors may lose significant efficiency or even cannot give an output of electricity. Therefore work has been done to improve the supercapacitor performance at low temperature. According to the reported literature, polyampholyte gel as electrolyte was synthesized which worked at low temperature [125]. Polyampholyte hydrogels can hinder the formation of ice and enhanced the mechanical properties and device efficiency at low temperature. A polyampholyte hydrogel-based supercapacitor delivered specific capacitance of 193 F g^{-1} at a current density of 0.5 A g^{-1} . The supercapacitor had 30 Wh kg^{-1} energy density while it maintained 10 Wh kg^{-1} at -30°C . In other work, Tao et al. reported cross-linked sodium alginate hydrogels which were flexible and self-healable and cold resistant at low temperature. Sodium alginate was cross-linked through catechol–borate ester bonding to form a hydrogel. Potassium chloride (KCl) was used to improve the ionic conductivity. Moreover, it was observed that dopamine grafting on sodium alginate improved the self-healing property and the electrochemical performance of supercapacitor was increased even at 10 times of cutting/healing cycles at room temperature. The hydrogels showed 85.7 mS cm^{-1} ionic conductivity at -10°C while supercapacitor maintained 80% capacitance at room temperature [126].

Previously, PVA GPEs were reported for supercapacitors. However, these polymer electrolytes have neither a tough physical performance nor self-healability. It is impossible to implant into different shapes and the deformation of supercapacitors and supercapattery for energy supply was reported. Therefore, Liao et al. reported mechanically tough and self-healable hydrogel electrolyte by micelle copolymerization of poly (acrylic acid) and octadecyl methacrylate in vinyl sponge (S-PAA). The preliminary mechanical tests of the hydrogel electrolyte such as stretching, pulling into films, supporting a 100 g weight, and repeated compression are shown in Fig. 11.11A, while stress–strain curves are given in Fig. 11.11B. This stress strength is higher than pure poly(acrylic acid)

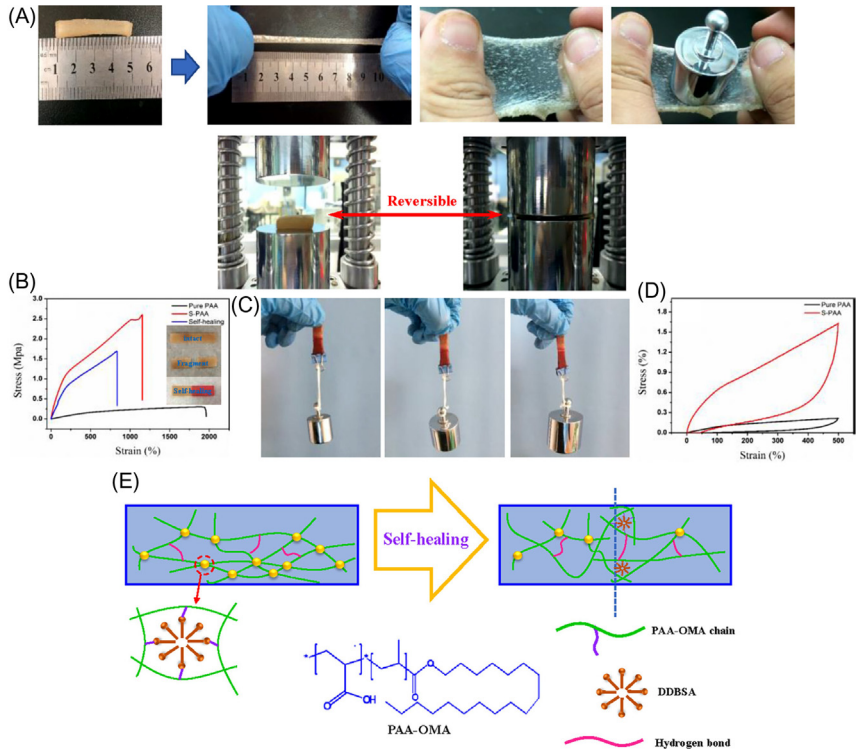


Figure 11.11 (A) preliminary mechanical tests of S-PAA, (B) stress–strain curves before and after self-healing, (C) loading with different weights, (D) loading–unloading curves at maximum strain of 500%, and (E) mechanism of self-healing of S-PAA hydrogel [127].

hydrogels, suggesting a tough hydrogel electrolyte. Fig. 11.11C reveals the lifting of 500 g weight without damage. The effect of self-healing for the physical resistance reflects on the stress–strain curves. S-PAA retained its performance even after an increase in stress strength elongation at break of self-healing (Fig. 11.11D). This suggests that sponge has no effect on the self-healing property of PAA and S-PAA can still work and is associated to the hydrophobic interactions and hydrogen bonding as shown in Fig. 11.11E. The micelles interact hydrophobically with the polymer chains at the fracture interface. The polymer chains migrate and entangle each other and further cross-link through hydrogen bonding to form a 3D network again [127]. The performance comparison of different hydrogel electrolytes is given in Table 11.2.

Table 11.2 Performance comparison of hydrogel electrolytes.

Hydrogel	Material	Method	Electrode	Specific capacitance (F g ⁻¹)	References
Poly(acrylamide) hydrogel electrolyte	Physical cross-linking by using NaMMT clay and magnesium trifluoromethanesulfonate as ion source	Free radical mechanism	Activated carbon, Acetylene black	29.48 at 30 mA g ⁻¹	[102]
Cellulose hydrogel electrolyte membranes	Cellulose, IL (<i>N, N</i> -dimethyl- <i>N</i> -ethylpiperazinium acetate	Solution casting	Activated carbon, Acetylene black	22 at 0.5 A g ⁻¹	[128]
Poly(acrylic acid) hydrogel electrolyte	Acrylic acid, H ₃ PO ₄ , and VSNPs as cross-linking agent	Free radical mechanism	CNTs/PPy	22 at 0.5 A g ⁻¹	[123]
Poly(acrylamide) hydrogel electrolyte	Acrylamide, methacrylated graphene oxide	Free radical mechanism	PANI	178.1 at 0.1 A g ⁻¹	[129]
PAMPS hydrogel electrolyte	Poly(2-acrylamido-2-methyl-1-propanesulfonic acid) (PAMPS) and MBA + NaMMT as cross-linkers. Hydrogel soaked in 4 M KOH	Free radical mechanism	N/A	22 at 10 mA g ⁻¹	[130]
PGA hydrogel electrolyte	PGA/ NaHCO ₃	Solution casting	PEDOT/Al ₂ O ₃ /YPGA	4.8 × 10 ⁻³ at 1 mA g ⁻¹	[131]
PVA hydrogel electrolyte	PVA/H ₃ PO ₄	Solution casting	CNT electrode	18 at 1 A g ⁻¹	[132]
Poly(acrylic acid) hydrogel electrolyte	Acrylic acid, H ₃ PO ₄ , and FeCl ₃ as cross-linking agent	Free radical mechanism	Graphite + PPy	87.4 at 0.5 A g ⁻¹	[133]
PVA/HEC hydrogel electrolyte	PVA/HEC	Solution mixing	CNTs/PANI	160 F g ⁻¹	[134]
PVA Hydrogel electrolyte	2-Acrylamido-2-methyl-1-propanesulfonic acid (AMPS) monomers in a swelling PVA with MMT	Polymerization	Activated carbon	201	[135]

VSNPs-PAM film hydrogel electrolyte	Cross-linked by vinyl hybrid silica nanoparticles (VSNPs)	Free radical polymerization	PPy@CNT papers	Not given	[136]
Poly(acrylic acid) hydrogel electrolyte	Acrylic acid and octadecyl methacrylate in vinyl-treated sponge (S-PAA).	Micelle copolymerization	PPy@CNTpaper	368 at 0.1 A g ⁻¹	[127]
PVA-g-PAA/KCl hydrogel electrolyte	Polyacrylic acid grafted polyvinyl alcohol (PVA-g-PAA) into a hydrogel in the presence of KCl and borax	Free radical polymerization	Activated carbon	85.4 at 1 A g ⁻¹	[137]
PVA/PAA blend hydrogel electrolyte	Cross-linking with glutaraldehyde and perchloric acid	Solution casting	Carbon electrode	60	[138]



11.3 Conclusion and future challenges

The current progress in supercapacitors and supercapattery using polymer electrolytes has been discussed in this chapter. This chapter introduces the basic concept of supercapacitors and supercapattery and includes a comprehensive discussion on the electrolytes involved. There has been a brief explanation of the types of electrolytes, such as aqueous, solid, and hydrogel, ionic conduction phenomena, methods of synthesis, and numerous techniques to improve the performance of the electrolytes. Aqueous polymer hydrogel electrolytes usually possess porous morphology, higher ionic conductivity, enhanced mechanical flexibility, and self-healability and are therefore helpful in the smooth transportation of ions due to free volume and porosity toward electrodes and increase the electrochemical performance of the device. Furthermore, electrolytes determine the potential window of the device and are useful for the electrostatic interactions and redox reactions occur at the electrodes. The correlation between the energy and power density of supercapacitors and supercapattery is the result of high electrochemical performances of electrode materials and ionic conductivity of the electrolyte materials. Therefore the polymer electrolytes have excellent potential as functional materials for supercapacitors and supercapattery. But the polymer electrolytes still need improvement in electrolytic ion diffusion and specific surface area reduction and enough cycling life of electrolyte materials which hinders the electrochemical efficiency of supercapacitors and supercapattery. The engineering design includes the current collectors, electrolytes, membrane separators, and counter electrodes, and the assembling of the devices needs a deeper investigation. It should be kept in mind that with improvements in energy densities, the principal advantage of supercapacitors and supercapattery, which are high rate capability and long cycle life, must not be sacrificed. Still the depth of knowledge about the compatibility of various polymer electrolytes, such as solid, gel, and hydrogel electrolytes, with different porous electrode materials is required.

Acknowledgments

This work is financially supported by Fundamental Research Grant Scheme (FRGS) from the Ministry of Education, Malaysia (FP062- 2018A) and Impact-Oriented Interdisciplinary Research Grant (IIRG007A-19IISS), University of Malaya, Malaysia.

References

- [1] J. Miller, A brief history of supercapacitors, *Battery + Energy Storage Technol.* (2007) 61.
- [2] H.I. Becker, Low voltage electrolytic capacitor: Google Patents (1957).
- [3] B.E. Conway, Transition from “supercapacitor” to “battery” behavior in electrochemical energy storage, *J. Electrochem. Soc.* 138 (6) (1991) 1539–1548.
- [4] P.J. Hall, M. Mirzaei, S.I. Fletcher, F.B. Sillars, A.J. Rennie, G.O. Shitta-Bey, et al., Energy storage in electrochemical capacitors: designing functional materials to improve performance, *Energy Environ. Sci.* 3 (9) (2010) 1238–1251.
- [5] R. Kötz, M. Carlen, Principles and applications of electrochemical capacitors, *Electrochim. Acta* 45 (15–16) (2000) 2483–2498.
- [6] S. Gao, L. Zhang, Y. Qiao, P. Dong, J. Shi, S. Cao, Electrodeposition of polyaniline on three-dimensional graphene hydrogel as a binder-free supercapacitor electrode with high power and energy densities, *RSC Adv.* 6 (64) (2016) 58854–58861.
- [7] Z.-A. Hu, Y.-L. Xie, Y.-X. Wang, L.-J. Xie, G.-R. Fu, X.-Q. Jin, et al., Synthesis of α -cobalt hydroxides with different intercalated anions and effects of intercalated anions on their morphology, basal plane spacing, and capacitive property, *J. Phys. Chem. C* 113 (28) (2009) 12502–12508.
- [8] F.S. Omar, A. Numan, N. Duraisamy, S. Bashir, K. Ramesh, S. Ramesh, Ultrahigh capacitance of amorphous nickel phosphate for asymmetric supercapacitor applications, *RSC Adv.* 6 (80) (2016) 76298–76306.
- [9] J. Iqbal, A. Numan, R. Jafer, S. Bashir, A. Jilani, S. Mohammad, et al., Ternary nanocomposite of cobalt oxide nanograins and silver nanoparticles grown on reduced graphene oxide conducting platform for high-performance supercapattery electrode material, *J. Alloy. Compd.* 821 (2020) 153452.
- [10] F.S. Omar, A. Numan, S. Bashir, N. Duraisamy, R. Vikneswaran, Y.-L. Loo, et al., Enhancing rate capability of amorphous nickel phosphate supercapattery electrode via composition with crystalline silver phosphate, *Electrochim. Acta* 273 (2018) 216–228.
- [11] S. Bashir, Y.Y. Teo, S. Ramesh, K. Ramesh, Synthesis, characterization, properties of N-succinyl chitosan-g-poly(methacrylic acid) hydrogels and in vitro release of theophylline, *Polymer* 92 (2016) 36–49.
- [12] Y. Shi, G. Yu, Designing hierarchically nanostructured conductive polymer gels for electrochemical energy storage and conversion, *Chem. Mater.* 28 (8) (2016) 2466–2477.
- [13] W. Zhang, X. Zhu, X. Chen, Y. Zhou, Y. Tang, L. Ding, et al., Cyano-bridged coordination polymer hydrogel-derived Sn–Fe binary oxide nanohybrids with structural diversity: from 3D, 2D, to 2D/1D and enhanced lithium-storage performance, *Nanoscale* 8 (18) (2016) 9828–9836.
- [14] Y. Zhao, B. Liu, L. Pan, G. Yu, 3D nanostructured conductive polymer hydrogels for high-performance electrochemical devices, *Energy Environ. Sci.* 6 (10) (2013) 2856–2870.
- [15] N.N. Sa’adun, R. Subramaniam, R. Kasi, Development and characterization of poly (1-vinylpyrrolidone-co-vinyl acetate) copolymer based polymer electrolytes, *Sci. World J.* (2014) 2014.
- [16] M.A.B.H. Susan, T. Kaneko, A. Noda, M. Watanabe, Ion gels prepared by in situ radical polymerization of vinyl monomers in an ionic liquid and their characterization as polymer electrolytes, *J. Am. Chem. Soc.* 127 (13) (2005) 4976–4983.
- [17] C.P. Fonseca, S. Neves, Characterization of polymer electrolytes based on poly (dimethyl siloxane-co-ethylene oxide), *J. Power Sources* 104 (1) (2002) 85–89.
- [18] W. Jia, Z. Li, Z. Wu, L. Wang, B. Wu, Y. Wang, et al., Graphene oxide as a filler to improve the performance of PAN-LiClO₄ flexible solid polymer electrolyte, *Solid. State Ion.* 315 (2018) 7–13.

- [19] Y.-J. Wang, Y. Pan, L. Wang, M.-J. Pang, L. Chen, Conductivity studies of plasticized PEO-Lithium chlorate-FIC filler composite polymer electrolytes, *Mater. Lett.* 59 (24–25) (2005) 3021–3026.
- [20] Y. Okamoto, T. Yeh, H. Lee, T. Skotheim, Design of alkaline metal ion conducting polymer electrolytes, *J. Polym. Sci. Part. A: Polym. Chem.* 31 (10) (1993) 2573–2581.
- [21] A.M. Regiani, G. de Oliveira Machado, J.F. LeNest, A. Gandini, A. Pawlicka, Cellulose derivatives as solid electrolyte matrixes. Paper presented at the Macromolecular Symposia (2001).
- [22] J. Chai, Z. Liu, J. Ma, J. Wang, X. Liu, H. Liu, et al., In situ generation of poly(vinylene carbonate) based solid electrolyte with interfacial stability for LiCoO₂ lithium batteries, *Adv. Sci.* 4 (2) (2017) 1600377.
- [23] A.B. Puthirath, S. Patra, S. Pal, M. Manoj, A.P. Balan, S. Jayalekshmi, Transparent flexible lithium ion conducting solid polymer electrolyte, *J. Mater. Chem. A* 5 (22) (2017) 11152–11162.
- [24] S.T. Gunday, E. Cevik, A. Yusuf, A. Bozkurt, Nanocomposites composed of sulfonated polysulfone/hexagonal boron nitride/ionic liquid for supercapacitor applications, *J. Energy Storage* 21 (2019) 672–679.
- [25] M. Hamsan, M. Shukur, M. Kadir, NH₄NO₃ as charge carrier contributor in glycerolized potato starch-methyl cellulose blend-based polymer electrolyte and the application in electrochemical double-layer capacitor, *Ionics* 23 (12) (2017) 3429–3453.
- [26] D.F. Vieira, C.O. Avellaneda, A. Pawlicka, Conductivity study of a gelatin-based polymer electrolyte, *Electrochim. Acta* 53 (4) (2007) 1404–1408.
- [27] S. Noor, A. Ahmad, I. Talib, M.Y.A. Rahman, Morphology, chemical interaction, and conductivity of a PEO-ENR50 based on solid polymer electrolyte, *Ionics* 16 (2) (2010) 161–170.
- [28] V.S. Kumaran, H. Ng, S. Ramesh, K. Ramesh, B. Vengadaesvaran, A. Numan, The conductivity and dielectric studies of solid polymer electrolytes based on poly(acrylamide-co-acrylic acid) doped with sodium iodide, *Ionics* 24 (7) (2018) 1947–1953.
- [29] S.B. Aziz, O.G. Abdullah, M.A. Rasheed, H.M. Ahmed, Effect of high salt concentration (HSC) on structural, morphological, and electrical characteristics of chitosan based solid polymer electrolytes, *Polymers* 9 (6) (2017) 187.
- [30] T. Bandara, D. Karunathilaka, J. Ratnasekera, L.A. De Silva, A. Herath, B. Mellander, Electrical and complex dielectric behaviour of composite polymer electrolyte based on PEO, alumina and tetrapropylammonium iodide, *Ionics* 23 (7) (2017) 1711–1719.
- [31] B. Jinisha, K. Anilkumar, M. Manoj, V. Pradeep, S. Jayalekshmi, Development of a novel type of solid polymer electrolyte for solid state lithium battery applications based on lithium enriched poly(ethylene oxide)(PEO)/poly(vinyl pyrrolidone)(PVP) blend polymer, *Electrochim. Acta* 235 (2017) 210–222.
- [32] P. Zhu, C. Yan, M. Dirican, J. Zhu, J. Zang, R.K. Selvan, et al., Li_{0.33}La_{0.557}TiO₃ ceramic nanofiber-enhanced polyethylene oxide-based composite polymer electrolytes for all-solid-state lithium batteries, *J. Mater. Chem. A* 6 (10) (2018) 4279–4285.
- [33] J. Bao, C. Tao, R. Yu, M. Gao, Y. Huang, C. Chen, Solid polymer electrolyte based on waterborne polyurethane for all-solid-state lithium ion batteries, *J. Appl. Polym. Sci.* 134 (48) (2017) 45554.
- [34] J. Adebahr, N. Byrne, M. Forsyth, D.R. Macfarlane, P. Jacobsson, Enhancement of ion dynamics in PMMA-based gels with addition of TiO₂ nano-particles, *Electrochim. Acta* 48 (14–16) (2003) 2099–2103.
- [35] C.-W. Liew, S. Ramesh, Comparing triflate and hexafluorophosphate anions of ionic liquids in polymer electrolytes for supercapacitor applications, *Materials* 7 (5) (2014) 4019–4033.

- [36] I. Nicotera, L. Coppola, C. Oliviero, M. Castriota, E. Cazzanelli, Investigation of ionic conduction and mechanical properties of PMMA–PVdF blend-based polymer electrolytes, *Solid. State Ion.* 177 (5–6) (2006) 581–588.
- [37] G. Pandey, Y. Kumar, S. Hashmi, Ionic liquid incorporated PEO based polymer electrolyte for electrical double layer capacitors: a comparative study with lithium and magnesium systems, *Solid. State Ion.* 190 (1) (2011) 93–98.
- [38] Y. Yusof, N. Majid, R. Kasmani, H. Illias, M. Kadir, The effect of plasticization on conductivity and other properties of starch/chitosan blend biopolymer electrolyte incorporated with ammonium iodide, *Mol. Cryst. Liq. Cryst.* 603 (1) (2014) 73–88.
- [39] E. Quartarone, P. Mustarelli, Electrolytes for solid-state lithium rechargeable batteries: recent advances and perspectives, *Chem. Soc. Rev.* 40 (5) (2011) 2525–2540.
- [40] Y. Wang, Recent research progress on polymer electrolytes for dye-sensitized solar cells, *Sol. Energy Mater. Sol. Cell* 93 (8) (2009) 1167–1175.
- [41] B. Scrosati, *Applications of Electroactive Polymers*, Vol. 75, Springer, 1993.
- [42] G. Swift, Directions for environmentally biodegradable polymer research, *Acc. Chem. Res.* 26 (3) (1993) 105–110.
- [43] S. Ramesh, R. Shanti, E. Morris, Discussion on the influence of DES content in CA-based polymer electrolytes, *J. Mater. Sci.* 47 (4) (2012) 1787–1793.
- [44] M. Rozali, A. Samsudin, M. Isa, Ion conducting mechanism of carboxy methylcellulose doped with ionic dopant salicylic acid based solid polymer electrolytes, *Int. J. Appl. 2* (4) (2012) 113–121.
- [45] I. Stepniak, M. Galinski, K. Nowacki, M. Wysokowski, P. Jakubowska, V.V. Bazhenov, et al., A novel chitosan/sponge chitin origin material as a membrane for supercapacitors—preparation and characterization, *Rsc Adv.* 6 (5) (2016) 4007–4013.
- [46] P. Perumal, P.C. Selvin, S. Selvasekarapandian, P. Sivaraj, K. Abhilash, V. Moniha, et al., Plasticizer incorporated, novel eco-friendly bio-polymer based solid bio-membrane for electrochemical clean energy applications, *Polym. Degrad. Stab.* 159 (2019) 43–53.
- [47] C.-W. Liew, S. Ramesh, Electrical, structural, thermal and electrochemical properties of corn starch-based biopolymer electrolytes, *Carbohydr. Polym.* 124 (2015) 222–228.
- [48] A. Arof, N. Shuhaimi, N. Alias, M. Kufian, S. Majid, Application of chitosan/iota-carrageenan polymer electrolytes in electrical double layer capacitor (EDLC), *J. Solid. State Electrochem.* 14 (12) (2010) 2145–2152.
- [49] A. Pawlicka, A.C. Sabadini, E. Raphael, D.C. Dragunski, Ionic conductivity thermogravimetry measurements of starch-based polymeric electrolytes, *Mol. Cryst. Liq. Cryst.* 485 (1) (2008) 804–816.
- [50] N. Salleh, S.B. Aziz, Z. Aspanut, M. Kadir, Electrical impedance and conduction mechanism analysis of biopolymer electrolytes based on methyl cellulose doped with ammonium iodide, *Ionics* 22 (11) (2016) 2157–2167.
- [51] J. Rodríguez, E. Navarrete, E.A. Dalchiele, L. Sánchez, J.R. Ramos-Barrado, F. Martín, Polyvinylpyrrolidone–LiClO₄ solid polymer electrolyte and its application in transparent thin film supercapacitors, *J. Power Sources* 237 (2013) 270–276.
- [52] C. Subramaniam, C. Ramya, K. Ramya, Performance of EDLCs using Nafion and Nafion composites as electrolyte, *J. Appl. Electrochem.* 41 (2) (2011) 197–206.
- [53] M.L. Verma, M. Minakshi, N.K. Singh, Synthesis and characterization of solid polymer electrolyte based on activated carbon for solid state capacitor, *Electrochim. Acta* 137 (2014) 497–503.
- [54] P. Perumal, K. Abhilash, P. Sivaraj, P.C. Selvin, Study on Mg-ion conducting solid biopolymer electrolytes based on tamarind seed polysaccharide for magnesium ion batteries, *Mater. Res. Bull.* 118 (2019) 110490.
- [55] M. Sasikumar, A. Jagadeesan, M. Raja, R.H. Krishna, P. Sivakumar, The effects of PVAc on surface morphological and electrochemical performance of P (VdF–HFP)-based blend solid polymer electrolytes for lithium ion-battery applications, *Ionics* 25 (5) (2019) 2171–2181.

- [56] S.B. Aziz, R.T. Abdulwahid, M.H. Hamsan, M.A. Brza, R.M. Abdullah, M.F. Kadir, et al., Structural, Impedance, and EDLC characteristics of proton conducting chitosan-based polymer blend electrolytes with high electrochemical stability, *Molecules* 24 (19) (2019) 3508.
- [57] N. Farhana, F.S. Omar, R. Shanti, Y. Mahipal, S. Ramesh, K. Ramesh, Iota-carrageenan-based polymer electrolyte: impact on ionic conductivity with incorporation of AmNTFSI ionic liquid for supercapacitor, *Ionics* (2019) 1–9.
- [58] P. Dhatarwal, R. Sengwa, Dielectric and electrical characterization of (PEO–PMMA)–LiBF₄–EC plasticized solid polymer electrolyte films, *J. Polym. Res.* 24 (9) (2017) 135.
- [59] F.M. Gray, J.R. MacCALLUM, C.A. Vincent, Poly(ethylene oxide)–LiCF₃SO₃–polystyrene electrolyte systems, *Solid. State Ion.* 18 (1986) 282–286.
- [60] T.B. Sahu, M. Sahu, S. Karan, Y. Mahipal, D. Sahu, R. Agrawal, Study of electrical and electrochemical behavior on copper ion conducting nano-composite polymer electrolyte, *Ionics* 24 (9) (2018) 2885–2892.
- [61] P. Chawla, S. Trivedi, K. Pandey, M. Tripathi, Dielectric studies of [PEO: CH₃COOLi]: graphite system synthesized by hot press and solution cast technique, *Proc. Natl Acad. Sci., India Sect. A: Phys. Sci* 88 (2) (2018) 187–193.
- [62] A. Chandra, Ion conduction behavior of hot-pressed nanocomposite polymer electrolytes: (1 – x)[70PEO: 30NaBr] + xSiO₂, *Polym. Bull.* 76 (2) (2019) 785–796.
- [63] S. Sharma, D. Pathak, N. Dhiman, R. Kumar, M. Kumar, FTIR, thermal and ionic conductivity studies of nanocomposite polymer electrolytes, *Surf. Innov.* 7 (1) (2018) 51–58.
- [64] Z. Huang, Q. Pan, D.M. Smith, C.Y. Li, Plasticized hybrid network solid polymer electrolytes for lithium-metal batteries, *Adv. Mater. Interfaces* 6 (2) (2019) 1801445.
- [65] Y. Yusof, M. Shukur, M. Hamsan, K. Jumbri, M. Kadir, Plasticized solid polymer electrolyte based on natural polymer blend incorporated with lithium perchlorate for electrical double-layer capacitor fabrication, *Ionics* (2019) 1–12.
- [66] P. Dhatarwal, R. Sengwa, S. Choudhary, Effectively improved ionic conductivity of montmorillonite clay nanoplatelets incorporated nanocomposite solid polymer electrolytes for lithium ion-conducting devices, *SN Appl. Sci.* 1 (1) (2019) 112.
- [67] Q. Ma, A. Chakrabarti, X. Mei, Z. Yue, H. Dunya, R. Filler, et al., New oligoether plasticizers for poly(ethylene oxide)-based solid polymer electrolytes, *Ionics* 25 (4) (2019) 1633–1643.
- [68] D. Li, X. Ji, X. Gong, F. Tsai, Q. Zhang, L. Yao, et al., The synergistic effect of poly(ethylene glycol)-borate ester on the electrochemical performance of all solid state Si doped-poly(ethylene glycol) hybrid polymer electrolyte for lithium ion battery, *J. Power Sources* 423 (2019) 349–357.
- [69] B. Li, Y. Liu, X. Zhang, P. He, H. Zhou, Hybrid polymer electrolyte for Li–O₂ batteries, *Green. Energy Environ.* 4 (1) (2019) 3–19.
- [70] N. Zhang, J. He, W. Han, Y. Wang, Composite solid electrolyte PEO/SN/LiAlO₂ for a solid-state lithium battery, *J. Mater. Sci.* 54 (13) (2019) 9603–9612.
- [71] K. Mishra, S. Hashmi, D. Rai, Nanocomposite blend gel polymer electrolyte for proton battery application, *J. Solid. State Electrochem.* 17 (3) (2013) 785–793.
- [72] M. Morita, T. Fujisaki, N. Yoshimoto, M. Ishikawa, Ionic conductance behavior of polymeric composite solid electrolytes containing lithium aluminate, *Electrochim. Acta* 46 (10–11) (2001) 1565–1569.
- [73] I. Osada, H. de Vries, B. Scrosati, S. Passerini, Ionic-liquid-based polymer electrolytes for battery applications, *Angew. Chem. Int. Ed.* 55 (2) (2016) 500–513.
- [74] J. Fu, Q. Lu, D. Shang, L. Chen, Y. Jiang, Y. Xu, et al., A novel room temperature POSS ionic liquid-based solid polymer electrolyte, *J. Mater. Sci.* 53 (11) (2018) 8420–8435.

- [75] K. Yang, Z. Liao, Z. Zhang, L. Yang, S.-i Hirano, Ionic plastic crystal-polymeric ionic liquid solid-state electrolytes with high ionic conductivity for lithium ion batteries, *Mater. Lett.* 236 (2019) 554–557.
- [76] Q. Lu, J. Fu, L. Chen, D. Shang, M. Li, Y. Xu, et al., Polymeric polyhedral oligomeric silsesquioxane ionic liquids based solid polymer electrolytes for lithium ion batteries, *J. Power Sources* 414 (2019) 31–40.
- [77] N. Fattah, H. Ng, Y. Mahipal, A. Numan, S. Ramesh, K. Ramesh, An approach to solid-state electrical double layer capacitors fabricated with graphene oxide-doped, ionic liquid-based solid copolymer electrolytes, *Materials* 9 (6) (2016) 450.
- [78] S. Selvalakshmi, T. Mathavan, S. Selvasekarapandian, M. Premalatha, Effect of ethylene carbonate plasticizer on agar-agar: $\text{NH}_4 \text{Br}$ -based solid polymer electrolytes, *Ionics* 24 (8) (2018) 2209–2217.
- [79] S. Ramesh, K.N. Bing, Conductivity, mechanical and thermal studies on poly(methyl methacrylate)-based polymer electrolytes complexed with lithium tetraborate and propylene carbonate, *J. Mater. Eng. Perform.* 21 (1) (2012) 89–94.
- [80] M. Ramlli, M. Maksud, M. Isa, Characterization of polyethylene glycol plasticized carboxymethyl cellulose-ammonium fluoride solid biopolymer electrolytes. Paper presented at the AIP Conference Proceedings (2017).
- [81] C. Ambika, K. Karuppasamy, D. Vikraman, J.Y. Lee, T. Regu, T.A.B. Raj, et al., Effect of dimethyl carbonate (DMC) on the electrochemical and cycling properties of solid polymer electrolytes (PVP-MSA) and its application for proton batteries, *Solid. State Ion.* 321 (2018) 106–114.
- [82] S. Gupta, P.K. Varshney, Effect of plasticizer concentration on structural and electrical properties of hydroxyethyl cellulose (HEC)-based polymer electrolyte, *Ionics* 23 (6) (2017) 1613–1617.
- [83] C.C. Sun, A.H. You, L.L. Teo, Characterizations of PMMA-based polymer electrolyte membranes with Al_2O_3 , *J. Polym. Eng.* 39 (7) (2019) 612–619.
- [84] M.Y. Chong, A. Numan, C.-W. Liew, H. Ng, K. Ramesh, S. Ramesh, Enhancing the performance of green solid-state electric double-layer capacitor incorporated with fumed silica nanoparticles, *J. Phys. Chem. Solids* 117 (2018) 194–203.
- [85] M. Rao, R. Koutavarapu, K.V. Kumar, Structural and electrochemical properties of ZrO_2 doped PVP-Na⁺ based nanocomposite polymer films, *Mater. Sci. Semicond. Process.* 89 (2019) 41–50.
- [86] G. Rajasudha, L.M. Jayan, P. Thangadurai, N. Boukos, V. Narayanan, A. Stephen, Polyindole-CuO composite polymer electrolyte containing LiClO_4 for lithium ion polymer batteries, *Polym. Bull.* 68 (1) (2012) 181–196.
- [87] M.Y. Chong, A. Numan, C.W. Liew, K. Ramesh, S. Ramesh, Comparison of the performance of copper oxide and yttrium oxide nanoparticle based hydroxyethyl cellulose electrolytes for supercapacitors, *J. Appl. Polym. Sci.* 134 (13) (2017).
- [88] A.R. Polu, H.-W. Rhee, Effect of TiO_2 nanoparticles on structural, thermal, mechanical and ionic conductivity studies of PEO12-LiTfDI solid polymer electrolyte, *J. Ind. Eng. Chem.* 37 (2016) 347–353.
- [89] K. Zhang, S. Mu, W. Liu, D. Zhu, Z. Ding, Y. Chen, A flexible NASICON-type composite electrolyte for lithium-oxygen/air battery, *Ionics* 25 (1) (2019) 25–33.
- [90] F. Chen, D. Yang, W. Zha, B. Zhu, Y. Zhang, J. Li, et al., Solid polymer electrolytes incorporating cubic $\text{Li}_7\text{La}_3\text{Zr}_2\text{O}_{12}$ for all-solid-state lithium rechargeable batteries, *Electrochim. Acta* 258 (2017) 1106–1114.
- [91] S.B. Aziz, W.O. Karim, K. Qadir, Q. Zafar, Proton ion conducting solid polymer electrolytes based on chitosan incorporated with various amounts of barium titanate (BaTiO_3), *Int. J. Electrochem. Sci.* 13 (2018) 6112–6125.

- [92] R. Jayaraman, P. Vickraman, N.M.V. Subramanian, A.S. Justin, AC impedance, XRD, DSC, FTIR studies on PbTiO₃ dispersoid pristine PVdF-co-HFP and PEMA blended PVdF-co-HFP microcomposite electrolytes, *J. Non Cryst. Solids* 435 (2016) 27–32.
- [93] S. Ibrahim, R. Ahmad, M.R. Johan, Conductivity and optical studies of plasticized solid polymer electrolytes doped with carbon nanotube, *J. Lumin.* 132 (1) (2012) 147–152.
- [94] C.M. Cholang, L.U. Krüger, R.D. Balboni, M.P. Rodrigues, F.C. Tavares, L.L. Peres, et al., Synthesis and characterization of solid polymer electrolyte based on poly(vinyl alcohol)/gum Arabic/LiClO₄, *Ionics* (2020) 1–8.
- [95] S.B. Aziz, M. Hamsan, R.M. Abdullah, R.T. Abdulwahid, M. Brza, A.S. Marif, et al., Protonic EDLC cell based on chitosan (CS): methylcellulose (MC) solid polymer blend electrolytes, *Ionics* (2020) 1–12.
- [96] S.K. Patla, R. Ray, K. Asokan, S. Karmakar, Investigation of ionic conduction in PEO–PVDF based blend polymer electrolytes, *J. Appl. Phys.* 123 (12) (2018) 125102.
- [97] Y.-J. Li, C.-Y. Fan, J.-P. Zhang, X.-L. Wu, A promising PMHS/PEO blend polymer electrolyte for all-solid-state lithium ion batteries, *Dalton Trans.* 47 (42) (2018) 14932–14937.
- [98] M.F.Z. Kadir, M. Hamsan, Green electrolytes based on dextran–chitosan blend and the effect of NH₄ SCN as proton provider on the electrical response studies, *Ionics* 24 (8) (2018) 2379–2398.
- [99] R. Manjuladevi, M. Thamilselvan, S. Selvasekarapandian, R. Mangalam, M. Premalatha, S. Monisha, Mg-ion conducting blend polymer electrolyte based on poly(vinyl alcohol)–poly(acrylonitrile) with magnesium perchlorate, *Solid. State Ion.* 308 (2017) 90–100.
- [100] S. Bashir, Y.Y. Teo, S. Ramesh, K. Ramesh, Physico-chemical characterization of pH-sensitive N-Succinyl chitosan-g-poly(acrylamide-co-acrylic acid) hydrogels and in vitro drug release studies, *Polym. Degrad. Stab.* 139 (2017) 38–54.
- [101] S. Bashir, Y.Y. Teo, S. Ramesh, K. Ramesh, M.W. Mushtaq, Rheological behavior of biodegradable N-succinyl chitosan-g-poly(acrylic acid) hydrogels and their applications as drug carrier and in vitro theophylline release, *Int. J. Biol. Macromol.* 117 (2018) 454–466.
- [102] S. Bashir, F.S. Omar, M. Hina, A. Numan, J. Iqbal, S. Ramesh, et al., Synthesis and characterization of hybrid poly(N, N-dimethylacrylamide) composite hydrogel electrolytes and their performance in supercapacitor, *Electrochim. Acta* 332 (2020) 135438.
- [103] N. Choudhury, S. Sampath, A. Shukla, Hydrogel–polymer electrolytes for electrochemical capacitors: an overview, *Energy Environ. Sci.* 2 (1) (2009) 55–67.
- [104] C. Zhong, Y. Deng, W. Hu, J. Qiao, L. Zhang, J. Zhang, A review of electrolyte materials and compositions for electrochemical supercapacitors, *Chem. Soc. Rev.* 44 (21) (2015) 7484–7539.
- [105] Y. Fang, B. Luo, Y. Jia, X. Li, B. Wang, Q. Song, et al., Renewing functionalized graphene as electrodes for high-performance supercapacitors, *Adv. Mater.* 24 (47) (2012) 6348–6355.
- [106] H. Gao, F. Xiao, C.B. Ching, H. Duan, High-performance asymmetric supercapacitor based on graphene hydrogel and nanostructured MnO₂, *ACS Appl. Mater. Interfaces* 4 (5) (2012) 2801–2810.
- [107] H. Wang, H. Yi, X. Chen, X. Wang, One-step strategy to three-dimensional graphene/VO₂ nanobelt composite hydrogels for high performance supercapacitors, *J. Mater. Chem. A* 2 (4) (2014) 1165–1173.

- [108] L. Pan, G. Yu, D. Zhai, H.R. Lee, W. Zhao, N. Liu, et al., Hierarchical nanostructured conducting polymer hydrogel with high electrochemical activity, *Proc. Natl. Acad. Sci.* 109 (24) (2012) 9287–9292.
- [109] P.-Y. Chen, N.-M.D. Courchesne, M.N. Hyder, J. Qi, A.M. Belcher, P.T. Hammond, Carbon nanotube–polyaniline core–shell nanostructured hydrogel for electrochemical energy storage, *RSC Adv.* 5 (48) (2015) 37970–37977.
- [110] S. Das, P. Chakraborty, S. Mondal, A. Shit, A.K. Nandi, Enhancement of energy storage and photoresponse properties of folic acid–polyaniline hybrid hydrogel by in situ growth of Ag nanoparticles, *ACS Appl. Mater. Interfaces* 8 (41) (2016) 28055–28067.
- [111] Y.-Y. Hong, Y.-C. Lu, Y.-K. Hsu, C.-C. Chen, L.-C. Chen, K.-H. Chen, Flexible supercapacitor based on polyaniline nanowires/carbon cloth with both high gravimetric and area-normalized capacitance, *J. Power Sources* 195 (13) (2010) 4418–4422.
- [112] J. Xu, L. Zhu, Z. Bai, G. Liang, L. Liu, D. Fang, et al., Conductive polypyrrole–bacterial cellulose nanocomposite membranes as flexible supercapacitor electrode, *Org. Electron.* 14 (12) (2013) 3331–3338.
- [113] Z. Wang, P. Tammela, P. Zhang, J. Huo, F. Ericson, M. Strømme, et al., Freestanding nanocellulose-composite fibre reinforced 3D polypyrrole electrodes for energy storage applications, *Nanoscale* 6 (21) (2014) 13068–13075.
- [114] G. Lee, D. Kim, D. Kim, S. Oh, J. Yun, J. Kim, et al., Fabrication of a stretchable and patchable array of high performance micro-supercapacitors using a nonaqueous solvent based gel electrolyte, *Energy Environ. Sci.* 8 (6) (2015) 1764–1774.
- [115] P. Li, Z. Jin, L. Peng, F. Zhao, D. Xiao, Y. Jin, et al., Stretchable all-gel-state fiber-shaped supercapacitors enabled by macromolecularly interconnected 3D graphene/nanostructured conductive polymer hydrogels, *Adv. Mater.* 30 (18) (2018) 1800124.
- [116] C.-C. Shih, Y.-C. Lin, M. Gao, M. Wu, H.-C. Hsieh, N.-L. Wu, et al., A rapid and green method for the fabrication of conductive hydrogels and their applications in stretchable supercapacitors, *J. Power Sources* 426 (2019) 205–215.
- [117] K. Wang, X. Zhang, C. Li, X. Sun, Q. Meng, Y. Ma, et al., Chemically crosslinked hydrogel film leads to integrated flexible supercapacitors with superior performance, *Adv. Mater.* 27 (45) (2015) 7451–7457.
- [118] M. Hu, Z. Li, G. Li, T. Hu, C. Zhang, X. Wang, All-solid-state flexible fiber-based MXene supercapacitors, *Adv. Mater. Technol.* 2 (10) (2017) 1700143.
- [119] L. Zang, Q. Liu, J. Qiu, C. Yang, C. Wei, C. Liu, et al., Design and fabrication of an all-solid-state polymer supercapacitor with highly mechanical flexibility based on polypyrrole hydrogel, *ACS Appl. Mater. Interfaces* 9 (39) (2017) 33941–33947.
- [120] H. Li, T. Lv, N. Li, Y. Yao, K. Liu, T. Chen, Ultraflexible and tailorable all-solid-state supercapacitors using polyacrylamide-based hydrogel electrolyte with high ionic conductivity, *Nanoscale* 9 (46) (2017) 18474–18481.
- [121] Q. Tang, M. Chen, G. Wang, H. Bao, P. Sáha, A facile prestrain–stick–release assembly of stretchable supercapacitors based on highly stretchable and sticky hydrogel electrolyte, *J. Power Sources* 284 (2015) 400–408.
- [122] Y. Huang, M. Zhong, F. Shi, X. Liu, Z. Tang, Y. Wang, et al., An intrinsically stretchable and compressible supercapacitor containing a polyacrylamide hydrogel electrolyte, *Angew. Chem. Int. Ed.* 56 (31) (2017) 9141–9145.
- [123] Y. Huang, M. Zhong, Y. Huang, M. Zhu, Z. Pei, Z. Wang, et al., A self-healable and highly stretchable supercapacitor based on a dual crosslinked polyelectrolyte, *Nat. Commun.* 6 (2015) 10310.
- [124] R. Na, Y. Liu, N. Lu, S. Zhang, F. Liu, G. Wang, Mechanically robust hydrophobic association hydrogel electrolyte with efficient ionic transport for flexible supercapacitors, *Chem. Eng. J.* 374 (2019) 738–747.

- [125] X. Li, L. Liu, X. Wang, Y.S. Ok, J.A. Elliott, S.X. Chang, et al., Flexible and self-healing aqueous supercapacitors for low temperature applications: polyampholyte gel electrolytes with biochar electrodes, *Sci. Rep.* 7 (1) (2017) 1685.
- [126] F. Tao, L. Qin, Z. Wang, Q. Pan, Self-healable and cold-resistant supercapacitor based on a multifunctional hydrogel electrolyte, *ACS Appl. Mater. Interfaces* 9 (18) (2017) 15541–15548.
- [127] H. Liao, F. Zhou, Z. Zhang, J. Yang, A self-healable and mechanical toughness flexible supercapacitor based on polyacrylic acid hydrogel electrolyte, *Chem. Eng. J.* 357 (2019) 428–434.
- [128] D. Kasprzak, I. Stępnia, M. Galiński, Electrodes and hydrogel electrolytes based on cellulose: fabrication and characterization as EDLC components, *J. Solid. State Electrochem.* 22 (10) (2018) 3035–3047.
- [129] X. Jin, G. Sun, G. Zhang, H. Yang, Y. Xiao, J. Gao, et al., A cross-linked polyacrylamide electrolyte with high ionic conductivity for compressible supercapacitors with wide temperature tolerance, *Nano Res.* 12 (5) (2019) 1199–1206.
- [130] J. Wang, X. Yu, C. Wang, K. Xiang, M. Deng, H. Yin, PAMPS/MMT composite hydrogel electrolyte for solid-state supercapacitors, *J. Alloy. Compd.* 709 (2017) 596–601.
- [131] M.G. Saborio, Š. Zukić, S. Lanzalaco, J. Casanovas, J. Puiggali, F. Estrany, et al., Prototyping flexible supercapacitors produced with biohydrogel, *Mater. Today Commun.* 16 (2018) 60–70.
- [132] Z. Yang, J. Deng, X. Chen, J. Ren, H. Peng, A highly stretchable, fiber-shaped supercapacitor, *Angew. Chem. Int. Ed.* 52 (50) (2013) 13453–13457.
- [133] Y. Guo, X. Zhou, Q. Tang, H. Bao, G. Wang, P. Saha, A self-healable and easily recyclable supramolecular hydrogel electrolyte for flexible supercapacitors, *J. Mater. Chem. A* 4 (22) (2016) 8769–8776.
- [134] M. Rosi, F. Iskandar, M. Abdullah, Khairurrijal, Hydrogel-polymer electrolytes based on polyvinyl alcohol and hydroxyethylcellulose for supercapacitor applications, *Int. J. Electrochem. Sci.* 9 (8) (2014) 4251–4256.
- [135] J. Wang, H. Chen, Y. Xiao, X. Yu, X. Li, PAMPS/PVA/MMT semi-interpenetrating polymer network hydrogel electrolyte for solid-state supercapacitors, *Int. J. Electrochem. Sci.* 14 (1) (2019) 1817–1829.
- [136] Y. Huang, M. Zhong, F. Shi, X. Liu, T. Zijie, W. Yukun, et al., A polyacrylamide hydrogel electrolyte enabled intrinsically 1000% stretchable and 50% compressible supercapacitor, *Angew. Chem. Int. Ed.* (2017).
- [137] Z. Wang, F. Tao, Q. Pan, A self-healable polyvinyl alcohol-based hydrogel electrolyte for smart electrochemical capacitors, *J. Mater. Chem. A* 4 (45) (2016) 17732–17739.
- [138] N. Choudhury, A. Shukla, S. Sampath, S. Pitchumani, Cross-linked polymer hydrogel electrolytes for electrochemical capacitors, *J. Electrochem. Soc.* 153 (3) (2006) A614–A620.

Applications of supercapattery

Syam G. Krishnan, Arulraj Arunachalam and Priyanka Jagadish

Graphene & Advanced 2D Materials Research Group (GAMRG), School of Science and Technology, Sunway University, Selangor, Malaysia

12.1 Introduction

The term “supercapattery” (SCAP) is the combination of two words: supercapacitor and battery. This arises owing to the property of certain transition oxide materials, chalcogenides, as well as other materials, that is, their charge storage property. Supercapacitors, typically divided into an electric double-layer capacitor (EDLC) and pseudocapacitors (PCs), differ in the energy storage process [1]. The energy released with the breakage of bonds in the electrode material, owing to the interaction of electrolyte/metal ions, will be stored in an electric double layer (EDL) in an EDLC. In PCs the storage of this energy will involve the EDL as well as the surface intercalation of the electrode, thereby providing improved energy density (E_s) than EDLCs. However, this improved energy density arises at the cost of inferior power density (P_s) owing to the slower response time to the ion intercalation in PCs. SCAP material involves deeper ion intercalation to the electrode surface. However, the intercalation is lower than the metal-ion intercalation involved in metal-ion batteries. Therefore the E_s of SCAP is higher than PCs with an almost identical power density of PCs thereby providing the possibility of bridging the research gap between SCs and metal-ion batteries [2].

SCAP involves deep surface intercalation of metal/electrolyte ions resulting in the redox process of electrode materials during electrochemical characterization. Electrochemical characterization of SCAP involves three processes: (1) cyclic voltammetry determining the process of charge storage; (2) galvanostatic charge–discharge for determining the practical capacitance; and (3) electrochemical impedance spectroscopy (EIS) for determining the characteristic resistances during the charge–discharge processes [3]. Usually, carbon materials such as carbon nanotubes (CNTs),

activated carbon (AC), graphene, and reduced graphene oxide (rGO) will be used for EDLC electrodes, whereas metal oxides such as RuO_2 and MnO_2 will be used as PC electrodes. The CV curves of both EDLC and PCs will be symmetrical and free of any redox peaks. However, PC material involves a redox reaction owing to the surface intercalation of electrodes and is not reflected in its CV. The CV of both the EDLC and PC is symmetrical thereby measuring similar instantaneous capacitance in each interval.

Metal oxides, such as CuO , Cu_2O , NiO , Co_3O_4 , V_2O_5 , CaO , and so on, as well as ternary metal cobaltites, such as MgCo_2O_4 , NiCo_2O_4 , CuCo_2O_4 , MnCo_2O_4 , etc., were utilized for SCAP applications [4,5]. The CV curves of these materials in aqueous electrolytes such as KOH , LiOH , Na_2SO_4 , HCl and so on show asymmetry in CV curves [6]. This asymmetry is owing to the deep surface intercalation of the metal/electrolyte ion causing the redox reaction. The area covered under the CV curves for the charge–discharge process will be different, thereby obtaining different capacitances in each instance. Therefore in SCAP, the capacitance measured is not instantaneous but the average. Therefore the instantaneous capacitance unit F g^{-1} should be changed to an average capacitance unit of mA h g^{-1} or C g^{-1} , thereby showing a battery-type charge-storage process [7].

SCAP materials are used for fabricating asymmetric supercapacitors (ASCs) combining SCAP and carbon materials as electrodes separated by a paper separator dipped in an electrolyte [8]. The energy density of these devices was higher than the EDLC devices. The several ASCs fabricated with SCAP electrodes are described below with due regard to their energy and power performances as well as cycling stability. The ASCs fabricated with metal oxides, TMCs, and chalcogenides were detailed in the upcoming section. As SCAP electrodes are involved in the fabrication of practical devices, the practical application of SCAP is termed as supercabattery (SCAB).



12.2 Metal oxide/metal hydroxide–based supercabattery

Metal oxides are chosen as SCAP electrodes for the stated reasons. Metal oxides, such as CuO , NiO , and Co_3O_4 possess multiple redox states, higher theoretical capacitance, appreciable electrical conductivity,

and higher ionic mobility. These factors are desired for electrode materials for SCAP electrodes. The voltage window (V) of this device is the combination of “V” of EDLC and SCAP materials. In three-electrode configuration, the optimum voltage window for carbon materials in aqueous electrolyte is 1.0–1.2 V. For metal oxide electrodes, the “V” is 0.4–0.6 V. Therefore the SCAB employing metal oxide and carbons as electrodes employing aqueous electrolyte-soaked separator shall deliver a “V” of 1.4–1.8 V. The SCABs fabricated employing these metal oxides as positive electrode materials are detailed below.

12.2.1 CuO supercabattery

CuO possesses material characteristics such as lower toxicity, relative abundance, is environmentally stable, and has the above-mentioned electrochemical properties. Furthermore, the theoretical capacitance of CuO is $\sim 1800 \text{ F g}^{-1}$. The first SCAB fabricated using CuO and AC as electrodes with 6 M KOH delivered a maximum energy density of 29.5 W h kg^{-1} with a power density of 800 W kg^{-1} [9]. The electrospinning method was used to synthesize CuO nanowires and the SCAB provided cycling stability of $\sim 98\%$ after 2000 cycles.

A three-dimensional (3D) CuO framework with appreciable surface area ($149 \text{ m}^2 \text{ g}^{-1}$) is synthesized by hydrothermal-assisted nanocasting [10]. CuO material consisted of highly ordered pores as well as nanowalls. The SCAB fabricated using 3D CuO electrode and AC as electrodes in 3 M KOH delivered an energy density of 19.7 W h kg^{-1} with impressive cycle life. The voltage window of the SCAB was 1.4 V combining the voltage window of both the electrodes. The 3D structure provided superior intercalation sites to achieve the appreciable energy density owing to its higher specific capacitance. 3D spherical CuO nanostructures were synthesized by a microwave-assisted solvothermal method [11]. These CuO structures provide a higher surface area ($\sim 168 \text{ m}^2 \text{ g}^{-1}$) and an appreciable capacitance (612 F g^{-1}) for three-electrode configuration. The SCAB of CuO//AC provided a working voltage of 1.6 V and an energy density of $\sim 27 \text{ Wh kg}^{-1}$ with $\sim 98\%$ of capacitance retention after 4000 cycles. The flower morphology comprising thin flakes proved to be efficient in this study as an efficient positive electrode in the SCAP.

A comparative energy storage performance study initiated the synthesis of different morphologies of CuO, viz., bud, flower, and plate-shaped nanostructures using a chemical method. The binder-free growth of CuO

nanoplate of nickel foam produced excellent capacitance properties in three-electrode configuration [12]. The “V” of SCAB was 1.6 V, thereby expecting a higher E_S . The SCAB fabricated using CuO nanoplate and AC electrodes showed an E_S of 29.4 Wh kg⁻¹ at a higher power density of 12.7 kW kg⁻¹. The binder-free approach is increasing the ion transport between the electrode–electrolyte interface and collaborating the utility of the active surface area of both the electrodes in SCAB for higher capacitance. Apart from these SCABs which utilized different morphologies of CuO as positive electrodes, there have been attempts to modify or decorate CuO with other materials and be used as a positive electrode. Doping of Cu with molybdenum will increase the conductivity of CuO and the research report proves that the capacitance increased up to 1392 F g⁻¹ [13]. The Mo–CuO//AC SCAB provided an excellent E_S of 36 Wh kg⁻¹ and provided capacitance retention of 81% after 5000 cycles.

Carbon composites of CuO were synthesized to improve its active surface area as well as its pore size (Fig. 12.1). Mesoporous carbon (MC) is combined with CuO to improve the conducting pathways of the metal oxide electrode and improve the energy storage properties. The CuO/MC composite improved the charge storage property of CuO, and the SCAB employing a

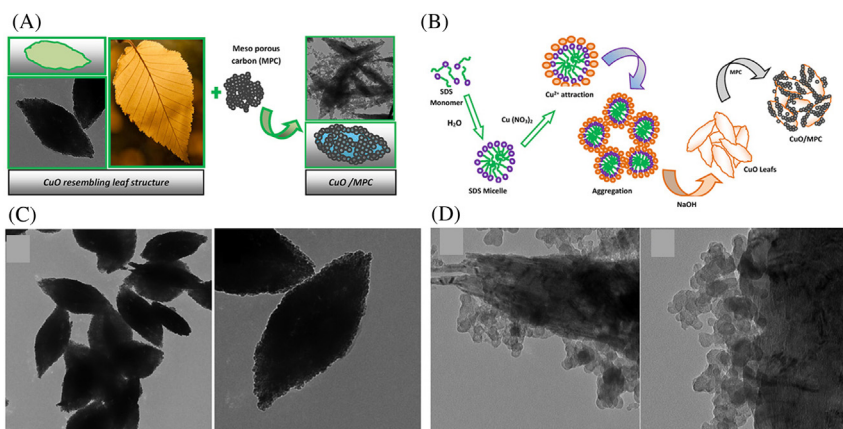


Figure 12.1 (A) Cartoon of the composite synthesis. (B) Schematic representation of the composite formation. (C) TEM images of the CuO. (D) TEM images of CuO-mesoporous carbon composite. Taken with permission from B. Saravanakumar, C. Radhakrishnan, M. Ramasamy, R. Kaliaperumal, A.J. Britten, M. Mkandawire, Copper oxide/mesoporous carbon nanocomposite synthesis, morphology and electrochemical properties for gel polymer-based asymmetric supercapacitors. *J. Electroanal. Chem.* 852 (2019) 113504. Copyright 2019, Elsevier publications.

polymer electrolyte (PVA-KOH) delivered an E_S of 26.6 Wh kg^{-1} [14]. However, the E_S of the device is inferior to the earlier mentioned CuO applications. Also, the mesoporous carbon content in the metal framework did not improve the cycling stability of the device. Only 69% of its initial capacitance is retained after 5000 cycles showing inferior capacitance retention.

Graphitic carbon-coated hollow CuO (H-CuO@GC) spheres are synthesized using a simple solvothermal technique [15]. These hollow spheres possessed a high specific surface area ($106 \text{ m}^2 \text{ g}^{-1}$), mesochannels, and higher pore volume. The H-CuO@GC//AC- SCAB delivered an appreciable E_S (38.6 Wh kg^{-1}) and appreciable cycling stability of $\sim 90\%$ after 10,000 cycles. Two such devices connected in series could light an LED of 2 V for almost 10 minutes showing an appreciable commercial potential.

The complex experimental approach of CuO nanotube arrays/Co(OH)₂/rGO on Cu wire (Fig. 12.2) is synthesized for the wearable application of SCABs using an in situ wet chemical approach [16]. The reason for using Co(OH)₂ for the composite is to increase the active surface area consisting of abundant faradic sites to achieve a higher capacitance. rGO is

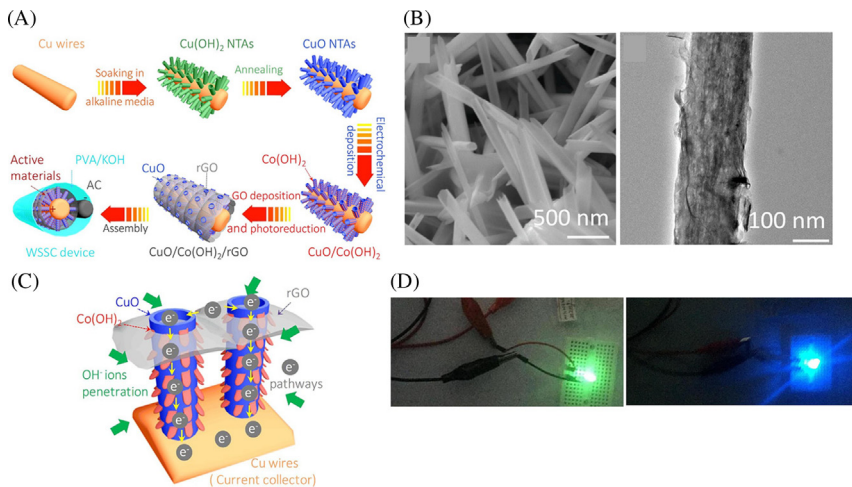


Figure 12.2 Schematics of the preparation of flexible CuO/Co(OH)₂/rGO nanotubes. (B) SEM and TEM images of nanotubes. (C) Schematics of energy storage in SCAB. (D) Power performance of SCABs. Taken with permission from W. Lan, X. Zhang, A. Zhai, W. Meng, H. Sheng, W. Dou, et al. Flexible CuO nanotube arrays composite electrodes for wire-shaped supercapacitors with robust electrochemical stability. *Chem. Eng. J.* 374 (2019) 181–188. Copyright 2019, Elsevier Publications.

used for improving the pathway of ion transfer as well as to decrease the dissolution of electrode material during the continuous charge–discharge process. The flexible SCAB with the CuO nanotube arrays/Co(OH)₂/rGO and AC as electrodes employing a PVA–KOH electrolyte demonstrated excellent cycling stability of 100% after 10,000 cycles and an excellent E_S . Three flexible SCABs in series could light an LED, showing its importance in wearable electronics. Research on improving the conductivity of CuO resulted in the chemical deposition of CuO on an rGO-coated sponge (SP) substrate prepared by a dip and dry method [17]. The electrode could scan at a higher voltage range of 200 mV s⁻¹. Using SP as an electrode substrate could facilitate the electrode flow throughout its 3D structures, thereby improving the electrolyte mobility in the substrate. The SCAP device fabricated with CuO-rGO@SP as a positive and rGO@SP as a negative electrode could achieve a higher potential window of 1.7 V. The E_S of the SCAP was determined to be $\sim 31 \text{ W h kg}^{-1}$ @ 1699 W kg⁻¹. The hierarchical porous structure of the electrode would improve the accessibility of electrolyte ions resulting in the utilization of active surface area of both the electrodes in SCAB. The thickness of the SCAP electrode should be maintained to the micrometer range and the electrode mass loading will be in the commercial aspect. Such a research attempt delivered a quasisolid state SCAB with CuO supported on La_{1-x}Sr_xCoO_{3-δ} (LSC, 0 ≤ x ≤ 0.8) as a positive and carbon cloth as a negative electrode working in a potential window of 1.4 V [18]. This SCAB utilizes PVA/KOH gel electrolyte and the device delivers a higher density of $\sim 3 \text{ mW cm}^{-3}$.

The research into the preparation of flexible SCAB resulted in the synthesis of Fe₂O₃ and CuO thin films as a cathode and an anode, respectively. The thin films were made using successive ionic layer adsorption and reaction (SILAR) and chemical bath deposition (CBD) methods [19]. A polymer gel electrolyte (carboxymethyl cellulose (CMC)-Na₂SO₄) is used for flexible SCAB fabrication showing a potential window of 2.0 V with a maximum E_S and P_S of 23 Wh kg⁻¹ and 19 kW kg⁻¹. The flexibility of the device was proved with a capacity retention of 89% after 180 degrees bending. However, the flexible SCAB could only retain 90% of its initial capacitance for 1000 cycles. The research attempts to prepare flexible wearable energy storage devices were reported too on CuO materials. A drop-casting approach is utilized to integrate caterpillar-like shaped CuO hierarchical structures on a flexible conductive woven textile substrate (CWTs) and electrochemically characterized as a binder-free

electrode. A redox-active electrolyte ($\text{K}_3\text{Fe}(\text{CN})_6$) is added into the 1 M KOH to improve the energy storage as well as the cycling capacity. The SCAB fabricated with this electrode operated in a voltage window of 1.5 V with an appreciable E_S [20].

The research interest in wearable electronics continues to explore CuO as one of its electrode materials. The complication of electrode fabrication for SCAB electrodes hinders its rapid commercialization. A 1D nanoarray electrode comprising both CuO nanowires and CoFe-layered double hydroxide nanoplatelets supported on the copper wire is synthesized [21]. The synthesis procedure is complex and the practical utility of these complex structures is questionable. However, the flexible material fabricated utilizing the complicated structure as one of the electrodes and AC as other with PVA-KOH gel electrolyte provides appreciable E_S and P_S . These sorts of fabrications techniques could be utilized for microelectronics energy storage devices.

Flexible supercapacitor research also developed the technique of the growth of CuO nanoflowers on carbon fiber fabric (CFF) [22]. These sorts of development techniques seem to be more commercially viable than earlier mentioned complex techniques (Fig. 12.3). A simple hydrothermal technique grows CuO nanoflowers on the CFF. A symmetric SCAB, fabricated with the CuO/CFF electrodes separated with separators and polyvinyl alcohol (PVA)-LiCl gel as an electrolyte, shows promising results as a flexible energy storage device. The voltage window of the device was ~ 1.6 V and could produce a maximum E_S of 4.66 W h kg^{-1} . Three such cells connected in series could light three green LEDs connected in parallel, each with a power rating of 2.3 V, 20 mA, for almost 5 minutes.

The research interest in the improvement of the conductivity as well as the rate capability of CuO resulted in the synthesis of $\text{Cu}_2\text{O}/\text{CuO}/\text{Co}_3\text{O}_4$ core-shell nanowires [23]. These core-shell structures were expected to improve the ionic transport pathways, its specific capacitance, and cycling stability. The SCAB fabricated using the composite electrode as a positive electrode and activated graphene (AG) as a negative electrode provided a voltage window of 1.4 V and a maximum energy density of 12 Wh kg^{-1} , which is not on a par with other metal oxide SCABs. These core-shell structures did not perform to expected results, showing inferior capacitance to the CuO nanowires reported earlier [24].

The SCABs fabricated utilizing CuO as a positive electrode couldn't be utilized for commercial applications. The research methods for

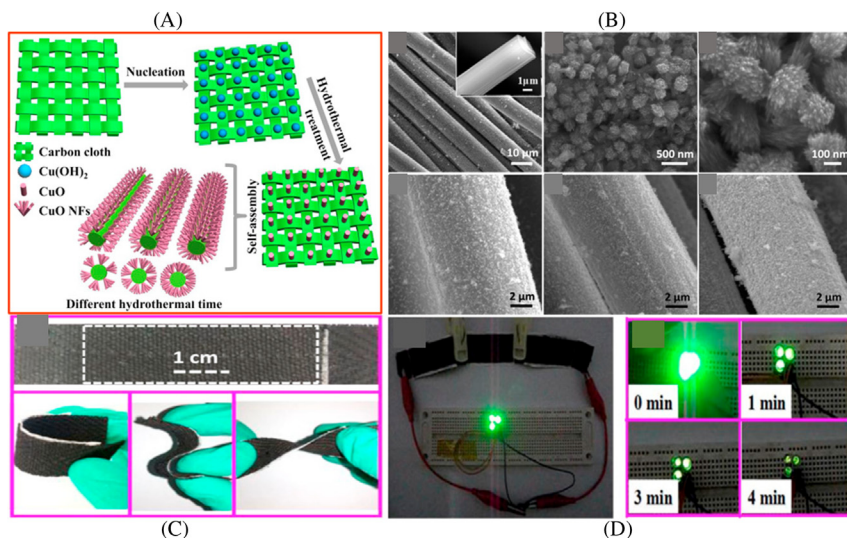


Figure 12.3 (A) Schematic diagram of growth of CuO nanoflowers on carbon cloth. (B) SEM images at various resolutions of CuO on carbon cloth. (C) Picture showing the thickness and flexibility of the SCAB. (D) Variation of power output from the device with time. Taken with permission from reference W. Xu, S. Dai, G. Liu, Y. Xi, C. Hu, X. Wang, CuO nanoflowers growing on carbon fiber fabric for flexible high-performance supercapacitors. *Electrochim. Acta* 203 (2016) 1–8. Copyright 2016, Elsevier publications.

improving the conductivity of CuO, its transport channels and its active surface area are more complex in nature. The synthesis of CuO for wearable electronics is not scalable and more innovative scalable research methods need to be adapted to develop a practical prototype of SCAB involving the CuO electrode.

12.2.2 NiO supercabattery

NiO is also a metal oxide which is largely explored for SCAP applications. This metal oxide possesses higher theoretical capacitance ($\sim 2573 \text{ F g}^{-1}$) and multiple oxidation states but these are combined with an inferior electrical conductivity. The research on NiO applications on SCAP electrodes focus on various synthesis methods, such as hydrothermal, electrospinning, precipitation, sol–gel, as well as other scalable techniques. Also, there are research reports of the development of composites of NiO with other metal oxides, as well as carbons such as graphene and AC to improve electrical conductivity.

Electrospun NiO fibers were used in fabricating a SCAB with aqueous electrolyte (6 M KOH) with an appreciable voltage window of 1.5 V [25]. The maximum E_S of the SCAB was reported to be $\sim 43 \text{ Wh kg}^{-1}$ and demonstrated appreciable cycling stability (88%) after 5000 GCD cycling. As the NiO structure was one-dimensional, it could focus on a controlled pathway of electrolyte/metal ions during electrochemical charge transfer processes. 3D NiO structures (microspheres with honeycomb structure) were synthesized using hydrothermal synthesis [26]. The fabricated SCAB device with rGO as a negative electrode delivered a voltage window of 1.5 V. The higher surface area ($257 \text{ m}^2 \text{ g}^{-1}$), as well as large pore volume ($1.64 \text{ cm}^3 \text{ g}^{-1}$), could have facilitated focused as well as rapid ion transport, thereby delivering an appreciable E_S (23.25 Wh kg^{-1}) at a P_S of 9.3 kW kg^{-1} .

Apart from surface area and morphology, the porosity of the electrode material also plays a significant part in energy storage. Porous NiO hierarchical structures were synthesized using a facile hydrothermal synthesis. This porous structure was used as a positive electrode and the porous carbon electrode synthesized using a template-assisted method as a negative electrode. The pore size for NiO and carbon was 6.7 nm and 5.1 nm, respectively. The SCAB was synthesized using these electrodes with aqueous electrolyte (6 M KOH) with an operating voltage window of 1.3 V. Temperature dependence of SCAB in temperature ranging from -20°C to 40°C is determined with NiO and AC as electrodes; the maximum efficiency of the device is determined at 40°C . The E_S of the device at 40°C (26.1 Wh kg^{-1}) was its maximum [27]. Alkaline polymer gel electrolyte (PVA-KOH) was used and the voltage window determined for the device was 1.6 V.

The exploration of the replacement of carbon materials with other transition metal oxides was also reported to improve the performance of SCAB with NiO as a positive electrode. A chemical route was employed to synthesize NiO and $\text{Ru}_{0.36}\text{V}_{0.64}\text{O}_2$ and these were used as positive and negative electrodes, respectively, for SCAB [28]. 1 M KOH was used as the electrolyte and the replacement of the carbon electrode improved the voltage window of the aqueous electrolyte, thereby improving the E_S . However, the voltage window of the device was 1.7 V and provided a maximum E_S of 23.0 Wh kg^{-1} .

Composites of NiO with graphene film were synthesized to increase the conductivity of the material. Hierarchical nitrogen-doped porous carbon nanotubes (HNPCNTs) were synthesized as a negative electrode and

the SCAB in KOH electrolyte (Fig. 12.4) [29]. The performance of the SCAB device was commendable, delivering 32 Wh kg^{-1} at 700 W kg^{-1} . The voltage window of the device is on the lower side (1.4 V) and the cycling stability of 94% was reported after 2000 charge–discharge cycles. To improve the conductivity as well as the cycling stability of the NiO material, NiO nanoparticles are uniformly deposited onto the 3D graphite-foam CNT forest substrate [30]. The SCAB device was fabricated utilizing the composite electrode and graphene–CNT electrode; 2 M KOH as electrolyte obtained a potential window of 1.4 V. The maximum E_S of the SCAB was determined to be 17 Wh kg^{-1} , providing capacitance retention of 94% after 2000 cycles.

Coordination polymer-derived nanomaterials also have been proved as energy storage applications (Fig. 12.5). NiO is synthesized from the cyano-bridged CPs using the thermal treatment and nanoporous carbon from the zeolithic imidazolate framework using a carbonization technique [31]. The NiO and porous carbon are utilized as positive and negative electrodes for SCAB fabrication and deliver a voltage window of 1.6 V in

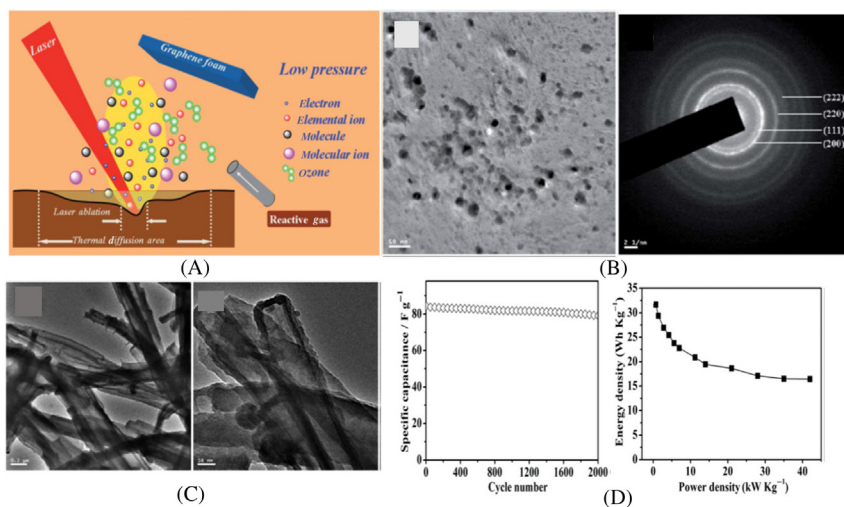


Figure 12.4 (A) Schematics for the synthesis of NiO/graphene composite. (B,C) TEM and SAED pattern of the NiO particle in NiO/GF. (D) Cycling stability and Ragone plot of the device, respectively. Taken with permission reference H. Wang, H. Yi, X. Chen, X. Wang, *Asymmetric supercapacitors based on nano-architected nickel oxide/graphene foam and hierarchical porous nitrogen-doped carbon nanotubes with ultrahigh-rate performance*. *J. Mater. Chem. A* 2 (2014) 3223–3230. Copyright 2015, Royal Society of Chemistry.

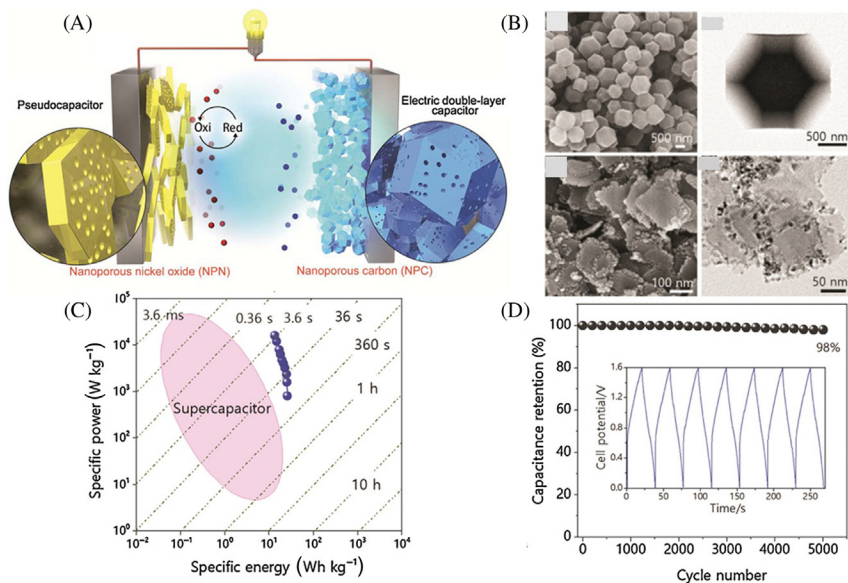


Figure 12.5 (A) Schematics of the working of NiO SCAB. (B) Various SEM and TEM images of NiO. (C) Ragone plot of the SCAB. (D) GCD curves and capacitance retention for 5000 CD cycles. Taken with permission from R.R. Salunkhe, M.B. Zakaria, Y. Kamachi, S.M. Alshehri, T. Ahamad, N.L. Torad, et al. *Fabrication of asymmetric supercapacitors based on coordination polymer derived nanoporous materials. Electrochim. Acta* 183 (2015) 94–99. Copyright 2015, Elsevier Publications.

6 M KOH. The maximum E_S obtained for the SCAB is 26 Wh kg⁻¹ with 98% of capacitance retention after 5000 cycles. The research attempts to bridge the NiO and graphene through Ni–O–C bands, resulting in the deposition of NiO quantum dots (~ 3 nm) on the graphene surface (NiO/Gh) [32]. The NiO/Gh//AC SCAB provided E_S is ~ 23 Wh kg⁻¹ with an operating voltage of 1.6 V and cycling stability of 87.2% retention after 5000 cycles. These NiO SCABs demonstrated the appreciable practical application of SCAP electrodes. Still, research innovations are required to commercialize NiO as an electrode material for high E_S commercial SCABs.

12.2.3 Co₃O₄ supercabattery

The theoretical capacitance of Co₃O₄ is high (~ 3560 F g⁻¹), which is higher than any other metal oxides for SCAP applications. Also, it possesses multiple oxidation states (+2 and +3) and appropriate redox potential (~ 0.5 V). However, its lower electrical conductivity hinders

achieving its higher theoretical capacity. Therefore research is focusing on the synthesis of various morphologies of Co_3O_4 with higher surface area as well as the focused ion transport layer to increase the electrolyte/metal ion contact with the electrode surface. This research also focuses on improving the conductivity of Co_3O_4 by combining it with materials with higher conductivity such as graphene and rGO to form its composites.

Electrospun Co_3O_4 nanowires were utilized as a cathode and have achieved almost 32% of its achieved capacitance in three-electrode characterization. The $\text{Co}_3\text{O}_4//\text{AC}$ SCAB could achieve a voltage window of 1.4 employing an aqueous electrolyte (6 M KOH) [33]. The E_S of SCAB was higher (47.6 W kg^{-1}) and the cycling stability of the materials was impressive demonstrating only 3% capacitance loss after 2000 cycles. Hard template synthesis of mesoporous Co_3O_4 is reported for $\text{Co}_3\text{O}_4//\text{AC}$ flexible SCAB. PVA-KOH electrolyte was utilized for this flexible SCAB delivering a voltage window of 1.5 V [34]. The E_S of the device is not compiled showing almost 90% capacitance retention after 5000 cycles. Also, the mechanical flexibility of the device is promising to retain almost the initial capacitance even after 180 degrees bending. Attempts to improve the E_S of Co_3O_4 SCABS developed porous carbon rather than the commercial AC using various synthesis methods for utility as a negative electrode. The solvothermal route developed Co_3O_4 nanowires on nickel foam and carbon aerogel microspheres, which were synthesized by using a condensation polymerization reaction [35]. The 3D structured carbon aerogels could provide improved ion intercalation and pathways for the improved capacitance. The two electrodes in SCAB were separated by a PVA-KOH soaked separator. The device voltage was fixed to be 1.5 V, the E_S of SCAB reported to be 17.9 Wh kg^{-1} with cycling stability of 85% after 2000 charge–discharge cycles.

A simple pyrolysis technique is used to synthesize an interconnected 3D flake structure morphology of Co_3O_4 from cobalt–oxalate complex thin structures [36]. Although, the three-electrode electrochemical characterization for SCAP application shows a higher capacitance (1500 F g^{-1}) in 2 M KOH electrolyte, the aqueous $\text{Co}_3\text{O}_4//\text{AC}$ SCAB does not show promising E_S ($\sim 15 \text{ kW kg}^{-1}$). The increase in capacitance, as well as E_S , corresponds to maximum utilization of the active surface area of both the electrodes.

Research in improving the transport channels of Co_3O_4 materials resulted in the construction of 3D nanostructures of Co_3O_4 nanowires by

the hydrothermal method [37]. The electrode prepared using this material showed an appreciable capacitance (642 F g^{-1}) in SCAP testing in the three-electrode configuration. The SCAB fabricated using this Co_3O_4 nanostructures and graphene hydrogel as electrodes in 3 M KOH as electrolyte showed a higher voltage window of 1.7 V. The E_S of the electrode was determined to be 31 Wh kg^{-1} for this aqueous SCAB.

Research attempts of using Co_3O_4 as a negative electrode in SCAB resulted in the synthesis of its polymer nanocomposites. A polymer nanocomposite of Co_3O_4 (Co_3O_4 @polypyrrole) along with Co_3O_4 nanowires as electrodes utilizing 1 M KOH is fabricated as SCAB [38]. The fabricated SCAB works in a potential window of 1.4 V and shows an E_S of $\sim 26 \text{ Wh kg}^{-1}$. The specific capacitance of the Co_3O_4 /polypyrrole composite was almost double the value ($\sim 320 \text{ F g}^{-1}$) of that of carbon electrodes, thus showing that its polymerization could produce an efficient negative electrode for SCAB.

Improving the conductivity of Co_3O_4 could deliver a higher capacitance as well as the E_S of the fabricated SCAB. Sequential deposition of Co_3O_4 nanoflakes onto spherical sponge-like porous rGO could deliver a maximum capacitance of 1112 F g^{-1} for a three-electrode system (Fig. 12.6) [39]. The SCAB fabricated with this composite electrode as a cathode and AC as an anode could deliver a maximum voltage window of 1.5 V. However, the maximum E_S obtained for the SCAB device was 23.3 Wh kg^{-1} , which is inferior to other Co_3O_4 SCABs reported here. Irrespective of its inferior E_S performance, the cycling stability of the device was commendable, retaining 100% capacitance retention after 20,000 charge–discharge cycles.

The improvement of surface area, as well as the conductivity of Co_3O_4 , could improve its energy storage property. One-step hydrothermal synthesis technique is used in the synthesis of 3D interconnected porous Co_3O_4 and graphene aerogel (GA) composite [40]. This composite electrode could deliver a higher specific capacitance of $\sim 1512 \text{ F g}^{-1}$ and a SCAB fabricated with Co_3O_4 /GA//GA electrode could work in a potential window of 1.6 V. The maximum E_S of this SCAB was also higher ($\sim 68 \text{ Wh kg}^{-1}$) with LiOH/PVA gel electrolyte. The cycling stability of the device also seems to be promising, demonstrating only $\sim 19\%$ capacitance loss after 5000 charge–discharge cycles.

Composites of Co_3O_4 are synthesized, citing the improvement in electrical conductivity thereby improving its charge storage parameters. $\text{Co}(\text{OH})_2$ is known for its higher redox reaction as well as higher theoretical capacitance. Co_3O_4 / $\text{Co}(\text{OH})_2$ composite is synthesized using

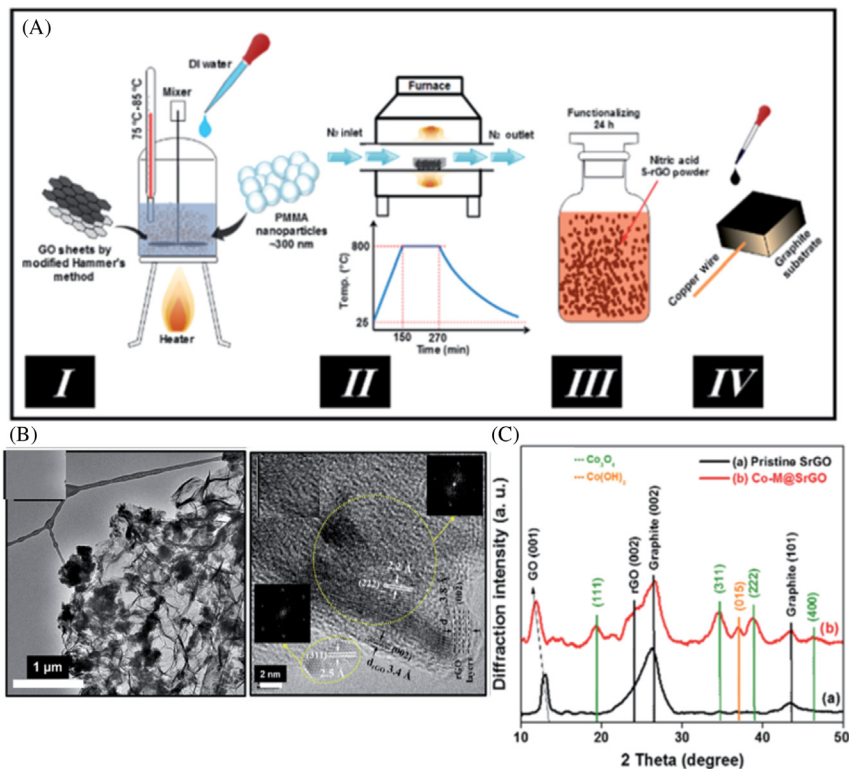


Figure 12.6 (A) Schematics of the synthesis process of the sponge like rGO. (B) TEM and HRTEM image of Co₃O₄@SrGO hybrid. (C) XRD patterns of the as prepared Co₃O₄@SrGO hybrid. *Reproduced from M. Qorbani, T.-C. Chou, Y.-H. Lee, S. Samireddi, N. Naseri, A. Ganguly, et al. Multi-porous Co₃O₄ nanoflakes@ sponge-like few-layer partially reduced graphene oxide hybrids: towards highly stable asymmetric supercapacitors. J. Mater. Chem. A 5 (2017) 12569–12577. Copyright, 2017, RSC publications.*

hydrothermal and electrodeposition methods [41]. A potential window of 1.5 V is observed for the Co₃O₄/Co(OH)₂//AC aqueous SCAB using 2 M KOH as an electrolyte. The maximum E_S of the SCAB obtained was $\sim 26 \text{ Wh kg}^{-1}$ and the cycling stability of the device was not reported. Co₃O₄@MnO₂ core–shell arrays were directly grown onto nickel foam as a part of improving the conductivity as well as oxidation states of Co₃O₄ [42]. Although the composite is characterized by higher surface area, the electrochemically active sites in the composite were lower, thereby resulting in a lower energy storage performance ($\sim 560 \text{ F g}^{-1}$). The SCAB with the composite electrode as a cathode and graphene as an anode could only deliver an E_S of $\sim 18 \text{ Wh kg}^{-1}$.

There are research reports on the synthesis of $\text{Co}_3\text{O}_4@\text{RuO}_2$ [43], $\text{Co}_3\text{O}_4@\text{MMoO}_4$ ($M = \text{Ni}, \text{Co}$) [44, 45], and $\text{NaCoPO}_4\text{-Co}_3\text{O}_4$ [46] as composite electrodes for supercapacitor applications. These electrodes improved the specific capacitance of Co_3O_4 due to its improvement in conductivity as well as oxidation states. As a SCAB device with both the aqueous and polymer electrolyte, the drastic improvement in the E_S was not observed, thereby validating the need for matching the pore size of electrodes with that of the electrolyte.

12.2.4 $\text{Cu}(\text{OH})_2$ supercapattery

Metal hydroxides are possessing similar energy storage properties compared to metal oxides. They possess improved theoretical capacitance and redox potential ideal for ion intercalation, thereby creating a potential difference for the charge storage. However, the problems associated with the metal hydroxides were poor rate capability, lower electrical conductivity, and lower energy densities. The commonly used metal hydroxides for SCAB applications are cobalt hydroxide ($\text{Co}(\text{OH})_2$) and nickel hydroxide ($\text{Ni}(\text{OH})_2$).

$\text{Co}(\text{OH})_2$ exists in two phases, α and β , depending on the arrangement of atoms in its crystal structure [47]. The β -phase consists of a hexagonal layered hydroxide with a similar structure to the pattern of brucite and pink ($a = 3.177 \text{ \AA}$ and $c = 4.653 \text{ \AA}$). The α -phase is similar to the brucite-like phase with the intercalation of water molecules between the sheets. Out of these two phases, $\beta\text{-Co}(\text{OH})_2$ is a promising supercapacitor electrode owing to its higher theoretical capacitance ($\sim 3460 \text{ F g}^{-1}$) and its natural abundance. However, its poor electrical conductivity, as well as inferior electroactive sites, limits the practical capacitance of the material. An oriented attachment strategy (Fig. 12.7) was involved in the synthesis of $\beta\text{-Co}(\text{OH})_2$ single layers with the thickness of the five-atom layer [48]. However, the CV shape of the practical device is symmetrical (Fig. 12.7), thereby showing a PC mechanism like SCAP and the assembled device is an ASC rather than an SCAB. The practical capacitance of the electrode is high (2025 F g^{-1}) for $\beta\text{-Co}(\text{OH})_2$ electrode and the solid-state ASC fabricated with N-doped graphene-based anode provided a working voltage of 1.8 V. The E_S of the device (98.9 Wh kg^{-1}) is on a par with the E_S of commercial SCs and the cycling stability of the device shown a mere $\sim 7\%$ of capacitance loss after 10,000 cycles.

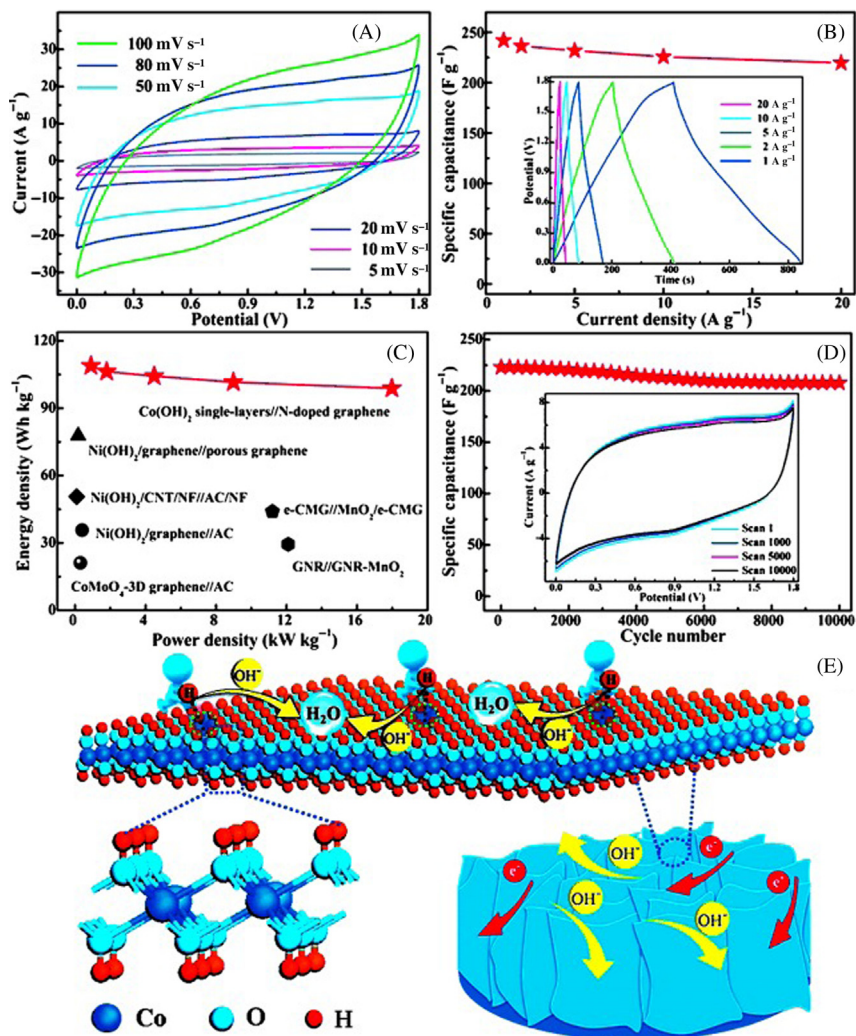


Figure 12.7 (A) CV curve of state ASCs. (B) GCD curves of the ASCs at different current densities and the variation of C_s with different current densities. (C) Ragone plot of the fabricated solid-state ASCs. (D) Schematics of energy storage process in single-layered Co(OH)_2 . Taken with permission from S. Gao, Y. Sun, F. Lei, L. Liang, J. Liu, W. Bi, et al. *Ultrahigh energy density realized by a single-layer β - Co(OH)_2 all-solid-state asymmetric supercapacitor*. *Angew. Chem. Int. Ed.* 53 (2014) 12789–12793. Copyright 2014, Wiley Publications.

The direct growth of Co(OH)_2 buds on Ni foam is reported and a higher specific capacitance of 2041 F g^{-1} is obtained in 6 M KOH electrolyte employing a three-electrode electrochemical characterization [49].

The CV curve shows a SCAP behavior and the aqueous SCAB fabricated with $\text{Co}(\text{OH})_2//\text{AC}$ with a voltage window of 1.6 V shows a maximum E_S of $\sim 20 \text{ Wh kg}^{-1}$, which is much inferior to the previously discussed device. Furthermore, the cycling stability of the device is inferior, retaining only $\sim 69\%$ after 1000 cycles of charge–discharge. The hydrothermal method was utilized to synthesize mace-like $\text{CNT}/\text{Co}(\text{OH})_2$ ordered arrays which delivered a maximum capacitance of $\sim 614 \text{ C g}^{-1}$ in three-electrode configuration in 2 M KOH [50]. The aqueous SCAB fabricated using this composite electrode and AC as electrodes could provide only a maximum energy density of 7.2 kW kg^{-1} with an operating cell voltage of 1.4 V.

Aqueous SCAB involving $\text{Co}(\text{OH})_2$ nanosheet arrays grown directly on nickel foam as a positive electrode (Fig. 12.8) and CNTs grown on nickel foam as negative electrode using electrodeposition technique was designed [51]. The E_S of the device was also not promising obtaining 19 Wh kg^{-1} with appreciable cycling stability of 96% after 7000 cycles. The voltage window of the device in 2 M KOH electrolyte was 1.5 V only and the CV curve of the SCAB shows more of a rectangular shape showing the dominance of EDLC property of CNTs than the intercalation capacitance of $\text{Co}(\text{OH})_2$.

Similar to the growth of $\text{Co}(\text{OH})_2$ on Ni foam, a combination of plasma-enhanced chemical vapor deposition (PECVD) and electrochemical deposition was employed to fabricate a graphene supported $\text{Co}(\text{OH})_2$ nanosheet ($\text{Co}(\text{OH})_2/\text{GNS}$) and AC on carbon filter paper (AC/CFP) as positive and negative electrodes, respectively. These composite electrodes, however, do not improve the charge storage performance of the SCABs. The maximum E_S obtained from this device was 19.3 Wh kg^{-1} in 1 M KOH as an electrolyte with a maximum working voltage of 1.6 V. The device provided stable cycling stability after 20,000 charge–discharge cycles.

$\text{Co}(\text{OH})_2$ is derived from MOFs using a solid–solid conversion process in the alkali solution. The prepared $\text{Co}(\text{OH})_2$ is porous in nature and shows a maximum C_S of $\sim 604 \text{ F g}^{-1}$ [52]. The SCAB fabricated with this metal hydroxide and AC as electrodes had a maximum working voltage of 1.4 V. However, the maximum E_S the device could attain was 13.6 Wh kg^{-1} , retaining only 80% of its initial capacitance after 2000 charge–discharge cycles. Apart from the superior performance of $\text{Co}(\text{OH})_2$ sheets with atomic layer thickness as ASCs, the other composite electrodes of $\text{Co}(\text{OH})_2$ do not produce an excellent E_S to recommend it as a commercial electrode material for SCAB.

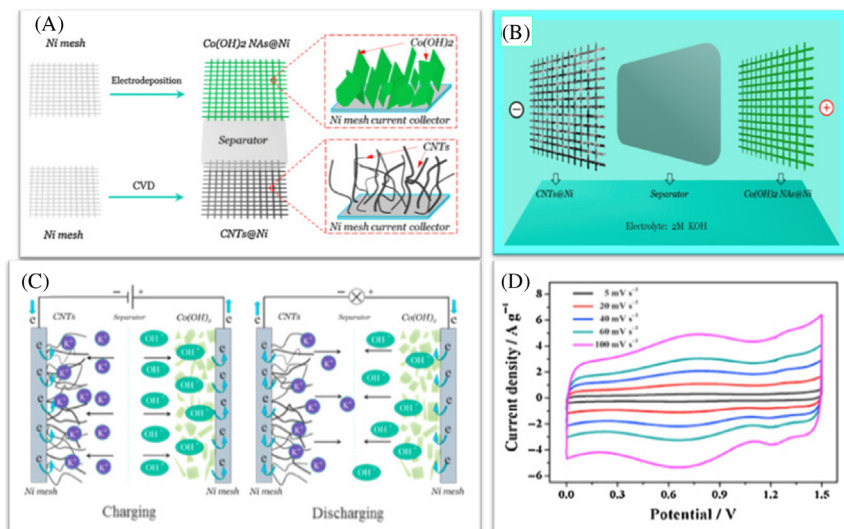


Figure 12.8 (A) Cartoon representation of the development of Co(OH)₂ nanoflakes on Ni foam. (B) Cartoon of SCAB fabrication of CNT and Co(OH)₂ as electrodes. (C) Schematics of the charge transfer process in the ASCs; and (D) the CV curve of SCAB device. Taken with permission from T. Peng, H. Wang, H. Yi, Y. Jing, P. Sun, X. Wang, Co(OH)₂ nanosheets coupled with cnt arrays grown on ni mesh for high-rate asymmetric supercapacitors with excellent capacitive behavior. *Electrochim. Acta* 176 (2015) 77–85. Copyright 2015, Elsevier Publications.

12.2.5 Ni(OH)₂ supercabattery

Ni(OH)₂ proves to be a good performing material for SCAP owing to its low cost, environmental friendliness, and higher theoretical capacitance. However, these characteristics do not support Ni(OH)₂ for its achievable capacitance particularly with higher scan rates owing to its poor electrical conductivity and lower cycling stability. For solving these problems several morphologies of Ni(OH)₂, such as nanotubes, nanoflowers, and hierarchical structure, were synthesized to improve the active surface area, porosity, and ion transportation. The highlighted performance of practical applications of SCAP is noted below.

The thermal chemical vapor deposition method is used to grow CNTs onto Ni Foams (CNT/NF) and a chemical bath deposition method is utilized to deposit Ni(OH)₂ nanostructures onto CNT/NF [53]. As the method is additive-free, the electrode tested for SCAP provided an excellent capacitance of 3300 F g⁻¹ in the three-electrode system utilizing KOH as an electrolyte. The SCAB consisting of this composite electrode

as a positive electrode and AC as a negative electrode delivered a voltage window of 1.8 V and a maximum E_S of 50.6 Wh kg⁻¹. This shows that the binder-free approach could increase the energy storage capability of the device. Further improvement in the energy density of the SCABs was achieved owing to the microwave synthesis of Ni(OH)₂/graphene composite as a cathode and porous carbon as an anode [54]. An improved E_S of ~78 Wh kg⁻¹ is obtained for the potential window of 1.6 V with cycling stability of ~94% after 3000 charge–discharge cycles.

A template-free spontaneous growth approach is used for the synthesis of β-Ni(OH)₂ on a nickel foam and to characterize it for SCAP applications [55]. The fabricated ASC using this as a cathode and AC using 6 M KOH electrolyte could produce a maximum E_S of ~36 Wh kg⁻¹ with a practical voltage window of 1.6 V. Attempts to stabilize the rate capability of α-Ni(OH)₂ material resulted in the substitution of Al with α-Ni(OH)₂ resulting in a higher specific capacitance (2080 F g⁻¹) for SCAP three-electrode configuration. The energy density of the aqueous SCAB using the α-Ni(OH)₂ and AC as electrodes shows an appreciable voltage window (1.6 V) and E_S (42 Wh kg⁻¹). However, the cycling stability of the device was still an issue; 82% after 1000 CD cycles.

The decay of capacitance of Ni(OH)₂ coated on Ni Foam using a chemical deposition method was studied for 1500 cycles and it was determined that only 5% of its initial capacitance is decreased [56]. The reason for the inferior capacitance of Ni(OH)₂ is determined to be the phase transformation and particle/crystal size growth. The hierarchical composite structures comprising Ni(OH)₂ nanowire–MnO₂ nanoflakes core–shell films prepared using the CBD technique proved to be effective in showing SCAP property in both neutral and alkaline electrolyte [57]. However, the capacitance of these complex structures was lower compared to the pristine Ni(OH)₂ structures, thus questioning the need for these complex structures to achieve lower practical capacitance than the parent compounds. Furthermore, the practical application of this electrode is not developed.

Similar attempts of modifying the conductivity of Ni(OH)₂ resulted in the single step coprecipitation synthesis method using coaxial CNT, thereby forming 3D CNT/Ni(OH)₂ nanostructures [58]. The SCAB fabricated using CNT/Ni(OH)₂ as a positive electrode and rGO as a negative electrode using 1 M KOH as electrolyte could deliver a maximum E_S of 35 Wh kg⁻¹ and a working voltage of 1.8 V. Further studies on tailoring the morphology of α-Ni(OH)₂ were performed with solvothermal

synthesis and it is determined that the CNT/Ni(OH)₂ microsphere could deliver a maximum capacitance of $\sim 1087 \text{ F g}^{-1}$ as a SCAP electrode in 6 M KOH [59]. The maximum E_S that the SCAB device with CNT/Ni(OH)₂//AC electrodes could deliver is $\sim 33 \text{ Wh kg}^{-1}$ with a voltage window of 1.6 V.

The binderless approach was performed to electrodeposit Ni(OH)₂ nanoflakes on Ni foam-supported vertically oriented graphene nanosheets. Although the three-electrode system measured a superior capacitance of 2215 F g^{-1} , the SCAB fabricated using this composite and AC as electrode could deliver a maximum E_S of $\sim 11 \text{ Wh kg}^{-1}$ with a voltage window of 1.4 V using 6 M KOH as an electrolyte. This also proves that the energy storage capability of a single electrode is not only the parameter for obtaining higher densities for the SCAB device. A similar example could be observed for the development of Ni(OH)₂ on a 3D carbon support of cellulose fiber with graphene. The synthesized material could provide a higher surface area ($\sim 426 \text{ m}^2 \text{ g}^{-1}$) and a higher specific capacitance (2276 F g^{-1}) in 2 M NaOH solution [60]. However, the maximum E_S of the SCAB device employing AC as a negative electrode and the composite electrode as a positive electrode is 15 Wh kg^{-1} with a voltage window of 1.6 V. The only advantage with this complex nanostructure is 100% capacitance retention after 5000 charge–discharge cycles.

The above performance evaluation provides a glance at the progress in material research of typically metal oxides for energy storage applications. Metal oxides and hydroxides, as well as their composites, are well explored to increase conductivity and the active surface area for improving the electron/ion transport between the electrode–electrolyte surface. Different material synthesis techniques, such as hydrothermal method, electrospinning, coprecipitation method, and chemical vapor deposition, were utilized to tailor the morphology as well as combining different metal oxides for improving the energy storage parameters. However, the achieved energy densities compiled above prove that further improvement is required in the performance of these materials to be commercialized as a SCAB device.

12.2.6 TMC supercapabattery

Cobalt in cobalt oxide (Co₃O₄) consists of two valences (+2 and +3) and consists of a spinel crystal structure. Although the theoretical capacitance of the Co₃O₄ is higher, its electrical conductivity is poor

($\sim 10^{-5} \text{ S cm}^{-1}$) and its higher toxicity and poor availability hinder its development as a commercial electrode material. Therefore research in increasing the conductivity as well as the content of Co in Co_3O_4 initiated synthesis of ternary metal cobaltites in which Co^{2+} ions of Co_3O_4 are replaced by eco-friendly, conductive, and redox-active elements such as Mn, Cu, Zn, Ca, Mg, Ni, and Fe to form MnCo_2O_4 , CuCo_2O_4 , CaCo_2O_4 , MgCo_2O_4 , NiCo_2O_4 , and FeCo_2O_4 , respectively. The theoretical capacity of these materials was similar to the theoretical capacitance of Co_3O_4 and the electrical conductivity is improved by an order or two. These materials are characterized by their energy storage capability as SCAP electrodes.

Out of these TMCs, NiCo_2O_4 is a widely researched material for SCAP electrodes. The theoretical capacitance of the electrode is higher and the electrical conductivity is two orders higher than Co_3O_4 . The hydrothermal method was utilized in developing porous NiCo_2O_4 flower-like nanostructures which delivered appreciable capacitance of 658 F g^{-1} in 6 M KOH [61]. The SCAB fabricated with this material as a positive and AC as a negative electrode could deliver a maximum E_S of $\sim 24 \text{ Wh kg}^{-1}$ with a voltage window of 1.4 V . The cycling stability of the device was promising, giving $\sim 95\%$ capacitance retention after $10,000$ cycles of CD cycling. A thermal decomposition method was used to synthesize NiCo_2O_4 mesoporous nanocrystals and achieved an improvement in maximum capacitance (764 F g^{-1}) [62]. The ASC fabricated with this mesoporous electrode and AC could deliver only a maximum E_S of $\sim 18 \text{ Wh kg}^{-1}$ with a maximum voltage of 1.7 V which is lower than the earlier fabricated device. Also, the cycling stability of the device is greater than $\sim 100\%$ showing that the activation period of the electrodes in the SCAB device is higher. However, this study revealed that varying the amount of HTAB could vary the homogeneity and porosity of the synthesized material. Recent studies revealed that hierarchical hollow NiCo_2O_4 nanospheres could deliver a maximum specific capacitance of 1229 F g^{-1} in a three-electrode system. The practical aqueous SCAB device with AC as a negative electrode and 1 M KOH as electrolyte could deliver a maximum E_S of $\sim 21 \text{ Wh kg}^{-1}$ with a maximum working voltage of 1.5 V [63]. One could also observe that the stability of the device was inferior ($\sim 87\%$ after 200 cycles) compared to earlier reported NiCo_2O_4 SCABS. Attempts to increase the conductivity, as well as the surface area, were studied via NiCo_2O_4 double-shell hollow spheres [64]. The aqueous SCAB fabricated using these core-shell structures as a

cathode and AC as an anode could deliver a maximum energy density of $\sim 35 \text{ Wh kg}^{-1}$ with a higher voltage window of 1.8 V with $\sim 90\%$ capacitance retention after 200 cycles.

Manganese cobaltite (MnCo_2O_4) is another ternary cobaltite constantly researched as an electrode material for energy storage applications owing to its higher theoretical capacitance ($\sim 3600 \text{ F g}^{-1}$) and improved electrical conductivity. MnCo_2O_4 nanoneedles were synthesized by a hydrothermal method which showed improved performance (1535 F g^{-1}) as a SCAP electrode. An appreciable E_S of $\sim 60 \text{ Wh kg}^{-1}$ is delivered by the SCAB consisting of MnCo_2O_4 as an anode and AC as a cathode [65]. The cycling stability (only $\sim 6\%$ loss after 12,000 cycles) and voltage window (1.5 V) of the device were determined. The electrospinning technique was used to synthesize nanofibers of MgCo_2O_4 and was used as an anode in the SCAB with an N-doped rGO electrode with KOH as electrolyte [66]. The one-dimensional structure is expected to provide focused electron transport in the electrode material, thereby improving its active surface area. The SCAB provided a higher working voltage (1.8 V) with higher E_S (54 Wh kg^{-1}) and appreciable cycling stability (85.2% of initial capacitance after 3000 CD cycles). These studies show that MnCo_2O_4 performs better than NiCo_2O_4 while using it as a positive electrode for SCAB.

Copper cobaltite (CuCo_2O_4) is another TMC researched for SCAP applications owing to its low cost and nontoxicity. Nanocasting from the silica template could synthesize mesoporous CuCo_2O_4 nanowires (Fig. 12.9) and their use as a SCAP electrode could deliver an initial capacitance of 1210 F g^{-1} [67]. The use of this as a positive electrode in a SCAB with AC as a negative electrode was explored and the device could achieve a potential window of 1.5 V and deliver an E_S of $\sim 43 \text{ kW kg}^{-1}$, showing 86% capacitance retention after 5000 charge–discharge cycles. Two of these SCABS in series could efficiently power 5 mm LEDs for 1 hour. CuCo_2O_4 nanostructures were fabricated on Ni wire using a simple hydrothermal method for wearable and as flexible SCABS [68]. The flexible SCABS were tested in 3 M KOH as a wearable device and showed cycling stability of $\sim 94\%$ after 4000 CD cycles. A porous nanowire network is synthesized using the electrospinning technique and determined an appreciable areal capacitance in a three-electrode system [69]. The $\text{CuCo}_2\text{O}_4//\text{AC}$ SCAB could operate at a voltage range of 1.5 V showing an appreciable E_S ($0.806 \text{ mWh cm}^{-3}$) and cycling stability of $\sim 82\%$ after 3000 cycles of charge–discharge cycles in 3 M KOH

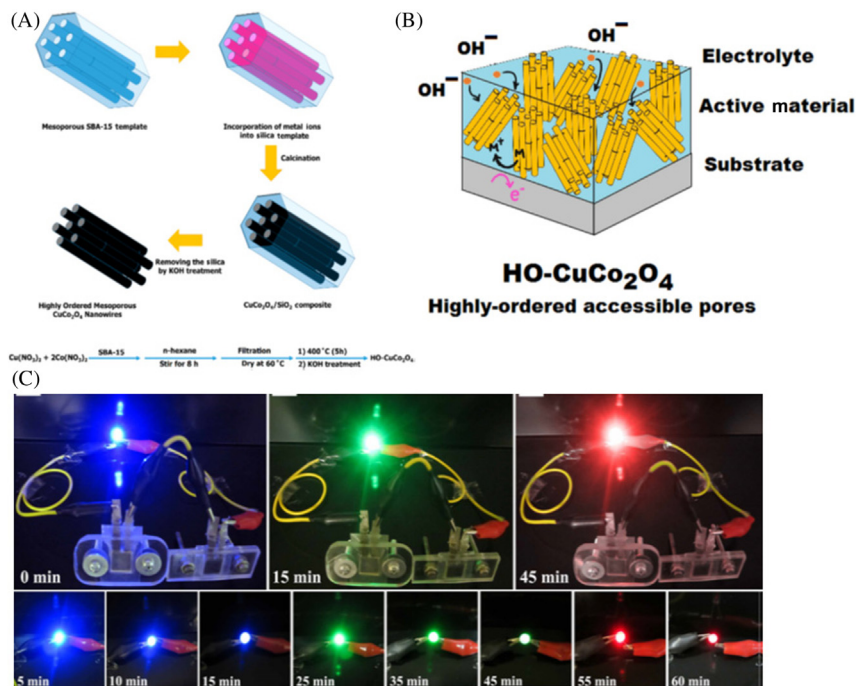


Figure 12.9 (A) Synthesis procedure of CuCo_2O_4 nanowires from mesoporous silica. (B) Schematics of charge storage process in the CuCo_2O_4 nanowires. (C) Photograph showing the energy and power capability of the device. Taken with permission from A. Pendashteh, S.E. Moosavifard, M.S. Rahmanifar, Y. Wang, M.F. El-Kady, R.B. Kaner, et al. Highly ordered mesoporous CuCo_2O_4 nanowires, a promising solution for high-performance supercapacitors. *Chem. Mater.* 27 (2015) 3919–3926. Copyright 2015, ACS Publications.

electrolyte. The other ternary metal cobaltites were characterized in a three-electrode system for SCAP applications. However, the TMCs such as CaCo_2O_4 and FeCo_2O_4 were not utilized as electrodes in SCAB fabrication.

MgCo_2O_4 , a TMC, also showed improved theoretical capacitance and electrical conductivity when utilized as a SCAB electrode. The reason for choosing Mg as an alternative to Co is its high availability, low toxicity, and higher redox potential. The hydrothermal method was used to synthesize MgCo_2O_4 and its rGO modification could increase its conductivity as well as the electrode stability [8]. The SCAB fabricated with rgO- MgCo_2O_4 //AC using 3 M KOH as electrolyte could work in a potential

window of 1.8 V and produce a maximum E_S of 31 Wh kg^{-1} with cycling stability of 99% after 3000 cycles of continuous charge–discharge cycles. Twinned hemispheres of ASCs were synthesized and this $\text{MgCo}_2\text{O}_4//\text{AC}$ SCAB provided 99% of charge–discharge cycling stability after 5000 cycles [70]. The voltage window of the device was 1.70 V and the device is fabricated with 2 M KOH as the electrolyte. The higher E_S of 81 Wh kg^{-1} is determined for the SCAB fabricated with porous MgCo_2O_4 nanoneedles as and rGO as electrodes [71]. PVA-KOH electrolyte is used as an electrolyte and the voltage window of this flexible SCAB was 1.50 V. Therefore ternary metal cobaltites with these appreciable energy densities over metal oxides could be considered as one of the prime candidates as an anode for SCABs.



12.3 Chalcogenides supercapacities

Metal chalcogenides (MCs) usually form due to the combination of transition elements placed on group IV to VII B in the periodic table with group VI A group elements such as Te, S, and Se, and form binary layered crystalline materials. The general formula for MCs is MX_2 ; where M is a transition element such as Ti, Zr, Hf, V, Nb, Ta, Mo, W, Tc and Re, and X is a chalcogen atom such as S, Se, and Te. The crystal structure of MCs is similar to semimetal pristine graphene; the bandgap for pristine graphene is almost zero whereas the bandgap of MCs depends on the material combination and usually lies between 0 and 2 eV. These MCs are characterized by high intercalation and active sites, short ion path lengths, improved conductivity and stability that can be utilized in supercapacitor or capattery applications. Typically metal sulfides, such as nickel sulfide (NiS_2 , NiS), copper sulfide (CuS), and cobalt sulfide (Co_3S_4 , CoS, CoS_2 , and Co_9S_8) are mainly used for SCAP applications. Also, binary metal sulfides such as NiCo_2S_4 , manganese cobalt sulfides, and molybdenum disulfide have also been utilized as SCAP electrodes. Transition metal selenides such as nickel selenide, copper selenide, molybdenum diselenide, and cobalt selenides were also explored for energy storage applications.

Nickel sulfide exists in different phases such as NiS, NiS_2 , Ni_3S_4 , Ni_7S_{10} , and Ni_9S_8 and in different morphologies. These different phases,

as well as morphologies, could coexist as a combination of these different phases. Therefore obtaining an even morphology with pure nickel sulfide in the same phase is a challenge. However, the theoretical capacitance and electrical conductivity of nickel sulfide are higher and the cost is low for characterizing its utility as a SCAP electrode.

An anion exchange reaction is utilized to synthesize NiS hierarchical hollow cubes (Fig. 12.10A) which provide improved capacitance ($\sim 875 \text{ F g}^{-1}$) in 2 M KOH electrolyte [72]. The NiS//CNF SCAB could deliver a maximum E_S of $\sim 35 \text{ Wh kg}^{-1}$ and 90.2% of cycling stability after 3000 cycles of CD cycles within the voltage range of 1.55 V. NiS microflowers were synthesized using a sulfuration and hydrothermal process and showed an improved charge storage property ($\sim 1123 \text{ F g}^{-1}$) (Fig. 12.10B) [73]. The SCABs fabricated with NiS microflower and AC as positive and negative electrodes, respectively, could produce a maximum E_S of 31 Wh kg^{-1} with a voltage window of 1.6 V and 100% cycling stability after 1000 GCD cycles. A facial sacrificial template method was used in the synthesis of NiS microflowers which delivered an excellent capacitance of $\sim 1315 \text{ F g}^{-1}$ in three-electrode characterization and the NiS//AC SCAB also delivered appreciable results [74]. The SCAB delivered a maximum E_S of $\sim 33 \text{ Wh kg}^{-1}$ within a working voltage window of 1.6 V. The cycling performance of the ASC was $\sim 87\%$ after 5000 CD cycles.

A composite of NiS₂/ZnS was successfully synthesized using a solvothermal method followed by a subsequent chemical sulfidation [75]. This composite electrode provided an appreciable capacitance of 1198 F g^{-1} in the three-electrode system. A maximum E_S of 28 Wh kg^{-1}

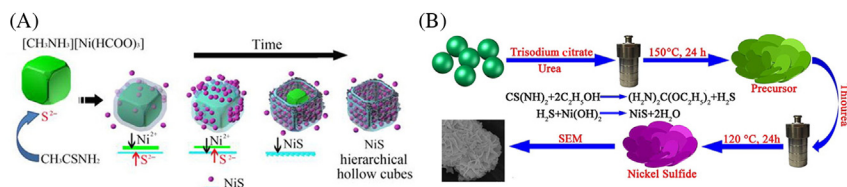


Figure 12.10 (A) Schematics for preparation of NiS hollow cubes. (B) Schematics for preparation of NiS microflowers. Taken with permission from X. Ma, L. Zhang, G. Xu, C. Zhang, H. Song, Y. He, et al. Facile synthesis of NiS hierarchical hollow cubes via Ni formate frameworks for high performance supercapacitors. *Chem. Eng. J.* 320 (2017) 22–28. B. Guan, Y. Li, B. Yin, K. Liu, D. Wang, H. Zhang, et al. Synthesis of hierarchical NiS microflowers for high performance asymmetric supercapacitor. *Chem. Eng. J.* 308 (2017) 1165–1173. Copyright 2017, Elsevier publications.

was obtained for the SCAB with NiS₂/ZnS//AC with an appreciable voltage window and cycling stability. Honeycomb-like nanosheet arrays of Ni₃S₂ were synthesized using hydrothermal sulfidation of nickel foam. The synthesized redox electrodes proved its electrochemical utility for SCAP application, delivering a maximum specific capacity of 151.2 mAh g⁻¹ [76]. The SCAB with AC and Ni₃S₂ as electrodes utilizing 2 M KOH as electrolyte could deliver a maximum E_S of 35.2 Wh kg⁻¹ within the working voltage of 1.6 V. NiS/Ni₃S₂ hybrids were synthesized on nickel foam using an economical solvothermal method [77]. A solid-state SCAB device using the composite electrode and AC as electrodes with PVA-KOH gel electrolyte was fabricated and showed an appreciable energy density of 0.289 m Wh cm⁻² with the voltage range 1.6 V. The cycling stability of the device was not appreciable with ~14% of capacitance loss after 8000 continuous charge–discharge cycles. Although these sorts of composite electrodes are synthesized for improving the E_S as well as the capacitance of the SCABS, a noticeable improvement for commercializing it as an electrode was not yet obtained.

Copper sulfide material is preferred as a chalcogenide owing to its higher electrical conductivity ($\sim 10^{-3}$ S cm⁻¹), low toxicity, and low cost. The nanostructured CuS network consisting of interconnected nanoparticles could produce an appreciable capacitance of ~ 50 mA h g⁻¹ as a SCAP electrode in 2 M KOH electrolyte [78]. The SCAB fabricated using AC as an anode and CuS as a cathode could work in a voltage window of 1.6 V delivering a maximum energy density of ~ 18 Wh kg⁻¹. Hollow microflowers of CuS were synthesized through a chemical route and the CuS//AC SCAB delivered an energy density of ~ 16 Wh kg⁻¹ with a working voltage of 1.55 V using 3 M KOH as electrolyte [79]. The practical cycling stability of the device is appreciable losing only ~20% of its initial capacitance after 20,000 cycles. A low-temperature solvothermal method was used to synthesize 3D CuS from an ionic liquid and fabricate a SCAB with AC as a negative electrode using 2 M KOH [80]. The voltage window of the device was 1.5 V and the maximum E_S delivered by the device was ~ 15 Wh kg⁻¹ with 88% capacitance retention after 4000 charge–discharge cycles.

Flexible SCABs are designed with CuS composite electrodes with 3D graphene as a cathode and 3D graphene as an anode in PVA-KOH electrolytes [81]. However, the energy density of this flexible device is not impressive (~ 7 Wh kg⁻¹) and it showed inferior cycling stability (77%

after 1000 cycles). This lower cycling stability was due to the decrease of the electrolyte during cycling. Dealloying of Ti–Cu amorphous alloy synthesized CuS nanosheets with higher surface areas [82]. This CuS nanosheet showed an improved performance compared with the other electrodes demonstrating a maximum achieved capacitance of $\sim 713 \text{ F g}^{-1}$. Therefore these sorts of synthesis strategies could increase the active surface area of the CuS materials to improve their performance. These performances show that the E_S of CoS is not comparable with NiS; tailoring its morphology and its conductivity will increase its energy storage performance.

In the metal oxide category, NiCo_2O_4 was discussed as a hot material for SCAP electrodes. The replacement of oxygen with sulfur in this spinel metal oxide could stretch the chemical bonds, thereby producing a more flexible structure for improved ion transport, and thereby improving the electrochemical storage properties [83]. This could decrease its optical band and increase the conductivity by two orders compared with NiCo_2O_4 [84]. There was a comparative study of the direct growth of NiCo_2S_4 nanostructures (nanowires and nanowires) on nickel foam with NiCo_2O_4 using the hydrothermal method. NiCo_2S_4 nanotubes show improved performance (1936 F g^{-1}) over the NiCo_2O_4 nanowires (1370 F g^{-1}) for SCAP electrodes. However, the practical SCAB device was not fabricated with the electrodes [85]. This comparative study gives a clear edge to NiCo_2S_4 over NiCo_2O_4 as a high-performance electrode in supercapatteries.

Mesoporous nanosheets synthesized using another chalcogenide (CuS_2) as a sulfur source using a one-step hydrothermal synthesis were utilized for SCAP testing [86]. The porous NiCo_2S_4 nanosheets consist of higher electrochemical active sites and are used as the positive electrode in SCAB with AC as a negative electrode and 3 M KOH as the electrolyte. The SCAB could deliver a maximum E_S of $\sim 26 \text{ Kw kg}^{-1}$ in a working voltage range of 1.6 V, retaining 86% of initial capacitance after 4000 cycles. Hollow mesoporous NiCo_2S_4 ellipsoids prepared by calcination and chemical transformation could deliver 495 F g^{-1} and showed SCAP properties [87]. The $\text{NiCo}_2\text{S}_4//\text{AC}$ SCAB produced a maximum E_S of $\sim 29 \text{ Wh kg}^{-1}$ with almost $\sim 96\%$ capacitance retention after 5000 charge–discharge cycles. The appropriate pore size and surface area for the active material could be attributed to the easy intercalation of OH^- ions, thereby increasing the energy storage property compared to the nanosheets.

Further improvement in the E_S of NiCo_2S_4 SCABs was obtained by synthesizing the polymer nanocomposites of the material with PANI [88]. The composite SCAP electrode could deliver a maximum specific capacitance of 1879 F g^{-1} in a three-electrode system. The flexible $\text{NiCo}_2\text{S}_4/\text{PANI//AC}$ SCAB and PVA-KOH gel electrolyte could deliver an E_S of 54 Wh kg^{-1} . The device could retain 88% of its initial capacitance after 2000 cycles of continuous charge–discharge cycles. Also, polypyrrole was used in synthesizing the polymer nanocomposites of NiCo_2S_4 ($\text{NiCo}_2\text{S}_4/\text{PPy}$) [89]. The synthesized twinned layer structure could deliver a higher specific capacitance (908 F g^{-1}) and the $\text{NiCo}_2\text{S}_4/\text{PPy//N-doped CNTs}$ SCAB could deliver a maximum E_S of $\sim 51 \text{ Wh kg}^{-1}$ in 2 M KOH showing the relevance of the polymer of NiCo_2S_4 to increase conductivity. The cycling stability of the device was superior showing $\sim 100\%$ retention after 2000 charge–discharge cycles compared to $\text{NiCo}_2\text{O}_4/\text{PANI//AC}$ SCAB. Therefore the polymer nanocomposites of NiCo_2S_4 could enhance conductivity and electron transport properties, thereby serving as a superior electrode material for a practical SCAB device.

Manganese cobalt sulfide (MnCo_2S_4) possesses appreciable intercalation charge storage properties, multiple oxidation states, and improved conductivity. A facile hydrothermal process and postsulfurization process are used to synthesize MnCo_2O_4 nanowires [90]. The electrode possesses higher C_S (2067 F g^{-1}) in a three-electrode configuration in a 3 M KOH electrolyte solution. $\text{MnCo}_2\text{S}_4/\text{rGO}$ SCAB could deliver a potential window of 1.6 V with an E_S of $\sim 31 \text{ Wh kg}^{-1}$ and 89% of capacitance retention after 5000 charge–discharge cycles. Further, graphene– MnCo_2O_4 nanocomposites with honeycomb structure were synthesized using chemical vapor deposition and electrodeposition synthesis [91]. The composite electrode showed appreciable capacitance (1938 F g^{-1}), however it was inferior to the earlier reported MnCo_2S_4 nanowires. The composite electrode with AC electrode and 6 M KOH as electrolyte was used to fabricate an ASC which could deliver a maximum E_S of $\sim 14 \text{ Wh kg}^{-1}$ within a working voltage range of 1.5 V. Further optimization of the synthesis technique and materials combination to form composites could enhance the performance of manganese cobalt sulfide and allow it to be considered as a commercial electrode material for practical SCABS.

Molybdenum selenide (MoS_2) is another MCs with a typical atomic structure, that is, three atomic layers are layered and combined with weak van der Waals forces. This weak binding force could help in the peeling of the MoS_2 layers and could create volume change during cycling, thereby

involving inferior cycling property. Furthermore, the adjacent van der Waal layer could decrease its conductivity, thereby suppressing its electrochemical performance. Therefore MoS_2 as an independent material could offer a lower capacitance, and material composites or intercalating other materials to layer separation is promising research to increase the capacitance of MoS_2 . Therefore composites such as $\text{MoS}_2@\text{CNT}$ [92], MoS_2 –graphene composite [93], and $\text{MoS}_2/\text{Mn}_3\text{O}_4$ hybrid [94] were synthesized for SCAP applications and electrochemically characterized in 3 M KOH. However, this research does not report the development of a SCAB device with these electrodes.

Three-dimensional MoS_2 nanospheres were assembled using a facile hydrothermal method with SiO_2 as a template [95]. A higher capacitance of 683 F g^{-1} is obtained for the SCAP electrode and the aqueous $\text{MoS}_2//\text{AC}$ SCAB delivers an E_S of $\sim 20 \text{ Wh kg}^{-1}$ in 2 M KOH with voltage window of 1.5 V. The cycling stability of this device was not reported. Reclaimed carbon nanofiber (RCF) was used to load MoS_2 and was tested as an anode in SCAP applications. The SCAB with MoS_2/RCF electrode as a cathode and MnO_2/RCF as a cathode produced a maximum E_S of 22.5 Wh kg^{-1} with a practical working voltage of 1.7 V [96]. The cycling stability of the device was a little inferior (81%) after 2000 cycles. Therefore these research studies show that the SCAB devices with MoS_2 electrodes require further optimizations to improve their cycling stability and decrease volume expansion with charge–discharge cycles for their practical use as SCAB electrodes.

12.4 Importance of supercabattery commercialization and applications

In the gap between metal ion batteries, especially LIBs, and capacitors are supercapacitors/ultracapacitors/EDLCs. The commercial supercapacitors available in the market utilize carbon or graphene as their electrode material. Therefore these devices are also known as power devices owing to their ability to release a large amount of stored energy for a limited period of time. The commercial supercapacitor devices and their performance indicators are given in Table 12.1. These performance indicators show that the working voltage, capacitance, and the resistance of the commercial device depend on the mass loading or volume of the electrode. Therefore to commercialize the SCAP electrodes as a working electrode, the mentioned factors have to be optimized (Table 12.1).

Table 12.1 Compilation of energy and power performance of commercially available supercapacitors.

Company	Capacitance (F)	Voltage (V)	ESR (m Ω)
Apowercap	55	2.70	—
Apowercap	450	2.70	—
Asahi Glass	1375	2.70	2.50
Fuji	1800	3.80	1.50
BatScap	2680	2.70	2.50
JSR Micro	1100	3.80	1.15
JSR Micro	2300	3.80	0.54
LS Mtron	3200	2.80	0.25
Loxus	3000	2.70	0.45
Loxus	2000	2.70	0.54
Nesscap	1800	2.70	0.55
Nesscap	3640	2.70	0.30
Nesscap	3160	2.70	0.40
Powerstor	2.20	2.50	4.57
Powerstor	65	16.20	7.00
Panasonic	0.10	2.30	0.08
Panasonic	50	5.50	0.08
Maxwell	2885	2.70	0.38
Maxwell	605	2.70	0.90
Yunasko	510	2.70	0.90
Yunasko	480	2.70	0.25
Yunasko	1275	2.75	0.11
Yunasko	7200	2.70	1.40
Yunasko	5200	2.70	1.50
Skeleton	3200	3.40	0.47
Skeleton	850	3.40	0.80
Vinatech	336	2.70	3.50
Vinatech	342	3.00	6.60

The energy market for portable energy storage is rising steeply owing to the depletion of fossil fuels and in order to control the emission of greenhouse gases. Electric vehicles in the market could be more commercialized with batteries with high energy densities. However, the batteries of these devices could achieve longer cycle life if the energy required for higher power operations could be optimized with a supercapacitor with higher power and energy densities. Also, the charging time of batteries is higher compared to supercapacitors. Therefore supercapacitors hold their space in energy storage markets. The cost of the materials is another factor that determines the fabrication of these devices. The E_S of supercapacitors

could be increased without lowering the power density using the mentioned low-cost SCAP materials.

The cost of high-purity carbon is almost $\$65 \text{ kg}^{-1}$ and the maximum capacitance it could produce per gram is 100 F [97]. Therefore material research into lowering the cost without affecting the performance is required in energy storage research. The increase in operating voltage of the device to $\sim 3.5 \text{ V}$ could reduce the cost of these devices. The companies mentioned in Table 12.1 focus on the development of advanced carbon materials such as graphene and CNTs and fabricating EDLC with it. However, the capacitance of these electrodes is not higher (~ 100 to 150 F g^{-1}), leading to difficulties in increasing the energy densities. Selecting SCAP materials with higher voltage operation as well as lower cost could be the future trend in the industry.

The potential energy storage market for SCs is ~ 1.34 billion year⁻¹ in the electronic industry for memory protection applications [98]. Furthermore, the application could extend to hybrid vehicles, the portable electronic device market, and power grid applications [99]. However, the most foreseen applications of SC/SCAB are replacing the traction batteries as well as inverter capacitors in electric vehicles for bus door opening and regenerative braking [100]. Another market opportunity for these devices is in the transportation sector, especially in engine starting, braking energy assimilation, electrical system and torque expansion, rapid power for start–stop processes, and hybrid electric drives for trucks and electric rail vehicles [101]. Furthermore, there are uses in backup applications, such as uninterrupted power supply, automated indicators in smart grids, and windmill blade pitch systems. The increased demand for various applications should decrease the cost of the devices as different types of SCs/SCABs will be commercially designed to meet the requirements.



12.5 Conclusion

The applications of SCAP materials are well summarized. The performances of various metal oxides, MCs, and ternary metal cobaltites in practical devices have been compiled. It was determined that the potential of these materials for development as commercial electrode material is

high. The voltage window for the fabricated practical devices in the lab scale is appreciable and the energy density of certain devices was higher than the commercially available devices. Therefore in the scenario of increasing green energy demands, the application of SCAP electrodes as a SCAB device shall bridge the energy gap between capacitors and batteries.

References

- [1] B.E. Conway, *Electrochemical supercapacitors, Scientific Fundamentals and Technological Applications*, 1997.
- [2] T. Brousse, D. Bélanger, J.W. Long, To be or not to be pseudocapacitive? *J. Electrochem. Soc.* 162 (2015) A5185–A5189.
- [3] R. Jose, S.G. Krishnan, B. Vidyadharan, I.I. Misnon, M. Harilal, R.A. Aziz, et al., Supercapacitor electrodes delivering high energy and power densities, *Mater. Today: Proc.* 3 (2016) S48–S56.
- [4] A. Afif, S.M. Rahman, A.T. Azad, J. Zaini, M.A. Islan, A.K. Azad, Advanced materials and technologies for hybrid supercapacitors for energy storage—a review, *J. Energy Storage* 25 (2019) 100852.
- [5] X. Zhao, L. Mao, Q. Cheng, J. Li, F. Liao, G. Yang, et al., Recent advances in two-dimensional spinel structured co-based materials for high performance supercapacitors: a critical review, *Chem. Eng. J.* (2020) 124081.
- [6] C. Zhong, Y. Deng, W. Hu, J. Qiao, L. Zhang, J. Zhang, A review of electrolyte materials and compositions for electrochemical supercapacitors, *Chem. Soc. Rev.* 44 (2015) 7484–7539.
- [7] P. Simon, Y. Gogotsi, B. Dunn, Where do batteries end and supercapacitors begin? *Science*. 343 (2014) 1210–1211.
- [8] S.G. Krishnan, M. Harilal, B. Pal, I.I. Misnon, C. Karupppiah, C.-C. Yang, et al., Improving the symmetry of asymmetric supercapacitors using battery-type positive electrodes and activated carbon negative electrodes by mass and charge balance, *J. Electroanal. Chem.* 805 (2017) 126–132.
- [9] B. Vidyadharan, I.I. Misnon, J. Ismail, M.M. Yusoff, R. Jose, High performance asymmetric supercapacitors using electrospun copper oxide nanowires anode, *J. Alloy. Compd.* 633 (2015) 22–30.
- [10] S.E. Moosavifard, M.F. El-Kady, M.S. Rahmanifar, R.B. Kaner, M.F. Mousavi, Designing 3D highly ordered nanoporous CuO electrodes for high-performance asymmetric supercapacitors, *Acs Appl. Mater. Inter.* 7 (2015) 4851–4860.
- [11] A.K. Mishra, A.K. Nayak, A.K. Das, D. Pradhan, Microwave-assisted solvothermal synthesis of cupric oxide nanostructures for high-performance supercapacitor, *J. Phys. Chem. C*. 122 (2018) 11249–11261.
- [12] V. Senthilkumar, Y.S. Kim, S. Chandrasekaran, B. Rajagopalan, E.J. Kim, J.S. Chung, Comparative supercapacitance performance of CuO nanostructures for energy storage device applications, *RSC Adv.* 5 (2015) 20545–20553.
- [13] W. Lv, L. Li, Q. Meng, X. Zhang, Molybdenum-doped CuO nanosheets on Ni foams with extraordinary specific capacitance for advanced hybrid supercapacitors, *J. Mater. Sci.* 55 (2020) 2492–2502.
- [14] B. Saravanakumar, C. Radhakrishnan, M. Ramasamy, R. Kaliaperumal, A.J. Britten, M. Mkwandawire, Copper oxide/mesoporous carbon nanocomposite synthesis, morphology and electrochemical properties for gel polymer-based asymmetric supercapacitors, *J. Electroanal. Chem.* 852 (2019) 113504.

- [15] J. Zhang, G. Zhang, W. Luo, Y. Sun, C. Jin, W. Zheng, Graphitic carbon coated CuO hollow nanospheres with penetrated mesochannels for high-performance asymmetric supercapacitors, *ACS Sustain. Chem. Eng.* 5 (2017) 105–111.
- [16] W. Lan, X. Zhang, A. Zhai, W. Meng, H. Sheng, W. Dou, et al., Flexible CuO nanotube arrays composite electrodes for wire-shaped supercapacitors with robust electrochemical stability, *Chem. Eng. J.* 374 (2019) 181–188.
- [17] D.P. Dubal, N.R. Chodankar, G.S. Gund, R. Holze, C.D. Lokhande, P. Gomez-Romero, Asymmetric supercapacitors based on hybrid CuO@reduced graphene oxide@sponge versus reduced graphene oxide@sponge electrodes, *Energy Technol.* 3 (2015) 168–176.
- [18] P. Liu, X. Weng, Z. Liu, Y. Zhang, Q. Qiu, W. Wang, et al., High-performance quasi-solid-state supercapacitor based on CuO nanoparticles with commercial-level mass loading on ceramic material $\text{La}_{1-x}\text{Sr}_x\text{CoO}_{3-\delta}$ as cathode, *ACS Appl. Energy Materials* 2 (2019) 1480–1488.
- [19] A.V. Shinde, N.R. Chodankar, V.C. Lokhande, A.C. Lokhande, T. Ji, J.H. Kim, et al., Highly energetic flexible all-solid-state asymmetric supercapacitor with Fe_2O_3 and CuO thin films, *RSC Adv.* 6 (2016) 58839–58843.
- [20] S.M. Cha, G. Nagaraju, S.C. Sekhar, J.S. Yu, A facile drop-casting approach to nanostructured copper oxide-painted conductive woven textile as binder-free electrode for improved energy storage performance in redox-additive electrolyte, *J. Mater. Chem. A* 5 (2017) 2224–2234.
- [21] Z. Li, M. Shao, L. Zhou, R. Zhang, C. Zhang, J. Han, et al., A flexible all-solid-state micro-supercapacitor based on hierarchical CuO@layered double hydroxide core-shell nanoarrays, *Nano Energy* 20 (2016) 294–304.
- [22] W. Xu, S. Dai, G. Liu, Y. Xi, C. Hu, X. Wang, CuO nanoflowers growing on carbon fiber fabric for flexible high-performance supercapacitors, *Electrochim. Acta* 203 (2016) 1–8.
- [23] M. Kuang, T.T. Li, H. Chen, S.M. Zhang, L.L. Zhang, Y.X. Zhang, Hierarchical $\text{Cu}_2\text{O}/\text{CuO}/\text{Co}_3\text{O}_4$ core-shell nanowires: synthesis and electrochemical properties, *Nanotechnology* 26 (2015) 304002.
- [24] B. Vidhyadharan, I.I. Misnon, R.A. Aziz, K.P. Padmasree, M.M. Yusoff, R. Jose, Superior supercapacitive performance in electrospun copper oxide nanowire electrodes, *J. Mater. Chem. A* 2 (2014) 6578.
- [25] M.S. Kolathodi, M. Palei, T.S. Natarajan, Electrospun NiO nanofibers as cathode materials for high performance asymmetric supercapacitors, *J. Mater. Chem. A* 3 (2015) 7513–7522.
- [26] X. Ren, C. Guo, L. Xu, T. Li, L. Hou, Y. Wei, Facile synthesis of hierarchical mesoporous honeycomb-like NiO for aqueous asymmetric supercapacitors, *ACS Appl. Mater. Inter.* 7 (2015) 19930–19940.
- [27] C. Yuan, X. Zhang, Q. Wu, B. Gao, Effect of temperature on the hybrid supercapacitor based on NiO and activated carbon with alkaline polymer gel electrolyte, *Solid. State Ion.* 177 (2006) 1237–1242.
- [28] C.-Z. Yuan, B. Gao, X.-G. Zhang, Electrochemical capacitance of NiO/RuO₂ 35V0.65O₂ asymmetric electrochemical capacitor, *J. Power Sources* 173 (2007) 606–612.
- [29] H. Wang, H. Yi, X. Chen, X. Wang, Asymmetric supercapacitors based on nano-architected nickel oxide/graphene foam and hierarchical porous nitrogen-doped carbon nanotubes with ultrahigh-rate performance, *J. Mater. Chem. A* 2 (2014) 3223–3230.
- [30] C. Guan, Y. Wang, Y. Hu, J. Liu, K.H. Ho, W. Zhao, et al., Conformally deposited NiO on a hierarchical carbon support for high-power and durable asymmetric supercapacitors, *J. Mater. Chem. A* 3 (2015) 23283–23288.

- [31] R.R. Salunkhe, M.B. Zakaria, Y. Kamachi, S.M. Alshehri, T. Ahamad, N.L. Torad, et al., Fabrication of asymmetric supercapacitors based on coordination polymer derived nanoporous materials, *Electrochim. Acta* 183 (2015) 94–99.
- [32] M. Jing, C. Wang, H. Hou, Z. Wu, Y. Zhu, Y. Yang, et al., Ultrafine nickel oxide quantum dots embedded with few-layer exfoliative graphene for an asymmetric supercapacitor: enhanced capacitances by alternating voltage, *J. Power Sources* 298 (2015) 241–248.
- [33] B. Vidyadharan, R.A. Aziz, I.I. Misnon, G. Anil Kumar, J. Ismail, M.M. Yusoff, et al., High energy and power density asymmetric supercapacitors using electrospun cobalt oxide nanowire anode, *J. Power Sources* (2014).
- [34] M. Zheng, L. Li, P. Gu, Z. Lin, W. Du, H. Xue, et al., High-performance flexible solid-state asymmetric supercapacitors based on ordered mesoporous cobalt oxide, *Energy Technol.* 5 (2017) 544–548.
- [35] W. Liu, X. Li, M. Zhu, X. He, High-performance all-solid state asymmetric supercapacitor based on Co_3O_4 nanowires and carbon aerogel, *J. Power Sources* 282 (2015) 179–186.
- [36] Y. Jiang, L. Chen, H. Zhang, Q. Zhang, W. Chen, J. Zhu, et al., Two-dimensional Co_3O_4 thin sheets assembled by 3D interconnected nanoflake array framework structures with enhanced supercapacitor performance derived from coordination complexes, *Chem. Eng. J.* 292 (2016) 1–12.
- [37] Y. Liang, Y. Yang, Z. Hu, Y. Zhang, Z. Li, N. An, et al., Three-dimensional cage-like Co_3O_4 structure constructed by nanowires for supercapacitor, *Int. J. Electrochem. Sci.* 11 (2016) 4092–4109.
- [38] J. Xu, T. Xiao, X. Tan, P. Xiang, L. Wu, et al., A new asymmetric aqueous supercapacitor: $\text{Co}_3\text{O}_4/\text{Co}_3\text{O}_4@$ polypyrrole, *J. Alloy. Compd.* 706 (2017) 351–357.
- [39] M. Qorbani, T.-c Chou, Y.-H. Lee, S. Samireddi, N. Naseri, A. Ganguly, et al., Multi-porous Co_3O_4 nanoflakes@sponge-like few-layer partially reduced graphene oxide hybrids: towards highly stable asymmetric supercapacitors, *J. Mater. Chem. A.* 5 (2017) 12569–12577.
- [40] H. Yan, J. Bai, M. Liao, Y. He, Q. Liu, J. Liu, et al., One-step synthesis of Co_3O_4 /Graphene aerogels and their all-solid-state asymmetric supercapacitor, *Eur. J. Inorg. Chem.* 2017 (2017) 1143–1152.
- [41] J. Mei, W. Fu, Z. Zhang, X. Jiang, H. Bu, C. Jiang, et al., Vertically-aligned Co_3O_4 nanowires interconnected with $\text{Co}(\text{OH})_2$ nanosheets as supercapacitor electrode, *Energy.* 139 (2017) 1153–1158.
- [42] M. Huang, Y. Zhang, F. Li, L. Zhang, Z. Wen, Q. Liu, Facile synthesis of hierarchical $\text{Co}_3\text{O}_4@$ MnO_2 core-shell arrays on Ni foam for asymmetric supercapacitors, *J. Power Sources* 252 (2014) 98–106.
- [43] J. Xu, Q. Wang, X. Wang, Q. Xiang, B. Liang, D. Chen, et al., Flexible asymmetric supercapacitors based upon Co_9S_8 nanorod/ $\text{Co}_3\text{O}_4@$ RuO_2 nanosheet arrays on carbon cloth, *ACS Nano.* 7 (2013) 5453–5462.
- [44] X.-J. Ma, L.-B. Kong, W.-B. Zhang, M.-C. Liu, Y.-C. Luo, L. Kang, Design and synthesis of 3D $\text{Co}_3\text{O}_4@$ MMoO_4 (M = Ni, Co) nanocomposites as high-performance supercapacitor electrodes, *Electrochim. Acta.* 130 (2014) 660–669.
- [45] W. Hong, J. Wang, P. Gong, J. Sun, L. Niu, Z. Yang, et al., Rational construction of three dimensional hybrid $\text{Co}_3\text{O}_4@$ NiMoO_4 nanosheets array for energy storage application, *J. Power Sources* 270 (2014) 516–525.
- [46] C. Wei, C. Cheng, B. Zhou, X. Yuan, T. Cui, S. Wang, et al., Hierarchically porous NaCoPO_4 - Co_3O_4 hollow microspheres for flexible asymmetric solid-state supercapacitors, *Part. Part. Syst. Character.* 32 (2015) 831–839.

- [47] J.R.S. Brownson, C. Lévy-Clément, Nanostructured α - and β -cobalt hydroxide thin films, *Electrochim. Acta* 54 (2009) 6637–6644.
- [48] S. Gao, Y. Sun, F. Lei, L. Liang, J. Liu, W. Bi, et al., Ultrahigh energy density realized by a single-layer β -Co(OH)₂ all-solid-state asymmetric supercapacitor, *Angew. Chem. Int. Ed.* 53 (2014) 12789–12793.
- [49] S. Yang, K. Cheng, K. Ye, Y. Li, J. Qu, J. Yin, et al., A novel asymmetric supercapacitor with buds-like Co(OH)₂ used as cathode materials and activated carbon as anode materials, *J. Electroanal. Chem.* 741 (2015) 93–99.
- [50] C. Wang, H. Qu, T. Peng, K. Mei, Y. Qiu, Y. Lu, et al., Large scale α -Co(OH)₂ needle arrays grown on carbon nanotube foams as free standing electrodes for supercapacitors, *Electrochim. Acta* 191 (2016) 133–141.
- [51] T. Peng, H. Wang, H. Yi, Y. Jing, P. Sun, X. Wang, Co(OH)₂ nanosheets coupled with cnt arrays grown on ni mesh for high-rate asymmetric supercapacitors with excellent capacitive behavior, *Electrochim. Acta* 176 (2015) 77–85.
- [52] Z. Wang, Y. Liu, C. Gao, H. Jiang, J. Zhang, A porous Co(OH)₂ material derived from a MOF template and its superior energy storage performance for supercapacitors, *J. Mater. Chem. A* 3 (2015) 20658–20663.
- [53] Z. Tang, Tang C-h, H. Gong, A high energy density asymmetric supercapacitor from nano-architected Ni(OH)₂/carbon nanotube electrodes, *Adv. Funct. Mater.* 22 (2012) 1272–1278.
- [54] J. Yan, Z. Fan, W. Sun, G. Ning, T. Wei, Q. Zhang, et al., Advanced asymmetric supercapacitors based on Ni(OH)₂/graphene and porous graphene electrodes with high energy density, *Adv. Funct. Mater.* 22 (2012) 2632–2641.
- [55] J. Huang, P. Xu, D. Cao, X. Zhou, S. Yang, Y. Li, et al., Asymmetric supercapacitors based on β -Ni(OH)₂ nanosheets and activated carbon with high energy density, *J. Power Sources* 246 (2014) 371–376.
- [56] G. Hu, C. Li, H. Gong, Capacitance decay of nanoporous nickel hydroxide, *J. Power Sources* 195 (2010) 6977–6981.
- [57] H. Jiang, C. Li, T. Sun, J. Ma, High-performance supercapacitor material based on Ni(OH)₂ nanowire-MnO₂ nanoflakes core-shell nanostructures, *Chem. Commun.* 48 (2012) 2606–2608.
- [58] R.R. Salunkhe, J. Lin, V. Malgras, S.X. Dou, J.H. Kim, Y. Yamauchi, Large-scale synthesis of coaxial carbon nanotube/Ni(OH)₂ composites for asymmetric supercapacitor application, *Nano Energy* 11 (2015) 211–218.
- [59] D. Wang, B. Guan, Y. Li, D. Li, Z. Xu, Y. Hu, et al., Morphology-controlled synthesis of hierarchical mesoporous α -Ni(OH)₂ microspheres for high-performance asymmetric supercapacitors, *J. Alloy. Compd.* 737 (2018) 238–247.
- [60] L.-L. Zhang, H.-H. Li, C.-Y. Fan, K. Wang, X.-L. Wu, H.-Z. Sun, et al., A vertical and cross-linked Ni(OH)₂ network on cellulose-fiber covered with graphene as a binder-free electrode for advanced asymmetric supercapacitors, *J. Mater. Chem. A* 3 (2015) 19077–19084.
- [61] H. Chen, J. Jiang, L. Zhang, T. Qi, D. Xia, H. Wan, Facilely synthesized porous NiCo₂O₄ flowerlike nanostructure for high-rate supercapacitors, *J. Power Sources* 248 (2014) 28–36.
- [62] C.-T. Hsu, C.-C. Hu, Synthesis and characterization of mesoporous spinel NiCo₂O₄ using surfactant-assembled dispersion for asymmetric supercapacitors, *J. Power Sources* 242 (2013) 662–671.
- [63] K. Xu, J. Yang, J. Hu, Synthesis of hollow NiCo₂O₄ nanospheres with large specific surface area for asymmetric supercapacitors, *J. Colloid Interface Sci.* 511 (2018) 456–462.

- [64] X. Li, L. Jiang, C. Zhou, J. Liu, H. Zeng, Integrating large specific surface area and high conductivity in hydrogenated NiCo_2O_4 double-shell hollow spheres to improve supercapacitors, *NPG Asia Materials*. 7 (2015). e165-e.
- [65] L. Kuang, F. Ji, X. Pan, D. Wang, X. Chen, D. Jiang, et al., Mesoporous $\text{MnCo}_2\text{O}_{4.5}$ nanoneedle arrays electrode for high-performance asymmetric supercapacitor application, *Chem. Eng. J.* 315 (2017) 491–499.
- [66] T. Pettong, P. Iamprasertkun, A. Krittayavathananon, P. Sukha, P. Sirisinudomkit, A. Seubsai, et al., High-performance asymmetric supercapacitors of MnCo_2O_4 nanofibers and n-doped reduced graphene oxide aerogel, *ACS Appl. Mater. Inter.* 8 (2016) 34045–34053.
- [67] A. Pendashteh, S.E. Moosavifard, M.S. Rahmanifar, Y. Wang, M.F. El-Kady, R.B. Kaner, et al., Highly ordered mesoporous CuCo_2O_4 nanowires, a promising solution for high-performance supercapacitors, *Chem. Mater.* 27 (2015) 3919–3926.
- [68] S. Gu, Z. Lou, X. Ma, G. Shen, CuCo_2O_4 nanowires grown on a Ni wire for high-performance, flexible fiber supercapacitors, *ChemElectroChem*. 2 (2015) 1042–1047.
- [69] Q. Wang, D. Chen, D. Zhang, Electrospun porous CuCo_2O_4 nanowire network electrode for asymmetric supercapacitors, *RSC Adv.* 5 (2015) 96448–96454.
- [70] Y. Wang, X. Ma, S. Li, J. Sun, Y. Zhang, H. Chen, et al., Facile solvothermal synthesis of novel MgCo_2O_4 twinned-hemispheres for high performance asymmetric supercapacitors, *J. Alloy. Compd.* (2019) 152905.
- [71] J. Xu, L. Wang, J. Zhang, J. Qian, J. Liu, Z. Zhang, et al., Fabrication of porous double-urchin-like MgCo_2O_4 hierarchical architectures for high-rate supercapacitors, *J. Alloy. Compd.* 688 (Part B) (2016) 933–938.
- [72] X. Ma, L. Zhang, G. Xu, C. Zhang, H. Song, Y. He, et al., Facile synthesis of NiS hierarchical hollow cubes via Ni formate frameworks for high performance supercapacitors, *Chem. Eng. J.* 320 (2017) 22–28.
- [73] B. Guan, Y. Li, B. Yin, K. Liu, D. Wang, H. Zhang, et al., Synthesis of hierarchical NiS microflowers for high performance asymmetric supercapacitor, *Chem. Eng. J.* 308 (2017) 1165–1173.
- [74] J. Zhao, B. Guan, B. Hu, Z. Xu, D. Wang, H. Zhang, Vulcanizing time controlled synthesis of NiS microflowers and its application in asymmetric supercapacitors, *Electrochim. Acta* 230 (2017) 428–437.
- [75] G.-C. Li, M. Liu, M.-K. Wu, P.-F. Liu, Z. Zhou, S.-R. Zhu, et al., MOF-derived self-sacrificing route to hollow NiS_2/ZnS nanospheres for high performance supercapacitors, *RSC Adv.* 6 (2016) 103517–103522.
- [76] H. Wang, M. Liang, D. Duan, W. Shi, Y. Song, Z. Sun, Rose-like Ni_3S_4 as battery-type electrode for hybrid supercapacitor with excellent charge storage performance, *Chem. Eng. J.* 350 (2018) 523–533.
- [77] F. Chen, H. Wang, S. Ji, V. Linkov, R. Wang, High-performance all-solid-state asymmetric supercapacitors based on sponge-like $\text{NiS}/\text{Ni}_3\text{S}_2$ hybrid nanosheets, *Mater. Today Energy* 11 (2019) 211–217.
- [78] W. Fu, W. Han, H. Zha, J. Mei, Y. Li, Z. Zhang, et al., Nanostructured CuS networks composed of interconnected nanoparticles for asymmetric supercapacitors, *Phys. Chem. Chem. Phys.* 18 (2016) 24471–24476.
- [79] Y. Liu, Z. Zhou, S. Zhang, W. Luo, G. Zhang, Controllable synthesis of CuS hollow microflowers hierarchical structures for asymmetric supercapacitors, *Appl. Surf. Sci.* 442 (2018) 711–719.
- [80] J. Zhang, H. Feng, J. Yang, Q. Qin, H. Fan, C. Wei, et al., Solvothermal synthesis of three-dimensional hierarchical CuS microspheres from a Cu-based ionic liquid precursor for high-performance asymmetric supercapacitors, *ACS Appl. Mater. Interfaces* 7 (2015) 21735–21744.

- [81] Z. Tian, H. Dou, B. Zhang, W. Fan, X. Wang, Three-dimensional graphene combined with hierarchical CuS for the design of flexible solid-state supercapacitors, *Electrochim. Acta* 237 (2017) 109–118.
- [82] W. Xu, Y. Liang, Y. Su, S. Zhu, Z. Cui, X. Yang, et al., Synthesis and properties of morphology controllable copper sulfide nanosheets for supercapacitor application, *Electrochim. Acta* 211 (2016) 891–899.
- [83] J. Yang, M. Ma, C. Sun, Y. Zhang, W. Huang, X. Dong, Hybrid NiCo₂S₄@MnO₂ heterostructures for high-performance supercapacitor electrodes, *J. Mater. Chem. A* 3 (2015) 1258–1264.
- [84] J. Xiao, L. Wan, S. Yang, F. Xiao, S. Wang, Design hierarchical electrodes with highly conductive NiCo₂S₄ nanotube arrays grown on carbon fiber paper for high-performance pseudocapacitors, *Nano Letters*. 14 (2014) 831–838.
- [85] L. Jinlong, L. Tongxiang, Y. Meng, S. Ken, M. Hideo, Performance comparison of NiCo₂O₄ and NiCo₂S₄ formed on Ni foam for supercapacitor, *Compos. Part. B: Eng.* 123 (2017) 28–33.
- [86] Z. Wu, X. Pu, X. Ji, Y. Zhu, M. Jing, Q. Chen, et al., High energy density asymmetric supercapacitors from mesoporous NiCo₂S₄ nanosheets, *Electrochim. Acta* 174 (2015) 238–245.
- [87] L. Hou, R. Bao, Z. Chen, M. Rehan, L. Tong, G. Pang, et al., Comparative investigation of hollow mesoporous NiCo₂S₄ ellipsoids with enhanced pseudo-capacitances towards high-performance asymmetric supercapacitors, *Electrochim. Acta* 214 (2016) 76–84.
- [88] X. He, Q. Liu, J. Liu, R. Li, H. Zhang, R. Chen, et al., High-performance all-solid-state asymmetrical supercapacitors based on petal-like NiCo₂S₄/polyaniline nanosheets, *Chem. Eng. J.* 325 (2017) 134–143.
- [89] Y. Zheng, J. Xu, X. Yang, Y. Zhang, Y. Shang, X. Hu, Decoration NiCo₂S₄ nanoflakes onto Ppy nanotubes as core-shell heterostructure material for high-performance asymmetric supercapacitor, *Chem. Eng. J.* 333 (2018) 111–121.
- [90] S. Liu, S.C. Jun, Hierarchical manganese cobalt sulfide core-shell nanostructures for high-performance asymmetric supercapacitors, *J. Power Sources* 342 (2017) 629–637.
- [91] M. Yu, X. Li, Y. Ma, R. Liu, J. Liu, S. Li, Nanohoneycomb-like manganese cobalt sulfide/three dimensional graphene-nickel foam hybrid electrodes for high-rate capability supercapacitors, *Appl. Surf. Sci.* 396 (2017) 1816–1824.
- [92] B. Hu, X. Qin, A.M. Asiri, K.A. Alamry, A.O. Al-Youbi, X. Sun, Synthesis of porous tubular C/MoS₂ nanocomposites and their application as a novel electrode material for supercapacitors with excellent cycling stability, *Electrochim. Acta* 100 (2013) 24–28.
- [93] K.-J. Huang, L. Wang, Y.-J. Liu, Y.-M. Liu, H.-B. Wang, T. Gan, et al., Layered MoS₂-graphene composites for supercapacitor applications with enhanced capacitive performance, *Int. J. Hydrogen Energy* 38 (2013) 14027–14034.
- [94] M. Wang, H. Fei, P. Zhang, L. Yin, Hierarchically layered MoS₂/Mn₃O₄ hybrid architectures for electrochemical supercapacitors with enhanced performance, *Electrochim. Acta* 209 (2016) 389–398.
- [95] Y.-P. Gao, K.-J. Huang, X. Wu, Z.-Q. Hou, Y.-Y. Liu, MoS₂ nanosheets assembling three-dimensional nanospheres for enhanced-performance supercapacitor, *J. Alloy. Compd.* 741 (2018) 174–181.
- [96] C. Zhao, Y. Zhou, Z. Ge, C. Zhao, X. Qian, Facile construction of MoS₂/RCF electrode for high-performance supercapacitor, *Carbon* 127 (2018) 699–706.
- [97] C.J. Barnhart, S.M. Benson, On the importance of reducing the energetic and material demands of electrical energy storage, *Energy Environ. Sci.* 6 (2013) 1083–1092.

-
- [98] M. Gidwani, A. Bhagwani, N. Rohra, Supercapacitors: the near future of batteries, *Int. J. Eng. Invent.* 4 (2014). 22-22.
 - [99] P. Denholm, J. Jorgenson, M. Hummon, T. Jenkin, D. Palchak, B. Kirby, et al., *Value of Energy Storage for Grid Applications*, National Renewable Energy Lab, Golden, CO, 2013.
 - [100] J. Liu, Addressing the grand challenges in energy storage, *Adv. Funct. Mater.* 23 (2013) 924–928.
 - [101] C. Heymans, S.B. Walker, S.B. Young, M. Fowler, Economic analysis of second use electric vehicle batteries for residential energy storage and load-levelling, *Energy Policy* 71 (2014) 22–30.



Supercapattery: technical challenges and future prospects

M.N.M. Ansari and Noor Afeefah Nordin

Institute of Power Engineering, Universiti Tenaga Nasional, Kajang, Malaysia



13.1 Introduction

Energy usually stems from fossil fuels and renewable sources such as wind, solar, and tide. However, the mass generation of energy from fossil fuels has caused a huge release of greenhouse gases and provoked immense concern about the environment. Thus researchers are attempting to replace fossil fuels with renewable energy and work on efficient ways for its storage. Concerning that, electrochemical energy storage (EES) was found to be prevalent in the literature for the past decade as it can be an appropriate alternative to produce energy at various scales [1]. In recent years, the use of sustainable/renewable sources of energy has become very indispensable due to the increasing demand for durable and high-power batteries. The durable power and power consumption in various energy sectors such as utilities, consumer electronics, solar PV grid, automobile industries, etc. require much higher energy sources compared to what is available at the moment [2]. Also, to meet the demand for next-generation electronic applications, optimizing the energy and power densities of electrochemical energy storage devices (EESD) with long cycle life is essential [3].

Batteries keep our appliances functioning the whole time. In other words, we can say that they have a high energy density, but they can yield extended hours to recharge when they run out of charge. For a speedy power supply and recharging (i.e., high power density), electrochemical capacitors, also known as supercapacitors, are utilized. One such usage is regenerative braking, used to regain power in cars and electric mass transit vehicles that would otherwise lose braking energy as heat. However, supercapacitors have a low energy density. Batteries and supercapacitors both depend on electrochemical processes, although dissimilar electrochemical

mechanisms govern their relative energy and power density [4]. Amid various energy storage technologies, supercapacitors are beneficial in numerous facets such as high power density and durability. Thus several applications, including electric and hybrid vehicles, smart grid, wireless sensor networks, and biomedical devices, have engaged supercapacitor-based energy storage systems [5].

Electrochemical measurements can distinguish between different types of energy storage materials and their underlying mechanisms [6]. The main focus of the development of this device is to overcome the problem of frequent fluctuations and variations in the energy output that finally leads to the exploration of electrode materials and electrolytes in EESD. As a result, the use of EESD, such as supercapacitors, batteries, or a combination of both such as “supercapatteries,” came into existence. Supercapatteries possess merits of both rechargeable batteries and supercapacitors, thus making them be considered as a vital choice to store energy over a specific period and retrieve it when required. Fig. 13.1. shows the

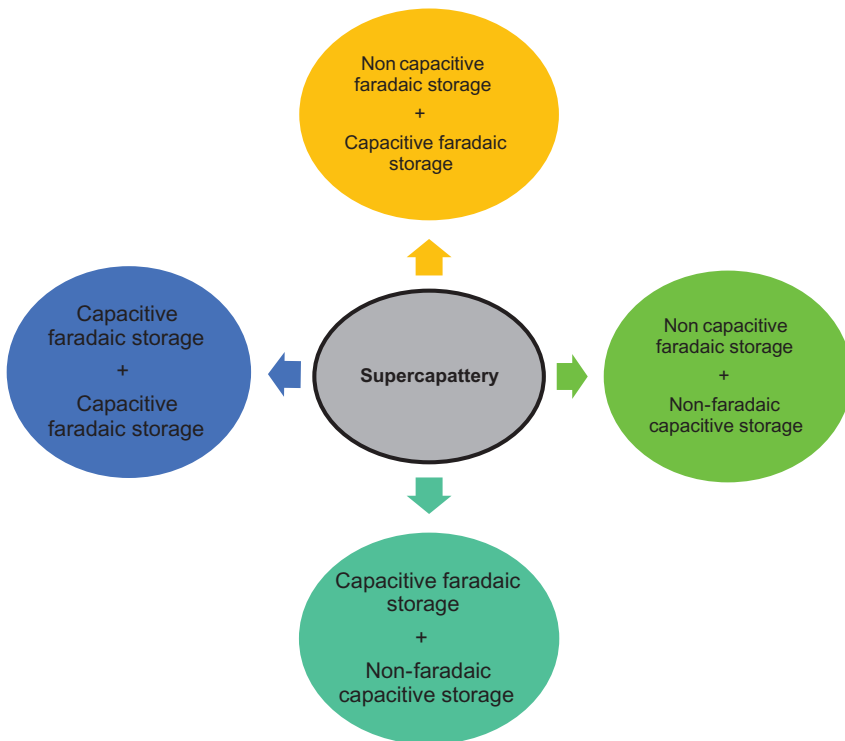


Figure 13.1 Classification of supercapattery.

classification of supercapatteries based on capacitive and faradaic storage. As an ideal EESD, supercapattery combines the high energy storage capability of conventional batteries with the high-power delivery capability of supercapacitors [7].

The recent popular trend of EES technologies includes rechargeable batteries, electrochemical capacitors (supercapacitors), and hybridization of batteries and capacitors (supercapattery and supercabattery). The ability to charge and discharge electric charge is the key foundation for all effective EES devices. The charge–discharge mechanisms, nevertheless, change considerably in terms of how and where the charge is stored. Electrode materials with EDL capacitance, pseudocapitance, or the Nernstian process can be applied in supercapatteries in which diverse types of electrode materials will give rise to diverse supercapatteries [3]. Supercapatteries can be constructed by numerous methods and have different properties based on the materials selected. One of the ways to construct a supercapattery is by the balanced coupling of a supercapacitor electrode with a battery electrode, or by constructing the electrodes from active materials that are adept in both capacitive and Nernstian charge storage. It can also be developed by supplementation of redox species in the electrolyte of a supercapacitor so that the device can store charge through both the Nernstian and capacitive mechanisms [8]. In constructing supercapattery, it is important to ascertain the charge storage mechanisms of the electrodes to be used to ensure its enhanced functioning in terms of energy storage and power output [3]. Fig. 13.2 shows a schematic illustration of a typical single-cell EES device.

Table 13.1 summarizes the combination of various types of supercapacitors and batteries to build a supercapattery. A supercapattery is a hybrid energy storage device (ESD), aggregating the high energy-storage potentiality of conventional batteries by using redox-active battery-grade

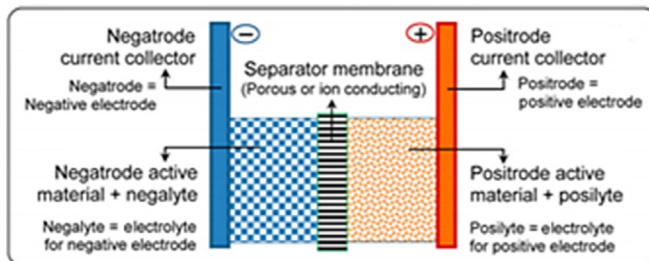


Figure 13.2 A single cell of typical electrochemical energy storage device [6].

Table 13.1 Summary of supercapattery properties [1].

Device	Supercapattery						Battery
	Supercapacitor			Hybrid			
	EDLC	Pseudocapacitor		Capacitive hybrid		Others (supercabattery)	
Electrode material	NFCS + NFCS	NFCS + CFS	CFS + CFS	NFCS + NCFS	CFS + NCFS	CFS + NCFS	NCFS + NCFS
Specific energy (Wh kg ⁻¹)	102 (IL), 6.7 (aq.) 10.2 (aq)	3.6 14.3	26.6	230 204	261 103 114	208.6	250
Max specific power (W g ⁻¹)	111.6	24.7 0.68	13	59 55	25 56	3	1.5
Cycling life (cycles)	> 10000	> 5000	> 5000	> 1000	> 1000	> 1000	< 1200
Electrolyte types	IL, aq.	aq.	aq.	IL	IL	Organic	Organic
References	[9,10]	[11]	[12]	[13]	[14]	[15]	(https://en.wikipedia.org/wiki/Lithium-ion_battery#cite_note-7)

aq., Aqueous; *CFS*, capacitive Faradaic storage = pseudocapacitive storage; *EDLC*, electric double-layer capacitor; *IL*, ionic liquid; *NCFS*, noncapacitive Faradaic storage = battery-type storage; *NFCS*, nonFaradaic capacitive storage = EDLC storage.

materials as a positive electrode with the high-power delivery capability and carbonaceous materials as a negative electrode. Thus combining the advantages of both batteries supercapacitors [16].

The development of the supercapattery was attained from a wide range of hybridization, and it is technically advanced by the hybridization of resources with the qualities of supercapacitors and batteries with different fundamental principles and technological prospects, as illustrated in Fig. 13.3. Usually it consists of battery-type materials as the anode and a capacitor-like electrode as the cathode. The wider operating voltage window of supercapattery is one of the main aspects that are accountable for the enhancement of energy density [16]. Redox-active materials that are highly porous in structure have the principle of EDL and faradaic charge

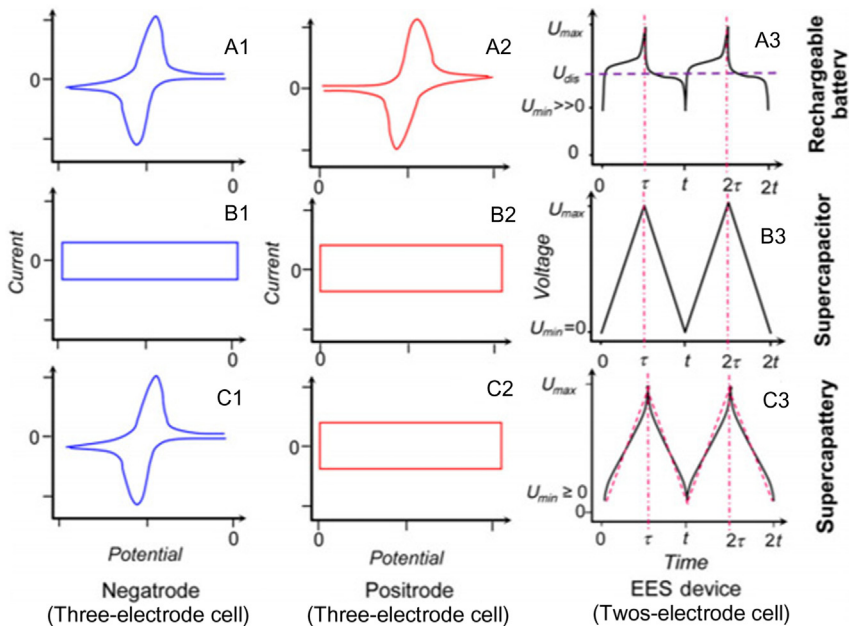


Figure 13.3 Potential windows of EES devices; (1,2) CVs of positrod and negatrod in a three-electrode cell and (3) GCDs of the two-electrode cell of (A) rechargeable battery, (B) supercapacitor, or (C) supercapattery [6]. * U_{max} and U_{min} : maximum and minimum cell voltages that can be reached during charging and discharging, respectively, without causing irreversible changes in the cell. U_{dis} : average-discharging voltage. τ and t : end times of the first charging and discharging cycle, $\tau \geq (t - \tau)$. 2τ and $2t$: end times of the second charging and discharging cycle, but not necessarily twice of τ and t . EES, electrochemical energy storage; GCD, galvanostatic–discharging.

storage mechanisms. Hence, these properties led to the possibility of constructing supercapattery from different types of materials [1]. Furthermore, pseudocapacitive materials are said to be a unique type of supercapattery electrode material due to their innately faradaic and capacitive properties.

This chapter discusses the scientific knowledge about supercapattery and highlights the technical challenges that are mainly focused on the electrode materials and their electronic properties, types of electrolytes, and corresponding electrochemical performances of the supercapatteries. In addition, it also focuses on the market potential and prospects of supercapatteries for various applications.



13.2 Technical challenges

Although supercapatteries appear to be an impressive invention with both the criteria of a supercapacitor and a battery in a single device, there are still some technical challenges confronted by the researchers. Several technical challenges are depicted in Fig. 13.4 and discussed below.

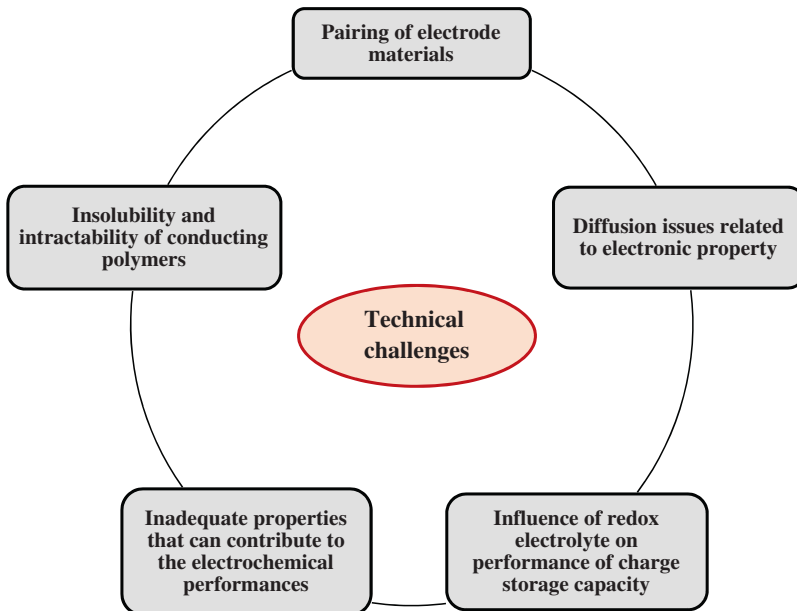


Figure 13.4 Technical challenges in supercapatteries.

13.2.1 Pairing of electrode materials

The EES technologies and the development of their materials have been broadly investigated in the current years regarding their exceptional and assured properties toward sustainable energy supply worldwide [17]. Rechargeable batteries are known to hold great energy capacities, whereas the supercapacitor has high-power capabilities and long cycle life spans. Nevertheless, each of the stated technologies alone is unable to meet all the requirements for effective commercialization owing to their limitations. Rechargeable batteries have been utilized in the initial progress of EES as the source of power in a broad variety of portable devices, such as electrical and electronic appliances, lighting in dark and remote areas, and for the ignition of internal combustion engines [18]. The ordinary batteries utilized are customarily made of nickel, cobalt, or iron-based and have a high capacity, good electrical conductivity, and many oxidation states for redox reactions [19]. Rechargeable batteries function by generating electricity from chemical energy through redox reactions at the anode and cathode, and this process is alterable for some time. In contrast with pseudocapacitive materials, the battery type electrode stores a significant amount of energy. The source of these rechargeable batteries is mostly from fossil fuels, and this needs to be replaced with some renewable energy to serve the need of world sustainability [20]. However, there are some inadequacies of rechargeable batteries that raised concern in the industry upon their service. The rechargeable batteries hold low power density, which allow them only limited types of application, particularly in high-power material/service. They also produces heat during usage, which could cause overheating, thermal runaway, and fire if not dissipated. Furthermore, rechargeable batteries have a very limited cycle life due to the absence of reversible redox reactions [3,17,21].

In a battery, the electrode where oxidation takes place is called the anode, whereas the electrode where reduction reaction takes place is called the cathode. The most favored electrodes are typically selected from plentiful and affordable materials that show effective electronic conductivity, excellent stability, and high catalytic activity [19]. Nevertheless, some applications also need the electrode material to display mixed ionic electronic conductivity, where both the ionic and electronic faults are rootless [22]. As one of the vital steps for supercapattery is the pairing of the electrode, it is essential to state the electrode type as it will affect the

specific energy, maximum specific power, and also cycling life of a supercapattery. Supercapattery can be achieved by many combinations of electrodes and electrolytes that ultimately mean to achieve the qualities of a supercapacitor (high specific power) and a battery (high specific energy) at the same time [23]. It is also necessary to think about sustainability, renewability, and “green chemistry” when picking materials for storage devices like electrodes or catalysts, especially when they are intended to be utilized in applications with large markets and potential.

Some of the materials that are generally used as the positive electrode in supercapattery are NiO [24], MnO₂ [25], Fe₂O₃ [26], and Co₃O₄ [28], respectively. Amid the group of transition metal oxides, Co₃O₄ has been one of the most appealing materials due to its abundance, high theoretical capacity, and reversibility [27]. However, Co₃O₄ nanoparticles were observed to inflict high particle accumulation that considerably decreases their functioning sites. Rapid capacity decline and structural deformation during charge–discharge reactions take place as a result of the ensuing accumulation. To tackle the setback, integrating graphene or multiwalled carbon nanotube as a highly conductive platform with Co₃O₄ is found to be efficient in decreasing the accumulation [16]. This is due to the properties of these carbon materials that can facilitate charge transfer mechanisms and avert the accumulation of nanoparticles. Therefore it increases the electrochemical surface area and cycling stability [29,30].

13.2.2 Diffusion issues related to electronic property

Due to the existence of diffusion limitation and energy barrier of solid materials, the conventional cathode electrode materials have only half of their available theoretical capacities. Among the important parameters in selecting the electrode material is for the structure to be facile for ion diffusion and electron transfer. As electrode materials have naturally weak electronic conductivity and substantially high solubility, this results in a great challenge for their explicit use as energy storage electrodes. The high electrochemical potential of devices can lead to high energy density. One of the approaches to tackle the problem is to merge these molecules with conductive and stable materials such as carbon or conducting polymers in a supercapacitor. Improvements in the electronic conductivity and ions mobility of electrode materials are of particular importance for their high-power applications. Carbon coating and doping are commonly used methods to improve electronic conductivity and ions diffusion [31].

Besides, defects can also affect the electronic structure of electrode materials. The presence of defects and vacancies strongly influences the properties of transition metal oxides, including electronic conductivity, electrode potential, and ionic transport [32].

It is not easy to develop supercapatteries due to some technical issues confronted in the field. Material selection, construction process, and cost are among the parameters that should be taken into account when inventing supercapattery as it would impact the efficiency of the product particularly when they are manufactured at a large scale [7,13,33]. Besides, it should also be considered to manufacture supercapatteries by using the present apparatus so as to not inflict a higher cost of production. Furthermore, thermal conditions have to be considered when planning supercapatteries that will be used for recurring rapid charge and discharge cycles. Ohmic self-heating might instigate the system to overheat and will lead to quick loss of performance.

13.2.3 Influence of redox electrolyte on performance of charge storage capacity

Electrolytes are the chief constituent of a supercapacitor device to hold a high power and energy density and long cycling life. The functioning of electrolytes is assessed primarily based on their ionic movement and conductivity. Compatibility between the electrolyte–electrode materials plays a vital role in attaining a high-performance device and affecting the overall electrochemical supercapattery performance [34,35]. Usually, the performance of a supercapacitor relies on the electrode composition and structure. This comprises the electrolyte ion absorption and desorption processes, manufacturing variations, device ratings, aging condition, and operating temperature. However, it is noticed that the effect of self-discharge is insignificant when the discharge current is comparatively higher. If the discharge current is lesser, self-discharge results in a significant energy loss and thus a drop in the delivered charge [5].

Normally, several types of electrolytes are employed in supercapacitor applications, namely aqueous and nonaqueous (ionic liquid and organic)-type electrolytes. These types of electrolytes affect cell operating potential. The aqueous electrolyte-based supercapatteries are the favored ones as they have excellent conductivity and are affordable. Nevertheless, the limit of the most aqueous electrolytes has a low decomposition voltage of water, that is, 1.23 V [6]. Consequently, most of the aqueous electrolytes-based supercapatteries work in the potential window of 0–1.2 V [7].

Aqueous electrolytes can be used in EES devices owing to their tremendously high conductivity, affordability, and ease of management. Despite that, it is reckoned to be a poor choice due to their small voltage window. Hence, most of the currently marketable supercapacitors decided to use carbon-based electrolyte to increase the voltage window but at the same time confront the issues of complex purification treatment under an unbendingly controlled environment to stay free of moistness [36,37].

The aqueous electrolytes are classified into three groups, namely, alkaline (KOH), acid (H_2SO_4), and neutral (Na_2SO_4) solutions. However, reports revealed that alkaline electrolyte is more favorable for use, as the acid ones tend to encounter corrosion problems over time. Therefore optimization of electrolyte concentration is vital for a supercapattery to ensure total competence of the EES device [20]. To date, there is still no perfect electrolyte found to be used for EES devices due to some of the advantages and disadvantages possessed by these electrolytes, as summarized in Table 13.2.

The solid type electrolyte can be utilized directly to split the positive and negative electrodes in EES devices electronically. However, it is more customary and pragmatic to use a thin membrane that is penetrable to a liquid electrolyte or its ions. The membrane should also be robust enough to inhibit direct contact between the two electrodes under pressure used to build the EES device [3]. To aid this mechanism, nanomaterials that have excellent chemical and physical properties are studied for their potential in energy storage applications. Advanced research on chemically modified materials at the molecular and atomic level would significantly improve the discoveries for energy storage applications [40].

Table 13.2 Types of electrolytes and their properties.

Type of electrolyte	Merit	Demerit	Example	References
Aqueous	High capacitance and conductivity	Narrow working voltage	HCl (acid), Na OH (alkaline), and Na_2SO_4 (neutral)	[23,38]
Ionic liquid/organic	High chemical and thermal stability, wide operating voltage	Low conductivity, small specific capacitance, toxic, flammable	(TEABF ₄) in ACN, [EMIM] [BF ₄]	[23,39]
Solid	No leakage	Low conductivity than liquid	PEO/LiCl	[23,38]

Bipolar stacking of the electrodes is presently analyzed to enhance the properties of EES devices, specifically supercapattery. The bipolar stacking is planned where the adjacent supercapattery cells are attached in a sequence by bipolar plates in the stack [6]. This pattern would allow nearly half of the titanium plate to be eliminated in contrast with the previous ones invented by using external cable connections. Previous work has found that the 19-cell stack is possible in scalable EES devices. However, the equilibrium between the plate weight and penetrability should be highly regarded because penetrability is directly linked to plate material thickness. For instance, internal short-circuiting would happen if bipolar plates were penetrable to ions in electrolytes [21]. The research carried out to tackle this problem employed titanium bipolar plates of 0.1-mm-thickness in the 19-cell stack that was targeted to avoid this permeability. Another study did some analyses on stackable bipolar pouch cells and proposed that lightweight carbon/polymer composite films can be an apt bipolar plate with the lowest thickness of 0.025 mm. The study was conducted on carbon black/polyethylene composite films that productively led to a very low electrolyte penetrability [41]. Although bipolar stacking designs can efficiently decrease the total weight of energy storage stacks, the equivalent series resistance (ESR) of stacked cells also needs to be taken into account. This is primarily because their ESR would sum up in the stack corresponding to the EES cells that are attached in sequence. It is observed that the discrepancy in manufacturing and cells with high ESR in the stack can instigate distorted galvanostatic charging–discharging (GCD), which would eventually lead to severe performance deprivation [6].

As one of the contemporary ESDs, the electric double-layer capacitor (EDLC) or pseudocapacitor has been broadly recognized in supercapacitor applications. The EDLCs are presently overshadowing the supercapacitor markets. It operates by depositing energy through the electrostatic collaboration between electrodes and electrolyte ions. Hence, a proper selection of the electrolyte to match the electrode materials is vital for an effective EDLC. It was also remarked that a supercapacitor in the form of a pseudocapacitor or EDLC would have high specific power but subsequently has lower specific energy compared to rechargeable batteries [42].

13.2.4 Inadequate properties that can contribute to the electrochemical performances

The amount of the conductive additives and polymer binder included in the electrode influence different properties and parameters of the EES

device performance. For instance, to increase the capacity of Li (Ni_{1/3}Co_{1/3}Mn_{1/3})O₂, the ionic conductivity, electronic conductivity, and porosity were investigated with different ratios of constituents [43]. One of the difficulties is the absence of proper current binders and surfactants for ink for a screen-printed electrode. This is because a high mass ratio of binders and surfactants needs to be incorporated into the ink to construct durable, thick printed layers, which increases resistivity when compared with electrocodeposited—carbon nanotube (ECP-CNT) composites. Also, the thickness of screen-printed electrodes needs to be more adaptable. Binder materials are responsible for holding the active material particles within the electrode in order to maintain a strong connection between the electrode and the contacts. A major function of the binder is to act as an active dispersion agent to connect the electrode and then steadily adhere them to the current collectors [44]. Binders generally must be insoluble in the electrolyte, flexible, chemically and electrochemically stable, and easy to apply to the electrodes. On another note, binders for positive cathode must be able to resist oxidation. Polyvinylidene fluoride (PVDF) was the most commonly used binder for both the anode and cathode of LIBs due to the excellent electrochemical and thermal stability and good adhesion between the current collectors and electrode films. However, the use of PVDF was limited due to some drawbacks, such as low flexibility, readily swollen at elevated temperatures, and the need for an organic solvent. Many researchers came out with alternative methods to manufacture composite electrodes with fewer binders or without binders to overcome the setback [35].

The lack of electronic conductivity and discharge capacity are also among the properties that contribute to the inefficiency of the EES device. The electrochemical performance of EES devices such as supercapacitors, especially based on redox inactive materials, can offer high power output, but the energy capacity would be relatively low. For this reason, hybridization of the properties of a supercapacitor and a battery in a single supercapattery is anticipated to hold high specific energy as in a battery and produce high specific power as in a supercapacitor. One of the fundamentals in supercapattery design is the redox electrode materials. The problems confronted by these materials are due to their innate characteristics, such as inadequate mechanical strength of conducting polymers and low conductivity of metal oxides [13].

The power density of a battery prepared in the nanoscale increases because of the short conveyance paths for ions and electrons. However,

the increased power density does not certainly transform nanoscale materials into oxide supercapacitors because their faradaic redox peaks and galvanostatic profiles stay battery-like. The performances of EES devices fluctuate due to the inconsistent techniques in evaluating their properties. The reasons for such inconsistencies are different instruments and methods of calculation used, different experiment setups, differences in electrode production, a different base used, and different test states applied [37]. Therefore to assess each of the device's performance, these factors must be crafted consistently to get reliable results and findings for the EES devices.

The launch of nanostructured materials such as carbon nanotube activated carbon (AC) and graphene as electrodes would result in the high power capability of the supercapattery. This is due to the inherent properties of the materials which are penetrable and, subsequently, present a large surface area. These nanostructured carbon materials also have low electrical resistance and are highly stable over a wide potential window. With regard to their characteristics, these materials are found to be perfect for utilization for polarizable electrodes [13].

Many pieces of research were conducted to increase the energy capacity of supercapacitors by increasing their charge capacity or cell voltage, and one of the potential methods is by using carbon nanotubes (CNTs). The CNT is among various nanostructured materials used to enhance the energy capacity of supercapacitors. The benefits of CNTs include high structural, electrical, mechanical and chemical properties [37]. The CNTs also hold high electrical conductivity that plays a part in the rapid movement of electrons within the electrode. The CNTs are well known for their exceptional mechanical properties. Thus they managed to ensure that the redox-active material could endure weariness and stress, which was instigated by the frequent intercalation and depletion of ions. Consequently, the electrode materials would have a longer cycle and tactfully solve the problem of rechargeable batteries in terms of their short life cycle [27]. However, large surface areas are attained by using highly porous materials and, when the pore size is not equaled to the radius of the solvated ion, those pores are not reachable and hence do not contribute to the capacitance [34].

13.2.5 Insolubility and intractability of conducting polymers

Conducting polymers are one of the nominee materials for supercapacitors owing to their excellent electrical conductivity, large pseudocapacitance,

and relatively low cost. Conducting polymers also require simple synthesis and processing conditions that make them easier to be utilized. Advances in nanotechnology have allowed the fabrication of versatile conducting polymer nanomaterials with improved performance for various applications. In contrast with bulk conducting polymers, the nanostructured conducting polymer has significantly high electrical conductivity, short ion transport path length, large surface area, and superior electrochemical activity. These properties make them apt to be used for energy storage and conversion applications [45]. The commonly used conducting polymers are polyaniline (PANI), polypyrrole (PPy), and poly[3,4-ethylene-dioxythiophene] (PEDOT). Conducting polymers could have a very large specific capacitance (SC) that is close to Ruthenium oxides, for example, 775 F g^{-1} for PANI, 480 F g^{-1} for PPy, and 210 F g^{-1} for PEDOT, respectively [45].

Some of the conducting polymers were utilized in various forms, namely nanosheets, nanorods, bulk powder, and nanowalls, and resulted in successful applications. The parameters that are highly affecting the physical properties of conducting polymers are their conjugation length, degree of crystallinity, and intra- and interchain interactions. However, the main challenge faced by conducting polymer is its insolubility and intractability. The majority of the conducting polymers are insoluble and need specific solvents to be solubilized entirely. The insolubility of conducting polymers would result in unstable suspension and would subsequently affect the electronic property of the device. In order to tackle the problem, the polymers were dispersed in solutions using a series of steps to remove the agglomerations and ensure a stable suspension [46]. Besides, conducting polymers are also being modified/hybridized with various heterogeneous material components to overcome their inherent limitations in terms of solubility, conductivity, and long-term stability.

In comparison with the aforementioned conducting polymers, PANI is considered to be the most promising supercapacitor electrode material. It has been extensively employed mainly because of the low cost of monomer, it is easily synthesized, environmentally friendly, and it has also reached higher specific capacitance than the carbon, but it is said to have meager stability [22]. Nevertheless, because of the repetitive cycles (e.g., charge/discharge process), swelling, and shrinkage, PANI is subject to rapid degradation in performance. To avoid this limitation, combining PANI with carbon materials has been proven to reinforce the stability of PANI as well as maximize the capacitance value. The stability of the conducting polymer

can also be enhanced by using H_2SO_4 electrolyte. The electrochemical capacitance and charge storage properties of conducting polymers have been analyzed by cyclic voltammetry (CV), electrochemical impedance spectroscopy, and chronopotentiometry. Nevertheless, conducting polymers have been found to have weak mechanical stability due to recurrent intercalation and depletion of ions during charging and discharging [38]. Hence, the right choice of materials for the conducting polymer is critical to ensure its compatibility in the system, and it could significantly enhance the properties of supercapatteries.



13.3 Prospects

This section reviews the requirements of supercapatteries from the existing ESDs like supercapacitors and batteries. The principal aim of this device is to develop the energy density with moderate power density through the hybridization of high-energy faradaic electrodes with high-power nonfaradaic electrodes. Numerous critical parameters concerned with the energy storage mechanism have been reviewed, which increases the prospect for many future developments. The progress of advanced ESDs is at the forefront of research aiming at a sustainable future [40].

The potential of developing materials with the energy density of batteries and the power density and cycle life of supercapacitors is an exhilarating path that has yet to be realized. One of the intriguing aspects of the field is whether to approach these targets by increasing the power density of battery materials or by increasing the energy density of supercapacitors. However, there needs to be clarity in the terminology applied along with appropriate measurements and analyses. Proper assessment of the new materials and their charge storage mechanisms will assist the advancements in this important field of electrical energy storage [4].

At this point, the development of battery and supercapacitor materials can support the growth of supercapatteries. Besides, novel engineering designs for supercapatteries such as bipolar stacking are essential to cross the gap between the laboratory setting and industrial manufacturing. Also, more significance needs to be given to the adaptive process for the manufacturing of supercapatteries using the prevailing equipment for commercial batteries and supercapacitors [1].

The abundance of an element is just one of the several standards dealing with its cost and availability. Therefore choosing elements from which to design eco-efficient electrodes or new technologies requires consideration of many other chemical and industrial facets [47]. The global energy crisis is compelling the scientists and researchers to explore alternative sources of energy, such as renewable and sustainable forms, instead of fossil fuels. Convenience is one of the significant markets for supercapatteries. These devices have the exceptional capacity to store a large amount of energy in a short time, provided the cyclical form of solar, wind, and wave type systems exist.

A group of researchers discovered that the Bi_2MoO_6 electrode displayed a possible extended window from 0.0 to 1.5 V, and subsequently, a proportioned supercapattery device was made to assess its marketable advances. For a proportioned supercapattery cell, Bi_2MoO_6 electrodes of a similar trait (including Ni – F and mass of Bi_2MoO_6) were used as negative and positive electrodes in the presence of a polypropylene separator in a plastic cylindrical tube. Table 13.2 shows the electrochemical performance of Bi_2MoO_6 supercapattery. It can be understood that the $\text{Bi}_2\text{MoO}_6//\text{Bi}_2\text{MoO}_6$ proportioned supercapattery device demonstrated an extraordinary energy density and power density of 45.6 Wh kg^{-1} and 0.989 kW kg^{-1} , respectively, which is impressive compared to the symmetrical cells described in several other earlier reports [48].

The researchers have stated that electrochemical charge storage mechanisms of the $\text{Bi}_2\text{MoO}_6//\text{Bi}_2\text{MoO}_6$ proportioned supercapattery with hydrangea-type Bi_2MoO_6 electrode exhibit a particular capacitance of 485 F g^{-1} at 5 A g^{-1} and stability of 82% over 5000 cycles [48]. These results show that Bi_2MoO_6 proportioned supercapattery has the capacity for many uses integrating utilities and devices.

Many works of literature have shown that supercapatteries have the enhanced electrochemical performance in terms of SC (F g^{-1}), energy density (Wh kg^{-1}), and power density (W kg^{-1}). Table 13.3 summarizes the various supercapatteries' performances, which provide the opportunity for many future improvements. Based on the previous research on CV, galvanostatic charge–discharge (CCD) of different electrode coupled with potassium hydroxide (KOH) electrolyte solution with different molar concentration is summarized in Table 13.3. Iqbal et al. [16] conducted a study on MWCNT- Co_3O_4 -Ag nanocomposite samples and achieved a maximum specific capacity of 83.88 C g^{-1} at 0.6 A g^{-1} of current density.

Table 13.3 BiMoO symmetrical supercapattery performance.

Type of supercapattery electrode	Energy density (Wh kg ⁻¹)	Power density (kW kg ⁻¹)	References
CS@Bi ₂ MoO ₆ //CS@Bi ₂ MoO ₆	10.8	0.410	[49]
RuO ₂ /graphene//RuO ₂ /graphene	11.0	0.076	[50]
Ni@FeCo ₂ O ₄ @MnO ₂ //Ni@FeCo ₂ O ₄ @MnO ₂	22.2	978.3	[51]
GR/BiVO ₄ //GR/BiVO ₄	45.69	800.0	[52]
Bi ₂ MoO ₆ //Bi ₂ MoO ₆	45.6	989	[48]

Furthermore, supercapattery assembled as MWCNT-Co₃O₄-Ag//AC achieved a high energy density of 16.5 Wh kg⁻¹ at a power density of 297.5 W kg⁻¹, which was credited due to the combination of MWCNT-Co₃O₄-Ag with AC [16]. Additionally, the life cycle test revealed that supercapattery was highly stable with superior long-term stability with a capacity retention of 93.1% of the initial value even after 3000 cycles.

A group of researchers effectively developed a symmetric device using C-Fe/PANI as a positive and negative electrode. This device displayed the energy and power densities of 41.3 Wh kg⁻¹ and 231.9 W kg⁻¹, respectively. Based on the power and energy density, it is proposed that the C-Fe/PANI symmetric device could be categorized as a supercapattery type of electrochemical power source [53] (Table 13.4).

In addition to this, a good focus has been given to strontium-based materials by pairing strontium phosphide/PANI (battery-grade material) with AC (capacitive material). This has presented a fantastic performance in terms of specific capacity (122.5 F g⁻¹), energy density (28.9 Wh kg⁻¹), and power density (5100 W kg⁻¹) [42]. A supercapattery device in the form of CR-2032 coin cell consisting of Co₃O₄ as the positive electrode and reduced graphene oxide as the negative electrode delivered a high energy density of 40 Wh kg⁻¹ at a power density of 742 W kg⁻¹. Also, the half-cell in the form of CR-2032 coin cell with Co₃O₄ as the anode and lithium metal as the counterelectrode exhibited stabilized lithium storage capacity of 620 mAh g⁻¹ with high coulombic efficiency [27].

In another study, an electrode material Bi₂O₃@MnO₂//Bi₂O₃@MnO₂ was tested for its electrochemical characterization and showed 350 F g⁻¹ of SC @10 A g⁻¹, which is better than that of its individual counterparts. Furthermore, the 28 Wh kg⁻¹ energy density at 1395 W kg⁻¹ power density of its symmetric electrochemical supercapattery is the summation of battery

Table 13.4 Summary of the performances of supercapattery.

Type of supercapattery electrode/retention capacity%	Electrolyte	Specific capacity (F g ⁻¹)	Energy density (Wh kg ⁻¹)	Power density (kW kg ⁻¹)	References
MWCNT-Co ₃ O ₄ -Ag//AC (93.1% @3000 cycles)	1 M KOH	150.9 @0.6 A g ⁻¹	16.5	0.297	[16]
C-Fe/PANI symmetric electrode (72%@10000 cycle, 5 A g ⁻¹)	6 M KOH	— @0.5 A g ⁻¹	41.3	0.232	[53]
Sr ₃ P ₂ /PANI//Ni foam//(battery-grade material) with activated carbon (capacitive material)	1 M KOH	221.5 @2 A g ⁻¹	28.90 10.95	1.02 5.10	[42]
Co ₃ O ₄ KOH rGO supercapattery	1 M KOH	—	40.0	0.742	[27]
Co ₃ O ₄ KOH Co ₃ O ₄ (98%@5000 cycles)		@0.5 A g ⁻¹	19.0	0.240	
Bi ₂ O ₃ @MnO ₂ grown on GR (72.41% @2000 cycles)	6 M KOH	144.7	28.93	1.395	[54]
Bi ₂ O ₃ /graphene nanocomposite (95% @1000 cycles)	6 M KOH	136.0 @ 0.5 A g ⁻¹	—	—	[55]
Co ₃ (PO ₄) ₂ .8H ₂ O/modified NF electrode (2.5 mM)/activated carbon electrode	1 M KOH	1029.5 @50 mA cm ⁻²	29.29	0.468	[33]
(Ni ₃ (PO ₄) ₂ -Ag ₃ PO ₄)/(82% @5000 cycles)	1 M KOH	868.9@1 A g ⁻¹	34.0	0.381	[56]
FeCoO//FeCoS electrode couple (97%@5000 cycles)		450.0 @2 A g ⁻¹	140.0	1.434	[57]
NiS ₂ -NiV ₂ S ₄ electrode couple (90%@10,000 cycles)	6 M KOH	141.8 @0.5 A g ⁻¹	19.4	0.140	[58]

and supercapacitor performance. The average capacity retention of 72.41% of the initial value after 2000 cycles, with specific capacity of 144.7 F g^{-1} is measured [54]. Graphene/ Bi_2O_3 nanocomposite material shows a SC of 136.76 F g^{-1} at a current density of 0.5 A g^{-1} which is found to be suitable for supercapacitor applications. Moreover, the synthesized nanocomposite electrode material has exhibited excellent cyclic stability ($>95\%$ over 1000 cycles), which may lead to applications in high-performance ESDs, such as supercapattery [55]. Shao et al. [33] used a binder-free $\text{Co}_3(\text{PO}_4)_2 \cdot 8\text{H}_2\text{O}$ /nickel foam substrate (NF) as the positive electrode and AC/NF as the negative electrode in a multilayer nano/microflake structure for supercapattery application. A maximum specific energy of 29.29 Wh kg^{-1} was acquired at a specific power of 468.75 W kg^{-1} with decent cyclic stability of 77.9% after 1000 cycles. Therefore $\text{Co}_3(\text{PO}_4)_2 \cdot 8\text{H}_2\text{O}$ is a good material for supercapattery functions [33].

The optimized $\text{Ni}_3(\text{PO}_4)_2\text{-Ag}_3\text{PO}_4$ nanocomposite-based electrode displayed an improved rate capability from 29% ($\text{Ni}_3(\text{PO}_4)_2$) to 78% capacity retention with a maximum specific capacity of 478 C g^{-1} at 1 A g^{-1} . The assembled 0.1 NAg//AC-based supercapattery attained a high energy density of 32.4 Wh kg^{-1} at a power density of 399.5 W kg^{-1} [56]. The electrochemical study on $\text{NiS}_2/\text{NiV}_2\text{S}_4//\text{AC}$ electrode supercapattery operated within a cell voltage of 1.6 V with good specific capacity (C_{sp}) value of 78 C g^{-1} (141.8 F g^{-1} at 0.5 A g^{-1}) and displayed high specific energy of 19.4 Wh kg^{-1} at a specific power of 140 W kg^{-1} . Furthermore, the hybrid device exhibited outstanding cycling stability of 90% for 10,000 charge–discharge cycles at a current density of 6 A g^{-1} [58].

The above discussions revealed that a good prospect of supercapattery electrodes is possible in the near future. There is a broad scope for research in the integration of hybrid supercapatteries with solar cells that could be flexible, lightweight, robust, and compact.



13.4 Market potential

This section aims to present a forecast of the market for supercapatterybased on the research and development in the past two decades concerning the understanding and enhancement of supercapattery performances.

The rapid decrease of the fossil fuels, rising demands of the electronic devices for numerous applications, and the intermittency of the renewable energy resource have incited society to build integrated energy storage systems [59]. The market for stationary batteries in several countries is increasing even though there are doubts about their prosperity. The necessity for power and energy storage is continuously growing throughout the world market. Technology is emerging with high speed, but well-known power devices are unable to handle the required necessities [54]. Supercapacitors have kindled great scientific attention due to their significance for energy storage [37]. Contemporary applications involve the automotive industry, hybrid transportation systems globally, grid stabilization, utility vehicles, and rail-system power models. The nearest future application for supercapattery is in energy storage and rapid charging. Many applications of this sort have already hit the market, and are transforming how we reflect on energy storage. Probably, the most crucial contemplation in our market economy is the price related to manufacturing conversion and storage devices, such as photovoltaic cells and batteries, which are now determined by both the abundance of the materials and the manufacturing processes [60]. It is necessary to think about sustainability, renewability, and green chemistry when picking materials for storage devices (e.g., electrodes, catalysts), particularly when used in applications with huge markets and volume (vehicles, grid) [47].

The supercapattery market is incentivized by the intensifying requirements for renewable energy solutions and reliability in the power output from the grid. As we discussed in the previous section, the supercapattery is a growing technology for several energy storage systems, and it is a member of the supercapacitor family, with its characteristic of possessing higher power density than batteries at the same time as having higher energy density compared with capacitors [7]. Supercapattery has a dominant market for the integration of solar PV panels and solar lighting devices. In general, power production through solar panels functions in both online and offline mode for which supercapatteries and supercapacitors are dependable choices. The supercapacitor market is expected to increase about 20% by 2020, and the requirement for this material is projected to reach around 416,000 units [61]. Supercapacitors evolved into supercapattery (hybrid device) with the development of contemporary nanomaterials, and the high energy and power density of supercapatteries have unlocked new application avenues. The potential of a supercapattery is being explored in a wide range of applications from portable electronics to hybrid electric vehicles (EV) [62].

Onsite electricity storage systems are found to be viable to upgrade the self-consumption ratios of electricity. To date, the lithium-ion batteries are being widely used for such technology [40]. However, the production capacities raised from the market uptake of EV seemed to lower the rates for lithium-ion battery packs which have been reported to have decreased from 320 US\$ kWh⁻¹ to 110 \$ kWh⁻¹ in 2020 [1,3]. This phenomenon subsequently resulted in the price drop of second-life batteries obtained from EV and Fisch-Haber et al. reported that the rate of these batteries would be priced at 55 US\$ kWh⁻¹ in 2020 [13,21]. Batteries for the improvement of self-consumption guarantee a better potential than the optimal scheduling of current appliances. An investigation conducted on 415 domestic households in Austria and Germany found that a 7.5 kWh battery can increase the self-consumed electricity of a 5 kW PV system by about 1000 kWh year⁻¹ on average [17].

The projected economic performance of PV battery has been the primary influence in the majority of the households [22,63,64]. Its economic performance is chiefly governed by the technology costs, regulatory regime, end-consumer electricity prices, insolation, and self-consumption ratio. The household electricity consumption directly affects the self-consumption ratio and is concurrently influenced by electricity consumption of advanced technology. Among the new technologies that have caught the attention of consumers are heat pumps and EV [47].

However, the emphasis is almost solely on electric cars. The EV's charging pattern has low compatibility with the PV production and has caused only a limited potential for enhanced self-consumption. The vehicle's battery is commonly charged in the late afternoon as a normal routine for a worker to return home. Since PV power could be temporarily stored to charge the EV and indirectly contributes to the economic progress, the market for an EV is worth noting, among other technologies. Due to its present dynamic diffusion, the deliberations of self-consumption enhancing technologies principally concentrates on stationary batteries [65].

Provided the vast market potential there appears to be in Southeast Asia, it is important to find the key drivers and impediments for the WHP market enlargement so that the related investors can well apprehend the developing tendency of WHP technologies. In Southeast Asia, the WHP market is determined on four major factors, namely, increasing electricity price and demand, government regulation and incentives, original equipment manufacturer (OEM)'s uptake of products, and supplier's

technology enhancement. These are recognized as the key growth drivers for WHP market development [61]. These key drivers are acknowledged mainly through the literature review below (Fig. 13.5).

The supercapacitors' market worldwide was estimated to be US\$ 834.33 million in 2019. The market is projected to reach US\$ 2.66 billion by 2025, registering a CAGR of 21.8%, from 2020 to 2025. Supercapacitors are at present replacing batteries in conventional electric cars as a consequence of their to its rapid charging and temperature stability properties. Besides, supercapacitors are more adaptable than traditional batteries and their highly stable power supply trait will create a significant demand for numerous applications in the developing markets, namely portable media gadgets, GPS, personal laptops, and mobile devices [61].

As the development of technology is significantly and vastly progressing, a renewable energy solution is getting higher in demand and consequently boost the market. As stated in the prior sections, supercapacitors are now classified as a developing technology for wide-ranging variations of the energy storage system. Supercapacitors hold higher power density in comparison with batteries and could present greater energy density than conventional capacitors [20]. Amongst the possible spheres for the application of supercapacitors are the solar PV panels and solar lighting. Since solar panels can be utilized in both online and offline modes, supercapacitors are discovered to be the right choice for this purpose [66].

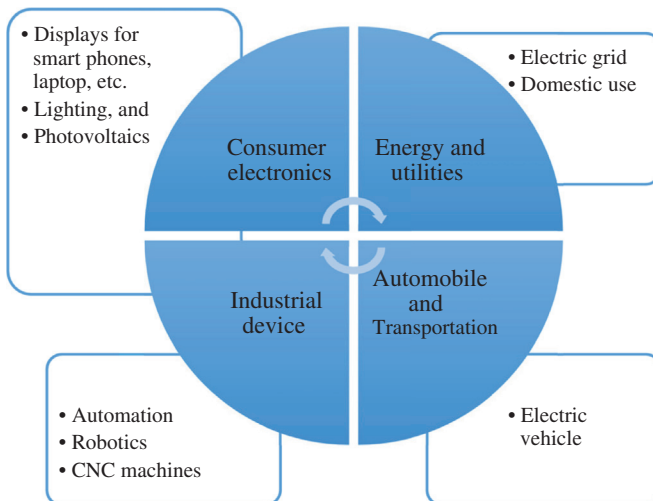


Figure 13.5 Market segments for supercapacities based on end user.

With a conservative prediction of 40% diffusion of supercapacitors in the market by 2020, the requirement for this sector is projected to touch approximately 416,000 units [61]. However, the higher cost imposed by supercapacitors has constrained the market from rising, although they have exceptional characteristics when compared to the traditional batteries [18]. End users are anticipating the supercapacitors to be priced at the range of lead–acid batteries to make it economically workable. Consequently, supercapacitors have fallen short of accomplishing the economic scale, a radical decrease in price is required [61].

The market for supercapatteries is wide in countless applications. One of the important markets is in the utilities. As the global energy crisis is giving more consideration toward the environmental issues, renewable energy in time will replace the use of fossil fuels for energy production [1]. Supercapacitors are among one of the answers to effectively store and recycle energy, as they can store energy originated from renewable sources like wind, tide, and solar.

One of the leading players in supercapacitors, Maxwell Technology, presented a grid energy storage subsystem in 2018 with a collaboration from Siemens to provide a cost-effective and efficient grid voltage and frequency support solution. A report by US Energy Storage Monitor Utility indicated that the scale energy storage is assured and the flourishing market of EES is anticipated to reach beyond US\$ 1 billion in 2020 in the United States alone. This consequently would provide a considerable market for supercapacitors. Further, supercapacitors are also used in security systems, such as for alarms, uninterruptible power supply (UPS) systems, as well as in solar power. Germany supported this technology by endorsing the use of supercapacitors in 80% of their customers with smart meters in 2020 [61].

The industry for automotives is swiftly mounting in China, and the government looks at this market as one of their pillar industries. It is projected by the Central Government of China that its automotive industry productivity would touch 30 million units by 2020 and would reach about 35 million units by 2025. The utilization of EV is developing internationally, and China is considered as the foremost adopter of the EV with their admirable technology development. China is also devoting billions of yuans to transport systems comprising a national high-speed railway network, bus rapid transit, and subways. Furthermore, China also contributed its technology for Shenzhen to follow improved bus systems. The World Resource Institute reported that Shenzhen received a subsidy

of US\$ 150,000 for each bus before 2016, which is more than 50% of each one. Besides, the utility workers in Japan are also integrating smart electricity meters as advised by their government to emphasize energy efficiency [61].

Five foremost contenders in the market own the supercapacitor and supercapattery business globally. They are Eaton Corporation PLC (Ireland), Maxwell Technologies Inc., (USA), Skeleton Technologies Inc., (Germany), Cap-XX Limited (Australia), and AVX Corporation (USA). The supercapacitors' market is challenging and competitive as it involves many major contenders. Some of the major contenders are presently overshadowing the market, and they are concentrating on the enlargement of the consumer base throughout foreign countries.

The above situation of the market requirements for this emerging field of energy storage systems, especially supercapattery, has motivated research to reach greater heights. These prospects for the supercapattery will undoubtedly pave the way for further progression and investments from many industry contenders. Moreover, this will encourage the researchers from institutes and universities to do more study and research in advancing this hybrid battery-supercapacitor energy storage system, which can have superior energy and power densities along with more capacity retention time.



13.5 Conclusion

This chapter elaborates the challenges and prospects in supercapattery and provides an insight into the need for supercapattery in our systems. The market potential of supercapattery, along with the market trend of supercapattery, have been reported. Though many established energy storage technologies are available, supercapattery has emerged as an eco-friendly and sustainable technology for the future. It is clear from all the research data that supercapattery is diverse and effective in various applications. The need for research in supercapattery can be justified by the limitations of the existing EESD. It is essential to develop supercapattery systems to overcome the drawbacks of EDLC or pseudocapacitors in order to increase the applicability range. Supercapattery can achieve more feasible and sustainable energy storing devices than the supercapacitors or LIB (lithium-ion batteries). Hence, the properties of these hybrid materials

can be altered based on the desired amount/capacity of each parameter according to the requirements of the end-product. Successful implementation of supercapattery in most of the typical applications such as solar power and EV/hybrid cars, consumer electronics, and industrial equipment depends majorly on the physicochemical characterization and type of electrode materials. Ultimately, this chapter delivers the existing challenges in the supercapattery field. In summary, the supercapattery possesses the high-energy potentiality of conventional batteries by using redox-active battery-grade materials as the positive electrode and the high-power delivery capability from carbonaceous materials as the negative electrode. There is a wide scope for research in the development of new advanced materials for supercapattery electrodes, which leads to a sustainable future.

Acknowledgments

Financial support from the Tenaga Nasional Berhad, UNITEN R&D Sdn.Bhd. (U-TV-RD-18–30), Universiti Tenaga Nasional (UNITEN) is gratefully appreciated. The TNB Seed Fund Program supported this study through the UNITEN R&D Sdn.Bhd. (URND) of the Universiti Tenaga Nasional (UNITEN) funded by the Tenaga Nasional Berhad, Malaysia.

References

- [1] L. Yu, G.Z. Chen, Supercapatteries as high-performance electrochemical energy storage devices, *Electrochem. Energy Rev.* (2020). Available from: <https://doi.org/10.1007/s41918-020-00063-6>.
- [2] E. Duraisamy, A. Prasath, V.S. Devi, M.N.M. Ansari, P. Elumalai, Sustainably-derived hierarchical porous carbon from spent honeycomb for high-performance lithium-ion battery and ultracapacitors, *Energy Storage* (2020) e136. Available from: <https://doi.org/10.1002/est.2.136>.
- [3] B. Akinwolemiwa, G.Z. Chen, A fundamental consideration for electrochemical engineering of supercapattery, *J. Brazil Chem. Soc.* 29 (5) (2018) 960–972.
- [4] P. Simon, Y. Gogotsi, B. Dunn, Where do batteries end and supercapacitors begin? *Science* 343 (6176) (2018) 1210–1211. Available from: <https://doi.org/10.1126/science.1249625>.
- [5] H.I. Bekker, V. Ferry, Low Voltage Electrolytic Capacitor. U.S. Patent, New York, 1957.
- [6] G.Z. Chen, Supercapacitor and supercapattery as emerging electrochemical energy stores, *Int. Mater. Rev.* 62 (4) (2017) 173–202. Available from: <https://doi.org/10.1080/09506608.2016.1240914>.
- [7] B. Saravanakumar, X. Wang, W. Zhang, L. Xing and W. Li. Holey two dimensional manganese cobalt oxide nanosheets as a high-performance electrode for supercapattery. *Chem. Eng. J.* 373, (2019) 547–555. <https://doi.org/10.1016/j.cej.2019.05.080>.

- [8] S. Balasubramaniam, A. Mohanty, S.K. Balasingam, S.J. Kim, A. Ramadoss, Comprehensive insight into the mechanism, material selection and performance evaluation of supercapatteries, *Nano-Micro Lett.* 12 (2020) 85. Available from: <https://doi.org/10.1007/s40820-020-0413-7>.
- [9] J. Hou, C. Cao, F. Idrees, et al., Hierarchical porous nitrogen doped carbon nanosheets derived from silk for ultrahigh-capacity battery anodes and supercapacitors, *ACS Nano* 9 (2015) 2556–2564. Available from: <https://doi.org/10.1021/nm506394r>.
- [10] A. Lewandowski, A. Olejniczak, M. Galinski, et al., Performance of carbon–carbon supercapacitors based on organic, aqueous and ionic liquid electrolytes, *J. Power Sources* 195 (2010) 5814–5819. Available from: <https://doi.org/10.1016/j.jpowsour.2010.03.082>.
- [11] X.H. Zhou, C. Peng, G.Z. Chen, 20V stack of aqueous supercapacitors with carbon (–), titanium bipolar plates and CNT polypyrrole composite (+), *AlChE J.* 58 (2012) 974–983. Available from: <https://doi.org/10.1002/aic.12632>.
- [12] Z.H. Huang, Y. Song, X.X. Xu, et al., Ordered polypyrrole nanowire arrays grown on a carbon cloth substrate for a high performance pseudocapacitor electrode, *ACS Appl. Mater. Inter.* 7 (2015) 25506–25513. Available from: <https://doi.org/10.1021/acsami.5b08830>.
- [13] L. Yu, G.Z. Chen, Redox electrode materials for supercapatteries, *J. Power Sources* 326 (2016) 604–612. Available from: <https://doi.org/10.1016/j.jpowsour.2016.04.095>.
- [14] S. Ortoboy, J.P. Alper, F. Rossi, et al., MnOx-decorated carbonized porous silicon nanowire electrodes for high performance supercapacitors, *Energy Environ. Sci.* 10 (2017) 1505–1516. Available from: <https://doi.org/10.1039/c7ee00977a>.
- [15] H.T. Zhou, X.H. Wang, H. Sheridan, et al., Boosting the energy density of 3D dual-manganese oxides-based li-ion supercabattery by controlled mass ratio and charge injection, *J. Electrochem. Soc.* 163 (2016) A2618–A2622. Available from: <https://doi.org/10.1149/2.0691613jes>.
- [16] J. Iqbal, A. Numan, S. Rafique, R. Jafer, S. Mohamad, K. Ramesh, et al., High performance supercapattery incorporating ternary nanocomposite of multi-walled carbon nanotubes decorated with Co₃O₄ nanograins and silver nanoparticles as electrode materials, *Electrochim. Acta* 278 (2018) 72–82. Available from: <https://doi.org/10.1016/j.electacta.2018.05.040>.
- [17] S. Zhang, N. Pan, Supercapacitors performance evaluation, *Adv. Energy Mater.* 5 (2015). Available from: <https://doi.org/10.1002/aenm.201401401>. 1401401.
- [18] K. Khan, A.K. Tareen, M.A.A.Q. Khan, Y. Zhang, Z. Ouyang, Z. Guo, et al., Going green with batteries and supercapacitor: two dimensional materials and their nanocomposites-based energy storage applications, *Prog. Solid. State Chem.* (2020). Available from: <https://doi.org/10.1016/j.progsolidstchem.2019.100254>.
- [19] Z. Liu, Y. Huang, Q. Yang, X. Li, Z. Huang, C. Zhi, Voltage issue of aqueous rechargeable metal-ion batteries, *Chem. Soc. Rev.* 49 (2020) 180–232. Available from: <https://doi.org/10.1039/c9cs00131j>.
- [20] T.M. Gur, Review of electrical energy storage technologies, materials and systems: challenges and prospects for large-scale grid storage, *Energy Environ. Sci.* (2018). Available from: <https://doi.org/10.1039/C8EE01419A>.
- [21] B. Evanko, S.J. Yoo, J. Lipton, Stackable bipolar pouch cells with corrosion-resistant current collectors enable high-power aqueous electrochemical energy storage, *Energy Environ. Sci.* 11 (2018) 2865–2875. Available from: <https://doi.org/10.1039/c8ee00546j>.
- [22] A.A. Alguail, A.H. Al-Eggiely, B.N. Grgur, Polyaniline–lead sulfate based cell with supercapattery behavior, *J. Saudi Chem. Soc.* 21 (2017) 575–582. Available from: <https://doi.org/10.1016/j.jscs.2017.01.002>.

- [23] B. Pal, S. Yang, S. Ramesh, V. Tangadurai, R. Jose, Electrolyte selection for supercapacitive devices: a critical review, *Nanoscale Adv.* 1 (2019) 3807. Available from: <https://doi.org/10.1039/c9na00374f>.
- [24] J. Lin, Y. Yan, X. Zheng, Z. Zhong, Y. Wang, J. Qi, et al., Designing and constructing core-shell $\text{NiCo}_2\text{S}_4/\text{Ni}_3\text{S}_2$ on Ni foam by facile one-step strategy as advanced battery-type electrodes for supercapattery, *J. Colloid Interface Sci.* 536 (2019) 456–462. Available from: <https://doi.org/10.1016/j.cis.2018.10.072>.
- [25] Q. Hu, M. Tang, M. He, N. Jiang, C. Xu, D. Lin, et al., Core-shell MnO_2/CoS nanosheets with oxygen vacancies for high-performance supercapattery, *J. Power Sources* 446 (2020) 227335. Available from: <https://doi.org/10.1016/j.jpowsour.2019.227335>.
- [26] L. Song, Y.H.F. Guo, Y. Jiao, Y. Li, Y. Liu, F. Gao, Mesoporous nickel-based zeolite capsule complex with Fe_3O_4 as electrode for advanced supercapacitor, *J. Nanomater.* Volume 2018 (2018). Available from: <https://doi.org/10.1155/2018/9813203>. Article ID 9813203.
- [27] K.O. Oyedotun, M.J. Madito, D.Y. Manyala, Synthesis of ternary NiCo-MnO_2 nanocomposite and its application as a novel high-energy supercapattery device, *Chem. Eng. J.* 335 (2018) 416–433. Available from: <https://doi.org/10.1016/j.cej.2017.10.169>.
- [28] V.S. Devi, M. Athika, E. Duraisamy, A. Prasath, A.S. Sharma, P. Elumalai, Facile sol-gel derived nanostructured spinel Co_3O_4 as electrode material for high-performance supercapattery and lithium-ion storage, *J. Energy Storage* 25 (2019) 100815. Available from: <https://doi.org/10.1016/j.est.2019.100815>.
- [29] A. Eatemadi, H. Daraee, H. Karimkhanloo, M. Kouhi, N. Zarghami, A. Akbarzadeh, et al., Carbon nanotubes: properties, synthesis, purification and medical applications. *Nanoscale Res. Lett.* 9 (393), 2014. Available from: <http://www.nanoscalelett/content/9/1/393>.
- [30] C. Lekakou, O. Moudam, F. Markoulidis, T. Andrews, J.F. Watts, G.T. Reed, Carbon-based fibrous EDLC capacitors and supercapacitors, *J. Nanotechnol.* 2011 (2011). Available from: <https://doi.org/10.1155/2011/409382>. Article ID 409382.
- [31] Y. Chen, J. Wang, H. Liu, M.N. Banis, R. Li, X. Sun, T-K. Sham, et al., Nitrogen doping effects on carbon nanotubes and the origin of the enhanced electrocatalytic activity of supported Pt for proton-exchange membrane fuel cell. 2011. Available from: <https://doi.org/10.1021/jp108864y>.
- [32] J. Hong, H. Gwon, S. Jung, Ku, K. Kang, *Electrochemical energy storage: next generation battery concepts*, *Electrochem. Soc.* 162 (2015) A2447–A2467.
- [33] H. Shao, N. Padmanathan, D. McNulty, C. O'Dwyer, K.M. Razeeb, Supercapattery based on binder-free $\text{Co}_3(\text{PO}_4)_2 \cdot 8\text{H}_2\text{O}$ multilayer nano/microflakes on nickel foam, *ACS Appl. Mater. Interfaces* 2016 (8) (2016) 28592–28598. Available from: <https://doi.org/10.1021/acsami.6b08354>.
- [34] J.M. Baptista, J.S. Sagu, U. Wijayantha, K.G.K. Lobato, Performance metrics and obstacles for the transition from lab to industrial scale – a critical approach, *Chem. Eng. J.* 374 (2019) 1153–1179. Available from: <https://doi.org/10.1016/j.cej.2019.05.207>.
- [35] L. Yu, G.Z. Chen, Ionic liquid-based electrolytes for supercapacitor and supercapattery, *Front. Chem.* (2019). Available from: <https://doi.org/10.3389/fchem.2019.00272>.
- [36] V. Egorov, C. O'Dwyer, Architected porous metals in electrochemical energy storage, *Curr. Opin. Electrochem.* 21 (2020) 201–208. Available from: <https://doi.org/10.1016/j.coelec.2020.02.01>.
- [37] R. Zhang, A. Palumbo, J.C. Kim, J. Ding, E.-H. Yang, Flexible graphene-, graphene-oxide-, and carbon-nanotube-based supercapacitors and batteries, *Ann. Phys.* (2019). Available from: <https://doi.org/10.1002/andp.201800507>. 1800507.

- [38] W. Raza, F. Raza, Y. Luo, K.-H. Kim, J. Yang, S. Kumar, et al., Recent advancements in supercapacitor technology, *Nano Energy* 52 (2018) 441–473. Available from: <https://doi.org/10.1016/j.nanoen.2018.08.013>.
- [39] L. Xia, L. Yu, D. Hu, G.Z. Chen, Electrolytes for electrochemical energy storage, *Mater. Chem. Front.* 1 (2017) 584–618. Available from: <https://doi.org/10.1039/C6QM00169F>.
- [40] X. Hu, W. Zhang, X. Liu, Y. Mei, Y. Huang, Nanostructured Mo-based materials for electrochemical energy storage, *Chem. Soc. Rev.* 44 (2015) 2376. Available from: <https://doi.org/10.1039/c4cs00350k>.
- [41] S. Biswas, A. Senju, R. Mohr, T. Hodson, N. Karthikeyan, K.W. Knehr, et al., Minimal architecture zinc-bromide battery for low cost electrochemical energy storage, *Energy Environ. Sci.* (2016). Available from: <https://doi.org/10.1039/C6EE02782B>.
- [42] M.Z. Iqbal, S. Alam, A.M. Afzal, M.J. Iqbal, K. Yaqoob, M.A. Kamran, et al., Binary composites of strontium oxide/polyaniline for high performance supercapattery devices, *Solid. State Ion.* 347 (2020) 115276. Available from: <https://doi.org/10.1016/j.ssi.2020.115276>.
- [43] Y.K. Lee. The effect of active material, conductive additives, and binder in a cathode composite electrode on battery performance. *Energies* 13, (2019) 658. Available from: <https://doi.org/10.3390/en12040658>.
- [44] X. Yan, Y. Zhang, K. Zhu, Y. Gao, D. Zhang, G. Chen, et al., Enhanced electrochemical properties of TiO₂(B) nanoribbons using the styrene butadiene rubber and sodium carboxyl methyl cellulose water binder, *J. Power Sources.* 246 (2014) 95–102. Available from: <https://doi.org/10.1016/j.jpowsour.2013.07.072>.
- [45] C. Peng, S. Zhang, D. Jewell, G.Z. Chen, Carbon nanotube and conducting polymer composites for supercapacitors, *Prog. Nat. Sci.* 18 (2008) 777–788. Available from: <https://doi.org/10.1016/j.pnsc.2008.03.002>.
- [46] P. Sengodu, A.D. Deshmukh, Conducting polymers and their inorganic composites for advanced Li-ion batteries: a review, *RSC Adv.* 5 (2015) 42109–42130. Available from: <https://doi.org/10.1039/C4RA17254J>.
- [47] P.V. Shinde, N.M. Shinde, J.M. Yun, R.S. Mane, K.H. Kim, Facile chemical synthesis and potential supercapattery energy storage application of Hydrangea-type Bi₂MoO₆, *ACS Omega* 4 (2019) 11093–11102. Available from: <https://doi.org/10.1021/acsomega.9b00522>.
- [48] K.J. Samdani, H.P. Jeong, W.J. Dong, T.L. Kang, Self-assembled Bi₂MoO₆ nanopetal array on carbon spheres toward enhanced supercapacitor performance, *ACS Sustain. Chem. Eng.* 6 (12) (2018) 16702–16712. Available from: <https://doi.org/10.1021/acssuschemeng.8b03988>.
- [49] L. Deng, J. Wang, G. Zhu, L. Kang, Z. Hao, Z. Lei, et al., RuO₂/graphene hybrid material for high performance electrochemical capacitor, *J. Power Sources* 248 (2014) 407–415.
- [50] L. Lin, S. Tang, S. Zhao, X. Peng, Ning Hu, Hierarchical three-dimensional FeCo₂O₄@MnO₂ core-shell nanosheet arrays on nickel foam for high-performance supercapacitor, *Electrochim. Acta* 228 (2017). Available from: <https://doi.org/10.1016/j.electacta.2017.01.022>.
- [51] L. Deng, J. Liu, Z. Ma, G. Fan, Z.H. Liu, Free-standing graphene/bismuth vanadate monolith composite as a binder-free electrode for symmetrical supercapacitors, *RSC Adv.* 8 (2018) 24796–24804. Available from: <https://doi.org/10.1039/C8RA04200D>.
- [52] M.N. Rantho, M.J. Madito, N. Manyala, Symmetric supercapacitor with supercapattery behavior based on carbonized iron cations adsorbed onto polyaniline, *Electrochim. Acta* 262 (2018) 82–96. Available from: <https://doi.org/10.1016/j.electacta.2018.01.001>.

- [53] D. Larcher, J.-M. Tarascon, Toward greener and more sustainable batteries for electrical energy storage, *Nat. Chem.* Volume 7 (2014). Available from: <https://doi.org/10.1038/NCHEM.2085>.
- [54] Z.A. Shaikh, P.V. Shinde, S.F. Shaikh, A.M. Al-Enizi, R.S. Mane, Facile synthesis of $\text{Bi}_2\text{O}_3@\text{MnO}_2$ nanocomposite material: a promising electrode for high performance supercapacitors, *Solid. State Sci.* 102 (2020) 106158. Available from: <https://doi.org/10.1016/j.solidstatesciences.2020.106158>.
- [55] A. Deepi, G. Srikesh, A.S. Nesaraj, Electrochemical performance of Bi_2O_3 decorated graphene nanocomposites for supercapacitor applications, *Nano-Structures Nano-Objects* 15 (2018) 10–16. Available from: <https://doi.org/10.1016/j.nanos.2018.03.003>.
- [56] F.S. Omar, A. Numan, S. Bashir, N. Duraisamy, R. Vikneswaran, Y.-L. Loo, et al., Enhancing rate capability of amorphous nickel phosphate supercapattery electrode via composition with crystalline silver phosphate, *Electrochim. Acta* 273 (2018) 216–228. Available from: <https://doi.org/10.1016/j.electacta.2018.03.136>.
- [57] S. Lalwani, A. Joshi, G. Singh, R.K. Sharma, Sulphur doped iron cobalt oxide nanocaterpillars: an electrode for supercapattery with ultrahigh energy density and oxygen evolution reaction, *Electrochim. Acta* 328 (2019) 135076. Available from: <https://doi.org/10.1016/j.electacta.2019.135076>.
- [58] R. Manikandan, C.J. Raj, K.H. Yu, B.C. Kim, Self-coupled nickel sulfide@nickel vanadium sulfide nanostructure as a novel high capacity electrode material for supercapattery, *Appl. Surf. Sci.* 497 (2019) 143778. Available from: <https://doi.org/10.1016/j.apsusc.2019.143778>.
- [59] H. Yang, Effects of supercapacitor physics on its charge capacity. *IEEE Trans. Power Electron.* 34 (1), 2019, 646–658. Available from: <https://doi.org/10.1109/TPEL.2018.2812882>.
- [60] I. Heng, F.W. Low, C., W. Lai, J.C. Juan, N. Amin, S.K. Tiong, High performance supercapattery with rGO/TiO₂ nanocomposites anode and activated carbon cathode, *J. Alloy. Compd.* 796 (2019) 13–24. Available from: <https://doi.org/10.1016/j.jallcom.2019.04.347>.
- [61] Mordor intelligence, <<https://www.mordorintelligence.com/industryreports/supercapacitor-market>> (accessed 1.05.20).
- [62] A. Mansour, C.H. Mohamed, B. Faouzi, Experimental study of a pack of supercapacitors used in electric vehicles, *Sci. World J.* (2017). Available from: <https://doi.org/10.1155/2017/6702838>. Article ID 6702838.
- [63] C.J. Akash, S.D. Zade, Disease prediction using machine learning, *Int. Res. J. Eng. Technol.* (2019). e-ISSN: 2395-0056.
- [64] C. Wang, J. Zhou, F. Du, Synthesis of highly reduced graphene oxide for supercapacitor, *J. Nanomater.* (2016). Available from: <https://doi.org/10.1155/2016/4840301>. Article ID 4840301.
- [65] R. Fachrizal, J. Munkhammar, Improved photovoltaic self-consumption in residential buildings with distributed and centralized smart charging of electric vehicles, *Energies* 13 (2020) 1153. Available from: <https://doi.org/10.3390/en13051153>.
- [66] B.K. Kim, S. Sy, A. Yu, J. Zhang, Electrochemical supercapacitors for energy storage and conversion, in: J. Yan. (Ed.), *Handbook of Clean Energy System*, 2015. Available from: <http://doi.org/10.1002/9781118991978.hces112>.

Index

Note: Page numbers followed by “f” and “t” refer to figures and tables, respectively.

A

AC. *See* Activated carbon (AC)
AC/CFP. *See* Activated carbon on carbon filter paper (AC/CFP)
Acetonitrile, 34–35
Activated carbon (AC), 50, 93, 94f, 102–107, 215–216, 311–312, 361
 electrochemical performance of NS@NVS//N,O-AC supercapattery, 105f
 nanocomposites, 184
Activated carbon on carbon filter paper (AC/CFP), 327
Activated graphene (AG), 317
Activated graphite fibers (EAGFs), 212
Active nanofillers, 282–283
Adsorption, 264–265
AEO-AC. *See* Alcohol ethoxylate–acryloyl chloride (AEO-AC)
AG. *See* Activated graphene (AG)
Agar–agar, 278
Alcohol ethoxylate–acryloyl chloride (AEO-AC), 295–296
Alkaline polymer gel electrolyte, 319
Aluminium ion batteries, 23
Aluminum oxide (Al_2O_3), 282
Amorphous nickel–cobalt–manganese hydride (NiCoMn-OH), 190
Aniline, 290
Anion exchange, 208, 335
Anionic clay, 199–200
Annealing process, 118–119
Anode, 5–6, 355–356
Aqueous electrolytes, 29–30, 258–259, 273–274, 357–358
Aqueous liquids, 273
Aromatic C-polymers, 66
Arrhenius theory, 276
Asymmetric supercapacitors (ASCs), 213, 233f, 312

B

Bacterial cellulose–PPy hydrogel composites, 291–292
Barium titanate (BaTiO_3), 283
Battery technology, traditional. *See also* Rechargeable batteries
 flow batteries, 21–22
 metal–air batteries, 22
 molten salt batteries, 22
Battery-grade
 electrode materials, 49
 materials, 51–58
 transition metal oxides, 55
Battery/batteries, 5–6, 6f, 8–9, 311
 electrode, 51–52
 flow, 14–15, 15f, 21–22
 Li-ion, 2–4, 259–260
 Li-ion solid-state, 23
 Li-oxygen, 4–5
 metal–air, 18, 22
 Na-S, 2–4, 15
Binary metal oxides (BMOs), 113–131, 115f, 132t
 for supercapattery applications, 120–131, 133t
 synthesis, 115–120, 117t
 electrodeposition method, 118–119
 hydrothermal/solvothermal technique, 115–116
 microwave-assisted technique, 116
 sonochemical method, 117–118
 template method, 119–120
Binder-free Ni–Co LDH electrode, 212–216
 cyclic voltammetry curves
 of hybrid supercapacitor, 214f
 of NiCo-LDH@NG/CC//NG/CC ASC device, 216f
 fabrication of NiCo-LDH on 3D porous Ni arrays, 215f

- Binder-free Ni–Co LDH electrode
(*Continued*)
synthetic route showing NiCo-SDBS-LDH@CFC, 213*f*
- Biodegradable host polymer, 277–278
- Biodegradable polymers, 277–278
- Biopolymers, 278
- Biosensors, 63–64
- Bipolar stacking, 359
- Blending, 284
- Block copolymers, 119–120
- BMOs. *See* Binary metal oxides (BMOs)
- 1-Butyl-1-methylpyrrolidinium tri(pentafluoroethyl)trifluorophosphate (BMPyrFAP), 102–103
- C**
- C-polymer/carbon/metal oxide, 80
- C-polymers. *See* Conducting polymers (CPs)
- CAES. *See* Compressed air energy storage (CAES)
- Calcination process, 116
- Calcium ion batteries, 23
- Capacitance, 53–54
- Capacitive behavior, 51
- Capacitive electrode, 47–48
material, 49
- Capacitive faradaic storage (CFS), 175
- Capacitive materials, 49–54
- Capacitors, 5–6
- Carbon, 255
aerogel microspheres, 322
black, 283
cloth, 290–291
surface morphology, 291*f*
coating, 356–357
composites, 314–315
doping, 356–357
materials, 141–142, 151–152
- Carbon fiber cloth (CFC), 213
- Carbon fiber fabric (CFF), 317
- Carbon material/LDH composites for supercapattery, 237–245
Co–Al LDH/rGO-3//AC ASC, 244*f*
formation process and structure of LDH/graphene composite, 243*f*
scanning electron microscope images, 240*f*
step-by-step growth of
nickel–aluminum LDH composite, 239*f*
- Carbon nanotubes (CNTs), 50, 93, 94*f*,
98–102, 99*f*, 151–154, 179–180,
201, 258–259, 283, 311–312, 341,
361
charge–discharge mechanism in
symmetric supercapattery device,
101*f*
fabrication of CNT–CuCo₂O₄@Ag||
AC supercapattery device, 103*f*
FESEM images, 100*f*
gold-containing ternary nanocomposites,
154
proton adsorption and intercalation,
104*f*
silver-containing ternary
nanocomposites, 153–154
- Carbon-based C-polymer composite, 78
- Carbon-based materials, 29–30, 182
- Carbon-based nanocomposite materials,
77–78
- Carbon-based nanoparticles, 283
- Carbon-based nanostructures, 77–78
- Carbonaceous C-polymer composite
materials, 73–74
- Carbonaceous electrode materials
AC and composites, 102–107
CNTs and composites, 98–102
graphene and composites, 95–98
- Carbonaceous materials, 50, 93, 94*f*, 106*t*,
151–158
CNTs, 152–154
GN, 155–158
- Carbonaceous nanocomposites for
supercapattery
carbonaceous electrode materials,
95–107
- Carbonaceous–polymer nanocomposites,
73–74
morphologies of carbonaceous
nanomaterials, 74*f*
- Carboxymethyl cellulose (CMC), 316–317
- Cathode, 5–6, 355–356

- CBD method. *See* Chemical bath deposition method (CBD method)
- CDP. *See* Cyclodextrin polymer (CDP)
- Cellulose, 278
- Cellulose acetate, 278
- Ceramic nanofillers. *See* Active nanofillers
- Ceramic nanoparticles, 282
- Ceramic-based solid polymer electrolyte (PEO/LiTFSI/LiAlO₂), 281–282
- CFC. *See* Carbon fiber cloth (CFC)
- CFF. *See* Carbon fiber fabric (CFF)
- CFS. *See* Capacitive faradaic storage (CFS)
- Chalcogenide–polymer nanocomposite, 74–75
- Chalcogenides SCAPs, 334–339
preparation of NiS hollow cubes, 335*f*
- Charge storage capacity, 357–359
- Charge storage mechanism, 202
in EDLCs, 31–32
in EES systems, 48–52
battery electrode, 51–52
electrical double-layer capacitive electrode, 50
pseudocapacitive electrode, 50–51
- Charge transfer reactions, 175
- Charge–discharge mechanisms, 202, 351
- Chemical bath deposition method (CBD method), 316–317
- Chemical energy
stockpiling, 6–7
storage, 18
- Chemical vapor deposition, 330
- Chitosan, 278
- CMC. *See* Carboxymethyl cellulose (CMC)
- CNTs. *See* Carbon nanotubes (CNTs)
- CNTs onto Ni Foams (CNT/NF), 328–329
- CNTs@manganese dioxide (MnO₂), 294
- Co–Al LDH. *See* Cobalt–Aluminum layered double hydroxides (Co–Al LDH)
- Cobalt (Co), 210
- Cobalt ferrites (CoFe₂O₄), 128
- Cobalt oxide (Co₃O₄), 120–121, 153–154, 185–189
Co₃O₄-based mixed oxides, 188–189
Co₃O₄-based nanocomposites, 186–188
SCAB, 321–325
synthesis process of sponge like rGO, 324*f*
- Cobalt–Aluminum layered double hydroxides (Co–Al LDH), 223–226
- Cobaltates (MCo₂O₄), 120–123
- Cobalt–Manganese LDH (Co–Mn LDH), 223–226
- Co–Mn LDH. *See* Cobalt–Manganese LDH (Co–Mn LDH)
- Composites, 95–98
- Compressed air, 13
- Compressed air energy storage (CAES), 13
- Conducting polymers (CPs), 63–64, 70*f*, 141, 158–165
based electrodes, 67–71
insolubility and intractability of, 361–363
nanocomposites of conducting polymer with nanomaterials, 77–85
polymer nanocomposite, 71–77
ternary composites of PANI, 158–163
ternary nanocomposites
of PPy containing noble metals, 163–164
of PTh or polymers containing noble metals, 164–165
types, 64–67
based on conductivity, 65–66
direct fabrication electrode, 83*f*
electrochemical performance of electrode fabrication, 68*t*
structural backbone, 66–67
- Conductive polymers, 29–30, 176
- Conductive woven textile substrate (CWTs), 316–317
- Conductivity, 65–66
extrinsically conducted polymer, 66
intrinsically conducted polymer, 66
- Conventional unitary metal oxides, 114
- Coordination polymer-derived nanomaterials, 320–321
- Copolymerization, 284–285
- Copper cobaltite (CuCo₂O₄), 332–333, 333*f*

- Copper cobaltite (CuCo_2O_4) (*Continued*)
pore access in highly ordered and disordered CuCo_2O_4 mesoporous materials, 122*f*
- Copper oxide (CuO), 181–182
CuO-based mixed oxides and nanocomposites, 182
SCAB, 313–318
cartoon of composite synthesis, 314*f*
growth of CuO nanoflowers on carbon cloth, 318*f*
preparation of flexible CuO/Co(OH)₂/rGO nanotunes, 315*f*
- Copper sulfide (CuS), 334
material, 336
- Copper(II) oxide (CuO), 282
- Coprecipitation method, 330
- Core@LDH core–shell particles, 227–229
- Core–shell 3D conducting hydrogels, 290
- Core–shell LDH, 226–237
CV for Co_3O_4 @LDH/GNS hybrid supercapacitor device, 234*f*
images of LDH-derived nanostructures, 227*f*
LDH-derived core–shell architectures, 228*f*
preparation
of Fe_3O_4 @C@Ni–Al-LDH core–shells, 230*f*
of MnCo_2O_4 @Ni(OH)₂ nanoflowers, 231*f*
route of polyaniline/LDH/carbon cloth core–shell structures, 236*f*
synthesis
of LDH microspheres, 237*f*
of NiCo-LDH@NiOOH core–shell heterostructures, 232*f*
- Corn starch, 278
- CPs. *See* Conducting polymers (CPs)
- Cu(OH)_2 SCAB, 325–327
cartoon representation of the development of Co(OH)_2 , 328*f*
CV curve of state ASCs, 326*f*
- CWTs. *See* Conductive woven textile substrate (CWTs)
- Cyclic voltammetry (CV), 97–98, 97*f*, 147–151, 153–154, 175–176, 202, 362–363
analysis, 295*f*
curves, 46, 186–187
- Cyclodextrin polymer (CDP), 77–78
- ## D
- De/sodiation process, 260–261
- Decaying process, 120–121
- Dedoping process, 52
- Deionized water (DI water), 258
- Delocalized electronic states, 63–64
- Density functional theory (DFT), 154
- Desorption, 264–265
- DFT. *See* Density functional theory (DFT)
- DI water. *See* Deionized water (DI water)
- Diethyl carbonate, 281
- Diffusion
diffusion-controlled process, 56
issues related to electronic property, 356–357
- Dimethyl carbonate (DMC), 281
- Direct synthesis, 203–208
- Dis/charge process, 260–261
- Dispersion, 276–277
- DMC. *See* Dimethyl carbonate (DMC)
- DMF. *See* *N*-dimethylformamide (DMF)
- Doping
degree, 63–64
process, 52
- Double layer capacitance, 35–36, 35*f*, 151–152
- Double-walled carbon nanotubes (DWCNTs), 98–100, 238–239
- DSSC. *See* Dye-sensitized solar cells (DSSC)
- Dunn's formula, 56
- DWCNTs. *See* Double-walled carbon nanotubes (DWCNTs)
- Dye-sensitized solar cells (DSSC), 283
- ## E
- EAGFs. *See* Activated graphite fibers (EAGFs)
- EC. *See* Ethylene carbonate (EC)

- ECP-CNT.
 See Electrocodeposited—carbon nanotube (ECP-CNT)
- EDL. *See* Electrical double layer (EDL)
- EDLC. *See* Electrical double-layer capacitor (EDLC)
- EDLCs. *See* Electrical dual layer capacitors (EDLCs)
- EDLE. *See* Electrical double-layer effect (EDLE)
- EEG. *See* Electrochemical exfoliated graphene (EEG)
- EES. *See* Electrochemical energy storage (EES)
- EESD. *See* Electrochemical energy storage devices (EESD)
- EIS. *See* Electrochemical impedance spectroscopy (EIS)
- Electric energy storage, 6–7
- Electric Power Research Institute (EPRI), 19–20
- Electric power storage, 5–6
- Electric vehicles (EVs), 259–260, 368
- Electrical conductivity, 93
- Electrical double layer (EDL), 29–30, 93, 311
 capacitive electrode, 50
 charge storage device, 271
 formation, 256–257
- Electrical double-layer capacitor (EDLC), 32–37, 50, 67, 111–113, 151–152, 175, 201, 256–257, 271–273, 278, 280–281, 311, 359
- Electrical double-layer effect (EDLE), 111–113
- Electrical dual layer capacitors (EDLCs), 27–28
 with charge separation at electrodes, 33*f*
 charge storage mechanism in, 31–32
 charging and discharging phases of, 33*f*
- Electrically “metal-like” CPs, 142–144
- Electroactive substrates, Ni–Co LDH
 growth on, 216–221
 cyclic voltammetry curves of fabricated HSC, 218*f*
 electrochemical performance of Ni–Co LDH/NF(2)//AC ASC, 219*f*
 fabrication process for synthesis of nickel–cobalt LDH, 220*f*
 FE-SEM, 225*f*
 synthesis process for Co–Mn layered double hydroxides, 224*f*
 XRD spectra obtained from Ni–Mn-LDH-H, 222*f*
- Electrochemical
 performances, 359–361
 processes, 8, 349–350
 signature, 52
 supercapacitors, 111–113
 supercapattery devices, 262
 techniques, 2–4
- Electrochemical capacitors (ECs).
 See Supercapacitors (SCs)
- Electrochemical deposition, 183–184, 327
- Electrochemical energy stockpiling, 6–7
- Electrochemical energy storage (EES), 16–17, 27–28, 111–113, 261–262, 349, 353*f*
 background, 28–29
 charge storage mechanism in EDLCs, 31–32
 ECs, 29–30
 electrical double-layer capacitor, 32–37
 principle of energy storage in ECs, 31
 pseudocapacitor, 37–39
 systems, 45–46
 charge storage mechanism in, 48–52
 and materials, 8–10, 10*f*
 technologies, 93
 types of pseudocapacitance, 39–41
- Electrochemical energy storage devices (EESD), 349
- Electrochemical exfoliated graphene (EEG), 77–78
- Electrochemical impedance spectroscopy (EIS), 153–154, 311–312
- Electrocodeposited—carbon nanotube (ECP-CNT), 359–360
- Electrode materials
 metal oxides as, 178–180
 pairing of, 355–356
- Electrode–electrolyte
 interface, 8–9, 111–113
 resistance, 38

- Electrodeposition, 118–119, 184, 207–208, 215–216
- Electrodes, 9–10
C-polymers based, 67–71, 71*f*
for supercapacitors, 73–74
- Electrolyte, 32, 271–273, 357, 358*t*
interface, 32
for supercapacitors and supercapattery, 273
- Electrolytic capacitors, 32–33
- Electromagnetic energy storage, 17
- Electromechanical devices, 63–64
- Electronics, 63–64
- Electrophoretic deposition (EPD), 72
- Electrosorption/electrodesorption, 38–39
- Electrospinning, 330
- Electrospun Co_3O_4 nanowires, 322
- Electrospun NiO fibers, 319
- Electrostatic
adsorption electrolyte ions, 50
capacitors, 32–33
charge separation, 175–176
interactions, 45–46
- ELIT, 271
- Emerging battery systems, 23
- EMIBF₄. *See* 1-Ethyl-3-methylimidazolium tetrafluoroborate (EMIBF₄)
- EMITFSI. *See* 1-Ethyl-3-methylimidazolium bis(trifluoromethyl sulfonyl)imide (EMITFSI)
- Energy density (E_s), 111–113, 262, 311
- Energy storage, 1–2, 4–5, 18, 28–29, 180
batteries and capacitors, 5–6
challenges and prospects of energy storage technologies
challenges of energy storage application, 18–19, 19*f*
prospects of energy storage technology development, 19–20, 20*f*
electrochemical energy storage systems and materials, 8–10
fundamentals of, 6–8
markets, 340–341
mechanism, 201–203
power *vs.* energy density characteristics, 5*f*
principle of energy storage in ECs, 31
systems costs and values, 20–21, 22*f*
technology development, 10–18, 12*f*
chemical energy storage, 18
electrochemical energy storage, 16–17
electromagnetic energy storage, 17
global energy storage capacity by technology type, 11*f*
heat storage, 15–16
mechanical energy storage, 11–15
technology frontiers, 21–23
emerging battery systems, 23
lithium-ion battery safety research, 22–23
solid-state battery R&D, 23
traditional battery technology, 21–22
typical electrical power profile, 3*f*
- Energy storage devices (ESD), 47–48, 74–75, 256–257, 283, 351–353
- EPD. *See* Electrophoretic deposition (EPD)
- EPRI. *See* Electric Power Research Institute (EPRI)
- Equivalent electrical circuit, 33–34, 34*f*
of EDLC cell, 37*f*
of pseudocapacitor, 39*f*
- Equivalent series resistance (ESR), 102–103, 359
- ESD. *See* Energy storage devices (ESD)
- ESR. *See* Equivalent series resistance (ESR)
- 1-Ethyl-3-methylimidazolium bis(trifluoromethyl sulfonyl)imide (EMITFSI), 258–259
- 1-Ethyl-3-methylimidazolium tetrafluoroborate (EMIBF₄), 258–259
- Ethylene carbonate (EC), 278–279
- 3,4-Ethylenedioxythiophene:poly(styrenesulfonate) (PEDOT:PSS), 164–165
- EVs. *See* Electric vehicles (EVs)
- Ex situ synthesis, 72
- Extrinsic pseudocapacitance, 56
- Extrinsic pseudocapacitive materials, 54
- Extrinsically conducted polymer, 66

F

Face centered cubic (fcc), 178
Faradaic energy storage, 38–39
 mechanism, 111–113
Faradaic processes, 39*f*, 82–84
Faradaic reactions, 45–46
fcc. *See* Face centered cubic (fcc)
Ferrites (MFe₂O₄), 123–128
 SEM image of CoFe₂O₄ nanotube
 arrays, 129*f*
 SEM results of ZnFe₂O₄ nanowall
 arrays, 127*f*
 synthesis process of porous CoFe₂O₄
 nanomesh arrays, 130*f*
Ferroelectric nanoparticles, 283
First thermodynamic law states, 6–7
Flexible hydrogel electrolytes, 292–301
Flexible supercapacitors, 292
 research, 317
Flow battery, 14–15, 15*f*, 21–22
Flywheel storage, 13
 energy storage rated power and
 discharge time, 14*f*
Fossil fuels, 349
Fossil production, 4–5
Free volume theory, 274–275
Fuel cells, 4–5, 18
Fullerene, 50
Futuristic room temperature ionic liquids,
 283

G

GA. *See* Glutaraldehyde (GA)
GA composite. *See* Graphene aerogel
 composite (GA composite)
Galvanostatic charge–discharge (GCD),
 50, 51*f*, 153–154, 175–176, 202,
 359
Gamma butyrolactone (γ -GBL), 102–103
GCD. *See* Galvanostatic charge–discharge
 (GCD)
Gel polymer electrolytes (GPEs), 271–273,
 285. *See also* Hydrogel electrolytes;
 Solid polymer electrolytes
Germanene, 255
Gibbs free energy, 7
Gibbs free energy change (ΔG), 9

Glutaraldehyde (GA), 292
GN. *See* Graphene (GN)
GO. *See* Graphene oxide (GO)
Gold (Au), 144–145
Gold NPs (Au NPs), 154
Gold-containing ternary nanocomposites,
 147
 and CNTs, 154
 CVs of NiCo₂O₄@Au at scan rates, 148*f*
 and GN, 158
 and PANI, 161
GPEs. *See* Gel polymer electrolytes (GPEs)
Graphene (GN), 50, 95–98, 141–142,
 155–158, 160, 201, 226–227, 341
 assembly of series connected CR2032
 coin cells, 98*f*
 gold-containing ternary nanocomposites,
 158
 sheets, 283
 silver-containing ternary
 nanocomposites, 156–157
 synthesis of graphene from graphite, 96*f*,
 241
Graphene aerogel composite (GA
 composite), 323
Graphene oxide (GO), 93
Graphene-based hydrogels, 289
Green chemistry, 355–356

H

HA-GPE. *See* Hydrogel poly(acrylamide)
 (HA-GPE)
hcp structures. *See* Hexagonal closed
 packed structures (hcp structures)
Heat storage, 15–16
Helmholtz plane/Stern layer capacitance,
 35–36
HEVs. *See* Hybrid electric vehicles (HEVs)
Hexagonal closed packed structures (hcp
 structures), 178
Hierarchical nitrogen-doped porous carbon
 nanotubes (HNPCNTs), 319–320
High dielectric constant polar solvents, 281
Hopping mechanism, 276
Host polymer types, 277–278
Hot-press technique, 280–281, 281*f*
HSC. *See* Hybrid supercapacitor (HSC)

- Hummer's method, 241
- Hybrid battery-supercapacitor energy storage system, 372
- Hybrid electric vehicles (HEVs), 28–29, 368
- Hybrid energy storage device, 47–48, 113–114
- Hybrid supercapacitor (HSC), 47–48, 175–178, 213, 215–216, 234–235, 271–273
- classification of electrochemical energy storage devices, 176*f*
 - prerequisites for supercapattery, 176–178
- Hybridization of metal oxides, 189–191
- metal oxide-based electrode composites, 191*t*
- Hydrated ruthenium oxide, 40
- Hydrazine, 265–266
- Hydro-talcite. *See* Anionic clay
- Hydrogel electrolytes, 285–301. *See also* Gel polymer electrolytes (GPEs); Solid polymer electrolytes
- flexible hydrogel electrolytes, 292–301
 - performance comparison, 300*t*
- Hydrogel poly(acrylamide) (HA-GPE), 295–297
- Hydrogels, 273
- structure of conducting, 293*f*
 - graphene-based, 289
 - polyaniline, 289–291
 - polypyrrole, 291–292
- Hydrogen
- bonding, 276–277
 - energy storage technologies, 18
- Hydrothermal method, 115–116, 330
- Hydrothermal/solvothermal synthesis, 115–116, 207
- Hydrous ruthenium oxide ($\text{RuO}_2 \cdot n\text{H}_2\text{O}$), 179
- I**
- IL electrolytes. *See* Ionic liquid electrolytes (IL electrolytes)
- Imidazolium, 283
- In situ polymerization process, 155–156
- In situ synthesis, 72
- Indirect synthesis, 203–204, 208–209
- Inert/passive/ceramic, 282
- Inorganic/active ceramic, 282
- Insolubility of conducting polymers, 361–363
- Intercalation, 51
- pseudocapacitance, 41, 56
 - pseudocapacitive materials, 55
 - system, 38–39
- Intractability of conducting polymers, 361–363
- Intrinsically conducted polymer, 66
- Ion conduction pattern
- Arrhenius theory, 276
 - free volume theory, 274–275
- Ion dipole, 276–277
- Ionic acid, 29–30
- Ionic liquid electrolytes (IL electrolytes), 36–37, 258–259
- Ionic liquids, 283
- Iron oxides (Fe_2O_4), 123–126
- K**
- κ -carrageenan, 278
- L**
- L-glutathione, 289
- Latent heat storage, 15–16
- Layered double hydroxide (LDH), 199–200, 265
- carbon material/LDH composites for supercapattery, 237–245
 - core-shell LDH, 226–237
 - energy storage mechanism, 201–203
 - nanostructures, 203–209
 - direct synthesis, 205–208
 - fabrication methods, 204*f*
 - indirect synthesis, 208–209
 - synthesis, 203–209
- structures, 200*f*
- transition metal LDH for supercapattery, 210–246
- Layered silicate nanocomposite, 75–76
- LCoS. *See* Levelized energy cost (LCoS)
- LDH. *See* Layered double hydroxide (LDH)
- Lead titanate (PbTiO_3), 283

- Levelized energy cost (LCoS), 20–21
- Lewis acid, 66
- Li-Fe-P batteries. *See* Lithium-iron-phosphate batteries (Li-Fe-P batteries)
- Li-NMC batteries. *See* Lithium-nickel-manganese-cobalt batteries (Li-NMC batteries)
- Li-oxygen batteries, 4–5
- Li-Ti batteries. *See* Titanium-lithium batteries (Li-Ti batteries)
- $\text{Li}_7\text{La}_3\text{Zr}_2\text{O}_{12}$. *See* Lithium lanthanum zirconium garnet (LLZO)
- LIBs. *See* Lithium-ion batteries (LIBs)
- LiCoO_2 electrode, crystallite size effect of, 55*f*
- Linear GCD, 53–54
- Liquid electrolytes, 273
- Lithium bis(fluorosulfonyl)imide, 283–284
- Lithium lanthanum zirconium garnet (LLZO), 282
- Lithium niobate (LiNbO_3), 283
- Lithium perchlorate (LiClO_4), 295–297
- Lithium-alumina (LiAl_2O_3), 282
- Lithium-ion batteries (LIBs), 2–4, 259–260
- safety research, 22–23
 - solid-state batteries, 23
- Lithium-iron-phosphate batteries (Li-Fe-P batteries), 16–17
- Lithium-nickel-manganese-cobalt batteries (Li-NMC batteries), 16–17
- Lithium-nitrogen (Li_2N), 282
- LLZO. *See* Lithium lanthanum zirconium garnet (LLZO)
- Low-potential deposition (UPD), 38–39
- M**
- Magnesium-based and proton-based EDLCs, 278–279
- Manganese (Mn), 210
- Manganese cobalt oxide (MnCo_2O_4), 230–232
- Manganese cobalt sulfide (MnCo_2S_4), 338
- Manganese cobaltite (MnCo_2O_4), 332
- Manganese dioxide (MnO_2), 183–185
- based nanocomposites, 184–185
 - nanoplate nickel foam electrode, 289
- Manganese ferrites (MnFe_2O_4), 128
- Manganites, 128–131
- Market potential, 367–372, 370*f*
- MC. *See* Mesoporous carbon (MC)
- MCs. *See* Metal chalcogenides (MCs)
- Mechanical degradation process, 77–78
- Mechanical energy storage, 6–7, 11–15
- CAES, 13
 - flow battery, 14–15
 - flywheel storage, 13
 - Na-S battery, 15
 - pumped hydro storage, 12
- Mechanical exfoliation, 241
- Memory effect, 203–204, 209
- Mesoporous carbon (MC), 314–315
- Mesoporous silica, 119
- Mesoporous ZnFe_2O_4 nanowall arrays, 126
- Metal carbides, 255
- Metal chalcogenides (MCs), 72, 74–75, 334
- MC-polymer nanocomposites, 72
- Metal hydroxides, 202–203, 325
- Metal ion capacitor (MIC), 261–262
- Metal monoxides (MO_x), 178
- Metal oxide-based composites materials, 79–80
- stretchable supercapacitor of graphene/PEDOT/ MnO_2 sponge ternary nanocomposite, 81*f*
- Metal oxide-based electrode composites, 191*t*
- Metal oxide/metal hydroxide-based SCAB, 312–334
- Co_3O_4 SCAB, 321–325
 - $\text{Cu}(\text{OH})_2$ SCAB, 325–327
 - CuO SCAB, 313–318
 - $\text{Ni}(\text{OH})_2$ SCAB, 328–330
 - NiO SCAB, 318–321
 - TMC SCAB, 330–334
- Metal oxide(s), 145–151, 312
- as electrode materials, 178–180
 - promising metal oxides, 178–179
 - rock salt (CoO) unit cell, 179*f*
 - technical issues with pure metal oxides, 179–180
 - electrodes, 180–189

- Metal oxide(s) (*Continued*)
 Co_3O_4 , 185–189
 CuO , 181–182
 MnO_2 , 183–185
 NiO , 180–181
 RuO_2 , 183
 V_2O_5 , 182–183
 gold-containing ternary nanocomposites, 147
 hybridization of, 189–191
 platinum-containing ternary nanocomposites, 147–151
 transition metal oxides, 146*f*
Metal transition oxides, 29–30
Metal-air batteries, 18, 22
Metal-organic frameworks (MOFs), 188–189
Metal/metal oxide thin film electrodes
 hybrid supercapacitors or supercapacities, 175–178
 hybridization of metal oxides, 189–191
 metal oxides as electrode materials, 178–180
 performance of metal oxide electrodes, 180–189
Methanol, 34–35
MIC. *See* Metal ion capacitor (MIC)
Microwave-assisted technique, 116
MOFs. *See* Metal-organic frameworks (MOFs)
Molten salt batteries, 22
Molten sodium, 15
Molten sulfur, 15
Molybdenum selenide (MoS_2), 338–339
Molybdenum trioxide (MoO_3), 178–179
Multiwalled carbon nanotubes (MWCNTs), 98–100, 141, 151–152, 152*f*, 153*f*, 238–239, 290
MXene. *See* Transition metal carbides (MXene)
- N**
N-dimethylformamide (DMF), 265–266
Na-S batteries, 2–4, 15
Nanocomposites, 71–72
 Co_3O_4 -based nanocomposites, 186–188, 187*f*, 188*f*
 of conducting polymer with nanomaterials
 carbon-based nanocomposite materials, 77–78
 metal oxide-based composite materials, 79–80
 MXene and transition metal dichalcogenides composites, 80–85
 CuO -based mixed oxides and, 182
 MnO_2 based nanocomposites, 184–185
Nanofillers, 282–283
Nanoflower morphology, 180–181
Nanomaterials, 54
 nanocomposites of conducting polymer with, 77–85
Nanoparticles (NPs), 141, 282–283
Nanosheets, 123, 181
Nanosized layered nickel hydroxide, 55
Nanotubes (NTs), 147
NASICON-structured LATP ($\text{Li}_{1+x}\text{Al}_x\text{Ti}_{2-x}(\text{PO}_4)_3$), 282
NCFS. *See* Noncapacitive faradaic storage (NCFS)
NEC. *See* Nippon Electric Company (NEC)
Nernstian process, 351
NF. *See* Nickel foam (NF)
NG. *See* Nitrogen-doped graphene (NG)
Ni/Co-DHM. *See* Nickel-cobalt double hydroxides microsphere (Ni/Co-DHM)
 $\text{Ni}(\text{OH})_2$ SCAB, 328–330
Nickel (Ni), 210
 nickel-based BMOs, 114–115
 sheet, 212–213
Nickel foam (NF), 103–104, 322
Nickel oxide (NiO), 48, 180–181
 SCAB, 318–321
 synthesis of NiO /graphene composite, 320*f*
 working of NiO SCAB, 321*f*
Nickel sulfide, 334–335

- Nickel–cobalt double hydroxides
 microsphere (Ni/Co-DHM),
 227–229
- Nickel–Cobalt layered double hydroxides
 (Ni–Co LDH), 210–226
 directly grown on electroactive
 substrates, 216–221
 electrodes prepared with binders,
 211–212
- Nickel–Manganese layered double
 heterostructures (Ni–Mn LDH),
 221–223
- Nickle cobaltite (NiCo_2O_4), 120–121
 structural arrangements of spinal, 121f
- Ni–Co LDH. *See* Nickel–Cobalt layered
 double hydroxides (Ni–Co LDH)
- Ni–Mn LDH. *See* Nickel–Manganese
 layered double heterostructures
 (Ni–Mn LDH)
- Nippon Electric Company (NEC), 271
- Nitrogen, 255
- Nitrogen-doped graphene (NG), 214–215
- Nitrogen–oxygen codoped porous carbon
 (NOPC), 189–190
- Non-Faradaic processes, 82–84
- Nonaqueous redox flow battery
 technologies, 21–22
- Nonaqueous-type electrolytes, 357–358
- Nonbiodegradable polymer. *See* Synthetic
 polymer
- Noncapacitive faradaic storage (NCFS),
 175
- Noncyclic C-polymers, 66
- NOPC. *See* Nitrogen–oxygen codoped
 porous carbon (NOPC)
- NPs. *See* Nanoparticles (NPs)
- NTs. *See* Nanotubes (NTs)
- O**
- Octadecyl methacrylate in vinyl sponge (S-
 PAA), 298–299, 299f
- OEM. *See* Original equipment
 manufacturer (OEM)
- Oligoether–based plasticizers, 281–282
- One-pot synthesis method, 118
- Optoelectronics, 63–64
- Organic electrolytes, 29–30, 273–274
- Organic liquids, 273
- Organic molecules, 119–120
- Original equipment manufacturer (OEM),
 369–370
- Oxidation, 40
 reduction process, 186
- P**
- p*-doped C-polymer, 66
- PA. *See* Polyacetylene (PA)
- PAAM hydrogels. *See* Polyacrylamide
 hydrogels (PAAM hydrogels)
- Palladium (Pd), 144–145
- Palladium-containing ternary
 nanocomposites, PANI, 161–162
- PAN. *See* Polyacrylonitrile (PAN)
- PAN-*b*-PEG-*b*-PAN copolymer, 284–285
- PANI. *See* Polyaniline (PANI)
- Passive nanofillers, 282–283
- PC. *See* Propylene carbonate (PC)
- PCs. *See* Pseudocapacitors (PCs)
- PDDA. *See* Poly(diallyl
 dimethylammonium chloride)
 (PDDA)
- PECVD. *See* Plasma-enhanced chemical
 vapor deposition (PECVD)
- PEDOT. *See* Poly(3,4-
 ethylenedioxythiophene) (PEDOT)
- PEDOT:PSS. *See* 3,4-
 Ethylenedioxythiophene:poly
 (styrenesulfonate) (PEDOT:PSS)
- PEG. *See* Polyethylene glycol (PEG)
- PEM. *See* Proton exchange membrane
 (PEM)
- PEMFC, 8–9
- PEO. *See* Poly(ethylene oxide) (PEO)
- PEO/LiTFSI/LiAlO₂. *See* Ceramic-based
 solid polymer electrolyte (PEO/
 LiTFSI/LiAlO₂)
- PEO/PDMS. *See* Poly(ethylene oxide)/
 poly(dimethyl siloxane) (PEO/
 PDMS)
- Permanent dipole, 276–277
- Phosphorene, 255
- Photoelectro-chemical processes, 8–9
- Photovoltaic system, 8–9
- PIL. *See* Poly(ionic liquid) (PIL)

- Piperidinium, 283
- Plasma-enhanced chemical vapor deposition (PECVD), 327
- Plasticization effect, 281–282
- Plasticizers, 281–282
- Platinum (Pt), 144–145
- Platinum-containing ternary nanocomposites, 147–151
- SEM images of Co_3O_4 , $\text{Co}_3\text{O}_4@\text{Pt}$, 150*f*
- Platinum-containing ternary nanocomposites, PANI, 162–163, 163*f*
- PMMA. *See* Poly(methylmethacrylate) (PMMA)
- Polarized “battery-type” electrode, 93
- Polarized “supercapacitor-type” electrode, 93
- Poly(2-hydroxyethyl methacrylate-comethyl methacrylate), 278
- Poly(3,4 ethylenedioxythiophene):poly(styrenesulfonate)/poly(vinyl alcohol)/poly(methacrylic acid) hydrogel electrode, 292
- Poly(acrylamide-co-acrylic acid), 276
- Poly(acrylic acid), 298–299
- Poly(diallyl dimethylammonium chloride) (PDDA), 241–242
- Poly(ethylene oxide) (PEO), 276, 278
- Poly(ethylene oxide)/poly(dimethyl siloxane) (PEO/PDMS), 275
- Poly(ionic liquid) (PIL), 283–284
- Poly(methylmethacrylate) (PMMA), 278
- Poly(phenylene)vinylene (PPV), 64, 141–144
- Poly(tri(4-(thiophen-2-yl)phenyl)amine) (pTTPA), 142–144
- Poly(vinyl alcohol)/poly(methacrylic acid)/phosphoric acid, 292
- Poly(vinyl chloride), 275
- Poly(vinyl pyrrolidone) (PVP), 278
- Poly(vinylidene fluoride-co-hexafluoropropylene) (PVdF-HFP), 278, 284–285
- Poly(3,4-ethylenedioxythiophene) (PEDOT), 141–144, 361–362
- Polyacetylene (PA), 64–65
- Polyacrylonitrile (PAN), 278
- Polyacrylamide, 278
- hydrogels, 294
- Polyacrylamide hydrogels (PAAM hydrogels), 294–295
- Polyacrylic acid hydrogels (PPA hydrogels), 295
- Polyampholyte hydrogels, 297–298
- Polyaniline (PANI), 64–65, 74–75, 141–144, 158–159, 235, 278, 289–290, 361–362
- hydrogels, 289–291
- supercapacitor, 292
- ternary composites of, 158–163
- gold-containing ternary nanocomposites, 161
- palladium-containing ternary nanocomposites, 161–162
- platinum-containing ternary nanocomposites, 162–163
- silver-containing ternary nanocomposites, 159–160
- Polyethylene glycol (PEG), 278
- Polyhedral oligomeric silsesquioxane (POSS), 283–284
- Polyheterocyclic C-polymers, 67
- Polymer electrolytes, 273–301
- GPEs, 285
- hydrogel electrolytes, 285–301
- ion conduction pattern
- Arrhenius theory, 276
- free volume theory, 274–275
- solid polymer electrolytes, 276–277
- Polymer/layered silicates nanocomposite, 75–77
- nanocomposite arises from interaction of layered silicates and polymers, 77*f*
- Polymer(s), 273–274, 361–362
- blends, 284
- containing noble metals, 164–165
- gels, 273
- nanocomposite, 71–77
- carbonaceous-polymer nanocomposites, 73–74
- chalcogenide-polymer nanocomposite, 74–75
- ex situ synthesis, 72

- polymer/layered silicates
 - nanocomposite, 75–77
 - in situ synthesis, 72
 - solids, 273
 - Polymeric backbone chain, 63–64
 - Polymeric matrix, 71–72
 - Polyphenylene (PPh), 64
 - Polypyrrole (PPy), 64–65, 67, 141–144, 278, 291–292, 294, 338, 361–362
 - containing noble metals, ternary nanocomposites of, 163–164
 - capacitance cycling performance, 165*f*
 - preparation procedure for GNS/AgNPs/PPY nanocomposites, 164*f*
 - hydrogels, 291–292
 - Polythiophene (PTh), 64–65, 67, 141–144, 164–165
 - ternary nanocomposites of, 164–165
 - CV curves of Ag-NW/PEDOT:PSS-NP, 166*f*
 - Polythiophene (P₃HT), 64
 - Polyvinyl alcohol (PVA), 75–76, 278, 293–294, 317
 - GPEs, 298–299
 - PVA-based hydrogels, 293–294
 - electrolytes, 293–294
 - Polyvinyl and polyvinyl alcohol, 75–76
 - Polyvinylidene fluoride (PVDF), 359–360
 - POSS. *See* Polyhedral oligomeric silsesquioxane (POSS)
 - Potassium chloride (KCl), 297–298
 - Potassium hydroxide (KOH), 293–294, 364
 - Potassium-ion batteries, 261
 - Potential-dependent pseudo-capacitance, 38
 - Power density (P_S), 262, 311
 - Power generation techniques, 1–2
 - PPA hydrogels. *See* Polyacrylic acid hydrogels (PPA hydrogels)
 - PPh. *See* Polyphenylene (PPh)
 - PPV. *See* Poly(phenylene)vinylene (PPV)
 - PPy. *See* Polypyrrole (PPy)
 - Propylene carbonate (PC), 281
 - Proton exchange membrane (PEM), 18
 - Pseudocapacitance, 175–176
 - types, 39–41
 - intercalation pseudocapacitance, 41
 - redox pseudocapacitance, 40
 - underpotential deposition, 39–40
 - Pseudocapacitive electrode, 50–51, 177–178
 - Pseudocapacitive materials, 47–58, 201
 - Li⁺ storage of Li₄Ti₅O₁₂ with capacitive currents, 57*f*
 - Pseudocapacitors (PCs), 31–32, 37–39, 38*f*, 175, 271–273, 292, 311, 359
 - Pseudocaps, 27–28
 - PTh. *See* Polythiophene (PTh)
 - pTTPA. *See* Poly(tri(4-(thiophen-2-yl)phenyl)amine) (pTTPA)
 - Pumped hydro storage, 12
 - Pumped hydroelectric plant, 4–5
 - Pumped storage power station, 11–12
 - PVA. *See* Polyvinyl alcohol (PVA)
 - PVAc/P(VdF-HFP)/lithium trifluoromethanesulfonate solid polymer electrolyte, 278–279
 - PVDF. *See* Polyvinylidene fluoride (PVDF)
 - PVdF-HFP. *See* Poly(vinylidene fluoride-co-hexafluoropropylene) (PVdF-HFP)
 - PVP. *See* Poly(vinyl pyrrolidone) (PVP)
 - Pyrrolidinium, 283
- ## Q
- Quasirectangular CV, 53–54
- ## R
- RCF. *See* Reclaimed carbon nanofiber (RCF)
 - Rechargeable batteries
 - function, 355
 - MXene in, 259–261
 - charge–discharge curves of 3D Ti₃C₂T_x film electrode, 261*f*
 - Rechargeable technology, 45–46
 - Reclaimed carbon nanofiber (RCF), 339
 - Reconstruction method, 209
 - Reduced graphene oxide (rGO), 93, 95–96, 156, 187–188, 241, 311–312
 - Reduction–oxidation (redox)
 - active metal oxides, 141

- Reduction–oxidation (redox) (*Continued*)
 electrolyte on performance of charge
 storage capacity, 357–359
 pseudocapacitance, 40
 for ruthenium oxide, 40*f*
 reactions, 37–38, 63–64, 256–257
 redox-active electrolyte species, 36–37
 redox-active materials, 353–354
- Renewable energy
 generation grid integration, 18
 production, 19–20
 resources, 45–46
- Renewable resources, 28–29
- Renewable sources, 349
- rGO. *See* Reduced graphene oxide (rGO)
- Room temperature ionic liquids, 283–284
- Ru–RuO₂ nanoparticles and activated carbon (Ru–RuO₂/AC), 190
- Ruthenium (Ru), 210
- Ruthenium dioxide, 176
- Ruthenium oxide (RuO₂), 183, 271
- Ruthenium redox, 40
- S**
- S-PAA. *See* Octadecyl methacrylate in vinyl sponge (S-PAA)
- SCAB. *See* Supercapattery (SCAB)
- SCAP. *See* Supercapattery (SCAP)
- SCs. *See* Supercapacitors (SCs)
- SDBS. *See* Sodium dodecylbenzene sulfonate (SDBS)
- Self-assembled 3D-interconnected porous network, 289
- Sensible heat storage, 15–16
- SIBs. *See* Sodium-ion batteries (SIBs)
- SILAR method. *See* Successive ionic layer adsorption and reaction method (SILAR method)
- Silicene, 255
- Silicon(IV) oxide (SiO₂), 282
- Silver (Ag), 144–145
 nanoparticles, 290
- Silver-containing ternary nanocomposites
 CNTs, 153–154
 GN, 156–157
 development of ternary nanocomposite, 157*f*
 GO containing functional groups, 155*f*
- PANI, 159–160
- Single-walled carbon nanotubes (SWCNTs), 93, 98–100, 99*f*, 151–152, 238–239
- SN. *See* Succinonitrile (SN)
- Sodium alginate, 297–298
- Sodium dodecylbenzene sulfonate (SDBS), 213
- Sodium sulfate–anionic polyurethane acrylates/polyacrylamide hydrogel electrolyte (Na₂SO₄-aPUA/PAAM hydrogel electrolyte), 294
- Sodium-ion batteries (SIBs), 260–261
- SOHIO. *See* Standard Oil of Ohia (SOHIO)
- Sol–gel synthesis, 205–206
- Solid electrode's bulk lattice, 41
- Solid polymer electrolytes, 276–277.
 See also Gel polymer electrolytes (GPEs); Hydrogel electrolytes copolymerization, 284–285
 host polymer types, 277–278
 hot-press technique, 280–281, 281*f*
 nanofillers, 282–283
 performance comparison, 286*t*
 plasticizers, 281–282
 polymer blends, 284
 room temperature ionic liquids, 283–284
 solution casting technique, 278–279
 synthetic host polymer, 278
- Solid-state battery R&D, 23
- Solid–solid conversion process, 327
- Solution casting technique, 278–279
 conventional, 279*f*
 modified, 280*f*
- Sonochemical method, 117–118
- Specific capacitance (SC), 361–362
- SPSU. *See* Sulfonated polysulfone (SPSU)
- Standard Oil of Ohia (SOHIO), 271
- Stibnium(III) oxide (Sb₂O₃), 282
- Successive ionic layer adsorption and reaction method (SILAR method), 316–317
- Succinonitrile (SN), 281–282
- Sulfonated polysulfone (SPSU), 275
- Supercapattery (SCAB), 312

- Supercapacitors (SCs), 8–9, 17, 27–30, 29*f*; 45–46, 67, 73–74, 111–113, 142–146, 175, 199, 256–257, 271–273, 294, 311, 349–350
- battery and supercapacitor comparison, 113*f*
- charge storage mechanism of supercapacitor materials, 112*f*
- development, 272*f*
- electrolytes for, 273
- MXene in, 256–259
- scan rate dependence on specific capacitance, 258*f*
- PANI, 292
- power density *vs.* energy density, 30*f*
- principle of energy storage in, 31
- Supercapattery (SCAP), 47–48, 113, 199, 271–273, 311, 351–353
- assembled supercapattery device, 47*f*
- BiMoO symmetrical SCAP
- performance, 365*t*
- BMOs for supercapattery applications, 133*t*
- cobaltites, 120–123
- ferrites, 123–128
- manganites, 128–131
- carbon material/LDH composites for, 237–245
- chalcogenides SCAPs, 334–339
- charge storage mechanism in EES systems, 48–52
- classification, 350*f*
- commercialization and applications, 339–341, 340*t*
- difference between pseudocapacitive and battery-grade materials, 52–58
- electrolytes for, 273
- future challenges, 302
- hybrid, 175–178
- market potential, 367–372, 370*f*
- metal oxide/metal hydroxide–based SCAB, 312–334
- MXene in, 261–266, 262*f*
- capacitance performance comparison of MXene electrode, 263*f*
- fabrication by LiF–HCl treatment, 264*f*
- performances, 366*t*
- polymer electrolytes, 273–301
- GPEs, 285
- hydrogel electrolytes, 285–301
- ion conduction pattern, 274–276
- solid polymer electrolytes, 276–277
- prerequisites for, 176–178
- prospects, 363–367
- Ragone plot of different energy storage devices, 46*f*
- technical challenges, 354–363, 354*f*
- diffusion issues related to electronic property, 356–357
- inadequate properties, 359–361
- insolubility and intractability of conducting polymers, 361–363
- pairing of electrode materials, 355–356
- redox electrolyte on performance of charge storage capacity, 357–359
- transition metal LDH for, 210–246
- binder-free Ni–Co LDH electrode, 212–216
- Ni–Co LDH directly grown on electroactive substrates, 216–221
- Ni–Co LDH electrodes prepared with binders, 211–212
- Surface redox reactions, 54, 175–176, 179
- Surface redox system, 38–39
- Surface-based faradaic reactions, 45–46
- Surfactants, 119–120
- Sustainable energy infrastructure, 2
- Sustainable/renewable sources, 349
- SWCNTs. *See* Single-walled carbon nanotubes (SWCNTs)
- Synthesized PANI hydrogels, 290
- Synthetic host polymer, 278
- Synthetic polymer, 278
- T**
- TEABF₄. *See* Tetraethylammonium tetrafluoroborate (TEABF₄)
- TEM. *See* Transmission electron microscopy (TEM)
- Template method, 119–120
- Template-free spontaneous growth approach, 329
- Ternary composites of PANI, 158–163
- Ternary nanocomposites

- Ternary nanocomposites (*Continued*)
 carbonaceous materials, 151–158
 conducting polymers, 158–165
 metal oxides, 145–151
 noble metals, 144–145
- Tetra ethylene glycol, 281
- Tetraethylammonium tetrafluoroborate (TEABF₄), 258–259
- Three-dimension (3D)
 CuO framework, 313
 graphene/VO₂ nanocomposite hydrogels, 289
- Titanium nitride nanotube (TiN), 213–214
- Titanium-lithium batteries (Li-Ti batteries), 16–17
- Titanium(IV) oxide (TiO₂), 282
- TMC, 312, 332–334
 supercapattery, 330–334
- TMDs. *See* Transition metal dichalcogenides (TMDs)
- TMO. *See* Transition metal oxides (TMO)
- Transition metal
 hydroxides, 203
 LDH for supercapattery, 210–246, 211*f*
- Transition metal carbides (MXene), 80–82, 255
 in rechargeable batteries, 259–261
 in SCs, 256–259
 structure and types of, 256, 256*f*
 in supercapattery, 261–266
 and transition metal dichalcogenides composites, 80–85
 electrochemical performance in terms of parameters, 85*t*
- Transition metal dichalcogenides (TMDs), 80–82
- Transition metal oxides (TMO), 50–51, 176
- Transmission electron microscopy (TEM), 295–296
- Triethylmethylammonium bromide, 283–284
- Two-dimension (2D)
 graphene, 255
 ionic lamellar structure, 199–200
- U**
Ultracapacitors, 17, 175
- Ultrasonic-microwave irradiation (US–MW), 278–279
- Underpotential deposition, 39–40, 51
- Uninterruptable power supply systems (UPS systems), 371
- Urea, 265–266
 hydrolysis, 206–207
- US–MW. *See* Ultrasonic-microwave irradiation (US–MW)
- V**
van der Waals, 41
 interactions, 289
- Vanadium oxide (VO₂), 289
- Vanadium pentoxide (V₂O₅), 182–183
- Vinyl hybrid silica nanoparticles (VSNPs), 294–295
- Vogel temperature, 274
- Vogel–Tamman–Fulcher models (VTF models), 274–275
- Voltage, 4–5
- VSNPs. *See* Vinyl hybrid silica nanoparticles (VSNPs)
- VTF models.
 See Vogel–Tamman–Fulcher models (VTF models)
- W**
William–Landel–Ferry models (WLF models), 274–275
- X**
X-ray absorption spectroscopy (XAS), 256–257
- Y**
Yttrium(III) oxide (Y₂O₃), 282
- Z**
Zeolitic imidazolate framework, 320–321
- Zirconium(IV) oxide (ZrO₂), 282
- ZnCo₂O₄
 surface characterization of mesoporous ZnCo₂O₄ microspheres, 124*f*
 surface studies of thin layered nanosheets, 125*f*
- ZnO–Au–NiO composites, 147